



THÈSE DE DOCTORAT D'AVIGNON UNIVERSITÉ

École Doctorale N° 536
AgroSciences & Sciences

Spécialité / Discipline de doctorat :
Chimie

INRAE-UMR 408 SQPOV
Sécurité et Qualité des Produits d'Origine Végétale

Présentée par
Julie-Anne FENGER

Les anthocyanes acylées en tant que colorants naturels

*Réactivité en solution aqueuse, complexation métallique
et stabilisation pour des applications alimentaires*

Acylated anthocyanins as natural colors

*Reactivity in aqueous solution, metal binding,
stabilization for food applications*

Soutenue publiquement le 26/03/2020 devant le jury composé de :

M. Victor de FREITAS, Professeur, REQUIMTE/LAQV, Porto **Rapporteur**

M. Sylvain GUYOT, Directeur de Recherche, INRAE-UR 1268 BIA, Rennes **Rapporteur**

Mme Véronique CHEYNIER, Directrice de Recherche, INRAE-UMR 1083 SPO, Montpellier **Examinatrice**

M. Stéphane QUIDEAU, Professeur, CNRS-UMR 5255, Université de Bordeaux **Examinateur**

M. Olivier DANGLES, Professeur, INRAE-UMR 408 SQPOV, Avignon Université **Directeur de thèse**

Abstract

Anthocyanins are ubiquitous plant pigments that exhibit bright colors from red to blue. Thus, they are good candidates to replace the synthetic food colors. However, the low stability of anthocyanin colors is a real hurdle to their industrial applications, especially under near neutral conditions required to express the blue color. A promising perspective is to resort to anthocyanins acylated by *p*-hydroxycinnamic acids, as these pigments develop color-stabilizing mechanisms (intramolecular copigmentation, self-association) based on strong π -stacking interactions between the anthocyanidin chromophore and the acyl residues. Therefore, this work investigates the structural transformations of acylated anthocyanins (proton transfer, water addition), their affinity to metal ions and their resistance to thermal degradation in the presence or absence of added metal ions. To that purpose, kinetic and thermodynamic studies by UV-visible spectroscopy are combined with the identification of degradation products by UPLC-DAD/MS.

The impact of the acyl residues (number, location, type) was deciphered from a series of isolated pigments from red cabbage and purple sweet potato. With the former, the acyl residue bound to the external glucose of the sophorose moiety provides a) optimal protection against attacks by H_2O , H_2O_2 and sulfite, b) improved affinity for metal ions, c) enhanced resistance against thermal degradation (for anthocyanins and their metal complexes). By contrast, caffeic acid, whether free or as an acyl residue (in purple sweet potato), accelerates the degradation of anthocyanins in spite of stabilizing the color.

Under moderate heating at pH 7, red cabbage anthocyanins were degraded into acylsophoroses, phloroglucinaldehyde-2-O-glucoside, protocatechuic acid, 3,5,7-trihydroxycoumarin derivatives, and 2,4,6-trihydroxyphenylacetic acid derivatives. Intramolecular acyl migration was also evidenced. The anionic base, a major colored form at pH 7, appears most vulnerable to autoxidation. The hydrogen peroxide thus produced is further involved in anthocyanin degradation. Overall, the tight binding of acylated anthocyanins to iron and aluminum ions and possibly the addition of natural antioxidants (*e.g.*, N-acetylcysteine) are promising perspectives for the development of stable natural blue colors.

Keywords: anthocyanin, hydroxycinnamic acid, natural color, iron, degradation, red cabbage, purple sweet potato

Résumé

Les anthocyanes sont des pigments d'origine végétale exprimant des couleurs vives allant du rouge au bleu. Ce sont donc de bons candidats pour remplacer les colorants alimentaires artificiels. Cependant, leur faible stabilité est un frein à ces applications, tout particulièrement en milieu neutre requis pour l'expression de la couleur bleue. Une perspective prometteuse est le recours aux anthocyanes acylées par les acides *p*-hydroxycinnamiques, car ces pigments développent des mécanismes protecteurs de la couleur (copigmentation intramoléculaire, auto-association) basés sur de fortes interactions d'empilement entre le chromophore et les résidus acyl. Ce travail étudie donc les transformations structurales d'anthocyanes acylées (transferts de proton, addition d'eau), leur affinité pour les ions métalliques et leur stabilité au cours d'un traitement thermique. Dans ce but, des études cinétiques et thermodynamiques par spectroscopie UV-visible sont combinées à l'identification de produits de dégradation par UPLC-DAD/MS.

L'impact des groupements acyl (nombre, position, type) a été étudié grâce à une gamme de pigments isolés du chou rouge et de la patate douce violette. Pour les premiers, les groupements acyl sur le sucre externe du groupement sophorose confèrent a) une protection optimale contre les attaques par H₂O, H₂O₂ and SO₃²⁻, b) une plus grande affinité pour les ions métalliques, c) une plus grande stabilité thermique (pour les pigments et leurs complexes). En revanche, l'acide caféique, qu'il soit libre ou bien sous forme de résidu acyl (cas des anthocyanes de la patate douce violette), accélère la dégradation des anthocyanes, bien qu'il stabilise la couleur.

Un traitement thermique modéré à pH 7 a converti les anthocyanes du chou rouge en acylsophoroses, phloroglucinaldéhyde-2-O-glucoside, acide protocatéchique, dérivés de la 3,5,7-trihydroxycoumarine et de l'acide 2,4,6-trihydroxyphenylacétique. Un phénomène de migration intramoléculaire de résidus acyl a également été mis en évidence. La base anionique, une forme colorée majeure à pH 7, apparaît comme la plus vulnérable à l'autoxydation. Le peroxyde d'hydrogène ainsi formé est également impliqué dans la dégradation des anthocyanes.

Globalement, nos résultats montrent que la forte association des anthocyanes acylées avec les ions du fer et de l'aluminium, voire l'ajout d'antioxydants naturels (par ex., la N-acétylcystéine), constituent des voies d'avenir pour le développement de colorants bleus naturels stables.

Mots-clés : anthocyane, acide hydroxycinnamique, dégradation, fer, colorant naturel, chou rouge, patate douce violette

Valorization

The present results were communicated through the following international communications, in the chronological order:

PUBLICATIONS IN PEER-REVIEWED JOURNALS

- Dangles, O., & **Fenger, J.-A.** (2018). The Chemical Reactivity of Anthocyanins and Its Consequences in Food Science and Nutrition. *Molecules*, 23(8), 1970. <https://doi.org/10.3390/molecules23081970>
- **Fenger, J.-A.**, Moloney, M., Robbins, R. J., Collins, T. M., & Dangles, O. (2019). The influence of acylation, metal binding and natural antioxidants on the thermal stability of red cabbage anthocyanins in neutral solution. *Food & Function*, 10(10), 6740–6751. <https://doi.org/10.1039/C9FO01884K>
- **Fenger, J.-A.**, Robbins, R. J., Collins, T. M., & Dangles, O. (2020). The fate of acylated anthocyanins in mildly heated neutral solution. *Dyes and Pigments*, 178, 108326. <https://doi.org/10.1016/j.dyepig.2020.108326>
- **Fenger, J.-A.**, Roux, H., Robbins, R. J., Collins, T. M., & Dangles, O. (2020). The influence of phenolic acyl groups on the color of purple sweet potato anthocyanins and their metal complexes. *Dyes and Pigments*, 108792. <https://doi.org/10.1016/j.dyepig.2020.108792>
- **Fenger, J.-A.**, Sigurdson, G. T., Robbins, R. J., Collins, T. M., Giusti, M. M., & Dangles, O. (2021). Acylated Anthocyanins from Red Cabbage and Purple Sweet Potato Can Bind Metal Ions and Produce Stable Blue Colors. *International Journal of Molecular Sciences*, 22(9), 4551. <https://doi.org/10.3390/ijms22094551>
- Denish, P. R., **Fenger, J.-A.**, Powers, R., Sigurdson, G. T., Grisanti, L., Guggenheim, K. G., Laporte, S., Li, J., Kondo, T., Magistrato, A., Moloney, M. P., Riley, M., Rusishvili, M., Ahmadiani, N., Baroni, S., Dangles, O., Giusti, M., Collins, T. M., Didzbalis, J., ... Robbins, R. J. (2021). Discovery of a natural cyan blue: A unique food-sourced anthocyanin could replace synthetic brilliant blue. *Science Advances*, 7(15), eabe7871. <https://doi.org/10.1126/sciadv.abe7871>

ORAL COMMUNICATIONS AT INTERNATIONAL CONGRESSES

- **J.-A. Fenger**, R. Robbins, T. Collins, O. Dangles (2019). Thermal degradation of red cabbage anthocyanins with different acylation pattern at neutral pH, and impact of metal binding. 10th International Workshop on Anthocyanins (IWA), San Michele all'Adige, Italy (9 Sept. 2019)
- O. Dangles, **J.-A. Fenger**, R. Robbins, T. Collins (2019). The influence of acylation on the color and pigment stability of red cabbage anthocyanins under neutral conditions. 10th IWA, San Michele all'Adige, Italy (10 Sept. 2019)

POSTER PRESENTED AT INTERNATIONAL CONGRESSES

- **J.-A. Fenger**, C. Barcliff, R. Robbins, T. Collins, O. Dangles (2018). Purple sweet potato anthocyanins: water addition, acid-base equilibria and chemical stability in acidic to mildly alkaline conditions. 29th International Conference on Polyphenols (ICP), Madison, Wisconsin, USA (July. 2018)

Remerciements / Acknowledgements

Cette thèse est le fruit de trois années enrichissantes et challengeantes,

First of all, I thank Rebecca J. Robbins for having led this ambitious project, and for her continuous guidance throughout my doctoral program. Thank to all the Mars and Wrigley teams for having invited me and trained me to their gum & confectionery processing facilities, and for their warm welcome.

Merci à Olivier Dangles, mon directeur de thèse, admirable sur tant d'aspects, qui m'a inspiré par sa culture scientifique et générale, sa structure intellectuelle, et émue pour ses valeurs humaines et son attachement aux traditions. Merci de m'avoir guidée tout au long de cette thèse, dans une liberté totale et inespérée. Merci infiniment pour la confiance que tu m'as accordée.

Merci aux membres du jury, Victor de Freitas, Sylvain Guyot, Véronique Cheynier et Stéphane Quideau pour leur patiente lecture de ce manuscrit. Un remerciement tout particulier pour Véronique Cheynier pour son support au cours de cette thèse, ses conseils lors des comités de suivi de thèse, et concernant la spectroscopie de masse. Merci aussi à Christian Ginies pour m'avoir transmis ses compétences sur cet outil, ainsi qu'à mes stagiaires ; et à Raphaël Lugan de m'avoir accordé sa confiance pour l'utilisation du ToF.

Merci à Catherine Renard et Carine Le Bourvellec pour leurs conseils lors des comités de suivi de thèse. Merci à Raphaël pour sa contribution au programme de conversion de la couleur, et à mes collègues Maxence, Sheiraz et Nathalie pour leur contribution à la vie du laboratoire.

Merci à ma famille bienveillante, à mes chères grand-mères. A Guillaume, mon grand frère, mon modèle. A mes parents, à mon père et son approbation discrète mais néanmoins précieuse. A mon oncle Daniel pour assouvir ma curiosité intellectuelle et m'avoir éveillé sur la physique, notamment l'énergie.

A Clément, une source de créativité inépuisable, mais surtout la source des solutions aux maux de ce monde. Merci pour ta « bienveillance inconditionnelle ».

Enfin, merci à mes amis écrivains, Mick, Valentin et Hugo, pour partager leur vision sensible et non consensuelle du monde.

A mes ami.e.s pour leur élan de vie et d'énergie, Adèle, Karine, Caroline, Mélanie, Luz, Fanny, Xavier, Fred et Greg.

*« Le monde ne sera pas détruit par ceux qui font le mal,
mais par ceux qui les regardent sans rien faire ».*

Albert Einstein

TABLE OF CONTENTS

Abstract	2
Valorization.....	4
Remerciements / Acknowledgements	6
Abbreviations and symbols	12
List of figures & tables	14
Introduction	25
Chapter 1. Literature review	29
1. The quest of a blue natural food color.....	30
1.1. The importance of food color	30
1.2. What is color?.....	30
1.3. The diversity and traditional uses of natural pigments	34
1.4. Natural & synthetic food colors	36
Food color regulation	38
2. Phenolic compounds	40
2.1. General properties	40
2.2. Flavonoids: structural diversity and functions in plants.....	40
2.3. Anthocyanin structure diversity, biosynthesis, occurrence and functions in plants ..	42
3. Anthocyanin color stability	51
3.1. Search methodology	51
3.2. The chemical reactivity of anthocyanins.....	51
The Chemical Reactivity of Anthocyanins and its Consequences in Food Science and Nutrition	52
1. Introduction	53
2. The Basis of Anthocyanin Chemistry	53
3. The Importance of Anthocyanin Chemistry in Food and Nutrition	76
References	81

3.2. The chemical reactivity of anthocyanins (continuation)	87
3.3. Color stability	100
References for chapter 1	105
Chapter 2. The influence of acylation, metal binding and natural antioxidants on the thermal stability of red cabbage anthocyanins in neutral solution	113
1. Introduction	115
2. Materials and methods	118
3. Results & discussion	122
3.1. Color loss and true anthocyanin degradation	122
3.2. Chalcone isomerization	126
3.3. Metal binding	129
3.4. Impact of dioxygen and antioxidants	132
3.5. Impact of acylation on the addition of hydrogen peroxide and bisulfite	133
3.6. Refined kinetic analysis	135
References	139
Supplementary Information	141
Chapter 3. The fate of acylated anthocyanins in neutral mildly heated solution	147
1. Introduction	160
2. Materials & methods	162
3. Results	164
3.1. Hydration and the reversible accumulation of the <i>trans</i> -chalcone	168
3.2. Deacylation & intramolecular acyl transfer	168
3.3. The oxidative products & degradation routes	171
4. Discussion	178
References	184
Supplementary Information	186
Chapter 4. Acylated anthocyanins from Red Cabbage and Purple Sweet Potato can bind metal ions and produce stable blue colors	201

1. Introduction	202
2. Results and Discussion.....	204
2.1. The Color and Spectral Properties of the Metal Complexes	204
2.2. Kinetic Analysis and Stoichiometry of Metal Binding	211
2.3. Competition between Metal Binding and Water Addition.....	215
2.4. Long-Term Stability of the Metal Complexes	218
3. Materials and Methods	219
3.1. Metal-Binding Experiments	219
3.1.1. Red Cabbage Anthocyanins	219
3.1.2. Purple Sweet Potato Anthocyanins	220
3.2. Kinetic Analyses	220
3.3. Colorimetric Data	220
3.4. High-Resolution Mass Spectrometry (HRMS)	220
3.5. Thermal Degradation.....	221
4. Conclusions	221
Supplementary Information.....	224
Chapter 5. The influence of phenolic acyl groups on the color of purple sweet potato anthocyanins and their metal complexes	237
1. Introduction	239
2. Materials and methods	240
3. Results and discussion.....	245
3.1. Structural transformations of PSP anthocyanins	245
3.2. Metal binding	249
3.3. Thermal stability	255
References	261
Supplementary information.....	263
Chapter 6. General discussion.....	276

1. Color expression.....	276
2. Color stability.....	278
3. Color stabilization by metal binding	284
4. Behavior of two-group extracts	288
5. Perspectives	289
References	297
Appendices	300

Abbreviations and symbols

A	Absorbance
A _f	Final absorbance
A _i	Initial absorbance
BHT	Butylated hydroxyanisole
C1	3,5,7-trihydroxycoumarin
C2	Protocatechuic acid
C3	2,4,6-trihydroxyphenylacetic acid
C4	Phloroglucinaldehyde
CD	Circular dichroism
Cf	Caffeic acid
CGA	Chlorogenic acid
Cy	Cyanidin
CZE	Capillary zone electrophoresis
DAA	Diacylated anthocyanins
DLS	Dynamic light scattering
Dp	Delphinidin
DPPH	2,2-diphenyl-1-picrylhydrazyl
EtOH	Ethanol
E131	Patent blue V (European Union regulation)
E132	Indigo carmine (FD&C 2)
E133	Brilliant blue (FD&C 1)
ESI	Electrospray Source Ionisation
FD&C	Food, drug and cosmetic Act regulation (USA)
Fe ²⁺ /Fe ³⁺	Ferrous/ferric ions
Fl	Ferulic acid
[M-H]	Molecular ion with loss of a proton, regardless of the charges
H	Hydrogen atom/ Proton (for MS ions)
HAT	Hydrogen atom transfer
HBA	Hydroxybenzoic acid
HCA	Hydroxycinnamic acid
HPLC	High pressure liquid chromatography
(HR)-MS	(High-resolution) mass spectrometry
HSO ₃ ⁻ /SO ₃ ²⁻	Sulfite/bisulfite ion

k	Rate constant
k'/k_{app}	Apparent rate constant
K	Thermodynamic equilibrium constant
K'/K_{app}	Apparent thermodynamic constant
K_{a1}	First acidity constant
K_{a2}	Second acidity constant
K_{h}	Hydration constant
K_{t}	Tautomerization constant
K_{i}	Isomerization constant
M	Molecular ion
MAA	Monoacylated anthocyanins
MM	Molar mass
MW	Molecular weight
NAA	Non-acylated anthocyanins
NMR	Nuclear magnetic resonance
pC	<i>p</i> -coumaric acid
Pn	Peonidin
PSPE	Purple sweet potato anthocyanin extract
PCA	Protocatechuic acid
PGA	Phloroglucinaldehyde
ppm	Part per million
RCE	Red cabbage extract
RP	Reverse phase
R_{t}^2	Retention time
Sh	Shoulder
Sp	Sinapic acid
TD-DFT	Time-dependent density functional theory
ToF	Time of flight detector
UPLC	Ultra-high performance liquid chromatography
USA	United States of America
UV	Ultra-violet
Δ	Delta, referring to a % variation, generally $(A_{\text{f}} - A_{\text{i}}) / A_{\text{i}}$
ϵ	Molar absorption coefficient
λ_{max}	Wavelength of maximal absorption
χ / \mathcal{X}	Fraction (molar unless specified)

List of figures & tables

CHAPTER 1

Fig. 1. Absorption spectra of natural pigments: the photosynthetic chlorophylls a and b; the accessory pigment β -carotene and the non-photosynthetic cyanidin-3,5-diglucoside (spectral data from Taniguchi, 2001 & Li, 1997)

Fig. 2. a) Sensitivity of cones and rods (dashed black line) to light, according to the wavelength (Bowmaker & Dartnall, 1980), b) CIE color matching functions $X(\lambda)$, $Y(\lambda)$, $Z(\lambda)$ defined for a standard colorimetric observer (CIE Standard, 2004).

Scheme 1. Occurrence of simultaneous physical and chemical phenomena impacting the color in a quartz cuvette, and associated hypothetical trajectories of the incident light rays.

Scheme 2. Structures of three synthetic blue food colors, brilliant blue and patent blue V (triarylmethane); and the oxo-indoline indigo carmine.

Scheme 3. Structures of hemisynthetic blue colors derived from anthocyanins: the Portisin (P) and Pyranomalvidin-3-galactoside (PD) dyes in their pyranoflavylum cation form, insert: picture of the PD solution at pH 2 (adapted from Araújo et al., 2018).

Scheme 4. Examples of structure of flavonoids

Scheme 5. Structure of the 6 main anthocyanin aglycones (anthocyanidins)

Scheme 6. Biosynthetic pathways of the synthesis of flavonoids and anthocyanins, example of pelargonidin and cyanidin. Adapted from Falcone Ferreyra, 2012 and Appelhagen, 2018. Enzyme abbreviations: PAL: phenylalanine ammonia-lyase; C4H: cinnamate-4-hydrogenase; 4CL: 4-coumarate-CoA ligase; CHS Chalcone synthase; CHI chalcone isomerase; F3H flavanone 3-hydroxylase; F3'H flavonoid-3'-hydroxylase; DFR dihydroflavonol 4-reductase; ANS anthocyanidin synthase.

Fig. 3. a) Pigmentation in *Arabidopsis thaliana* leaves due to anthocyanin accumulation, b) Anthocyanin localization in *A. thaliana* leaves epidermal cells (Kubo et al., 1999), c) Epidermal cells of *Rhoeo discolor* (*Tradescantia spathacea*) after plasmolysis. The vacuoles (pink) have shrunk. Size: ca. 450 μm (Innsbruck, 2004).

Table 1. Anthocyanin structure and content in common foodstuffs.

Fig. 4. Calculated absorption spectra of the flavylum, neutral base and anionic base of purple sweet potato anthocyanin P12: Pn-3-(Cf,Fl)Soph-5-Glc

Scheme 7. Anthocyanins with various glycosylation and acylation patterns from a) red cabbage leaves, b) black carrot roots and c) butterfly pea flower.

Fig. 5. a) Evolution of the number of research items for “Anthocyanins AND stability” in the “Food science & technology field”, vs. control (all fields). Source: Web of Science. b) Evolution of the number of research items in 3 major research areas for “Anthocyanins and Stability”.

Scheme 8. Electrophilic and nucleophilic sites of anthocyanin forms

Scheme 9. The two routes followed by the flavylum cation in aqueous solutions: the acid/base equilibria (top) and hydration equilibria (bottom), and association thermodynamic constants (adapted from Pina et al., 2012).

Table 3. Thermodynamic and kinetic constants used to describe the physico-chemical behavior of anthocyanins.

Fig 5. Distribution diagram of pigments PA (*left*), P1 (*center*) and P4 (*right*) at $t = 0$ (top) and at equilibrium (Moloney et al., 2018). —: flavylium ion, —: neutral base, —: anionic base, —: colorless forms (25°C).

Scheme 10. A. Coordination of Fe^{2+} by *o*-diphenol rings and subsequent electron transfer in the presence of oxygen generating the Fe^{3+} -polyphenol complex; B. Coordination of Fe^{3+} by polyphenols, subsequent iron reduction and semiquinone formation, and reduction of Fe^{3+} to form a quinone species and Fe^{2+} . R=H, OH (from Perron & Brumaghim, 2009).

Table 4. Anthocyanin degradation products isolated and characterized by NMR.

Scheme 11. Electrophilic addition of H_2O_2 to flavylium – water (hemiketal) or alcohol adducts resulting in mono-oxygenation (consistent by ^{18}O labelling and MS analysis, Satake & Yanase, 2018)

Scheme 12. Nucleophilic addition of H_2O_2 to the flavylium ion resulting in dioxygenation (not consistent by ^{18}O labeling and MS analysis, Satake & Yanase, 2018)

Table 5. Electrochemical and chemical and thermodynamical constants of different HCAs.

Scheme 13. Structure of different hydroxycinnamic acids

Scheme 14. Three types of caffeic acid dimers. *Left*: major lactone dimers identified in Antolovich et al., 2004. *Center*: tetrahydrofuran derivative identified in Fulcrand et al., 1994, stereoisomers not represented. *Right*: 2,3-dihydro-1,4-benzodioxan-type caffeicins identified in Cilliers & Singleton, 1991.

Scheme 15. π - π Stacking interactions in anthocyanins and their complexes. (A) intermolecular copigmentation, (B) self-association, (C) intramolecular copigmentation in acylated anthocyanins, (D) self-association of acylated anthocyanins, (E) intercalation in intermolecular copigmentation, and (F) copigmentation in metal–anthocyanin complexes, from Trouillas et al., 2016a).

LITERATURE REVIEW

Figure 1. Flavylium ions are weak diacids.

Figure 2. (I) Absorption spectra of Cat-Mv3Glc: pH jump from pH = 1.0 (100% flavylium) to pH 3.00, 3.59, 4.50, 5.70, 5.96, 6.25, and 7.15, respectively. Spectra recorded 10 ms after mixing (negligible water addition). (II) Spectra of the components obtained by mathematical decomposition. From [4] with permission of the *American Chemical Society*.

Figure 3. Flavylium ions are hard electrophiles reacting at C2 with O-centered nucleophiles, such as water (water addition followed by formation of minor concentrations of chalcones).

Figure 4. Simulations of the pH dependence of the apparent rate constant (A) and relative magnitude (B) of color loss. Selected values for parameters: $\text{p}K_{\text{a}1} = 4$, $\text{p}K_{\text{a}1} = 7$, $\text{p}K'_{\text{h}} = 2.5$, $k_{\text{h}} = 0.1 \text{ s}^{-1}$, $k'_{-\text{h}} \approx k_{\text{h}}/K'_{\text{h}}$.

Figure 5. (I) Spectral changes of Cat-Mv3Glc between 10 ms and 9 s following a pH jump from pH = 1 to pH = 2.45; half-life of flavylium = 2.4 s. (II) pH jump from pH = 1 to pH = 4.5; half-life of quinonoid bases = 53.3 s. At pH = 6, the half-life of quinonoid bases \approx 30 min. From reference [4] with permission of the *American Chemical Society*.

Figure 6. Flavylium ions are soft electrophiles that react at C4 with S- and C-centered nucleophiles, such as bisulfite and 4-vinylphenols.

Figure 7. Anthocyanin hemiketals are nucleophiles reacting with carbocations (Ar = catechol ring).

Figure 8. Pathways of anthocyanin degradation.

Figure 9. Possible mechanisms of anthocyanin degradation with pre-formed hydrogen peroxide.

Figure 10. Possible mechanisms of anthocyanin degradation without pre-formed hydrogen peroxide.

Table 1. Antioxidant activity of malvidin 3-*O*- β -D-glucoside (oenin) and related pigments: reduction of the DPPH (2,2-diphenyl-1-picrylhydrazyl) radical (MeOH, 25 °C, ¹ and ²) and inhibition of heme-induced peroxidation of linoleic acid (0.1 mM linoleic acid in acetate buffer + 2 mM Tween-20, 0.1 μ M metmyoglobin, pH = 4, 37 °C, ³). From reference [29].

Figure 11. Possible mechanisms for the antioxidant activity of anthocyanins in food and in the gastrointestinal tract.

Figure 12. Co-pigmentation of malvin (malvidin 3,5-diglucoside, 50 μ M) by rutin bis(hydrogensuccinate) (mixture of 3 regioisomers, 200 equiv.). (A) pH = 3.5, malvin + co-pigment at T = 15.5 (1), 25.0 (2), 35.0 (3), 44.2 (4) °C, malvin alone at T = 25.3 °C (5). (B) pH = 0.9, T = 25.0 °C, malvin alone (1), malvin + co-pigment (2). Adapted from reference [35].

Figure 13. Acylated anthocyanins: discrimination of intramolecular co-pigmentation (type 1) and self-association (types 2 and 3) by circular dichroism (pink or blue CD spectra depending on the chirality of the stacks). From [34] with permission of the *Royal Society of Chemistry*.

Figure 14. Triacylated (B) vs. non-acylated (A) *Morning glory* (*Pharbitis nil*) anthocyanins: equilibrium distribution of anthocyanin species in aqueous solution. Red solid line: flavylium ion, blue solid line: neutral base, dotted green line: total colorless forms. Parameters for plots are $pK_h^* = 2.30$, $pK_{a1} = 4.21$ (A); $pK_h^* = 4.01$, $pK_{a1} = 4.32$ (B). From [36,37].

Figure 15. (A) 3',4'-Dihydroxy-7-*O*- β -D-glucopyranosyloxyflavylium (50 μ M) in a pH 4 buffer (0.1 M acetate), red spectrum: before hydration, blue spectrum: 10 min after addition of Al³⁺ (4 equiv.); (B) equilibrium distribution of species in aqueous solution. Red solid line: flavylium ion, blue dotted line: neutral base, dotted green line: total colorless forms, blue solid line: Al³⁺ complex. Parameters for plots are $pK_h^* = 3.42$, $pK_{a1} = 4.72$, $K_M = 2 \times 10^{-4}$. From [39].

Figure 16. (A) Frontier MOs of the flavylium ion of cyanidin (from reference (Anouar et al., 2012a)) and its most representative mesomeric forms in the ground state (left) and first excited state (right). (B) The fate of free anthocyanins in the excited state (from references [54,56]).

Figure 17. The influence of co-pigmentation on the fate of anthocyanins in the excited state. (A) Intermolecular co-pigmentation (from reference [57]). (B) Intramolecular co-pigmentation (from reference [58]).

Table 2. Serum pharmacokinetic profiles of cyanidin 3-glucoside (C3G) and its metabolites in humans after the consumption of 500 mg ¹³C-labelled C3G. From reference [3] (in red is the reference compound and its most abundant metabolites).

CHAPTER 2

Fig. 1. A: Color loss at pH 7, 50°C. Pigment A (+), P1 (●), P4 (■). B: Anthocyanin loss (residual flavylium ion after acidification to pH 1 – 2 and 48h stabilization at room temperature).

Fig. 2. Distribution diagrams for pigments A, 1 and 4 at equilibrium. —: flavylium ion, —: neutral base, —: anionic base, ---: colorless forms (25°C). Calculated apparent rate constants of water addition (from eqn. (4) in text) and corresponding half-life values at 25°C.

Fig. 3. A: Spectra of the iron complexes of pigment A, P2 and P5 (1 equiv. Fe²⁺, pH 7, 25°C). B: Maximal amplitude in the development of the iron complex's visible band as a function of the metal/pigment molar ratio.

Fig. 4. A & B: Color loss at pH 7, 50°C. C & D: Residual fraction of anthocyanin (colored + colorless forms, spectroscopic titration in acidified samples after 1h-incubation at RT) at pH 7, 50°C. Pigment alone (■), pigment + 0.6 equiv. Fe²⁺ (+), pigment + 5 equiv. NAC (▲). A & C: PA, under argon (+). B & D: P4.

Fig. 5. Color changes in P6 solutions at pH 7, 50°C following addition of Fe²⁺ (0.6 equiv.) and storage over 24h (pigment concentration = 50 μM).

Fig. 6. Kinetics of bleaching (pH 7, room temperature). A: After addition of H₂O₂ (103 equiv.). B: After addition of sodium bisulfite (5 equiv.). ○: PA, +: P2, —: P5, — —: red cabbage extract.

Fig. 7. Kinetic analysis of the thermal stability of P1 at pH 7, 50°C. X_n (■, fraction of colored forms): r = 0.999, X_h (●, fraction of colorless hydrated forms): r = 0.982, X_d (▲, fraction of colorless degradation products): r = 0.942. Curve-fitting according to eqns (1) – (3) gave the following optimized rate constants: k_{DA} = 0.193 (± 0.013), k_h = 1.77 (± 0.12), k_{-h} = 0.58 (± 0.06) h⁻¹.

Table 1. Distribution of colored forms / hemiketal + cis-chalcone / trans-chalcone / degradation products (D) after 2h of heating at 50°C, pH 7 for pigment A, P1 and P4. First part of Table 1 gathers molar absorption coefficients and absorbance values used in the calculations.

Table 2. Rate constants of hydrogen peroxide (103 equiv.) and bisulfite (5 equiv.) addition to anthocyanins at pH 7, room temperature.

Table 3. Kinetic analysis of thermal degradation at 50°C. Apparent rate constants k_{DA}, k_h and k_{-h} refer to the degradation of the colored forms, and to the hydration and dehydration steps, respectively.

Scheme 1. The red cabbage anthocyanins studied in this work.

Scheme 2. Structural transformations of anthocyanins in acidic to neutral aqueous solution.

Scheme 3. The protocol for assessing the distribution of species in a neutral anthocyanin sample after thermal treatment.

Scheme 4. A simplified kinetic scheme for analyzing the thermal degradation of anthocyanins in neutral solution.

Fig. 1-SI Spectroscopic monitoring of color loss at pH 7, 50°C. **A:** Pigment A (+), P1 (○), P4 (■), **B:** same pigments in the presence of 0.6 equiv. Fe²⁺.

Fig. 2-SI **A:** The slow conversion of the *trans*-chalcone to flavylium ion (25°C) after acidification to pH 1-2 of samples uptaken after a 2h period of thermal treatment at pH 7, 50°C. A₀ = absorbance immediately after acidification. PA (+), P1 (○), P4 (■), RCE (X). First-order curve fitting gives: k_{obs} (x10⁻³, h⁻¹) = 106.0 ± 2.3 (PA), 31.7 ± 0.1 (P1), 37.4 ± 0.6 (P4) and 31.4 ± 0.7 (RCE). **B:** —: intact pigment A (control, pure flavylium), — —: sample immediately after acidification (flavylium + Ct + degradation products), — — —: sample after incubation for 48h (flavylium + degradation products). **C:** Normalized spectrum of the *trans*-chalcone deduced from the spectra of part B.

Fig. 3-SI Kinetic simulations for the degradation of pigment A at pH 7, 50°C. First graph: curve-fitting of the experimental data. Graphs 1-3: simulations from parameters reported in Table. X_n: —, X_h: — —, X_d: — — —.

Fig. 4-SI Kinetic simulations for the degradation of P4 at pH 7, 50°C. First graph: curve-fitting of the experimental data. Graphs 1-3: simulations from parameters reported in Table. X_n: —, X_h: — —, X_d: — — —.

Table 1-SI Apparent rate constants and amplitudes of color loss at pH 7 deduced from mono- or biexponential curve-fitting (r > 0.999).

CHAPTER 3

Scheme 1-SI. a) Structural transformations of anthocyanins in aqueous solutions.

Fig 1-SI. Species distribution at a) pH 7 and b) pH 8, calculated at 25°C from the acidity and hydration thermodynamic constants [3].

Fig 2-SI. UV-visible and mass spectra of the pigments and their *trans*-chalcones. P4 isomer obtained after heating for 24h at 50°C, pH 7.

Fig 3-SI. a) Formation of the *trans*-chalcone (Ct) of PA (●) and irreversible degradation of the flavylium ion (AH⁺) (■). b) Estimated fractions of *trans*-chalcone and degradation products (D) from PA, P1, P4 after 2h at pH 7, 50°C. c) Same data calculated after 2h and 24h.

Table 1-SI. Product quantification in PA, P1 and P4 solutions after 24h at pH 7, 50°C.

Scheme 2-SI. Proposed fragmentation pattern for ion [M-H]⁻ *m/z* 481 attributed to C3(Glc)-C2 from PA.

Fig 4-SI. UV, MS and MS² spectra of the coumarin derivatives from PA (*m/z* 679) and P1 (*m/z* 825), structure proposals.

Fig 5-SI. Identification data for compound **1'** = *p*-coumaroylsophorose from P1 (major isomer at R_t = 4.55 min): a) DAD spectrum. b) MS and MS² spectra ([M-H]⁻ *m/z* 487). c) MS chromatogram of the isomers. d) Structure proposal.

Fig 6-SI. a) UPLC-DAD-MS data for compound **1**. b) UV, MS and MS² spectrum of **1** (*m/z* 345). c) Structure proposal.

Fig 7-SI. Identification data for a minor compound from PA and P1: a) UPLC-MS data. b) MS and MS² spectra ([M-H]⁻ *m/z* 463). c) Structure proposal for C7 glucoside. d and e) Data for an unidentified isomer.

Fig 8-SI. Identification data for compounds **8** C6-(*p*C)Soph from P1 (*m/z* 675.1564) and **7'** C6-Soph from PA (*m/z* 529.1190). a) UPLC-MS data; b and c) MS and MS² spectra in b) PA and c) P1.

Fig 9-SI. Identification data for compounds **9**, **6'** and **3''**: a) UPLC/MS data. b) MS and MS² spectra of **9** (*m/z* 597). c) MS and MS² spectra of **6'** (*m/z* 743). d) Tentative structures for C7 derivatives.

Fig 10-SI. Impact of Fe²⁺ addition on pigment degradation (1h stabilization at pH 1.2).

Fig 11-SI. Chromatograms at 280 nm of P1 solution after 24h at pH 7, 50°C without and with added H₂O₂; a) 1 molar equiv.; b) 10³ molar equiv. c) DAD spectrum, MS and MS² data of unidentified compound at *m/z* 625.

Fig 12-SI. Chromatograms of the pigment solutions after prolonged thermal degradation: 24h (in black) vs. 72h (in red).

Scheme 3-SI. A possible mechanism for the formation of the coumarin derivatives.

Scheme 4-SI. Possible intramolecular transesterification of the Sp residue at C2-OH to the stable C6-OH position in pigment P4. Intermediate positions are possible but would not accumulate. The *p*C was not mobile.

Scheme 5-SI. Possible intramolecular transesterification of the *p*C residue at C6-OH to the neighboring C5-OH position in the *p*C-sophorose. Both species are present as α and β anomers, and are in apparent equilibrium (in a stable ratio over time). When bound to the chromophore, the *p*C was not mobile.

CHAPTER 4

Scheme 1. Structure of the 6 red cabbage anthocyanins studied and gathered according to color stability, *i.e.* G2 > G1.

Fig. 1. International Commission on Illumination's (CIE) CIELAB (L*a*b*) space

Scheme 2. Binding of the anionic base to Fe²⁺ (similar with Al³⁺) followed by autoxidation to Fe³⁺. L: ligands completing the octahedral coordination sphere (water, phosphate, possibly 1 or 2 additional anthocyanin molecules).

Fig. 2. UV-visible spectra of P5 at pH 7, its pure anionic base (Am, calculated) and its Fe²⁺ and Al³⁺ complexes (1 equiv.). Right: color patches calculated from the absorption spectra.

Scheme 3. Chromatic coordinates a* and b* for P5 and its Al³⁺ complex at pH 7, 50 μM, compared to brilliant blue (concentration in ppm).

Fig 3. Color patches for the free pigments and metal - pigment complexes at pH 7 (50 μM pigment + 1 equiv. metal ion), color calculated from the L*a*b coordinates, brilliant blue reference at two concentrations (from Robbins et al., 2016).

Table 1. Spectral characteristics of the Fe²⁺ and Al³⁺ complexes with PA, PB, P2 and P5 (1 equiv. metal ion).

Table 2. Kinetic analysis of metal binding (1 equiv. metal ion). Spectroscopic monitoring at 670 nm.

Fig. 4. a) Kinetics of free Fe²⁺ autoxidation monitored at 295 nm in the absence of anthocyanin (grey dotted line) and in the presence of PA (1 equiv. Fe²⁺, red dashed line, secondary axis). PA + Fe²⁺ binding monitored at 670 nm (2 equiv. Fe²⁺, red, plain line). b) Spectra of PA + 2 equiv. Fe²⁺ (left) and Fe²⁺ alone (right) at different time points (pH 7 phosphate buffer).

Fig. 5. Amplitude of the iron complex's visible band for pigments P2 and P5 as a function of the iron/anthocyanin molar ratio. PA (○), P2 (+), P5 (●), PB (□).

Table 3. HR-MS analysis of metal – pigment complexes (pH 7 phosphate buffer).

Scheme 2. A 3D representation of the 1:3 Al³⁺ - PB complex. Geometry optimization in vacuum by molecular mechanics (MM+) followed by semi-empirical quantum mechanics calculations (PM3). HyperChem 5.1 software (Hypercube, Waterloo, Canada).

Fig. 6. Spectral changes observed after addition of a pigment + Fe²⁺ (1 equiv.) mixture to a pH 4.25 acetate buffer. *Top:* Spectra at time zero (—), after 60 s (—) and at the end of the kinetic run (—). *Bottom:* spectral monitoring at 525 (P3) or 530 (PB) nm (free pigment, —) and at 670 nm (iron complex, —).

Fig. 7. Kinetics of color loss in solutions of iron – anthocyanin complexes at pH 7 and room temperature (C = 50 μM + 1 equiv. Fe²⁺), ▲: PA (582 nm), □: P1 (595 nm), ●: P4 (656 nm), ■: PB (656 nm).

Table 4. Period of time for 25% pigment loss at pH 7, 50°C. a) Color loss, b) Pigment degradation (% of the initial flavylum). Note: for some pigments, a 50% loss was not reached over 8h.

Fig. 7. Rate of pigment loss for the isomeric P3 and PB at pH 7, 50°C, in the absence (left) and presence (right) of 0.6 equiv. Fe²⁺.

Fig 1-SI. ba Absorption spectra of pigments P3 and PB before and after complexation to Fe²⁺ at pH 7 (phosphate 10mM, pigment 40μM). —: Px, ---: Px + 1 eq. Fe²⁺. b) Binding kinetics at pH 7 with 1 equiv. Fe²⁺.

Fig 2-SI. Amplitude of the complex's visible band as a function of the metal/ligand molar ratio.

Fig. 3-SI. Iron - P5 binding at pH 1 (1 equiv. iron). Top, left: slow binding after addition of Fe³⁺. Bottom, left: fast binding after addition of Fe²⁺. Right: initial and final visible spectra.

Fig 4-SI. Spectroscopic monitoring of metal - anthocyanin binding. a) Fe²⁺, b) Al³⁺

Fig 5-SI. pH dependence of the UV-visible spectra of PB and P3 in the presence of Fe^{2+} (1 equiv.). For a given pH, the UV-visible spectrum was recorded after maximal binding.

Fig. 6-SI. Kinetics of trans-chalcone accumulation from PB at pH 7, 50°C in the absence (top) or presence (bottom) of Al^{3+} (1 equiv.) showing the inhibition of Ct formation from the PB- Al complex

Fig. 7-SI. Detection of P5-Fe^{3+} and P5-Al^{3+} complexes by HRMS with ToF detection (direct infusion, pH 7 phosphate buffer).

Fig. 8-SI. ToF detection of $\text{PB}_3\text{-Al}^{3+}$ trimeric complex by HRMS with ToF detection (direct infusion, pH 7 phosphate buffer).

Table 1-SI. HR-MS analysis of metal – pigment complexes (pH 7 phosphate buffer).

Fig 8-SI. Rate of color loss (top) and pigment loss (bottom) in solutions of PA, P1, P4 and PB at pH 7, 50°C, in the absence (black plain line) and presence (grey dashed line) of 0.6 equiv. Fe^{2+} .

Table 1-SI. L^*a^*b values of PA and P5 at pH 7 in the absence or presence of 1 equiv. metal ion.

Fig 9-SI. Comparison between the picture of the cuvette (left) and color patch calculated from the L^*a^*b coordinates (right)

Fig 13-SI. Spectral properties of common synthetic pigments and color patches calculated from the $L^*a^*b^*$ coordinates published in US 2016/0015067 A1.

Fig 14-SI. Anthocyanin-metal kinetic binding constants obtained from $k_{\text{obs}} = k_1 \cdot M + k_{-1}$, and association constant $K = k_1/k_{-1}$. In P2 (left) and P5 (right), at $C = 40 \mu\text{M}$ (pH 7), $20 \mu\text{M}$ (pH 8).

CHAPTER 5

Scheme 1. Structure of the purple sweet potato anthocyanins studied.

Table 1. Thermodynamic and rate constants for the structural transformations of the PSP anthocyanins (25°C).

Fig. 1. UV-visible spectra of pure colored forms for peonidin derivatives PA', P9a, P11 and P12. —: flavylium ion, —: neutral base, —: anionic base.

Fig 2. UV-visible spectra of pigment P9b (Cya, Acyl = Cf, HB) and P10 (Pn, Acyl = Cf, Cf), at pH 7, its pure anionic base (Am, calculated) and its Fe^{2+} and Al^{3+} complexes (1 equiv.).

Fig. 4. The kinetics of metal binding to P9b and P10 (pH 7, 2 equiv. metal ion). ■: Monitoring in the UV range (370 nm), ●: Monitoring in the visible range (Fe^{2+} : 670 nm, Al^{3+} : 550 nm).

Table 2. Kinetic analysis of metal – ligand binding (pH 7, 0.01 M phosphate buffer, 25°C).

Scheme 2. Proposed structure for the 1:1 P10 - Fe^{2+} complex (left) and the 1:1 P9b - Fe^{2+} (right, $n = 2$ (initially) or 3 (after autoxidation)).

Fig 5. Kinetics of **a**) color loss and **b**) thermal degradation (pH 7, 50°C). PA (Cya, no acyl, grey), PA' (Peo, no acyl, black), P10 (Peo, Cf, Cf, green), PA' + equiv. 2 Cf (orange).

Fig. 6. UPLC-DAD-MS analysis of the degradation products at pH 7, 50°C. Chromatograms at 520 nm and ion current for the major ion of compounds 1a and 2a. a) **P12** after 8h ($[\text{M-2H}]^-$ ion: m/z 1123). Formation of two-electron oxidized isomeric pigments **2a** and **2b** (m/z 1121). b) **P4** after 24h ($[\text{M-2H}]^-$ ion: m/z 1123), with formation of caffeic acid addition pigments **1a** and **1b** (m/z 1301).

Fig. 1-SI. Spectroscopic titrations of P10 in the acidic pH range at equilibrium (**a**) and in near neutral solutions (**b**): $\text{pK}'_a = 3.53 (\pm 0.03)$, $\text{pK}_{a2} = 7.16 (\pm 0.05)$. pH dependence of the hydration kinetics in the

acidic pH range (c): $pK_{a1} = 4.11 (\pm 0.06)$. The solid lines are the results of the curve-fitting procedures (Moloney et al., 2018).

Fig 2-SI. Speciation diagrams of PSP anthocyanins at equilibrium (calculated from the values of pK_{a1} , pK_{a2} and pK'_h). —: flavylium ion, —: neutral base, —: anionic base, —: total colorless forms.

Fig 3-SI. UV-visible spectra of free caffeic acid, P9a, P9b, P10 (plain black lines) and their Fe^{2+} complexes (dashed gray lines) at pH 7. Caffeate spectrum (in red). λ_{max} are indicated, in nm.

Fig 4-SI. Evidence for 1:1 binding for P9b and 1:3 binding for the caffeic acid.

Fig 5-SI. Thermal stability of four peonidin derivatives at pH 7, 50°C: PA' (3-O-sophorosyl-5-O-glucosyl-peonidin), P10 (Cf,Cf), P11 (Cf,HB), P12 (Cf, Fl). a) Color loss, b) Pigment degradation.

Fig 6-SI. Thermal stability of 3-O-sophorosyl-5-O-glucosyl-cyanidin PA, 3-O-sophorosyl-5-O-glucosyl-peonidin PA' and the dicaffeoylated P10 in the presence (dotted lines) or absence (solid lines) of added Fe^{2+} (pH 7, 50°C). PA: 0.6 equiv.; PA' and P10: 1.5 equiv.

Fig 7-SI. Color (top) and thermal (bottom) stability of red cabbage (red) and purple sweet potato (black) extracts (pH 7, 50°C).

Fig 8-SI. DAD absorption spectra of P4 and cross-coupling products **1a** and **1b** (m/z 1301).

Fig 9-SI. Thermal degradation of P12 (pH 7, 50°C). UPLC-DAD-MS analysis showing the formation of new isomeric pigments (**2**) resulting from P12 – caffeic acid oxidative coupling. Chromatograms with detection at 520 nm at t = 0h, 8h and 24h. b) DAD absorption spectra of P12 and pigments **2a** and **2b**.

Table 1-SI. Spectroscopic data of selected ligands and their Fe^{2+} and Al^{3+} complexes deduced from the binding kinetics (initial vs. final spectra). Hyperchromic shift $HS = (A_{max,f} - A_{max,0})/A_{max,0}$. Bathochromic shift $BS = \lambda_{max,f} - \lambda_{max,0}$. Metal/anthocyanin molar ratio = 1.

CHAPTER 6.

Fig 1. Color patches calculated from the L*a*b coordinates of 4 pigments and their metal complexes (1 molar equiv., 50 μ M).

Table 1. a) Coefficients of linear regressions correlating the physicochemical parameters of 16 anthocyanins with the type of phenolic acyl moieties. b) Coefficients of linear regressions correlating the pK'_a of 16 anthocyanins with the position of the phenolic acyl moieties.

Fig 2. Thermal degradation of a) PA (in grey) and two monoacylated anthocyanins P1: pC (in black), P3: Sp (in blue); and b) PA' (in black) and two diacylated caffeoylated anthocyanins P11: HBA (in dashed red), Cf; P12: Fl, Cf (in dashed grey).

Fig 3. Example of biexponential fitting for the irreversible consumption of a monoacylated pigment, normalized absorbance at the flavylium λ_{max} .

Table 2. t_{75} of pigment loss at pH 7 for various pigments. ^a Pigments alone, ^b in the presence of 0.6 or 1 equiv. Fe^{2+} . NB: for several pigments, t_{50} was not reached over 24h.

Scheme 1. Skeletons of the degradation products detected, in green.

Table 3. Spectroscopic features of the metal chelates formed from various cyanidin derivatives at pH 7 after addition of 1 equiv. Fe^{2+} .

Table 4. Compared behavior of 4 types of anthocyanins.

Scheme 2. Hypothetical triacylated anthocyanin and the covalent bonds (in red) allowing free rotation for the development of π -stacking interactions between cyanidin and HCA moieties. The total number of degrees of free rotation is 5 (HCA1), 6 (HCA2a) and 7 (HCA2b).

Scheme 3. The most probable organization of the metal complexes of NAA, MAA and DAA (a mixture of 1:1 and 1:2 complexes), and 1:3 complexes expected for Cf or detected for PB.

Table 5. Relative content in the RCE anthocyanins, and 2-groups classification by stability.

Table 6. Fraction of anthocyanins based on their acylation number and calculated pK'_a values.

Fig 4. Rate of color loss (left) and pigment loss (right) of P6 at 50°C, in pH 7 phosphate buffer (black plain line), P6 with 1 equiv. Fe^{3+} (dotted line), P6 with 1 equiv. Fe^{3+} + 10 equiv. N-acetylcysteine (NAC, dashed yellow line), and P6 with 1 equiv. Fe^{3+} + 10 equiv. NAC + 10 equiv. rutin (dashed green line). The NAC compensates for the Fe^{3+} -induced degradation; and rutin further stabilizes the pigment and the color. The absorbance was initially higher with rutin ($A_0 = 1.42$ vs. 1.32).

Fig 5. Fraction in each specie relatively to the flavylium, and k_{obs} of color loss in the presence of 10^3 equiv. H_2O_2 , at room temperature.

APPENDICES

Table 1-A. Data for color repeatability and reproducibility of the absorbance in the visible region, for P5 at pH 7.

Table 2-A. Maximum wavelength (λ_{max}) and molar absorption coefficient (ϵ) of the pigments studied in pH 1 aqueous solutions.

Table 3-A. Regulatory information of E 163 Anthocyanins¹ as food color, (EU) No 231/2012.

Table 4-A. List of the natural pigments authorized in foods in the European Union

Table 5-A. Major patents on blue color made from anthocyanins

Table 6-A. a) Structural features, b) Physico-chemical constants, of the 14 isolated anthocyanins studied. In PSPE and RCE: pondered constants based on the extract composition. Data used in the multiple linear regression.

Appendix 1. Determination of the composition of four anthocyanin extracts in UHPLC-MS/DAD.

Appendix 1.1. Red Cabbage Extract (*Brassica oleracea L., capitata rubra*)

Appendix 1.2. Purple Sweet Potato Extract (*Ipomoea batatas L.*)

Appendix 1.3. Black Carrot Extract (*Daucus carota L.*)

Appendix 1.4. Elderberry Extract (*Sambucus nigra L.*)

Fig 5-A. Solvent effects on the UV-vis spectra of red cabbage anthocyanins acylated with sinapic acid. Spectral features recorded at 0.1 M aqueous HCl and methanol 0.1 % HCl. 50 μ M pigments. Anthocyanins show *negative solvatochromism*: as the excited state of the flavylium is less polar than ground state, in less polar solvents than H_2O (MeOH), the energetic gap between HOMO/LUMO is minimized, and the pigment λ_{max} is superior (e.g. +13 nm for PA).

Table 7. pK'_a of pigment PB at 50 μ M (in 10 mm quartz cuvette) and 500 μ M (in 1 mm quartz cuvette), in 10 mM citrate buffer, with and without 0.1M KCl. The pK'_a values were slightly smaller at the 10-fold concentration (500 μ M).

Fig 6. Color stability of P5 at pH 7 in the absence or presence of Fe^{2+} or Fe^{3+} (1 equiv.). t=0 after complexation (plain lines), t=20 days (dotted lines). P5 (blue), P5+ Fe^{2+} (black), P5+ Fe^{3+} (red). b) Blue index of the corresponding solutions: $\Sigma A(480 \text{ nm} - 750 \text{ nm})$.

Fig 7-A. Spectra of the solutions at pH 7 of PA, P1 and P4 after 24h at pH7, 50°C, corresponding to the residual color in the absence and presence of 0.6 equiv. Fe^{2+} .

Fig. 8-A. ANOVA for the residual flavylum content after 4h, 8h and 24h at pH7, 50°C inter-pigment comparison: differences are significant at 4h and 24h.

Fig 9-A. Kinetics of trans-chalcone accumulation at pH 7, 50°C for pigments PA, PB and P4, showing the very slow formation in the case of P4. Maximum Ct concentration is reached after 0.5-1h for PA, 2h for PB and is not reached over 24h for P4 where the Ct formation is slower than its degradation.

Fig 10-A. Kinetics of pigment loss of P1 and P6 at pH 7 (in black) and pH 8 (in red), at 50°C. The disinnapoylated pigment P6 is more impacted by the pH variations than the p-coumaroylated pigment P1. P1 fraction in anionic base is 7.4% at pH 7 and 44% at pH 8 ($\text{pK}_{a2} = 7.2$). P6 fraction in anionic base is 13% at pH 7 and 60% at pH 8 ($\text{pK}_{a2} = 7.2$).

Fig 11-A. Rate of color loss (left) and pigment loss (right) of P1 under air (■) and under an inert atmosphere (▲).

Fig 12-A. Fraction of residual flavylum after 1 hour in the presence of 10^3 equiv. H_2O_2 at pH 7, room temperature. The flavylum was recovered by acidification to pH 1.2, and spectrum was captured 1min after acidification (black) and 24h after (grey), at room temperature.

1 minute after acidification, the difference in the fraction of colorless species between PA and P2 does not dramatically impact the residual flavylum. However, after 24h at pH 1.2, the flavylum of acylated anthocyanins is recovered in much higher amounts, and thus seems more resistant to the action of H_2O_2 and its derivatives formed at acidic pH than the non-acylated flavylum.

Fig 13-A. Rate of color loss of RCE, in pH 7 phosphate buffer at room temperature. Top: aqueous buffer, bottom: 60% sucrose buffer. The apparent hydration rate was surprisingly 3-fold higher in sucrose syrup than in aqueous solution. The equilibrium is insignificantly shifted.

Fig 14-A. UV-visible spectra of the complexes of pigments P9b and P10 in the presence of Al^{3+} or Fe^{2+} at pH 7, after reaching the complexation plateau. Blue lines: 1 equiv. metal ion, dotted orange lines: 2 equiv. metal ion.

Script 1-A. Fitting model used to determine the k_h , k_{-h} and pK_{a1} , with the Scientist® software (Micromath, INC., Salt Lake City, USA).

Script 2-A. Exponential models used with the Scientist® software.

Script 3-A. Binding model followed by a first order decay

Method 1. Determination of the overall hydration and acidity constant pK'_a of 2 groups within an extract

Fig 9-A. $A(\text{AH}^+)$ as a function of the pH used for the determination of pK'_a of 2 groups within the extract.

Method 2. Calculation of the pure spectra of an individual anthocyanin.

Fig 10-A. Calculated spectra the 3 forms: flavylum, neutral base and anionic base of 6 individual PSPE pigments, at $t=0$.

Fig 11 to 16-A. Data fitting for the determination of pK'_a , k_h , k_{-h} , pK'_h , pK_{a1} and pK_{a2} constants, for pigment PA', P9a, P9b, P10, P11 and P12 isolated from the purple sweet potato extract.

Method 3. Prediction of acylated anthocyanin color at any pH in the range 1 to 8

Fig 17-A. Predicted spectra vs. actual spectra for P5 (top) and P2 (bottom), at a theoretical $t=0$.

Fig 18-A. Color patches of P5 at equilibrium (note: this pigments underwent slow metal complexation leading to a bathochromic shift (presence of trace metal in the water and buffers), c) Pictures of the cuvettes of P5, taken after 1 day, i.e. at the equilibrium

Fig 19-A. a) $L^*a^*b^*$ coordinated of P2. b) Color patches of P2 at $t=0$ (top) and at equilibrium (note: this pigments underwent slow metal complexation leading to a bathochromic shift (presence of trace metal in the water and buffers), c) Pictures of the cuvettes of P2 taken after 1 day, i.e. at the equilibrium, NB: hydration was too fast for pictures, and the solutions are partially hydrated. The same method was used with the spectra at equilibrium, and for the pigment PA (not presented here).

Introduction

Over the last years, the food color industry has been rapidly growing and is expected to continue growing 10% to 15% annually (Cortez et al., 2017), outreaching the growth of the overall food additive industry (+3.4%)¹. This growth is driven by the rise in the consumption of transformed products (Kearney, 2010) and the ever improving offer and supply by ingredients companies. In addition, there has been a continuing demand for health-promoting food products, as well as sustainable and eco-friendly foods, ingredients and packaging², witnessed by the “clean label” trend and the “natural” claim (Hilton, 2017). A catalyst of the consumers’ distrust about the E-numbers in the European Union (EU) was the “Southampton Six” study (McCann et al., 2007), which assessed the effect synthetic colors used in confectionery products on children attention and hyperactivity disorders (van Gunst & Roodenburg, 2019). As a result, the European Union has increased its labeling requirements for several food colors. Globally, the transition toward natural ingredients in food extends to the cosmetic and care products (Barbulova et al., 2015; Soto et al., 2015).

In this context, the segment of natural colors is promising. By contrast to the petroleum-derived synthetic ingredients, natural colors are directly extracted from living organisms (plants, algae, fungi, bacteria or animals), and can be modified by only physical or biological processes (e.g. drying, fermentation, but no chemical reaction). Since 2003, among the global patents present technical solutions to produce natural colors, 12 target the blue color (Table 4-Appendix).

In order to satisfy the new consumers expectations, in 2015 and 2016, the Nestlé and Mars Inc. companies both committed to removing all artificial colors and flavors from their confectionery products^{3,4}. To date, several synthetic colors have successfully been replaced by natural alternatives. For example, red is obtained with carminic acid, lycopene or annatto; yellows and oranges with carotenoids; pinks with betanins or anthocyanin extracts; brown

² Food Liquid Colors Market - Global Industry Analysis, Size, Share, Growth, Trends, and Forecast 2019 – 2027 2016. Retrieved 5/08/2019. <https://www.transparencymarketresearch.com/food-liquid-colors-market.html>

³ Press release of the Nestlé company. 2015. Retrieved 5/08/2019. <https://www.nestleusa.com/media/pressreleases/nest1%C3%A9-usa-commits-to-removing-artificial-flavors-and-fda-certified-colors-from-all-nest1%C3%A9-chocolate-candy-by-the-end-of-20>

⁴ Press release of the Mars Incorporated company. 2016. Retrieved 5/08/2019. <https://gateway.mars.com/m/69d4da3d183f114c/original/POLICY-Mars-to-Remove-All-Artificial-Colors-From-Its-Human-Food-Portfolio.pdf>

with malt/caramels and black with carbon black. However, the blue and green colors are challenging: no natural source is able to mimic the vibrant blue hues displayed by the synthetic blue pigments brilliant blue FCF (FD&C 1, E133) or indigo carmine (FD&C 2, E132). Extracts from the spirulina microalgae can be purified so as to produce a blue color. However, it exhibits only restricted shades of cyan blue, that are slightly greener than the synthetic colors. Pure copper salts also produce a cyan color, but are not considered suitable for food applications.

For several years, the Mars Wrigley Company has been leading a program aiming at replacing the synthetic blues in their confectionary products by a natural alternative. Among the potential blue sources, anthocyanins were identified as the best candidate. Anthocyanins are non photo-synthetic plant pigments belonging to the polyphenolic compounds. Some of them exhibit blue colors at mildly alkaline pH (pH > 7.5 - 8.5). In addition, they are already used as foods colors (pink and purples), so they are available on the market, and are not regulatory restricted (see Table 3-A in Appendix). They are also abundant in nature: present in many edible parts of plants and quite concentrated in cultivated plants (Oplatowska-Stachowiak & Elliott, 2017). However, some obstacles still hinder their development: their lower stability, the cost of the raw materials and their limited current market availability.

A consortium of several universities with complementary research activities has been exploring the color expression of anthocyanins, from the molecular orbitals modeling by TD-DFT (time-dependent density functional theory) calculations, to the color measurement in model products. The Micronutrients, Reactivity and Digestion team from the UMR SQPOV (Security and Quality of Plant-based Products) was invited to characterize the physico-chemical properties of isolated anthocyanins from various food sources. This collective research effort contributed to build theoretical knowledge on anthocyanins structure and assembly, color expression and stability, reactivity, as well as their potential production through biological engineering. In this purpose, the industrial partner the Mars Wrigley Company isolated fourteen different anthocyanins from different vegetable extracts.

Anthocyanins exhibit a blue color in two conditions: in mildly alkaline solutions (pH 7.5 - 9.0), or in the presence of metal ions such as Fe^{2+} or Al^{3+} (at pH 6 - 8). Pure anthocyanins in neutral aqueous solutions rapidly lose their color, with half lives of a few hours (Moloney et al., 2018). The overall color loss actually results from the combination of reversible and irreversible reactions. The two components are not always distinguished in the

literature, pointing to the need to design methods in that purpose. The reversible reactions are well documented (Pina et al., 2012b), and are mainly governed by intra- and intermolecular interactions between the aromatic acyl moieties and the chromophore (Trouillas et al., 2016a). However, the irreversible component of the degradation, resulting from autoxidative and hydrolytic mechanisms is less known at neutral pH. The high oxidation rate of phenols at neutral pH is expected to contribute to the degradation of anthocyanins (C. Li & Hoffman, 1999). Several degradation products have been characterized (e.g. the phenolic acid, the phloroglucinaldehyde, 2,4,6-trihydroxyphenylacetic acid derivatives), but the specific routes followed at neutral pH remain poorly documented. Indeed, the reactivity at pH 7 is complex as is results of the combined reactivity of five major species in equilibrium. Neutral pH is common in food and cosmetic products, deciphering the reaction mechanisms at neutral pH may therefore open new stabilization strategies with various applications.

Besides, anthocyanin binding to metal ions, which is favored at circumneutral pH is one of the most efficient color stabilization mechanisms in nature, together with the copigmentation and self-association. Metal binding produces blue colors over a wider range of pH, and increases their color stability. The conformational features of such complexes e.g. the flower metalloanthocyanins have been characterized in NMR and circular dichroism (Yoshida et al., 2009), and has gained a recent interest with molecular dynamics tools (Estévez et al., 2019; Trouillas et al., 2016). Three main questions are thus:

- 1) What is the contribution of anthocyanins phenolic acyl residues to the color expression and stability at circumneutral pH?
- 2) What are the major degradation products and pathways of anthocyanins at neutral pH?
- 3) What is the impact of acylation on metal–anthocyanin binding and color expression?

To that purpose, the reversible transformations and color expression of isolated pigments and extracts were investigated over the pH range 1 – 9, in UV-visible (UV-vis) absorption spectroscopy. Their irreversible degradation was accelerated by a mild thermal treatment at 50°C. Kinetic analyses were used to characterize both the color loss and pigment degradation. Finally, products identification was carried out in UPLC-DAD/MS.

The first chapter reviews the current literature on the degradation routes of anthocyanins at all pH. Chapter 2 presents the kinetic study of the irreversible degradation of

different anthocyanins at pH 7. These results were published in the journal *Food & Function* (Fenger et al., 2019).

Then, the degradation products detected were tentatively identified and quantified in Chapter 3. These results were published in the journal *Dyes & Pigments*.

Anthocyanin-metal complexes color and conformation were explored in UV-visible photoabsorption spectroscopy and mass spectrometry, in particular their color expression, stability and stoichiometry. The contribution of the phenolic acyls number and position in red cabbage anthocyanins is presented in Chapter 4. A case of competition between two sites of metal binding (cyanidin vs. caffeic acid) observed purple sweet potato anthocyanins is also presented, in Chapter 5.

These results are discussed in Chapter 6. The analytical tools used to determine the color stability of individual pigments was extended to more complex anthocyanin extracts. To that end, the composition of four extracts (red cabbage, purple sweet potato, black carrot and elderberry) was determined in UPLC-MS/DAD (Appendix 3).

Chapter 1. Literature review

1. THE QUEST OF A BLUE NATURAL FOOD COLOR

1.1. The importance of food color

The color of food is an important criterion of acceptability (Clydesdale, 1993). In particular, consumers associate the color with sensory characteristics (intensity of aroma and taste, in particular sweetness), hedonicity (Christensen, 1983), and quality parameters, such as an food safety and an adequate (mild) processing (Delgado-Vargas et al., 2002). In children, food color has been shown to be a major criterion for food classification (Matheson et al., 2002). Although researchers state that raw foods color intensity correlates with their richness in micronutrients, namely anthocyanins, the consumers mental association between food color and freshness/nutrients density is still little documented at the research level.

The blue color is the favorite color in the USA⁵ and in Europe⁶, but few studies have assessed the psychological impact of blue color in foodstuffs. The blue color in food may reduce the appetite, however this perception is very product-dependent. For example in mint chewing gums, the blue color is perceived as “refreshing” (Labbe et al., 2009). In other types of confectionaries, blue is generally used as in a mixture with other bright colors.

1.2. What is color?

This section aims at explain what color is, before dealing with more practical aspects of the color and its optimization. The definition of color is not as obvious as it seems. Color is defined as "*a phenomenon of light visual perception that enables one to differentiate otherwise identical objects*"⁷, which is essentially a property: the discrimination property. It is thus a mental, not physical phenomenon. More descriptive definitions exist for the color: "*the aspect of the appearance of objects (and light sources) that may be described in terms of hue, lightness, and saturation*", or "*a specific combination of hue, saturation, and lightness or brightness*". Color can arise from the selective absorption of light by materials containing dyes or pigments, or to purely physical phenomena such as selective reflection and scattering. To exist, color thus requires a light source, enlightening an object and the human eye.

Light is a combination of monochromatic electromagnetic radiations emitted by a source (the sun, a fire, an electric light bulb) and interfering with matter, including gases,

⁵ The Psychology of Color: A Designer's Guide to Color Association & Meaning. 2015. Retrieved 5/08/2019. <https://zevendesign.com/color-association/#blue>

⁶ Color trends in Europe. 2016. Retrieved 5/08/2019. https://www.coatingsworld.com/issues/2016-12-01/view_europe-reports/color-trends-in-europe

⁷ Merriam Webster online dictionary. Retrieved 2/06/2020. <https://www.merriam-webster.com/dictionary/color>

liquids and particles suspended in these systems, as well as solids. As a reference for light emission in research and the industry, the standard illuminant D65 corresponding to a natural light reaching the earth surface at noon (at the summer solstice on the Cancer tropic, by an uncloudy day). It corresponds to a color temperature of 6504 K (CIE Standard, 2004) and is described as a cold white. The standard light sources are polychromatic, so they comprise all the colors.

Pigments are molecules (organic or inorganic) that selectively absorb radiations. For instance, many transition metal (*e.g.*, Mn, Fe, Co, Ni, and Cu) complexes absorb visible light and the resulting color is modulated by the metal-ligand interactions. Interactions between the metal's *d* orbitals and the ligand's frontier orbitals cause the *d* layer to split into two energy levels. Upon excitation by a photon whose energy ($E = hc/\lambda$) matches the gap between the two energy levels, an electron from the lower level is transferred to the upper level (incomplete for transition metals). When a radiation is absorbed by pigments, all the other wavelengths of the exciting light are transmitted, and the initial white light (all wavelengths) is changed into a "colored" light lacking specific wavelengths.

The criterion for organic molecules to absorb visible light is to display extensive electron delocalization bringing the frontier orbitals HOMO and LUMO in close proximity. Upon light irradiation, a HOMO electron is transferred to the LUMO orbital. For pigments, the HOMO-LUMO gap, in other words, the absorbed photon's energy, lies in the range 1.6 – 3.3 eV, corresponding to a wavelength in the range 380 - 750 nm, the "visible region". With highly conjugated systems such as anthocyanins, other molecular orbitals (HOMO-1, HOMO-2, LUMO+1, LUMO+2 etc...) can contribute to the absorption of visible light. Moreover, solute - solvent interactions and molecular vibration cause monochromatic transitions to degenerate into absorption bands. Finally, several acid-base forms and/or tautomers, each having distinct absorption bands, can be present.

An absorption band is typically characterized by two major parameters: the wavelength of maximal absorption λ_{max} (in nm), characteristic of the pigment's color, and the molar absorption coefficient (in $\text{M}^{-1} \text{cm}^{-1}$) at λ_{max} noted ϵ_{max} , characteristic of the color intensity. However, the whole visible spectrum $\epsilon = f(\lambda)$ is necessary to qualify the color expressed. The major colorimetric parameters can be determined therefrom, in particular, the hue indicating the type of color, and the chroma, a characteristic of color purity.

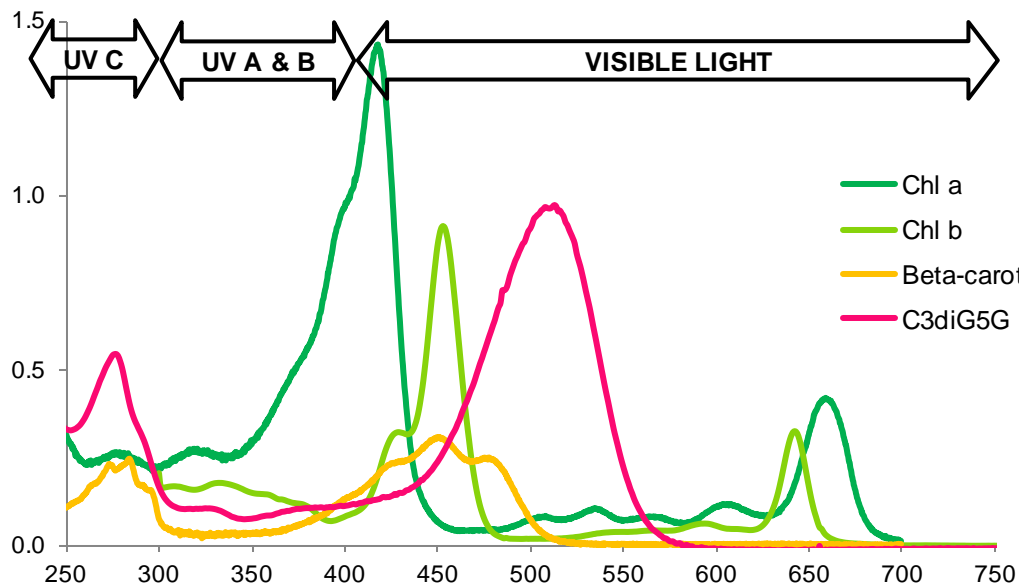


Fig. 1. Absorption spectra of natural pigments: the photosynthetic chlorophylls a and b; the accessory pigment β -carotene and the non-photosynthetic cyanidin-3,5-diglucoside (spectral data from Taniguchi, 2001 & Li, 1997)

The human eyes are equipped with photosensitive cells on the retina: the cones and rods. In both cases, pigments are associated with photoreceptor proteins (called iodopsins or photopsins for the cones, and rhodopsins for the rods). These pigments, for example the 11-*cis*-retinal in rods, play a key role in the mechanism of vision. The visual transduction occurs at three levels: a membrane which offers a large surface thanks to a ciliated structure in cones, a high number of fine discs inside the rods; the cytoplasm composition; and finally the synaptic end of the cell. Briefly, in rods, photons induce the *cis-trans* isomerization of the 11-*cis*-retinal, modifying the structure of the rhodopsin, activating a transducin bound to the rhodopsin, inducing the opening of the cellular GPMc into GMP. In absence of GMPc, the sodium channels close, resulting in membrane hyperpolarization, thus inhibiting the glutamate transmitter. In absence of glutamate, the bipolar cells are activated, and transmit electric pulses to the visual cortex through the optic nerve, perceived as light (Baylor, 1996). Overall, the photons transmitted by the object we see excite pigmented cells of our retina, which converts the optical signal into a conscious sensory perception. It is admitted that the three major iodopsins types are sensitive to specific light radiations, enabling a trichromic vision in mammals, but this is still object of researches, as other photoreceptors may exist in part of the population. In addition, genetic variations explain part of the interindividual variability, namely daltonism, wh is due to the inactivity of one or several types of iodopsins.

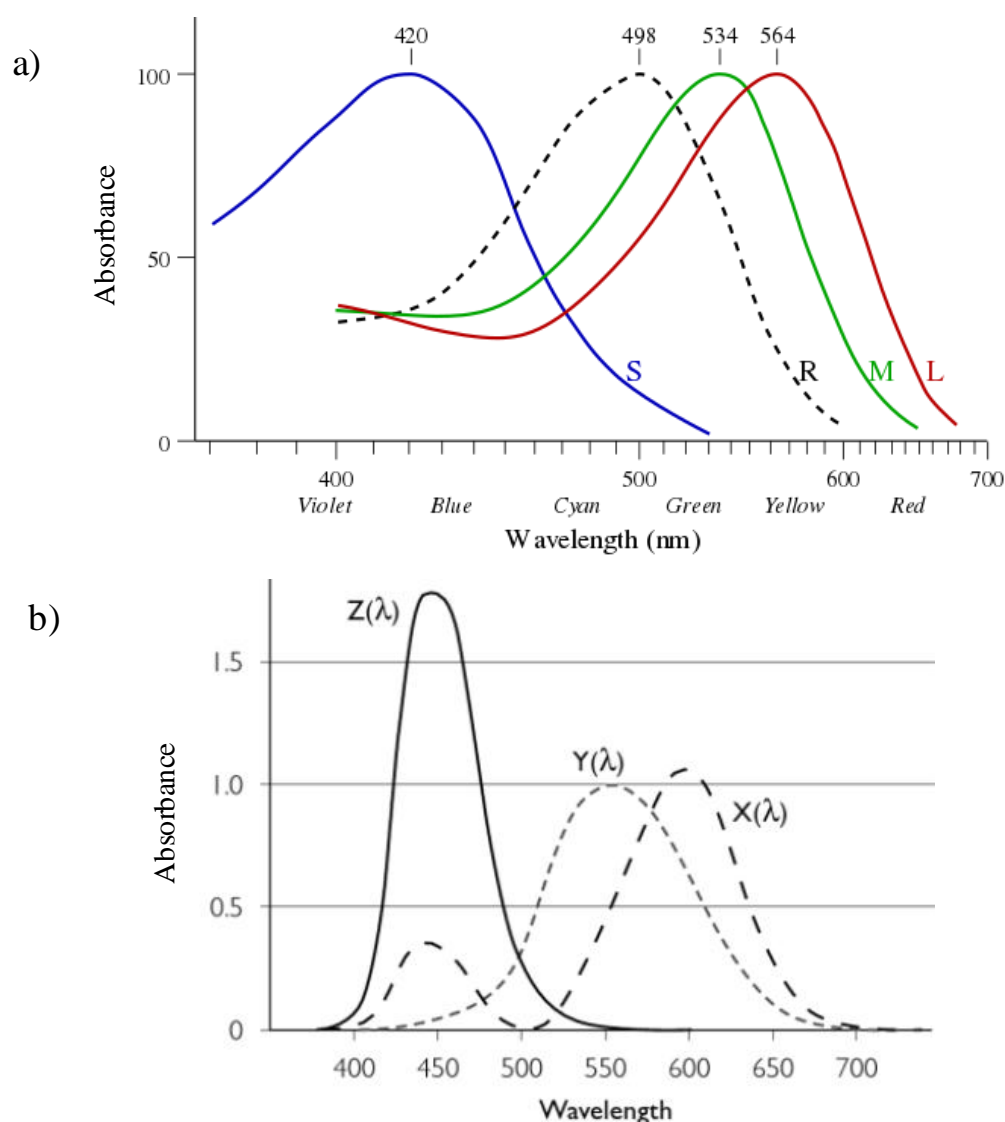
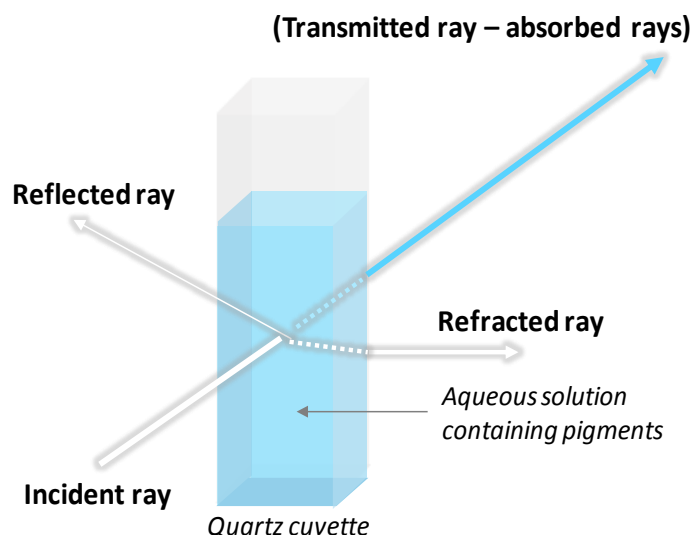


Fig. 2. a) Sensitivity of cones and rods (dashed black line) to light, according to the wavelength (Bowmaker & Dartnall, 1980), b) CIE color matching functions $X(\lambda)$, $Y(\lambda)$, $Z(\lambda)$ defined for a standard colorimetric observer (CIE Standard, 2004).

This work explores the color expressed by aqueous solutions containing hydrosoluble pigments. To quantify and qualify the pigments in aqueous solutions, a spectrophotometric analysis is used. The pigments are placed in glass or quartz containers that minimize the light - surface interactions (reflection, refraction). The horizontal incident light beam (intensity I_0) is partially absorbed by the pigments and partially transmitted (intensity I_t) (Scheme 1). The absorbance A is calculated from the transmission ratio $A = \log(I_t/I_0)$. A is an additive value, linearly related to the pigment concentration C (mol/L), through the well-established Beer-Lambert's law: $A = \epsilon \times l \times C$, with l the optical pathlength (cm) of the cell, and ϵ the molar

absorption coefficient characteristic of the pigment. A was measured within the linear range of this relationship ($A < 1.2$). Color actually combines physical phenomena (selective reflection, scattering). Reflection and refraction are surface properties that are minimized with quartz cells typically used in UV-visible spectroscopy, but light scattering can occur if large particles are present (e.g., colloids, precipitates).



Scheme 1. Occurrence of simultaneous physical and chemical phenomena impacting the color in a quartz cuvette, and associated hypothetical trajectories of the incident light rays.

1.3. The diversity and traditional uses of natural pigments

Nature offers a full range of organic and inorganic pigments. Organic pigments are found in all the living reign: plants (e.g., chlorophylls, carotenoids...), fungi (e.g., anthraquinones), bacteria (e.g., phycocyanin, anthraquinones) and animals (hemoglobin, carminic acid). In comparison to inorganic pigments, organic pigments are generally much more vulnerable to heat and oxidation.

HISTORY

Natural pigments have been traditionally used as coloring agents by human communities since ancient times. The earliest pigments were ground mineral pigments, used in caves in Africa as far back as 350-400 000 years BC. Later, ca. 2500 BC, the Egyptians invented the so-called “Egyptian Blue” by melting a copper-rich mineral with lime and sand at 850-950°C. Used in paintings, it is considered the first synthetic pigment. The use of plants for dyeing simultaneously appeared in China.

During the Middle Ages in Europe, pigments from tinctorial plants were used in painting and textile dyeing, for instance anthraquinones (*e.g.*, alizarin) were extracted from the Garancia (*Rubia tinctorium*); the yellow luteolin from *Reseda luteola* L., the red α -crocin from the saffron stigmas. Some of them were even produced by hemisynthesis, for example the indigo blue, obtained by transformation of indican found in the leaves of woad (*Isatis tinctoria* L.). The extracted precursor is transformed into leuco-indigo by alkaline reduction, then oxidized by air into indigo. The traditional process using the European pastel was progressively replaced since the XVth century thanks to the discovery of a new source of indigo coming from Asia, the indigo tree (*Indigofera tinctoria*). Like other pigments from exotic sources (*e.g.*, the cochineal (*Dactylopius coccus*), the achiote (*Bixa orellana*)), their production was industrialized in the European colonies until the XVIIIth century.

MODERN TIMES: SYNTHETIC PIGMENTS

In the late XIXth and early XXth century, benefiting from advances in organic chemistry and thanks to the Industrial Revolution, a successful chemical industry created a range of synthetic pigments finding applications in the coloring industry (paints, inks, textile dyeing). The first industrial productions of synthetic pigments date back to the 1910's: azo pigments (mono- and diazoic yellows and oranges), blue phtalocyanins, indigoids, triarylmethane etc. (Eastaugh et al., 2007; Herbst et al., 2005). Most synthetic pigments are based on aniline and nitrobenzene, both ultimately derived from the petroleum naphthas.

As of 2008, synthetic food colors represented 42% of the market share, *vs.* 27% for natural food colors⁸. chemical modification can also be used to provide a specific property based on an extracted pigment, for example the sulfonation of the indigotin that makes it water-soluble. Their synthetic nature raises the question of their biological compatibility and toxicity. The toxicological assessment is required for authorization by the food safety & health authorities.

Besides, the chemical synthesis can produce pigments that are identical to their natural versions, therefore called "natural identical". It is the case of carotenoids and anthraquinones, such as carminic acid. They may have a similar biological effect to their counterparts extracted from plants, provided that the extracted compounds are pure and not used as a "totum" of compounds, their production has a different environmental impact, associated with

⁸ Transparency Market Research. Retrieved 2/08/2020. <https://www.transparencymarketresearch.com/food-colors-market.html>.

petroleum extraction as a raw material, high energetic expenditures required for the petroleum cracking, use of solvents for compounds purification, etc.

1.4. Natural & synthetic food colors

Food colors have two primary uses: i) to color a non-colored food (e.g. sugar candies, syrups and spirituous), or ii) to correct the color of transformed food, due to their processing. Among the array of synthetic pigments developed by the chemical industry, some were authorized in food and became commonly used in the food processing industry, e.g. carmine red in sausages, erythrosine in canned cherries, and various colors in candies and chewing gums.

In the food industry, pigments and dyes are referred to as “food colors”. Strictly speaking, a pigment refers to a substance that is insoluble in the medium in which it is incorporated, and therefore stays in a crystalline or particulate form, while “dye” or “color” refers to a soluble coloring agent (Herbst et al., 2005). A mineral color is thus always a pigment, while an organic color can be a dye or a pigment. Some mineral compounds can be used as pigments in foods, but only calcium carbonate (CaCO_3) and titanium dioxide (TiO_2) are authorized as white pigments, the latter being a controversial ingredient (Shakeel et al., 2016).

LAKES

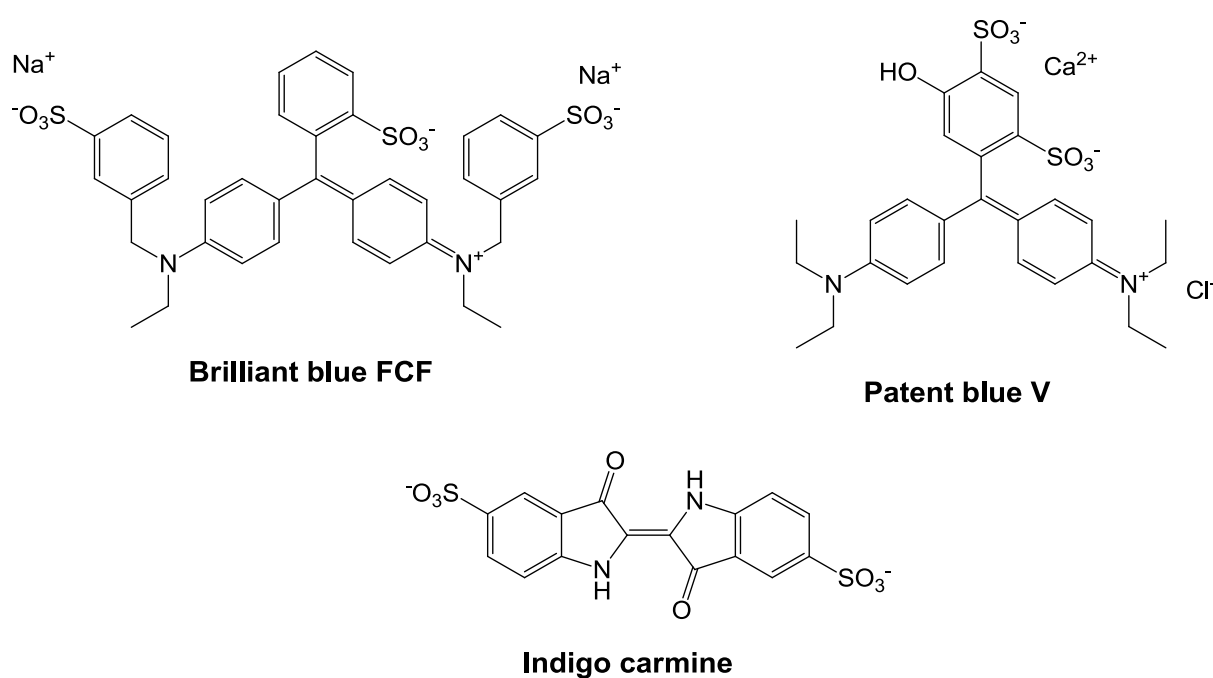
When mixing soluble food colors with aluminum chloride and sodium carbonate, the so-called “aluminum lakes” are produced (Lehto et al., 2017). They are usually prepared from synthetic sulfonylated azo-compounds or triarylmethane (brilliant blue, indigo carmine, tartrazine, sunset yellow and allura red). Following binding to Al^{3+} , the pigments precipitate (Yuan et al., 2019). They become water- insoluble but are oil-dispersible, thanks to their stable low particle size. They are therefore usually dispersed in edible oils, sugar syrups, propylene glycol and glycerin or waxes. They offer a high color stability as well as a homogenous, uniform and reproducible aspect in mixtures.

BLUE PIGMENTS

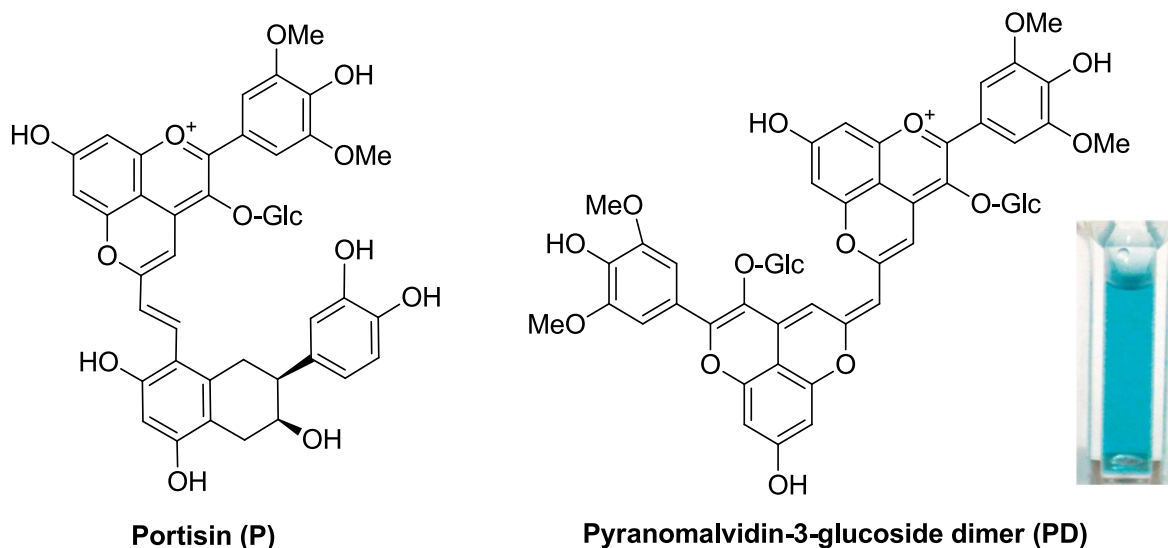
In the food and beverages industries, the blue color is scarce. It is thus generally obtained with synthetic colors. The structures of three of them are provided in Scheme 2. Among them, Patent Blue V is present in several blue and purple candies as well as in green spirituous liquors, it is however not authorized in the USA. Brilliant Blue FCF is commonly

used in drinks: mint syrup, "blue wine" and blue spirits, as well as in confectionary products. Finally, the indigotine or indigo carmine, a natural-identical pigment, is less common in food products.

Other semi-synthetic blue pigments were identified in aged portwine, called portisins (Scheme 3). They are derived from anthocyanins (red at acidic pH), by the addition of e.g. pyruvic acid to form carboxypyrananthocyanins (orange). Then, reaction with good nucleophiles (vinylphenol or vinylcatechin), leads to the blue portisin and portisin dimers (Mateus et al., 2004; J. Oliveira et al., 2010). The latter are the only known organic pigment to date, that exhibit a blue color at acidic pH.



Scheme 2. Structures of three synthetic blue food colors, brilliant blue and patent blue V (triarylmethane); and the oxo-indoline indigo carmine.



Scheme 3. Structures of hemisynthetic blue colors derived from anthocyanins: the Portisin (P) and Pyranomalvidin-3-glucoside dimer (PD) dyes in their pyrano-flavylium cation form, insert: picture of the PD solution at pH 2 (adapted from Araújo et al., 2018).

Food color regulation

GLOBAL FOOD COLORS REGULATION

Food colors are regulated by the local institutions: the FDA (Food and Drugs Administration) in the USA; and in the European union (EU), the European Food Safety Authority (EFSA) and the European Chemicals Agency (ECA) laying down the regulation REACH (Registration, Evaluation, Authorization and Restriction of Chemicals) (EC n° 1907/2006⁹). This European regulation aims at a transparency and the protection of the population of any harmful substance, following the principle "no data no market" (Lehto et al., 2017). In the EU, among the 39 authorized color additives, 9 are synthetic, and 6 of them have a labeling requirement (see below) (Appendices II and III of Regulation (EU) No. 1333/2008¹⁰, usage specifications in Regulation (EU) No. 231/2012). In the US, 7 synthetic colors are authorized ("certified"). In both zones, these additives are subject to restricted conditions of use and limiting specifications for use. For example, the synthetic blue dye Brilliant Blue FCF is limited in the US with an ADI (Acceptable Daily Intake) of 6 mg/kg, and 12 mg/kg in the EU. Some natural colors also have a maximum level in the EU (curcumin; carminic acid; lycopene and lutein), while in the USA, they are submitted to the

⁹ REACH <https://eur-lex.europa.eu/legal-content/EN/TXT/PDF/?uri=CELEX:32006R1907&from=EN>

¹⁰ Regulation (EU) No. 1333/2008 <https://eur-lex.europa.eu/LexUriServ/LexUriServ.do?uri=OJ.L:2008:354:0016:0033:en:PDF>

GMP (good manufacturing practices), i.e. they can be used at a level not higher than necessary to achieve the intended purpose.

In the EU, an interventional study tested the impact of mixtures of 6 different artificial food colors (AFCs) and benzoic acid (a preservative) on children, suggesting a correlation between one mixture and ADHD (attention deficit and hyperactivity disorders) (McCann et al., 2007). Since this study, known as the “Southampton Six”, a scientific opinion was published by the EFSA ANS panel (European Food Safety Authority, 2008). It concluded that the findings of the study cannot be used as a basis for altering the ADI of the respective food colors or sodium benzoate due to several weaknesses in the methodology and data consistency. In spite of this scientific opinion, the EFSA reassessed the regulation of these synthetic food colors, and requires on the label of foods containing one of the 6 AFCs among Sunset yellow (E 110); Quinoline yellow (E 104); Carmoisine (E 122); Allura red (E 129); Tartrazine (E 102) and Ponceau 4R (E 124) (Smith, 2015) the following label “*name or E number of the color(s): may have an adverse effect on activity and attention in children*”. Today, the distrust about the E-numbers leads the European consumers to avoid E-numbers, belongs to the Clean label trend (van Gunst & Roodenburg, 2019). This movement advocates an overall higher transparency, the use of a minimal number of ingredients, and the avoidance of synthetic ones. However, food experts say that the consumers are generally unaware of the consequences of removing the E-numbers, for example the shorter shelf life and reduced quality (including appearance, texture, taste and smellà (van Gunst & Roodenburg, 2019).

ANTHOCYANINS REGULATION

In the USA, according to the FDA regulation, anthocyanins are permitted as food colorants under the category of fruit (21CFR73.250) or vegetable (21CFR73.260) juice color. In the EU, several anthocyanin extracts are authorized in food, and are all labeled as E163. They can be used *quantum satis*, with specifications restricting the residual presence of extraction solvents and heavy metals (EU No 1129/2011). The authorized sources in the EU are: 163(ii) Grape skin extract (Enociania, Eno); 163(iii) Blackcurrant extract; 163(iv) Purple corn color; 163(v) Red cabbage color; 163 (vi) Black carrot extract; 163 (vii) Purple sweet potato color; 163 (viii) Red radish color; 163(ix) Elderberry color; 163(x) Hibiscus color. Aluminum lakes thereof are authorized.

2. PHENOLIC COMPOUNDS

2.1. General properties

Phenolic compounds are plant secondary metabolites that bear at least one phenolic ring (C_6H_5OH). They exist as mono-, oligo- and polymers. Phenols and polyphenols are ubiquitous to green plant cells. They are also major contributors to Earth's biomass, as they include the polymer lignin, the major component of wood with cellulose. They are also abundant in plant-based food (fruits, vegetables, cereals). Because the word "polyphenol" is sometimes used abusively, it is worth referring to its most recent definition: "*The term "polyphenol" should be used to define plant secondary metabolites derived exclusively from the shikimate-derived phenylpropanoid and/or the polyketide pathway(s), featuring more than one phenolic ring and being devoid of any nitrogen-based functional group in their most basic structural expression.*" (Quideau, 2011).

Polyphenols are plant secondary metabolites, i.e. they are not involved in normal growth, development, and reproduction. Instead, they play diverse biological roles, including redox status regulation, antibacterial, inhibition of viral enzymes, genes activation, etc. (Havsteen, 2002). Their functions are rooted in the chemical properties of phenolic rings themselves (Quideau, 2011): i) hydroxyl groups are hydrophilic and can establish hydrogen bonds as donors and acceptors. ii) Phenyl rings is typically hydrophobic and can establish van der Waals interactions with other similar (weakly polar, polarizable) structures. iii) thanks to their H-donating capacity phenols are powerful antioxidants (Dangles, 2012). The enhanced electron-/H-atom-donating properties of polyphenols such as flavonoids provide them a higher antioxidant activity than simple phenols. iv) Catechol and pyrogallol rings have the ability to bind metal ions thanks to their adjacent hydroxyl groups.

2.2. Flavonoids: structural diversity and functions in plants

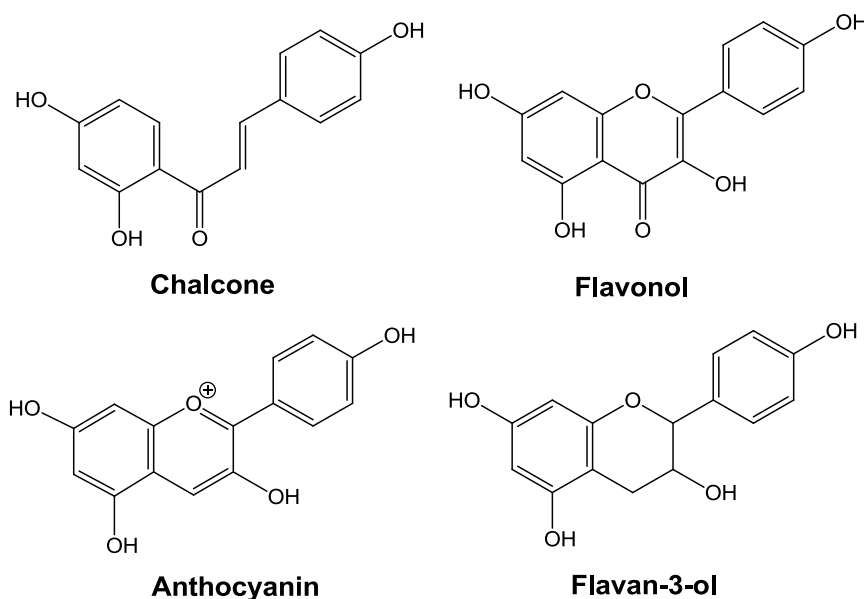
FLAVONOIDS STRUCTURE

Flavonoids are the largest class of phenolic compounds, with more than 4000 different flavonoids already identified (Harborne & Williams, 2000). They are based on a core $C_6C_3C_6$ structure (Scheme 4). They are divided in subclasses that differ by the C-ring substitution: phenolic acids, flavonoids, stilbenes, tannins, lignans, coumarins, curcuminoids, and quinones

(Basli, Belkacem, & Amrani, 2017). Within a sub-class, various substitutions increase the structural diversity, the hydroxylation and O-methylation (on the A- and B-rings), and O-glycosylation. Flavonoid C-rings include i) chromones, either saturated (flavanones) or unsaturated (flavones, flavonols), ii) the saturated chromanes (flavan-3-ols) and iii) aromatic pyrylium cations (anthocyanins).

They all show two major absorption bands: the band II in the UV region (240 - 290 nm), and the band I (300 - 380 nm, depending on the C-ring conjugation and B-ring substitution). Three structural features determine the energy of the absorption band II: the π -conjugation, orbital (de)localisation, and mesomeric (+M) effects of the hydroxyl moieties (Anouar et al., 2012b). Thanks to a continuous π -electrons delocalization throughout the A, B and C rings, anthocyanin absorption band ranges between 480 and 540 nm (fully protonated flavylium form), making them visible to the human eye.

The strong UV-absorption property of flavonoids serves the photo-protective role in plants leaves (Nichelmann & Bilger, 2017).

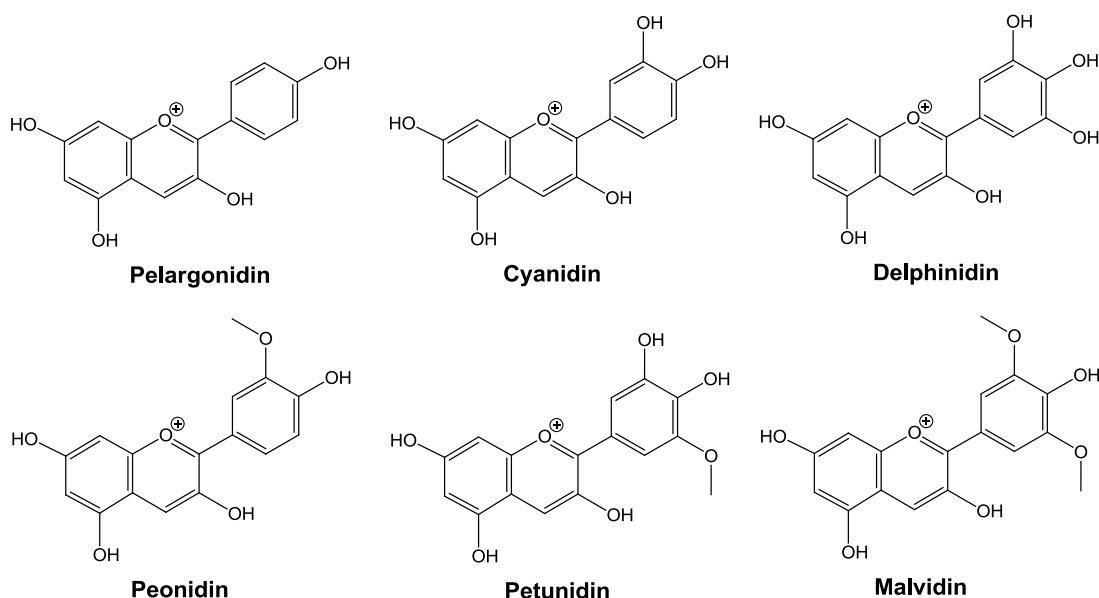


Scheme 4. Examples of structure of flavonoids.

2.3. Anthocyanin structure diversity, biosynthesis, occurrence and functions in plants

2.3.1. ANTHOCYANIN STRUCTURE

Anthocyanins are a subclass of flavonoids built on the 2-phenylbenzopyrylium (flavylium) skeleton, which is the chromophore. In plants, anthocyanins are mainly found as O-glycosides. As of August 2008, 644 different anthocyanins have been reported (Andersen & Jordheim, 2010; Veitch & Grayer, 2011). Their structural diversity arises from the B-ring substitution, and from the number, type and site of glycosylation and acylation. There are 6 main types of natural anthocyanidins (Scheme 5) (Timberlake, 1980). Their diversity and distribution in nature is discussed at section 2.3.4.



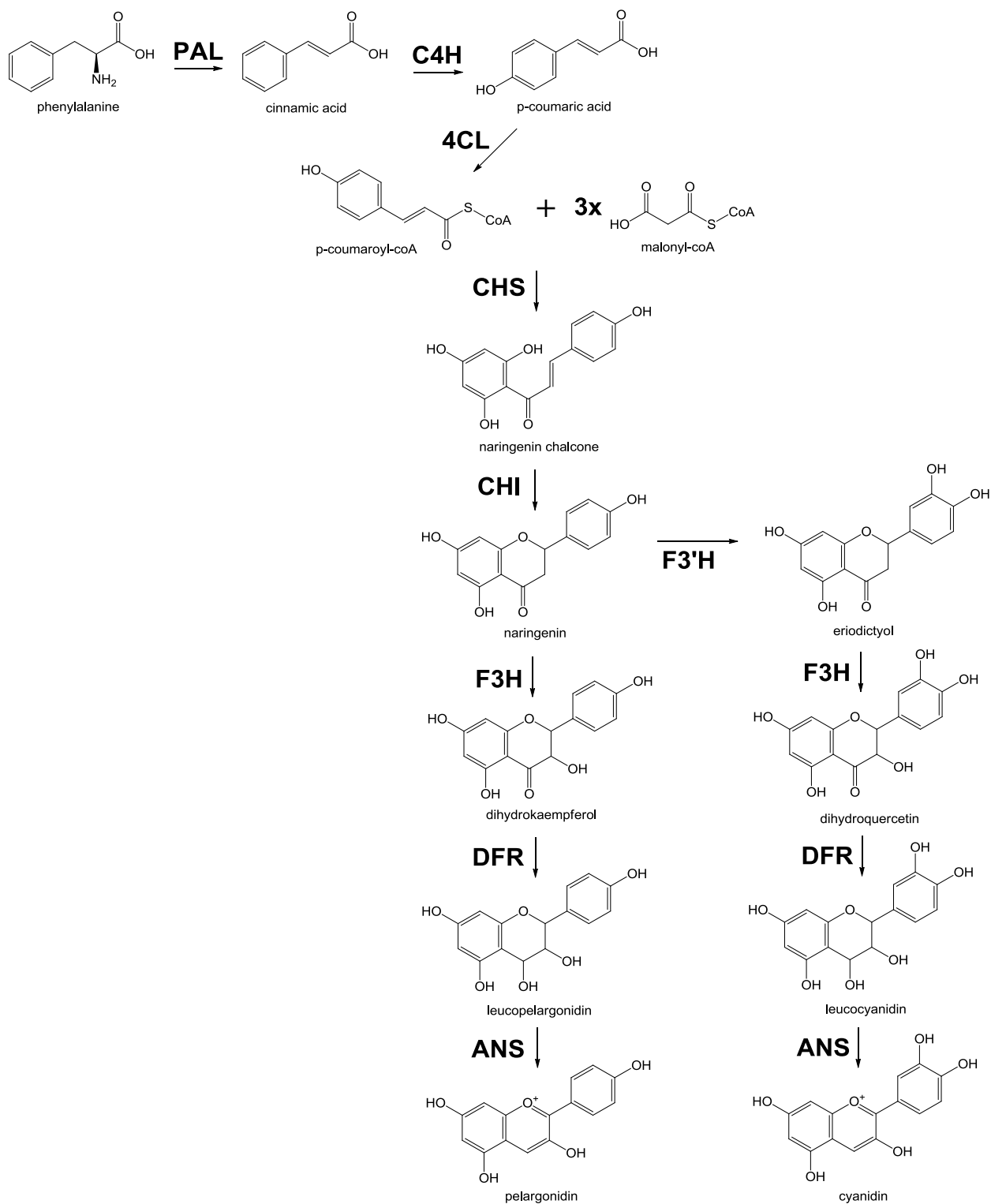
Scheme 5. Structure of the 6 main anthocyanin aglycones (anthocyanidins).

2.3.2. ANTHOCYANIN BIOSYNTHESIS

Anthocyanins and the other flavonoids are present in cell vacuoles, but they are synthesized by a multi-enzyme complex localized at the surface of the endoplasmic reticulum, and delivered by in vesicles to the vacuoles or to the extracellular cell wall. Flavonoids are synthesized through the phenylpropanoid pathway, a continuation of the shikimate pathway. The phenylpropanoid pathway starts with the conversion of L-phenylalanine into *p*-coumaroyl-CoA (Winkel, 2006) (Scheme 6). Then, *p*-coumaroyl-CoA is condensed with 3 equiv. of malonyl-CoA into the naringenin chalcone (a tetrahydrochalcone). It is then

cyclized into naringenin (a flavanone) from which the biosynthetic pathway branches out to the different flavonoid classes. If not hydroxylated at 3' and/or 5'-OH, naringenin is hydroxylated at C3 into dihydrokaempferol, which is reduced into a leucoanthocyanidin (flavan-3,4-diol), the leucopelargonidin. It is generally admitted that leucoanthocyanidins are finally converted to anthocyanins by anthocyanidin synthase (ANS). Finally, glycosyltransferases convert anthocyanidins into anthocyanins. Optionally, cytoplasmic and vacuolar acyltransferases catalyze the acylation steps, with either acyl-coenzyme A thioesters or acyl-sugars as acyl donors (Appelhagen et al., 2018).

This biosynthetic pathway has been gradually elucidated by using plant models whose genome is known, e.g. *Arabidopsis thaliana* or *Nicotiana tabacum*, and by selectively knocking out biosynthetic genes. It is still an object of research open to refinement. A recent in vitro study shows that ANS from vine (*Vitis vinifera*) actually only catalyzes the 3-hydroxylation of 3,4-leucoanthocyanidins into flavan-3,3,4-triols (Zhang et al., 2019). It opens the possibility to produce anthocyanins by bioengineering in the so-called “microbial cell factories” and “plant cell factories” (Appelhagen et al., 2018). For example, the anthocyanin concentrations reached in transgenic tobacco cell lines were two-fold that of blackberries or aronia.



Scheme 6. Biosynthetic pathways of the synthesis of flavonoids and anthocyanins, example of pelargonidin and cyanidin. Adapted from Falcone Ferreyra, 2012 and Appelhagen, 2018. Enzyme abbreviations: PAL: phenylalanine ammonia-lyase; C4H: cinnamate-4-hydrogenase; 4CL: 4-coumarate-CoA ligase; CHS Chalcone synthase; CHI chalcone isomerase; F3H flavanone 3-hydroxylase; F3'H flavonoid-3'-hydroxylase; DFR dihydroflavonol 4-reductase; ANS anthocyanidin synthase.

2.3.3. ANTHOCYANIN FUNCTIONS IN PLANTS

Anthocyanins can occur naturally in diverse plant vegetative structures, from underground storage organs to stems, leaves, flowers and fruits. They play important roles in the regulation of biotic stress (insects, bacteria, viruses) and abiotic stress (UV light, high-intensity light, drought, cold/heat). Anthocyanins serve various roles in plants, physiological functions (photoprotection and antioxidant activity) as well as an ecological role by repelling of the predators and parasite insects by producing unexpected or undesirable visible colors (Archetti, 2000).

There is empirical evidence of the protection against the photo-oxidative damage exerted by anthocyanins in leaves (Steyns et al., 2002). This protection would result from the interception of a portion of supernumerary photons that would otherwise strike the chloroplasts, thus increasing the ROS production and ROS-triggered damage. Anthocyanins indeed specifically absorb green radiations (Hatier & Gould, 2008). This photoprotective role seems especially important in young leaves that are not yet equipped with the photosynthetic apparatus, or in autumn leaves, when the photosynthetic apparatus is broken down and the nutrients reabsorbed. However the UV-absorbing function is not the primary role for anthocyanins in planta (Landi et al., 2015), as anthocyanins are not universal in this reign, and most other flavonoids exhibit a superior UV absorption. Acylated anthocyanins are not particularly located in the exposed leaves, but rather in roots and fruits and flowers, where they may not play a photoprotective role. In leaves, the localization of anthocyanins storage, in epidermal and/or mesophyll cells (Fig 3) is in agreement with this light-screening role.

The reduction of the photo-oxidative stress is another major property of anthocyanins. They show a high scavenging capacity for active oxygen resulting from the photo-excitation of chlorophyll, the Mehler reaction and the photorespiration (Gould et al., 2002). Also, anthocyanins are excellent scavengers of reactive oxygen species (ROS) and transition metal ions, superior to other flavonoids (Yamasaki et al., 1996). Although anthocyanins are mainly located in the cell vacuole, thus separated from the organelles where oxidative stress occurs (chloroplasts, mitochondria), they are able to regulate the H₂O₂ content thanks to the diffusion of the latter through the vacuole membrane (Hatier & Gould, 2008). This redox regulation highly depends on the pigment structure: the cyanidin aglycone is 10 times more efficient than its sophoroside (Yamasaki et al., 1996). Finally, foliar anthocyanins also regulate redox enzymes (LOX, POD) (Cásedas et al., 2018) and the sugar metabolism, (Landi et al., 2015).

In angiosperms, their additional presence in fruits and flowers, both wild and cultivated, attest of the coevolution of plant pigments (including carotenoids) with insects and animals (Archetti, 2000; Harborne & Williams, 2000). In flowers for instance, the exhibition of bright colors and UV absorption helps attracting pollinating insects, and this may have contributed to the broad variety of anthocyanin structures and colors found in flowers (Yoshida et al., 2009). In fruits, the role of animals in seed dispersal may explain the high concentration of anthocyanins that make them more visible.

Overall, the physiological roles of anthocyanins contribute to delaying the senescence phenomenon, and thus to increasing plants life expectancy. In addition to reproductive function associated with their presence in fruits and flowers, anthocyanins bring important evolutionary advantages to plants. Finally, in other organs of cultivated plants consumed as vegetables (roots, tubers, leaves and stems), the varieties rich in anthocyanin have rather been selected by humans for their health effects and/or their visual attractiveness than for their benefits for the plant.

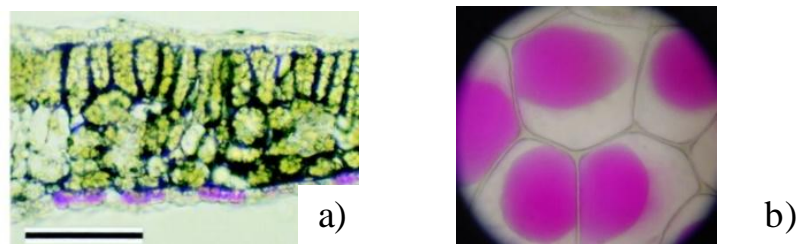


Fig. 3. a) Anthocyanin localization in *Arabidopsis thaliana* leaves epidermal cells (Kubo et al., 1999), b) Epidermal cells of *Rhoeo Discolor* (*Tradescantia spathacea*) after plasmolysis. The vacuoles (pink) have shrunk. Size: ca. 450 μm (Innsbruck, 2004).

2.3.4. ANTHOCYANIN OCCURRENCE IN PLANTS

Given their various functions in plants, anthocyanins are ubiquitous in both the mono- and dicotyledons, although their type and concentration vary considerably (Table 1). For example, cyanidin prevails in leaves, while delphinidin prevails in flowers. In leaves, they accumulate in the cells of the upper epidermis (Fig 3 b)). In plant cells, anthocyanins are localized in vacuoles (Fig 3 b)). Although the vacuolar sap is very dilute, it contains the bulk of the cell's content in K^+ , Ca^{2+} (10^4 times more concentrated than in the cytosol), Cl^- , sugars, organic acids, enzymes and other solutes. Functions of vacuoles include storage for sugars,

proteins and solutes, defense (alkaloids, enzymes), toxic avoidance (storage of heavy metals), pH and ionic homeostasis, pigmentation and macromolecule recycling during senescence (Taiz, 1992).

Edible plants offer a variety of anthocyanin structures. The most common sources and their content is provided in Table 1. The distribution of the six most common anthocyanidins in fruits and vegetables is: Cya 50%, Dp 12%, Pg 12%, Pn 12%, Pt 7% and Mv 7% (Lawrence et al., 1939). The most common glycosylation site is at C3-OH, most frequently by glucose, but also by galactose or rhamnose, disides (sophorose (Glc-1,2-Glc), sambubiose (Xyl-1,2-Glc), rutinose (Glc-1,6-Mal) or trisides (e.g. the Xyl-1,2-Glc-1,6-Gal sequence in black carrot, Scheme 7). The additional glucosylation in C5-OH is also common (e.g. in black carrot, purple potato, red radish), and significantly increases the pigment solubility. More rarely anthocyanins can also be glycosylated at the C7-, C3'- or C5'-OH groups. The glycosidic moieties can be acylated by phenolic (*p*-hydroxycinnamic, *p*-hydroxybenzoic) acids and/or by aliphatic acids, e.g., acetic, and malonic (Wallace & Giusti, 2013). Flowers anthocyanins exhibit particular glycosylation-acylation sequences (Timberlake & Bridle, 1982; Yoshida et al., 2009b). There are however exceptions of permanently colored leaves containing polyacylated anthocyanins, for example in the *Commelinaceae Tradescuntia* gender. For example, the anthocyanin found in *Tradescuntia pallida* (purple secretia) is the cyanidin-3,7,3'-triglucoside with one feruloyl residue on each sugar.

Besides the type of anthocyanin, the concentration varies considerably: berries are amongst the richest sources of anthocyanins. For example, anthocyanin concentrations in aronia and elderberry reach 1.4 - 1.5 g / 100 g fresh weight (Table 1). Some common foods have a flesh which is rich in anthocyanins: purple corn (Cya-3-Glc), black carrots (Cya-3-Samb-5-Glc), purple kohlrabi, etc. Other have anthocyanins gathered in their skin, for example the lychee fruit (Cya-3-Glc, Cya-3-Gal, Pg-3-Rha, Pg-3,5-diGlc), eggplant (Dp-3-pC-Rha-Glc-5-Glc), grape (Mv-3-Glc, Mv-3,5-diGlc and others), plums (Cya-3-Rut), red radish (Pg-3-Soph-5-Glc), etc.

2.3.5. ANTHOCYANIN STRUCTURE & COLOR PROPERTIES

At acidic pH (pure flavylium form), anthocyanins display a visible absorption band with λ_{\max} between 480 (Pg) and 530 nm (Dp, Pt). This value is modulated by the B-ring

hydroxylation and methoxylation pattern and by the glycosylation and acylation patterns (Giusti et al., 1999; Gregory T. Sigurdson et al., 2018). However, the color variety displayed by anthocyanins in nature is largely due to their acid-base properties, as the flavylium ion is a weak diacid in the natural pH domain (pH 2 – 8). From the flavylium ion, the loss of one phenolic protons yields the neutral base, and the loss of the second one yields the anionic base. At this stage, the focus is simply put on the consequences of this feature for the resulting color. The spectra of the 3 individual forms are displayed on Fig 4, they show the strong bathochromic shift associated with each proton loss (occurring at $\text{pH} \approx 4$ and $\text{pH} \approx 7$) (Pina et al., 2012b). The 3-sophorosyl-5-glucosyl-cyanidin and peonidin derivatives of red cabbage and purple sweet potato exhibit a blue anionic base (Fig 4), which is rather uncommon (Moloney et al., 2018). The structure/color stability relationship is detailed at section 3.2.4.

Table 1. Anthocyanin structure and content in common foodstuffs.

Source	Aglycone	% MG*	% DG*	% Acylation	Anthocyanin content**	Moisture
Strawberry ¹	Pg	93	8	1-9	21-40	91
Blackberry ¹	Cy	90	10	6	244	87
Red currant ¹	Cy	2	41 +TG	0	12.8	87
Chokeberry/aronia ¹	Cy	100	0	0	1480	72
Elderberry ^{1,2}	Cy	71-95	4-29	54	1375	82
Plum ¹	Cy	77	23	1	19-124	87.4
Apple (Gala) ¹	Cy	100	0	0	2.3	86
Cranberry ¹	Cy, Pn	77	23	50	140	87
Grape (red) ^{1,6}	Mv, Pn, Dp	28	71	18-22	27-120	80.4
Blueberry ¹	Dp, Mv, Pt	100	0	4-13	131-155	89
Red radish ¹	Pg	0	0 +TG	100	100	96
Red cabbage ¹	Cy	0	0 +TG	85	322	91
Red onion ¹	Cy	69	31	77	46.4-49	88
Black carrot ⁵	Cy	100***	0	82	1.5-17.7	87.3
Eggplant ¹	Cy	83	16	0	86	92
Purple corn ⁷	Cy, Pn	100	0	<10	-	-
Purple potato ³ sweet	Cy, Pn	0	0 +TG	51-86	6.5-29.1	-
Black bean ¹	Dp, Pg	81	19	0	213	10
Soybean seed coat ⁴	Cy > Dp, Pg	100	0	NA	353	40

¹ (X. Wu et al., 2006); ² (Veberic et al., 2009) ; ³ (Montilla et al., 2010) ; ⁴ (Jhan et al., 2016); ⁵ (Montilla et al., 2011), ⁶ (Gómez- Alonso et al., 2007); ⁷ (P. Jing & Giusti, 2007)

*MG: monoglucoside (3-Glc); DG: diglucoside (3,5diGlc); TG = triglycosylated (at C3-OH)

**Expressed as mg/100 g fresh weight, from HPLC analysis, as Cya-3-Glc equivalent

***Glycosylation at C3-OH by (Xyl-Glc)-Gal

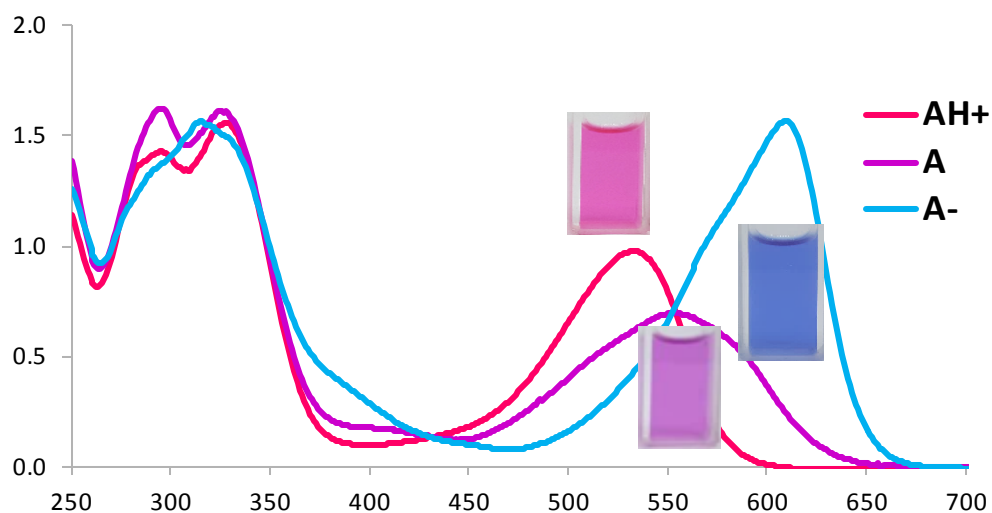
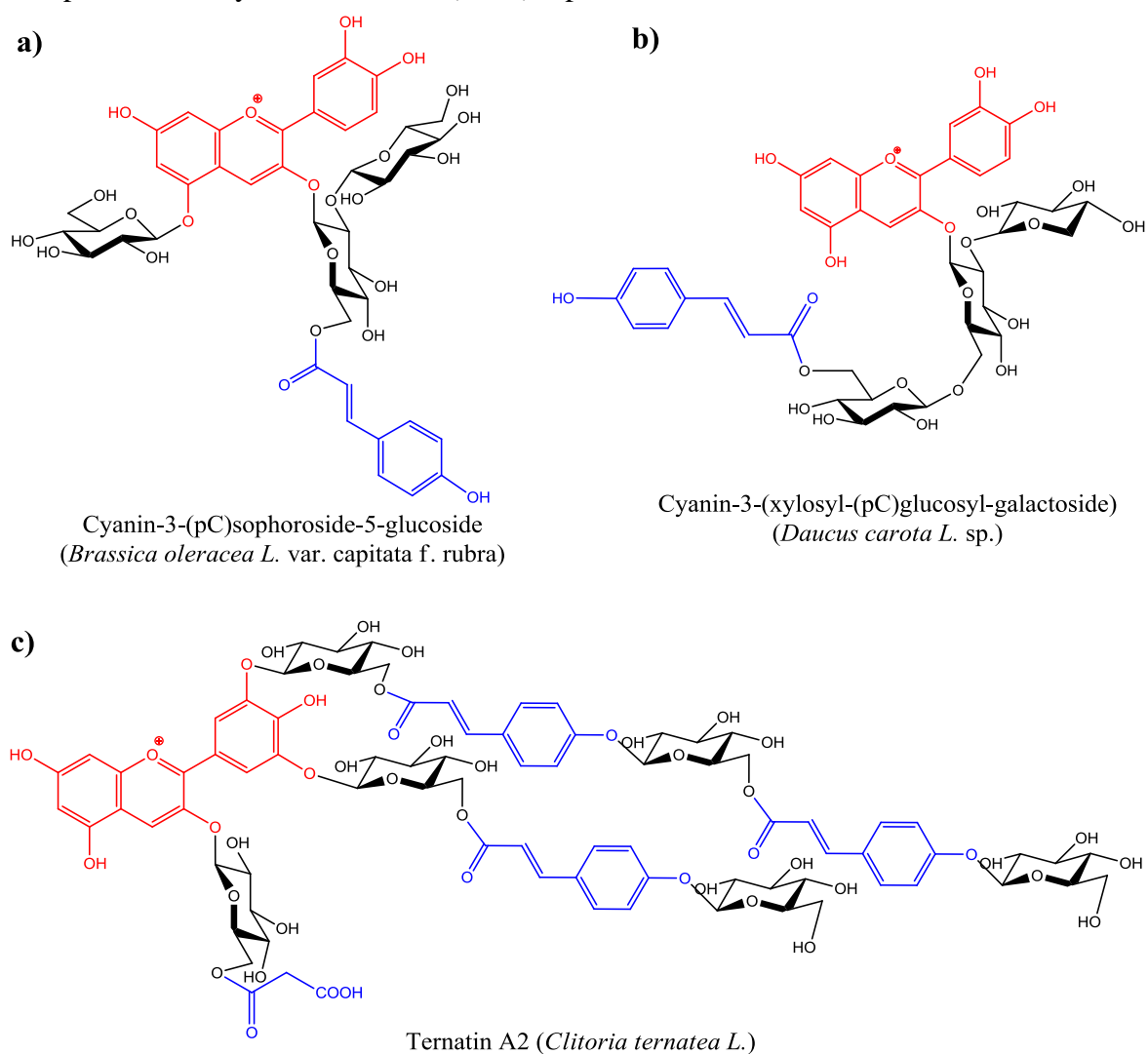


Fig. 4. Calculated absorption spectra of the flavylium, neutral base and anionic base of purple sweet potato anthocyanin P12: Pn-3-(Cf,Fl)Soph-5-Glc



Scheme 7. Anthocyanins with various glycosylation and acylation patterns from a) red cabbage leaves, b) black carrot roots and c) butterfly pea flower.

3. ANTHOCYANIN COLOR STABILITY

From the applied research perspective, the challenge is thus to identify and produce the most similar natural food color to the synthetic colors, namely Brilliant Blue FCF. Some anthocyanins produce blue colors, but several technical hurdles currently limit their use in food and cosmetic applications, namely: a limited number of anthocyanins are able to produce blue colors (mostly in flowers); in the case of edible sources (red cabbage, purple sweet potato), the conditions for blue expression are very specific, as blue require the deprotonation of the B-ring. Two conditions thus produce a blue color: i) at a mildly alkaline pH (7.5 - 9.0), where the powerful reducing properties of anthocyanins lead to their destruction; or ii) in the presence of metal ions, over a broader range of pH, this solution operating only for cyanidin, delphinidin and petunidin derivatives. In both cases, the color stability remains the major challenge to tackle.

3.1. Search methodology

Articles search was executed with the databases Science Direct, American Chemical Society, Royal Society of Chemistry and Google Scholar. According to Web of Science, 1991 - 2017 research on anthocyanin stability mainly related to the following fields: food science & technology category (1,769), applied chemistry (752), nutrition & dietetics (418), agriculture (310) and chemical engineering (171). Since 2015, there has been as rapid increase in the number of publications related to anthocyanins stability/degradation and reactivity, which is likely driven by the industrial need for natural food colors, and the technical challenges associated. Although the pH of most biological fluids is close to neutrality, few studies have addressed the issue of anthocyanin stability under neutral conditions. They are rather carried out in the pH range 3 to 6, corresponding fruit preparations, wine and dairy products. For this literature review, studies at all pH and all temperatures are included, so as to build a complete picture of anthocyanin degradation. Only the degradation of individual pigments and structurally characterized extracts are considered. The degradation products of phenolic acids are also briefly reviewed, as they occur as acyl residues and could impact the stability of anthocyanins.

3.2. The chemical reactivity of anthocyanins

This section presents the literature review on the general reactivity of anthocyanin, that was published as the first review of a special issue of the journal *Molecules* (Dangles & Fenger, 2018). Following the review, more specific information on the structural transformations, major degradation products and mechanisms in simple models is provided.

Review

The Chemical Reactivity of Anthocyanins and its Consequences in Food Science and Nutrition

Olivier Dangles * and Julie-Anne Fenger

University of Avignon, INRA, UMR408, 84000 Avignon, France; julie-anne.fenger@univ-avignon.fr

* Correspondence: olivier.dangles@univ-avignon.fr; Tel.: +33-490-144-446

Received: 6 July 2018; Accepted: 31 July 2018; Published: 5 August 2018

Abstract: Owing to their specific pyrylium nucleus (C-ring), anthocyanins express a much richer chemical reactivity than the other flavonoid classes. For instance, anthocyanins are weak diacids, hard and soft electrophiles, nucleophiles, prone to developing π -stacking interactions, and bind hard metal ions. They also display the usual chemical properties of polyphenols, such as electron donation and affinity for proteins. In this review, these properties are revisited through a variety of examples and discussed in relation to their consequences in food and in nutrition with an emphasis on the transformations occurring upon storage or thermal treatment and on the catabolism of anthocyanins in humans, which is of critical importance for interpreting their effects on health.

Keywords: anthocyanin; flavylum; chemistry; interactions

1. INTRODUCTION

Anthocyanins are usually represented by their flavylium cation, which is actually the sole chemical species in fairly acidic aqueous solution ($\text{pH} < 2$). Under the pH conditions prevailing in plants, food and in the digestive tract (from $\text{pH} = 2$ to $\text{pH} = 8$), anthocyanins change to a mixture of colored and colorless forms in equilibrium through acid–base, water addition–elimination, and isomerization reactions [1, 2]. Each chemical species displays specific characteristics (charge, electronic distribution, planarity, and shape) modulating its reactivity and interactions with plant or food components, such as the other phenolic compounds. This sophisticated chemistry must be understood to interpret the variety of colors expressed by anthocyanins and the color changes observed in time and to minimize the irreversible color loss signaling the chemical degradation of chromophores. The chemical reactivity of anthocyanins is also important to interpret their fate after ingestion and their effects on health, as anthocyanins may be consumed as a complex mixture of native forms, derivatives, and degradation products, which themselves can evolve in the digestive tract [3].

2. THE BASIS OF ANTHOCYANIN CHEMISTRY

2.1. Anthocyanins Are Weak Diacids

Due to conjugation with the electron-withdrawing pyrylium ring, the phenolic OH groups of the flavylium ion at C4', C5, and C7 are fairly acidic [1, 2]. In terms of structure–acidity relationships, it is clear that C7-OH is the most acidic group with a $\text{p}K_{\text{a}1}$ of ca. 4, i.e., 6 $\text{p}K_{\text{a}}$ units below the phenol itself. The corresponding neutral quinonoid base (Figure 1) can thus be considered to be the prevailing tautomer. At higher pH levels, a second proton loss from C4'-OH ($\text{p}K_{\text{a}2} \approx 7$ for common anthocyanins) yields the anionic base with maximized electron delocalization over the three rings. Along this deprotonation sequence, the wavelength of maximal visible absorption typically shifts by 20–30 nm ($\text{AH}^+ \rightarrow \text{A}$), then by 50–60 nm ($\text{A} \rightarrow \text{A}^-$) (Figure 2), and the corresponding color turns from red to purple-blue [4].

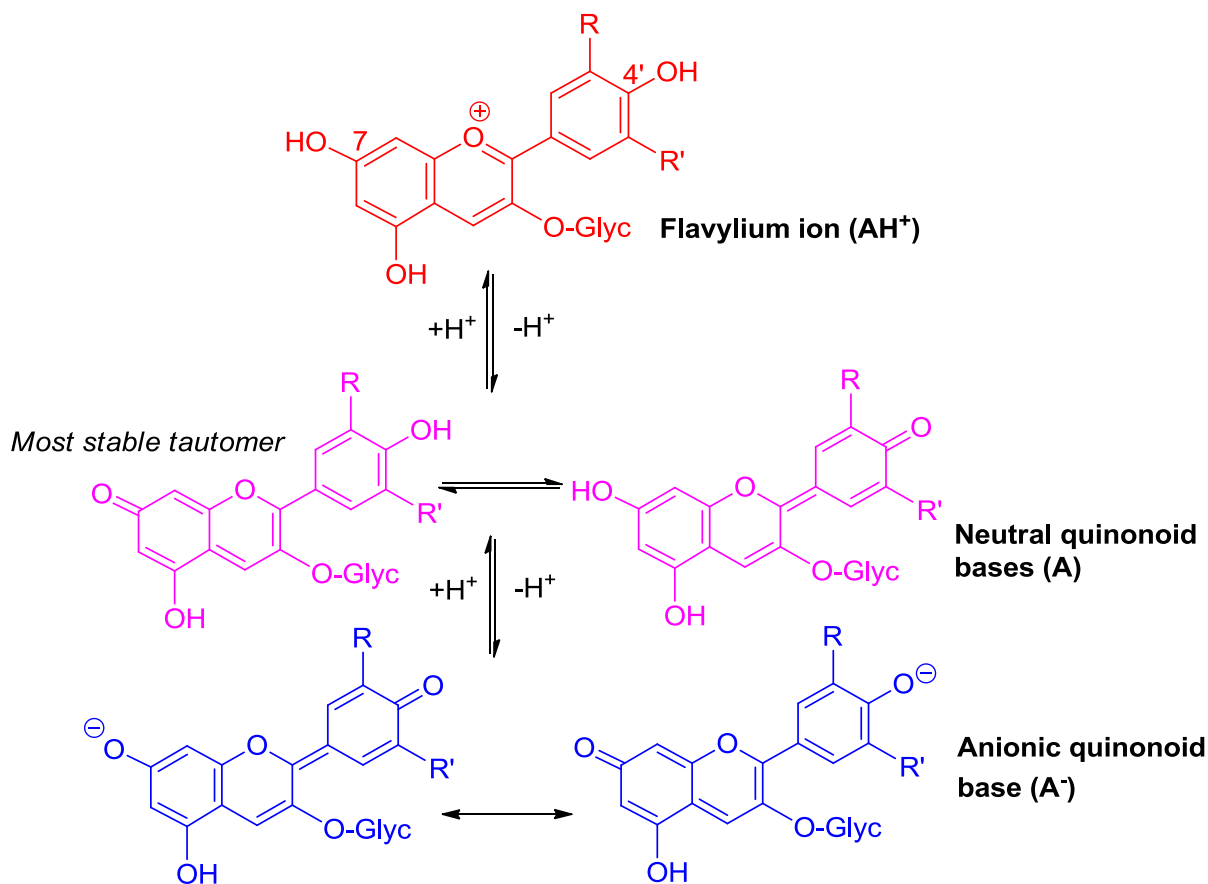


Figure 1. Flavylium ions are weak diacids.

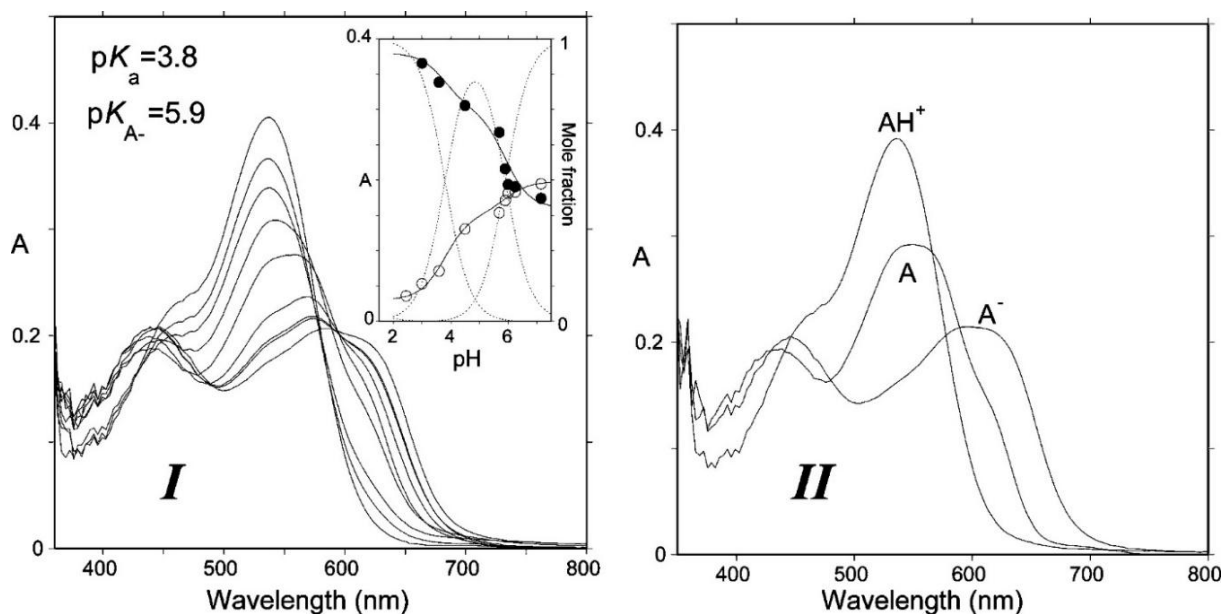


Figure 2. (I) Absorption spectra of Cat-Mv3Glc: pH jump from pH = 1.0 (100% flavylium) to pH 3.00, 3.59, 4.50, 5.70, 5.96, 6.25, and 7.15, respectively. Spectra recorded 10 ms after mixing (negligible water addition). (II) Spectra of the components obtained by mathematical decomposition. From [4] with permission of the *American Chemical Society*.

2.2. Anthocyanins Are Hard and Soft Electrophiles

By analogy with enones, the C2 and C4 atoms of the pyrylium ring can be regarded as hard and soft electrophilic centers, respectively. Hence, they respectively react with hard (O-centered) and soft (S- and C-centered) nucleophiles, the first mechanism being driven by local charges and the second one by interactions between the frontier molecular orbitals (HOMO of nucleophiles and LUMO of electrophiles).

2.2.1. NUCLEOPHILIC ADDITION AT C2

Water addition is the ubiquitous process taking place within aqueous anthocyanin solutions [1, 2]. It leads to the colorless hemiketal (Figure 3) and can be characterized by the thermodynamic hydration constant K_h , or as an acceptable approximation (chalcones making only a minor contribution, typically less than 20%, of the total pool of colorless forms), by the apparent constant K'_h connecting the flavylum ion and the colorless forms taken collectively. With common anthocyanins, pK'_h lies in the range of 2–3, which means that hydration is thermodynamically more favorable than proton transfer ($pK'_h < pK_{a1}$). Fortunately, it is also much slower, and its pH-dependent kinetics can be quantified by the apparent rate constant of hydration (k_{obs}) (Equation (1), $h = [H^+]$, χ_{AH} = mole fraction of AH^+ within the mixture of colored forms [2,5]):

$$k_{obs} = k_h \chi_{AH} + k'_{-h} h = \frac{k_h}{1 + K_{a1}/h + K_{a1}K_{a2}/h^2} + k'_{-h} h \quad (1)$$

k_h is the absolute rate constant of water addition, k'_{-h} is the apparent rate constant of water elimination (from the mixture of hemiketal and *cis*-chalcone in fast equilibrium), and $K'_h \approx k_h/k'_{-h}$ (*trans*-chalcone neglected). Equation (1) can be easily understood by keeping in mind that the flavylum ion is the sole colored form that is electrophilic enough to directly react with water.

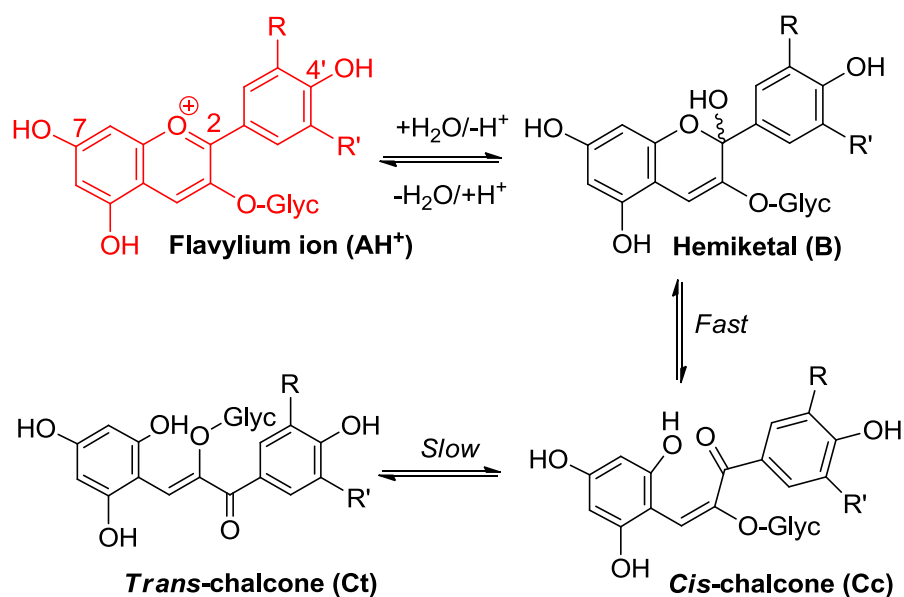


Figure 3. Flavylium ions are hard electrophiles reacting at C2 with O-centered nucleophiles, such as water (water addition followed by formation of minor concentrations of chalcones).

At a given pH, the initial visible absorbance (A_0) (no colorless forms) and the final visible absorbance (A_f) (hydration equilibrium established) can be easily related through Equation (2):

$$\frac{A_f}{A_0} = \frac{1 + K_{a1}/h + K_{a1}K_{a2}/h^2}{1 + (K_{a1} + K'_h)/h + K_{a1}K_{a2}/h^2} \quad (2)$$

Thus, the magnitude of color loss can be expressed as (Equation (3)):

$$\frac{A_0 - A_f}{A_0} = \frac{K'_h/h}{1 + (K_{a1} + K'_h)/h + K_{a1}K_{a2}/h^2} \quad (3)$$

From typical values for the rate and thermodynamic constants of common anthocyanins, simulations of the pH dependence of the apparent rate constant and percentage of color loss can be constructed (Figure 4). The plots clearly show that the reversible color loss due to water addition to the flavylium ion becomes slower at higher pH (less flavylium in solution), whereas its magnitude becomes larger because of the higher stability of the colorless forms. The typical time-dependence of the visible spectrum during water addition is shown in Figure 5 [4].

Near neutrality water addition is so slow (fraction of flavylum ion < 0.1%) that the colored forms (mixtures of neutral and anionic bases) can, in principle, persist for hours. However, such a reasoning ignores the irreversible mechanisms of color loss taking place near neutrality as the anionic base is obviously much more sensitive to autoxidation (non-enzymatic oxidation by O₂ triggered by transition metal traces) than the flavylum ion. These mechanisms will be addressed in Section 2.4.1.

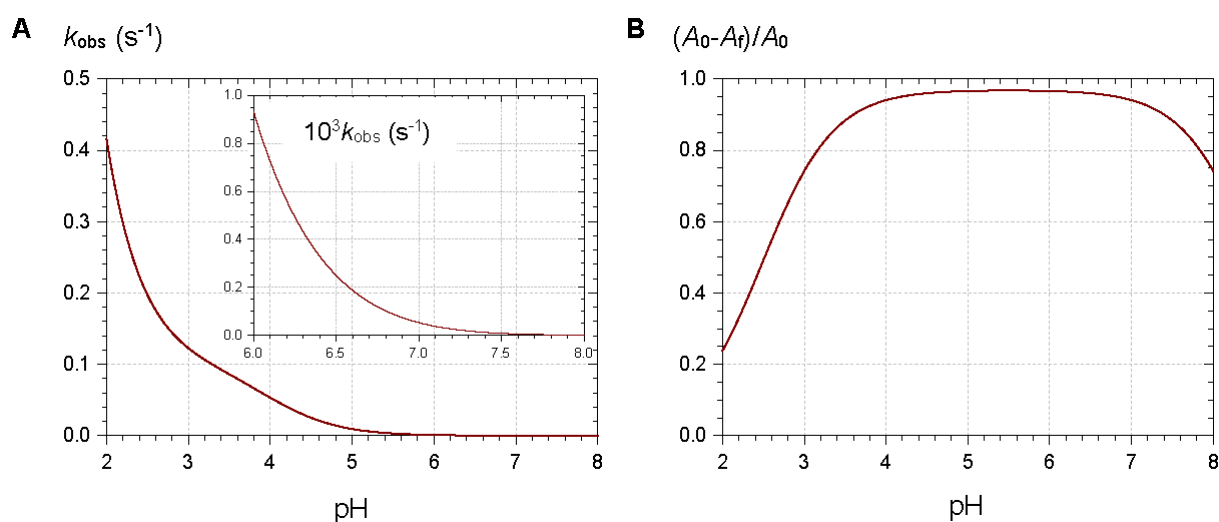


Figure 4. Simulations of the pH dependence of the apparent rate constant (**A**) and relative magnitude (**B**) of color loss. Selected values for parameters: $pK_{a1} = 4$, $pK_{a1} = 7$, $pK'_h = 2.5$, $k_h = 0.1 \text{ s}^{-1}$, $k'_{-h} \approx k_h/K'_h$.

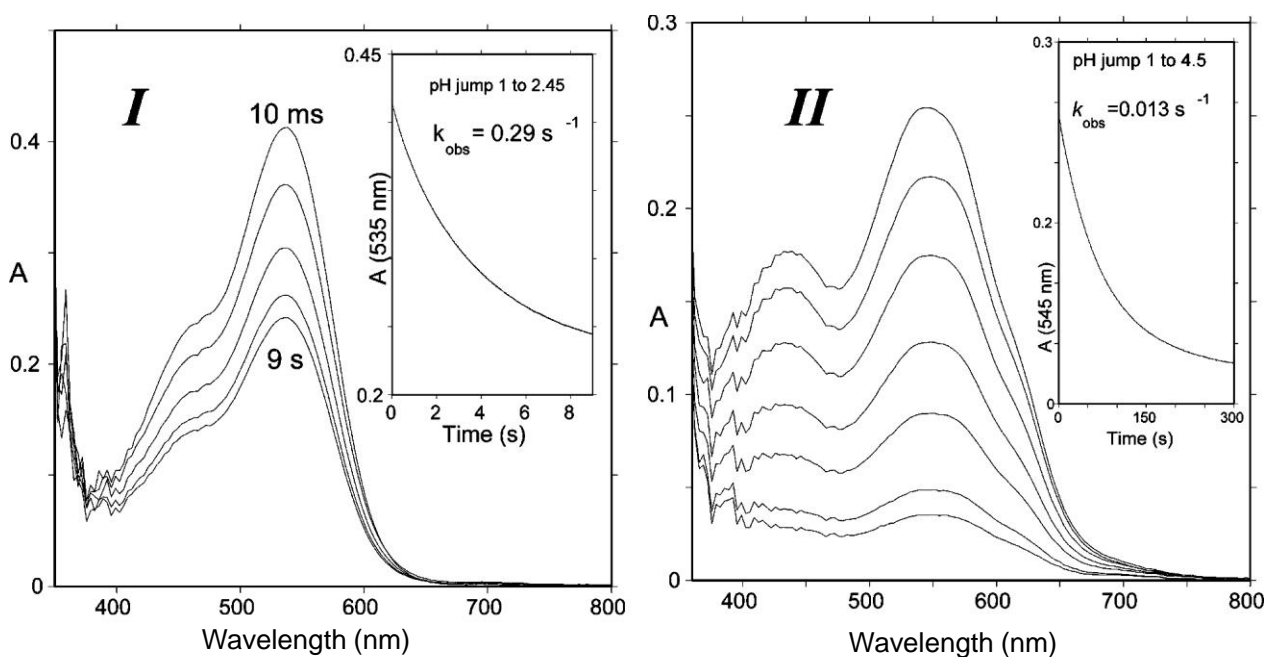


Figure 5. (I) Spectral changes of Cat-Mv3Glc between 10 ms and 9 s following a pH jump from pH = 1 to pH = 2.45; half-life of flavylum = 2.4 s. (II) pH jump from pH = 1 to pH =

4.5; half-life of quinonoid bases = 53.3 s. At pH = 6, the half-life of quinonoid bases \approx 30 min. From reference [4] with permission of the *American Chemical Society*.

2.2.2. NUCLEOPHILIC ADDITION AT C4

Bisulfite is an antimicrobial and anti-browning agent that is frequently used in the food industry. As a S-centered nucleophile, it reversibly reacts with the flavylium ion at C4, thus yielding colorless adducts (Figure 6) [6]. No such adducts have been identified so far by simply reacting anthocyanins with natural thiols such as cysteine and glutathione (GSH). Unlike bisulfite, which is actually the conjugated base of SO_2 ($\text{p}K_a \approx 1.8$) and can coexist with the flavylium ion under acidic conditions, thiolate anions ($\text{p}K_a = 8-9$) are usually formed at much higher pH levels where the flavylium ion is only present as traces.

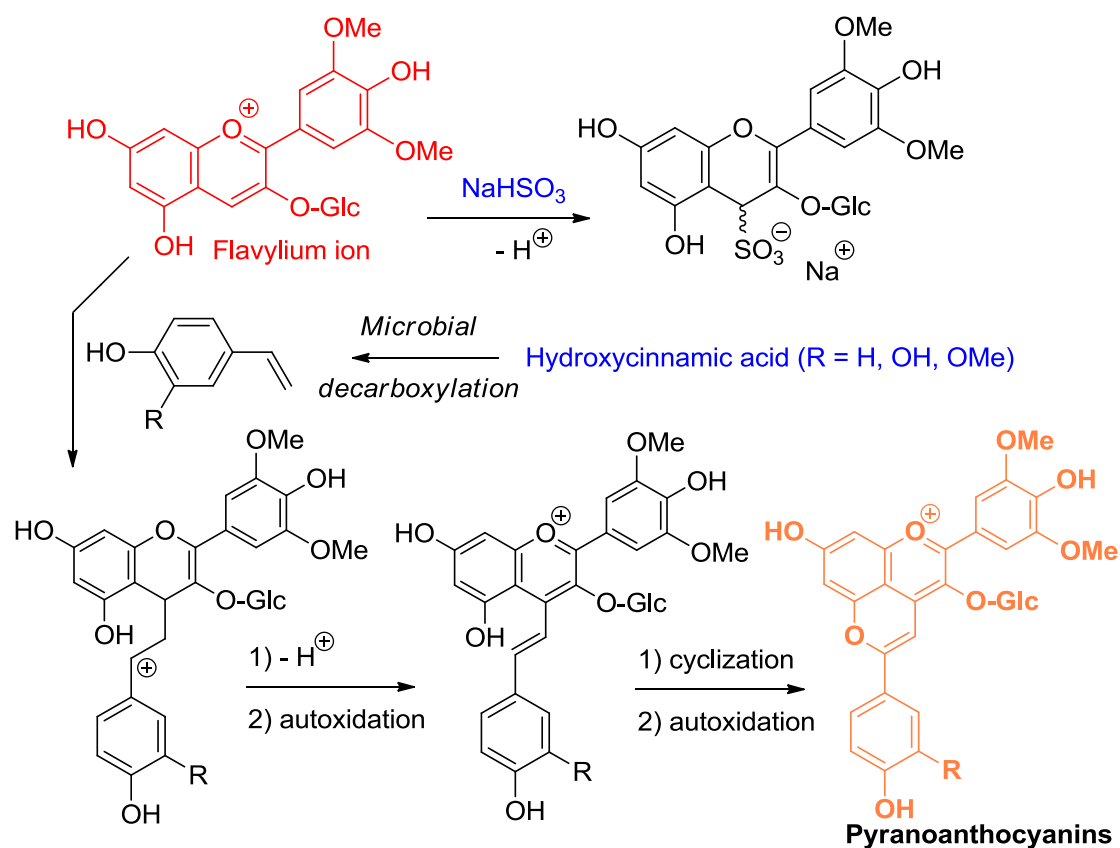


Figure 6. Flavylium ions are soft electrophiles that react at C4 with S- and C-centered nucleophiles, such as bisulfite and 4-vinylphenols.

A variety of C-centered nucleophiles are also known to add to the flavylium ion, and this chemistry underlies the color changes observed in red wine upon aging [7]. In this context, the most important C-centered nucleophiles are electron-rich C–C double bonds, such as 4-vinylphenols (4-hydroxystyrenes), formed upon microbial decarboxylation of 4-

hydroxycinnamic acids (Figure 6) and the enol forms of various aldehydes and ketones such as pyruvic acid and ethanal (acetaldehyde) [8,9]. In the process, new pigments, called pyranoanthocyanins, are formed, which are resistant to nucleophilic addition at C2 and C4 [10–12]. Their color (shifted to orange-red, compared to the corresponding flavylum ion) is thus more stable. Through their nucleophilic C6- and C8-atoms, flavanols and proanthocyanidins can also add to the electrophilic C4 center of anthocyanins [13]. However, the flavene intermediate thus formed is not accumulated and evolves through two possible routes: (a) under strongly acidic conditions (pH = 2), protonation at C3 allows a second nucleophilic attack by a nearby phenolic OH group of the tannin to yield a colorless product (see Section 2.3. for a similar mechanism); or (b) under moderately acidic conditions (pH = 3–6), dehydration with concomitant formation of an additional pyrane ring is favored and a new pigment bearing a xanthylium chromophore is formed.

With its enediol structure, ascorbate (vitamin C) can also react with flavylum ions at C4 but the corresponding adducts have not been reported so far.

2.3. Anthocyanin Hemiketals Are Nucleophiles

Basic organic chemistry teaches that electron-donating substituents of benzene rings accelerate aromatic electrophilic substitutions (S_{EAr}) and orient the entering electrophiles to the *ortho* and *para* positions. In that perspective, the phloroglucinol (1,3,5-trihydroxybenzene) ring (A-ring) of anthocyanins must be especially favorable to S_{EAr} as the three O-atoms combine their electronic effects to increase the reactivity of C6 and C8. However, the pyrylium ring (C-ring) of the flavylum ion (and, to a lesser degree, the enone moiety of chalcones) is strongly electron-withdrawing, so that only the hemiketal is expected to react by S_{EAr} .

Here, again, wine chemistry provides interesting examples of S_{EAr} between anthocyanins and various carbocations derived from other wine components (Figure 7) [7]. For instance, wine pigments in which anthocyanins and flavanols are linked through an ethylidene bridge between their C6- and/or C8-atoms are formed by double S_{EAr} between A-rings and ethanol [14,15]. The likely intermediates in the reaction are the 6- or 8-vinyl-flavanol and the 6- or 8-vinyl-anthocyanin hemiketals, the protonation of which delivers a benzylic cation that is directly involved in the S_{EAr} reaction. Of course, in addition to the

cross reaction products, anthocyanin–ethylidene–anthocyanin and flavanol–ethylidene–flavanol adducts can also form oligomers and mixed oligomers [16]. Even, pyranoanthocyanins stemming from the nucleophilic attack of vinyl-phenols at C4 of anthocyanins can be produced.

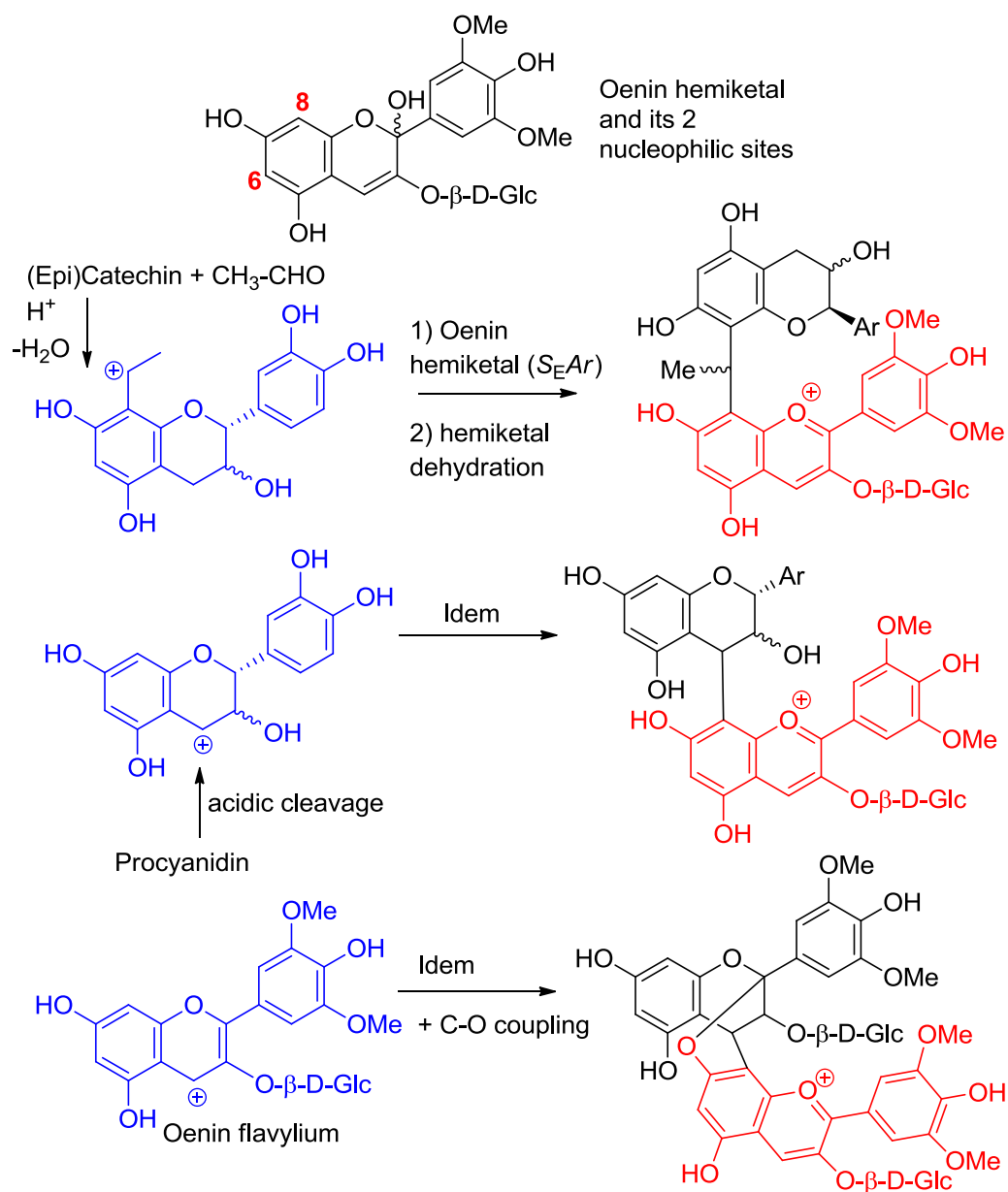


Figure 7. Anthocyanin hemiketals are nucleophiles reacting with carbocations (Ar = catechol ring).

Flavanol carbocations formed by acidic cleavage of the inter-flavan linkage of proanthocyanidins also react with anthocyanin hemiketals by S_EAr [17]. Interestingly, both direct and ethylidene-bridged flavanol–anthocyanin adducts are more purple than the native

anthocyanin, but only the latter expresses a color that is stable, i.e., a flavylum nucleus that is less sensitive to water addition [4,18]. A possible explanation is that ethylidene-bridged flavanol–anthocyanin adducts are prone to non-covalent self-association by π -stacking, which provides a less aqueous environment for the flavylum nuclei.

Water elimination from the anomeric C-atom of the ellagitannin vescalagin (abundant in oak barrels) also delivers a carbocation for direct coupling with wine anthocyanins [19] and subsequent modest protection against water addition [20]. Finally, the anthocyanin hemiketal can react with the flavylum ion itself, and this pathway provides a route for anthocyanin oligomerization, a poorly documented mechanism as the corresponding oligomers are probably difficult to evidence and quantify. However, an oenin trimer has been found in Port wine, and its structure has been fully elucidated by NMR [21]. The two linkages are of the C4–C8 type. As in the direct flavanol–anthocyanin coupling (see Section 2.2.2.), flavene intermediates evolve by C–O coupling and only the lower unit remains colored. Similar oligomers also occur with 3-deoxyanthocyanidins, e.g., in red sorghum, but the detailed structures remain unknown [22]. Anthocyanin hemiketals can also react by Michael addition with *o*-quinones formed by two-electron oxidation of catechols, such as epicatechin [13] and caffeoyltartaric acid [23].

2.4. Anthocyanins Are Electron-Donors

Many polyphenols, especially those containing electron-rich catechol (1,2-dihydroxybenzene) or pyrogallol (1,2,3-trihydroxybenzene) nuclei are good electron- or H-donors. Electron transfer is typically faster when the pH is raised, i.e., when the fraction of phenolate anion (a much better electron-donor than the parent phenol) increases. Electron transfer from phenols is involved in their oxidation mechanisms and also underlies the most common mechanism of antioxidant activity, i.e., the reduction of reactive oxygen species (ROS) involved in oxidative stress from plants to humans. Anthocyanins are known to be thermally unstable, especially under neutral conditions, and various degradation products have been identified. Their antioxidant activity has been also established in various chemical models. However, detailed knowledge on the mechanisms involved and on the relative contributions of the different colored and colorless forms is still missing.

2.4.1. OXIDATION

Anthocyanins are among the least thermally stable flavonoids. Anthocyanidins, the corresponding aglycones, are actually only stable under highly acidic conditions and are extensively degraded in less than one hour under physiological conditions (pH = 7.4, 37 °C) [24,25]. From the structure of the degradation products, it is clear that a combination of hydrolytic and autoxidative pathways operate, leading to cleavage of the C2–C1', C2–C3 and C3–C4 bonds (Figure 8) [13, 26, 27]. A mechanism involving pre-formed hydrogen peroxide actually accounts for the formation of some cleavage products (Figure 9). The critical step is the addition of H₂O₂ (a hard nucleophile) at C2 of the flavylum ion, followed by Baeyer–Villiger rearrangement, which opens routes for cleavage of the C2–C1' and C2–C3 bonds [13,26]. However, the preliminary formation of H₂O₂ remains unclear and must involve the direct autoxidation of anthocyanins. Thus, an alternative mechanism beginning by electron or H-atom transfer (mediated by unidentified transition metal traces) from the anionic or neutral base to O₂ would deliver a highly delocalized radical that is susceptible to O₂ addition at different centers (Figure 10). The cleavage of hydroperoxide intermediates thus formed could also yield the degradation products detected.

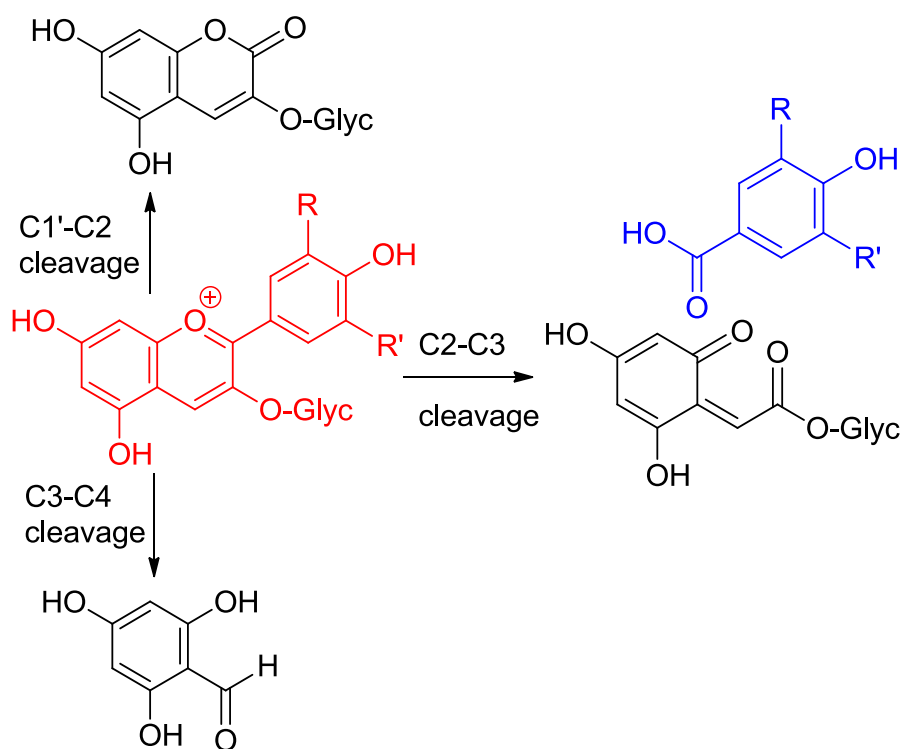


Figure 8. Pathways of anthocyanin degradation.

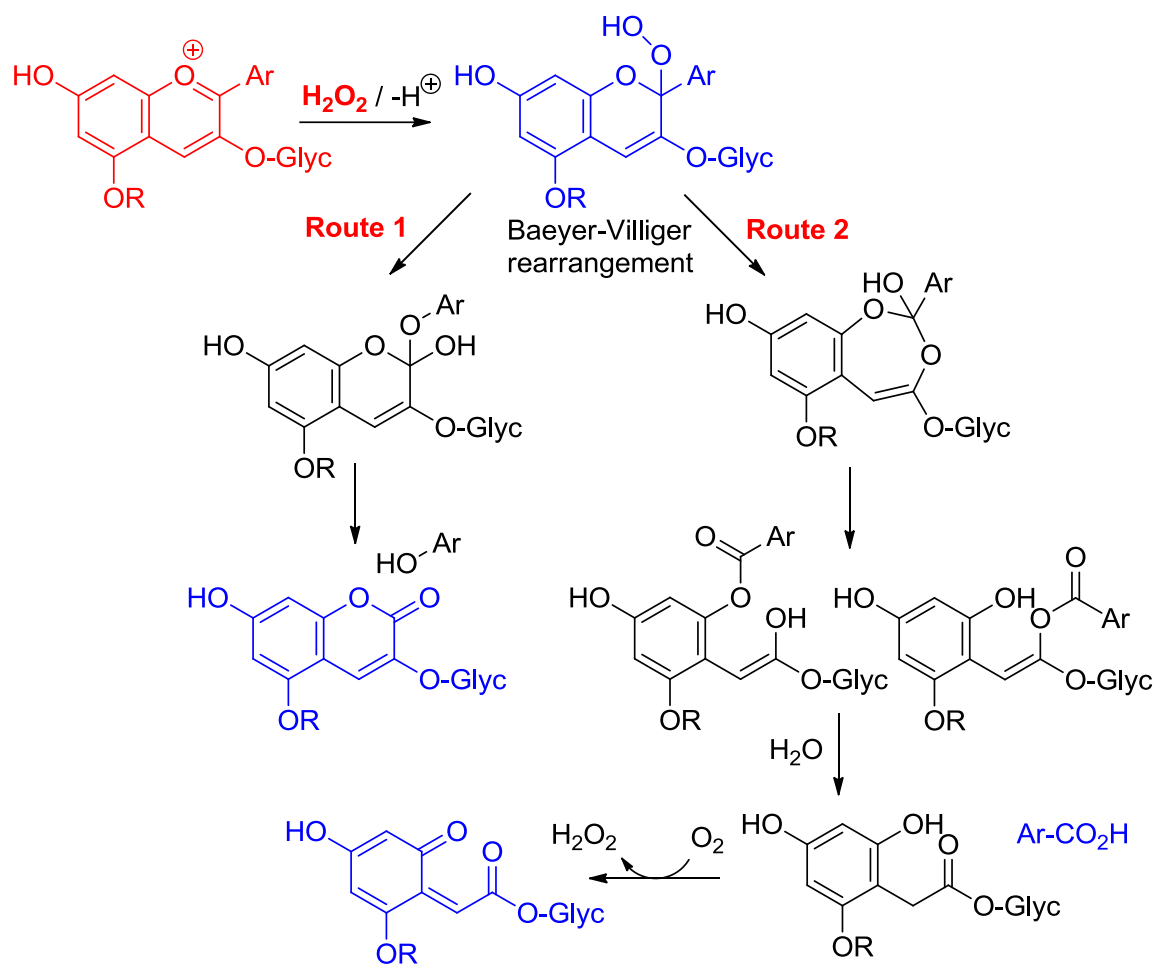


Figure 9. Possible mechanisms of anthocyanin degradation with pre-formed hydrogen peroxide.

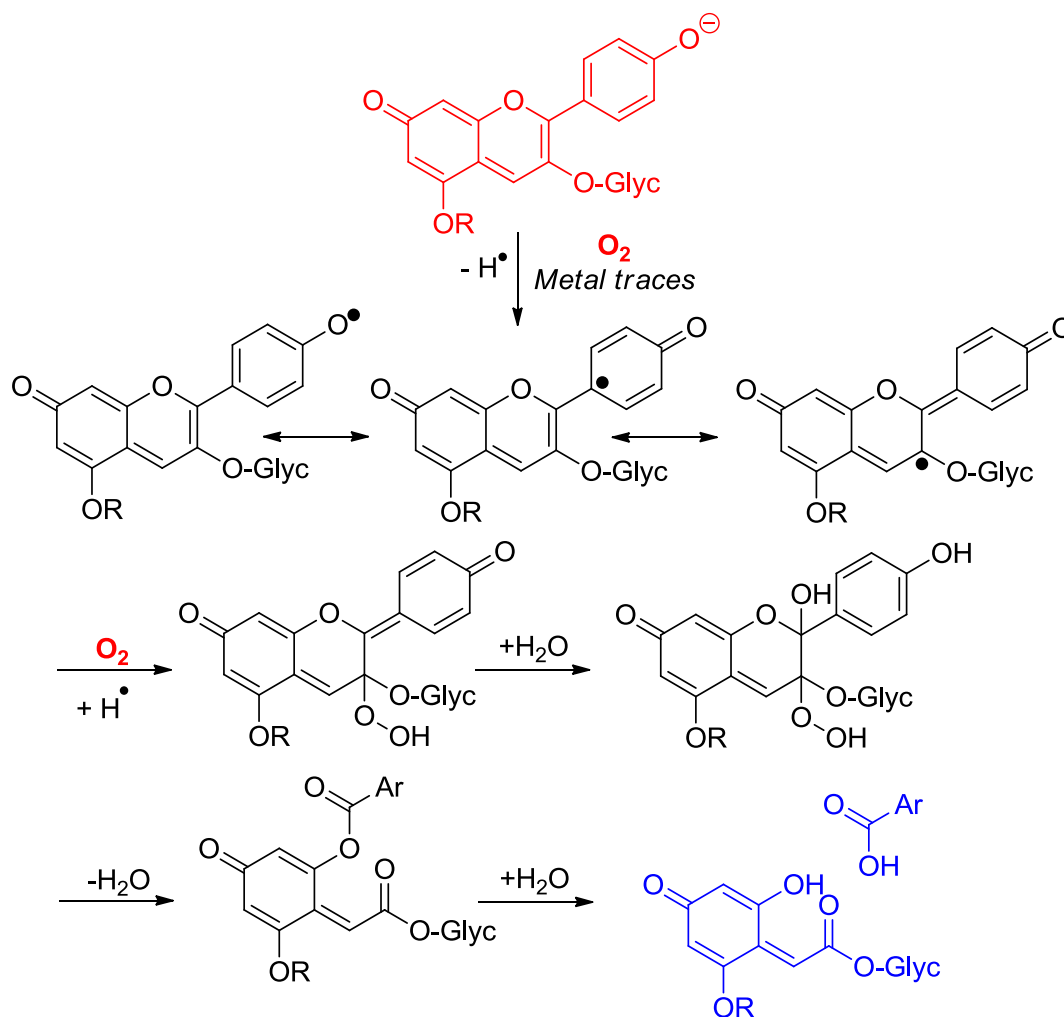


Figure 10. Possible mechanisms of anthocyanin degradation without pre-formed hydrogen peroxide.

2.4.2. ANTIOXIDANT ACTIVITY

Anthocyanins under their native forms can transfer electrons to ROS and could, therefore, provide protection to important oxidizable biomolecules, such as polyunsaturated fatty acids (PUFAs), proteins, and DNA. The relevance of such phenomena is probably much higher in food preservation than in nutrition and health, given the current knowledge on anthocyanin bioavailability (see Section 3). In this section, we simply mention that anthocyanins can indeed effectively reduce one-electron oxidants such as the stable radical DPPH (2,2-diphenyl-1-picrylhydrazyl). Structure–activity relationships show that hydroxylation at C3' and C5' increases the H-donating capacity, thus suggesting that the B-ring is primarily involved in electron donation [28]. Comparing oenin and the flavanol catechin shows that the transfer of the first (most labile) H-atom to DPPH is roughly as fast for both flavonoids but that oenin reduces at least twice as many radicals than catechin (Table

1) [29]. This advantage must be rooted in the extensive oxidative degradation undergone by oenin during the DPPH-scavenging process with the transient formation of intermediates (possibly, syringic acid) retaining a substantial electron-donating activity. It is also remarkable that the wine pigments combining the oenin and catechin units retain a high but contrasting DPPH-scavenging activity [29]: the direct coupling between the two flavonoid units results in a faster first H-atom transfer (higher k_1) but markedly lowers the total number of radicals reduced (n_{tot}), whereas the coupling through an ethylidene bridge apparently leaves each unit free to independently react with DPPH (k_1 almost unchanged, approximate additivity in the n_{tot} value), as observed with the equimolar oenin–catechin mixture (Table 1).

Table 1. Antioxidant activity of malvidin 3-*O*- β -D-glucoside (oenin) and related pigments: reduction of the DPPH (2,2-diphenyl-1-picrylhydrazyl) radical (MeOH, 25 °C, ¹ and ²) and inhibition of heme-induced peroxidation of linoleic acid (0.1 mM linoleic acid in acetate buffer + 2 mM Tween-20, 0.1 μ M metmyoglobin, pH = 4, 37 °C, ³). From reference [29].

Antioxidant	n_{tot} ¹	k_1/s^{-1} ²	IC ₅₀ / μ M ³
Oenin	11.26 (\pm 0.08)	910 (\pm 70)	0.68
Catechin	4.86 (\pm 0.03)	1200 (\pm 110)	0.27
Oenin + Catechin (1:1)	14.04 (\pm 0.10)	1160 (\pm 330)	nd
(<i>R</i>)-Catechin-8-CHMe-8-Oenin	14.56 (\pm 0.03)	1000 (\pm 320)	0.15
(<i>S</i>)-Catechin-8-CHMe-8-Oenin	14.61 (\pm 0.18)	600 (\pm 120)	0.41
Catechin-4,8-Oenin	7.16 (\pm 0.08)	5120 (\pm 1050)	0.60

¹ Antioxidant stoichiometry (number of DPPH radicals reduced per antioxidant molecule). ² Rate constant for the transfer of the first H-atom from antioxidant to DPPH. ³ Antioxidant concentration for a doubling of the period of time required for the accumulation of a fixed concentration of polyunsaturated fatty acid (PUFA) hydroperoxides (conjugated dienes).

Oenin, catechin, and wine pigments were also compared for their ability to inhibit the peroxidation of linoleic acid induced by dietary heme iron in acidic micelle solutions, a chemical model of postprandial oxidative stress in the stomach [29]. As hydrophilic antioxidants, polyphenols are known to act at the initiation stage by reducing the hypervalent iron species (Fe^{IV}) involved in the generation of propagating lipid peroxy radicals (Figure 11)

[30] which, on the other hand, are directly reduced by the typical chain-breaking amphiphilic antioxidant α -tocopherol (vitamin E). The highly hydrophilic oenin was found to be less potent than catechin in the inhibition, but coupling both flavonoids via an ethylidene bridge improves their efficiency (Table 1).

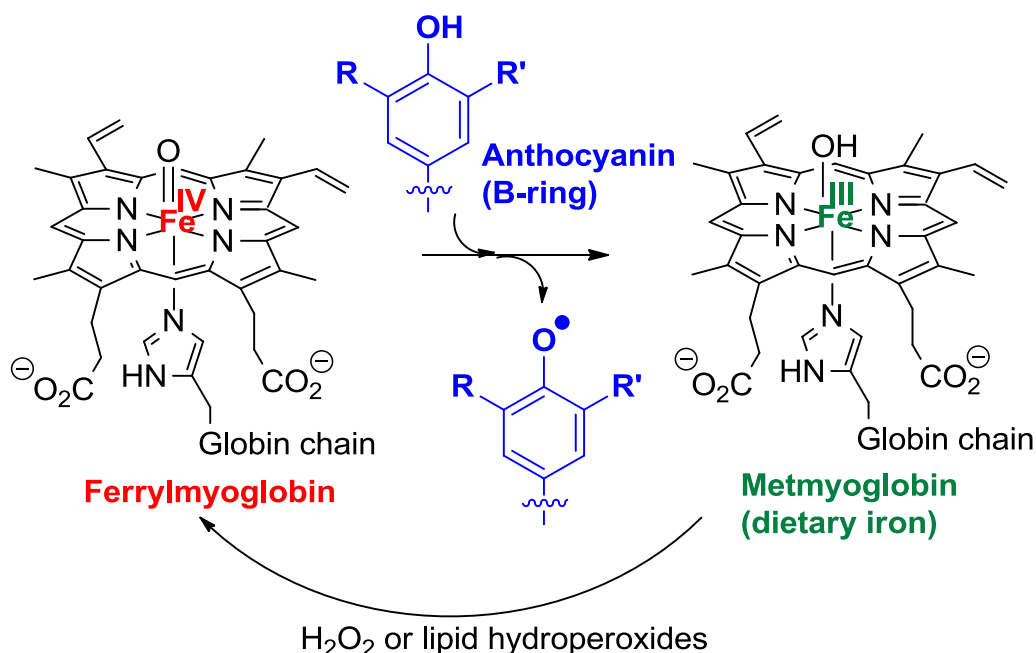


Figure 11. Possible mechanisms for the antioxidant activity of anthocyanins in food and in the gastro-intestinal tract.

Acylation by electron-rich hydroxycinnamic acids, such as sinapic and ferulic acids, potentiates the capacity of anthocyanins to inhibit the diazo-initiated autoxidation of styrene in acetonitrile. In particular, a higher rate constant and stoichiometric factor of radical scavenging were obtained for acylated (*vs.* non-acylated) anthocyanins [31]. Curiously, this trend could not be confirmed for the peroxidation of linoleic acid in micelles, as if the intrinsic differences in electron-donating activity were counterbalanced by differences in the partition of anthocyanins between micelles and the aqueous phase.

2.5. Anthocyanin Complexes

Phenolic nuclei have an intrinsic ability to develop molecular (non-covalent) interactions as they combine flat polarizable apolar surfaces (the aromatic nuclei) for strong dispersion interactions and polar OH groups that are susceptible to acting as H-bond donors and acceptors.

2.5.1. SELF-ASSOCIATION AND CO-PIGMENTATION

One of the most remarkable properties of the anthocyanin chromophores is their ability to develop π -stacking interactions [32–34], mostly driven by dispersion interactions and the concomitant favorable release of water molecules from the solvation shells of the interacting nuclei, known as the hydrophobic effect. Owing to their planar structures and extended electron delocalization over the three rings, the colored forms are much more prone to π -stacking interactions than the colorless forms, for which such interactions, although not necessarily absent, are typically neglected. Examples of π -stacking interactions with anthocyanins are self-association and binding between anthocyanins and other phenols, a phenomenon called co-pigmentation. The affinity of co-pigments for a given anthocyanin (as measured by the corresponding thermodynamic binding constant) decays along the series: planar flavonoids (flavones, flavonols) > non-planar flavonoids (catechins), hydroxycinnamic acids > hydroxybenzoic acids [32]. As for self-association, it is stronger for the neutral base than for the flavylium ion and the anionic base, as the latter stacks are destabilized by charge repulsion.

The spectral consequences of co-pigmentation are summarized in Figure 12 with malvin (malvidin 3,5-di-*O*- β -glucoside) and a highly water-soluble rutin (quercetin 3-*O*- β -rutinoside) derivative [35]. In strongly acidic solutions (negligible water-to-flavylium addition), π -stacking interactions between the two partners promote bathochromism as a consequence of co-pigment-to-pigment charge transfer. Changes in color intensity simply reflect differences between the molar absorption coefficients of free and bound pigments. Under the mildly acidic conditions typically encountered in natural media, pigment–co-pigment interactions also promote hyperchromism, which can be understood as a shift in the now established flavylium–hemiketal equilibrium toward the colored form, which is selectively stabilized by its association with the co-pigment. This combination of bathochromic and hyperchromic shifts makes co-pigmentation one of the most important mechanisms for color variation and stabilization in plants. It can also be noted that heating

usually attenuates the hyperchromic shift (Figure 12) as a consequence of the exothermic character of co-pigmentation ($\Delta H^0 < 0$).

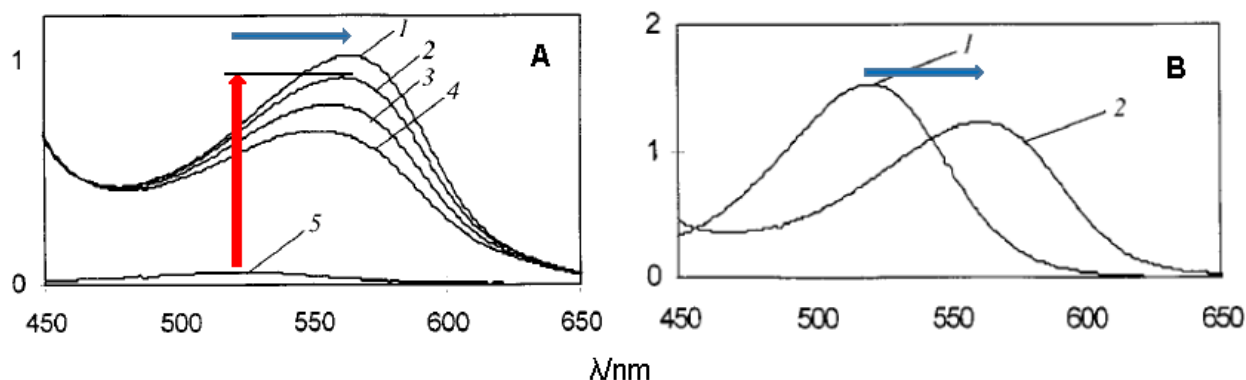


Figure 12. Co-pigmentation of malvin (malvidin 3,5-diglucoside, 50 μM) by rutin bis(hydrogensuccinate) (mixture of 3 regioisomers, 200 equiv.). (A) pH = 3.5, malvin + co-pigment at T = 15.5 (1), 25.0 (2), 35.0 (3), 44.2 (4) $^{\circ}\text{C}$, malvin alone at T = 25.3 $^{\circ}\text{C}$ (5). (B) pH = 0.9, T = 25.0 $^{\circ}\text{C}$, malvin alone (1), malvin + co-pigment (2). Adapted from reference [35].

The possibility of developing π -stacking interactions increases with the acylation of anthocyanins on their glycosyl moieties by hydroxycinnamic acid (HCA) residues. Indeed, depending on the location and number of HCA residues, different spatial arrangements can be observed (Figure 13) [34]:

- Intramolecular co-pigmentation: π -stacking interactions promote a conformational folding of the pigment bringing one or more HCA residue(s) into contact with the chromophore;
- Enhanced self-association: the HCA residues can stabilize the chiral stacking of chromophores evidenced by circular dichroism.

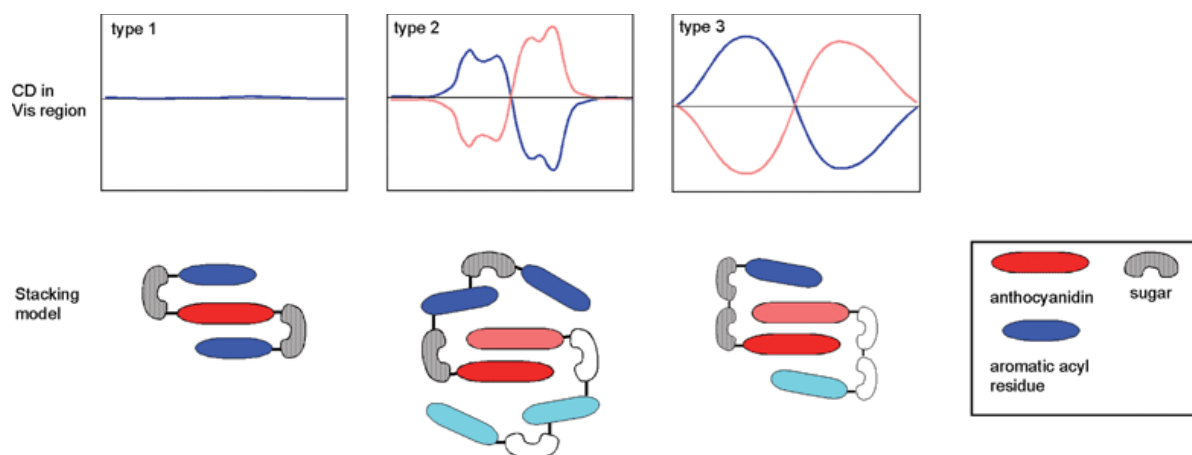


Figure 13. Acylated anthocyanins: discrimination of intramolecular co-pigmentation (type 1) and self-association (types 2 and 3) by circular dichroism (pink or blue CD spectra depending on the chirality of the stacks). From [34] with permission of the *Royal Society of Chemistry*.

In such assemblies, the flavylium nucleus has restricted access to the water solvent. Consequently, the thermodynamics of water addition are less favorable (increased pK'_h), and the percentage of colored forms at equilibrium increases [5,36–38]. For instance, at pH = 3, ca. 90% of the triacylated *Morning glory* pigment is still in colored form (mostly flavylium) vs. 15% for its non-acylated counterpart (Figure 14). Its vulnerability to water addition prevents the non-acylated pigment from accumulating the neutral quinonoid base at higher pH levels, and the corresponding solutions are almost colorless. In contrast, 30% of the triacylated pigment is present as the colored neutral base at pH = 5. Moreover, the π -stacking interactions developed by the triacylated flavylium ion induce a 20 nm bathochromic shift of its λ_{max} compared to its non-acylated counterpart.

Anthocyanins with an *o*-dihydroxy substitution on their B-ring (cyanidin, delphinidin, and petunidin derivatives) also bind hard metal ions, such as Al^{3+} and Fe^{3+} , in mildly acidic to neutral solution. As the anthocyanin binds as the quinonoid base with additional proton loss from C3'-OH, bathochromism is observed with additional ligand-to-metal charge transfer with Fe^{3+} (Figure 15).

At least in mildly acidic solution, metal binding is restricted to the colored forms and thus efficiently competes with the hydration equilibrium, thereby preventing the formation of the colorless forms. In the most sophisticated assemblies, metal binding and π -stacking interactions combine, thus providing the most common mechanism towards the formation of

stable blue colors [34,40,41]. In the so-called metalloanthocyanins, a fixed metal–pigment–co-pigment stoichiometry of 2:6:6 is observed: three anthocyanins bind to each metal ion and two equivalent complexes assemble by left-handed π -stacking interactions between the chromophores. Then, three pairs of flavone or flavonol co-pigments in left-handed π -stacking intercalate between the pairs of stacked anthocyanins. In this intercalation, right-handed pigment–copigment π -stacking occurs. Large-scale aggregation of acylated anthocyanins can also result in the formation of highly colored assemblies within the vacuole (the so-called anthocyanin vacuolar inclusions) [42], the organelle where anthocyanins are stored in plant cells.

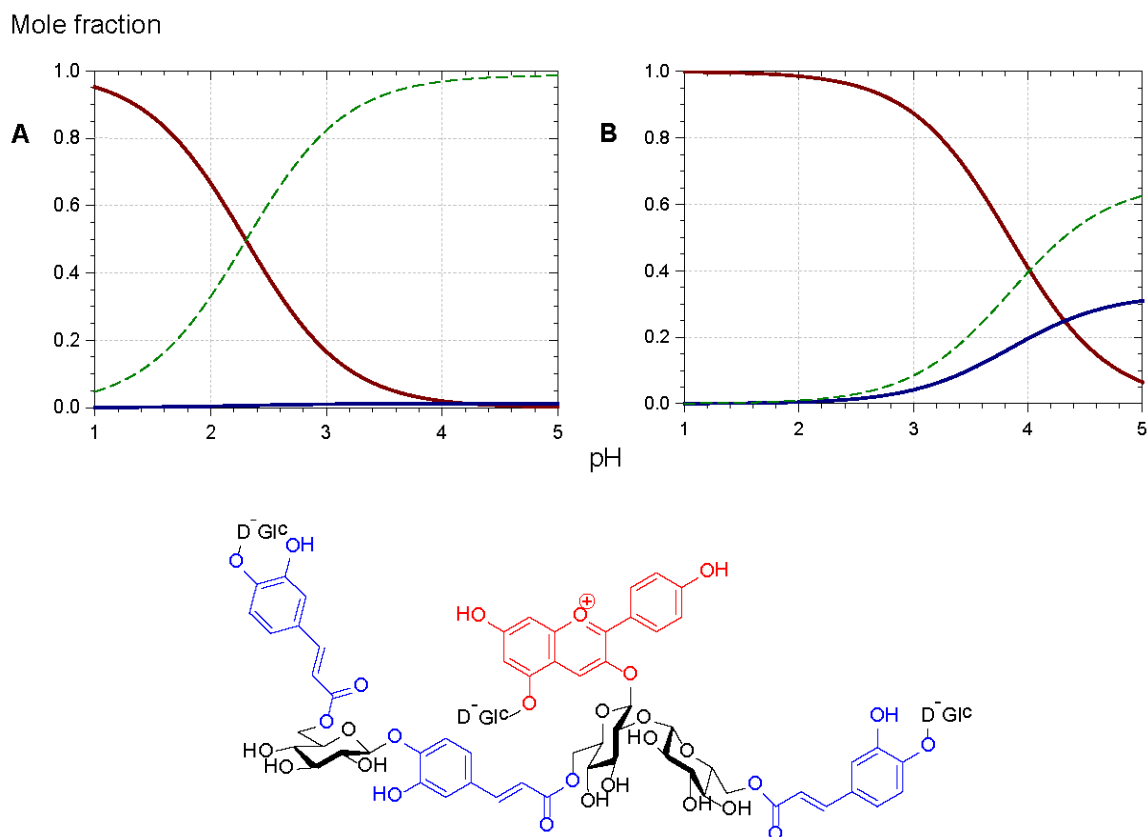


Figure 14. Triacylated (**B**) vs. non-acylated (**A**) *Morning glory* (*Pharbitis nil*) anthocyanins: equilibrium distribution of anthocyanin species in aqueous solution. Red solid line: flavylium ion, blue solid line: neutral base, dotted green line: total colorless forms. Parameters for plots are $pK'_h = 2.30$, $pK_{a1} = 4.21$ (**A**); $pK'_h = 4.01$, $pK_{a1} = 4.32$ (**B**). From [36,37].

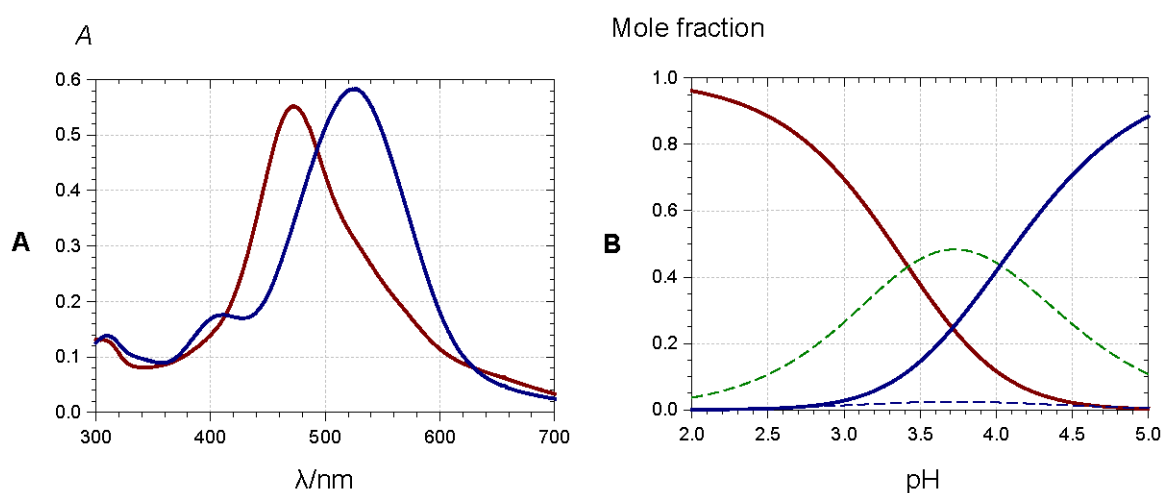


Figure 15. (A) 3',4'-Dihydroxy-7-O- β -D-glucopyranosyloxyflavylium (50 μ M) in a pH 4 buffer (0.1 M acetate), red spectrum: before hydration, blue spectrum: 10 min after addition of Al^{3+} (4 equiv.); (B) equilibrium distribution of species in aqueous solution. Red solid line: flavylium ion, blue dotted line: neutral base, dotted green line: total colorless forms, blue solid line: Al^{3+} complex. Parameters for plots are $pK'_h = 3.42$, $pK_{a1} = 4.72$, $K_M = 2 \times 10^{-4}$. From [39].

2.5.2. BINDING TO BIOPOLYMERS

Despite the potential significance of such associations in food chemistry and nutrition, the ability of anthocyanins to bind proteins and polysaccharides is still poorly documented at the molecular level. This paragraph focuses on anthocyanins (glycosides), although anthocyanidins are also commonly investigated. Indeed, aglycones are chemically unstable in mildly acidic and neutral conditions and may be substantially degraded over the duration of analysis.

Saturation transfer difference (STD)-NMR was used to probe the binding of cyanidin and delphinidin 3-glucosides to pectin from citrus fruits (MM = 111 kDa) [43]. Indeed, magnetization transfer (requiring proton pairs distant by less than 0.5 nm) from irradiated pectin protons to anthocyanin protons provided direct evidence that the two partners are in close contact. STD titrations at pH = 4.0 and pH = 1.5 suggest that the flavylum ion has a higher affinity for pectin than the hemiketal. Assuming the Scatchard model (n identical binding sites having the same binding constant, K_b), pectin was found to bind 180–600 anthocyanin units depending on the selected anthocyanin and pH. The corresponding K_b values are very weak ($<10^3 \text{ M}^{-1}$). Thus, the picture emerging from this study is that anthocyanins (as individual species or non-covalent oligomers) provide a coating of the pectin's surface through the development of very weak interactions (van der Waals contacts, H-bonds).

The quenching of intrinsic protein fluorescence by increasing ligand concentrations is a classical method to probe ligand–protein binding and to extract binding parameters. As anthocyanins typically absorb light at the protein's excitation and emission wavelengths, corrections for these inner-filter effects should be applied [44], which are not systematic [45] and thus lead to discrepancies in K_b values as well as in enthalpy and entropy changes. With human serum albumin (HSA), a globular protein, 1:1 binding is observed with a K_b in the order of 10^5 M^{-1} [44,45], meaning a moderate affinity. The influence of the pH (from pH = 4 to pH = 7.4) on the binding strength is very modest [44]. Competition with probes of a known binding site (ibuprofen, warfarin) enables location of the anthocyanin binding site, a hydrophobic pocket lined by positively charged amino-acid residues (Arg, Lys) for possible accommodation of the anionic base [45]. As for the weakly structured salivary proteins, interaction with malvidin-3-glucoside (probed by STD-NMR) was found to be much weaker

($K_b \approx 500 \text{ M}^{-1}$) and largely pH-independent (same affinity at pH = 1.0 and pH = 3.4), which suggests that the hemiketal and flavylum ions bind with close affinities [46]. Electrospray ionization MS revealed the formation of soluble aggregates involving 2–6 anthocyanin units and 1–4 peptides (proline-rich proteins or histatin). STD-NMR was also used to investigate the binding of keracyanin (cyanidin 3-rutinoside) to wheat flour gliadins at pH = 2.5 [47]. Protons C2'-H, C5'-H, C6-H and C8-H appear to be primarily involved in the binding. At this low pH, the corresponding aglycone (cyanidin) is stable and can be also investigated. Its affinity for gliadins appears higher based on the strong shielding of its proton signals when gliadins are added (confirmed by the large retention of cyanidin in the centrifugation pellet: up to 80% vs. only 8% for keracyanin). However, STD-NMR did not point protons specifically involved in the interaction. Cyanidin 3-glucoside expresses a rather high affinity for sodium caseinate (NaCas) [48]. Two binding sites were identified at pH = 2 and pH = 7, one of high affinity ($K_b \approx 1-7 \times 10^6 \text{ M}^{-1}$ depending on pH and T) and a second of lower affinity ($K_b \approx 2-7 \times 10^5 \text{ M}^{-1}$). For both sites, the binding was found to be exothermic at pH = 7 but endothermic at pH = 2 and thus is driven by a favorable entropy, which could point to a large contribution of the hydrophobic effect. Interestingly, NaCl addition gradually cancels cyanidin 3-glucoside–NaCas binding at pH = 7 but has no effect at pH = 2. In contrast to the high affinity of cyanidin 3-glucoside for NaCas, malvidin 3-glucoside only weakly binds to α - and β -caseins [49] and to β -lactoglobulin [50] (1:1 binding with $K_b < 10^3 \text{ M}^{-1}$).

Unlike co-pigmentation, the binding of anthocyanins to biopolymers does not trigger spectacular spectral changes. For instance, in the presence of various polysaccharides [51], no change in the wavelength of maximal visible absorption (λ_{max}) was observed. Interactions of anthocyanins with cellulose, oat bran, and lignin is associated with a weak hypochromic effect, whereas an opposite effect (weak hyperchromism) is observed with highly methylated apple pectins. Sugar beet pectins have been shown to promote strong bathochromism in solutions of blackcurrant anthocyanins (cyanidin and delphinidin glycosides), but this effect is due to endogenous iron ions (bound to the polysaccharide) forming blue chelates with the pigments [52]. In agreement with the small spectral changes observed, the binding of anthocyanins to pectin does not significantly affect the thermodynamic constants of the acid–base and hydration equilibria [43]. In other words, all anthocyanin forms (colored or colorless) bind pectin with close affinities. This apparent discrepancy with the STD-NMR data (stronger flavylum–pectin binding) might be due to anthocyanin self-association, which probably is significant in the concentrated solutions used in the STD-NMR experiments. In

contrast, the flavylium cation of the pyranoanthocyanin portisin is strongly stabilized by interactions with anionic wood lignosulfates as evidenced by its much weaker acidity in the presence of the polysaccharide ($pK_{a1} = 6.6$ vs. 4.6 for portisin alone) [53].

2.6. Anthocyanins in the Excited State

Although their main function is to absorb visible light and express color, anthocyanins are intrinsically poorly fluorescent with quantum yields typically lower than 4×10^{-3} (meaning that less than one photon out of 250 absorbed is actually re-emitted) [54]. Indeed, the fate of anthocyanins after absorption, i.e., once in the excited state, is a difficult question that must be addressed by sophisticated fast techniques, such as time-resolved fluorescence and transient absorption-emission spectroscopies. In the HOMO \rightarrow LUMO transition accompanying the absorption of visible light by the flavylium ion, electron transfer from the B-ring to the A-/C-rings takes place (Figure 16) (Anouar et al., 2012a). In the excited state, the flavylium ion is a strong acid ($pK_a < 0$) that transfers a proton to the solvent on a picosecond timescale (20 ps for pelargonin at pH = 1) [54,56]. In the next step, the quinonoid base in the excited state is deactivated by a combination of radiative (fluorescence) and non-radiative (heat) processes and then captures a proton in the ground state to form the ground state flavylium ion. In other words, the quinonoid base is responsible for the (weak) fluorescence observed for anthocyanins even in strongly acidic solution. In the presence of a co-pigment, other mechanisms (Figure 17) supersede the fast flavylium deprotonation observed with free anthocyanins [57] in the following ways: (a) within the complex in the excited state, through ultrafast internal conversion (<1 ps) via a low-energy co-pigment-to-pigment charge transfer state, resulting in static fluorescence quenching; and (b) for the fraction of free anthocyanin, diffusion-controlled electron transfer from the co-pigment to the flavylium ion in the excited state, resulting in dynamic fluorescence quenching. The mechanism of energy dissipation by ultrafast internal conversion has been confirmed for the folded conformation of a cyanidin glycoside acylated by *p*-coumaric acid [58]. In addition, fast energy transfer to the chromophore following absorption of UV light by the acyl residue operates (Figure 17), thereby conferring acylated anthocyanins to have an important role in plant photoprotection.

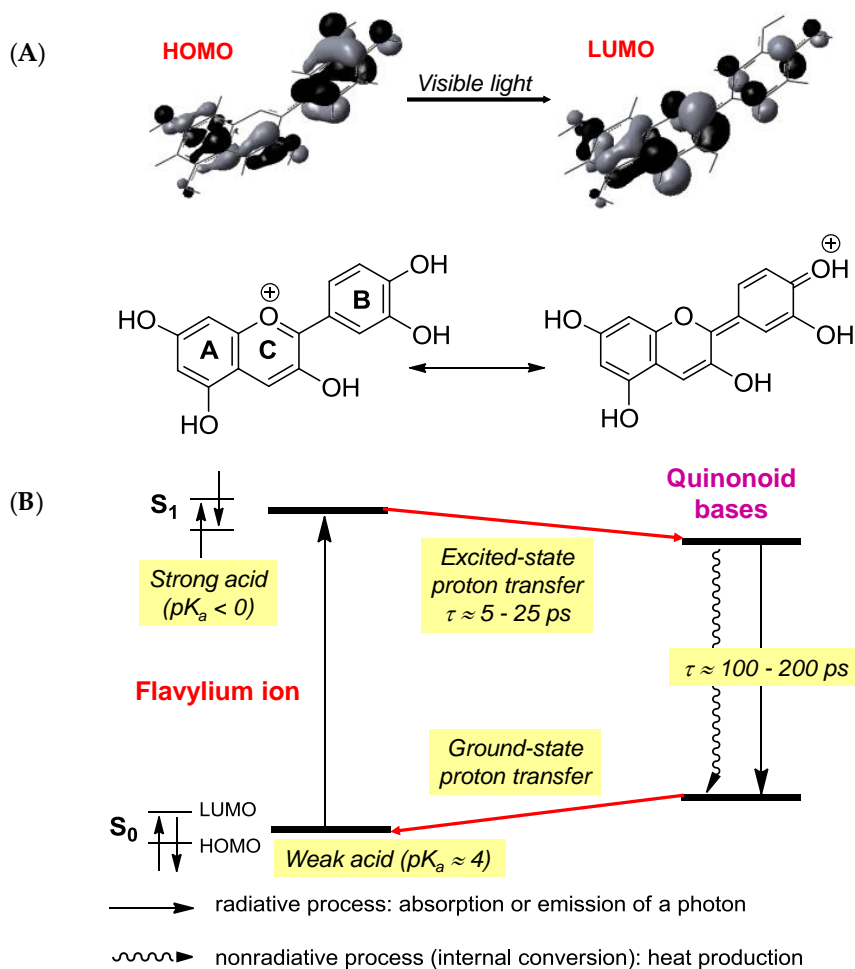


Figure 16. (A) Frontier MOs of the flavylium ion of cyanidin (from reference (Anouar et al., 2012a)) and its most representative mesomeric forms in the ground state (left) and first excited state (right). (B) The fate of free anthocyanins in the excited state (from references [54,56]).

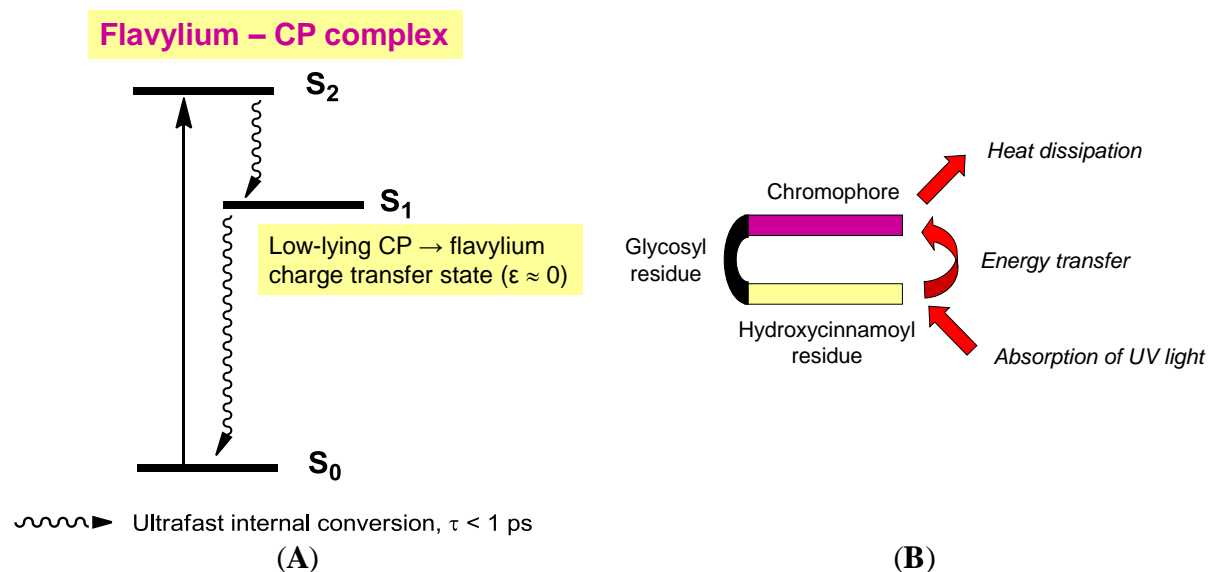


Figure 17. The influence of co-pigmentation on the fate of anthocyanins in the excited state. (A) Intermolecular co-pigmentation (from reference [57]). (B) Intramolecular co-pigmentation (from reference [58]).

3. THE IMPORTANCE OF ANTHOCYANIN CHEMISTRY IN FOOD AND NUTRITION

3.1. Formulation of anthocyanins for food applications

Anthocyanin degradation typically occurs during thermal processing and storage. The knowledge on anthocyanin–biopolymer interactions can be applied to devise formulations for improved chemical stability. Degradation studies aimed at demonstrating the protection afforded by biopolymers may be limited to monitoring the color loss under given conditions of pH, temperature, and light exposure. More information is obtained when samples are also acidified to pH 1–2 for quantification of the residual flavylum ions by HPLC or by UV-visible spectroscopy. With this approach, color loss (directly observed at the monitoring pH), which combines the reversible water addition and irreversible phenomena (hydrolysis, autoxidation), and true anthocyanin loss (irreversible component), can be distinguished.

In the simplest experiments involving modeling beverages, solutions of anthocyanins and soluble biopolymers are heated, and their color or residual anthocyanin concentration is monitored as a function of time. For instance, yeast mannoproteins (0.5% *w/w* for both anthocyanins and mannoproteins) increase the half-life of color loss by a factor of 5.4 in experiments conducted at pH = 7 and T = 80 °C or 126 °C (modeling pasteurization or sterilization) [59]. Similarly, the color loss in solutions of purple carrot anthocyanins at pH = 3.0 and T = 40 °C (in light) was shown to be inhibited by the addition of gum arabic (0.05–5.0%) with maximal stability observed at 1.5% (50% color retention after 5 days, vs. 20% in control) [60]. Similar observations were made with pectins or whey proteins (1%), the best result being obtained with heat-denatured whey proteins (70% color retention after 7 days at 40 °C, vs. 20% in control) [61]. In these works, fluorescence quenching experiments suggest that color protection involves direct interactions between anthocyanins and proteins (including the glycoprotein of gum arabic). However, the mechanism of protection remains largely unknown. It may be speculated that biopolymers mostly act by providing a more hydrophobic environment to anthocyanins, resulting in slower hydrolysis (despite the weak impact on the hydration equilibrium itself, see Section 2.5.2) and/or by scavenging transition metal traces acting as initiators/catalysts of anthocyanin autoxidation.

A more sophisticated approach consists of preparing solid micro- or nanoparticles as delivery systems for anthocyanins. For instance, nanoparticles of whey proteins and beet pectin can be loaded with anthocyanin extracts with a higher efficiency (55%) when

anthocyanins are added prior nanoparticle formation [62]. However, when dispersed in pH 4 solution, these nanoparticles do not show improved color stability. Particles of chitosan and carboxymethylchitosan (CMC) loaded with anthocyanins (size \approx 200 nm, encapsulation efficiencies ranging from 16 to 44% depending on the CMC/chitosan proportions) can be simply prepared by mixing at pH = 5–6 followed by centrifugation [63]. The thermal stability of encapsulated anthocyanins was shown to greatly improve: 12% degradation after 3 days at 40 °C, vs. 90% in the control (no particles). Similar protection was observed in samples exposed to white light for 10 days (–20% vs. –80%). Sulfonated polysaccharides, such as dextran sulfate and carrageenans, can also be used to encapsulate bilberry anthocyanins from acidic solutions (pH \approx 3) with high efficiency and improved stability [64,65]. The binding of isotherms and HPLC analysis showed that the binding is selective of anthocyanins (the other phenols remaining in solution) and is stronger when the sulfonation degree is higher. These data strongly suggest that the encapsulation is driven by ionic flavylum–sulfate interactions. Interestingly, the nanoparticles are gradually dissociated under near neutral conditions modeling the small intestine, which is desirable for subsequent intestinal absorption. Combining chitosan and cellulose nanocrystals at pH 2–3 also allows the formation of nanoparticles with high affinity for anthocyanins (up to 94% encapsulation) [66]. When cellulose is replaced by sodium tripolyphosphate, a reticulating agent for the polycationic chitosan chain, gel microcapsules (size \approx 34 μ m, encapsulation yield \approx 33%) are formed. Finally, large hydrogel particles (size \approx 2–3 mm) combining alginate and pectin can be used for encapsulation of anthocyanin-rich extracts under acidic conditions (pH = 1–3), and they are released upon dissolution at higher pH [67]. When exposed to white light, the half-life values of anthocyanins in hydrogel, hydrogel particles dispersed in pH 3 solution, and in a control solution (pH = 3) were 630 h, 277 h, and 58 h, respectively.

Interestingly, anthocyanin-rich blackcurrant extracts can be incorporated into bread [68]. Replacing wheat flour by a mixture of gluten and starch led to markedly decreased anthocyanin concentrations (especially, for delphinidin glycosides, which are most sensitive to oxidation). This suggests that other flour proteins (e.g., albumins, globulins) and non-starch polysaccharides (e.g., hemicelluloses, β -glucans) may be important to provide chemical stability to anthocyanins in such matrices.

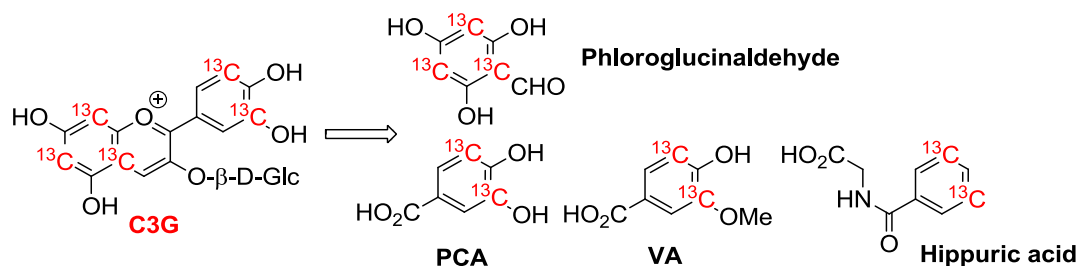
3.2. The Fate of Anthocyanins in Humans, Consequences on the Possible Effects on Health

The bioavailability of phenolic compounds has been largely elucidated over the last decades [69]. This knowledge, which is crucial to the interpretation of the possible effects on health, encompasses the bioaccessibility (the release of phenols from the food matrix during digestion), intestinal absorption, metabolism, transport, distribution to tissues, and excretion of dietary phenols and their metabolites. Anthocyanins have emerged as poorly bioavailable micronutrients as judged from the low concentrations (generally, <0.1 μM) of native forms (mostly, anthocyanidin glucosides) and anthocyanidin conjugates detected in the general blood circulation [70,71]. These derivatives are formed in the small intestine after enzymatic hydrolysis by membrane-bound lactate phlorizin hydrolase or by cytosolic β -glucosidase, and subsequent conjugation by *O*-glucuronidation, *O*-methylation, and/or *O*-sulfonylation. The detection of native forms in the blood circulation is not equivalent to other flavonoid glucosides and could be due to partial absorption from the stomach. This early absorption has been demonstrated in cell and animal models [72–74] and has been proposed to involve the organic anion transporter bilitranslocase in the gastric epithelium [72].

Most importantly, recent investigations, in particular using ^{13}C -labelled compounds [3], have shown that the bulk of the ingested amount of anthocyanins is actually converted into simple phenolic compounds (Table 2), as a consequence of (a) the chemical instability (under near neutral conditions) of anthocyanins and, especially, of anthocyanidins [24] and (b) the extensive catabolism by the colonic microbiota of the fraction reaching the large intestine. These simple metabolites, which themselves can be further conjugated by intestinal and hepatic enzymes, have been found in the blood circulation in much higher concentration than anthocyanidin derivatives [3,75].

Table 2. Serum pharmacokinetic profiles of cyanidin 3-glucoside (C3G) and its metabolites in humans after the consumption of 500 mg ¹³C-labelled C3G. From reference [3] (in red is the reference compound and its most abundant metabolites).

Compound	<i>n</i>	<i>C</i> _{max} /nM	<i>t</i> _{max} /h	<i>t</i> _{1/2} /h	AUC ₀₋₄₈ /nM h
Cyanidin-3-glucoside (C3G)	5	141 (±70)	1.8 (±0.2)	0.4	279 (±170)
Protocatechuic acid (PCA)	8	146 (±74)	3.3 (±0.7)	9.9 (±3.4)	1377 (±760)
Phloroglucinaldehyde	4	582 (±536)	2.8 (±1.1)	nd	7882 (±7768)
PCA-sulfates	8	157 (±116)	11.4 (±3.8)	31.9 (±19.1)	1180 (±349)
Vanillic acid (VA)	2	1845 (±838)	12.5 (±11.5)	6.4	23319 (±20650)
VA-sulfates	4	430 (±299)	30.1 (±11.4)	nd	10689 (±7751)
Ferulic acid	7	827 (±371)	8.2 (±4.1)	21.4 (±7.8)	17422 (±11054)
Hippuric acid	8	1962 (±1389)	15.7 (±4.1)	95.6 (±77.8)	46568 (±30311)



In agreement with the strong *in vivo* catabolism of anthocyanins, *in vitro* digestion models have shown that whereas anthocyanins are readily released into the acidic gastric compartment and relatively stable, they undergo substantial degradation in the near neutral upper intestinal compartment, possibly because of autoxidation [76,77]. However, this chemical instability could be overestimated in *in vitro* models, as the O₂ content is higher than under real physiological conditions. As a striking example, protocatechuic acid (PCA, 3,4-dihydroxybenzoic acid), recovered in blood and fecal samples, was shown to represent more than 70% of the ingested dose of the cyanidin *O*-glucosides from blood orange juice [75]. Interestingly, PCA can be formed by chemical oxidative degradation of anthocyanins and anthocyanidins (Figures 8–10). However, it must be noted that anthocyanins bearing an

electron-rich B-ring (e.g., cyanidin and delphinidin glycosides) must be much more prone to oxidative degradation than, for instance, pelargonidin derivatives [78], which indeed could be detected in higher concentrations (0.2–0.3 μM) in the blood [79].

In the digestive tract, anthocyanins may also modulate the digestion and uptake of nutrients by interacting with intestinal α -glucosidase [80]. They could, as well, attenuate oxidative stress in the digestive tract, for instance, by inhibiting the peroxidation of dietary lipids induced by heme iron [29,81]. After intestinal absorption, anthocyanin derivatives are probably transported in the blood in moderate association with serum albumin [45] before distribution to tissues, which, again, could involve bilitranslocase, as evidenced in the kidneys of rats [82].

Most importantly, it must be kept in mind that the degradation products of anthocyanins, which are formed in the digestive tract and are generally much more abundant than the residual anthocyanidin derivatives, could mediate most of the potential health effects of anthocyanins [83,84], which remains intriguing given their chemical simplicity [3] (Table 2). However, redox-active compounds, such as PCA, could indeed participate in regulating the expression of genes associated with transcription factors susceptible to redox activation. Such mechanisms could, at least partly, underline the induction of antioxidant defense via the Nrf2 pathway and the reduction of inflammation via NF- κ B inhibition observed in cells and in rodents with cyanidin derivatives [85] or PCA itself [86].

Author Contributions: O.D. and J.-A. F. analyzed the literature and wrote the paper.

Conflicts of Interest: The authors declare no conflict of interest.

REFERENCES

1. Pina, F.; Melo, M.J.; Laia, C.A.T.; Parola, A.J.; Lima, J.C. Chemistry and applications of flavylum compounds: A handful of colours. *Chem. Soc. Rev.* **2012**, *41*, 869–908, doi:10.1039/C1CS15126F.
2. Pina, F. Chemical applications of anthocyanins and related compounds. A source of bioinspiration. *J. Agric. Food Chem.* **2014**, *62*, 6885–6897, doi:10.1021/jf404869m.
3. De Ferrars, R.M.; Czank, C.; Zhang, Q.; Botting, N.P.; Kroon, P.A.; Cassidy, A.; Kay, C.D. The pharmacokinetics of anthocyanins and their metabolites in humans. *Br. J. Pharmacol.* **2014**, *171*, 3268–3282, doi:10.1111/bph.12676.
4. Nave, F.; Petrov, V.; Pina, F.; Teixeira, N.; Mateus, N.; de Freitas, V. Thermodynamic and kinetic properties of a red wine pigment: Catechin-(4,8)-malvidin-3-*O*-glucoside. *J. Phys. Chem. B* **2010**, *114*, 13487–13496, doi:10.1021/jp104749f.
5. Moloney, M.; Robbins, R.J.; Collins, T.M.; Kondo, T.; Yoshida, K.; Dangles, O. Red cabbage anthocyanins: The influence of D-glucose acylation by hydroxycinnamic acids on their structural transformations in acidic to mildly alkaline conditions and on the resulting color. *Dyes Pigment.* **2018**, *158*, 342–352, doi:10.1016/j.dyepig.2018.05.057.
6. Berké, B.; Chèze, C.; Vercauteren, J.; Deffieux, G. Bisulfite addition to anthocyanins: Revisited structures of colourless adducts. *Tetrahedron Lett.* **1998**, *39*, 5771–5774.
7. Fulcrand, H.; Dueñas, M.; Salas, E.; Cheynier, V. Phenolic reactions during wine making and aging. *Am. J. Enol. Vitic.* **2006**, *57*, 289–297.
8. Oliveira, J.; Mateus, N.; de Freitas, V. Previous and recent advances in pyranoanthocyanins equilibria in aqueous solution. *Dyes Pigment.* **2014**, *100*, 190–200, doi:10.1016/j.dyepig.2013.09.009.
9. Vallverdú-Queralt, A.; Meudec, E.; Ferreira-Lima, N.; Sommerer, N.; Dangles, O.; Cheynier, V.; Guernevé, C.L. A comprehensive investigation of guaicacyl-pyranoanthocyanin synthesis by one-/two-dimensional NMR and UPLC–DAD–ESI–MSn. *Food Chem.* **2016**, *199*, 902–910, doi:10.1016/j.foodchem.2015.12.089.
10. Oliveira, J.; Fernandes, V.; Miranda, C.; Santos-Buelga, C.; Silva, A.; de Freitas, V.; Mateus, N. Color properties of four cyanidin-pyruvic acid adducts. *J. Agric. Food Chem.* **2006**, *54*, 6894–6903, doi:10.1021/jf061085b.
11. Cruz, L.; Petrov, V.; Teixeira, N.; Mateus, N.; Pina, F.; Freitas, V.D. Establishment of the chemical equilibria of different types of pyranoanthocyanins in Aqueous solutions: Evidence for the formation of aggregation in pyranomalvidin-3-*O*-coumaroylglucoside-(+)-catechin. *J. Phys. Chem. B* **2010**, *114*, 13232–13240, doi:10.1021/jp1045673.
12. Vallverdú-Queralt, A.; Biler, M.; Meudec, E.; Guernevé, C.L.; Vernhet, A.; Mazauric, J.-P.; Legras, J.-L.; Loonis, M.; Trouillas, P.; Cheynier, V.; et al. *p*-Hydroxyphenyl-pyranoanthocyanins: An experimental and theoretical investigation of their acid–Base properties and molecular interactions. *Int. J. Mol. Sci.* **2016**, *17*, 1842, doi:10.3390/ijms17111842.
13. Dueñas, M.; Fulcrand, H.; Cheynier, V. Formation of anthocyanin–flavanol adducts in model solutions. *Anal. Chim. Acta* **2006**, *563*, 15–25, doi:10.1016/j.aca.2005.10.062.
14. Lee, D.F.; Swinny, E.E.; Jones, G.P. NMR identification of ethyl-linked anthocyanin–flavanol pigments formed in model wine ferments. *Tetrahedron Lett.* **2004**, *45*, 1671–1674, doi:10.1016/j.tetlet.2003.12.110.

15. Li, L.; Zhang, M.; Zhang, S.; Cui, Y.; Sun, B. Preparation and antioxidant activity of ethyl-linked anthocyanin-flavanol pigments from model wine solutions. *Molecules* **2018**, *23*, 1066.
16. Vallverdú- Queralt, A.; Meudec, E.; Eder, M.; Lamuela- Raventos, R.M.; Sommerer, N.; Cheynier, V. The hidden face of wine polyphenol polymerization highlighted by high-resolution mass spectrometry. *ChemistryOpen* **2017**, *6*, 336–339, doi:10.1002/open.201700044.
17. Salas, E.; Fulcrand, H.; Meudec, E.; Cheynier, V. Reactions of anthocyanins and tannins in model solutions. *J. Agric. Food Chem.* **2003**, *51*, 7951–7961, doi:10.1021/jf0345402.
18. Dueñas, M.; Salas, E.; Cheynier, V.; Dangles, O.; Fulcrand, H. UV–visible spectroscopic investigation of the 8,8-methylmethine catechin-malvidin 3-glucoside pigments in aqueous solution: Structural transformations and molecular complexation with chlorogenic acid. *J. Agric. Food Chem.* **2006**, *54*, 189–196, doi:10.1021/jf0516989.
19. Quideau, S.; Jourdes, M.; Lefeuvre, D.; Montaudon, D.; Saucier, C.; Glories, Y.; Pardon, P.; Pourquier, P. The chemistry of wine polyphenolic C-glycosidic ellagitannins targeting human topoisomerase II. *Chem.-A Eur. J.* **2005**, *11*, 6503–6513, doi:10.1002/chem.200500428.
20. Chassaing, S.; Lefeuvre, D.; Jacquet, R.; Jourdes, M.; Ducasse, L.; Galland, S.; Grelard, A.; Saucier, C.; Teissedre, P.-L.; Dangles, O.; et al. Physicochemical studies of new anthocyano-ellagitannin hybrid pigments: About the origin of the influence of oak C-glycosidic ellagitannins on wine color. *Eur. J. Org. Chem.* **2010**, 55–63, doi:10.1002/ejoc.200901133.
21. Oliveira, J.; da Silva, M.A.; Jorge Parola, A.; Mateus, N.; Brás, N.F.; Ramos, M.J.; de Freitas, V. Structural characterization of a A-type linked trimeric anthocyanin derived pigment occurring in a young Port wine. *Food Chem.* **2013**, *141*, 1987–1996, doi:10.1016/j.foodchem.2013.04.091.
22. Geera, B.; Ojwang, L.O.; Awika, J.M. New highly stable dimeric 3-deoxyanthocyanidin pigments from sorghum bicolor leaf sheath. *J. Food Sci.* **2012**, *77*, C566–C572, doi:10.1111/j.1750-3841.2012.02668.x.
23. Sarni-Manchado, P.; Cheynier, V.; Moutounet, M. Reactions of polyphenoloxidase generated caftaric acid o-quinone with malvidin 3-O-glucoside. *Phytochemistry* **1997**, *45*, 1365–1369, doi:10.1016/S0031-9422(97)00190-8.
24. Fleschhut, J.; Kratzer, F.; Rechkemmer, G.; Kulling, S.E. Stability and biotransformation of various dietary anthocyanins in vitro. *Eur. J. Nutr.* **2006**, *45*, 7–18, doi:10.1007/s00394-005-0557-8.
25. Cabrita, L.; Petrov, V.; Pina, F. On the thermal degradation of anthocyanidins: Cyanidin. *RSC Adv.* **2014**, *4*, 18939–18944, doi:10.1039/C3RA47809B.
26. Lopes, P.; Richard, T.; Saucier, C.; Teissedre, P.-L.; Monti, J.-P.; Glories, Y. Anthocyanone a: A quinone methide derivative resulting from malvidin 3-O-glucoside degradation. *J. Agric. Food Chem.* **2007**, *55*, 2698–2704, doi:10.1021/jf062875o.
27. Sadilova, E.; Carle, R.; Stintzing, F.C. Thermal degradation of anthocyanins and its impact on color and in vitro antioxidant capacity. *Mol. Nutr. Food Res.* **2007**, *51*, 1461–1471, doi:10.1002/mnfr.200700179.
28. Kähkönen, M.P.; Heinonen, M. Antioxidant activity of anthocyanins and their aglycons. *J. Agric. Food Chem.* **2003**, *51*, 628–633, doi:10.1021/jf025551i.
29. Goupy, P.; Bautista-Ortin, A.-B.; Fulcrand, H.; Dangles, O. Antioxidant activity of wine pigments derived from anthocyanins: Hydrogen transfer reactions to the DPPH radical and inhibition of the heme-induced peroxidation of linoleic acid. *J. Agric. Food Chem.* **2009**, *57*, 5762–5770, doi:10.1021/jf900841b.

30. Achat, S.; Rakotomanomana, N.; Madani, K.; Dangles, O. Antioxidant activity of olive phenols and other dietary phenols in model gastric conditions: Scavenging of the free radical DPPH and inhibition of the haem-induced peroxidation of linoleic acid. *Food Chem.* **2016**, *213*, 135–142, doi:10.1016/j.foodchem.2016.06.076.
31. Matera, R.; Gabbanini, S.; Berretti, S.; Amorati, R.; De Nicola, G.R.; Iori, R.; Valgimigli, L. Acylated anthocyanins from sprouts of *Raphanus sativus* cv. Sango: Isolation, structure elucidation and antioxidant activity. *Food Chem.* **2015**, *166*, 397–406, doi:10.1016/j.foodchem.2014.06.056.
32. Trouillas, P.; Sancho-García, J.C.; De Freitas, V.; Gierschner, J.; Otyepka, M.; Dangles, O. Stabilizing and modulating color by copigmentation: Insights from theory and experiment. *Chem. Rev.* **2016**, *116*, 4937–4982, doi:10.1021/acs.chemrev.5b00507.
33. Mori, M.; Miki, N.; Ito, D.; Kondo, T.; Yoshida, K. Structure of tecophilin, a tri-caffeoylanthocyanin from the blue petals of *Tecophilaea cyanocrocus*, and the mechanism of blue color development. *Tetrahedron* **2014**, *70*, 8657–8664, doi:10.1016/j.tet.2014.09.046.
34. Yoshida, K.; Mori, M.; Kondo, T. Blue flower color development by anthocyanins: From chemical structure to cell physiology. *Nat. Prod. Rep.* **2009**, *26*, 884, doi:10.1039/b800165k.
35. Alluis, B.; Pérol, N.; El hajji, H.; Dangles, O. Water-soluble flavonol (= 3-Hydroxy-2-phenyl-4H-1-benzopyran-4-one) derivatives: Chemical synthesis, colouring, and antioxidant properties. *Helv. Chim. Acta* **2000**, *83*, 428–443, doi:10.1002/(SICI)1522-2675(20000216)83:2<428:AID-HLCA428>3.0.CO;2-J.
36. Dangles, O.; Saito, N.; Brouillard, R. Anthocyanin intramolecular copigment effect. *Phytochemistry* **1993**, *34*, 119–124.
37. Dangles, O.; Saito, N.; Brouillard, R. Kinetic and thermodynamic control of flavylum hydration in the pelargonidin-cinnamic acid complexation. Origin of the extraordinary flower color diversity of *Pharbitis nil*. *J. Am. Chem. Soc.* **1993**, *115*, 3125–3132, doi:10.1021/ja00061a011.
38. Figueiredo, P.; George, F.; Tatsuzawa, F.; Toki, K.; Saito, N.; Brouillard, R. New features of intramolecular copigmentation by acylated anthocyanins. *Phytochemistry* **1999**, *51*, 125–132, doi:10.1016/S0031-9422(98)00685-2.
39. Mora-Soumille, N.; Al Bittar, S.; Rosa, M.; Dangles, O. Analogs of anthocyanins with a 3',4'-dihydroxy substitution: Synthesis and investigation of their acid–base, hydration, metal binding and hydrogen-donating properties in aqueous solution. *Dyes Pigment.* **2013**, *96*, 7–15, doi:10.1016/j.dyepig.2012.07.006.
40. Kondo, T.; Yoshida, K.; Nakagawa, A.; Kawai, T.; Tamura, H.; Goto, T. Structural basis of blue-colour development in flower petals from *Commelina communis*. *Nature* **1992**, *358*, 515–518, doi:10.1038/358515a0.
41. Shiono, M.; Matsugaki, N.; Takeda, K. Phytochemistry: Structure of the blue cornflower pigment. *Nature* **2005**, *436*, 791, doi:10.1038/436791a.
42. Kallam, K.; Appelhagen, I.; Luo, J.; Albert, N.; Zhang, H.; Deroles, S.; Hill, L.; Findlay, K.; Andersen, Ø.M.; Davies, K.; et al. Aromatic decoration determines the formation of anthocyanic vacuolar inclusions. *Curr. Biol.* **2017**, *27*, 945–957, doi:10.1016/j.cub.2017.02.027.
43. Fernandes, A.; Brás, N.F.; Mateus, N.; de Freitas, V. Understanding the molecular mechanism of anthocyanin binding to pectin. *Langmuir* **2014**, *30*, 8516–8527, doi:10.1021/la501879w.
44. Cahyana, Y.; Gordon, M.H. Interaction of anthocyanins with human serum albumin: Influence of pH and chemical structure on binding. *Food Chem.* **2013**, *141*, 2278–2285, doi:10.1016/j.foodchem.2013.05.026.

45. Tang, L.; Zuo, H.; Shu, L. Comparison of the interaction between three anthocyanins and human serum albumins by spectroscopy. *J. Lumin.* **2014**, *153*, 54–63, doi:10.1016/j.jlumin.2014.03.004.
46. Ferrer-Gallego, R.; Soares, S.; Mateus, N.; Rivas-Gonzalo, J.; Escribano-Bailón, M.T.; Freitas, V.D. New anthocyanin-human salivary protein complexes. *Langmuir* **2015**, *31*, 8392–8401, doi:10.1021/acs.langmuir.5b01122.
47. Mazzaracchio, P.; Tozzi, S.; Boga, C.; Forlani, L.; Pifferi, P.G.; Barbiroli, G. Interaction between gliadins and anthocyan derivatives. *Food Chem.* **2011**, *129*, 1100–1107, doi:10.1016/j.foodchem.2011.05.084.
48. Casanova, F.; Chapeau, A.-L.; Hamon, P.; de Carvalho, A.F.; Croguennec, T.; Bouhallab, S. pH- and ionic strength-dependent interaction between cyanidin-3-*O*-glucoside and sodium caseinate. *Food Chem.* **2018**, *267*, 52–59, doi:10.1016/j.foodchem.2017.06.081.
49. He, Z.; Xu, M.; Zeng, M.; Qin, F.; Chen, J. Interactions of milk α - and β -casein with malvidin-3-*O*-glucoside and their effects on the stability of grape skin anthocyanin extracts. *Food Chem.* **2016**, *199*, 314–322, doi:10.1016/j.foodchem.2015.12.035.
50. He, Z.; Zhu, H.; Xu, M.; Zeng, M.; Qin, F.; Chen, J. Complexation of bovine β -lactoglobulin with malvidin-3-*O*-glucoside and its effect on the stability of grape skin anthocyanin extracts. *Food Chem.* **2016**, *209*, 234–240, doi:10.1016/j.foodchem.2016.04.048.
51. Mazzaracchio, P.; Pifferi, P.; Kindt, M.; Munyaneza, A.; Barbiroli, G. Interactions between anthocyanins and organic food molecules in model systems. *Int. J. Food Sci. Technol.* **2004**, *39*, 53–59.
52. Buchweitz, M.; Carle, R.; Kammerer, D.R. Bathochromic and stabilising effects of sugar beet pectin and an isolated pectic fraction on anthocyanins exhibiting pyrogallol and catechol moieties. *Food Chem.* **2012**, *135*, 3010–3019, doi:10.1016/j.foodchem.2012.06.101.
53. Araújo, P.; Basílio, N.; Azevedo, J.; Fernandes, A.; Mateus, N.; Pina, F.; de Freitas, V.; Oliveira, J. Colour modulation of blue anthocyanin-derivatives. Lignosulfonates as a tool to improve the water solubility of natural blue dyes. *Dyes Pigment.* **2018**, *153*, 150–159, doi:10.1016/j.dyepig.2018.02.019.
54. Moreira, P.F.; Giestas, L.; Yihwa, C.; Vautier-Giongo, C.; Quina, F.H.; Maçanita, A.L.; Lima, J.C. Ground- and excited-state proton transfer in anthocyanins: From weak acids to superphotoacids. *J. Phys. Chem. A* **2003**, *107*, 4203–4210, doi:10.1021/jp027260i.
55. Anouar, E.H.; Gierschner, J.; Duroux, J.-L.; Trouillas, P. UV/Visible spectra of natural polyphenols: A time-dependent density functional theory study. *Food Chem.* **2012**, *131*, 79–89, doi:10.1016/j.foodchem.2011.08.034.
56. Ferreira da Silva, P.; Lima, J.C.; Quina, F.H.; Maçanita, A.L. Excited-state electron transfer in anthocyanins and related flavylum salts. *J. Phys. Chem. A* **2004**, *108*, 10133–10140, doi:10.1021/jp047300d.
57. Rodrigues, R.F.; Ferreira da Silva, P.; Shimizu, K.; Freitas, A.A.; Kovalenko, S.A.; Ernsting, N.P.; Quina, F.H.; Maçanita, A. Ultrafast internal conversion in a model anthocyanin-polyphenol complex: Implications for the biological role of anthocyanins in vegetative tissues of plants. *Chem.-A Eur. J.* **2009**, *15*, 1397–1402, doi:10.1002/chem.200801207.
58. Ferreira da Silva, P.; Paulo, L.; Barbařina, A.; Elisei, F.; Quina, F.H.; Maçanita, A.L. Photoprotection and the photophysics of acylated anthocyanins. *Chem.-A Eur. J.* **2012**, *18*, 3736–3744, doi:10.1002/chem.201102247.

59. Wu, J.; Guan, Y.; Zhong, Q. Yeast mannoproteins improve thermal stability of anthocyanins at pH 7.0. *Food Chem.* **2015**, *172*, 121–128, doi:10.1016/j.foodchem.2014.09.059.
60. Chung, C.; Rojanasasithara, T.; Mutilangi, W.; McClements, D.J. Enhancement of colour stability of anthocyanins in model beverages by gum arabic addition. *Food Chem.* **2016**, *201*, 14–22, doi:10.1016/j.foodchem.2016.01.051.
61. Chung, C.; Rojanasasithara, T.; Mutilangi, W.; McClements, D.J. Enhanced stability of anthocyanin-based color in model beverage systems through whey protein isolate complexation. *Food Res. Int.* **2015**, *76*, 761–768, doi:10.1016/j.foodres.2015.07.003.
62. Arroyo-Maya, I.J.; McClements, D.J. Biopolymer nanoparticles as potential delivery systems for anthocyanins: Fabrication and properties. *Food Res. Int.* **2015**, *69*, 1–8, doi:10.1016/j.foodres.2014.12.005.
63. Ge, J.; Yue, P.; Chi, J.; Liang, J.; Gao, X. Formation and stability of anthocyanins-loaded nanocomplexes prepared with chitosan hydrochloride and carboxymethyl chitosan. *Food Hydrocoll.* **2018**, *74*, 23–31, doi:10.1016/j.foodhyd.2017.07.029.
64. Klimaviciute, R.; Navikaite, V.; Jakstas, V.; Ivanauskas, L. Complexes of dextran sulfate and anthocyanins from *Vaccinium myrtillus*: Formation and stability. *Carbohydr. Polym.* **2015**, *129*, 70–78, doi:10.1016/j.carbpol.2015.04.038.
65. Navikaite, V.; Simanaviciute, D.; Klimaviciute, R.; Jakstas, V.; Ivanauskas, L. Interaction between κ - and ι -carrageenan and anthocyanins from *Vaccinium myrtillus*. *Carbohydr. Polym.* **2016**, *148*, 36–44, doi:10.1016/j.carbpol.2016.04.059.
66. Wang, W.; Jung, J.; Zhao, Y. Chitosan-cellulose nanocrystal microencapsulation to improve encapsulation efficiency and stability of entrapped fruit anthocyanins. *Carbohydr. Polym.* **2017**, *157*, 1246–1253, doi:10.1016/j.carbpol.2016.11.005.
67. Guo, J.; Giusti, M.M.; Kaletunç, G. Encapsulation of purple corn and blueberry extracts in alginate-pectin hydrogel particles: Impact of processing and storage parameters on encapsulation efficiency. *Food Res. Int.* **2018**, *107*, 414–422, doi:10.1016/j.foodres.2018.02.035.
68. Sivam, A.S.; Sun-Waterhouse, D.; Perera, C.O.; Waterhouse, G.I.N. Exploring the interactions between blackcurrant polyphenols, pectin and wheat biopolymers in model breads; a FTIR and HPLC investigation. *Food Chem.* **2012**, *131*, 802–810, doi:10.1016/j.foodchem.2011.09.047.
69. Del Rio, D.; Rodriguez-Mateos, A.; Spencer, J.P.E.; Tognolini, M.; Borges, G.; Crozier, A. Dietary (Poly) phenolics in human health: Structures, bioavailability, and evidence of protective effects against chronic diseases. *Antioxid. Redox Signal.* **2013**, *18*, 1818–1892, doi:10.1089/ars.2012.4581.
70. Kay, C.D. Aspects of anthocyanin absorption, metabolism and pharmacokinetics in humans. *Nutr. Res. Rev.* **2006**, *19*, 137–146, doi:10.1079/NRR2005116.
71. Manach, C.; Williamson, G.; Morand, C.; Scalbert, A.; Rémésy, C. Bioavailability and bioefficacy of polyphenols in humans. I. Review of 97 bioavailability studies. *Am. J. Clin. Nutr.* **2005**, *81*, 230S–242S, doi:10.1093/ajcn/81.1.230S.
72. Passamonti, S.; Vrhovsek, U.; Mattivi, F. The interaction of anthocyanins with bilitranslocase. *Biochem. Biophys. Res. Commun.* **2002**, *296*, 631–636, doi:10.1016/S0006-291X(02)00927-0.
73. Fernandes, I.; Freitas, V.D.; Reis, C.; Mateus, N. A new approach on the gastric absorption of anthocyanins. *Food Funct.* **2012**, *3*, 508–516, doi:10.1039/C2FO10295A.

74. Talavéra, S.; Felgines, C.; Texier, O.; Besson, C.; Lamaison, J.-L.; Révész, C. Anthocyanins are efficiently absorbed from the stomach in anesthetized rats. *J. Nutr.* **2003**, *133*, 4178–4182, doi:10.1093/jn/133.12.4178.
75. Vitaglione, P.; Donnarumma, G.; Napolitano, A.; Galvano, F.; Gallo, A.; Scalfi, L.; Fogliano, V. Protocatechuic acid is the major human metabolite of cyanidin-glucosides. *J. Nutr.* **2007**, *137*, 2043–2048, doi:10.1093/jn/137.9.2043.
76. Bouayed, J.; Deuber, H.; Hoffmann, L.; Bohn, T. Bioaccessible and dialysable polyphenols in selected apple varieties following in vitro digestion vs. their native patterns. *Food Chem.* **2012**, *131*, 1466–1472, doi:10.1016/j.foodchem.2011.10.030.
77. Tagliazucchi, D.; Verzelloni, E.; Bertolini, D.; Conte, A. In vitro bio-accessibility and antioxidant activity of grape polyphenols. *Food Chem.* **2010**, *120*, 599–606, doi:10.1016/j.foodchem.2009.10.030.
78. Woodward, G.; Kroon, P.; Cassidy, A.; Kay, C. Anthocyanin stability and recovery: Implications for the analysis of clinical and experimental samples. *J. Agric. Food Chem.* **2009**, *57*, 5271–5278, doi:10.1021/jf900602b.
79. Mullen, W.; Edwards, C.A.; Serafini, M.; Crozier, A. Bioavailability of pelargonidin-3-*O*-glucoside and its metabolites in humans following the ingestion of strawberries with and without cream. *J. Agric. Food Chem.* **2008**, *56*, 713–719, doi:10.1021/jf072000p.
80. McDougall, G.J.; Fyffe, S.; Dobson, P.; Stewart, D. Anthocyanins from red wine—Their stability under simulated gastrointestinal digestion. *Phytochemistry* **2005**, *66*, 2540–2548, doi:10.1016/j.phytochem.2005.09.003.
81. Dangles, O. Antioxidant activity of plant phenols: Chemical mechanisms and biological significance. *Curr. Org. Chem.* **2012**, *16*, 1–23.
82. Vanzo, A.; Terdoslavich, M.; Brandoni, A.; Torres, A.M.; Vrhovsek, U.; Passamonti, S. Uptake of grape anthocyanins into the rat kidney and the involvement of bilitranslocase. *Mol. Nutr. Food Res.* **2008**, *52*, 1106–1116, doi:10.1002/mnfr.200700505.
83. Tsuda, T. Dietary anthocyanin-rich plants: Biochemical basis and recent progress in health benefits studies. *Mol. Nutr. Food Res.* **2012**, *56*, 159–170, doi:10.1002/mnfr.201100526.
84. De Pascual-Teresa, S. Molecular mechanisms involved in the cardiovascular and neuroprotective effects of anthocyanins. *Arch. Biochem. Biophys.* **2014**, *559*, 68–74, doi:10.1016/j.abb.2014.04.012.
85. Hwang, Y.P.; Choi, J.H.; Yun, H.J.; Han, E.H.; Kim, H.G.; Kim, J.Y.; Park, B.H.; Khanal, T.; Choi, J.M.; Chung, Y.C.; et al. Anthocyanins from purple sweet potato attenuate dimethylnitrosamine-induced liver injury in rats by inducing Nrf2-mediated antioxidant enzymes and reducing COX-2 and iNOS expression. *Food Chem. Toxicol.* **2011**, *49*, 93–99, doi:10.1016/j.fct.2010.10.002.
86. Wang, D.; Wei, X.; Yan, X.; Jin, T.; Ling, W. Protocatechuic acid, a metabolite of anthocyanins, inhibits monocyte adhesion and reduces atherosclerosis in apolipoprotein E-deficient mice. *J. Agric. Food Chem.* **2010**, *58*, 12722–12728, doi:10.1021/jf103427j.



3.2. The chemical reactivity of anthocyanins (continuation)

As exposed in the review, the chemical reactivity of anthocyanins in aqueous solution is very versatile given the multiple properties of the anthocyanidin nucleus (Scheme 8). It shows an acidic character (flavylium ion: C7-OH, C4'-OH, possibly C5-OH), electrophilic properties (flavylium ion: at C2 and C4), nucleophilic properties (hemiketal and anionic base, at C3, C6 and C8), and electron-donating capacity (potentially all forms but the flavylium ion). The relatively poor stability of anthocyanin colors in near neutral solution stems from this high reactivity.

This section aims at reviewing the current knowledge on the **degradation pathways** of anthocyanins in aqueous conditions in the pH range 1 to 9. The reversible chemistry of anthocyanins is only briefly commented here as the fundamental reactions involved and their thermodynamic and kinetic bases are well understood and accepted (Pina et al., 2012b). These reactions (proton transfer, water addition and subsequent isomerization) determine the distribution of anthocyanins as mixtures of colored and colorless forms in aqueous solution (Moloney et al., 2018).

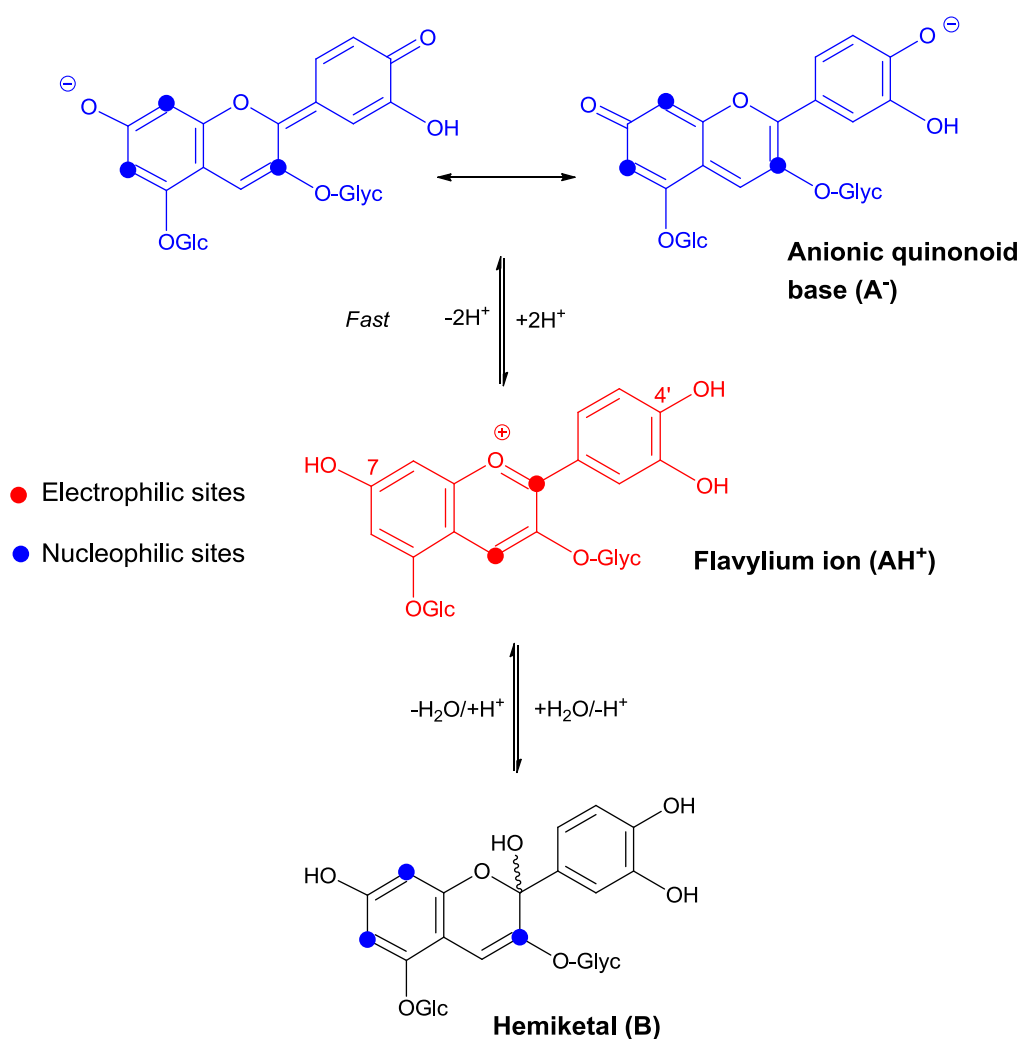
3.2.1. THE REVERSIBLE STRUCTURAL TRANSFORMATIONS

Aqueous solution of anthocyanins are typically prepared by diluting an acidic concentrated solution of pigment (100% flavylium) into a buffered solution at a given pH. Anthocyanins immediately form a mixture of colored species (the flavylium ion, the neutral base and the anionic base) in an equilibrium governed by the 2 thermodynamic constants of deprotonation of the flavylium ion (Scheme 9). Over time, this initial mixture evolves through three steps yielding colorless forms: water addition to the flavylium ion forming the hemiketal (the major colorless form at the equilibrium), the hemiketal cycle – chain tautomerization forming the *cis*-chalcone, and the *cis*-chalcone isomerization into the *trans*-chalcone (Pina et al., 2012b).

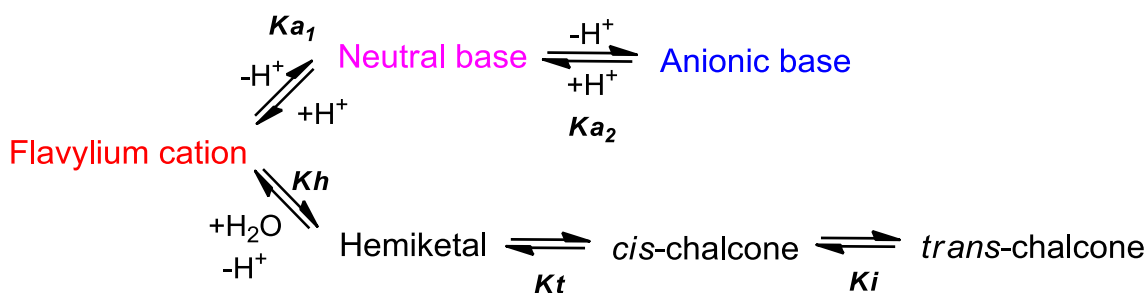
These reactions evolve toward an equilibrium state combining the colored and colorless forms. The two acidity constants (pK_a ca. 4 and 7), barely depend on anthocyanin structure, whereas the thermodynamic constants governing the other reactions depend on the anthocyanin structure (Moloney et al., 2018; Pina, 2014b)). For example, water addition is favored (faster, more complete) when C5-OH is glycosylated (Gregory T. Sigurdson et al.,

2018), and inhibited by acylation by phenolic acids (see section 3.3.2). This inhibition is strongly dependent on the number and location of the acyl residues (Moloney et al., 2018; Trouillas et al., 2016a).

The rate-limiting step toward the equilibrium is the *cis*-chalcone isomerization into the *trans*-chalcone, e.g., $k_i \approx 10^{-4}$ s for malvidin-3-5, diglucoside (Pina et al., 2012b). At room temperature, the formation of *trans*-chalcone (Ct) is slow and minor, but upon heating, the endothermic Ct accumulation becomes significant (Brouillard & Lang, 1990). It was recently reported that with complex (polyglycosylated, polyacylated) anthocyanins, this reaction can be much slower than with simple glucosides (J. Mendoza et al., 2018).



Scheme 8. Electrophilic and nucleophilic sites of anthocyanin forms



Scheme 9. The two competitive routes followed by the flavylium cation in aqueous solutions: the acid/base equilibria (top, kinetic products) and hydration equilibria (bottom, thermodynamic products), and related thermodynamic constants (adapted from Pina et al., 2012).

Table 3. Thermodynamic and kinetic constants used to describe the physico-chemical behavior of anthocyanins.

Reaction	Thermodynamic constant	Kinetic constant
$AH^+ = A + H^+$	K_{a1} First acidity constant	Fast
$A = A^- + H^+$	K_{a2} Second acidity constant	Fast
$AH^+ + H_2O = B + H^+$	K_h Hydration constant	k_h Hydration / k_{-h} dehydration rate
$B = C_c$	K_t Tautomerization constant	Fast
$C_c = C_t$	K_i Isomerization constant	k_i Isomerization rate k_{-i} constants
$AH^+ + H_2O = B + C_c + H^+$	K'_h Apparent hydration constant (pseudo-equilibrium)	k'_h Apparent hydration k'_{-h} /dehydration rate constants
$AH^+ = A + B + C_c + C_t + H^+$	K'_a Overall acidity constant	

Three domains of pH can be distinguished: At pH 1 – 2: flavylium form is nearly pure and hydration is thermodynamically unfavorable, thus negligible. At pH 2 – 6: a mixture of flavylium ion and neutral base prevails, and hydration becomes thermodynamically favorable. The apparent rate constant of hydration decays when the pH is increased, as the electrophilic flavylium ion is the sole anthocyanin species undergoing water addition. At pH 6 – 8: a mixture of neutral and anionic bases prevails, and hydration becomes very slow. Works at pH > 8 are rare due to the high sensitivity of anthocyanins to autoxidation in alkaline solution, i.e. the non-enzymatic oxidation by O₂ initiated by transition metal traces (Salgado Mendoza et al., 2017).

The pH-dependence of the composition at equilibrium can be represented on speciation diagrams (Fig 5). The fraction of colored species, which represents the color intensity of the solution, is simply the sum of the fractions: $\chi_{\text{colored species}} = \chi_{\text{AH}^+} + \chi_{\text{A}} + \chi_{\text{A}^-}$.

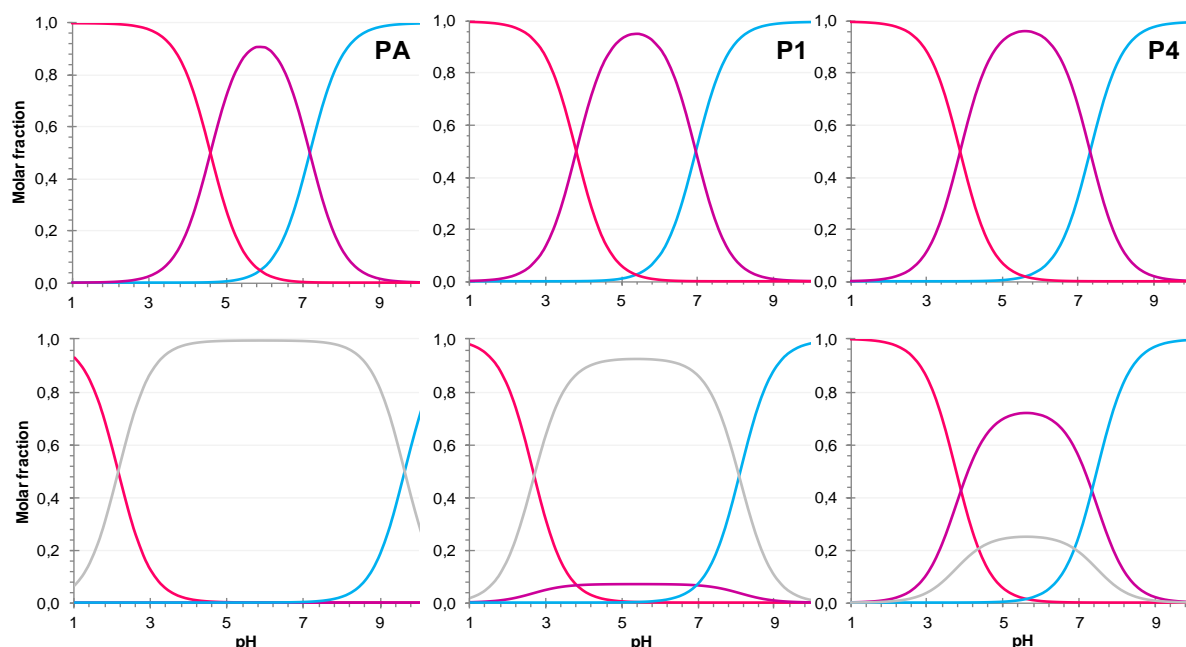
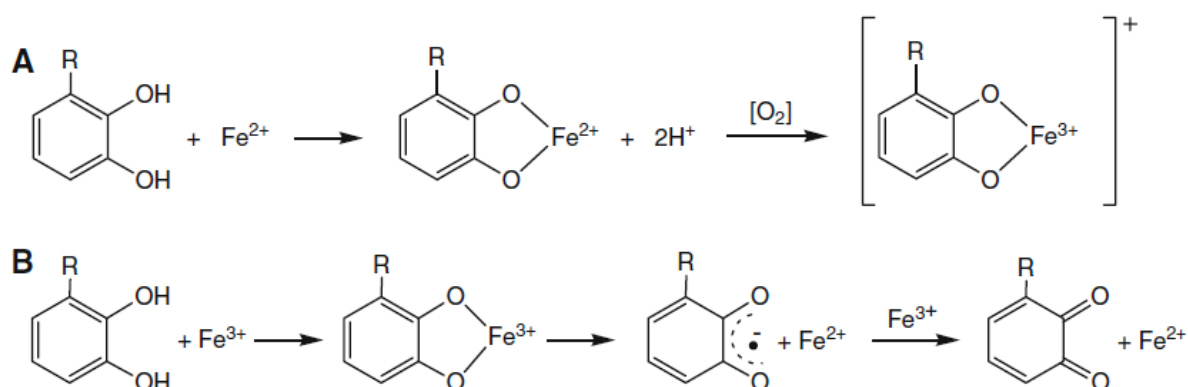


Fig 5. Distribution diagram of pigments red cabbage PA (nonacylated, *left*), P1 (monoacylated, *center*) and P4 (diacylated, *right*) at $t = 0$ (top) and at equilibrium (Moloney et al., 2018). —: flavylum ion, —: neutral base, —: anionic base, —: colorless forms (25 °C).



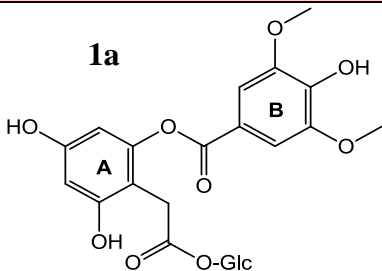
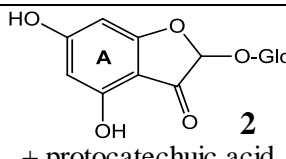
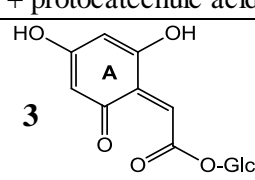
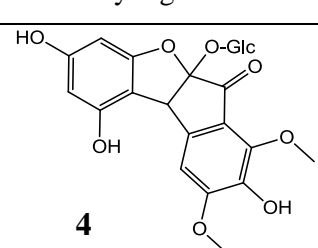
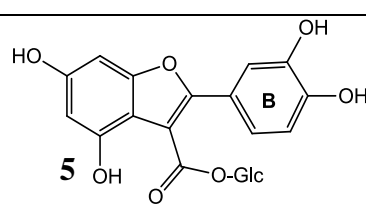
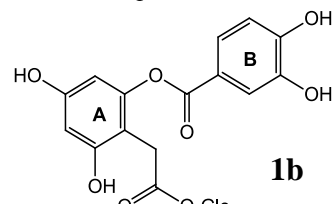
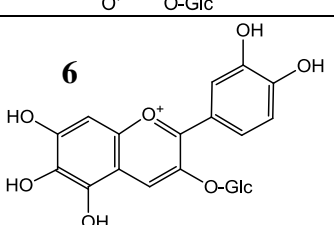
Scheme 10. A. Coordination of Fe^{2+} by *o*-diphenol rings (catechols) and subsequent electron transfer in the presence of oxygen generating the Fe^{3+} -polyphenol complex; B. Coordination of Fe^{3+} by polyphenols, subsequent iron reduction and to form semiquinone and *o*-quinone species. R=H, OH (from Perron & Brumaghim, 2009).

3.2.2. DEGRADATION PATHWAYS AND PRODUCTS

Anthocyanidins, which are the product of acid-catalyzed or enzymatic hydrolysis of glycosidic bonds, are highly unstable, and were shown to rapidly decompose into phloroglucinaldehyde and the corresponding phenolic acid (Seeram et al., 2001; Tanchev & Ioncheva, 1976, 1976). Anthocyanins are more stable at pH 1 than at higher pH, suggesting that the colorless species are intermediates in the irreversible degradation. By contrast, the glycosylated anthocyanins are much more stable and studying their degradation requires long periods of time (days, weeks or even months) or specific conditions (e.g., heating, high pH, irradiation, addition of oxidants). The different products characterized and whose structure was confirmed by NMR are listed in Table 4.

Anthocyanins (Malvidin-3-glucoside, cyanidin-3-glucoside and their 3,5-diglucoside homologs) show the same degradation products as their aglycones. In particular, the phenolic acids produced by C2-C3 cleavage (residue of the B-ring, protocatechuic acid or syringic acid), and phloroglucinaldehyde (or its 2-O-glucoside) produced by C3-C4 cleavage (residue of the A-ring) (Cabrita et al., 2014; Lopes et al., 2007; Piffaut et al., 1994; Sadilova et al., 2007; Sinela et al., 2017; Tsuda et al., 1996). Their identification is easily achieved thanks to available commercial references. These two products are however not complementary, suggesting distinct simultaneous pathways (with elimination of CO or CO₂). Other degradation products identified retain the full 15 C-atoms of the flavonoid skeleton, among them: compounds **1a/1b** and **5** (Géza Hrazdina & Franzese, 1974; Kamiya et al., 2014), compound **4** (Es-Safi et al., 2008) and 6-hydroxycyanidin 3-glucoside (Stebbins, 2016) (Table 4). Compounds **1a/1b** were detected under their reduced form. By contrast, product **5**, which may result from the hydrolysis of 1a/1b, was detected under two oxidized isomers (Lopes et al., 2007). In a recent article using ¹⁸O-labeling experiments (Satake & Yanase, 2018), the likely mechanism for the formation of **1b** from cyanidin 3-O-glucoside and H₂O₂ was unveiled (Schemes 11 & 12).

Table 4. Anthocyanin degradation products isolated and characterized by NMR.

Reference	Pigment & Conditions	Products identified	Mechanisms proposed
Hrazdina & Franzese, 1974	Mv-3Glc Aqueous H ₂ O ₂	 1a	Bayer-Villiger oxidation
Tsuda <i>et al.</i> , 1996	Cy-3Glc Free radical initiator, air, 37°C, pH 7	 2 + protocatechuic acid	Oxidation by peroxy radicals (from aerobic decomposition of azo compound)
Lopes <i>et al.</i> , 2007	Mv-3Glc pH 2.5	 3 (<i>Z</i>) + (<i>E</i>)-isomers + syringic acid	Bayer-Villiger oxidation
Es-Safi <i>et al.</i> , 2008	Mv-3Glc EtOH	 4	Cyclization of <i>trans</i> -chalcone + autoxidation
Terahara <i>et al.</i> , 2009	8 acylated PSP anthocyanins Fermented red vinegar	diacylated sophorose	Not determined
Kamiya <i>et al.</i> , 2014	Cy-3Glc Free radical initiator, air, 60°C, pH 7	 5	Nucleophilic attack of hemiketal to H ₂ O ₂
Satake & Yanase, 2018	Aqueous H ₂ O ₂ / H ₂ ¹⁸ O ₂	 1b	5 prevails in EtOH 1b prevails in H ₂ O
Stebbins, 2016	Cy-3Glc Ascorbic acid pH 3.6	 6	Fenton reaction followed by hydroxyl radical attack

Other degradation products were proposed, for which the structure was not fully characterized. For example, phloroglucinol was proposed to result from the thermal degradation of Mv-3Glc and Mv-3,5-diGlc at pH 3, according to MS analysis (Piffaut et al., 1994). The 3-glucosides and 3,5-diglucosides of 3,5,7-trihydroxycoumarin were detected from several anthocyanins and identified by TLC with an authentic reference compound and by spectral comparison in 5 solvents (Géza Hrazdina & Franzese, 1974) and later by HPLC-MS (Malien-Aubert et al., 2002). The coumarin derivatives were proposed to be generated by Bayer-Villiger oxidation with elimination of the B-ring, observed in presence of added H₂O₂ (Hrazdina & Franzese, 1974). Finally, in the presence of ascorbic acid, a 6-hydroxylation product of cyanidin 3-Glc was characterized (compound **6**). Its formation was proposed to involve the hydroxyl radical (Fenton reaction with H₂O₂ generated by ascorbate oxidation and iron traces) (Stebbins, 2016).

The mechanisms for the thermal degradation of anthocyanins are only partly understood. As polyphenols, anthocyanins are sensitive to oxidation by air. These pathways may be initiated by iron or copper traces (Nkhili et al. 2014) via one-electron or two-electron oxidation steps, the second mechanism being generally restricted to polyphenols having catechol or pyrogallol groups, *e.g.* delphinidin, cyanidin and petunidin glycosides.

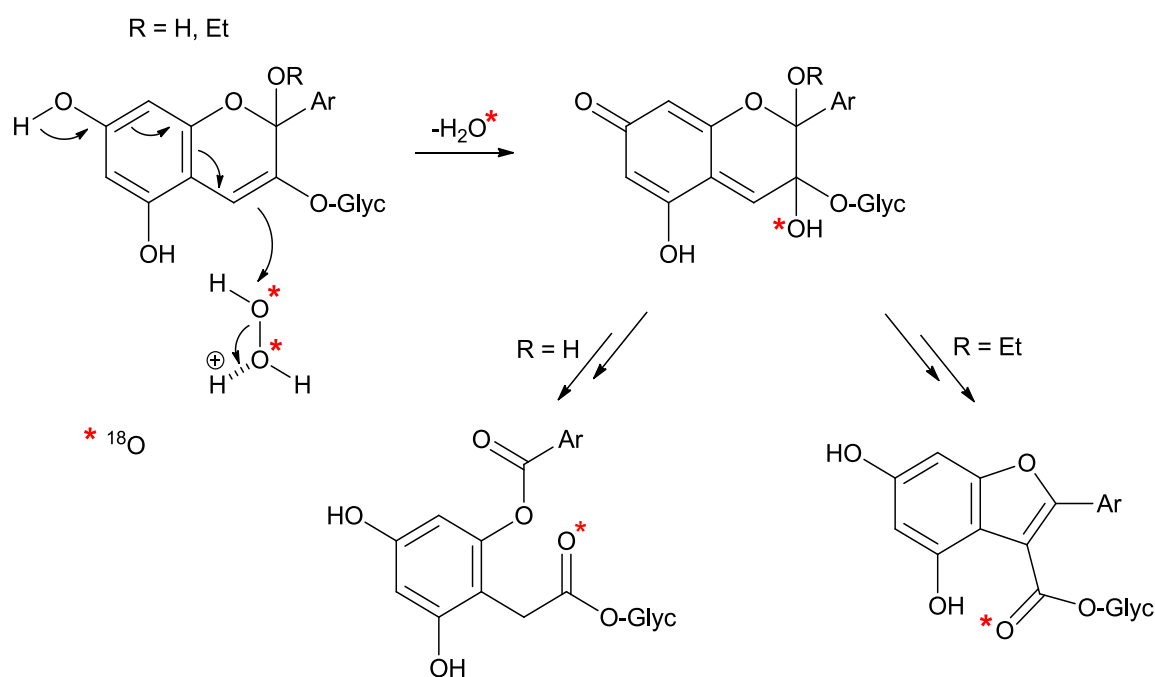
In the one-electron route, aryloxy radicals are formed, which could either add O₂ to eventually lead to hydroperoxide intermediates or recombine to form dimers. To our knowledge, no such dimers (formed upon oxidative dimerization) have been identified with anthocyanins. In parallel, superoxide is produced, which then either disproportionates or undergoes a second one-electron transfer, both steps resulting in H₂O₂ production. In the two-electron route, hydrogen peroxide can also be directly produced, while the polyphenol is converted into an *o*-quinone, a strong electrophile, which could then react with any nucleophile in the medium. To our knowledge, no anthocyanin-derived *o*-quinone intermediates have been evidenced so far, possibly because of their too high reactivity.

The more advanced stage of anthocyanin degradation involving H₂O₂ produced upon the first stage is better known, typically from works directly using H₂O₂ as a reagent. In this context, H₂O₂ can have three distinct fates:

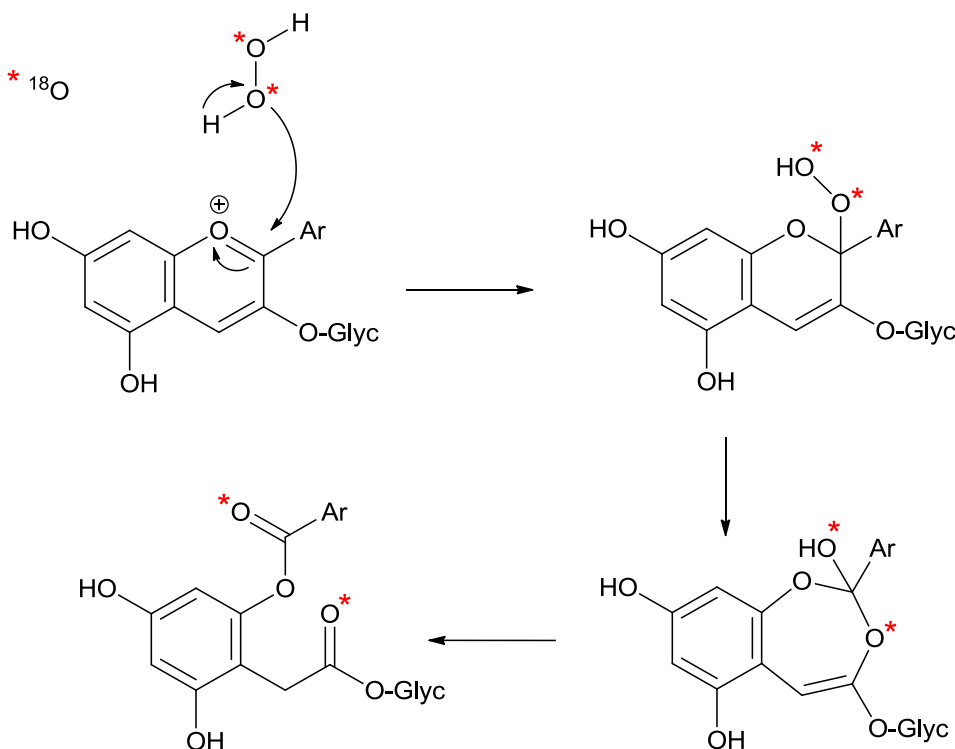
- In the presence of Fe^{2+} (deliberately added or simply contaminating the medium), it produces a highly reactive hydroxyl radical (Fenton reaction), which can trigger one-electron oxidation and/or aromatic hydroxylation. An example of the latter case has been reported: a 6-hydroxy derivative is formed when cyanidin 3-Glc is treated by ascorbate (a H_2O_2 generator upon autoxidation) in an acidic aqueous solution (Stebbins, 2016).

- H_2O_2 can react as a hard nucleophile attacking the electrophilic flavylum C2 site, as proposed in early works (Hrazdina, 1970; Lopes et al., 2007). This adduct would undergo a Bayer-Villiger rearrangement cleaving the C2-C3 bond and forming products that have been characterized by NMR (Table 4). Derivatives of 3,5,7-trihydroxycoumarin could also form via this route (Hrazdina & Franzese, 1974).

- H_2O_2 can react as an electrophile attacking the nucleophilic hemiketal C3 site, as more recently proposed and confirmed by ^{18}O labeling (Satake & Yanase, 2018), Scheme 11 and 12. As the product distribution is similar in both routes, it may be claimed that the proposal of H_2O_2 reacting as an electrophile is now more convincing. Moreover, it also provides an interpretation for the C-ring contraction observed in EtOH.



Scheme 11. Electrophilic addition of H_2O_2 to flavylum – water (hemiketal) or alcohol adducts resulting in mono-oxygenation (consistent by ^{18}O labelling and MS analysis, Satake & Yanase, 2018)



Scheme 12. Nucleophilic addition of H_2O_2 to the flavylum ion resulting in dioxygenation (not consistent by ^{18}O labeling and MS analysis, Satake & Yanase, 2018)

3.2.3. THE ROLE OF ACYLATION IN THE REACTIVITY OF ANTHOCYANINS

In the literature, the thermal stability of anthocyanins acylated by hydroxycinnamic acid (HCA) residues is usually associated to strong π -stacking interactions between the chromophore and the acyl residues (Malien-Aubert et al., 2001). Indeed, the most stable extracts at pH 3 - 5 were also the richest in diacylated anthocyanins. In anthocyanins only differing by the structure of the acyl residues, differences in thermal stability were also observed. For example, a study evidenced an impact of the methoxylation degree of the HCA residues on the thermal stability of acylated anthocyanins from black carrot at pH 1, with a stability ranked as $\text{Sp} < \text{pC} < \text{Fl}$ (Sadiłova et al., 2006). Moreover, the thermal stability of acylated red cabbage anthocyanins at pH 6 was also ranked as $\text{Sp} < \text{pC} \approx \text{Fl}$ (Wiczowski et al., 2013). In addition, the *trans* \rightarrow *cis* photo-isomerization of the HCA residues was proposed to be a factor of instability in (poly)acylated anthocyanins under irradiation (Yoshida et al., 2003). Hence, we briefly compare here the reactivity of free HCAs.

Radical-scavenging experiments and electrochemical methods like cyclic voltammetry provide information on the reduction potential of phenols and their mechanisms of electron

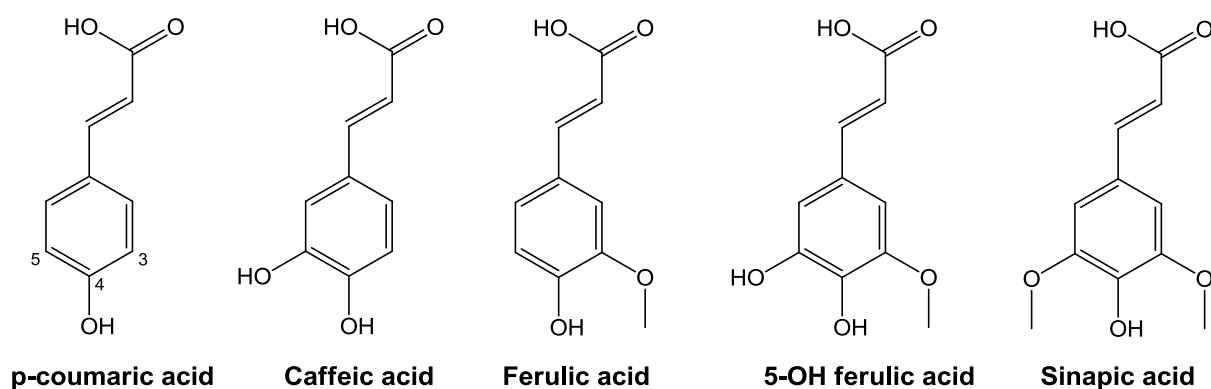
and H-atom transfers (ET, HAT) (Teixeira et al., 2013). HAT from phenols forms an aryloxy radical (ArO•) stabilized by resonance. The mechanism at stake for phenolic acids was reported to be PCET (proton-coupled electron transfer) (Foti, 2007) or SPLET (sequential proton loss - electron transfer) (Amorati et al., 2006). Overall, these mechanisms are favored when the bond dissociation energy (BDE) of the phenolic O-H group and the reduction potential (or peak potential E_p , see Table 5) are low. The pK_a of the phenolic proton does not clearly correlate with the electron-donating capacity, although a lower pK_a means a higher fraction of more reducing phenolate ion at a given pH (Foti et al., 2004; Roche et al., 2005). The reducing capacity follows the order: Sp > Cf > Fl > pC (Teixeira et al., 2013). However, the redox activity of caffeic acid has specificities as it can undergo two-electron oxidation to the corresponding *o*-quinone and bind transition metal ions, a first step to inner sphere electron transfer (Scheme 10) (Perron & Brumaghim, 2009).

In the HCA series, sinapic acid is the most sensitive to one-electron oxidation, and sinapoyl residues are also the least efficient at providing stability to acylated anthocyanins. This suggests that oxidation of HCA residues contributes to anthocyanin degradation. To our knowledge, the relative stability of anthocyanins bearing caffeoyl residues is not documented. However, the free radical scavenging capacity of diacylated anthocyanins and their acylsophorose released upon fermentation revealed the strong and additive contribution of phenolic acid residues according to: Cf > Fl \approx HB \approx no acyl (Terahara et al., 2009).

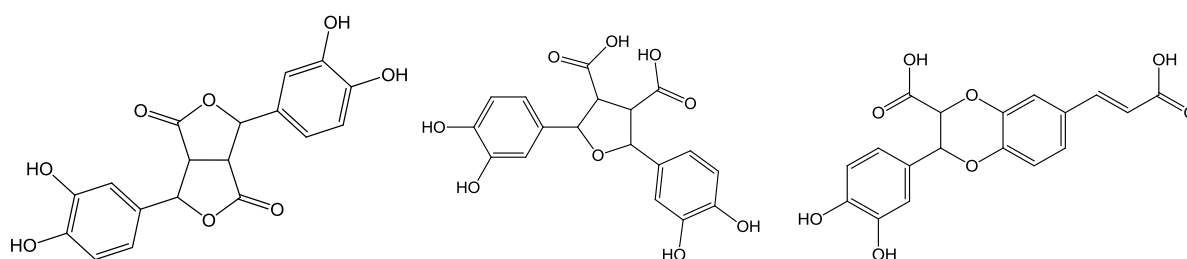
Table 5. Parameters for assessing the redox activity of hydroxycinnamic acids.

	pK_{a2} ^a in H ₂ O	BDE ^b (kcal/mol) in EtOH	k_{obs} ^b ($\times 10^{-5} s^{-1}$) in EtOAc	E_p (mV) pH 7.4 ^c , 7.8 ^d
<i>p</i> -coumaric acid	8,37	79,6	<	+736 ^d +335 +447 ^c
Ferulic acid	8,65	81,3	20	+410 ^d +183 ^c
Caffeic acid	8,32	79,2	600	+142 ^d
Sinapic acid	9,21	75,2	1000	+188 +295 ^c

^a Phenolic OH (Ozkorucuklu et al., 2009) ^b(Amorati et al., 2006) ^c(Gaspar et al., 2009) ^d(L. Li et al., 2018), k_{obs} = apparent rate constant of phenol oxidation. E_p = Reduction peak potential.



Scheme 13. Structure of the different hydroxycinnamic acids



Scheme 14. Three types of caffeic acid dimers. *Left:* bis-lactone type (Antolovich et al., 2004). *Center:* tetrahydrofuran type (Fulcrand et al., 1994), stereoisomers not represented. *Right:* 2,3-dihydro-1,4-benzodioxan type called caffeicins (Cilliers & Singleton, 1991).

Regarding the **degradation products**, caffeic acid forms a broad range of covalent C-C and C-O dimers involving the corresponding *o*-quinone as an intermediate (Bernillon et al., 2004; Cilliers & Singleton, 1991; Roche et al., 2005). Decarboxylation and further oxidation were also evidenced (Nkhili et al., 2014). Ferulic acid was also reported to form dimers and trimers, in the presence of a azo generator of free radicals at pH 7.4 (Roche et al., 2005) and by periodate and Fenton oxidation (Antolovich et al., 2004). In presence of an H₂O₂-peroxidase system at pH 6.5, several novel cross-coupling Fl – Cf and Sp – Cf products were reported (Arrieta-Baez & Stark, 2006). All HCAs react with the Fenton reagent to produce the corresponding benzaldehydes as major products (Antolovich et al., 2004). The main products identified in the photolysis of pC are protocatechuic acid (PCA, pointing to aromatic hydroxylation), 4-hydroxybenzylalcohol and oxalacetic acid (Li et al., 2018).

3.2.4. STRUCTURE/STABILITY RELATIONSHIPS

The structural features of anthocyanins, i.e. the glycosylation and acylation pattern and the B-ring substitution, are known to impact their color stability. However, systematic studies on the structure/stability relationships are scarce and the structural diversity increases the complexity. Besides, the glycosylation and acylation pattern are embedded. The color stability at a given pH actually reflects two distinct phenomena: the susceptibility of anthocyanins to water addition (reversible) and their oxidizability (leading to irreversible degradation). The structural features protecting the chromophore against water addition (*e.g.*, acylation by HCA residues) may differ from those stabilizing it against oxidation.

It is generally accepted that anthocyanins with complex patterns of glycosylation and acylation exhibit remarkable stability to pH changes, heat treatment and light exposure (Giusti & Wrolstad, 2003). The favorable influence of acylation on the reversible color loss is well-known (Trouillas et al. 2016), but its possible influence on the irreversible component of color loss remains poorly documented, especially at higher pH, where the reactivity of the phenolic acid residues could become significant. We emphasize the following trends:

Glycosylation at C5 increases the susceptibility to water addition. For example, the overall acidity constant pK'_a (overall hydration + first proton transfer, $K'_a = K'_h + K_{a1}$) of Mv-3-Glc is 2.55 *vs.* 1.7 - 2.1 for Mv-3,5-diGlc (Pina et al., 2012b, p. 201). Compared to Glc, a bulky disaccharide moiety at C3-OH, *e.g.* sophorose, provides a modest stabilization, whereas the type of sugar has no clear impact (Sigurdson et al., 2018).

The impact of the B-ring substitution is marginal on the susceptibility to water addition (Leydet et al., 2012) but more pronounced on the oxidizability (electron-donating capacity). Delphinidin and cyanidin aglycones are less stable than pelargonidin (Pereira et al., 1997), with a similar observation on the corresponding 3-O-glucosides *in vitro* ($t_{50}(\text{Cy3G}) = 1.8\text{h}$, $t_{50}(\text{Pg3G}) = 2.1\text{h}$) (Sadilova et al., 2007) and *in vivo* (Braga et al., 2018). The stability of anthocyanins with different B-ring and glycosylation patterns was assessed in saliva: Cy and Pg glycosides were more stable than their Dp and Pt homologs (Kamonpatana et al., 2012). The stability of di- and trisaccharides slightly exceeded that of monosaccharides.

Acylation by HCAs efficiently protects the flavylum ion against hydration and the protection is usually greatly improved when a second acyl residue is introduced, in agreement with the formation of sandwich-like conformations in which one acyl residue is stacked onto

each anthocyanidin face (Moloney et al., 2018; Yoshida et al., 2000). The contribution of HCAs to oxidative pathways is little documented (Sadilova et al., 2007).

3.2.5. CONCLUSION

The instability of anthocyanins during storage and/or processing is a major limitation to their applications as natural colors, in spite of their great potential. Their color stability is affected by a combination of reversible and irreversible pathways. Their chemical stability, represented by the irreversible component of color loss, involves a combination of autoxidative and hydrolytic mechanisms. Both phenomena largely depend on the anthocyanin structure. Among the parameters impacting the rate of color loss, several environmental factors are also critical. They are reviewed in the next section.

3.3. Color stability

3.3.1. INSTABILITY DURING INDUSTRIAL FOOD PROCESSING

In the food processing industry, several ingredients containing anthocyanins can be added to contribute to the color of the finished products. Natural extracts used in a coloring purpose are considered as coloring foods, whereas after a selective enrichment (by a factor higher than 6) they are considered as food colors (additive regulation). Their color is particularly important in fruit preparations (juices, syrups, jams and jellies). From the elaboration of the ingredient (extraction, stabilization step) to its addition in the finished product (matrix interactions, stabilization step), anthocyanins degradation can occur. Degradation may continue throughout the entire product shelf-life. For the color to stay acceptable over 18 months, color changes should be minor, i.e. $\Delta E < 5$, with ΔE being the color difference (deduced from coloric parameters) between t_0 and t ; $\Delta E = \sqrt{(L - L_0)^2 + (a - a_0)^2 + (b - b_0)^2}$.

Several recent reviews summarize the factors that impact the stability of anthocyanins (Castañeda-Ovando et al., 2009; Cavalcanti et al., 2011; Cortez et al., 2017; Tierno & Galarreta, 2016). The destabilizing factors include i) physical factors: a high temperature, light exposure, high hydrostatic pressure; and ii) (bio)chemical factors, especially the presence of oxidants (e.g. oxygen, ozone), pro-oxidant compounds (e.g. ascorbic acid, transition metals), nucleophiles (sulfites in wine, water, hydrogen peroxide), and the enzymes. Controlling these factors is important to improve color stability.

A critical step in the food processing industry is microbial stabilization, which aims at extending the duration of product storage before consumption. For extracts preparations, as anthocyanins are thermo-sensitive, the extracts are generally freeze-dried (Delgado-Vargas et al., 2002). However, in finished product, pasteurization and sterilization remain common stabilization processes, that will alter the color of products rich in anthocyanins. Among thermal processes, steaming appears as the softest treatment (-29% anthocyanin content), followed by boiling (-41%) and then blanching (-59%) (Patras et al., 2010). Other microbial stabilization techniques exist, that also diminish anthocyanin stability. For instance, in the wine-making process, the addition of sulfites for preservation actually induce the bleaching of free anthocyanins. Finally, the compounds naturally present in the plant sources (phenolic compounds, endogenous enzymes (polyphenol oxidase, glucosidase...), other redox active

compounds) can destabilize anthocyanins, or stabilize them (de Aguiar Cipriano et al., 2015). It would be interesting to compare the relative contribution of these factors in a given process.

Several natural mechanisms of anthocyanin stabilization are known: copigmentation, reviewed in (Trouillas et al., 2016a), and binding to metal ions, reviewed in (Yoshida, 2009). In plant, the isolation of anthocyanins in the vacuoles, which are delimited compartments of controlled composition contributes to the color stabilization. Indeed, the high local concentration favors copigmentation and self-association. In these conditions, the simultaneous presence of anthocyanins, other flavonoids and metal cations also allows the formation of sophisticated supramolecular assemblies, called metalloanthocyanins (Yoshida et al., 2009). In these structures, 3 anthocyanin molecules bind a metal ion (Mg^{2+} , Fe^{3+} or Al^{3+}) via their B-ring, while 3 flavone copigments are inserted between the anthocyanidin nuclei, and stabilized by π -stacking (Yoshida et al., 2009). The dimerization of such complexes results in final aggregates having a fixed 2:6:6 metal-pigment-copigment stoichiometry.

3.3.1. STABILIZATION BY COPIGMENTATION & SELF-ASSOCIATION

Copigmentation consists in the spontaneous association of the planar anthocyanidin nucleus (the pigment) with a colorless phenol (the copigment), through weak (non-covalent) interactions of the two rings facing each other (Trouillas et al., 2016a). The driving force of copigmentation is mostly a combination of dispersion (the stabilizing component of van der Waals interactions) and the hydrophobic effect (the thermodynamically favorable desolvation of weakly polar surfaces when they associate in water due to the concomitant release of high-energy water molecules from the solvation shells to the bulk solvent). In phenol – phenol interactions, this association is called π -stacking: the interacting aromatic nuclei are typically parallel with an offset to minimize the electrostatic repulsion between their π -electrons. Thanks to their wide planar polarizable chromophore, anthocyanins are particularly prone to π -stacking interactions with copigments such as flavones and flavonols glycosides ($K > 10^3 M^{-1}$) or to a lesser extent, hydroxycinnamic acids ($K = 2 - 4 \times 10^2 M^{-1}$) (Trouillas et al., 2016a). In mildly acidic solution, copigmentation causes both a hyperchromic shift (increase in the visible absorbance) and a bathochromic shift (increase in the λ_{max} of the visible band). The former is simply ascribed to a shift of the hydration equilibrium to the flavylium ion, which is selectively stabilized by its π -stacking interactions with the copigment. The latter is more subtle and possibly involves copigment-to-pigment charge transfer interactions (Trouillas et

al., 2016a) and/or conformational distortions (*e.g.*, rotation about C2-C1' or about the glycosidic bonds) due to the stacked copigment molecule (Rusishvili et al., 2019). Overall, copigmentation slows down hydration and thus the related color loss, results in a higher mole fraction of colored forms at equilibrium and in a bluing effect. This sole phenomenon might explains up to 30 - 50% of the color in wine (Boulton, 2001).

Intramolecular copigmentation operates in anthocyanins acylated by HCAs. The conformational folding bringing the two nuclei in van der Waals contact is favored by an appropriate balance between flexibility and rigidity in the sugar spacer. As such, the efficiency of intramolecular copigmentation is very dependent on the glycosidation and acylation sites, and on the type of sugar spacer (linear or branched) (Yoshida et al., 2009).

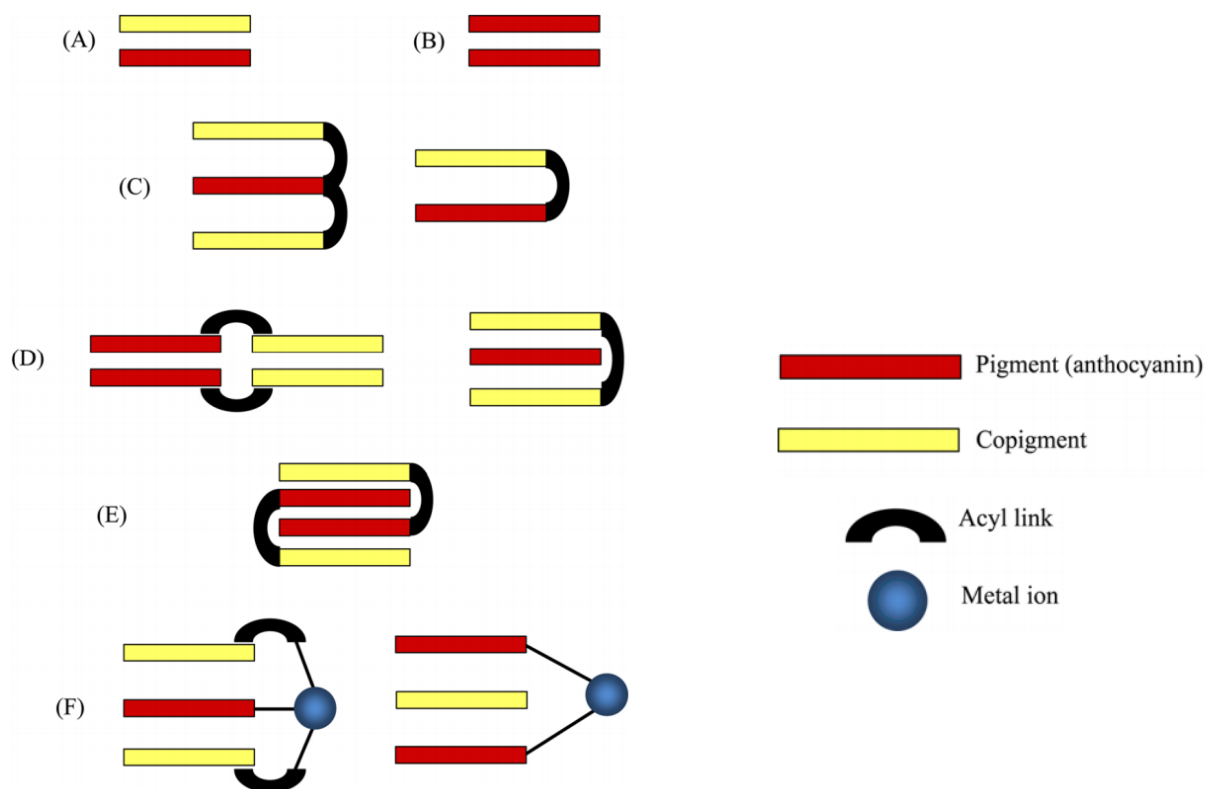
Finally, π -stacking interactions can also develop between 2 (or more) anthocyanidin nuclei and indeed self-association of anthocyanins also participates in color stabilization. Anthocyanin acylation not only allows intramolecular copigmentation but also strengthens self-association. The two mechanisms can be distinguished by circular dichroism (Yoshida et al., 2009).

With red cabbage and purple sweet potato anthocyanins, the bulkiness of the 3-O-sophorosyl moiety should in principle favor intramolecular copigmentation over self-association. However, Cotton effects in the visible range, which is typical of stacked anthocyanidin nuclei, are observed with diacylated red cabbage anthocyanins, especially when acyl residues display methoxy groups (Sp > Fl > pC) (Moloney et al., 2018). The different cases of π -stacking interactions are depicted on Scheme 15.

Anthocyanins exhibiting the highest color stability are found in flowers, owing to polyacylation (up to 4 phenolic acyl residues) of sugars at C3, C7, C3' or 5'-OH positions. Examples of anthocyanins stabilized mainly by intramolecular copigmentation (C) include the ternatins (polyacylated at C3' and C5'); the monoacylated alatanin is reported to be mainly stabilized by self-association, in the (E) "nested" conformation, and others combine intra- and intermolecular copigmentation, *e.g.* the tecophilin (triacylated at C7) (Yoshida et al., 2009).

The acylated anthocyanins found in the edible parts of the purple varieties of cabbage, potato, carrots, radish and grape, are simpler, bearing only one or two phenolic acid residues. Overall, it was reported that any extension of the π -conjugated system beyond the phenolic ring (*e.g.*, conjugation through the 2,3-double bond of flavonoids, substitution by electron-

donating hydroxyl and methoxyl groups) has a positive impact on copigmentation (Trouillas et al., 2016a). In particular, for a given anthocyanin, the copigmentation binding constant increases in the order: pC < Fl < Sp, and HBA is a weaker copigment than HCAs. The intensity of copigmentation is weaker at higher temperature, due to its exothermic nature.



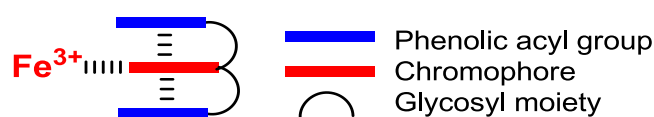
Scheme 15. π - π Stacking interactions in anthocyanins and their complexes. (A) intermolecular copigmentation, (B) self-association, (C) intramolecular copigmentation in acylated anthocyanins, (D) self-association of acylated anthocyanins, (E) intercalation in intermolecular copigmentation, and (F) copigmentation in metal-anthocyanin complexes, from Trouillas et al., 2016.

3.3.3. STABILIZATION BY METAL COMPLEXATION

Cyanidin, delphinidin and petudinin glycosides are able to bind hard metal ions (*e.g.*, Fe^{3+} , Al^{3+} , Ga^{3+}), thus forming stable soluble complexes (Sigurdson et al., 2016; (Yoshida et al., 2009b). Even in mildly acidic solution, the protons at C3'-OH and C4'-OH are removed upon binding and the anthocyanidin adopts the *p*-quinonemethide structure typical of the anionic base. The main consequences are: a) a strong bluing effect, b) a hyperchromic effect (as the anionic base is the colored form having the highest molar absorption coefficient) and c) an improved resistance to water addition. However, unlike copigmentation complexes, metal - anthocyanin complexes are dissociated at acidic pH ($\text{pH} < 3 - 4$), which restricts the application of this phenomenon to color stabilization. In addition, an excess of Fe^{3+} appears damaging to color (G.T. Sigurdson et al., 2016).

Cooperation between copigmentation (“vertical”) and metal binding (“horizontal”) (Scheme 16) is expected to modulate the color and greatly enhance its stability. This approach appears relevant with acylated cyanidin glycosides from vegetables.

Besides, the addition of biopolymers: proteins, natural or modified polysaccharides was reported to stabilize anthocyanins (and other phenolic compounds) through direct interactions or microencapsulation (Fang & Bhandari, 2010). Electrostatic interactions and hydrogen bonding were proposed to be important driving forces in these associations (Chung et al., 2015; Lang et al., 2019); (W. Wang et al., 2017).



Scheme 16. The cooperation between intramolecular copigmentation through vertical π -stacking interactions and horizontal metal binding, modulates the color and greatly enhance its stability in neutral solution.

REFERENCES FOR CHAPTER 1

- Amorati, R., Pedulli, G. F., Cabrini, L., & Landi, L. (2006). Solvent and pH Effects on the Antioxidant Activity of Caffeic and Other Phenolic Acids. *J. Agric. Food Chem.*, *54*(8), 2932–2937.
- Andersen, Ø. M., & Jordheim, M. (2010). 3.16 - Chemistry of Flavonoid-Based Colors in Plants. In H.-W. (Ben) Liu & L. Mander (Eds.), *Comprehensive Natural Products II* (pp. 547–614). Elsevier. <https://doi.org/10.1016/B978-008045382-8.00086-1>
- Anouar, E. H., Gierschner, J., Duroux, J.-L., & Trouillas, P. (2012). UV/Visible spectra of natural polyphenols: A time-dependent density functional theory study. *Food Chemistry*, *131*(1), 79–89. <https://doi.org/10.1016/j.foodchem.2011.08.034>
- Antolovich, M., Bedgood, D. R., Bishop, A. G., Jardine, D., Prenzler, P. D., & Robards, K. (2004). LC-MS Investigation of Oxidation Products of Phenolic Antioxidants. *Journal of Agricultural and Food Chemistry*, *52*(4), 962–971. <https://doi.org/10.1021/jf0349883>
- Appelhagen, I., Wulff-Vester, A. K., Wendell, M., Hvoslef-Eide, A.-K., Russell, J., Oertel, A., Martens, S., Mock, H.-P., Martin, C., & Matros, A. (2018). Colour bio-factories: Towards scale-up production of anthocyanins in plant cell cultures. *Metabolic Engineering*, *48*, 218–232. <https://doi.org/10.1016/j.mben.2018.06.004>
- Archetti, M. (2000). The Origin of Autumn Colours by Coevolution. *Journal of Theoretical Biology*, *205*(4), 625–630. <https://doi.org/10.1006/jtbi.2000.2089>
- Arrieta-Baez, D., & Stark, R. E. (2006). Modeling suberization with peroxidase-catalyzed polymerization of hydroxycinnamic acids: Cross-coupling and dimerization reactions. *Phytochemistry*, *67*(7), 743–753. <https://doi.org/10.1016/j.phytochem.2006.01.026>
- Baylor, D. (1996). How photons start vision. *Proceedings of the National Academy of Sciences*, *93*(2), 560–565. <https://doi.org/10.1073/pnas.93.2.560>
- Bernillon, S., Guyot, S., & Renard, C. M. G. C. (2004, May 15). *Detection of phenolic oxidation products in cider apple juice by high-performance liquid chromatography electrospray ionisation ion trap mass spectrometry*. Rapid Communications in Mass Spectrometry. <https://doi.org/10.1002/rcm.1430>
- Boulton, R. (2001). The Copigmentation of Anthocyanins and Its Role in the Color of Red Wine: A Critical Review. *American Journal of Enology and Viticulture*, *52*(2), 67–87.
- Bowmaker, J. K., & Dartnall, H. J. (1980). Visual pigments of rods and cones in a human retina. *The Journal of Physiology*, *298*, 501–511.
- Braga, A. R. C., Murador, D. C., de Souza Mesquita, L. M., & de Rosso, V. V. (2018). *Bioavailability of anthocyanins: Gaps in knowledge, challenges and future research*. <https://pubag.nal.usda.gov/catalog/6362194>
- Brouillard, R., & Lang, J. (1990). The hemiacetal–cis-chalcone equilibrium of malvin, a natural anthocyanin. *Canadian Journal of Chemistry*, *68*(5), 755–761. <https://doi.org/10.1139/v90-119>
- Cabrera, L., Petrov, V., & Pina, F. (2014). On the thermal degradation of anthocyanidins: cyanidin. *RSC Advances*, *4*(36), 18939–18944. <https://doi.org/10.1039/C3RA47809B>
- Cásedas, G., González-Burgos, E., Smith, C., López, V., & Gómez-Serranillos, M. P. (2018). Regulation of redox status in neuronal SH-SY5Y cells by blueberry (*Vaccinium myrtillus* L.) juice, cranberry (*Vaccinium*

macrocarpon A.) juice and cyanidin. *Food and Chemical Toxicology*, 118, 572–580. <https://doi.org/10.1016/j.fct.2018.05.066>

Castañeda-Ovando, A., Pacheco-Hernández, Ma. de L., Páez-Hernández, Ma. E., Rodríguez, J. A., & Galán-Vidal, C. A. (2009). Chemical studies of anthocyanins: A review. *Food Chemistry*, 113(4), 859–871. <https://doi.org/10.1016/j.foodchem.2008.09.001>

Cavalcanti, R. N., Santos, D. T., & Meireles, M. A. A. (2011). Non-thermal stabilization mechanisms of anthocyanins in model and food systems—An overview. *Food Research International*, 44(2), 499–509. <https://doi.org/10.1016/j.foodres.2010.12.007>

Chung, C., Rojanasathara, T., Mutilangi, W., & McClements, D. J. (2015). Enhanced stability of anthocyanin-based color in model beverage systems through whey protein isolate complexation. *Food Research International*, 76, 761–768. <https://doi.org/10.1016/j.foodres.2015.07.003>

CIE Standard. (2004). *Colorimetry — Part 1: CIE standard colorimetric observers* | CIE. <http://www.cie.co.at/publications/colorimetry-part-1-cie-standard-colorimetric-observers-0>

Cilliers, J. J. L., & Singleton, V. L. (1991). Characterization of the products of nonenzymic autoxidative phenolic reactions in a caffeic acid model system. *Journal of Agricultural and Food Chemistry*, 39(7), 1298–1303. <https://doi.org/10.1021/jf00007a021>

Cortez, R., Luna-Vital, D. A., Margulis, D., & Gonzalez de Mejia, E. (2017). Natural Pigments: Stabilization Methods of Anthocyanins for Food Applications: Stabilization of natural pigments.... *Comprehensive Reviews in Food Science and Food Safety*, 16(1), 180–198. <https://doi.org/10.1111/1541-4337.12244>

Dangles, O. (2012, March). *Antioxidant Activity of Plant Phenols: Chemical Mechanisms and Biological Significance* [Text]. <https://doi.org/info:doi/10.2174/138527212799957995>

Dangles, O., & Fenger, J.-A. (2018). The Chemical Reactivity of Anthocyanins and Its Consequences in Food Science and Nutrition. *Molecules*, 23(8), 1970. <https://doi.org/10.3390/molecules23081970>

de Aguiar Cipriano, P., Ekici, L., Barnes, R. C., Gomes, C., & Talcott, S. T. (2015). Pre-heating and polyphenol oxidase inhibition impact on extraction of purple sweet potato anthocyanins. *Food Chemistry*, 180, 227–234. <https://doi.org/10.1016/j.foodchem.2015.02.020>

Delgado-Vargas, F., Paredes-Lopez, O., & Paredes-Lopez, O. (2002). *Natural Colorants for Food and Nutraceutical Uses*. CRC Press. <https://doi.org/10.1201/9781420031713>

Eastaugh, N., Walsh, V., Chaplin, T., & Siddall, R. (2007). *Pigment Compendium: A Dictionary of Historical Pigments*. Routledge.

Es-Safi, N.-E., Meudec, E., Bouchut, C., Fulcrand, H., Ducrot, P.-H., Herbette, G., & Cheynier, V. (2008). New Compounds Obtained by Evolution and Oxidation of Malvidin 3- O -Glucoside in Ethanolic Medium. *Journal of Agricultural and Food Chemistry*, 56(12), 4584–4591. <https://doi.org/10.1021/jf8001872>

Falcone Ferreyra, M. L., Rius, S. P., & Casati, P. (2012). Flavonoids: biosynthesis, biological functions, and biotechnological applications. *Frontiers in Plant Science*, 3. <https://doi.org/10.3389/fpls.2012.00222>

Fang, Z., & Bhandari, B. (2010). Encapsulation of polyphenols – a review. *Trends in Food Science & Technology*, 21(10), 510–523. <https://doi.org/10.1016/j.tifs.2010.08.003>

Foti, M. C. (2007). Antioxidant properties of phenols. *Journal of Pharmacy and Pharmacology*, 59(12), 1673–1685. <https://doi.org/10.1211/jpp.59.12.0010>

- Foti, M. C., Daquino, C., & Geraci, C. (2004). Electron-Transfer Reaction of Cinnamic Acids and Their Methyl Esters with the DPPH• Radical in Alcoholic Solutions. *The Journal of Organic Chemistry*, 69(7), 2309–2314. <https://doi.org/10.1021/jo035758q>
- Fulcrand, H., Cheminat, A., Brouillard, R., & Cheynier, V. (1994). Characterization of compounds obtained by chemical oxidation of caffeic acid in acidic conditions. *Phytochemistry*, 35(2), 499–505. [https://doi.org/10.1016/S0031-9422\(00\)94790-3](https://doi.org/10.1016/S0031-9422(00)94790-3)
- Gaspar, A., Garrido, E. M., Esteves, M., Quezada, E., Milhazes, N., Garrido, J., & Borges, F. (2009). New insights into the antioxidant activity of hydroxycinnamic acids: Synthesis and physicochemical characterization of novel halogenated derivatives. *European Journal of Medicinal Chemistry*, 44(5), 2092–2099. <https://doi.org/10.1016/j.ejmech.2008.10.027>
- Giusti, M. M., Rodríguez-Saona, L. E., & Wrolstad, R. E. (1999). Molar Absorptivity and Color Characteristics of Acylated and Non-Acylated Pelargonidin-Based Anthocyanins. *Journal of Agricultural and Food Chemistry*, 47(11), 4631–4637. <https://doi.org/10.1021/jf981271k>
- Giusti, M. M., & Wrolstad, R. E. (2003). Acylated anthocyanins from edible sources and their applications in food systems. *Biochemical Engineering Journal*, 14(3), 217–225. [https://doi.org/10.1016/S1369-703X\(02\)00221-8](https://doi.org/10.1016/S1369-703X(02)00221-8)
- Gómez-Alonso, S., Fernández-González, M., Mena, A., Martínez, J., & García-Romero, E. (2007). Anthocyanin profile of Spanish *Vitis vinifera* L. red grape varieties in danger of extinction. *Australian Journal of Grape and Wine Research*, 13(3), 150–156. <https://doi.org/10.1111/j.1755-0238.2007.tb00245.x>
- Gould, K. S., Neill, S. O., & Vogelmann, T. C. (2002). A unified explanation for anthocyanins in leaves? In *Advances in Botanical Research* (Vol. 37, pp. 167–192). Academic Press. [https://doi.org/10.1016/S0065-2296\(02\)37049-6](https://doi.org/10.1016/S0065-2296(02)37049-6)
- Harborne, J. B., & Williams, C. A. (2000). Advances in flavonoid research since 1992. *Phytochemistry*, 55(6), 481–504.
- Hatier, J.-H., & Gould, K. (2008). Anthocyanin Function in Vegetative Organs. In *Anthocyanins, Biosynthesis, Functions, and Applications* (pp. 1–19). https://doi.org/10.1007/978-0-387-77335-3_1
- Havsteen, B. H. (2002). The biochemistry and medical significance of the flavonoids. *Pharmacology & Therapeutics*, 96(2), 67–202. [https://doi.org/10.1016/S0163-7258\(02\)00298-X](https://doi.org/10.1016/S0163-7258(02)00298-X)
- Herbst, W., Hunger, K., Wilker, G., & Winter, R. (2005). Polycyclic Pigments. In *Industrial Organic Pigments* (pp. 421–566). John Wiley & Sons, Ltd. <https://doi.org/10.1002/3527602429.ch3>
- Hrazdina, G. (1970). Oxidation of the anthocyanidin-3,5-diglucosides with H₂O₂: The structure of malvone. *Phytochemistry*, 9(7), 1647–1652. [https://doi.org/10.1016/S0031-9422\(00\)85290-5](https://doi.org/10.1016/S0031-9422(00)85290-5)
- Hrazdina, Géza, & Franzese, A. J. (1974). Oxidation products of acylated anthocyanins under acidic and neutral conditions. *Phytochemistry*, 13(1), 231–234. [https://doi.org/10.1016/S0031-9422\(00\)91300-1](https://doi.org/10.1016/S0031-9422(00)91300-1)
- Jhan, J.-K., Chung, Y.-C., Chen, G.-H., Chang, C.-H., Lu, Y.-C., & Hsu, C.-K. (2016). Anthocyanin contents in the seed coat of black soya bean and their anti-human tyrosinase activity and antioxidative activity. *International Journal of Cosmetic Science*, 38(3), 319–324. <https://doi.org/10.1111/ics.12300>
- Jing, P., & Giusti, M. M. (2007). Effects of Extraction Conditions on Improving the Yield and Quality of an Anthocyanin-Rich Purple Corn (*Zea mays* L.) Color Extract. *Journal of Food Science*, 72(7), C363–C368. <https://doi.org/10.1111/j.1750-3841.2007.00441.x>

- Kamonpatana, K., Giusti, M. M., Chitchumroonchokchai, C., MorenoCruz, M., Riedl, K. M., Kumar, P., & Failla, M. L. (2012). Susceptibility of anthocyanins to ex vivo degradation in human saliva. *Food Chemistry*, *135*(2), 738–747. <https://doi.org/10.1016/j.foodchem.2012.04.110>
- Klassen, K. M., Borleis, E. S., Brennan, L., Reid, M., McCaffrey, T. A., & Lim, M. S. (2018). What People “Like”: Analysis of Social Media Strategies Used by Food Industry Brands, Lifestyle Brands, and Health Promotion Organizations on Facebook and Instagram. *Journal of Medical Internet Research*, *20*(6), e10227. <https://doi.org/10.2196/10227>
- Kubo, H., Peeters, A. J. M., Aarts, M. G. M., Pereira, A., & Koomneef, M. (1999). ANTHOCYANINLESS2, a Homeobox Gene Affecting Anthocyanin Distribution and Root Development in Arabidopsis. *The Plant Cell*, *11*(7), 1217–1226. <https://doi.org/10.1105/tpc.11.7.1217>
- Labbe, D., Almiron-Roig, E., Hudry, J., Leathwood, P., Schifferstein, H. N. J., & Martin, N. (2009). Sensory basis of refreshing perception: Role of psychophysiological factors and food experience. *Physiology & Behavior*, *98*(1–2), 1–9. <https://doi.org/10.1016/j.physbeh.2009.04.007>
- Landi, M., Tattini, M., & Gould, K. S. (2015). Multiple functional roles of anthocyanins in plant-environment interactions. *Environmental and Experimental Botany*, *119*, 4–17. <https://doi.org/10.1016/j.envexpbot.2015.05.012>
- Lang, Y., Li, E., Meng, X., Tian, J., Ran, X., Zhang, Y., Zang, Z., Wang, W., & Li, B. (2019). Protective effects of bovine serum albumin on blueberry anthocyanins under illumination conditions and their mechanism analysis. *Food Research International*, *122*, 487–495. <https://doi.org/10.1016/j.foodres.2019.05.021>
- Lawrence, W. J. C., Price, J. R., Robinson, G. M., & Robinson, R. (1939). The distribution of anthocyanins in flowers, fruits and leaves. *Philosophical Transactions of the Royal Society of London. Series B, Biological Sciences*, *230*(567), 149–178. <https://doi.org/10.1098/rstb.1939.0006>
- Lehto, S., Buchweitz, M., Klimm, A., Straßburger, R., Bechtold, C., & Ulberth, F. (2017). Comparison of food colour regulations in the EU and the US: a review of current provisions. *Food Additives & Contaminants: Part A*, *34*(3), 335–355. <https://doi.org/10.1080/19440049.2016.1274431>
- Leydet, Y., Gavara, R., Petrov, V., Diniz, A. M., Jorge Parola, A., Lima, J. C., & Pina, F. (2012). The effect of self-aggregation on the determination of the kinetic and thermodynamic constants of the network of chemical reactions in 3-glucoside anthocyanins. *Phytochemistry*, *83*, 125–135. <https://doi.org/10.1016/j.phytochem.2012.06.022>
- Li, L., Zhang, M., Zhang, S., Cui, Y., & Sun, B. (2018). Preparation and Antioxidant Activity of Ethyl-Linked Anthocyanin-Flavanol Pigments from Model Wine Solutions. *Molecules*, *23*(5), 1066. <https://doi.org/10.3390/molecules23051066>
- Lopes, P., Richard, T., Saucier, C., Teissedre, P.-L., Monti, J.-P., & Glories, Y. (2007). Anthocyanone A: A Quinone Methide Derivative Resulting from Malvidin 3-O-Glucoside Degradation. *Journal of Agricultural and Food Chemistry*, *55*(7), 2698–2704. <https://doi.org/10.1021/jf062875o>
- Malien-Aubert, C., Dangles, O., & Amiot, M. J. (2001). Color Stability of Commercial Anthocyanin-Based Extracts in Relation to the Phenolic Composition. Protective Effects by Intra- and Intermolecular Copigmentation. *Journal of Agricultural and Food Chemistry*, *49*(1), 170–176. <https://doi.org/10.1021/jf000791o>
- Malien-Aubert, C., Dangles, O., & Amiot, M.-J. (2002). Influence of Procyanidins on the Color Stability of Oenin Solutions. *Journal of Agricultural and Food Chemistry*, *50*(11), 3299–3305. <https://doi.org/10.1021/jf011392b>

- Mateus, N., Oliveira, J., Haettich-Motta, M., & de Freitas, V. (2004). New Family of Bluish Pyranoanthocyanins. *Journal of Biomedicine and Biotechnology*, 2004(5), 299–305. <https://doi.org/10.1155/S1110724304404033>
- Mendoza, J., Basílio, N., Pina, F., Kondo, T., & Yoshida, K. (2018). Rationalizing the Color in Heavenly Blue Anthocyanin. A Complete Kinetic and Thermodynamic Study. *The Journal of Physical Chemistry. B*, 122(19), 4982–4992. <https://doi.org/10.1021/acs.jpccb.8b01136>
- Moloney, M., Robbins, R. J., Collins, T. M., Kondo, T., Yoshida, K., & Dangles, O. (2018). Red cabbage anthocyanins: The influence of d-glucose acylation by hydroxycinnamic acids on their structural transformations in acidic to mildly alkaline conditions and on the resulting color. *Dyes and Pigments*, 158, 342–352. <https://doi.org/10.1016/j.dyepig.2018.05.057>
- Montilla, E. C., Arzaba, M. R., Hillebrand, S., & Winterhalter, P. (2011). Anthocyanin Composition of Black Carrot (*Daucus carota* ssp. *sativus* var. *atrorubens* Alef.) Cultivars Antonina, Beta Sweet, Deep Purple, and Purple Haze. *Journal of Agricultural and Food Chemistry*, 59(7), 3385–3390. <https://doi.org/10.1021/jf104724k>
- Montilla, E. C., Hillebrand, S., Butschbach, D., Baldermann, S., Watanabe, N., & Winterhalter, P. (2010). Preparative Isolation of Anthocyanins from Japanese Purple Sweet Potato (*Ipomoea batatas* L.) Varieties by High-Speed Countercurrent Chromatography. *Journal of Agricultural and Food Chemistry*, 58(18), 9899–9904. <https://doi.org/10.1021/jf101898j>
- Nichelmann, L., & Bilger, W. (2017). Quantification of light screening by anthocyanins in leaves of *Berberis thunbergii*. *Planta*, 246(6), 1069–1082. <https://doi.org/10.1007/s00425-017-2752-2>
- Nkhili, E., Loonis, M., Mihai, S., Hajji, H. E., & Dangles, O. (2014). Reactivity of food phenols with iron and copper ions: binding, dioxygen activation and oxidation mechanisms. *Food & Function*, 5(6), 1186–1202. <https://doi.org/10.1039/C4FO00007B>
- Oliveira, J., Azevedo, J., Silva, A. M. S., Teixeira, N., Cruz, L., Mateus, N., & de Freitas, V. (2010). Pyranoanthocyanin Dimers: A New Family of Turquoise Blue Anthocyanin-Derived Pigments Found in Port Wine. *Journal of Agricultural and Food Chemistry*, 58(8), 5154–5159. <https://doi.org/10.1021/jf9044414>
- Ozkorucuklu, S. P., Beltrán, J. L., Fonrodona, G., Barrón, D., Alsancak, G., & Barbosa, J. (2009). Determination of Dissociation Constants of Some Hydroxylated Benzoic and Cinnamic Acids in Water from Mobility and Spectroscopic Data Obtained by CE-DAD. *Journal of Chemical & Engineering Data*, 54(3), 807–811. <https://doi.org/10.1021/jc800595x>
- Patras, A., Brunton, Nigel. P., O'Donnell, C., & Tiwari, B. K. (2010). Effect of thermal processing on anthocyanin stability in foods; mechanisms and kinetics of degradation. *Trends in Food Science & Technology*, 21(1), 3–11. <https://doi.org/10.1016/j.tifs.2009.07.004>
- Pereira, G. K., Donate, P. M., & Galembeck, S. E. (1997). Effects of substitution for hydroxyl in the B-ring of the flavylum cation. *Journal of Molecular Structure: THEOCHEM*, 392, 169–179. [https://doi.org/10.1016/S0166-1280\(97\)90395-X](https://doi.org/10.1016/S0166-1280(97)90395-X)
- Perron, N. R., & Bru maghim, J. L. (2009). A Review of the Antioxidant Mechanisms of Polyphenol Compounds Related to Iron Binding. *Cell Biochemistry and Biophysics*, 53(2), 75–100. <https://doi.org/10.1007/s12013-009-9043-x>
- Piffaut, B., Kader, F., Girardin, M., & Metche, M. (1994). Comparative degradation pathways of malvidin 3,5-diglucoside after enzymatic and thermal treatments. *Food Chemistry*, 50(2), 115–120. [https://doi.org/10.1016/0308-8146\(94\)90106-6](https://doi.org/10.1016/0308-8146(94)90106-6)

- Pina, F. (2014). Chemical Applications of Anthocyanins and Related Compounds. A Source of Bioinspiration. *Journal of Agricultural and Food Chemistry*, *62*(29), 6885–6897. <https://doi.org/10.1021/jf404869m>
- Pina, F., Melo, M. J., Laia, C. A. T., Parola, A. J., & Lima, J. C. (2012). Chemistry and applications of flavylum compounds: a handful of colours. *Chemical Society Reviews*, *41*(2), 869–908. <https://doi.org/10.1039/C1CS15126F>
- Quideau, S. (2011). *Plant Polyphenols: Chemical Properties, Biological Activities, and Synthesis*. *50*, 586 – 621. <https://doi.org/10.1002/anie.201000044>
- Roche, M., Dufour, C., Mora, N., & Dangles, O. (2005). Antioxidant activity of olive phenols : mechanistic investigation and characterization of oxidation products by mass spectrometry. *Organic & Biomolecular Chemistry*, *3*(3), 423–430. <https://doi.org/10.1039/B416101G>
- Rusishvili, M., Grisanti, L., Laporte, S., Micciarelli, M., Rosa, M., J. Robbins, R., Collins, T., Magistrato, A., & Baroni, S. (2019). Unraveling the molecular mechanisms of color expression in anthocyanins. *Physical Chemistry Chemical Physics*, *21*(17), 8757–8766. <https://doi.org/10.1039/C9CP00747D>
- Sadilova, E., Carle, R., & Stintzing, F. C. (2007). Thermal degradation of anthocyanins and its impact on color and in vitro antioxidant capacity. *Molecular Nutrition & Food Research*, *51*(12), 1461–1471. <https://doi.org/10.1002/mmfr.200700179>
- Sadilova, E., Stintzing, F. C., & Carle, R. (2006). Thermal Degradation of Acylated and Nonacylated Anthocyanins. *Journal of Food Science*, *71*(8), C504–C512. <https://doi.org/10.1111/j.1750-3841.2006.00148.x>
- Salgado Mendoza, P., Melin, V., Alborno, M., Mansilla, H., Vidal, G., & Contreras, D. (2017). Effects of pH and substituted 1,2-dihydroxybenzenes on the reaction pathway of Fenton-like systems. *Applied Catalysis B: Environmental*, *226*. <https://doi.org/10.1016/j.apcatb.2017.12.035>
- Satake, R., & Yanase, E. (2018). Mechanistic studies of hydrogen-peroxide-mediated anthocyanin oxidation. *Tetrahedron*, *74*(42), 6187–6191. <https://doi.org/10.1016/j.tet.2018.09.012>
- Seeram, N. P., Bourquin, L. D., & Nair, M. G. (2001). Degradation Products of Cyanidin Glycosides from Tart Cherries and Their Bioactivities. *Journal of Agricultural and Food Chemistry*, *49*(10), 4924–4929. <https://doi.org/10.1021/jf0107508>
- Shakeel, M., Jabeen, F., Shabbir, S., Asghar, M. S., Khan, M. S., & Chaudhry, A. S. (2016). Toxicity of Nano-Titanium Dioxide (TiO₂-NP) Through Various Routes of Exposure: a Review. *Biological Trace Element Research*, *172*(1), 1–36. <https://doi.org/10.1007/s12011-015-0550-x>
- Sigurdson, Gregory T., Robbins, R. J., Collins, T. M., & Giusti, M. M. (2018). Impact of location, type, and number of glycosidic substitutions on the color expression of o-dihydroxylated anthocyanidins. *Food Chemistry*, *268*, 416–423. <https://doi.org/10.1016/j.foodchem.2018.06.079>
- Sigurdson, G.T., Robbins, R. J., Collins, T. M., & Giusti, M. M. (2016). Evaluating the role of metal ions in the bathochromic and hyperchromic responses of cyanidin derivatives in acidic and alkaline pH. *Food Chemistry*, *208*, 26–34. <https://doi.org/10.1016/j.foodchem.2016.03.109>
- Sinela, A., Rawat, N., Mertz, C., Achir, N., Fulcrand, H., & Dormier, M. (2017). Anthocyanins degradation during storage of Hibiscus sabdariffa extract and evolution of its degradation products. *Food Chemistry*, *214*, 234–241. <https://doi.org/10.1016/j.foodchem.2016.07.071>
- Stebbins, N. B. (2016). Ascorbic acid-catalyzed degradation of cyanidin-3- O-β-glucoside: Proposed mechanism and identification of a novel hydroxylated product. *Journal of Berry Research*, *6*(2), 175–187. <https://doi.org/10.3233/JBR-160132>

- Taiz, L. (1992). The Plant Vacuole. *Journal of Experimental Biology*, 172(1), 113–122.
- Tanchev, S., & Ioncheva, N. (1976). Products of Thermal Degradation of the Anthocyanins Cyanidin-3-glucoside, Cyanidin-3-rutinoside and Cyanidin-3-sophoroside. *Food / Nahrung*, 20(10), 889–893. <https://doi.org/10.1002/food.19760201006>
- Teixeira, J., Gaspar, A., Garrido, E. M., Garrido, J., & Borges, F. (2013). Hydroxycinnamic Acid Antioxidants: An Electrochemical Overview. *BioMed Research International*, 2013, 1–11. <https://doi.org/10.1155/2013/251754>
- Terahara, N., Matsui, T., Minoda, K., Nasu, K., Kikuchi, R., Fukui, K., Ono, H., & Matsumoto, K. (2009). Functional New Acylated Sophoroses and Deglycosylated Anthocyanins in a Fermented Red Vinegar. *Journal of Agricultural and Food Chemistry*, 57(18), 8331–8338. <https://doi.org/10.1021/jf901809p>
- Tierno, R., & Galarreta, J. I. R. de. (2016). Influence of Selected Factors on Anthocyanin Stability in Colored Potato Extracts. *Journal of Food Processing and Preservation*, 40(5), 1020–1026. <https://doi.org/10.1111/jfpp.12682>
- Timberlake, C. F. (1980). Anthocyanins—Occurrence, extraction and chemistry. *Food Chemistry*, 5(1), 69–80. [https://doi.org/10.1016/0308-8146\(80\)90065-5](https://doi.org/10.1016/0308-8146(80)90065-5)
- Timberlake, C. F., & Bridle, P. (1982). Chapter 5 - Distribution of Anthocyanins in Food Plants. In P. Markakis (Ed.), *Anthocyanins As Food Colors* (pp. 125–162). Academic Press. <https://doi.org/10.1016/B978-0-12-472550-8.50009-3>
- Trouillas, P., Sancho-García, J. C., De Freitas, V., Gierschner, J., Otyepka, M., & Dangles, O. (2016). Stabilizing and Modulating Color by Copigmentation: Insights from Theory and Experiment. *Chemical Reviews*, 116(9), 4937–4982. <https://doi.org/10.1021/acs.chemrev.5b00507>
- Tsuda, T., Ohshima, K., Kawakishi, S., & Osawa, T. (1996). Oxidation products of cyanidin 3-O-β-d-glucoside with a free radical initiator. *Lipids*, 31(12), 1259. <https://doi.org/10.1007/BF02587910>
- Veberic, R., Jakopic, J., Stampar, F., & Schmitzer, V. (2009). European elderberry (*Sambucus nigra* L.) rich in sugars, organic acids, anthocyanins and selected polyphenols. *Food Chemistry*, 114(2), 511–515. <https://doi.org/10.1016/j.foodchem.2008.09.080>
- Veitch, N. C., & Grayer, R. J. (2011). Flavonoids and their glycosides, including anthocyanins. *Natural Product Reports*, 28(10), 1626–1695. <https://doi.org/10.1039/C1NP00044F>
- Wallace, T. C., & Giusti, M. M. (2013). *Anthocyanins in Health and Disease*. CRC Press.
- Wang, W., Jung, J., & Zhao, Y. (2017). Chitosan-cellulose nanocrystal microencapsulation to improve encapsulation efficiency and stability of entrapped fruit anthocyanins. *Carbohydrate Polymers*, 157, 1246–1253. <https://doi.org/10.1016/j.carbpol.2016.11.005>
- Wiczowski, W., Szawara-Nowak, D., & Topolska, J. (2013). Red cabbage anthocyanins: Profile, isolation, identification, and antioxidant activity. *Food Research International*, 51(1), 303–309. <https://doi.org/10.1016/j.foodres.2012.12.015>
- Winkel, B. S. J. (2006). The Biosynthesis of Flavonoids. In E. Grotewold (Ed.), *The Science of Flavonoids* (pp. 71–95). Springer New York. https://doi.org/10.1007/978-0-387-28822-2_3
- Wu, X., Beecher, G. R., Holden, J. M., Haytowitz, D. B., Gebhardt, S. E., & Prior, R. L. (2006). Concentrations of anthocyanins in common foods in the United States and estimation of normal consumption. *Journal of Agricultural and Food Chemistry*, 54(11), 4069–4075. <https://doi.org/10.1021/jf060300l>

- Yamasaki, H., Uefuji, H., & Sakihama, Y. (1996). Bleaching of the Red Anthocyanin Induced by Superoxide Radical. *Archives of Biochemistry and Biophysics*, *332*(1), 183–186. <https://doi.org/10.1006/abbi.1996.0331>
- Yoshida, K., Mori, M., & Kondo, T. (2009). Blue flower color development by anthocyanins : from chemical structure to cell physiology. *Natural Product Reports*, *26*(7), 884–915. <https://doi.org/10.1039/B800165K>
- Yoshida, K., Okuno, R., Kameda, K., Mori, M., & Kondo, T. (2003). Influence of E,Z-isomerization and stability of acylated anthocyanins under the UV irradiation. *Biochemical Engineering Journal*, *14*(3), 163–169. [https://doi.org/10.1016/S1369-703X\(02\)00217-6](https://doi.org/10.1016/S1369-703X(02)00217-6)
- Yoshida, K., Toyama, Y., Kameda, K., & Kondo, T. (2000). Contribution of each caffeoyl residue of the pigment molecule of gentiodelphin to blue color development. *Phytochemistry*, *54*(1), 85–92. [https://doi.org/10.1016/S0031-9422\(00\)00049-2](https://doi.org/10.1016/S0031-9422(00)00049-2)
- Yuan, D., Wang, C., Liu, Y., Lei, S., & Wen, Y. (2019). Mechanism Study of the Formation of Indigo Carmine–Aluminum Hydroxide Lake for Food Use. *Journal of Food Science*, *84*(11), 3129–3139. <https://doi.org/10.1111/1750-3841.14809>
- Zhang, J., Trossat-Magnin, C., Bathany, K., Delrot, S., & Chaudière, J. (2019). Oxidative Transformation of Leucocyanidin by Anthocyanidin Synthase from *Vitis vinifera* Leads Only to Quercetin. *Journal of Agricultural and Food Chemistry*, *67*(13), 3595–3604. <https://doi.org/10.1021/acs.jafc.8b06968>

Chapter 2. The influence of acylation, metal binding and natural antioxidants on the thermal stability of red cabbage anthocyanins in neutral solution

Julie-Anne Fenger,^a Micheal Moloney,^a Rebecca J. Robbins,^b Tom M. Collins,^c
Olivier Dangles^{a*}

^a J.-A. Fenger, M. Moloney, O. Dangles, Avignon University, INRA, UMR408, 84000 Avignon, France.

^b R. J. Robbins, Mars Wrigley Confectionery, 1132 W Blackhawk Street, Chicago, IL 60642, USA

^c T. M. Collins, Mars Wrigley Confectionery, 800 High St., Hackettstown, NJ 07840, USA

Food &
Function




PAPER

[View Article Online](#)
[View Journal](#)



Cite this: DOI: 10.1039/c9fo01884k

The influence of acylation, metal binding and natural antioxidants on the thermal stability of red cabbage anthocyanins in neutral solution†

Julie-Anne Fenger,^a Micheal Moloney,^a Rebecca J. Robbins,^b Thomas M. Collins^c
and Olivier Dangles  ^{a*}

Abstract

The main red cabbage anthocyanins (pigments) are cyanidin glycosides bearing one or two acyl groups derived from hydroxycinnamic acids (HCAs). Through π -stacking interactions with the cyanidin chromophore, the HCA residues have a deep influence on the color expressed and its stability. In this work, a series of non-, mono- and diacylated anthocyanins were investigated in neutral solution (pH 7 and 8), where the pigments exhibit purple to blue colors. Under such conditions, the gradual color loss observed is a combination of two distinct processes involving the cyanidin nucleus: reversible water addition and irreversible autoxidation. By acidification to $\text{pH} < 2$, the colorless forms stemming from water addition (hemiketal and chalcones) are converted to the red flavylum ion, thereby permitting the selective monitoring of the irreversible contribution. The kinetics of color loss and of true pigment degradation could thus be recorded for each pigment. The influence of iron – cyanidin binding and of antioxidants (caffeic acid, N-acetylcysteine) was also investigated. A complete kinetic analysis combining the anthocyanin colored and colorless forms and the degradation products is provided. Overall, it appears that acylation is critical to color stability. For instance, the nonacylated pigment is rapidly bleached as a result of fast water addition and its iron complex is too unstable to provide protection. By contrast, the diacylated pigments are efficiently protected against hydration but much more moderately against autoxidation, which on the other hand is inhibited by efficient iron binding and addition of N-acetylcysteine. Finally, the diacylated pigments are much more resistant to bleaching by hydrogen peroxide (possibly produced by cyanidin autoxidation) and bisulfite (a common food preservative).

1. INTRODUCTION

Anthocyanins (plant pigments) whose glycosyl moieties are acylated by hydroxycinnamic acid (HCA) residues (Scheme 1) are known to exhibit more stable colors than their nonacylated counterparts. (L. Li et al., 2018; Matera et al., 2015; Moloney et al., 2018) This color stability is observed across the range of food-compatible pHs (from 2 to 8), making acylated anthocyanins from edible sources promising candidates for development as natural red, purple and blue food colors.

HCA residues contribute to color stability through π -stacking interactions with the anthocyanidin chromophore (evidenced by long-range correlations in NOESY NMR spectra) and, depending on anthocyanin structure, involves individual anthocyanin molecules (intramolecular copigmentation) or noncovalent dimers (self-association) and possibly higher oligomers. (Pyysalo & Kuusi, 1973; Trouillas et al., 2016a) The prevalence of intramolecular copigmentation or self-association is governed by the shape of the acylated sugar (*e.g.*, extended *vs.* more compact disaccharides), the acylation site (on a given sugar) and the site at which the acylated sugar is attached to the chromophore. (Pyysalo & Kuusi, 1973) Through these π -stacking interactions, the flavylum nucleus is protected against the reversible addition of water at the hard electrophilic site C2, which yields the colorless hemiketal and chalcone forms (Scheme 2). Generally, the presence of a second HCA residue brings a larger increase in color stability than the first one, which is attributed to π -stacking interactions developing on both sides of the chromophore within a "sandwich-like" structure. (Dangles et al., 1993c; Moloney et al., 2018) Moreover, anthocyanidin - HCA interactions promotes bathochromic shifts in the pigments' visible absorption band and thus also participate in color variation.

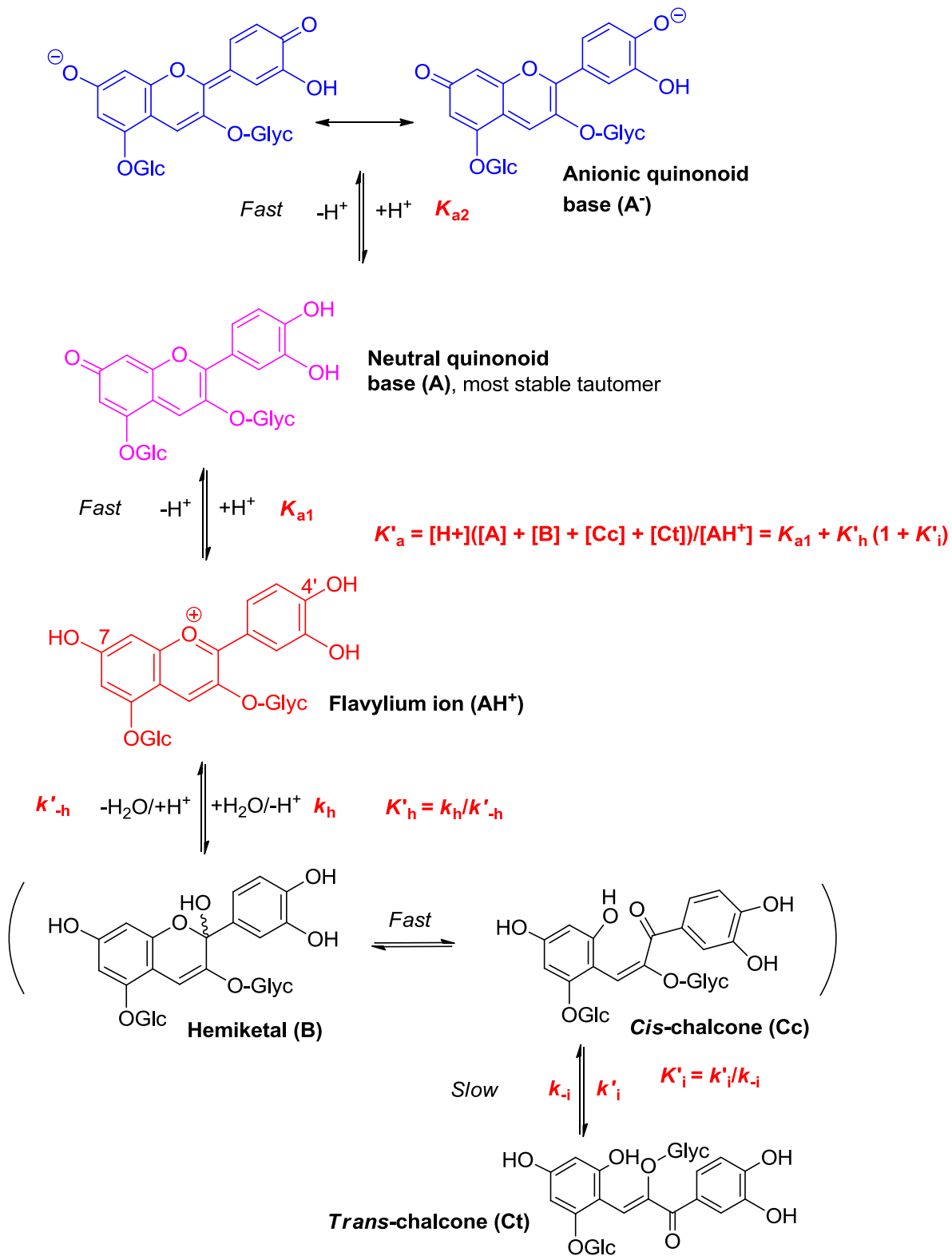
Besides pH and copigmentation / self-association, the color of anthocyanins can be modulated by metal cations. (G.T. Sigurdson et al., 2016) For instance, owing to their catechol group (B-ring), cyanidin glycosides can bind Fe^{2+} , Fe^{3+} and Al^{3+} . Due to concomitant proton loss and increased electron delocalization, metal - anthocyanin binding also triggers a bathochromic shift of the visible absorption band (up to +100 nm at pH 6). (Pyysalo & Kuusi, 1973; G.T. Sigurdson et al., 2016; Trouillas et al., 2016a)

Color loss during industrial food processing can be due to other nucleophiles than water, namely bisulfite (a common food preservative) and hydrogen peroxide. The latter may be formed upon the autoxidation of oxygen-sensitive compounds, such as L-ascorbate and plant phenols bearing a catechol or pyrogallol ring, like caffeic and gallic acids.⁸ The soft bisulfite

ion reversibly adds to the soft electrophilic site C4 of the flavylum cation, yielding a chromen-4-sulfonate.⁹ To limit the oxidative degradation of anthocyanins at neutral pH, antioxidants, such as thiols, can be used. For instance, glutathione (0.5 g L⁻¹) increases the stability of anthocyanins in blackberry juice.¹⁰

In neutral solution, acylated anthocyanins from red and purple varieties of vegetables (red cabbage, purple sweet potato, purple cauliflower) have great potential for use as blue colors. Red cabbage is particularly interesting for its high content (> 80%) in acylated anthocyanins,¹¹ particularly in diacylated anthocyanins (37% in the extract studied in this work), known for their higher color stability. While the color stability of anthocyanins has been broadly studied, their irreversible degradation in near neutral solution is still poorly documented. Under neutral conditions, acylated anthocyanins display a higher fraction of neutral and anionic quinonoid bases (the major colored forms at pH 6 - 8) than nonacylated anthocyanins, which are predominantly under the hemiketal and chalcone forms. (Moloney et al., 2018) At pH > 7, the anionic base becomes the major colored form and a significant fraction of anionic chalcone may also be present.^{12,13} Both anionic species are probably much better electron donors, and thus more vulnerable to autoxidation (nonenzymatic oxidation by O₂ under the mediation of transition metal traces), than the corresponding neutral forms. The overall rate of anthocyanin degradation is thus expected to reflect the initial distribution of colored and colorless forms, as well as their relative sensitivity to the oxidative/hydrolytic pathways leading to colorless products.

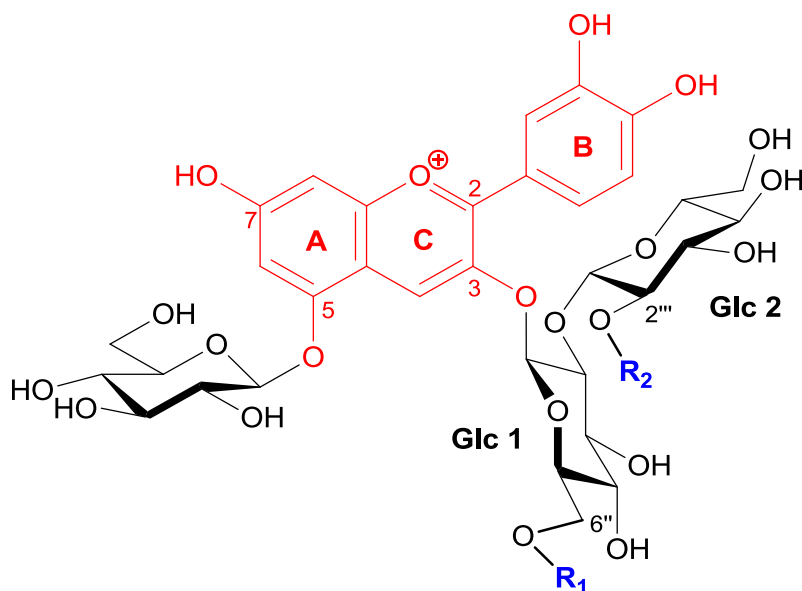
In this work, a selection of red cabbage anthocyanins (RCAs, mostly, pigments A, 1 and 4, see Scheme 1), from nonacylated to diacylated, has been investigated for its thermal stability in neutral dilute solution (pH 7 or 8). The kinetics of color loss and true anthocyanin degradation have been monitored in the presence or absence of added Fe²⁺ and of two common antioxidants caffeic acid and N-acetylcysteine (NAC). The corresponding curves have been quantitatively analyzed to extract kinetic parameters and information on the mechanisms at work. The influence of acylation a) on the reversible or irreversible color loss, and b) on the susceptibility of the cyanidin chromophore to nucleophilic attack by bisulfite or H₂O₂, is discussed.



Scheme 2. Structural transformations of anthocyanins in acidic to neutral aqueous solution.

2. MATERIALS AND METHODS

Anthocyanins were studied in dilute aqueous solutions (typically, 50 μM), thus minimizing self-association.



Pigment	R ₁	R ₂
A	H	H
1	<i>p</i> -Coumaroyl (R = R' = H)	H
2	Feruloyl (R = OMe, R' = H)	H
4	<i>p</i> -Coumaroyl	Sinapoyl
5	Feruloyl	Sinapoyl
6	Sinapoyl (R = R' = OMe)	Sinapoyl

Scheme 1. The red cabbage anthocyanins studied in this work.

2.1. Chemicals

Individual red cabbage anthocyanins (isolated and characterized according to previously reported procedures¹⁴) and the red cabbage extract (RCE) were provided by Mars Wrigley Confectionery (Hackettstown, NJ, USA). Based on UPLC/DAD analysis (data not shown), RCE contains *ca.* 7% pigment A (noted PA), 56% monoacylated anthocyanins and 37% diacylated anthocyanins, a composition in good agreement with the literature.¹¹ Stock solutions (5 mM) of pigment were prepared in aqueous 0.01 M HCl (pH \approx 2). Cyanin (cyanidin-3,5-O-diglucoside), N-acetylcysteine, caffeic acid, NaHSO₃, aqueous H₂O₂,

FeSO₄·7H₂O, NaH₂PO₄·2H₂O and Na₂HPO₄·7H₂O were all purchased from Sigma-Aldrich Co. HPLC-grade water was used in all experiments. RCE was purified on a Bondelut C18 cartridge. Solvents for purification contained 0.01 M HCl. The extract was washed with 2 volumes of water, 2 volumes of MeOH/H₂O (15/85) and eluted with MeOH/H₂O (30/70). The anthocyanin fractions were mixed, concentrated under vacuum and lyophilized. A 6 mM solution of the purified RCE fraction (in cyanin equivalent) was prepared in aqueous 0.05 M HCl (pH ≈ 1.3).

2.2. UV-visible spectroscopy

Absorption spectra were recorded on diode-array spectrometers (Agilent 8453 or Specord S600) in thermostated magnetically stirred quartz cuvettes (1 cm pathlength).

2.3. Thermal degradation

Thermal degradation was performed at 50°C in sealed pyrex bottles protected from light to avoid photodegradation and placed in a thermostated water bath. At time zero, the anthocyanin was diluted to 50 μM directly in the preheated 10 mM phosphate buffer. Aliquots were taken up at time zero and at regular time intervals over 8h and finally at 24h. The samples were immediately cooled in an ice bath to stop the thermal degradation. As a control in the absence of degradation, the UV-visible spectrum of the pigment was recorded after dilution to 50 μM in 0.05 M HCl.

For degradation experiments with added Fe²⁺, a stock Fe²⁺ solution in aqueous 1 mM HCl (pH ≈ 3) was freshly prepared and a small volume added to a final concentration of 0.6 molar equivalent *vs.* anthocyanin. The binding was fast and accompanied by the development of a large visible band in the range 600 – 750 nm characteristic of the iron-pigment complex. (G.T. Sigurdson et al., 2016) The selected Fe²⁺ concentration was sufficient to reach near maximal binding while minimizing the concentration of unbound iron ions in solution.

The thermal degradation experiments were performed in triplicate for P1 and P4 at pH 7, and in duplicate for pigment A. The degradation in the presence of antioxidants and under modified atmosphere were performed once. To establish the modified atmosphere, series of freeze/thaw cycles were performed with the buffer in a Schlenk tube, enabling full degassing. Argon was then added to atmospheric pressure. Stock solutions (15 mM) of antioxidants

(caffeic acid, N-acetylcysteine) in aqueous 1 mM HCl (pH \approx 3) were prepared and added (antioxidant/anthocyanin molar ratio = 3) to the anthocyanin solution at $t = 0$.

2.4. Kinetics of color loss and anthocyanin degradation

The fraction of residual colored forms in the heated near neutral solution was calculated as $X_n = A_{\max}(t)/A_{\max}(0)$ and plotted *vs.* time. For assessing the true anthocyanin degradation (irreversible component of the observed color loss), the aliquots were then acidified to pH \sim 1.2 with 2M HCl for conversion of all anthocyanin forms (colored + colorless) into the flavylium ion. A UV-visible spectrum was recorded after 1 min, allowing the fast regeneration of the flavylium ion from the quinonoid bases, hemiketal and *cis*-chalcone. However, as the *cis-trans* isomerization of chalcones is very slow, especially with acylated anthocyanins,¹⁵ much longer periods of time are required for the overall conversion of the *trans*-chalcone into the flavylium ion. Monitoring flavylium regeneration at pH 1.2 over up to 140h at 25°C showed that at least 80% of the final plateau value was reached after 48h for both P1 and P4. Hence, a second spectrum was recorded 48h after acidification to determine the residual flavylium concentration. The residual fraction of flavylium ion X_a was calculated as for X_n and plotted *vs.* time.

For experiments with added Fe^{2+} , the spectra were simply recorded 1 min after acidification to avoid further pigment degradation. Indeed, Fe^{2+} autoxidation to Fe^{3+} is fast in near neutral solution⁸ and Fe^{3+} thus formed is an oxidant at low pH. Fortunately, independent UPLC-DAD analysis (data not shown) revealed that iron binding largely inhibits the formation of the *trans*-chalcone. Hence, in experiments with added Fe^{2+} , a 1 min-period is sufficient to ensure the conversion of most colorless forms into the flavylium ion.

2.5. Additions of hydrogen peroxide and bisulfite

Red cabbage anthocyanins were compared in bleaching tests involving sodium bisulfite (5 equiv.) and hydrogen peroxide (10^3 equiv., *i.e.* a large excess to achieve a strong color loss in less than 1h). To that purpose, 1.5 mL of phosphate buffer (10 mM, pH 7) were placed into the spectrometer cell and a small volume of a concentrated stock solution of anthocyanin was rapidly added (final concentration = 50 μM), immediately followed by a small volume of concentrated aqueous H_2O_2 (0.6 M) or sodium bisulfite (0.015 M). Spectra were recorded immediately every 2 to 5 s over 50 min with H_2O_2 , and every 0.5 s over 1 min with bisulfite.

2.6. Kinetics of trans-chalcone isomerization

In a first step, the *trans*-chalcones (Ct) of PA, P1, P4 and of the whole red cabbage extract were accumulated by heating at 50°C, pH 7 for 2h. This duration was sufficient to provide significant Ct concentrations, while limiting the rate of irreversible degradation. Then, aliquots were cooled down and acidified to pH 1 by concentrated HCl. UV-visible spectra showing the regeneration of the flavylum ion were recorded every hour over 7 days and the visible absorbance plotted as a function of time.

2.7. Mathematical analysis

The Scientist[®] software (Micromath, Salt Lake City, USA) was used for all curve-fitting calculations. Most curves of color loss could be analyzed according to a first-order model. The apparent rate constant (k_{obs}) and absorbance amplitude (ΔA) were calculated. For the kinetics in the presence of Fe^{2+} and for the irreversible degradation kinetics, a biexponential model was used, yielding one set of parameters ($k_1, \Delta A_1$) for the fast component and another one ($k_2, \Delta A_2$) for the slow component.

The Scientist[®] software was also used for the simultaneous analysis of the fractions of colored (X_n), colorless hydrated (X_h) and colorless degraded (X_d) species. A kinetic model assuming an apparent first-order for the degradation pathways was built (eqns (1) – (3)) and used for the simultaneous curve-fitting analysis of the time-dependence of the three fractions.

$$-dX_n/dt = (k_{DA} + k_h)X_n - k_{-h}X_h \quad (1)$$

$$-dX_h/dt = (k_{DB} + k_{-h})X_h - k_hX_n \quad (2)$$

$$dX_d/dt = k_{DA}X_n + k_{DB}X_h \quad (3)$$

The procedure gave access to the optimized values of the four adjustable parameters: the rate constants of apparent hydration (k_h) and dehydration (k_{-h}), and the rate constants of irreversible degradation for the colored forms (k_{DA}) and for the colorless forms (k_{DB}). As the calculation provided negligible values for k_{DB} , this rate constant was set at zero for the final assessment of the other three rate constants.

3. RESULTS & DISCUSSION

In red cabbage anthocyanins, acylation occurs on the compact sophorosyl moiety (Glc- β -1,2-Glc) at C3-OH, more specifically at C6 of the internal Glc (HCA = *p*-coumaric, ferulic or sinapic acid) and/or at C2 of the external Glc (HCA = sinapic acid) (Scheme 1). (Matera et al., 2015; Moloney et al., 2018; Torskangerpoll & Andersen, 2005)⁶ The latter sinapoyl residue is critical to the sensitivity of RCAs to water addition. (Moloney et al., 2018) The structure of acylated RCAs favors the conformational folding of the HCA residues onto the cyanidin nucleus, known as intramolecular copigmentation. (Pyysalo & Kuusi, 1973; Trouillas et al., 2016a) Self-association may also contribute to the color stability of acylated anthocyanins, as evidenced by the circular dichroism spectra of the diacylated red cabbage pigments in mildly alkaline aqueous solution, which display a Cotton effect in the visible range. (Moloney et al., 2018) Based on the Cotton effect intensity, self-association increases with the number of methoxyl groups on the internal acyl residue (within the *p*-coumaric, ferulic, sinapic series). These π -stacking interactions have a huge impact on the pH-dependent distribution of colored and colorless forms and are thus expected to deeply modulate both color stability and the rate of the pigments' thermal degradation.

3.1. Color loss and true anthocyanin degradation

The curves of color loss for PA, P1 and P4 were built by sampling over 8h (Fig. 1A). As expected, the color of diacylated P4 is much more stable than that of monoacylated P1, itself more stable than that of nonacylated PA, in agreement with the literature. (Moloney et al., 2018) A more accurate spectroscopic monitoring over 2h (Fig. 1A-SI) gave the following first-order rate constants of color loss at pH 7: 6.9 h⁻¹ for PA, 4.1 h⁻¹ for P1 and 0.8 h⁻¹ for P4 (Table 1-SI).

At pH 8, P1 color was more stable ($t_{1/2}$ = 1.5 h) than at pH 7 ($t_{1/2}$ = 0.4 h) (data not shown). The same trend is observed with P4 ($t_{1/2}$ = 7.0 h at pH 8 vs. 3.8 h at pH 7). However, the opposite holds for P6 ($t_{1/2}$ = 5.6 h at pH 8 vs. 6.0 h at pH 7). The faster degradation of P6 at pH 8 might reflect the higher sensitivity to autoxidation of the second electron-rich sinapoyl residue. Moreover, in control experiments at pH 7 and 8, sinapic acid was actually rapidly consumed with concomitant formation of covalent dimers (evidenced by UPLC-DAD-MS analysis, data not shown) whereas *p*-coumaric acid was mostly unchanged.

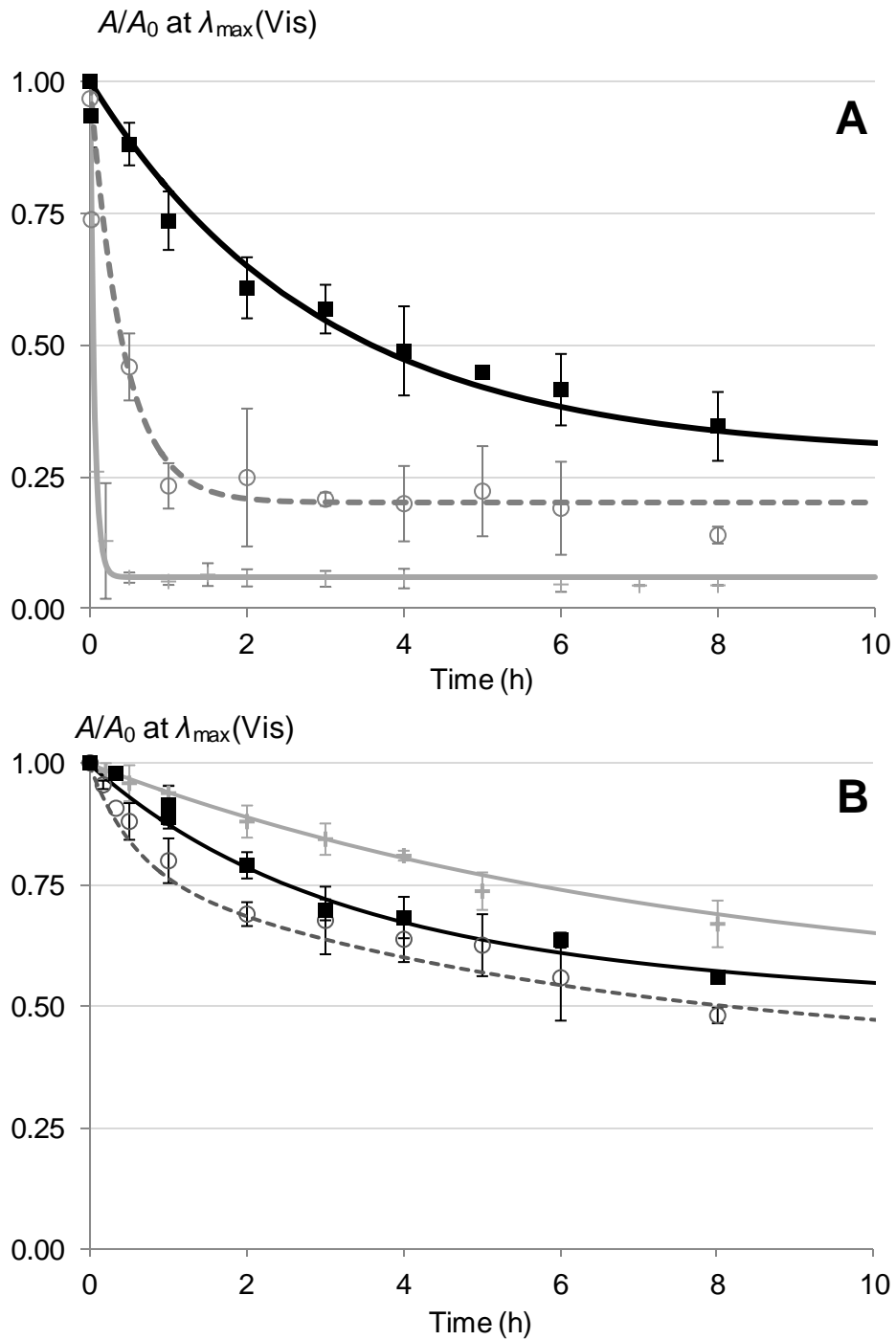


Fig. 1. A: Color loss at pH 7, 50°C. Pigment A (+), P1 (○), P4 (■). **B:** Anthocyanin loss (residual flavylium ion after acidification to pH 1 – 2 and 48h stabilization at room temperature).

The color loss observed likely results from a combination of the reversible water addition (and subsequent isomerization reactions, Scheme 2) and of irreversible reactions that are expected to be slower than the hydration process under acidic conditions but could actually compete with it under neutral conditions. Indeed, water addition is very slow at pH 7 – 8, as the electrophilic flavylum ion is in trace amounts, and autoxidation is probably relatively fast, as electron-rich anthocyanin forms (mostly, the anionic base, but also the chalcone anion) are present. The residual color of the solutions after 24h at pH 7, 50°C was pale yellow for PA, light blue/violet for P1, and blue/violet for P4 and P6.

Among the structural transformations of anthocyanins (Scheme 2), water addition (hydration) is the step that is most critically influenced by acylation. Indeed, π -stacking interactions (intramolecular copigmentation and/or self-association) slow down the nucleophilic addition of water at C2 and consequently lower k_h and thus K'_h and the global acidity constant K'_a .¹

The distribution diagrams of the colored and colorless species are represented on Fig. 2 for pigment A, P1 and P4. For PA, water addition to AH^+ is much more favorable than proton loss, and the neutral base A does not accumulate. By contrast, for P4, under mildly acidic conditions, the neutral base A is more abundant than the global pool of colorless forms. An intermediate situation is observed with P1 (the neutral base can accumulate but remains less abundant than the hemiketal and chalcones). At equilibrium at pH 7, the colored forms (a near 1:1 mixture of neutral and anionic bases) are essentially absent with PA and represent no more than 15% with P1. By contrast, they remain largely dominant (*ca.* 80%) with P4. However, these percentage values are theoretical (deduced from K'_a , K_{a1} and K_{a2}) because the kinetics of water addition is very slow at pH 7, meaning that the equilibrium state is not reached before the onset of irreversible reactions combining hydrolysis and autoxidation. Indeed, AH^+ is the sole electrophilic species susceptible to react with water. Hence, the apparent rate constant of water addition can be expressed as eqn. (4) (χ_{AH} = mole fraction of AH^+ within the mixture of colored forms in fast equilibrium, $h = [H^+]$):

$$k_{obs} = k_h \chi_{AH} + k'_{-h} h = \frac{k_h}{1 + K_{a1}/h + K_{a1}K_{a2}/h^2} + k'_{-h} h \quad (4)$$

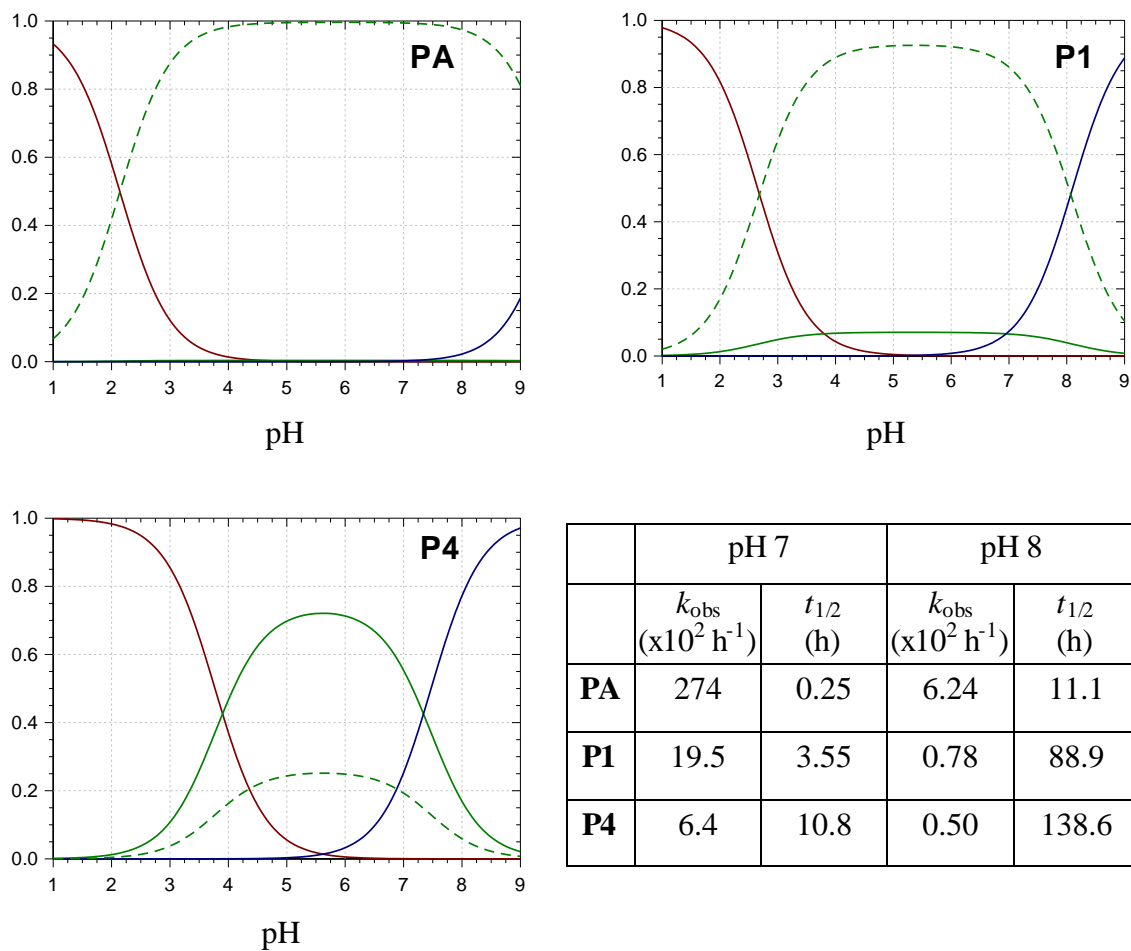


Fig. 2. Distribution diagrams for pigments A, 1 and 4 at equilibrium. —: flavylium ion, —: neutral base, —: anionic base, - - -: colorless forms (25°C). Calculated apparent rate constants of water addition (from eqn. (4) in text) and corresponding half-life values at 25°C.

Eqn (4) (in fact, a simplified version neglecting the 2nd proton transfer) can be used to estimate pK_{a1} , k_h and k'_{-h} from experiments conducted in the pH range 3 – 5 where hydration is relatively fast and degradation negligible. (Moloney et al., 2018) However, it can also be used for estimating the apparent rate constant of pure hydration (in absence of degradation) under neutral conditions (Fig. 2). For instance, calculated k_{obs} values at pH 7, 25°C were estimated at 0.20 h⁻¹ for P1 and 0.06 h⁻¹ for P4. Under the same conditions, the experimental curves recorded upon direct spectroscopic monitoring over 2h required biexponential analysis for quantitative exploitation, which suggests more complex processes combining hydration and degradation. The rate constants of the fast component were estimated at 1.42 h⁻¹ for P1 and 0.32 h⁻¹ for P4 (Table 1-SI), *i.e.* 6 – 7 times larger than the theoretical values assuming pure hydration. Therefore, it is clear that degradation participates from the start in the slow color loss observed under neutral conditions.

The contribution of irreversible reactions to the global color loss observed under neutral conditions is fully confirmed by cooling the samples to room temperature, acidifying them to pH 1-2, waiting for the complete conversion of the residual colored and colorless forms to the flavylum ion, and eventually plotting the final flavylum concentration as a function of time (Fig. 1B). The decays now observed only reflect the irreversible component of the color loss recorded at pH 7 and 50°C. Interestingly, the differences between the pigments are not significant, suggesting that if the acyl residues are efficient at protecting the cyanidin nucleus against the reversible addition of water, they seem much less efficient at inhibiting the irreversible pathways leading to cyanidin degradation. In other words, π -stacking interactions prevent anthocyanins from water addition but may not protect them against oxidative degradation. Thus, the differences in the rates of color loss between acylated and nonacylated anthocyanins would be mostly attributable to differences in susceptibility to the reversible water addition. A more complete kinetic analysis (see below) permits to refine the interpretations.

3.2. Chalcone isomerization

Upon heating at 50°C, the *trans*-chalcone (usually a minor colorless form at room temperature) readily accumulates at pH 7 (as evidenced by UPLC-DAD analysis, data not shown). After sample uptake, cooling to room temperature and acidification to pH 1 – 2 for spectroscopic titration of the residual flavylum ion, the residual *trans*-chalcone was still

observed after a 1h incubation at room temperature. Indeed, the slowest step in the structural transformations of anthocyanins is the *cis-trans* isomerization of chalcones.^{12,13} To accurately quantify the true degradation of anthocyanins, the full recovery of the flavylium ion is required. The rate of chalcone isomerization was thus determined for PA, P1 and P4 after accumulating the colorless forms over 2h at pH 7, 50°C.

Following the pH jump, the kinetics during the first 30s shows the fast regeneration of the flavylium ion from the hemiketal and *cis*-chalcone (Table 1, Scheme 3). Then, the very slow Ct isomerization was monitored over up to 3 days to reach the plateau corresponding to full flavylium regeneration (Fig. 2-SI). With the 3 major anthocyanins studied, a 48h period is sufficient to convert *ca.* 80% of the residual anthocyanins into the flavylium ion. Acylation has a significant impact on the rate of flavylium regeneration at room temperature. It is higher with PA ($k_{\text{obs}} = 0.11 \text{ h}^{-1}$) than with P1 and P4 ($k_{\text{obs}} \approx 0.03 - 0.04 \text{ h}^{-1}$). Surprisingly, chalcone isomerization with pigment A (cyanidin-3-sophoroside-5-glucoside, $t_{1/2} \approx 5\text{h}$) is much slower than with malvin (malvidin-3,5-diglucoside, $t_{1/2} = 17.5 \text{ min}$),¹² meaning that the bulky sophorosyl moiety strongly inhibits the reaction. With the sterically hindered Heavenly blue anthocyanin (a sophorose moiety at C3-OH acylated by 3 glucosylated caffeoyl residues), chalcone isomerization is even much slower than with RCAs, requiring more than 2 weeks for complete flavylium regeneration.(J. Mendoza et al., 2018)

From absorbance measurements along the process of heating over 2h at pH 7, acidification and kinetic monitoring of the *trans*-chalcone \rightarrow flavylium conversion (Scheme 3), the distribution at pH 7 of the colored forms (a mixture of neutral and anionic bases in fast acid-base equilibrium), hemiketal + *cis*-chalcone (in fast cycle-chain equilibrium), *trans*-chalcone and degradation products (D) could be estimated for PA, P1 and P4 (Table 1). As expected, after 2h at pH 7, 50°C, the percentage of residual colored forms is much higher for the acylated pigments (*ca.* 36% for P4 *vs.* 7% for PA) and the reverse holds for the colorless hydrated forms (resp. *ca.* 16 and 6 % of B + Cc and Ct for P4 *vs.* *ca.* 39 and 21% for pigment A). However, the protection against hydration exerted by the HCA residues apparently does not extend to autoxidation and the percentage of degradation is even slightly higher for P4 (42%) than for PA and P1 (34%).

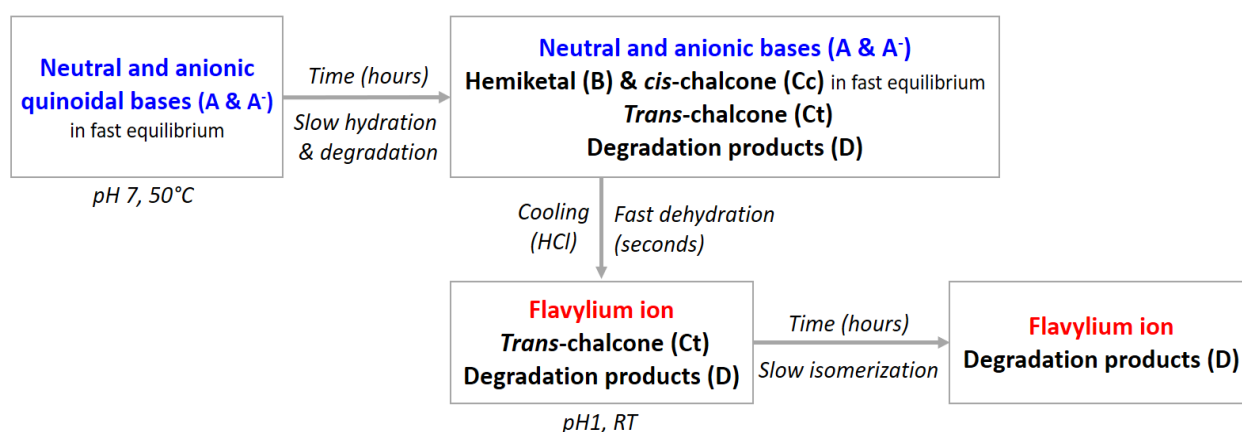
Table 1. Distribution of colored forms / hemiketal + *cis*-chalcone / *trans*-chalcone / degradation products (D) after 2h of heating at 50°C, pH 7 for pigment A, P1 and P4. First part of Table 1 gathers molar absorption coefficients and absorbance values used in the calculations.^a

	$\epsilon_{\text{AH}}(\text{pH } 1)^b$	$\epsilon_{\text{obs}}(\text{pH } 7)^b$	A_1^c	A_7^d	A_{li}^e	A_{lf}^f
PA	21990	10400	1.17	0.036	0.531	0.776
P1	16590	9400	0.906	0.104	0.435	0.597
P4	17620	11000	1.15	0.259	0.601	0.665

	C_{tot}	[A + A ⁻], %	[AH ⁺] _i	[AH ⁺] _f	[D], %	[Ct], %	[B + Cc], %
PA	53.2	3.5, 6.6	24.1	35.3	17.9, 33.6	11.1, 20.9	20.7, 38.9
P1	54.6	11.1, 20.3	26.2	36.0	18.6, 34.0	9.8, 17.9	15.2, 27.8
P4	65.3	23.5, 36.1	34.1	37.7	27.5, 42.2	3.6, 5.5	10.6, 16.2

^a All concentrations in μM , ϵ values in $\text{M}^{-1} \text{cm}^{-1}$. ^b Values estimated from our previous work.¹

^c pH 1, no degradation. ^d pH 7 after 2h at 50°C. ^e pH 1, initial value just after acidification. ^f pH 1, final value. *Method:* concentrations are deduced from the following relationships: $A_1 = \epsilon_{\text{AH}} C_{\text{tot}} \Rightarrow C_{\text{tot}}$; $A_{\text{lf}} = \epsilon_{\text{AH}} [\text{AH}^+]_{\text{lf}} \Rightarrow [\text{AH}^+]_{\text{lf}}$; $C_{\text{tot}} = [\text{AH}^+]_{\text{lf}} + [\text{D}] \Rightarrow [\text{D}]$; $A_{\text{li}} = \epsilon_{\text{AH}} [\text{AH}^+]_{\text{li}} \Rightarrow [\text{AH}^+]_{\text{li}}$; $C_{\text{tot}} = [\text{AH}^+]_{\text{li}} + [\text{Ct}] + [\text{D}] \Rightarrow [\text{Ct}]$; $A_7 = \epsilon_{\text{obs}} [\text{A} + \text{A}^-] \Rightarrow [\text{A} + \text{A}^-]$; $C_{\text{tot}} = [\text{A} + \text{A}^-] + [\text{B} + \text{Cc}] + [\text{Ct}] + [\text{D}] \Rightarrow [\text{B} + \text{Cc}]$.



Scheme 3. The protocol for assessing the distribution of species in a neutral anthocyanin sample after thermal treatment.

3.3. Metal binding

Addition of Fe^{2+} (1 equiv.) to a solution of anthocyanin in dilute phosphate buffer (pH 7) results in the fast development of a large low-energy visible band characteristic of the complex (Fig. 3A). The binding is accompanied by the fast autoxidation of Fe^{2+} to Fe^{3+} (confirmed by the observation that the final spectra are identical after addition of Fe^{2+} or Fe^{3+}), as already observed with other polyphenols having a catechol nucleus.⁸ Total iron binding is achieved at low metal/anthocyanin molar ratio (< 1 , Fig. 3B), which suggests the formation of complexes in which several anthocyanin molecules are bound to metal ions (*e.g.*, 1:2 and 1:3 Fe^{3+} - anthocyanin complexes or higher aggregates). Surprisingly, although the HCA residues are not expected to strongly interact with metal ions, the complex's visible band is more intense with P5 than with P2 or PA, and the λ_{max} value is much higher (650 nm *vs.* 590 nm, Fig. 3A). On the other hand, self-association of the cyanidin nuclei under neutral conditions (evidenced by Cotton bands in the visible circular dichroism spectra) is much more important with the diacylated red cabbage anthocyanins than with their non- and monoacylated counterparts. (Moloney et al., 2018) Hence, it may be speculated that iron-anthocyanin aggregates are more easily formed from P5 than from P2 or PA. Under these conditions, no precipitation of the complexes was observed over a storage period of 3 months at room temperature.

The half-life of color for the Fe^{2+} complexes of P1 and P4 is respectively 4 and 7 times larger than that of the free pigments (Figs 4B & 1B-SI). With their quinonoid structure, the metal complexes do not undergo water addition, and are probably less prone to autoxidation. A similar strong color stabilization was obtained with the whole RCA extract. For P6, although Fe^{2+} increases the half-life of color by only a factor 2-3 (a possible consequence of the higher oxidizability of the sinapoyl - *vs.* *p*-coumaroyl - moiety), the strong influence of Fe^{2+} on the color expressed and its stability is obvious (Fig. 5). By contrast, no color stabilization is observed with PA (Fig. 4A). Again, HCA residues are critical to the stability of the iron complexes (possibly by promoting the formation of aggregates) and the corresponding color.

Diacylated P4 only has a slightly higher thermal stability in the presence of iron ions (Fig. 4D), again suggesting that the color stabilization observed at pH 7 mostly reflects a protection against hydration, rather than against true (irreversible) degradation. By contrast, P1 and even more so PA (Fig. 4C) are more rapidly degraded following Fe^{2+} addition. This suggests that P4 efficiently sequesters iron ions (possibly within aggregates of high

stoichiometry), while leakage of iron ions from the weaker complexes formed with PA and P1 may initiate autoxidation.

In the acidified samples, the wavelength of the flavylum absorption maximum decreased by up to 9 nm for diacylated P6 over 24h at pH 7, 50°C, *vs.* only 5 nm for P4, and less than 1 nm for P1 and PA. This hypsochromic shift is ascribed to the partial hydrolysis of the hydroxycinnamoyl residues (confirmed by UPLC-DAD-MS analysis, data not shown). As expected, the decrease in $\lambda_{\max}(\text{AH}^+)$ was larger at pH 8 than at pH 7 (P4: -8 nm at pH 8), pointing to a faster deacylation at higher pH, in agreement with the base-catalyzed hydrolysis of ester bonds. With P4, the addition of Fe^{2+} cancelled the hypsochromic shift. The strong iron – P4 binding could thus inhibit the deacylation reaction. On the whole anthocyanin extract, Fe^{2+} accelerated the irreversible degradation in agreement with the dominant contribution of non- and monoacylated pigments (representing 64% of the anthocyanins). Overall, Fe^{2+} ions exert a dual impact on red cabbage anthocyanins: on the one hand, it stabilizes the blue color of acylated pigments by forming stable complexes that prevent the oxidation of the anionic bases and the hydrolysis of the acyl moieties. On the other hand, loosely bound Fe^{2+} promotes the irreversible degradation of non- and monoacylated pigments.

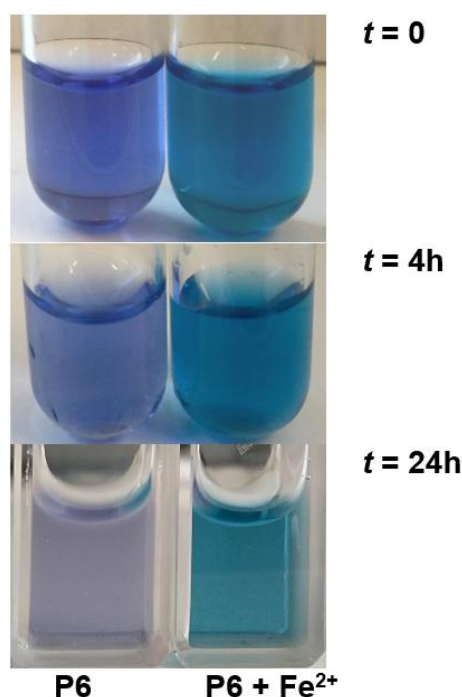


Fig. 5. Color changes in P6 solutions at pH 7, 50°C following addition of Fe^{2+} (0.6 equiv.) and storage over 24h (pigment concentration = 50 μM).

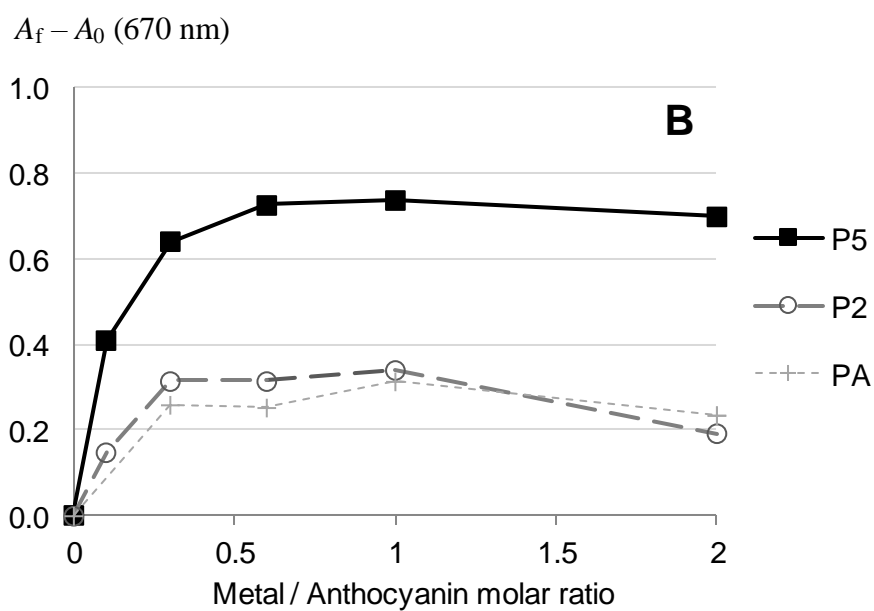
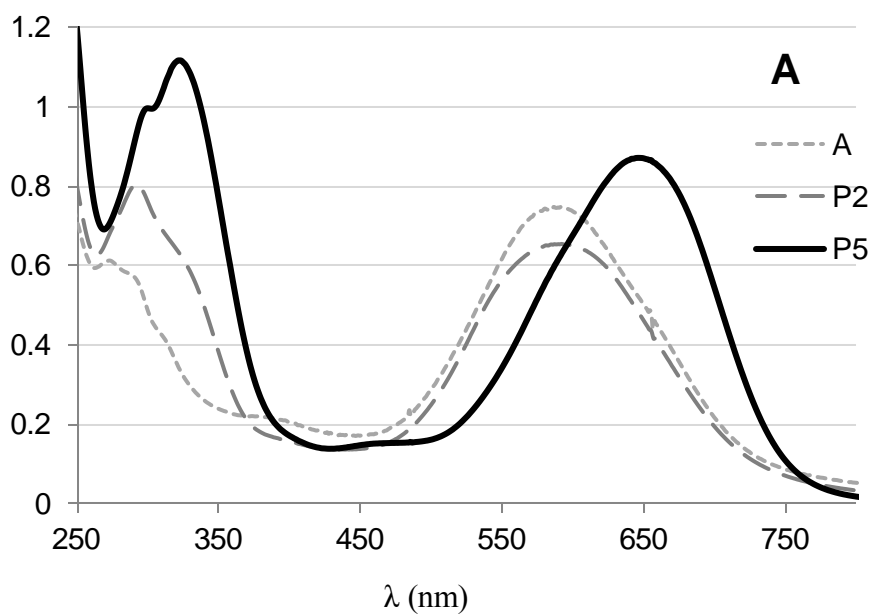


Fig. 3. **A:** Spectra of the iron complexes of pigment A, P2 and P5 (1 equiv. Fe^{2+} , pH 7, 25°C). **B:** Maximal amplitude in the development of the iron complex's visible band as a function of the metal/pigment molar ratio.

3.4. Impact of dioxygen and antioxidants

To inhibit the irreversible degradation of anthocyanins, naturally occurring antioxidants (caffeic acid, N-acetylcysteine), an inert atmosphere and a metal-chelating buffer (citrate) were tested. As expected, when the samples were heated under rarefied O₂ conditions (argon atmosphere), pigment degradation was much slower (see Fig. 4C for PA). This is evidence for the contribution of oxidative degradation pathways.

Caffeic acid (3 equiv.) has essentially no impact on both color and pigment content, although a slight destabilization could be detected in the long term (> 24h, data not shown). Similar observations were made with other phenols bearing catechol or pyrogallol groups (protocatechuic acid, methylgallate). Under the present conditions (pH 7, 50°C), caffeic acid can produce H₂O₂ upon autoxidation⁸ and this pro-oxidant effect could cancel out the expected antioxidant protection.

More interestingly, NAC (5 equiv.), while having no influence on the color stability of PA (governed by the hydration kinetics, Fig. 4A), exerts a strong protection against its degradation (Fig. 4C). As P4 is much less sensitive to water addition than pigment A, its color loss at pH 7 has a strong irreversible component (autoxidation), which is significantly inhibited by NAC (Fig. 4B). This protection is confirmed in the acidified samples (Fig. 4D). Overall, NAC inhibits anthocyanin degradation at pH 7 but this favorable influence is translated into a more stable color only for the acylated anthocyanins that are efficiently protected against hydration.

A similar stabilization by thiols was observed with blackcurrant anthocyanins at pH 7. Glutathione, dihydrolipoid acid and L-cysteine enabled to double the residual amount of anthocyanins after 4h at 37°C. The effect was stronger with the anthocyanins that are more susceptible to oxidation (delphinidin > cyanidin).¹⁷ The antioxidant effect of NAC may be ascribed to its ability to reduce reactive oxygen species (including H₂O₂) involved in anthocyanin autoxidation.¹⁸

Finally, citrate (10 mM) added to the phosphate buffer slowed down the irreversible degradation of PA (70% residual pigment at t = 24h, vs. only 40% in pure phosphate buffer, data not shown), a likely consequence of its ability to chelate unidentified transition metal traces initiating cyanidin autoxidation. Although still poorly documented, the combination of metal-chelating buffers and thiols has potential for stabilizing anthocyanin colors in food matrices.

A/A_0 at $\lambda_{\max}(\text{Vis})$

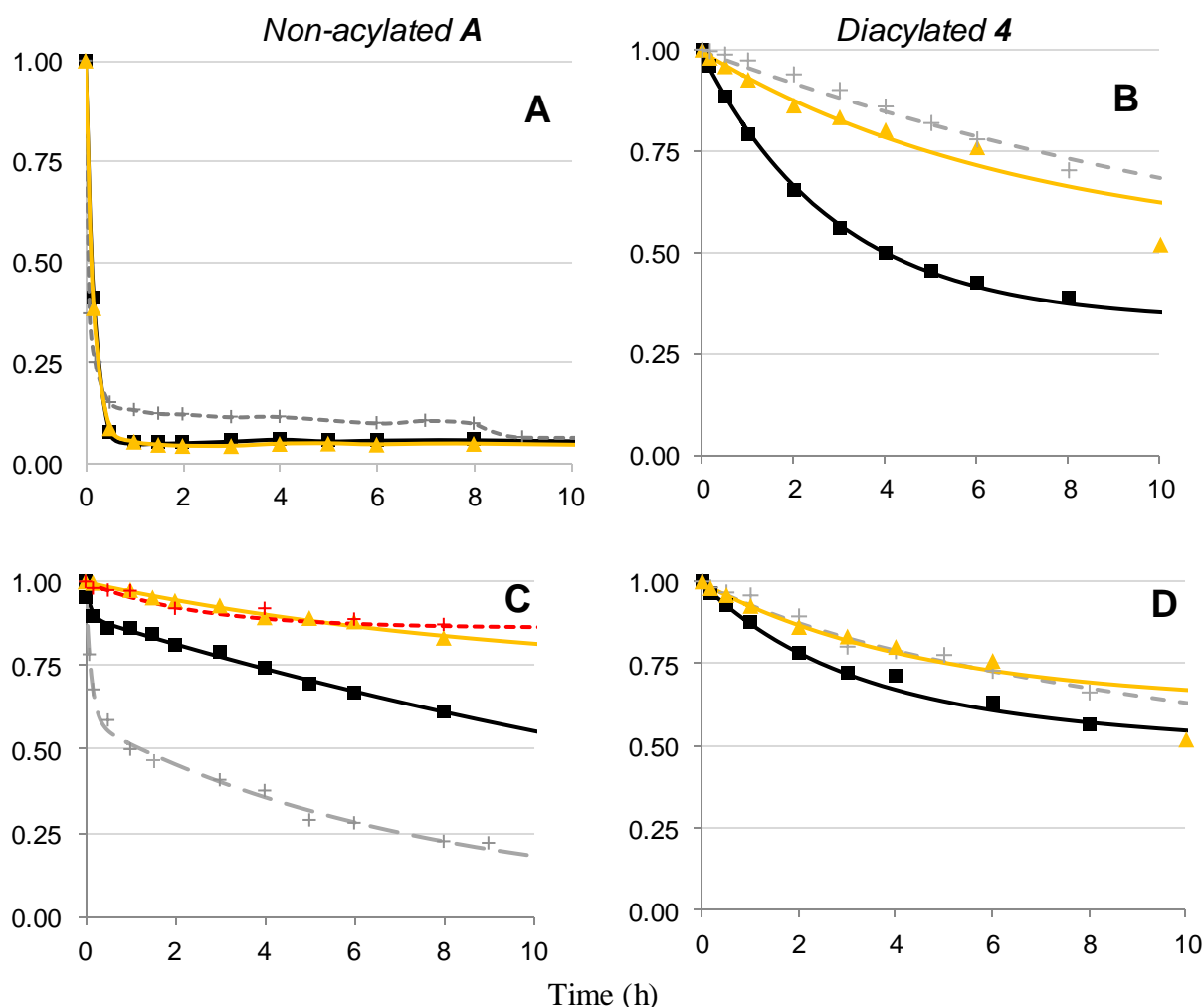


Fig. 4. A & B: Color loss at pH 7, 50°C. C & D: Residual fraction of anthocyanin (colored + colorless forms, spectroscopic titration in acidified samples after 1 h-incubation at RT) at pH 7, 50°C. Pigment alone (■), pigment + 0.6 equiv. Fe^{2+} (+), pigment + 5 equiv. NAC (▲). A & C: PA, under argon (+). B & D: P4.

3.5. Impact of acylation on the addition of hydrogen peroxide and bisulfite

The presence of aromatic acyl moieties protects the flavylium from the nucleophilic addition of water. (Moloney et al., 2018) At pH 7, two other common nucleophiles possibly involved in anthocyanin bleaching were tested: a hard one, hydrogen peroxide, reacting at C2,¹⁹ and a soft one, the bisulfite ion, reacting at C4.⁹ Recently, H_2O_2 was also proposed to react as an electrophile at C3 of the nucleophilic hemiketal.²⁰

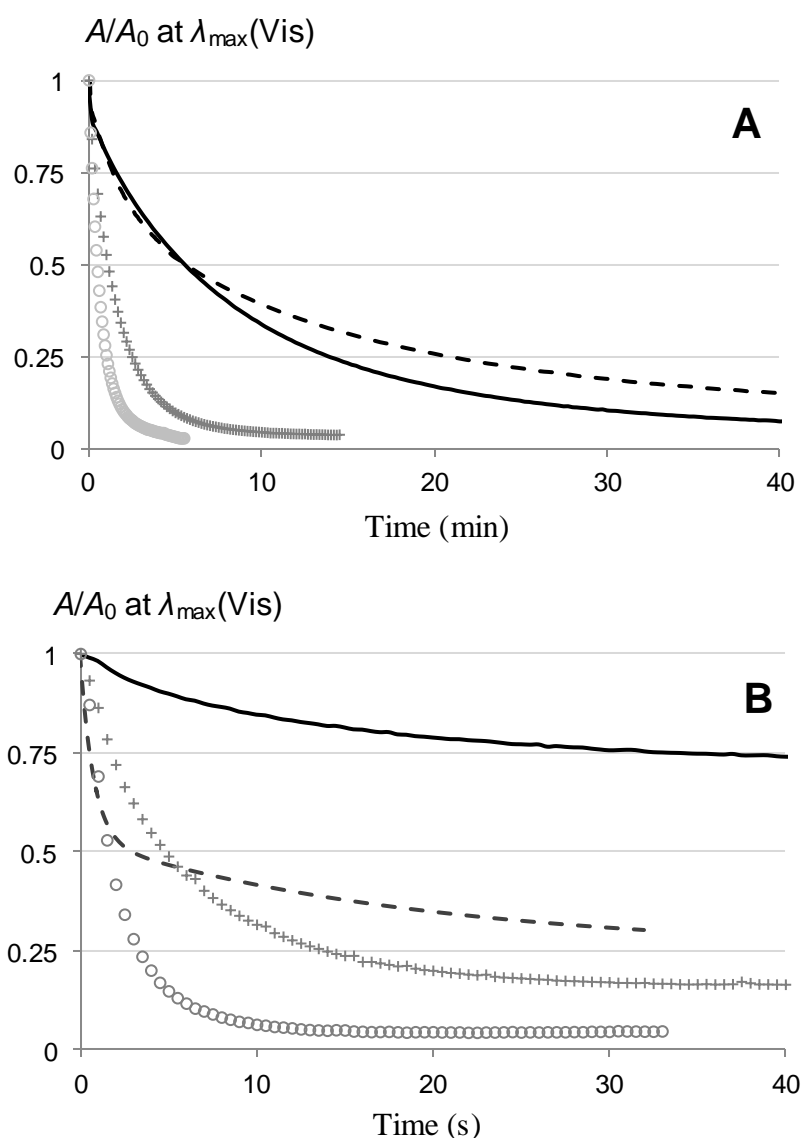


Fig. 6. Kinetics of bleaching (pH 7, room temperature). **A:** After addition of H_2O_2 (10^3 equiv.). **B:** After addition of sodium bisulfite (5 equiv.). \circ : PA, $+$: P2, $—$: P5, $- -$: red cabbage extract.

At pH 7, bisulfite adds to cyanidin much more rapidly than H_2O_2 (Fig. 6). As expected, the presence of aromatic acyl groups clearly hinders the addition of both nucleophiles. Compared with nonacylated PA, P5 reacts with H_2O_2 (10^3 equiv.) 11 times less rapidly, *vs.* only 4.8 times for P2 (Table 2). For P5 and P2, the color loss following the addition of bisulfite (5 equiv.) is 6.7 and 2.7 times faster than for PA, respectively. In the case of the fully reversible bisulfite addition, the acyl groups shift the position of the equilibrium toward the colored forms, whose percentage is 73% for P5, 17% for P2 and 4.6% for PA. The corresponding binding constants could be estimated (Table 2), showing that the affinity of

bisulfite for P5 is decreased by a factor 74 compared to PA, *vs.* only a factor 4.4 for P2. These stabilization factors are of the same magnitude as for the rate constant of water addition, which is respectively 29 and 2 times smaller for P5 and P2 than for PA. (Moloney et al., 2018) These observations show that acyl groups protect the cyanidin chromophore against nucleophilic additions, not only at C2 (hard nucleophiles) but also at C4 (soft nucleophiles).

3.6. Refined kinetic analysis

For each thermal degradation, two kinetics were monitored: a) the color loss (fraction of colored species at pH 7, noted X_n), and b) the irreversible degradation (fraction of residual flavylum recovered after acidification to pH 1 and 48h of stabilization, noted X_a). At pH 7, both the hydrated and degraded forms (respective fractions = X_h and X_d) contribute to the species distribution and one has: $X_n + X_h + X_d = 1$. After acidification to pH 1, the colored forms (a mixture of neutral and anionic bases at pH 7) and the hydrated forms are both converted into the flavylum ion (fraction X_a) and one now has: $X_a + X_d = 1$. After direct spectroscopic determination of X_n and X_a (*e.g.*, from curves on Fig. 1A and Fig. 1B, resp.), X_h and X_d can be easily calculated: $X_h = X_a - X_n$, $X_d = 1 - X_a$. The apparent rate constants of hydration (k_h) and dehydration (k_{-h}), and the rate constants of irreversible degradation for the colored forms (k_{DA}) and the colorless forms (k_{DB}) can be estimated from the simultaneous curve-fitting of X_n , X_h and X_d *vs.* time according to eqns (1) – (3) (Scheme 4, Table 3). The calculations provided negligible values for k_{DB} for all samples. This is an indication that under neutral conditions the colorless forms undergo minor degradation. An example of kinetic analysis (P1, pH 7) is shown on Fig. 7.

Table 2. Rate constants of hydrogen peroxide (10^3 equiv.) and bisulfite (5 equiv.) addition to anthocyanins at pH 7, room temperature.

Pigment	k_{obs} (s^{-1})	X_{eq} (%) ^a	K (M^{-1})	k_{obs} (min^{-1})
	Bisulfite	Bisulfite	Bisulfite	H ₂ O ₂
PA	0.40	4.6	1.0×10^5	1.46 (± 0.01)
P2	0.16 (± 0.02)	17	2.3×10^4	0.63 (± 0.01)
P5	0.06 (± 0.01)	73	1.6×10^3	0.13 (± 0.01)
RCE ^b	0.44 ± 0.04	37		1.33 (± 0.03)
	0.05 ± 0.04			0.05 (± 0.01)

^a Percentage of residual anthocyanin at equilibrium ($N = 3$).

^b Biexponential decay ($N = 3$).

Table 3. Kinetic analysis of thermal degradation at 50°C. Apparent rate constants k_{DA} , k_h and k_{-h} refer to the degradation of the colored forms, and to the hydration and dehydration steps, respectively.

k (h^{-1})	Pigment A	P1	P4
k_{DA} ($\times 10^{-3}$), pH 7	546 (± 39)	193 (± 13)	83 (± 5)
k_h , pH 7	14.0 (± 0.5)	1.77 (± 0.12)	0.14 (± 0.02)
k_{-h} , pH 7	1.16 (± 0.10)	0.58 (± 0.06)	0.20 (± 0.06)
k_{DA} ($\times 10^{-3}$), pH 8	-	411 (± 58)	85 (± 3)
k_h , pH 8	-	1.4 (± 0.3)	22 (± 3) $\times 10^{-3}$
k_{-h} , pH 8	-	0.61 (± 0.18)	^c
k_{DA} ($\times 10^{-3}$), pH 7 + Fe^{2+} ^a	5110 (± 380) ^b	218 (± 11)	62 (± 5)
k_h , pH 7 + Fe^{2+} ^a	6.41 (± 0.47) ^b	0.56 (± 0.10)	^c
k_{-h} , pH 7 + Fe^{2+} ^a	0.39 (± 0.03) ^b	0.80 (± 0.17)	^c

^a Fe^{2+} /anthocyanin molar ratio = 0.6. ^b Additional adjustable parameter = fraction of Fe^{2+} -bound colored forms = 0.11 (± 0.01). ^c Too low to estimate.

The data of Table 3 permit to distinguish the impacts of the acyl groups on hydration (rate constant k_h) and on degradation (rate constant k_{DA}) and thereby to refine the interpretations. As expected, acyl groups markedly slow down water addition, k_h for diacylated P4 being smaller by 2 orders of magnitude than for nonacylated PA. However, despite the almost superimposed curves featuring flavylum consumption for PA, P1 and P4 (Fig. 1B), acylation does protect the cyanidin chromophore against degradation, k_{DA} for P4 being smaller by a factor 6 - 7 than for PA. This paradox can be explained from eqn (5) governing the time dependence of the flavylum fraction $X_a = X_h + X_n$ (degradation of colorless forms neglected, $k_{DB} = 0$):

$$-dX_a/dt = k_{DA}X_n \quad (5)$$

If acylation actually inhibits degradation (lower k_{DA}), it also inhibits hydration (higher fraction of colored forms at pH 7, X_n). Hence, compensation in the $k_{DA}X_n$ product results in similar rates of flavylum consumption, irrespective of the acylation pattern. In other words, under neutral conditions, the nonacylated anthocyanin benefits from a relative protection by being more rapidly converted into colorless hydrated forms, as the latter are much more

resistant to degradation than the colored forms. Overall, it seems clear that π -stacking interactions involving the acylated anthocyanins not only hinder water addition (and other nucleophilic addition to the C-ring) but also protect the cyanidin nucleus against degradation. This complex process must start by electron transfer from the anionic base to O_2 under the mediation of transition metal traces (autoxidation). Hydrogen peroxide thus produced would then rapidly add to the cyanidin nucleus, followed by the irreversible formation of colorless products.^{19,20} As shown in this work, HCA residues actually slow down H_2O_2 addition. Our kinetic analysis also suggests that they, at least moderately, inhibit cyanidin autoxidation. If H_2O_2 is indeed a key intermediate in the irreversible degradation of anthocyanins, then the slight reduction in the rate of irreversible degradation observed in this work may result from the hindrance of H_2O_2 addition onto the chromophore. Data in Table 3 also suggest that the double positive effect of acylation (slower hydration, slower degradation) is maintained at pH 8 and in the presence of Fe^{2+} .

The $Q_h = k_h/k_{-h}$ ratio is the apparent thermodynamic constant of the global hydration equilibrium under neutral conditions. From a simple manipulation of the global and individual acidity constants, one can write:

$$Q_h = \frac{k_h}{k_{-h}} = \frac{[B] + [Cc] + [Ct]}{[A] + [A^-]} = \frac{K'_a / K_{a1} - 1}{1 + K_{a2} / h} \quad (6)$$

The Q_h values at pH 7, either calculated from eqn (6) at 25°C (using the literature values for the acidity constants (Moloney et al., 2018)) or experimentally determined at 50°C, are actually very different: $Q_h(25^\circ C) = 173, 16.3$ and 4.0 vs. $Q_h(50^\circ C) = 12, 3.1$ and 0.7 for PA, P1 and P4, respectively. Although the temperature difference precludes rigorous comparison, it seems that our kinetic model leads to underestimate Q_h . Kinetic simulations show that assuming a participation of the colorless forms in the degradation ($k_{DB} \neq 0$) permits to correct this discrepancy (Figs. 3&4-SI). More specifically, decreasing the rate constant of dehydration (with concomitant increase of Q_h by a factor *ca.* 10) while introducing a rate constant for the degradation of the colorless forms *ca.* 10 times smaller than for the colored forms gave curves close to experiment.

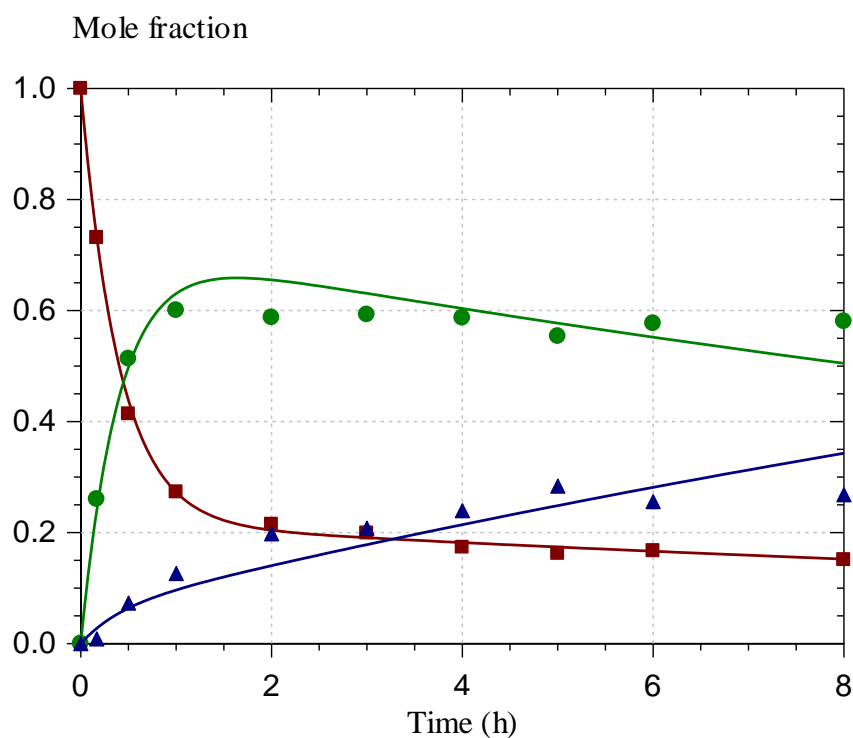
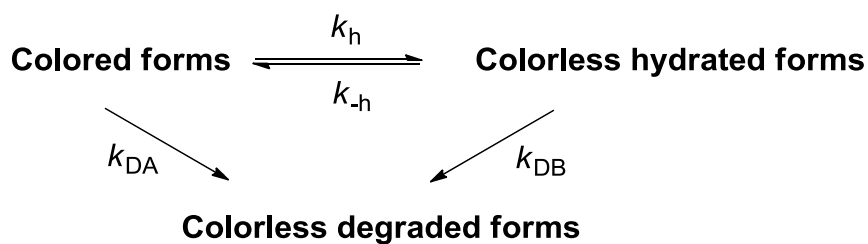


Fig. 7. Kinetic analysis of the thermal stability of P1 at pH 7, 50°C. X_n (■, fraction of colored forms): $r = 0.999$, X_h (●, fraction of colorless hydrated forms): $r = 0.982$, X_d (▲, fraction of colorless degradation products): $r = 0.942$. Curve-fitting according to eqns (1) – (3) gave the following optimized rate constants: $k_{DA} = 0.193 (\pm 0.013)$, $k_h = 1.77 (\pm 0.12)$, $k_{-h} = 0.58 (\pm 0.06) \text{ h}^{-1}$.



Scheme 4. A simplified kinetic scheme for analyzing the thermal degradation of anthocyanins in neutral solution.

Conclusions

In summary, modulating pH around neutrality and adding metal ions permit to achieve stable blue colors with diacylated red cabbage anthocyanins. Acylation not only protects the cyanidin nucleus against water addition but also against bleaching by H₂O₂ and the bisulfite ion. Compared to the nonacylated pigment, these favorable effects concur to making the color of acylated anthocyanins (especially the diacylated ones) much more stable under neutral conditions. Paradoxically, during degradation, the total pool of anthocyanin forms (colored + colorless) is largely unaffected by acylation because the colorless forms, more abundant with the nonacylated anthocyanin, are also more resistant to autoxidation.

For an improved stabilization, the priority should be set at protecting the electron-rich anionic base against autoxidation. Strategies based on natural phenolic antioxidants seem limited given the susceptibility of such compounds to autoxidation (with concomitant H₂O₂ production), turning them into pro-oxidants. More promising alternatives include a) tight binding to hard metal ions, which lowers the electron density of the chromophore, b) the use of natural thiols and chelating buffers (as long as metal binding is not considered), possibly in combination.

Conflicts of interest

There are no conflicts to declare.

REFERENCES

- 1 M. Moloney, R. J. Robbins, T. M. Collins, T. Kondo, K. Yoshida and O. Dangles, Anthocyanins: the influence of D-glucose acylation by hydroxycinnamic acids on their structural transformations in acidic to mildly alkaline conditions and on the resulting color, *Dyes Pigm.*, 2018, 158, 342–352.
- 2 E. Sadilova, R. Carle, F. C. Stintzing, Thermal degradation of anthocyanins and its impact on color and in vitro antioxidant capacity, *Mol. Nutr. Food Res.*, 2007, 51, 1461–1471.
- 3 F. C. Stintzing, A. S. Stintzing, R. Carle, B. Frei and R. E. Wrolstad, Color and antioxidant properties of cyanidin-based anthocyanin pigments, *J. Agric. Food Chem.*, 2002, 50, 6172–6181.

- 4 K. Yoshida, M. Mori and T. Kondo, Blue flower color development by anthocyanins: from chemical structure to cell physiology, *Nat. Prod. Rep.*, 2009, 26, 884–915.
- 5 P. Trouillas, J. C. Sancho-García, V. De Freitas, J. Gierschner, M. Otyepka and O. Dangles, Stabilizing and modulating color by copigmentation: insights from theory and experiment, *Chem. Rev.*, 2016, 116, 4937–4982.
- 6 O. Dangles, N. Saito and R. Brouillard, Kinetic and thermodynamic control of flavylum hydration in the pelargonidin-cinnamic acid complexation. Origin of the extraordinary flower color diversity of *Pharbitis nil*, *J. Am. Chem. Soc.*, 1993, 115, 3125–3132.
- 7 G. T. Sigurdson, R. J. Robbins, T. M. Collins and M. M. Giusti, Evaluating the role of metal ions in the bathochromic and hyperchromic responses of cyanidin derivatives in acidic and alkaline pH, *Food Chem.*, 2016, 208, 26–34.
- 8 E. Nkhili, M. Loonis, S. Mihai, H. E. Hajji and O. Dangles, Reactivity of food phenols with iron and copper ions: binding, dioxygen activation and oxidation mechanisms, *Food Funct.*, 2014, 5, 1186–1202.
- 9 B. Berké, C. Chèze, J. Vercauteren and G. Deffieux, Bisulfite addition to anthocyanins: revisited structures of colourless adducts, *Tetrahedron Lett.*, 1998, 39, 5771–5774.
- 10 N. B. Stebbins, L. R. Howard, R. L. Prior, C. Brownmiller and A. Mauromoustakos, Stabilization of anthocyanins in blackberry juice by glutathione fortification, *Food Funct.*, 2017, 8, 3459–3468.
- 11 P. Mizgier, A. Z. Kucharska, A. Sokół-Lętowska, J. Kolniak-Ostek, M. Kidoń and I. Fecka, Characterization of phenolic compounds and antioxidant and anti-inflammatory properties of red cabbage and purple carrot extracts, *J. Funct. Foods*, 2016, 21, 133–146.
- 12 F. Pina, M. J. Melo, C. A. T. Laia, A. J. Parola and J. C. Lima, Chemistry and applications of flavylum compounds: a handful of colours, *Chem. Soc. Rev.*, 2012, 41, 869–908.
- 13 F. Pina, Chemical applications of anthocyanins and related compounds. A source of bioinspiration, *J. Agric. Food Chem.* 2014, 62, 6885–6897.
- 14 N. Ahmadiani, R. J. Robbins, T. M. Collins and M. M. Giusti, Molar absorptivity (ϵ) and spectral characteristics of cyanidin-based anthocyanins from red cabbage, *Food Chem.*, 2016, 197, 900–906.
- 15 J. Mendoza, N. Basílio, F. Pina, T. Kondo and K. Yoshida, Rationalizing the color in Heavenly blue anthocyanin: A complete kinetic and thermodynamic study, *J. Phys. Chem. B*, 2018, 122, 4982–4992.
- 16 K. Torskangerpoll and Ø. M. Andersen, Colour stability of anthocyanins in aqueous solutions at various pH values, *Food Chem.*, 2005, 89, 427–440.
- 17 T. Eidenberger, Stabilized anthocyanin compositions, US patent 20120328755A2, 2012.
- 18 Y. Samuni, S. Goldstein, O. M. Dean and M. Berk, The chemistry and biological activities of N-acetylcysteine, *Biochim. Biophys. Acta - Gen. Subj.*, 2013, 1830, 4117–4129.
- 19 P. Lopes, T. Richard, C. Saucier, P.-L. Teissedre, J.-P. Monti and Y. Glories, Anthocyanone A: A quinone methide derivative resulting from malvidin 3-O-glucoside degradation, *J. Agric. Food Chem.*, 2007, 55, 2698–2704.
- 20 R. Satake and E. Yanase, Mechanistic studies of hydrogen-peroxide-mediated anthocyanin oxidation, *Tetrahedron*, 2018, 74, 6187–6191.

Chapter 2.

The influence of acylation, metal binding and natural antioxidants on the thermal stability of red cabbage anthocyanins in neutral solution

SUPPLEMENTARY INFORMATION

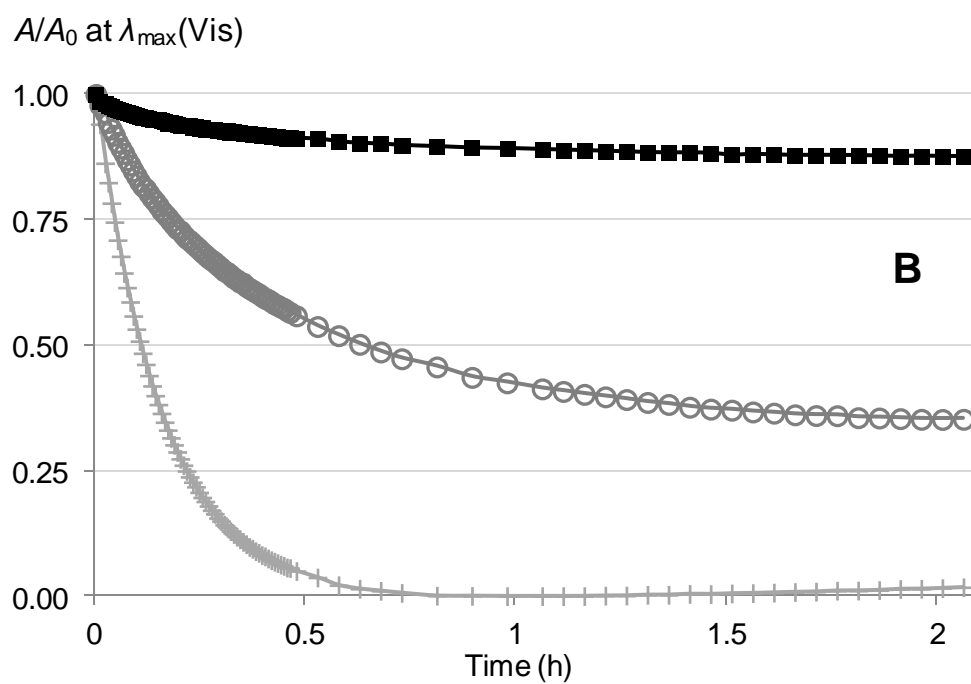
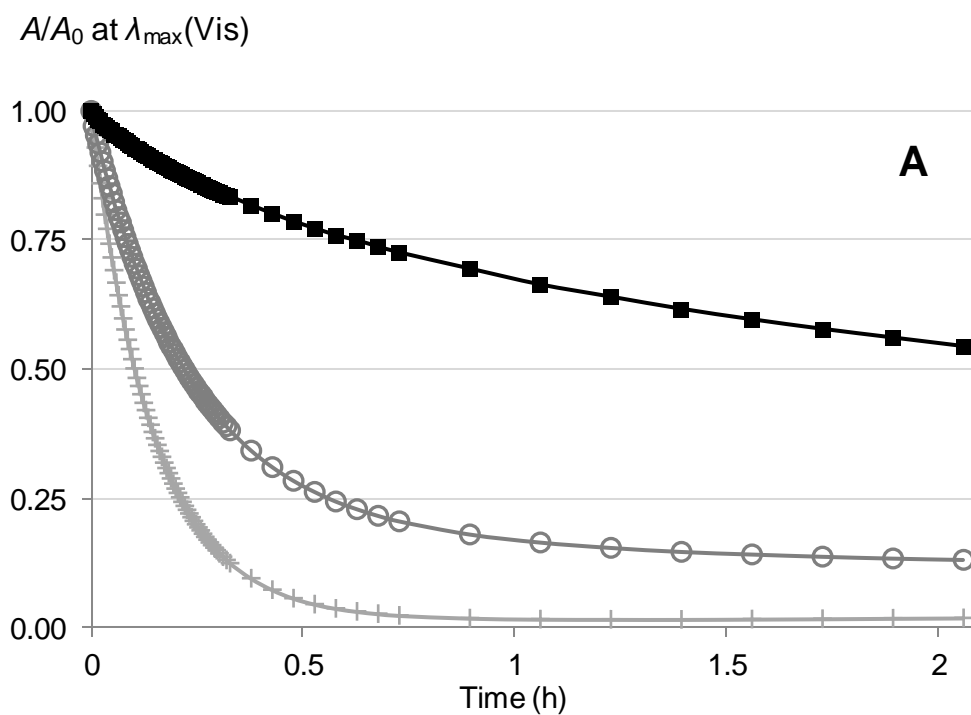


Fig. 1-SI Spectroscopic monitoring of color loss at pH 7, 50°C. **A:** Pigment A (+), P1 (○), P4 (■), **B:** same pigments in the presence of 0.6 equiv. Fe^{2+} .

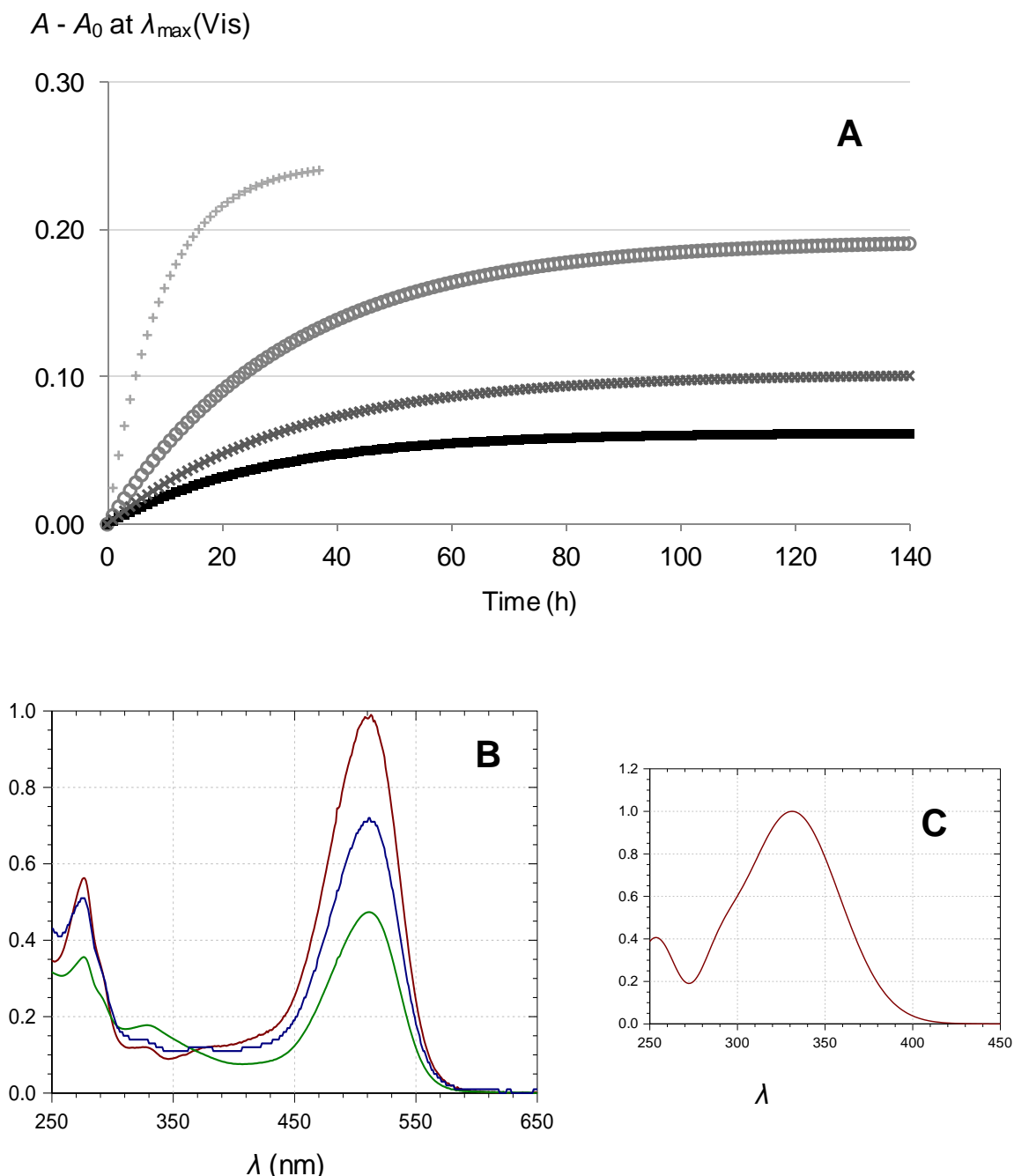


Fig. 2-SI A: The slow conversion of the *trans*-chalcone to flavylum ion (25°C) after acidification to pH 1-2 of samples uptaken after a 2h period of thermal treatment at pH 7, 50°C. A_0 = absorbance immediately after acidification. PA (+), P1 (o), P4 (■), RCE (X). First-order curve fitting gives: k_{obs} ($\times 10^{-3}$, h^{-1}) = 106.0 ± 2.3 (PA), 31.7 ± 0.1 (P1), 37.4 ± 0.6 (P4) and 31.4 ± 0.7 (RCE). **B:** —: intact pigment A (control, pure flavylum), —: sample immediately after acidification (flavylum + Ct + degradation products), —: sample after incubation for 48h (flavylum + degradation products). **C:** Normalized spectrum of the *trans*-chalcone deduced from the spectra of part B.

Simulation	k_{DA} / h^{-1}	k_{DB} / h^{-1}	k_h / h^{-1}	k_{-h} / h^{-1}	Q_h
1	0.5	0	10	1	10
2	0.5	0.5	10	1	10
3	0.5	0.05	10	0.1	100

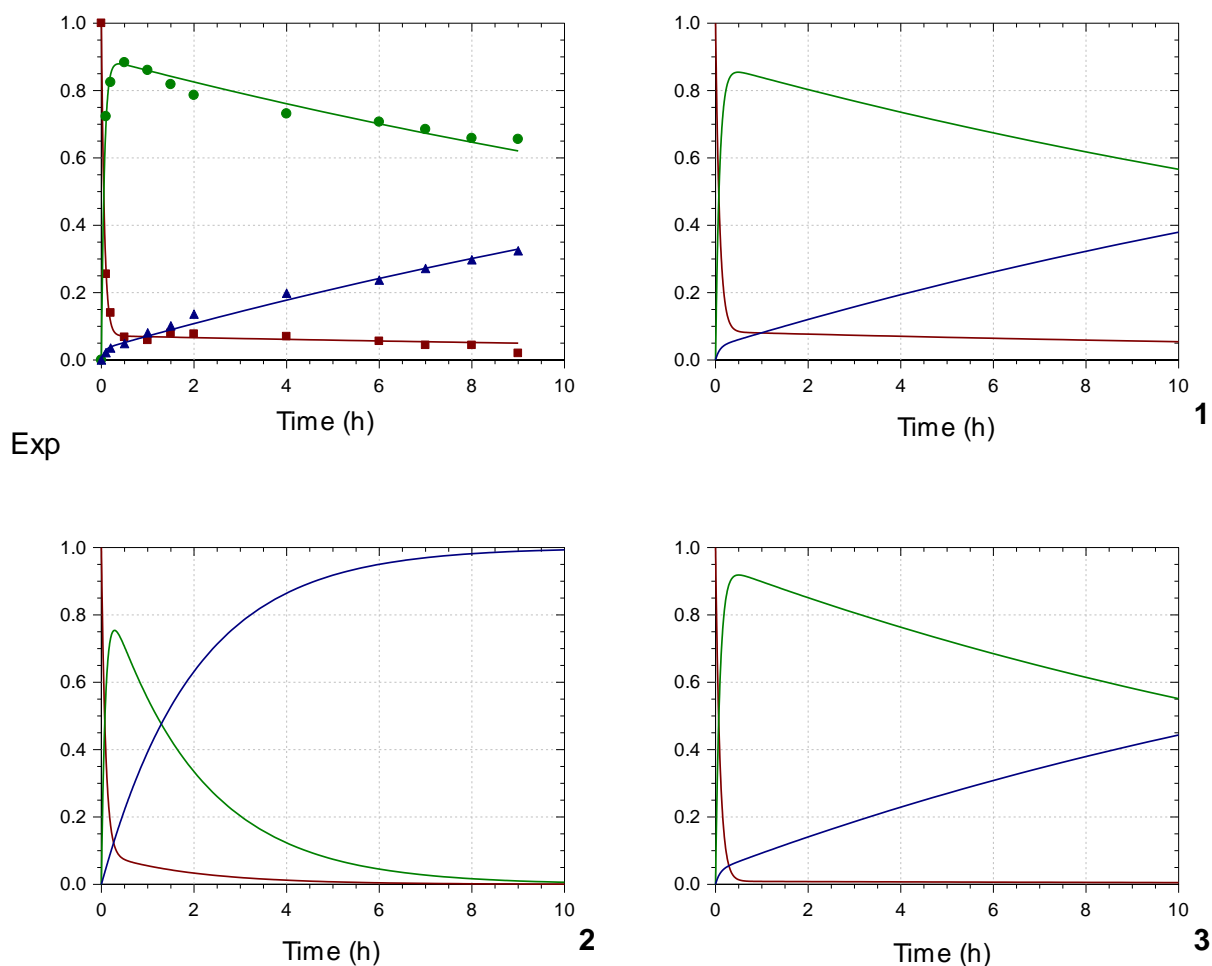
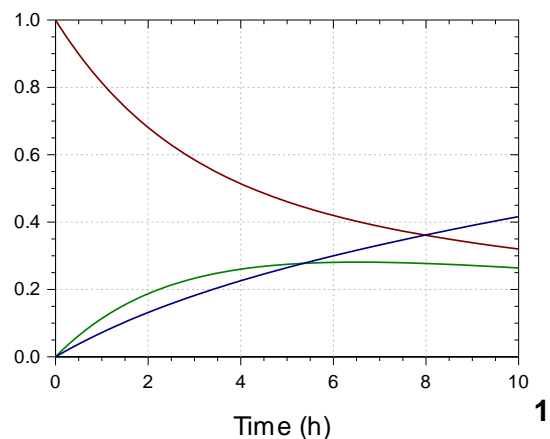
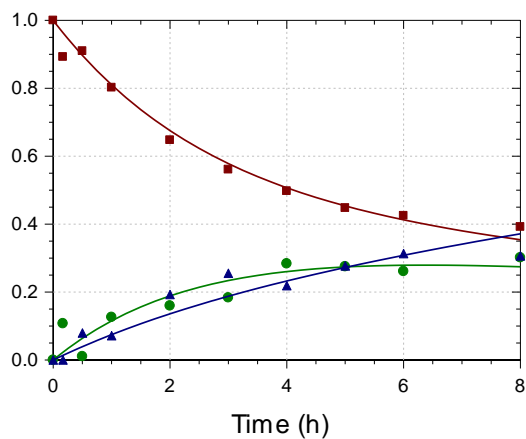


Fig. 3-SI Kinetic simulations for the degradation of pigment A at pH 7, 50°C. First graph: curve-fitting of the experimental data. Graphs 1-3: simulations from parameters reported in Table. X_n : —, X_h : —, X_d : —.

Simulation	k_{DA} / h^{-1}	k_{DB} / h^{-1}	k_h / h^{-1}	k_{-h} / h^{-1}	Q_h
1	0.08	0	0.14	0.2	0.7
2	0.08	0.08	0.14	0.2	0.7
3	0.08	0.008	0.08	0.01	8



Exp.

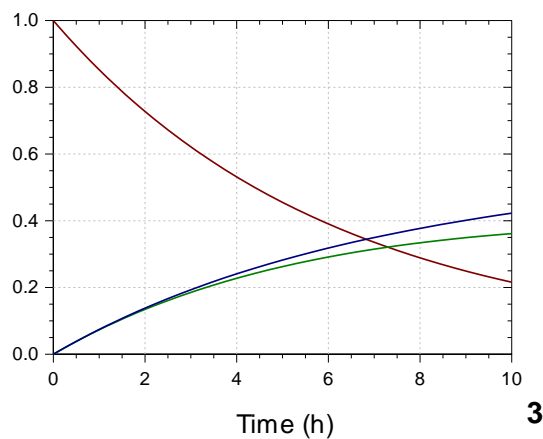
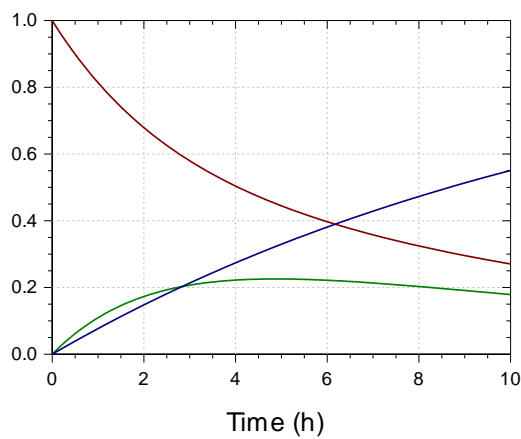


Fig. 4-SI Kinetic simulations for the degradation of P4 at pH 7, 50°C. First graph: curve-fitting of the experimental data. Graphs 1-3: simulations from parameters reported in Table. X_n : —, X_h : —, X_d : —.

Table 1-SI Apparent rate constants and amplitudes of color loss at pH 7 deduced from mono- or biexponential curve-fitting ($r > 0.999$).

	PA	P1	P4
k_{obs} (h^{-1}), 25°C	-	1.42 (± 0.06) ^a 0.11 (± 0.03)	0.32 (± 0.02) ^a 0.04 (± 0.01)
ΔA , 25°C	-	0.66 (± 0.02) 0.12 (± 0.02)	0.199 (± 0.009) 0.35 (± 0.01)
k_{obs} (h^{-1}), 50°C	6.89 (± 0.01)	4.05 (± 0.03)	0.80 (± 0.02) 8.1 (± 0.5)
ΔA , 50°C	0.98 (± 0.01)	0.85 (± 0.01)	0.49 (± 0.01) 0.06 (± 0.01)
k_{obs} (h^{-1}), Fe^{2+} (0.6 equiv.), 50°C	6.19 (± 0.04)	2.55 (± 0.02)	-
ΔA , Fe^{2+} (0.6 equiv.), 50°C	<i>ca.</i> 1	0.64 (± 0.01)	<i>ca.</i> 0.1

^a Calculated k_{obs} values (pure hydration) at 25°C = 0.195 (P1) and 0.064 (P4) h^{-1} .

Chapter 3. The fate of acylated anthocyanins in neutral mildly heated solution

This chapter was published in the journal *Dyes and Pigments* (Fenger et al., 2020). As it invokes a technique that was not detailed in the first articles, the UPLC-MS, a detailed materials and methods section is proposed prior to the publication. It provides additional information for the reader on the pigments used, their purity, the detection of anthocyanins in mass spectrometry with an ion trap and Q-ToF detector.

1. Parameters for the LC-MS analysis

The individual pigments were initially stored in HCl 0.1 M of known mass concentration. They were diluted to stock solutions of 5 mM in HCl 0.05M for the further analyses. The pigments were analyzed in UPLC-MS/DAD to determine their purity. The LC and MS parameters used are in Table 1. Unless specified, the MS information refers to the ion trap system. The LC gradient Q was used in all quantification analyses of anthocyanins degradation products, whereas gradients IDA and ID14 were used for their identification. The latter provide a better separation of the early-eluted compounds.

Table 1. a) LC parameters, b) Major LC gradients used (named gradients 1 and 2 in the article).

a)

LC system	Acquity UPLC System
	BEH C18 Acquity UPLC
Column	50 x 2.1 mm, 1.7 μ m + VanGuard Pre-Column
Column temperature	30°C
Sample temperature	10°C
Flow rate	0.4 mL/min
Binary solvent system	
Mobile phase A	Water + 1% Formic acid
Mobile phase B	Acetonitrile + 1% Formic acid
Injection volume	5 μ L, full loop

b)

Gradient Q		Gradient ID14		Gradient IDA	
Time (min)	%B	Time (min)	%B	Time (min)	%B
0	6	0	2	0	2
5	12	12	24	2,5	2
10	24	14	80	7	8
12	80	15	80	10	24
14	80	16	2	12	80
15	6	18	2	13	80
18	6			14	2
				16	2

Table 2. MS/DAD parameters used with a) the ion trap, b) the Q-ToF.

MS system	Bruker Daltonics HCT ultra
MS type	Ion trap
Ionization system	Electrospray ionization (ESI)
Collision gas	N ₂ (40 psi)
Capillary voltage	1800V (ESI+), 2200V (ESI-)*
Desolvation temperature	365°C
Desolvation gas flow rate	9 L/min
Acquisition mode	Ultrascan
Precursor ion scans range	m/z 80-1500*
Average target mass	m/z 500*
<i>DAD parameters</i>	
λ range	240-600 nm
*For HCA calibration: m/z=50-500; target m/z=200	

MS system	Waters Synapt G2-Si
MS type	Q-ToF
Ionization system	Electrospray ionization (ESI)
Collision gas	N ₂ (40 psi)
Capillary voltage	800V (ESI-)
Cone voltage	5 V
Desolvation temperature	500°C
Desolvation gas flow rate	13 L/min
Acquisition mode	Ultrascan , 0.2 s ⁻¹
Resolution	Enhanced 40 000
Precursor ion scans range	m/z 50-1500

The purity was calculated according to equation (1).

$$\text{Pigment purity} = \frac{\text{Pigment}}{\text{Pigment} + \text{Other anthocyanins}} \quad (4)$$

The contaminants include the other anthocyanins. When phenolic compounds other than anthocyanins were present in significant amount, their identity was determined and they were quantified as contaminants, with an appropriate reference. Cyanin (Cya-3-Glc-5-Glc, Sigma Aldrich Co.) was used as reference for DAD quantification.

2. Compounds quantification

The calibration curves were set down to minimal concentrations of 0.5 μM , because below this concentration, the S/N of anthocyanins was <8 . The linear regressions were set with an intercept, so to determine the LOD and LOQ. The quantification was then based on linear regressions without intercept, and based on the single coefficient a , for more clarity and because the contribution of the intercept was negligible (e.g. for pC 0.23 μM and for Sp 0.57 μM).

The LOD (limit of detection) and LOQ (limit of quantification) for this UPLC method were determined: for pC and Sp by the repetition of 3 standard curves, the standard deviation of the intercept was calculated. The LOD is the concentration range equivalent to this error, deduced from the curve linear regression coefficient. The LOD value was multiplied by 10 to get the LOQ value. The obtained LOQ for pC is 8.9 μM , and 10.5 μM for Sp.

For the cyanin, with only a duplicate calibration curve, the LOD was determined from the S/N (signal to noise) ratio. The minimum acceptable S/N = 5 was chosen, giving the minimum detectable peak area. From the calibration curve, it corresponds to a concentration of 3 μM , which was defined as the LOD.

Table 3. Regression parameters of the compounds quantified in DAD.

Compound	Abbrev.	RT (min)	λ_{\max} (sh)	Area range (nm)	Linear regression a, R ²	Concentration range (μ M)
p-coumaric acid*	pC	3.4	309	300-330	890 0.997	0.5-100
Ferulic acid	Fl	4.5	322	300-330	635 0.999	0,5-100
Sinapic acid*	Sp	4.9	323	300-330	401 0.999	0.5-100
Caffeic acid	Cf	4.4	323	300-330	592.0 0.999	0,5-100
Chlorogenic acid	CGA	1	326	300-330	166.4 0.999	2-1000
Protocatechuic acid	C2	1.1	295(269)	280	3.48 0.999	0.5-100
Phloroglucinaldehyde	C4	2.9	293	270-320	75.0 0.998	5-100
Cyanin**	Cy	1.4	512	460-560	1325 0.999	5-200

Quantification elution profile: 0' 6%; 5' 12% B phase, cleaning and equilibration

*Average of triplicate, ** Average of duplicate

3. Initial purity

The purity of the isolated anthocyanins ranged between 75% and 93%, mostly due to the presence of derived anthocyanins: in P4 and P5, some presence of the neighboring peak from the initial semi-prep LC elution. In the diacylated anthocyanins, some deacylation products, were present, e.g. in P6: PA and PB, and traces of isomers. In addition, the product of hydrolysis of the glucose at C5 is frequently detected, and is eluted later than the initial pigment. It may result from hydrolysis slowly occurring at acidic pH, during the storage at cold temperature or during sampling. Additional contaminants were initially present, such as Sp-Glc in PB (m/z 385, λ_{\max} = 329), and Sp-Soph (m/z 377). In PA some 301 (λ_{\max} = 297 nm).

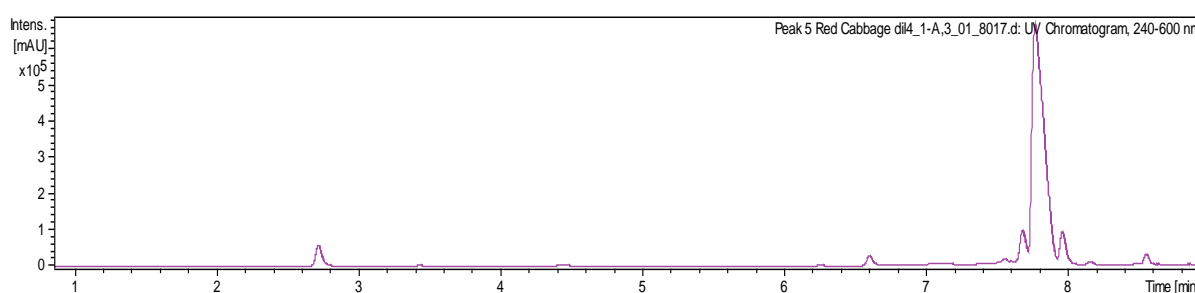
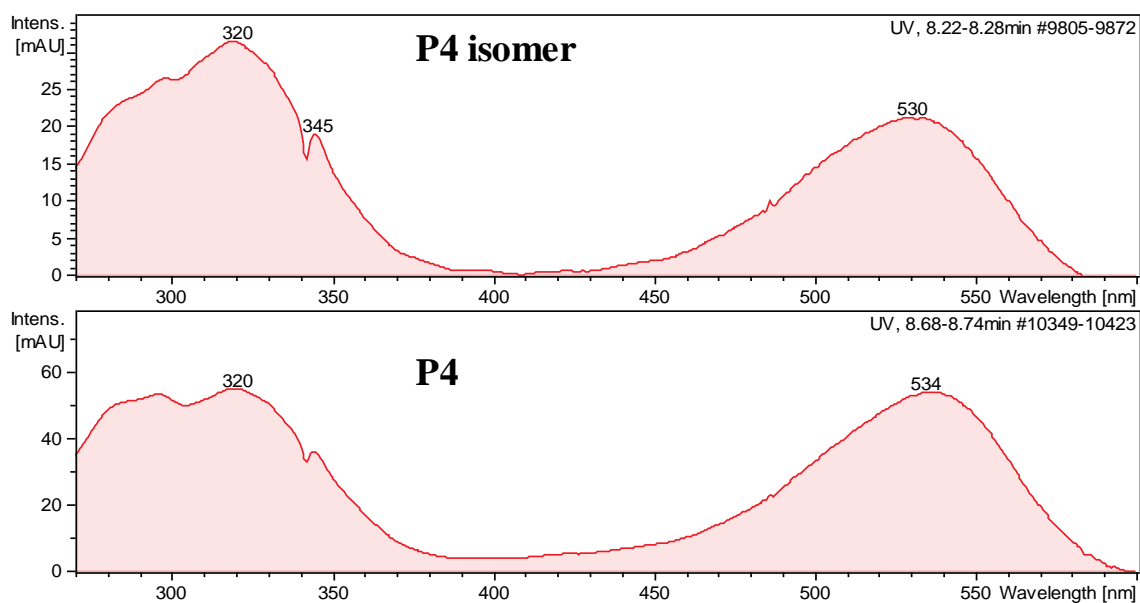
**Fig 1.** Contaminants in P5 (Rt = 7.8 min): P2 (2.7 min), P4 (7.65 min), and P6 (8.0 min), and P5 Glc hydrolysis at C5 (8.6 min).

Table 4. Pigment initial purity by UPLC-DAD quantitation.

Abbrev.	RT (min)	Lmax (nm)	Purity %*	% Peak A	% Peak B
Cyanin	1,3-1,5	512	98%	-	-
PA	1,1	514	94%	-	-
PB	2,6	531	98%	-	-
P1	6,5	523	89%	4,5%	-
P2	7,0	524	88%	5,3%	-
P3	7	525	93%	3,3%	-
P4	7,55	536	75%	<	5,5%
P5	7,75	536	81%	<	5,0%
P6	7,8	538	91%	<	4,6%

Above 50 μM , the spectra produced by the DAD provide a sufficient sensibility to be used to determine λ_{max} and ratios between UV band and visible band. For example, for P4 and its regioisomer ($C_0 = 200 \mu\text{M}$; $C(24\text{h}) = 32 \mu\text{M}$), there is a clear hypsochromic shift of ca. 4 nm.

**Fig 2.** Absorption spectrum in DAD of P4 and its isomer, used for the calculation of the A_{530}/A_{320} ($= 0.68$ for the P4 isomer, $= 0.98$ for P4).

FURTHER DEVELOPMENTS IN DAD ANALYSIS

A discrepancy between UPLC-DAD and UV-vis quantification was observed, but only for the acylated anthocyanins (P1 and even more P4). By default, all anthocyanins were quantified as cyanin equivalent, the only commercial individual pigment, for which, as it is diglucosylated, the ϵ is expected to be comparable. However, this common reference supposes the same molar absorption coefficient, independently on the acylation pattern. Actually, the ϵ of the individual pigments determined in the literature on the same pigments, isolated at the Ohio State University, reveals differences (Table 4).

a)

Pigment	Structure	Epsilon
Cyanin	Cya-3-Glc-5-Glc	27500
A	Cya-3-[Glc-2-Glc]-5-Glc	25540
1	Cya-3-[Glc(6-pC)-2-Glc]-5-Glc	20260
2	Cya-3-[Glc(6-Fl)-2-Glc]-5-Glc	18200
3	Cya-3-[Glc(6-Sp)-2-Glc]-5-Glc	21800
B	Cya-3-[Glc-2-Glc(2-Sp)]-5-Glc	13700
4	Cya-3-[Glc(6-pC)-2-Glc(2-Sp)]-5-Glc	16900
5	Cya-3-[Glc(6-Fl)-2-Glc(2-Sp)]-5-Glc	15120
6	Cya-3-[Glc(6-Sp)-2-Glc(2-Sp)]-5-Glc	12730

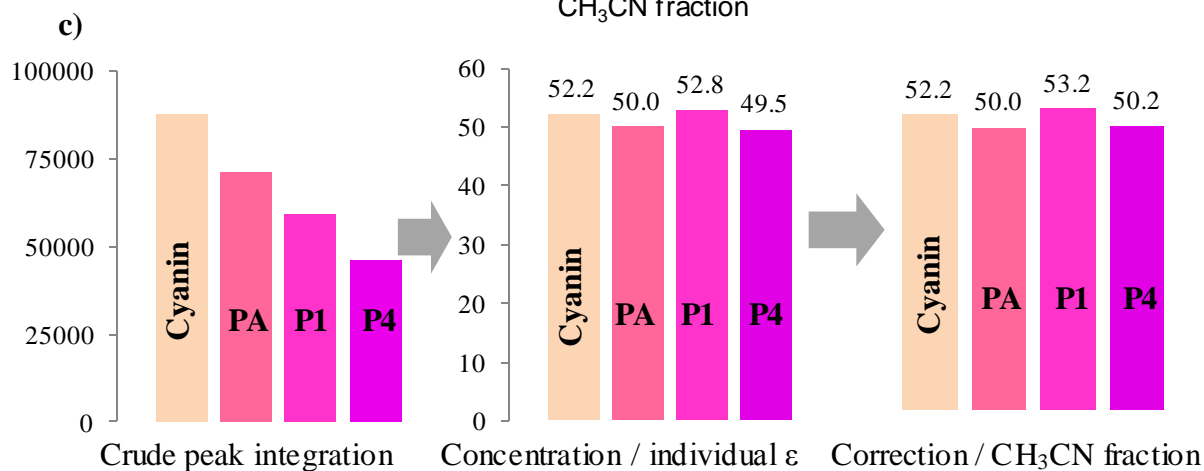
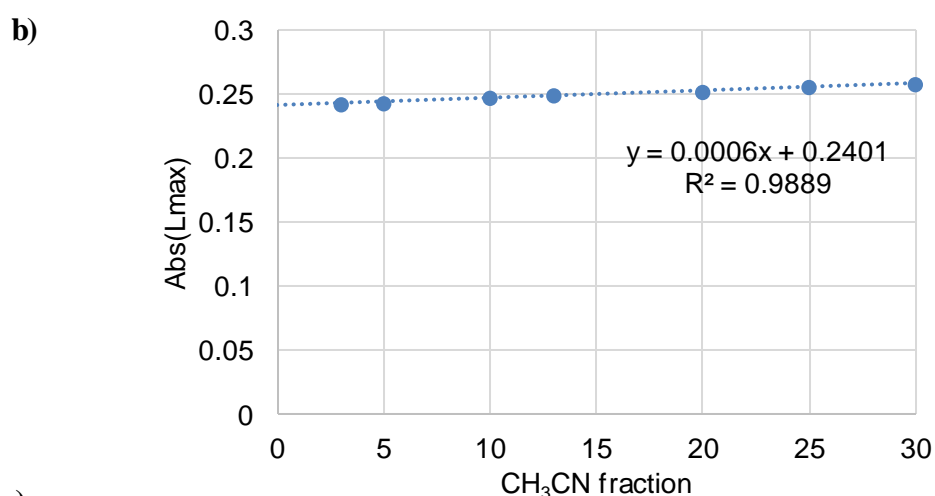


Fig 3. a) Molar absorption coefficient of the individual RCE anthocyanins (Ahmadiani et al., 2016). b) Impact of acetonitrile (CH_3CN) fraction on the absorbance of the flavylum at pH 2.22 (1% Formic acid in H_2O). The fraction of acetonitrile at the retention time of the flavylum was 8.5% (cyanin), 13% (PA), 16.3% (P1) and 18% (P4). c) Correction of i) the bias due to individual pigments molar absorption coefficient (ϵ), ii) the bias due to the CH_3CN fraction.

4. Ions detection in MS

The typical fragmentation patterns observed with anthocyanins analyzed in these conditions are in Table 5. With the ion trap, the resolution was of ca. 0.5 m/z. The glucose moiety at C5-OH is the most labile. As second fragment, the acyl loss, and the loss of the sophorose(+acyl) moiety.

Table 5. MS ions and fragments detected for the 8 RCE anthocyanins and the cyanin reference.

Pigment	MW (g/mol)	m/z [M+-2H]-	m/z [M]+	MS(2) -	MS(3) -	MS(2) +	MS(3) +
Cyanin	612	609-663 ^a	-	663>465-627	627>265-285-447-465	-	-
PA	774	771	773	771>609-815	609>285-339	287-449-611	137-213
PB	980	977	979	977,1>6,9-815,1	609>339		287
P1	920	917	919	917>447-755	755>609	287-449-757	287
P2	950	947	949	947>785	785>284-339-609	287-449-757	287
P3	980	977	979	979>815	339, 609, 815	287-449-757	287
P4	1126	1123	1125	1123>755-961	961>419-755	963, 287	963, 287
P5	1156	1153	1155	1153>785-992	992>339-785	287, 449, 993, 1156	287
P6	1186	1183-1201	1185	1219>1185	1185>977-1021	449-1023	287

^a[M+Cl] ion; >: fragments into. Ions are ranked in decreasing order of intensity.

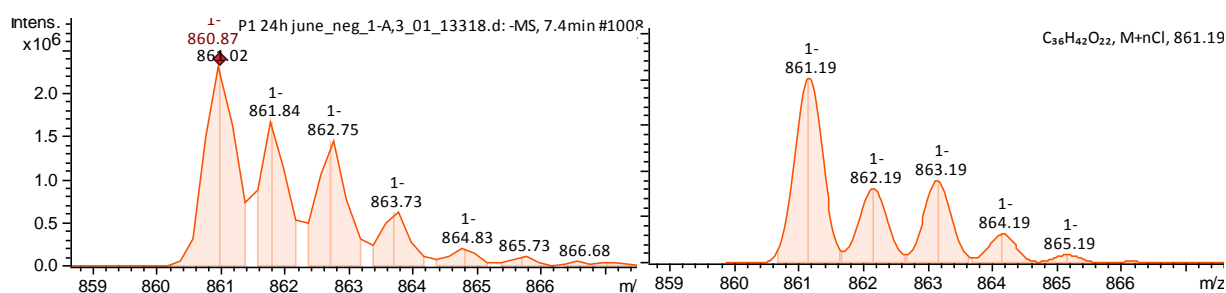
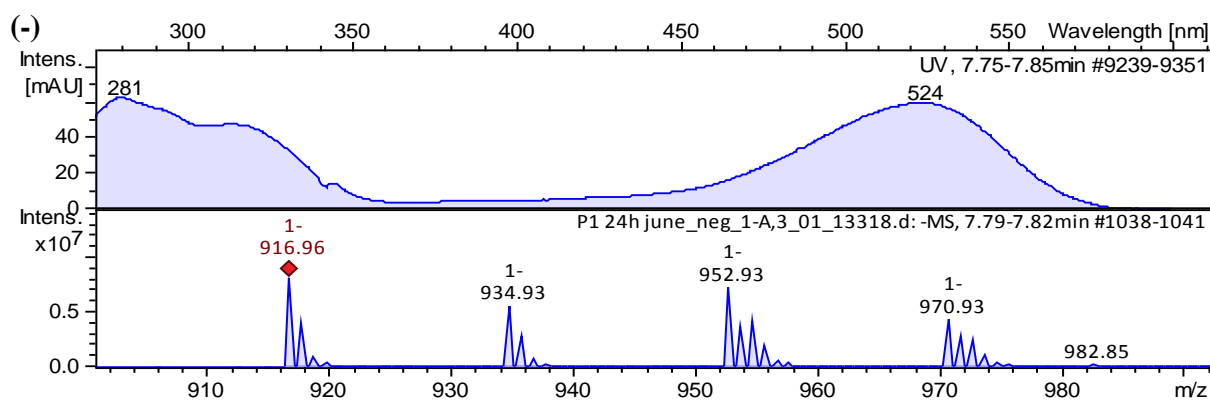
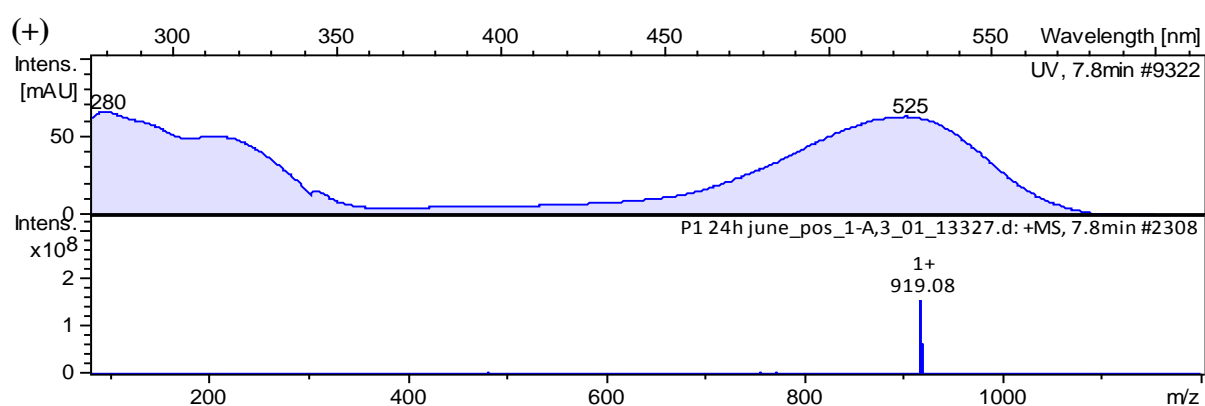


Fig 3. Confirmation of compound Cl adduct with the isotopic pattern, example of C1-3-[Glc(pC)-2-Glc]-5-Glc Cl adduct in P1 after 24h, C = 200 μ M. Left: ions detected (ion trap), right: calculated mass pattern (Bruker DataAnalysis software). ³⁷Cl : 24.23%, ¹³C : 1.1%.



m/z	z	I (AU)	% / P1	Ion type	Name
916.95	1-	2625299	100%	$[M-2H]^-$	P1
952.92	1-	2213201	84%	$[M-H+Cl]^-$	Cl ⁻ adduct
934.93	1-	1724506	66%	$[M+H_2O-H]^-$	P1 hemiketal
970.91	1-	1305271	50%	$[M+H_2O-H+Cl]^-$	Hemiketal Cl ⁻ adduct
954.88	1-	1203114	46%	$[M+Cl]^-$	P1 ³⁷ Cl ⁻ adduct isotope
917.92	1-	1201748	46%	$[M-2H]^-$	P1 ¹³ C isotope
953.89	1-	1193309	45%	$[M+Cl]^-$	P1 ³⁶ Cl ⁻ adduct isotope



m/z	z	I (AU)	% / P1	Ion type	Name
919.06	1+	56588860	100%	$[M]^+$	P1
920.05	1+	30021766	53%	$[M]^+$	P1 ¹³ C isotope
921.04	1+	10076229	18%	$[M]^+$	P1 ¹³ C isotope
922.04	1+	2545383	4%	$[M]^+$	P1 ¹³ C isotope

Fig 4. Typical MS patterns detected for pigment P1 (MW = 919 g/mol). In (-) mode: m/z $[M^+-2H]^+ = [M-2H]^- = 917$, a major chloride adduct m/z $[M+Cl-H]^- = 971$, the hemiketal in rapid equilibrium (sometimes referred to as "H₂O adduct"), and a Cl⁻ adduct of the hemiketal. NB: 983 = traces of P2 chloride adduct. In (+) mode: no K⁺, Na⁺ adducts, solely the detection of the flavylum ion and its high proportion of isotopes.

Typically, compounds identification was executed in 3 steps:

1. *UPLC-DAD data collection: compound chemical class*

The LC information (retention time, λ_{\max}) are collected from the DAD chromatogram.

2. *MS data collection: fragments identification*

The MS information is analyzed: the m/z, the isotopic pattern, the neutral losses from the fragments in MS² and MS³. In Fig 3, the calculated and measured isotopic patterns of a chloride adduct of a coumarin derivative are compared as example.

3. *MS data collection: raw formula confirmation*

When the precise mass (from Q-ToF analysis) was available, the raw formula of the compound proposed was compared to the mass actually detected. The compound formula was confirmed when the error was < 10.

Table 6. Example of confirmation of the raw formula of the 3 coumarin derivatives, by calculating the error between the m/z of the ion detected (detected mass) and the calculated mass of the [M-H]⁻ corresponding to the formula proposed (ion mass).

Peak	Compound detected	Ion selected	Formula	Ion mass	Neutral mass	Detected mass	Error (ppm)
2'	C1-3-Soph	[M-H] ⁻	C ₂₁ H ₂₆ O ₁₅	517.1185	518.1263	517.1182	0.6
6	C1-3-Soph-5-Glc	[M-H] ⁻	C ₂₇ H ₃₆ O ₂₀	679.1710	680.1788	679.1707	0.4
4'	C1-3-(pC)Soph-5-Glc	[M-H] ⁻	C ₃₆ H ₄₂ O ₂₂	825.2076	826.2154	825.2071	0.6

The fate of acylated anthocyanins in neutral mildly heated solution

Julie-Anne Fenger,^{a*} Rebecca J. Robbins,^b Thomas M. Collins,^c Olivier Dangles^{a*}

^a Avignon University, INRAE, UMR408, 84000 Avignon, France

^b Mars Wrigley, 1132 W Blackhawk Street, Chicago, IL 60642, USA





^c Retired



Dyes and Pigments
Volume 178, July 2020, 108326



The fate of acylated anthocyanins in mildly heated neutral solution

Julie-Anne Fenger ^a  , Rebecca J. Robbins ^b, Thomas M. Collins ¹, Olivier Dangles ^a  

 [Show more](#)

<https://doi.org/10.1016/j.dyepig.2020.108326>

Abstract

In neutral solution, anthocyanins acylated by hydroxycinnamic acids typically exhibit attractive blue colors and a higher resistance to color loss compared to their nonacylated homologs. However, they remain vulnerable to a poorly understood combination of oxidative and hydrolytic reactions that strongly contribute to color loss and limits their industrial applications. In this work, the thermal degradation of isolated red cabbage anthocyanins (0, 1 or 2 acyl groups) at pH 7 was investigated by UPLC-DAD-MS (low- and high-resolution). Non-oxidative alterations, including deacylation and intramolecular acyl transfer, were observed and found very dependent on the number and position of the acyl group(s) as well as on the presence of iron ions. At intermediate and advanced thermal degradation, several oxidative mechanisms were evidenced that lead to protocatechuic acid, phloroglucinaldehyde 2-O-glucoside, acylglycosides and derivatives of 2,4,6-trihydroxyphenylacetic acid and 3,5,7-trihydroxycoumarin. Based on the product distribution observed and on the impact of added Fe^{2+} ions and H_2O_2 , possible degradation mechanisms are discussed. They likely start with a one- or two-electron transfer from the anionic base (a major colored form in neutral solution) to O_2 . The hydrogen peroxide produced could then further react as an electrophile with the anionic base and/or the hemiketal (major colorless hydrated form).

This contribution to understanding the degradation mechanisms of anthocyanins around neutrality can open up new stabilization strategies to extend the range of their food applications to neutral media.

1. INTRODUCTION

Anthocyanins are plant pigments expressing a wide array of red to blue colors depending on pH and the presence of other species susceptible to interact with the anthocyanidin chromophore, such as phenolic compounds (copigments) and metal ions (Trouillas et al., 2016a). In particular, anthocyanins and their complexes can express attractive blue colors around neutral pH (G.T. Sigurdson et al., 2016). This is the case of 3-O-sophorosyl-5-O-glucosylcyanidin and peonidin derivatives commonly found in purple vegetables (*e.g.*, red cabbage) (Moloney et al., 2018). Most importantly, purple vegetables are typically rich in anthocyanins acylated by *p*-hydroxycinnamic acids (HCA), which increase color stability and participate in color diversification. However, at neutral and mildly alkaline pHs, color loss remains relatively fast, which is a serious hurdle to industrial development.

Color loss in anthocyanin solutions at $\text{pH} > 2$ is due to the reversible water addition to the flavylum ion (with concomitant accumulation of a colorless hemiketal and pale yellow *cis*- and *trans*-chalcones) and to a combination of irreversible routes (hydrolytic and oxidative pathways) typically resulting in cleavage of the C-ring (Dangles & Fenger, 2018). The color stability of diacylated anthocyanins is much higher than for non- or mono-acylated anthocyanins (Fenger et al., 2019; Moloney et al., 2018; G. T. Sigurdson et al., 2017). Indeed, the HCA residues can develop π -stacking interactions with the anthocyanidin chromophore (intramolecular copigmentation + self-association), thereby protecting it against water addition (Trouillas et al., 2016a). By contrast, the rate of irreversible degradation at pH 7 barely depends on the acylation pattern in the case of red cabbage anthocyanins (Fenger et al., 2019). Indeed, diacylation results in a higher proportion of the colored anionic base at pH 7, which is probably a much better electron donor (thus more vulnerable to autoxidation) than the neutral colorless forms more readily accumulated from the weakly acylated pigments.

The mechanisms of irreversible degradation have been mainly investigated at acidic pH (Cabrita et al., 2014; Es-Safi et al., 2008; Fleschhut et al., 2006; Sadilova et al., 2007; Seeram et al., 2001; Sinela et al., 2017) and only a few studies were also carried out at neutral pH in the presence of radical initiators, H_2O_2 or ascorbate (a H_2O_2 generator by autoxidation) (Satake & Yanase, 2018; Stebbins, 2016). In the pH range 2 - 4, anthocyanins were reported to be degraded into B-ring + C2 (*e.g.*, protocatechuic acid) and A-ring + C4 (*e.g.*, phloroglucinaldehyde) fragments, C3 being probably eliminated as CO_2 . The colorless species, in particular the chalcones, were proposed to be intermediates in the irreversible

degradation of anthocyanins at acidic pH (Cabrita et al., 2014; Sinela et al., 2017). At pH 7 – 8, the electrophilic flavylum ion (a diacid with $pK_a \sim 4$ and 7) is in trace amounts so that water addition is very slow (Pina, 2014). Anthocyanins are thus mostly a mixture of neutral / anionic bases, with low concentrations of hemiketal and neutral / anionic *cis*- and *trans*-chalcones ($pK_a \sim 8$) gradually appearing (JMendoza et al., 2018).

At pH 7, more stable blue colors can be obtained with cyanidin derivatives in the presence of metal ions such as Fe^{2+} , Fe^{3+} and Al^{3+} (Buchweitz et al., 2013). Upon metal binding, the anthocyanidin chromophore adopts a *p*-quinonemethide structure, which unlike the flavylum ion does not undergo water addition with concomitant color loss. In spite of this color stabilization, irreversible degradation occurs over a prolonged storage. Addition of Fe^{2+} was reported to be actually protective with diacylated anthocyanins, which strongly bind iron (a possible consequence of the strong π -stacking interactions), but unexpectedly deleterious for the non- and monoacylated homologs, suggesting that iron leakage from the corresponding less stable complexes results in a prooxidant effect (Fenger et al., 2019).

Unraveling the degradation mechanisms of anthocyanins around neutrality can open up specific stabilization strategies for anthocyanins used as blue colors. Therefore, this study aims at identifying the main products of irreversible degradation at pH 7. A set of 3 anthocyanins from red cabbage (from non- to diacylated) was thermally degraded at neutral pH, 50°C. The role of O_2 , added Fe^{2+} and hydrogen peroxide in these mechanisms was investigated. Based on the product distribution observed and on the impact of added Fe^{2+} ions and H_2O_2 , possible degradation mechanisms are discussed.

2. MATERIALS & METHODS

2.1. Materials

Red cabbage anthocyanins were isolated from red cabbage by preparatory LC according to already published procedures (Ahmadiani et al., 2016). The pigments investigated in this work encompass a nonacylated anthocyanin (PA) and its homologs with a *p*-coumaroyl (pC) residue (P1) and an additional sinapoyl (Sp) residue (P4). PA: cyanidin-3-O-[Glc-2-O-Glc]-5-O-Glc, P1: cyanidin-3-O-[(6-O-pC)-Glc-2-O-Glc]-5-O-Glc, and P4: cyanidin-3-O-[(6-O-pC)-Glc-2-O-(2-O-Sp)-Glc]-5-O-Glc. Stock solutions (5 mM) of pigment were prepared in aqueous 0.01 M HCl (metal-trace grade). Aqueous H₂O₂, FeSO₄·7H₂O, NaH₂PO₄·2H₂O, Na₂HPO₄·7H₂O and the following standards for LC quantification, cyanin (cyanidin-3,5-O-diglucoside), *p*-coumaric acid and sinapic acid, were all obtained from Sigma-Aldrich (St Louis, MO, USA). HPLC-MS grade water was used in all experiments.

For each pigment, the fraction of colored and colorless species at equilibrium at pH 7 (Scheme 1-SI, Fig. 1-SI) was calculated using the global acidity constant of the flavylium ion (formation of the neutral base + colorless forms) and the two stepwise acidity constants (sequential formation of the neutral and anionic bases) (Moloney et al., 2018).

The thermal degradation of anthocyanins was performed at 50°C in a thermostated water bath protected from light, as already described (Fenger et al., 2019). The initial anthocyanin concentration in the 0.01 M phosphate buffer was 5x10⁻⁵ M. Aliquots were taken up at regular time intervals over 8h and at 24 and 72h. The total concentration in residual pigment was quantified with a UV-Vis spectrophotometer (Agilent 8453) immediately after cooling and acidification to pH 1.0 – 1.5 (fast conversion of the residual colored forms, hemiketal and *cis*-chalcone into the flavylium ion) and 6 to 50h later (additional conversion of the *trans*-chalcone) (Fig. 2-SI).

2.2. Product identification and quantification

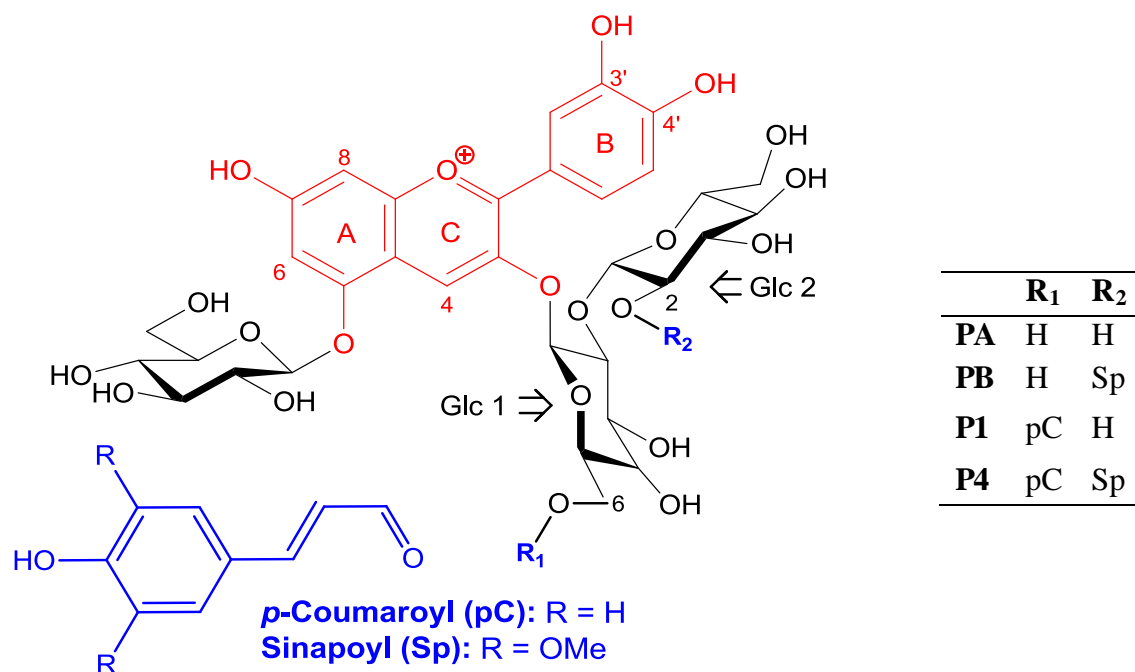
The acidified and stabilized samples were analyzed with an Acquity UPLC (Waters Corporation, Milford, USA) equipped with a binary solvent delivery manager and a diode array detector (DAD). Samples (5 µL) were injected onto an Acquity UPLC BEH C18 reversed phase column (50x2.1 mm, 1.7 µm) set at 30°C. Phase A (1% HCO₂H in H₂O) and B

(1% HCO₂H in MeCN) were eluted at 0.4 mL/min. Unless otherwise specified, all chromatograms are presented at 280 nm after 24h at pH 7, 50°C. Only peaks with S/N > 8 on the 280 nm chromatogram were considered for identification. For P1 and P4, gradient 1 (%B: 0 min: 2%, 12 min: 24%, 14-15 min: 80%, 16-18 min: 2%) was used. For PA, gradient 2 (%B: 0-2.5 min: 2%, 7 min: 8%, 10 min: 24%, 13 min: 80%, 14-16 min: 2%) enabled a better separation of the more polar degradation products.

The UPLC system was coupled with a ESI-Q-trap HCT Ultra (Bruker Daltonics, Bremen, Germany) in ultrascan mode. The capillary voltage was -1.8 kV (positive mode) or 2.2 kV (negative mode) with a 80-1500 *m/z* scanning interval at a speed of 26x10³ *m/z* s⁻¹. Desolvation was conducted with N₂ at 365°C, 40 psi, 540 L/h. Cone voltage was 40 V, and the fragmentation amplitude was 1.2 V.

For confirmation of raw formulae, three samples of P1 (t = 0, 24h, 24h in the presence of Fe²⁺) were also analyzed on a Waters Acquity UPLC system coupled with a Waters Synapt G2-Si High Resolution Mass Spectrometer (HRMS) equipped with an ESI source (Waters Co.). The source and desolvation temperatures were set at 120°C and 500°C, respectively. Desolvation was also conducted with N₂ at 500°C (40 psi) at 800 L h⁻¹. The capillary and cone voltages were set at 0.8 kV and 5 V, respectively. The scan range was *m/z* 50–1500 with a spectrum acquisition every 0.2 s and a resolution of 4x10⁴. Mass scale was corrected during acquisition using leucine enkephalin (Sigma-Aldrich). Data were acquired using the MassLynx™ (V4.2) software in continuum mode. The *m/z* accuracy (Δ , in ppm) of the parent ions was calculated as the relative difference to their expected monoisotopic ion.

Anthocyanin were quantified as cyanin equivalent with a correction factor accounting for the differences in molar absorption coefficient at $\lambda_{\max}(\text{Vis})$ between the pigments (Ahmadiani et al., 2016). The monoacylsophorose compounds and coumarin derivatives were quantified in HCA equivalent and phloroglucinaldehyde (PGA) derivatives in PGA equivalent.



Scheme 1. Structures of the red cabbage anthocyanins studied in this work

3. RESULTS

At pH 7 and 50°C, the color stability of diacylated anthocyanin P4 and its iron complex is much higher than that of its non- and mono-acylated counterparts PA and P1 (Fenger et al., 2019). However, the global color loss is the result of a reversible component featuring water addition to the flavylium ion (and subsequent isomerization steps) and of an irreversible component of true oxidative degradation. The latter component can be appreciated by reversing the former through reacidification to pH 1 - 1.5, so as to convert all colored and colorless forms into the flavylium ion. Hence, the time dependence of the residual flavylium percentage solely reflects the rate of oxidative degradation occurring in neutral solution (Fig. 2-SI). After 24h, the percentage of residual flavylium ion lies in the range 40 - 60% and is mostly independent of the acylation pattern. Product identification was then carried out (Fig. 1, Table 1).

Three types of products were distinguished: a) colorless species resulting from reversible water addition (*trans*-chalcones), b) new pigments, *i.e.* isomers and deacylation products (Fig. 2), c) products of oxidative degradation. In addition, the composition of P1 and P4 solutions after degradation over 24h was determined under different conditions: addition of Fe²⁺, addition of hydrogen peroxide, inert atmosphere. Finally, degradation routes are proposed and discussed.

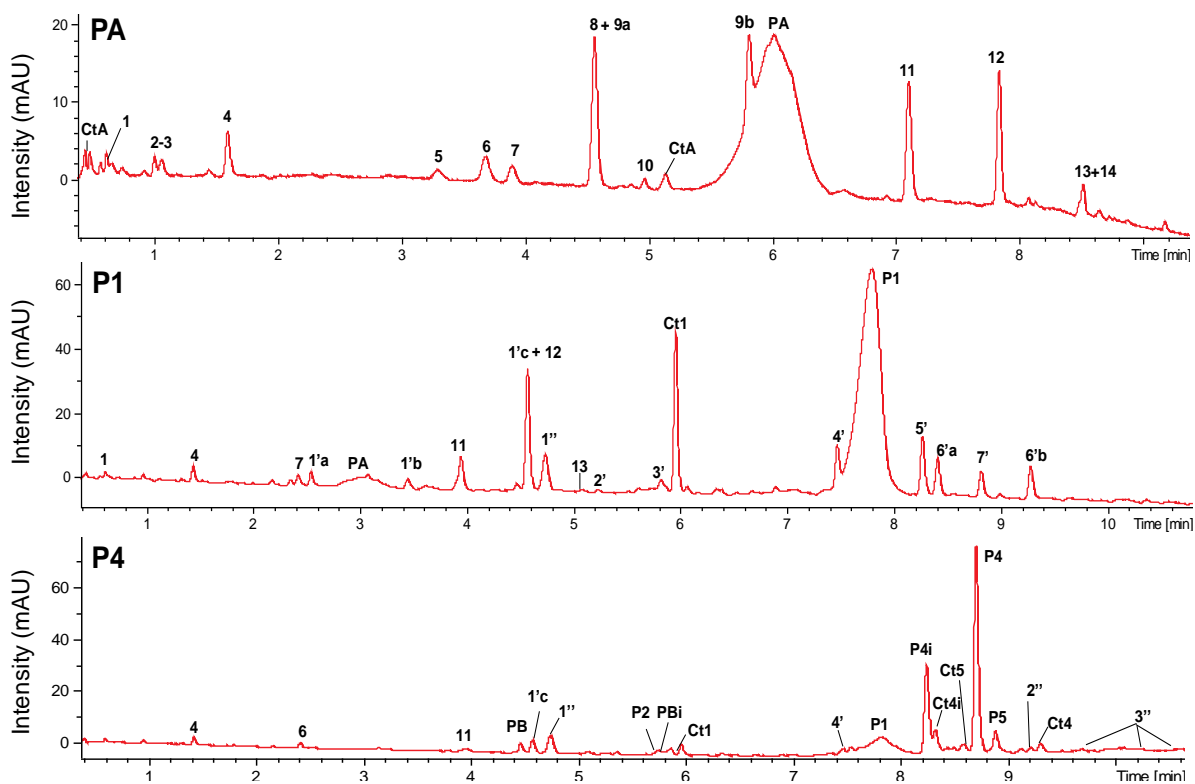


Fig. 1. Chromatograms of the solutions of PA (gradient 2), P1 and P4 (gradient 1) after 24h at pH 7, 50°C (detection at 280 nm). Additional anthocyanins present: PB (from P4): cyanidin-3-O-[(Glc-2-O-(2-O-Sp)-Glc]-5-O-Glc, P2 (contaminant): cyanidin-3-O-[(6-O-pC)-Glc-2-O-Glc]-5-O-Glc, P5 (contaminant): cyanidin-3-O-[(6-O-FI)-Glc-2-O-(2-O-Sp)-Glc]-5-O-Glc. At the elution pH ~ 2.2, the flavylum ions are coeluted with the hemiketal and *cis*-chalcone [M-H+H₂O]⁻ with which they are in fast equilibrium.

Table 1. Selection of ions detected in the solutions of PA, P1 and P4 after 24h at pH 7, 50°C. Products numbered according to elution order with the following convention: product p potentially present in all 3 samples, product p' potentially present in P1 and P4 samples, product p'' specifically present in P4 samples (see Fig. 1).

#	R _t (min)	Proposal	λ _{max} (nm)	m/z (-)	Ion type (-)	MS2 (-)	MS3 (-)
PA: Cya-3-[O-Glc-2-O-Glc]-5-O-Glc (gradient 2)							
1	0.67	C3-Glc	275	345	[M-H] ⁻	345 → 165 (-Glc-H ₂ O); 139 (-Glc-CO ₂); 183 (-Glc)	-
2-3	1.07	Unid.	291 325	643 1253	[M+Cl] ⁻ [2M-H] ⁻	1253 → 1055; 1235; 893; 643 → 527; 617	1055 → 893; 783; 551 527 → 445; 783; 365
4	1.60	C2	258	109	[M-H-CO ₂] ⁻	-	-
5	3.25	C1-3-Soph -5-Glc	325	715	[M+Cl] ⁻	715 → 517 (-Cl-Glc); 679 (-Cl)	517 → 247; 191; 337
6	3.65	C4-Glc	289	315	[M-H] ⁻	315 → 153 (-Glc)	153 → 125 (-CO)
7	3.95	Unid.	293	361	-	-	-
8	4.55	C6-Soph	275	529	[M-H] ⁻	529 → 409, 205 (-Soph)	-
9a	4.55	C7-Soph	278	597	[M-H] ⁻	597 → 272 (-Soph-H); 417 (-Glc-H ₂ O); 297; 555 (-CH ₂ CO)	272 → 231; 258; 175
10	4.95	Unid.	270 430	757	-	757 → 551 (-Glc-CO ₂); 595 (-Glc); 713 (-CO ₂)	551 → 371 (-Glc-H ₂ O); 227; 281
9b	5.78	C7-Soph	278	597	[M-H] ⁻	597 → 272 (-Soph-H); 417 (-Glc-H ₂ O); 297; 555 (-CH ₂ CO)	272 → 231; 258; 175
CtA	5.15	PA Ct	330	789	[M-H] ⁻	789 → 627; 517; 285	627 → 285; 517; 241
PA	5.8-6.3	PA	510	807 825	[M+Cl-H] ⁻ Id.+H ₂ O	807 → 771; 609 825 → 789; 627	771 → 609; 285; 447 789 → 627; 517; 285; 447
11	7.20	C3-Glc -Soph-C2	269	805	[M-H] ⁻	805 → 463 (-Soph-H ₂ O) 651 (-C2-H ₂ O); 327 (-C2-Soph-H ₂ O)	463 → 327 (-C2); 299 (-pC-H ₂ O); 165 (-C2-Glc)
12	7.88	C3-Glc-C2	ND	481	[M-H] ⁻	481 → 345 (-C2); 327 (-C2-H ₂ O); 463 (-H ₂ O)	345 → 165 (-Glc-H ₂ O); 139 (-Glc-CO ₂); 183 (-Glc); 327 (-H ₂ O)
13	8.47	Cya-5-Glc	ND	447	[M-2H] ⁻	447 → 285 (-Glc)	285 → 257
14	8.50	C5-Glc	328	463	[M-H] ⁻	463 → 419; 257; 445	419 → 213
P1: Cya-3-O-[(6-O-pC)-Glc-2-O-Glc]-5-O-Glc (gradient 1)							
1'a	2.53	pC-Soph	310	487	[M-H] ⁻	487 → 469 (-H ₂ O)	469 → 205; 307 (-Glc); 265
1'b	3.44	pC-Soph	310	487	[M-H] ⁻	487 → 469 (-H ₂ O)	469 → 205; 307 (-Glc); 265
1'c	3.92	pC-Soph	310	487	[M-H] ⁻	487 → 469 (-H ₂ O)	469 → 205; 307 (-Glc); 265

1'd	4.55	pC-Soph	310	487	[M-H] ⁻	487 → 469 (-H ₂ O)	469 → 205; 307 (-Glc); 265
2'	5.21	C1-3-Soph	310	553	[M+Cl] ⁻	553 → 499 (-Cl-H-H ₂ O); 517 (-Cl-H)	517 → 499 (-H ₂ O); 235; 295; 179
3'	5.80	Unid.	ND	498	-	498 → 301 (Cya + O); 336; 463 (Cya-Glc + O)	301 → 165 (-C4 or C2); 257 (-CO ₂); 137
Ct1	5.97	P1 Ct	310	935 971	[M-H] ⁻ [M+Cl] ⁻	935 → 773; 755; 663; 447; 285; 971 → 935	663 → 517; 247; 935 → 773; 755; 663; 285
4'	7.45	C1-3- (pC)Soph-5- Glc	317	825	[M-H] ⁻	825 → 663 (-Glc)	663 → 517 (-pC); 247; 191
P1	7.81	P1	524	917	[M-2H] ⁻	917 → 755 (-Glc)	755 → 609 (-pC); 339; 284; 309
5'	8.27	C3- (pC)Soph- Glc-C2	308	951	[M-H] ⁻	951 → 623 (-C3-Glc); 463 (-pC-Soph-H ₂ O)	463 → 327 (-C2); 301 (-Glc); 165 (-C2-Glc)
6'a	8.40	C7-(pC)Soph	318	743	[M-H] ⁻	743 → 659; 597 (-pC); 272 (-pC-Soph-H)	659 → 479 (-Glc-H ₂ O); 335
7'	8.83	C6-(pC)Soph	ND	675	[M-H] ⁻	675 → 529 (-pC); 409; 205 (-pC-Soph)	529 → 511 (-H ₂ O); 409; 349 (-Glc-H ₂ O); 205 (-Soph)
6'b	9.30	C7-(pC)Soph	318	743	[M-H] ⁻	743 → 659; 597 (-pC); 272 (-pC-Soph-H)	659 → 479 (-Glc-H ₂ O); 335
P4: Cya-3-O-[(6-O-pC)-Glc-2-O-(2-O-Sp)-Glc]-5-O-Glc (gradient 1)							
PB	4.46	PB	530	1013	[M+Cl-H] ⁻	1013 → 977 (-Cl); 815 (-Glc)	977 → 609 (-Glc)
1''	4.76	pC acid	309	119	[M-H-CO ₂] ⁻	-	-
P2	5.76	P2 (cont.)	530	983	[M+Cl-H] ⁻	983 → 947 (-Cl); 785 (-Glc)	947 → 785 (-Glc)
PBi	5.88	PB isomer	530	1013	[M+Cl-H] ⁻	1013 → 977 (-Cl); 815 (-Cl-Glc)	977 → 609 (-Sp-Glc); 339
P4i	8.12	P4 isomer	530	1159 1123	[M+Cl-H] ⁻ [M-2H] ⁻	1159 → 1123 (-Cl) 1123 → 961 (-Glc)	961 → 755 (-Sp); 737 (-Sp-H ₂ O); 285 (Cya)
Ct4	8.34	P4 Ct	320	1141	[M-H] ⁻	1141 → 977 (-pC-H ₂ O); 869	977 → 853; 935 (-Sp); 469; 285 (Cya)
P4	8.71	P4	534	1123	[M-2H] ⁻	1123 → 961 (-Glc)	961 → 755 (-Sp); 737 (-Sp-H ₂ O); 285 (Cya)
P5	8.89	P5 (cont.)	534	1189	[M+Cl-H] ⁻	1189 → 1153 (-Cl)	1153 → 991 (-Glc); 785 (-Glc-Sp); 947 (-Sp)
2''	9.19	C1-Glc- (Sp,pC) Soph	ND	1067	[M+Cl] ⁻	1067 → 1031 (-Cl)	1031 → 869 (-Glc); 663 (-Glc-Sp); 825 (-Sp); 517 (-Sp-pC-Glc)
Ct4i	9.31	P4 Ct isomer	320	1141	[M-H] ⁻	1141 → 977 (-pC-H ₂ O); 869; 855	869 → 663 (-Sp); 715; 645 (-Sp-H ₂ O); 503
3''a	10.0	C7-(Sp,pC) Soph	ND	949	[M-H] ⁻	949 → 865; 931; 782	931 → 725; 515; 359
3''b	10.6	C7-(Sp,pC) Soph	ND	949	[M-H] ⁻	949 → 865; 931; 782	865 → 711; 847; 539
3''c	11.1	C7-(Sp,pC) Soph	ND	949	[M-H] ⁻	949 → 865; 931; 782	931 → 545; 739; 311

3.1. Hydration and the reversible accumulation of the *trans*-chalcone

The fractions of colored and colorless species at the hydration equilibrium (Scheme 1-SI, Fig. 1-SI) are strongly dependent on the acylation pattern. From the global (hydration included) and specific (sequential proton transfers) acidity constants of the flavylum ion at 25°C (Moloney et al., 2018) it is estimated that PA is almost colorless at pH 7 (99% hemiketal B + chalcones). By contrast, the fraction of colored forms is higher for P1 (*ca.* 15%) and P4 (*ca.* 80% colored forms, of which 55% anionic base).

In heated samples (50°C), the residual *trans*-chalcone (Ct) can be detected by UPLC-DAD-MS when the analyses are performed rapidly after acidification. Indeed, its conversion into the flavylum ion is strongly retarded by the slow *cis-trans* isomerization. The PA *trans*-chalcone (CtA) was detected with $\lambda_{\max} = 330$ nm (Fig. 3-SI), close to the malvidin-3,5-diGlc Ct, at 335 nm (Preston & Timberlake, 1981)). After 1h, the fraction of Ct reaches *ca.* 29% for PA (Fig. 2-SI). By comparison, at pH 6, the Ct fraction accumulated from the triacylated heavenly blue anthocyanin, which has the same glycosidation pattern as the red cabbage pigments, is 32% (Mendoza et al., 2018).

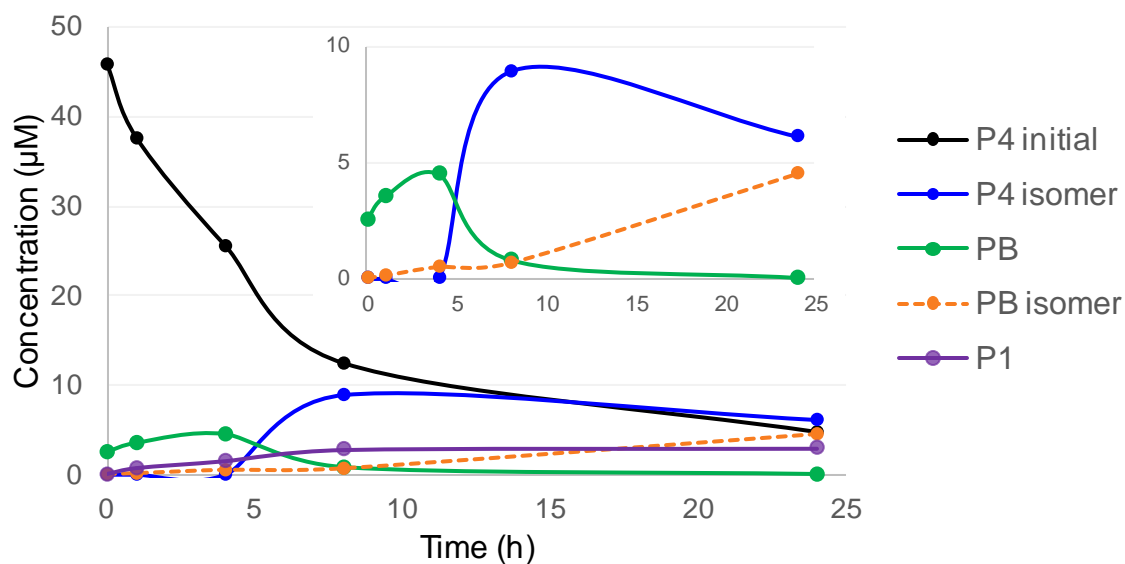
3.2. Deacylation & intramolecular acyl transfer

The acyl groups undergo hydrolysis and intramolecular migration (*trans*-esterification) at pH 7 and 8. After 24h at pH 7, the total yield of these anthocyanin derivatives amounts to 7% for P1 and 28% for P4 (Table 2). The hydrolysis of the protecting acyl moieties must reduce the color stability (Trouillas et al., 2016).

The λ_{\max} values of P1 and P4 in the visible range after a 24h period of heating at pH 7 were shifted by -1 nm and -6 nm respectively, while the λ_{\max} of PA remained unchanged. The decrease in λ_{\max} is ascribed to deacylation, at a rate corresponding to the fraction of deacylation products (PA, PB, P1). P1 and PB are respectively formed upon loss of the Sp and pC residues (Fig. 2). When P1 and PB are heated separately under the same conditions, 37% PA is formed from PB after 24h, *vs.* only 14% from P1. This suggests that the Sp residue (at C2-OH of Glc-2) is more prone to hydrolysis than the pC residue (at C6-OH of Glc-1). Investigations with sucrose acylated by fatty acids (pH 7 – 10) also concluded that esters of primary alcohols are more resistant to saponification than esters of secondary alcohols (Thévenet et al., 1999). Anthocyanin deacylation was observed previously in red cabbage extracts. Over storage, a decrease in the diacylated anthocyanins was compensated by an

increase in the non- and monoacylated ones (Wiczowski et al., 2015). The kinetic monitoring shows that PB is formed from P4 over the first 4 hours, and that isomers of both P4 and PB are formed later (Fig. 2).

A



B

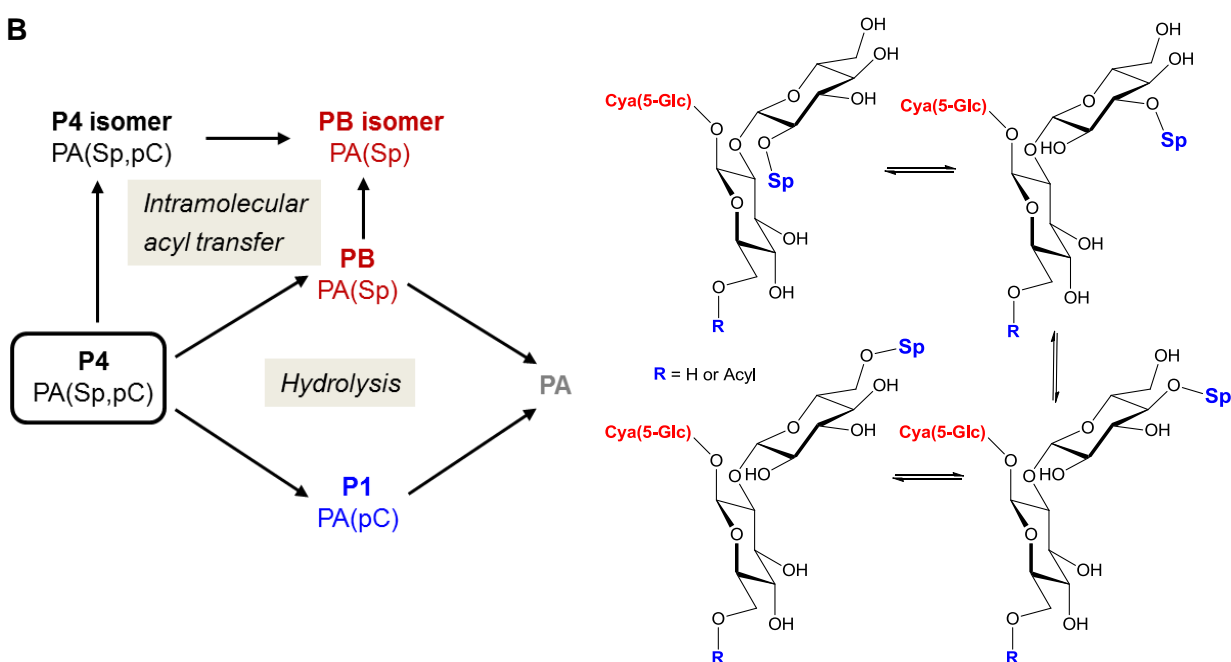
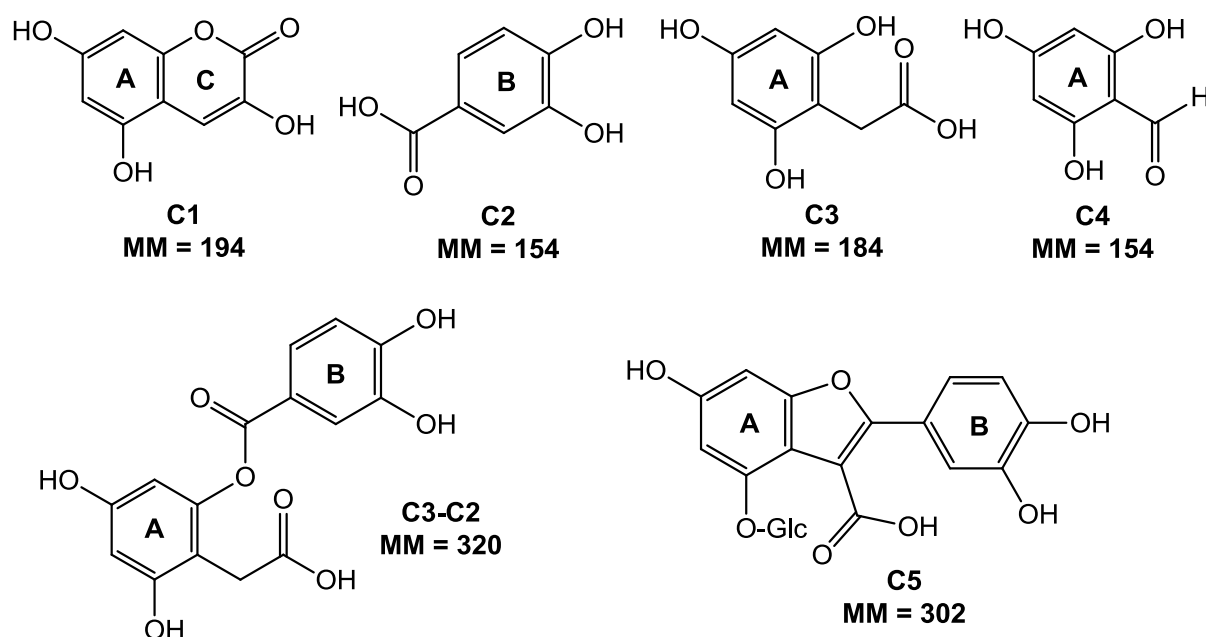


Fig. 2. A: Kinetic monitoring of deacylation and intramolecular acyl transfer for diacylated pigment P4 (pH 7, 50°C, *insert for easier visual appreciation*). **B:** Kinetic scheme and hypothetical intramolecular acyl transfer routes within the sophorose moiety (Glc-2).

Table 2. Quantification by UPLC-DAD of anthocyanin degradation and of the new pigments formed in PA, P1 and P4 solutions after thermal treatment (24h, pH 7, 50°C) in the absence or presence of Fe²⁺. Concentrations in μM of cyanin equivalent (corrected for differences in molar absorption coefficient between pigments).

	Pigment						Pigment + Fe ²⁺ (0.6 equiv.)					
	PA		P1		P4		PA		P1		P4	
	t=0	t=24h	t=0	t=24h	t=0	t=24h	t=0	t=24h	t=0	t=24h	t=0	t=24h
PA	51.5	12.7	2.5	3.0			51.4	1.5	2.4	0.7		
PB					0.8	1.4					2.3	0.5
P1			54.9	25.4	1.4	3.6			56.5	2.8	3.8	1.1
P1 isomer				0.5								
P4 isomer					0.4	9.1					1.3	0.6
P4					51.7	8.1					53.4	13.5
Total anthocyanins	51.5	12.7	57.4	28.9	54.2	22.2	51.4	1.5	58.9	3.4	60.8	15.7
Acyl loss (%)			4.6	5.2	4.0	8.9			4.3	1.2	10.7	2.6
Acyl transfer (%)				0.6	0.8	16.8					1.4	0.5

Upon heating at pH 7 and 8, a major P4 isomer accumulates (Table 2, Fig. 3-SI). It displays a lower λ_{max} (-4 nm) than P4. Two other isomers are also detected, both remaining very minor. By contrast, P1 isomerization is marginal (< 2%). The hypothesis of *cis-trans* isomerization of the HCA residues can be ruled out, first because the samples were heated in the dark, and second, because it would also have occurred with P1. Hence, the P4 isomers are believed to form upon migration (*trans*-esterification) of a HCA residue within the same Glc. As acyl migration within P1 is negligible, it can be assumed that the labile acyl residue of P4 is the sinapoyl residue at C2'-OH. Similar phenomena were reported for aliphatic esters of sucrose in alkaline aqueous solution (Thévenet et al., 1999) with a clear trend of acyl groups to shift from secondary to primary positions. Overall, our data demonstrate that the sinapoyl residue of P4 is more sensitive to both hydrolysis and *trans*-esterification than the *p*-coumaroyl residue.



Scheme 2. Proposed core structures for the major compounds detected (see Table 1). C1 = 3,5,7-trihydroxycoumarin, C2 = protocatechuic acid, C3 = 2,4,6-trihydroxyphenylacetic acid, C4 = phloroglucinaldehyde. Core structures C6 (MM = 205) and C7 (MM = 274) remain unidentified.

3.3. The oxidative products & degradation routes

The products of irreversible degradation of PA, P1 and P4 were characterized by UPLC-MS-DAD (Table 1). Several groups of compounds only differ by the presence of the acyl and/or glucose moieties, and share common fragments in MS² and MS³. In this case, a common core was assumed and tentatively identified (Scheme 2).

3.3.1. CONFIRMED STRUCTURES

Compound **4** is detected in PA, P1 and P4 solutions. Its characteristics are identical to those of a commercial standard of protocatechuic acid (noted C2). Besides, C2 formation upon degradation of cyanidin derivatives was reported several times (Cabrita et al., 2014; Sadilova et al., 2007). Compound **4** is therefore confidently identified as protocatechuic acid.

Compound **2''** is detected in P4 solution only. The commercial standard of *p*-coumaric acid (pC) displays the same characteristics. In HRMS, the [M-H]⁻ ion at *m/z* 163.0401 is also detected ($\Delta = 3.6$ ppm). Compound **2''**, which is expected from the hydrolysis of P4 into PB, is therefore confidently identified as *p*-coumaric acid.

3.3.2. PROBABLE STRUCTURES

Compounds **5**, **4'** and **2''** were respectively detected in PA, P1 and P4 solutions (Fig. 4-SI). They are thought to be derivatives of 3,5,7-trihydroxycoumarin (noted C1). The λ_{\max} of **5** (329 nm) is in agreement with that of the 3,5-O-diglucoside derivative of C1 formed upon treatment of malvidin 3,5-di-O-glucoside (malvin) by H₂O₂ in neutral solution (Hrazdina & Franzese, 1974). As for **4'**, its λ_{\max} (317 nm) is close to that of free *p*-coumaric acid (310 nm) and in agreement with the reported 3-O-(*p*-coumaroyl)glucoside of C1 (λ_{\max} = 315 nm) (Géza Hrazdina & Franzese, 1974). In HRMS, **4'** is detected as [M-H]⁻ at *m/z* 825.2071, in agreement with the calculated monoisotopic value (Δ = 2.2 ppm). Among the fragments identified: the successive losses of Glc to *m/z* 663.1552, and of *p*-coumaroylsophorose down to *m/z* 193.0127. The nonacylated coumarin (**5**) is also detected from P1 after an extended thermal treatment of 96h. Its raw formula is confirmed by HRMS: *m/z* 715.1473 ([M+Cl]⁻) and 679.1707 ([M-H]⁻, Δ = 2.2 ppm). The fragment at *m/z* 553 (from [M+Cl]⁻) likely results from the loss of Glc at C5-OH. By analogy, **2''** must be the diacylated coumarin C1-3-(*p*C,*Sp*)Soph-5-Glc. The following fragments substantiate this hypothesis: 869 ([M-H-Glc]⁻), 825 ([M-H-Sp]⁻), 663 ([M-H-Glc-Sp]⁻) and 517 ([M-H-Glc-Sp-*p*C]⁻). Surprisingly, coumarin derivatives were not detected from anthocyanins that are not glycosylated at C5-OH (Géza Hrazdina & Franzese, 1974). In the absence of added H₂O₂, these products remain in low amounts (<1% of the initial pigment concentration, Table 1-SI).

A series of compounds having a *m/z* of +34 compared to the native pigments were detected. The compounds, noted **12**, **11** and **5'**, display similar UV spectra and produce common fragments at *m/z* 463, 345, 327 and 301. Compound **11**, detected from the 3 pigments, is proposed to be C3(Glc,Soph)-C2, an analog of structures formed upon reacting anthocyanins with H₂O₂ (Satake & Yanase, 2018) or upon their azo-initiated autoxidation (Kamiya et al., 2014). Alternatively, a two-electron oxidized analog was identified in the autoxidation of malvidin 3-O-glucoside in acidic solution (Géza Hrazdina & Franzese, 1974; Lopes et al., 2007). From the [M-H]⁻ ion of compound **12** (C3(Glc)-C2), the loss of C2 and/or H₂O followed by the loss of Glc and/or H₂O or CO₂, was observed (Scheme 2-SI). The *p*-coumaroyl analog (**5'**, *m/z* 951) yields fragments at *m/z* 623 (loss of C3 + Glc) and 463 (loss of *p*C + Soph + H₂O). Second fragmentations of the latter ion give fragments with *m/z* 327 (loss of C2), 301 (loss of Glc) and 165 (loss of C2 + Glc). In HRMS, **5'** is detected at *m/z* 951.2438 (C₄₂H₄₇O₂₅, Δ = 3.3 ppm). Finally, **12** (*m/z* 481) is identified as C3(Glc)-C2. Overall, these compounds are proposed to be (acyl)glycosides of 2-(3,4-dihydroxy)-benzoyloxy-4,6-dihydroxyphenylacetic acid.

Several isomers of compound **1'** (m/z 487) were detected from P1 (Fig. 5-SI). The two major ones **1'c** and **1'd** (m/z 487.1454 in HRMS, corresponding to $C_{21}H_{27}O_{13}$, $\Delta = 0.5$ ppm) were also detected from P4. They mostly fragment by losing H_2O . In MS3, the additional loss of Glc is observed yielding a fragment ion at m/z 307. In ESI(+), ions of m/z 511 and 527, respectively corresponding to the Na^+ and K^+ adducts, were detected. Compound **1'** is proposed to be pC-sophorose released by hydrolysis of 1-O-acylglycosides formed during oxidative degradation pathways. Four diacylsophoroses from purple sweet potato anthocyanins were reported and their structures confirmed by NMR (Terahara et al., 2009). No MS fragmentation data have been reported yet. The pC-sophorose isomers are likely a mixture of regioisomers produced by migration of pC to a neighboring OH group, each potentially present as a mixture of α and β anomers (Scheme 4-SI).

As intramolecular acyl migration is negligible for P1, the pC moiety appears labile in the cleavage products only. Thus, it seems that the acyl–cyanidin π -stacking interactions developed by P1 inhibit acyl migration within the sophorose moiety. Only one diacylsophorose (m/z 693) in low concentration ($< 0.5 \mu M$) could be detected from P4, in agreement to the relatively high sensitivity of the sinapoyl residue to hydrolysis. However, free sinapic acid remains undetected and must be quickly consumed, while free *p*-coumaric acid is detected in P4 solution (Table 1-SI). Consistently, under the same conditions, free sinapic acid undergoes extensive oxidative dimerization after 24h (22% residual content, unpublished data) while *p*-coumaric acid is much more stable (78% residual content).

From a 50 μM pigment solution, the pC-sophorose concentration after a 72h heating reached 11.2 μM and 6 μM from P1 and P4, respectively. The concentration did not plateau, suggesting a high stability of these compounds. Overall, acylglycosides come up as useful indicators of the oxidative degradation of acylated anthocyanins in neutral solution.

Compound **6** is detected with the 3 pigments. Its main fragment (m/z 153) reflects the loss of glucose. The additional loss of 28 (m/z 125) is a decarbonylation step expected for aldehydes. A probable structure for **6** is phloroglucinaldehyde 2-O-glucoside. The formula is in agreement with the detected molecular ion at m/z 315.0714 ($\Delta = 0.7$ ppm) and the aglycone at m/z 153.0203. Phloroglucinaldehyde and its glucoside were frequently reported as anthocyanin degradation products involving the A-ring (Cabrita et al., 2014; Piffaut et al., 1994; Sadilova et al., 2007). Compound **6** accounts for *ca.* 10% of all products present at 24h in PA, P1 and P4 solutions (Table 1-SI).

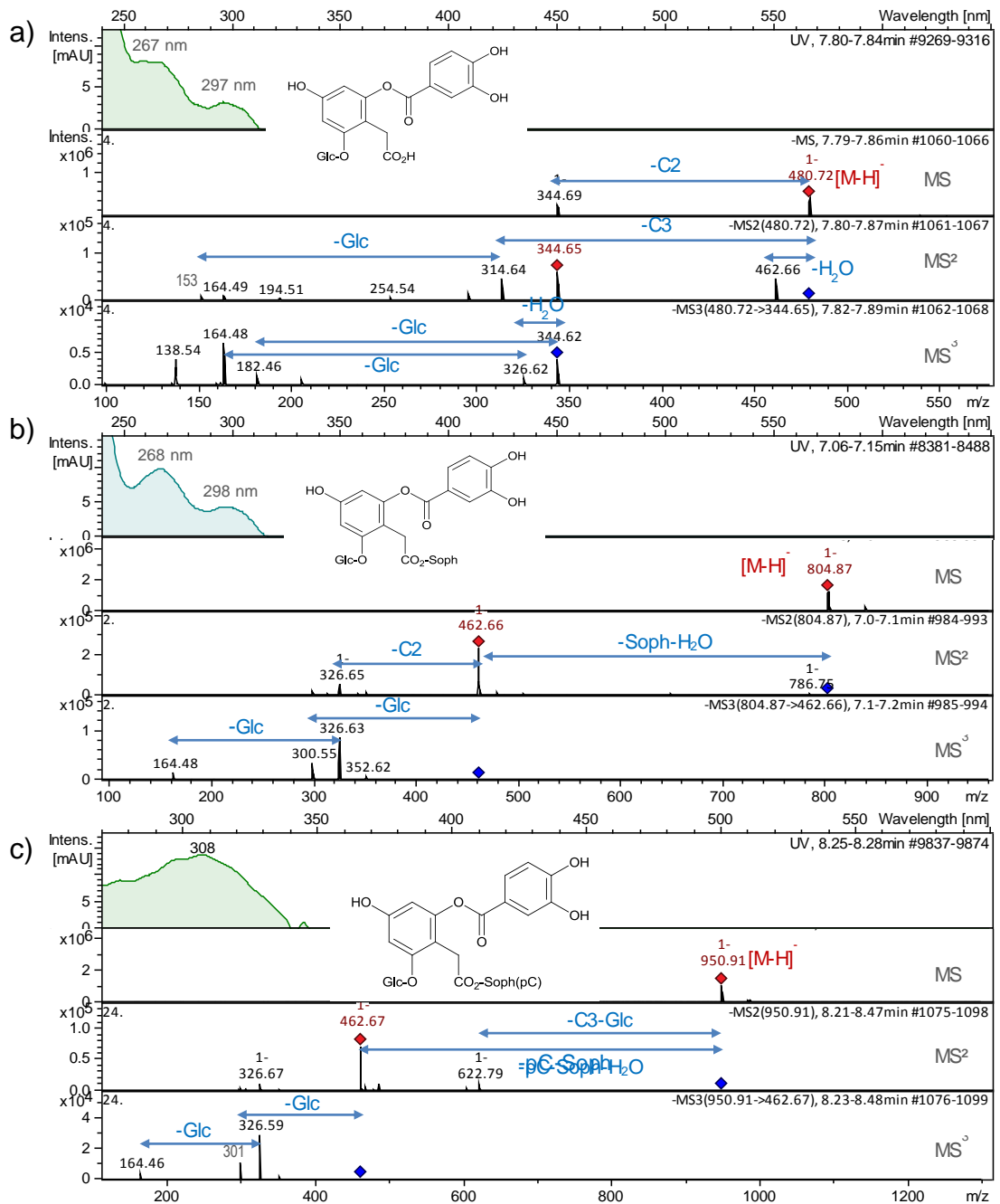


Fig. 3. UV- visible, MS and MS² spectra of a) C3Glc-C2 from PA (m/z 481); b) C3(Soph,Glc)-C2 from PA (m/z 805); c) C3(pCSoph,Glc)-C2 from P1 (m/z 951).

3.3.3. TENTATIVE STRUCTURES

For the following compounds, no literature data is available. However, the structures proposed are compatible with at least two features among raw formula from high resolution MS, MS2 fragments and UV-visible spectrum.

Compound **1** is detected with the 3 pigments (Fig. 6-SI). The $[M-H]^-$ ion undergoes the loss of Glc but also the concomitant loss of Glc + H₂O, with subsequent decarboxylation. This fragmentation pattern is close to that of C3(Glc)-C2 (**12**, Scheme 2-SI). Based on these characteristics, **1** is proposed to be 2-glucosyloxy-4,6-dihydroxyphenylacetic acid (C3Glc). Compound **1** is probably produced by hydrolysis of the C3-C2 derivatives identified above (**11** and **12**). HRMS confirmed the raw formula proposed for **1**: C₁₄H₁₈O₁₀ (m/z 345.0810, $\Delta = 3.4$ ppm). This group of products is mostly detected from the nonacylated anthocyanin (6.6% of the initial pigment concentration at 24h, Table 1-SI).

3.3.4. OTHER COMPOUNDS

Compound **14** is a minor product detected in PA solution. Its fragmentation pattern mainly consists in the loss of CO₂ and water (Fig. 7-SI). A closely related structure (same core noted C5) was reported previously in the reaction of cyanidin 3-O-glucoside with H₂O₂ in a water/ethanol mixture (Satake & Yanase, 2018). It is consistent with the raw formula deduced from m/z 463.1051 in HRMS ($\Delta = 1.0$ ppm).

Compounds **8** and **7'** are sophorosides of the same unidentified aglycone noted C6 (m/z 205.0131 for C₁₀H₅O₅, $\Delta = 2.9$ ppm, Fig. 8-SI). The chemical formulas of **8** (m/z 529.1190, $\Delta = 0.7$ ppm) and its *p*-coumaroyl ester **7'** (m/z 675.1564, $\Delta = 0.4$ ppm) are respectively C₂₂H₂₆O₁₅ and C₃₁H₃₂O₁₇.

Similarly, compounds **9**, **6'** and **3''** are sophorosides of the same structure noted C7 (m/z 272.0323, even value detected as a fragment with both mass spectrometers, Fig. 9-SI), which has no equivalent in the literature. The raw formula of C7 (C₁₄H₁₀O₆) is compatible with the ions detected for **6'** and **9** at the respective m/z values of 743.1816 and 597.1461 ($\Delta = 1.0$ and 0.9 ppm). C7 derivatives could be produced by a multistep mechanism starting with the electrophilic addition of H₂O₂ to the anionic base at position C3. Compounds **9**, **6'** and **3''** are all detected as mixtures of 2 or 3 isomers. While acyl transfer can be proposed for **6'** and **3''** to account for this observation, the isomerization of **9** remains unexplained. Moreover, the

absence of glucose at C5-OH, which is normally not labile in neutral solution, is surprising. Hence, the structure proposed in Fig. 9-SI must be regarded as tentative.

3.4. MEDIUM EFFECTS

The major products - other than anthocyanins - detected after 24h in PA, P1 and P4 are quantified in Table 1-SI. Besides the products of acyl migration, protocatechuic acid (C2) and phloroglucinaldehyde-2-glucoside (C4-Glc) come up as major products. The putative C6 and C7 derivatives are also relatively abundant (*ca.* 10% of the initial pigment concentration).

Fe²⁺ prevents the accumulation of the *trans*-chalcones through the formation of metal complexes resistant to water addition. More surprising is the almost total inhibition of P4 isomerization and deacylation. Higher concentrations of oxidation products, *e.g.* C7 derivatives **6'**, were detected in Fe²⁺-supplemented P1 solutions (Fig. 10-SI) in agreement with Fe²⁺ promoting P1 autoxidation (Fenger et al., 2019). This trend is not observed with P4.

Addition of H₂O₂ (1 equiv.) to P1 solution leads to a much higher concentration of pC-sophorose and coumarin derivatives and C3-C2 derivatives (Fig. 3). Addition of H₂O₂ in large excess (10³ equiv.) induces a fast consumption of the anthocyanin even in the absence of thermal treatment. Under both conditions, pC-sophorose and C1 derivatives are the major products. Moreover, a major, yet unidentified, product (*m/z* 625 and 312, fragment at 183 corresponding to C3) is specifically formed (Fig. 11-SI).

Under argon atmosphere (low O₂ level), more residual pigment is present after 24h and the known oxidation products of P1 and PA are very minor (Fig. 4).

Finally, in order to identify late degradation products of anthocyanins, the heating period was extended to 72h. The chromatograms (Fig. 12-SI) show the accumulation of protocatechuic acid from all three pigments, and of the pC-sophorose isomers and coumarin *p*-coumaroylglycoside from P1 and P4 (as after addition of 1 equiv. H₂O₂).

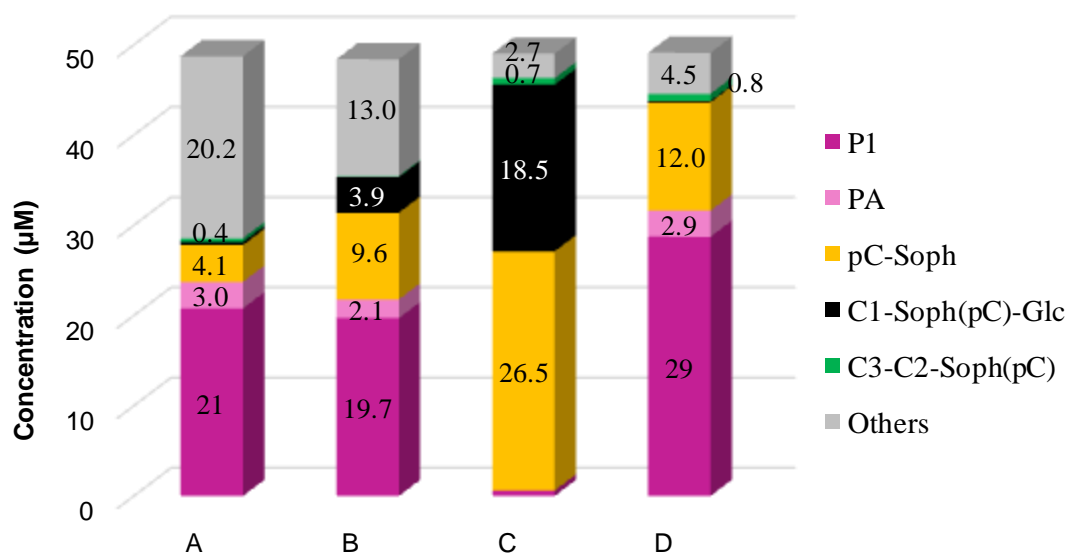


Fig. 4. Distribution of degradation products from P1 after 24h at pH 7, 50°C. **A:** P1. **B-C:** Impact of added H₂O₂ (**B:** 1 equiv., **C:** 10³ equiv.), **D:** Impact of an argon atmosphere.

Interestingly, none of the P4 degradation products bears the sinapoyl residue (except traces of diacylsophorose). Again, the Sp residue is not only more prone to intramolecular migration than the pC residue, but also more labile or more reactive.

4. DISCUSSION

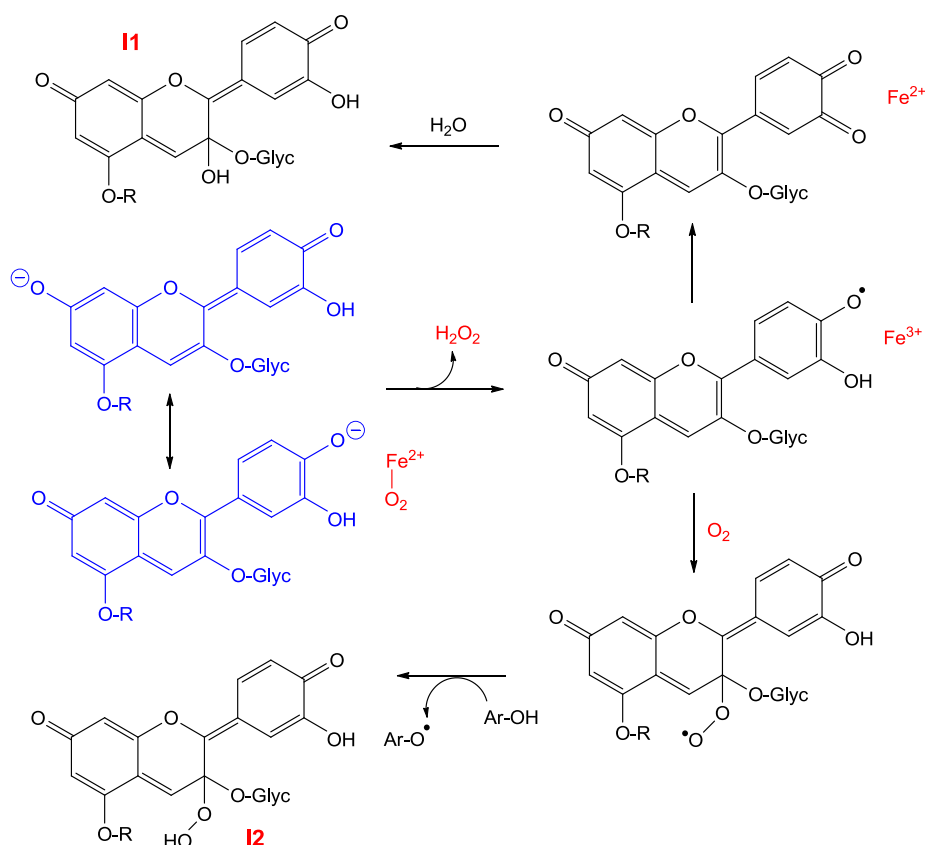
At neutral pH, anthocyanins are a mixture of neutral and anionic bases slowly evolving into a mixture of hemiketal and chalcones. Upon moderate heating in neutral solution, red cabbage anthocyanins evolve by acyl hydrolysis and intramolecular transfer. The migration of the sinapoyl group (at C2-OH of Glc-2) appears specific to an acyl residue borne by a secondary C-atom. It is proposed to shift to the primary C-atom (C6-OH, major isomer) through the 2 intermediate secondary C-atoms (C3-OH and C4-OH, minor isomers). As most acylated anthocyanins display their acyl groups at primary C-atoms, this type of isomerization is generally not observed and constitutes a remarkable feature of red cabbage anthocyanins. Interestingly, when these anthocyanins are bound to iron, the sinapoyl residue loses its mobility. The well-known propensity of HCA residues for developing π -stacking interactions with the anthocyanidin nucleus (Moloney et al., 2018; Trouillas et al., 2016a) could be intensified within these complexes, given the capacity of iron to coordinate up to 3 anthocyanin ligands (Estévez et al., 2019), thereby increasing the rigidity of the HCA residues and inhibiting their migration.

For red cabbage anthocyanins, the rate of anthocyanin consumption (oxidative degradation) in neutral solution is not significantly different for the di- and monoacylated pigments, and unexpectedly slightly faster than for the nonacylated one (Fenger et al., 2019). This observation was interpreted by assuming that PA is rapidly converted into the colorless forms (by reversible water addition), which are much more resistant to autoxidation than the electron-rich anionic base (far more abundant in solutions of acylated anthocyanins) (Fenger et al., 2019).

Upon degradation of an extract of purple sweet potato containing acylated 3-O-sophorosyl-5-O-glucosylpeonidins (caffeoyl, feruloyl and *p*-hydroxybenzoyl residues), the monoacylated anthocyanins appeared more stable than the diacylated ones (Xu et al., 2015). However, part of this apparent stability could be due to the partial hydrolysis of diacylated anthocyanins, thereby replenishing the pool of monoacylated anthocyanins.

We recently showed that Fe^{2+} addition strongly slows down the rate of color loss in P4 solution at pH 7, mostly because the *p*-quinonemethide structure of P4 in the complex does not undergo water addition (Fenger et al., 2019). This is consistent with Fe^{2+} addition inhibiting the formation of the *trans*-chalcone. Besides its strong influence on the reversible

color loss, Fe^{2+} addition caused a modest slowing down of the early stage (up to 10h at pH 7, 50°C) of irreversible degradation for P4, while the opposite holds for PA and P1 (Fenger et al., 2019). This difference was ascribed to the higher stability of the iron – P4 (vs. iron – P1) complex due to enhanced π -stacking interactions, while leakage of iron from the iron – P1 complex probably accelerates autoxidation. However, 24h after iron addition, no protection of P4 against irreversible degradation could be evidenced (Table 2). On the other hand, the accumulation of oxidation products in iron-supplemented solutions obviously remains more modest in P4 than in P1 solution (Fig. 10-SI).



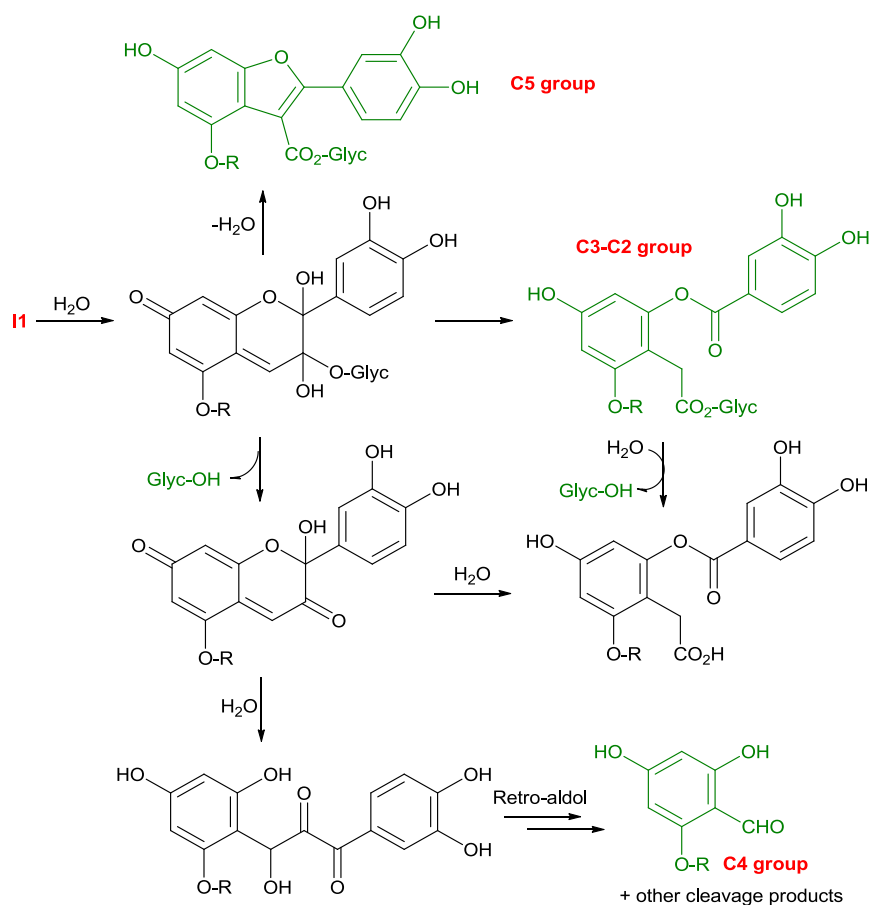
Scheme 3. Proposed mechanisms for the early stages of anthocyanin autoxidation in neutral solution.

Our recent kinetic analysis suggests that the colored forms are primarily involved in the oxidative degradation at pH 7 (Fenger et al., 2019), which is consistent with the anionic base being probably a much better electron donor than the other (neutral) species. We thus assume that the first step consists in an electron transfer from A^- to O_2 under the mediation of transition metal traces, most probably Fe^{2+} . The aryloxy radical thus formed can evolve through 2 distinct pathways (Scheme 3):

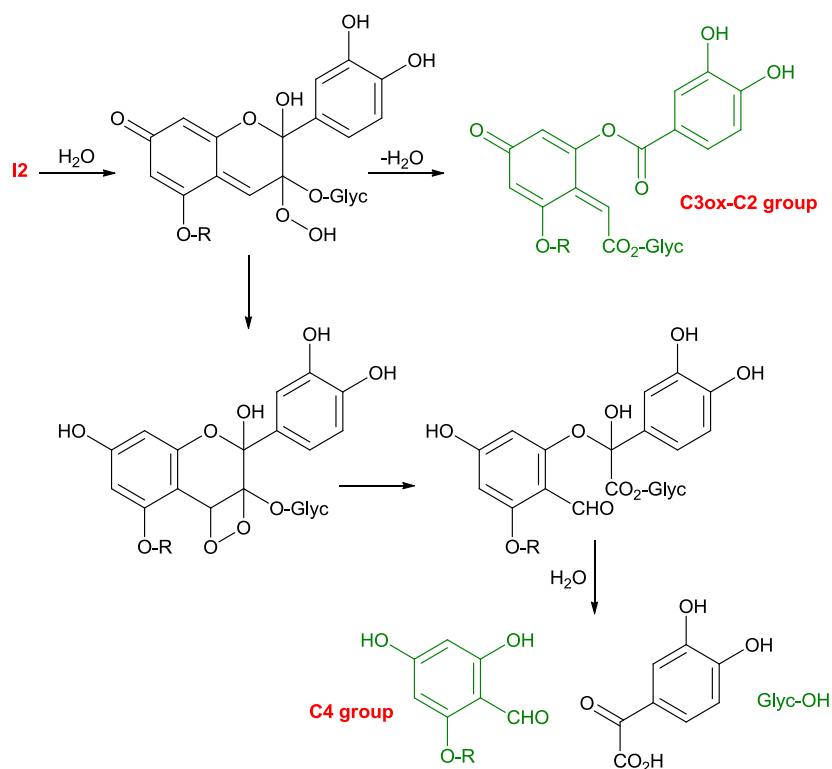
a) A second electron transfer to form a highly electrophilic *o*-quinone intermediate (pathway specific to B-rings having a 3',4'-dihydroxy substitution such as cyanidin derivatives) with concomitant generation of H₂O₂. Then, the *o*-quinone is expected to add a water molecule, thereby leading to intermediate I1.

b) Addition of O₂ with formation of a highly reactive peroxy radical, which will rapidly abstract a labile H-atom from a second anthocyanin molecule, thus yielding intermediate I2, a hydroperoxide.

Intermediates I1 and I2 may have different fates, some leading to products identified in this work or in the literature. In particular, I1 can add a second water molecule and form an intermediate already postulated to result from the electrophilic attack of H₂O₂ to the hemiketal in acidic solution (Satake & Yanase, 2018). From this intermediate, two end-products (belonging to the C3-C2 and C5 groups) duly identified by NMR can be produced (Scheme 4). Alternatively, elimination of the glycosyl group at C3-OH is feasible. More generally, the conversion of the glycosidic bond at C3-OH into an ester bond opens up a route for the release of the glycosyl group in neutral solution through simple hydrolysis.



Scheme 4. Proposed mechanisms for the fate of intermediate I1.



Scheme 5. Proposed mechanisms for the fate of intermediate I2.

Similar mechanisms can be written from I2 (Scheme 5). In this case, C3-C2 compounds are also expected, although in a two-electron oxidized version. Such a compound (two (*Z,E*) isomers) was indeed fully identified by NMR in the autoxidation of malvidin 3-O-glucoside in acidic solution (Lopes et al., 2007). With a malvidin derivative (no catechol ring), the two-electron oxidation pathway is quenched and O₂ addition is actually the most likely fate for the aryloxy radical. However, with the cyanidin derivatives investigated in this work, only the reduced version was evidenced, an indication that the two-electron oxidation pathway is privileged (Schemes 3 & 4) and/or that H₂O₂ addition to the anthocyanins also occurs (see below). Alternatively, formation of a 1,2-dioxetane ring (with concomitant re-aromatization of the A-ring) might open up a route for the formation of C4 derivatives (Scheme 5). Phloroglucinaldehyde and its glycosides are actually classical markers of anthocyanin degradation (Fleschhut et al., 2006; Sadilova et al., 2007). They could be formed by other routes, such as H₂O₂ addition to C3ox (free acid), followed by decarboxylation, or retro-aldol condensation from C-ring-opened intermediates (Scheme 4).

Hydrogen peroxide produced in the autoxidation step probably participates in the oxidative degradation (as suggested by the experiments with added H₂O₂), either by electrophilic attack onto the anionic base or hemiketal (C3 position), or by nucleophilic attack

onto the flavylum ion (C2 position) or chalcone (Bayer-Villiger reaction). The first route has been convincingly demonstrated in acidic solution from labelling experiments (reaction with $\text{H}_2^{18}\text{O}_2$ or in H_2^{18}O) (Satake & Yanase, 2018). It leads to intermediate II (also produced by two-electron oxidation and subsequent water addition, Scheme 3) or its water adduct. The second route has the additional advantage to rationalize the formation of the coumarin derivatives. On the one hand, these products are detected at pH 5 – 7 but not at pH < 3 (Géza Hrazdina & Franzese, 1974), which is not consistent with a mechanism involving the flavylum ion. On the other hand, addition of H_2O_2 indeed promotes their formation, *e.g.* **4'** (Fig. 4). Overall, the second route remains possible, although coumarins might be also produced through autoxidation of the anionic base (Scheme 3-SI). However, complementary products derived from the B-ring (*p*-hydroquinones in the Bayer-Villiger rearrangement, *p*-quinones in the autoxidation route) were not detected.

Finally, no direct participation of the HCA residues in the oxidative degradation could be evidenced and analyses by UPLC-DAD-MS and by capillary zone electrophoresis failed to detect anthocyanin dimers or higher oligomers.

Conclusions

Under the conditions where anthocyanins express blue colors, *i.e.* pH 7 in the presence of metal ions or pH 8, they undergo oxidative and hydrolytic pathways that alter the color and restrict their applications. The irreversible degradation of acylated red cabbage anthocyanins at 50°C leads to several groups of products, among which phloroglucinaldehyde-2-glucoside, *p*-coumaroylsophorose (a mixture of regioisomers) and derivatives of 2-(3,4-dihydroxy)benzoxyloxy-4,6-dihydroxyphenylacetic acid are the major ones. Overall, the acylglycosides (*p*-coumaroylsophorose in this work) appear particularly stable and thus constitute suitable markers of the irreversible degradation of acylated anthocyanins.

In addition, the diacylated red cabbage anthocyanins appear remarkably prone to isomerization by intramolecular acyl transfer, a phenomenon that is evidenced for the first time.

Overall, the irreversible degradation of anthocyanins in neutral solution is probably kinetically controlled by an initial step of one- or two-electron autoxidation of the anionic

base. The major oxidation products are thus proposed to derive either from the oxidized anionic base itself or from an electrophilic attack of H₂O₂ (produced in the autoxidation step) to the anionic base.

For the development of anthocyanin extracts as food colorants in neutral media, the priority should be set at providing protection against autoxidation, for instance by the formation of stable redox-inert metal complexes or by adding suitable antioxidants.

Acknowledgements

The HRMS analyses were carried out on the ESI-Q-trap of the *Metaboscope* Platform funded by the European Fund for Regional Development, the French Ministry of Research, Higher Education and Innovation, the Region Provence-Alpes-Côte d'Azur, the Departmental Council of Vaucluse and the Urban Community of Avignon. The authors gratefully thank Christian Ginies for his support in the MS analyses, and Dr. Véronique Cheynier for helpful discussion.

REFERENCES

- Ahmadiani, N., Robbins, R. J., Collins, T. M., & Giusti, M. M. (2016). Molar absorptivity (ϵ) and spectral characteristics of cyanidin-based anthocyanins from red cabbage. *Food Chemistry*, *197*, 900–906. <https://doi.org/10.1016/j.foodchem.2015.11.032>
- Buchweitz, M., Brauch, J., Carle, R., & Kammerer, D. R. (2013). Colour and stability assessment of blue ferric anthocyanin chelates in liquid pectin-stabilised model systems. *Food Chemistry*, *138*(2–3), 2026–2035. <https://doi.org/10.1016/j.foodchem.2012.10.090>
- Cabrera, L., Petrov, V., & Pina, F. (2014). On the thermal degradation of anthocyanidins: cyanidin. *RSC Advances*, *4*(36), 18939–18944. <https://doi.org/10.1039/C3RA47809B>
- Dangles, O., & Fenger, J.-A. (2018). The Chemical Reactivity of Anthocyanins and Its Consequences in Food Science and Nutrition. *Molecules*, *23*(8), 1970. <https://doi.org/10.3390/molecules23081970>
- Es-Safi, N.-E., Meudec, E., Bouchut, C., Fulcrand, H., Ducrot, P.-H., Herbette, G., & Cheynier, V. (2008). New Compounds Obtained by Evolution and Oxidation of Malvidin 3- O -Glucoside in Ethanolic Medium. *Journal of Agricultural and Food Chemistry*, *56*(12), 4584–4591. <https://doi.org/10.1021/jf8001872>
- Estévez, L., Sánchez-Lozano, M., & Mosquera, R. A. (2019). Complexation of common metal cations by cyanins: Binding affinity and molecular structure. *International Journal of Quantum Chemistry*, *119*(6), 1–11. <https://doi.org/10.1002/qua.25834>
- Fenger, J.-A., Moloney, M., Robbins, R. J., Collins, T. M., & Dangles, O. (2019). The influence of acylation, metal binding and natural antioxidants on the thermal stability of red cabbage anthocyanins in neutral solution. *Food & Function*, *10*(10), 6740–6751. <https://doi.org/10.1039/C9FO01884K>
- Fleschhut, J., Kratzer, F., Rechkemmer, G., & Kulling, S. E. (2006). Stability and biotransformation of various dietary anthocyanins in vitro. *European Journal of Nutrition*, *45*(1), 7–18. <https://doi.org/10.1007/s00394-005-0557-8>
- Hrazdina, G., & Franzese, A. J. (1974). Oxidation products of acylated anthocyanins under acidic and neutral conditions. *Phytochemistry*, *13*(1), 231–234. [https://doi.org/10.1016/S0031-9422\(00\)91300-1](https://doi.org/10.1016/S0031-9422(00)91300-1)
- Idaka, E., Yamakita, H., Ogawa, T., Kondo, T., Yamamoto, M., & Goto, T. (1987). Structure of Three Diacylated Anthocyanins Isolated from Red Cabbage, *Brassica oleracea*. *Chemistry Letters*, *16*(6), 1213–1216. <https://doi.org/10.1246/cl.1987.1213>
- Kamiya, H., Yanase, E., & Nakatsuka, S. (2014). Novel oxidation products of cyanidin 3-O-glucoside with 2,2'-azobis-(2,4-dimethyl)valeronitrile and evaluation of anthocyanin content and its oxidation in black rice. *Food Chemistry*, *155*, 221–226. <https://doi.org/10.1016/j.foodchem.2014.01.077>
- Lopes, P., Richard, T., Saucier, C., Teissedre, P.-L., Monti, J.-P., & Glories, Y. (2007). Anthocyanone A: A Quinone Methide Derivative Resulting from Malvidin 3-O-Glucoside Degradation. *Journal of Agricultural and Food Chemistry*, *55*(7), 2698–2704. <https://doi.org/10.1021/jf062875o>
- Mendoza, J., Basílio, N., Pina, F., Kondo, T., & Yoshida, K. (2018). Rationalizing the Color in Heavenly Blue Anthocyanin. A Complete Kinetic and Thermodynamic Study. *The Journal of Physical Chemistry. B*, *122*(19), 4982–4992. <https://doi.org/10.1021/acs.jpcc.8b01136>
- Moloney, M., Robbins, R. J., Collins, T. M., Kondo, T., Yoshida, K., & Dangles, O. (2018). Red cabbage anthocyanins: The influence of d-glucose acylation by hydroxycinnamic acids on their structural transformations in acidic to mildly alkaline conditions and on the resulting color. *Dyes and Pigments*, *158*, 342–352. <https://doi.org/10.1016/j.dyepig.2018.05.057>
- Piffaut, B., Kader, F., Girardin, M., & Metche, M. (1994). Comparative degradation pathways of malvidin 3,5-diglucoside after enzymatic and thermal treatments. *Food Chemistry*, *50*(2), 115–120. [https://doi.org/10.1016/0308-8146\(94\)90106-6](https://doi.org/10.1016/0308-8146(94)90106-6)

- Pina, F. (2014). Chemical Applications of Anthocyanins and Related Compounds. A Source of Bioinspiration. *Journal of Agricultural and Food Chemistry*, 62(29), 6885–6897. <https://doi.org/10.1021/jf404869m>
- Preston, N. W., & Timberlake, C. F. (1981). Separation of anthocyanin by high-performance liquid chromatography. *Journal of Chromatography*, 214, 222–228.
- Sadilova, E., Carle, R., & Stintzing, F. C. (2007). Thermal degradation of anthocyanins and its impact on color and in vitro antioxidant capacity. *Molecular Nutrition & Food Research*, 51(12), 1461–1471. <https://doi.org/10.1002/mnfr.200700179>
- Satake, R., & Yanase, E. (2018). Mechanistic studies of hydrogen-peroxide-mediated anthocyanin oxidation. *Tetrahedron*, 74(42), 6187–6191. <https://doi.org/10.1016/j.tet.2018.09.012>
- Seeram, N. P., Bourquin, L. D., & Nair, M. G. (2001). Degradation Products of Cyanidin Glycosides from Tart Cherries and Their Bioactivities. *Journal of Agricultural and Food Chemistry*, 49(10), 4924–4929. <https://doi.org/10.1021/jf0107508>
- Sigurdson, G. T., Robbins, R. J., Collins, T. M., & Giusti, M. M. (2017). Effects of hydroxycinnamic acids on blue color expression of cyanidin derivatives and their metal chelates. *Food Chemistry*, 234, 131–138. <https://doi.org/10.1016/j.foodchem.2017.04.127>
- Sinela, A., Rawat, N., Mertz, C., Achir, N., Fulcrand, H., & Dornier, M. (2017). Anthocyanins degradation during storage of Hibiscus sabdariffa extract and evolution of its degradation products. *Food Chemistry*, 214, 234–241. <https://doi.org/10.1016/j.foodchem.2016.07.071>
- Stebbins, N. B. (2016). Ascorbic acid-catalyzed degradation of cyanidin-3- O- β -glucoside: Proposed mechanism and identification of a novel hydroxylated product. *Journal of Berry Research*, 6(2), 175–187. <https://doi.org/10.3233/JBR-160132>
- Terahara, N., Matsui, T., Minoda, K., Nasu, K., Kikuchi, R., Fukui, K., Ono, H., & Matsumoto, K. (2009). Functional New Acylated Sophoroses and Deglycosylated Anthocyanins in a Fermented Red Vinegar. *Journal of Agricultural and Food Chemistry*, 57(18), 8331–8338. <https://doi.org/10.1021/jf901809p>
- Thévenet, S., Wernicke, A., Belniak, S., Descotes, G., Bouchu, A., & Queneau, Y. (1999). Esterification of unprotected sucrose with acid chlorides in aqueous medium: kinetic reactivity versus acyl- or alkyloxycarbonyl-group migrations. *Carbohydrate Research*, 318(1), 52–66. [https://doi.org/10.1016/S0008-6215\(99\)00079-8](https://doi.org/10.1016/S0008-6215(99)00079-8)
- Trouillas, P., Sancho-García, J. C., De Freitas, V., Gierschner, J., Otyepka, M., & Dangles, O. (2016). Stabilizing and Modulating Color by Copigmentation: Insights from Theory and Experiment. *Chemical Reviews*, 116(9), 4937–4982. <https://doi.org/10.1021/acs.chemrev.5b00507>
- Wiczowski, W., Szawara-Nowak, D., & Topolska, J. (2015). Changes in the content and composition of anthocyanins in red cabbage and its antioxidant capacity during fermentation, storage and stewing. *Food Chemistry*, 167(Supplement C), 115–123. <https://doi.org/10.1016/j.foodchem.2014.06.087>
- Xu, J., Su, X., Lim, S., Griffin, J., Carey, E., Katz, B., Tomich, J., Smith, J. S., & Wang, W. (2015). Characterisation and stability of anthocyanins in purple-fleshed sweet potato P40. *Food Chemistry*, 186, 90–96. <https://doi.org/10.1016/j.foodchem.2014.08.123>
- Zhang, J.-L., Luo, C.-L., Zhou, Q., & Zhang, Z.-C. (2018). Isolation and identification of two major acylated anthocyanins from purple sweet potato (*Ipomoea batatas* L. cultivar Eshu No. 8) by UPLC-QTOF-MS/MS and NMR. *International Journal of Food Science & Technology*, 53(8), 1932–1941. <https://doi.org/10.1111/ijfs.13780>

Chapter 3.

The fate of acylated anthocyanins in mildly heated neutral solution

SUPPLEMENTARY INFORMATION

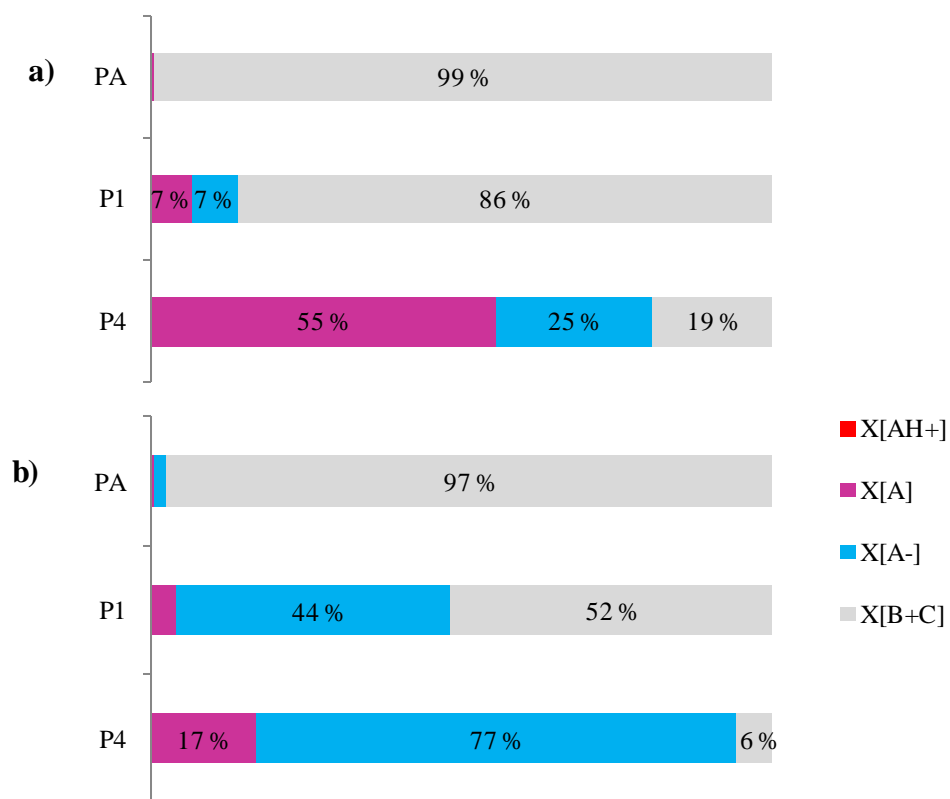
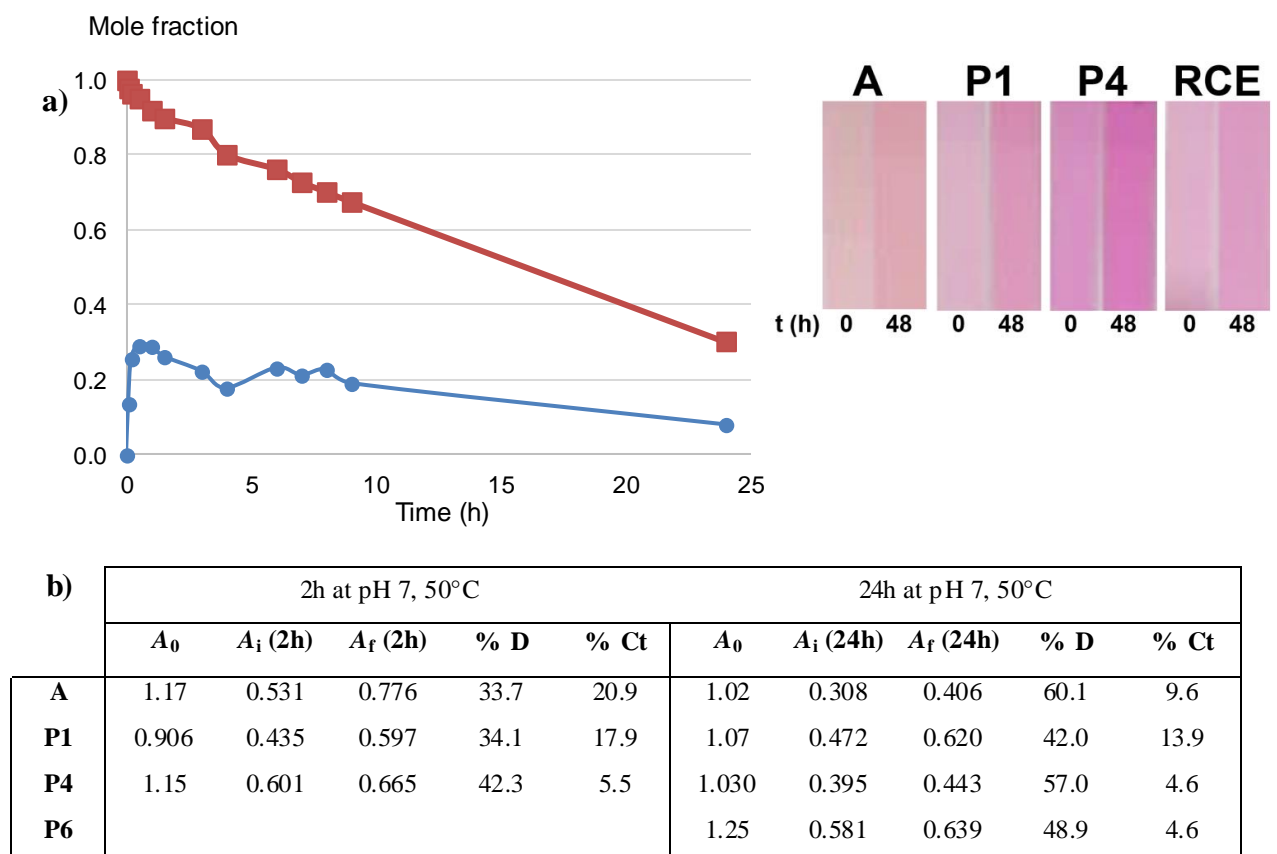


Fig. 1-SI. Species distribution at a) pH 7 and b) pH 8, calculated at 25°C from the acidity and hydration thermodynamic constants [3].



Only the flavylium absorbs at λ_{max} vis (510 to 530 nm). A_0 = absorbance of the total flavylium concentration at $t = 0$, $A(2h)$: residual concentration after 2h heating (including degradation products D), A_i = absorbance recorded 1 min after acidification, A_f = absorbance in the same sample, after 48h stabilization at room T, and conversion of Ct into AH^+ ; % D = $100 \times (A_0 - A_f) / A_0$ and % Ct = $100 \times (A_f - A_i) / A_0$.

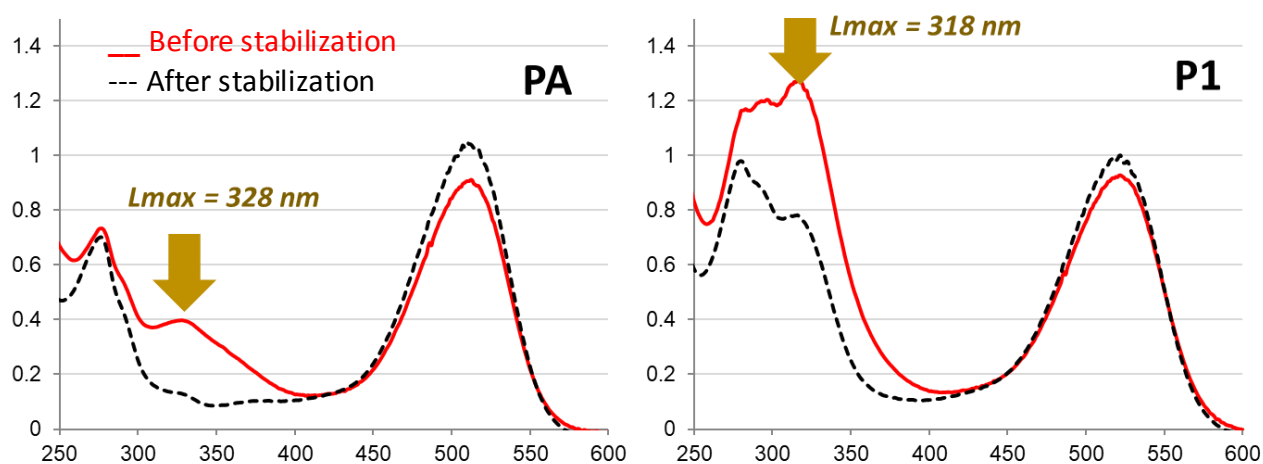
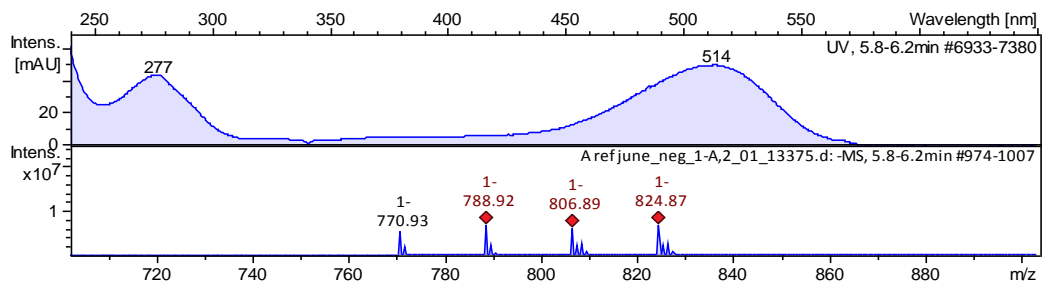
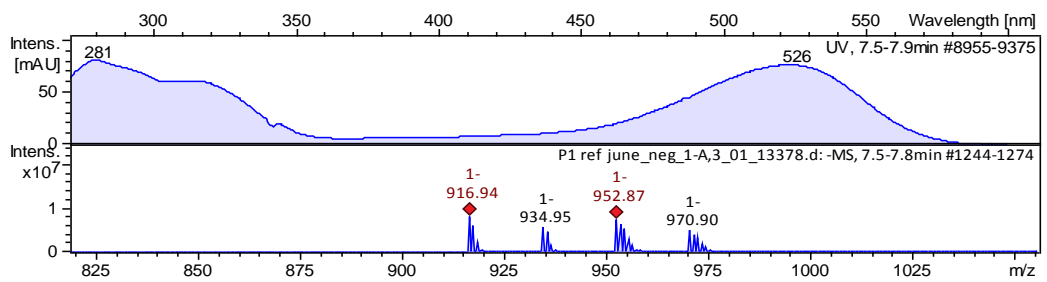


Fig. 2-SI. a) Evolution of the residual flavylium ion (AH^+) of pigment PA (■) over heating at pH 7, 50°C and formation of the trans-chalcone of PA (CtA) (●). The residual flavylium ion obtained after 48h stabilization includes the fraction of Ct. After 1 min: total concentration = AH^+ + Ct + D (degradation products), and after 48h: total concentration = AH^+ + D. CtA accumulates over 1h and then undergoes degradation. b) Estimated fractions of trans-chalcone and degradation products (D) from PA, P1, P4 after 2h and 24h at pH 7, 50°C.

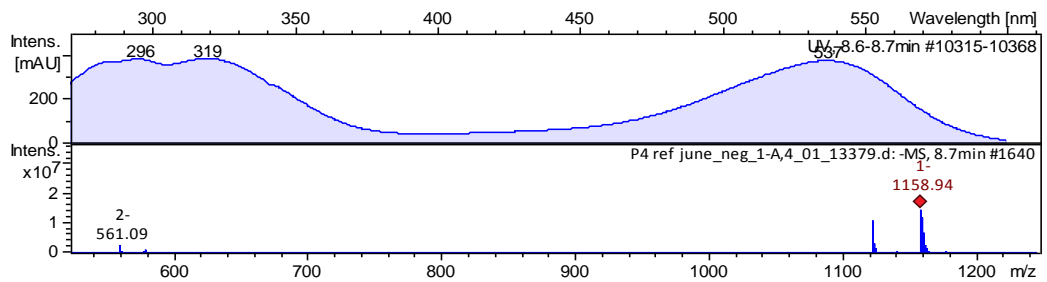
PA



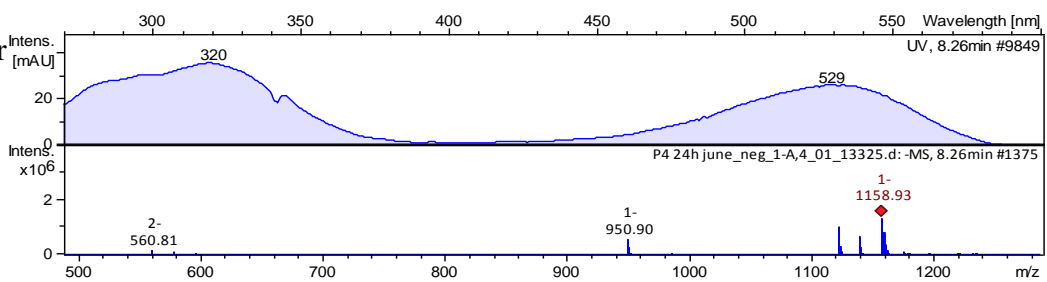
P1



P4



P4 isomer



(Continued next page)

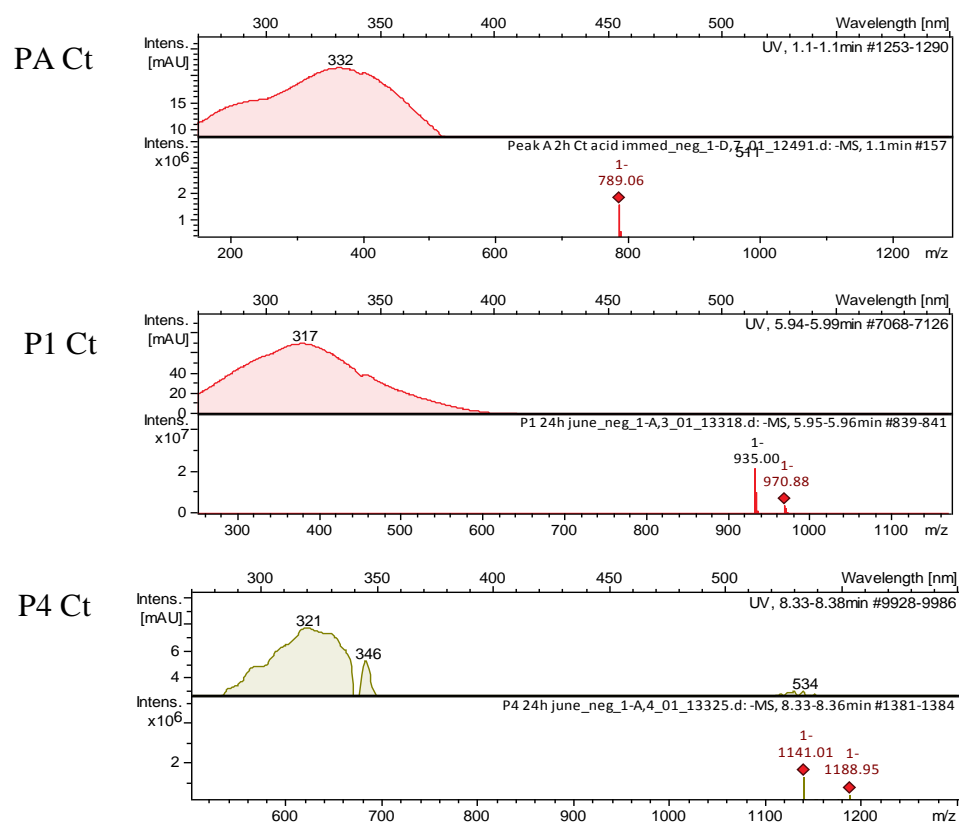


Fig. 3-SI. UV-visible and mass spectra of the pigments and their *trans*-chalcones. P4 isomer obtained after heating for 24h at 50°C, pH 7.

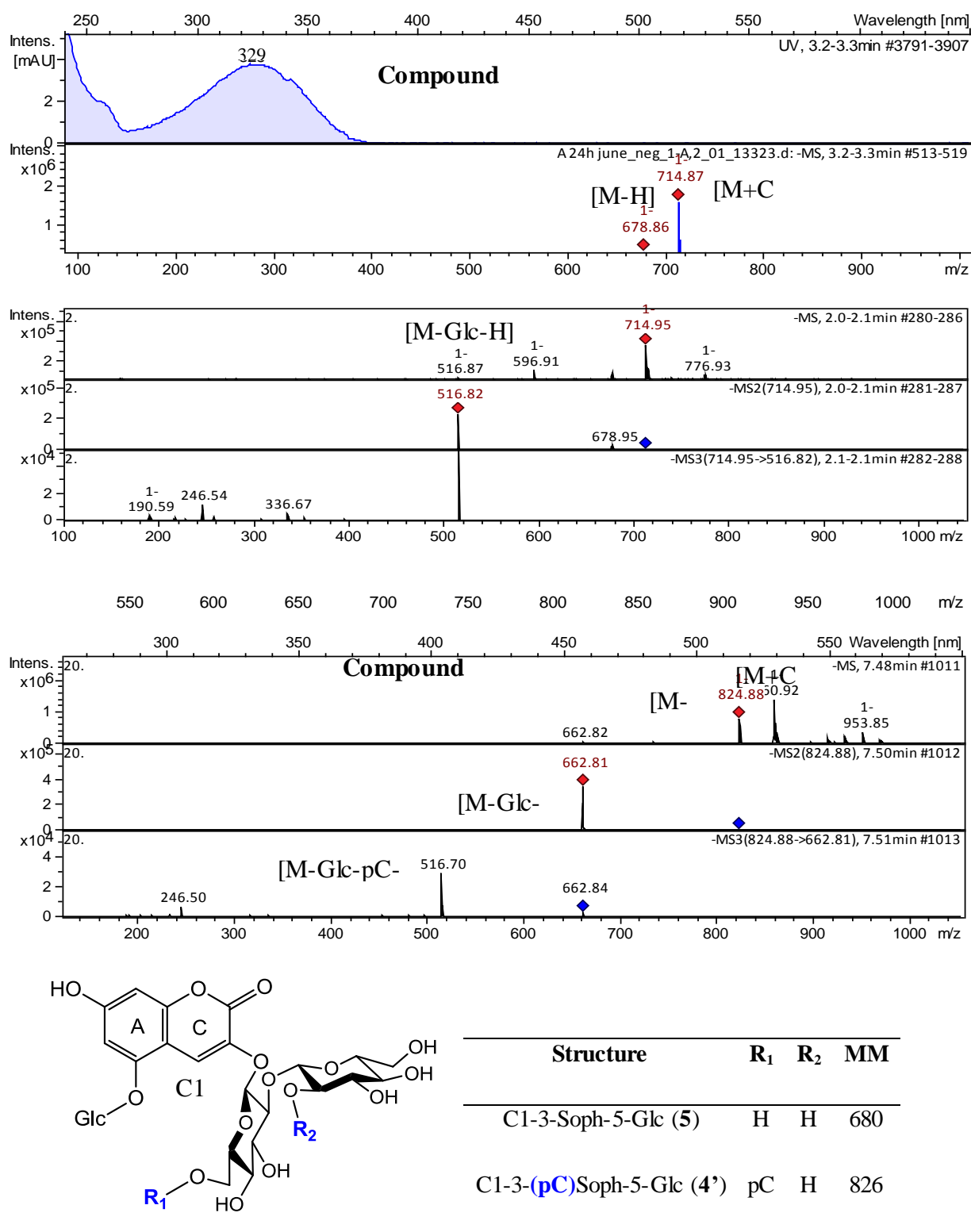


Fig. 4-SI. DAD, MS and MS² data for the coumarin derivatives from PA and P1.

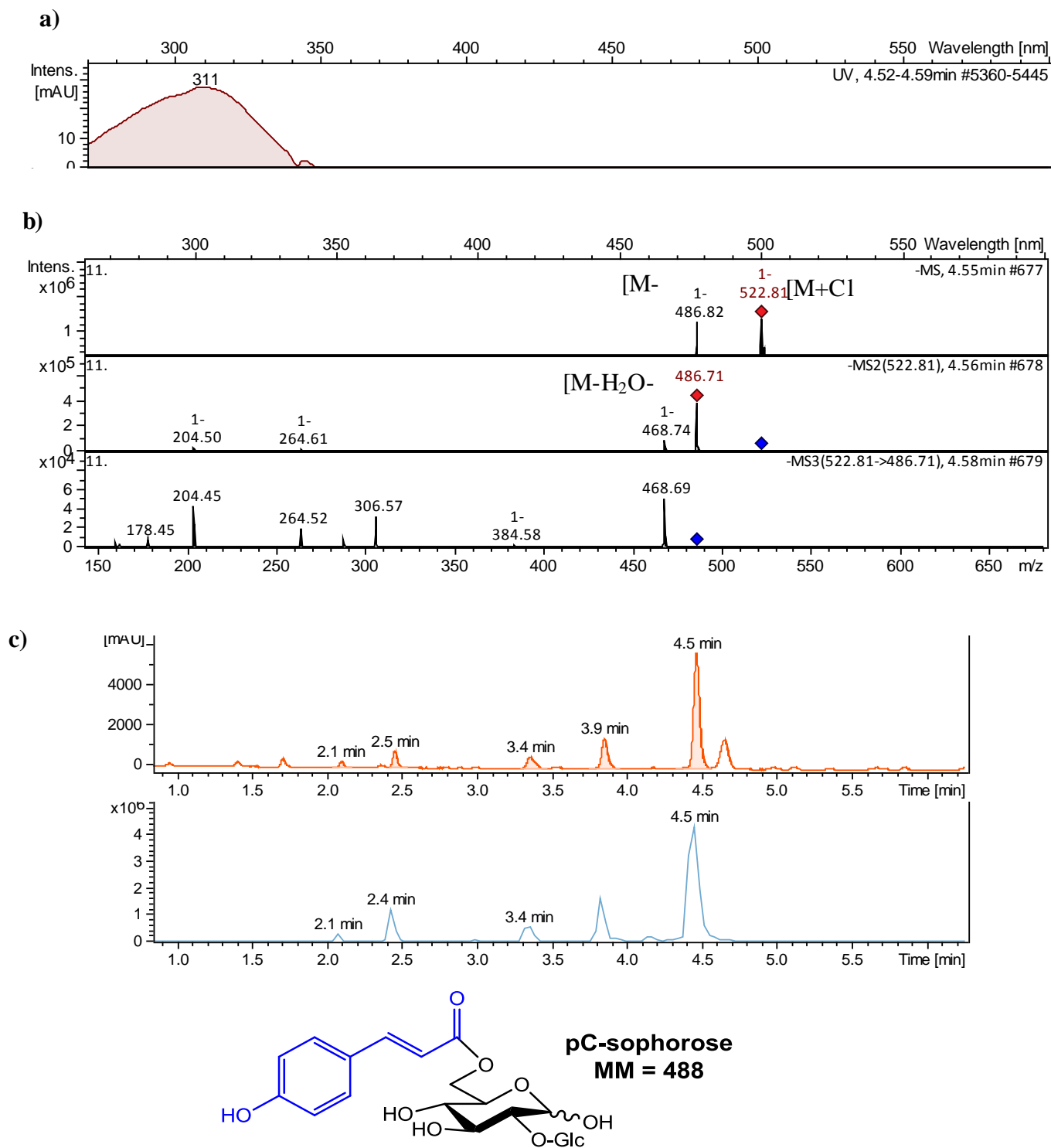


Fig. 5-SI. Identification of p-coumaroylsophorose (**1'**) from P1 (major isomer at $R_t = 4.55$ min): a) DAD spectrum. b) MS and MS² data. c) Chromatograms of the isomers.

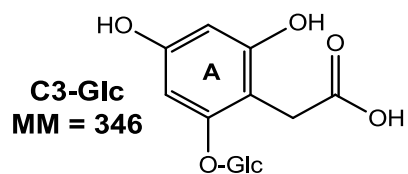
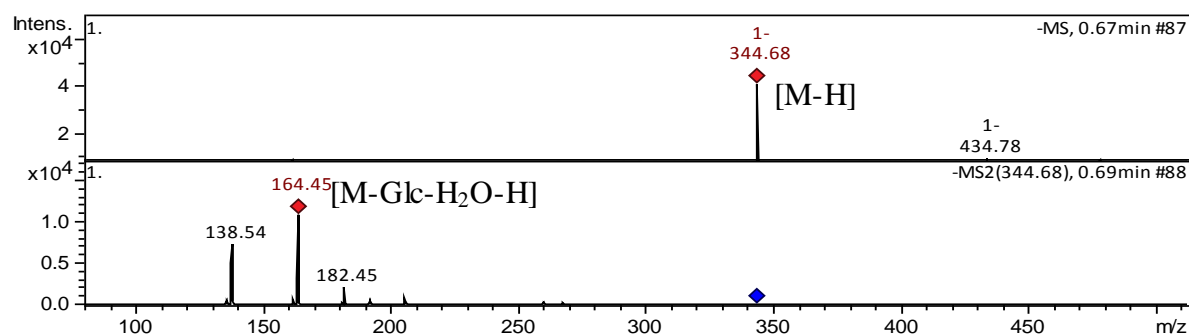
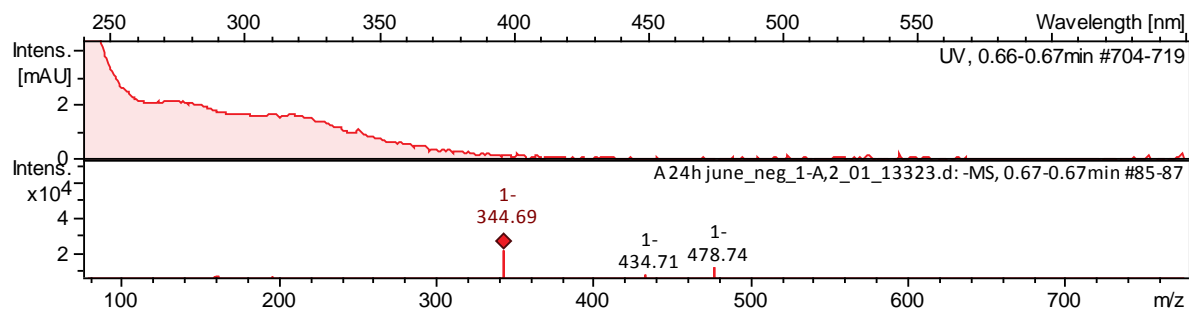


Fig. 6-SI. DAD, MS and MS2 data for compound **1** (from PA and P1)

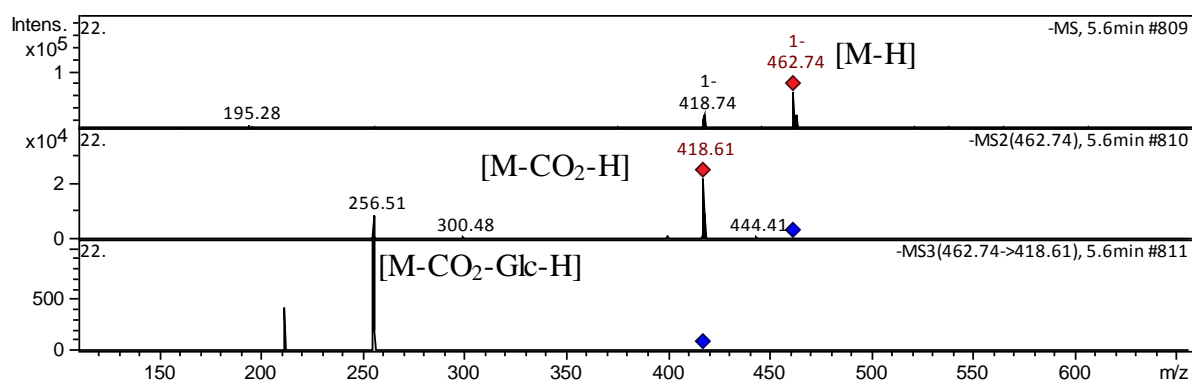


Fig. 7-SI. MS, MS2 and MS3 data for compound **14** detected in PA and P1 solutions.

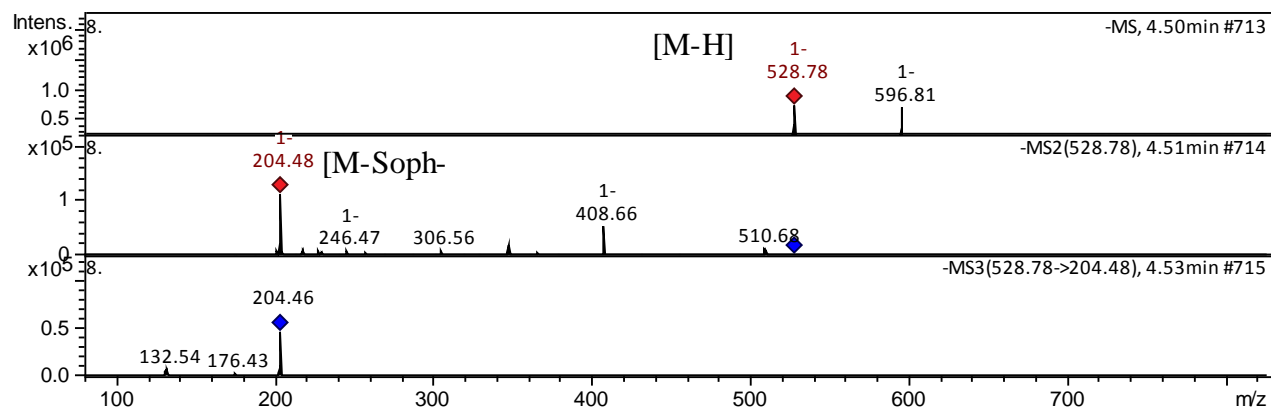


Fig 8-SI. MS, MS2 and MS3 data for compound **8** (C6-Soph) from PA.

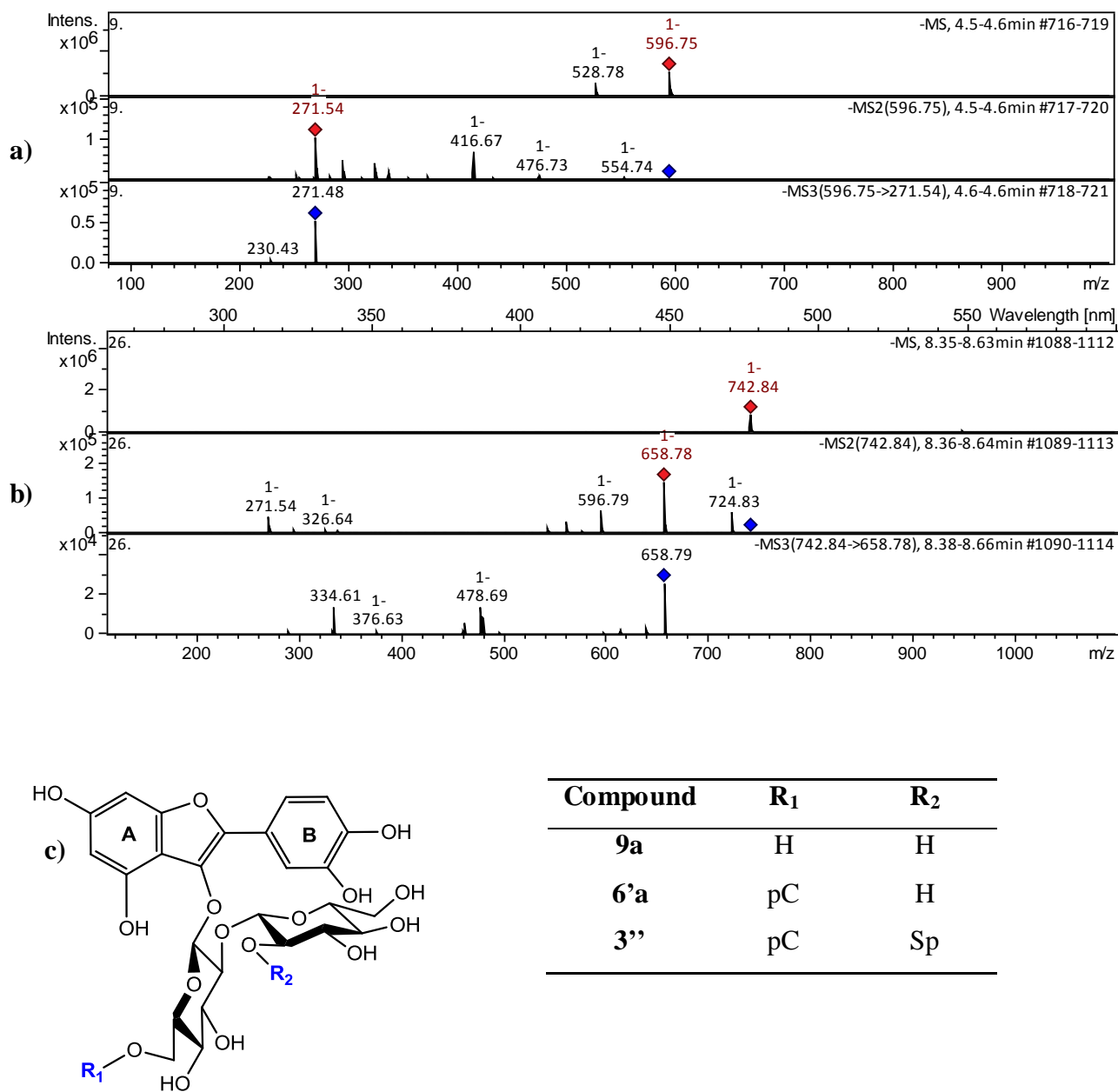


Fig. 9-SI. MS and MS2 data of **a)** compound **9a** (m/z 597) and **b)** compound **6'a** (m/z 743).
c) Tentative structures for C7 derivatives.

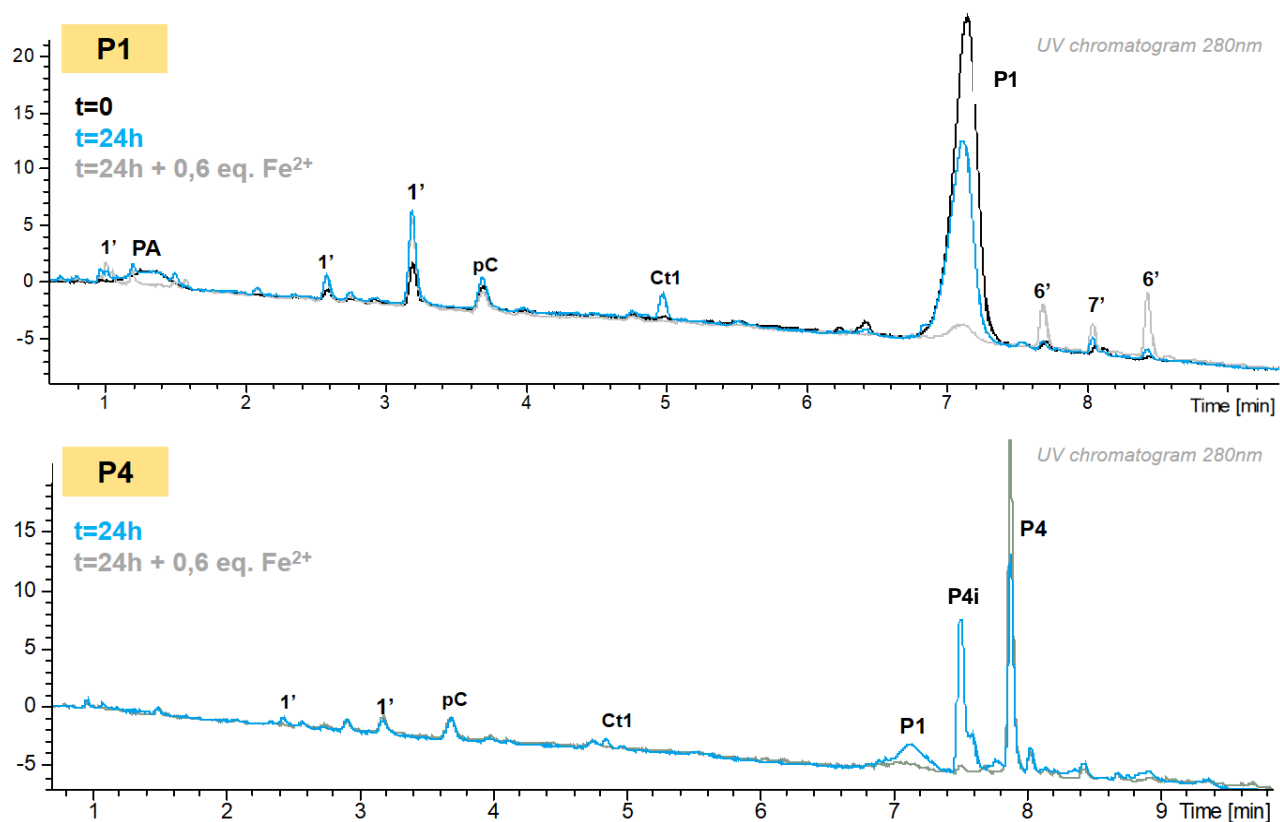


Fig. 10-SI. Impact of Fe²⁺ addition on pigment degradation (UPLC analysis 1h after acidification to pH 1.2)

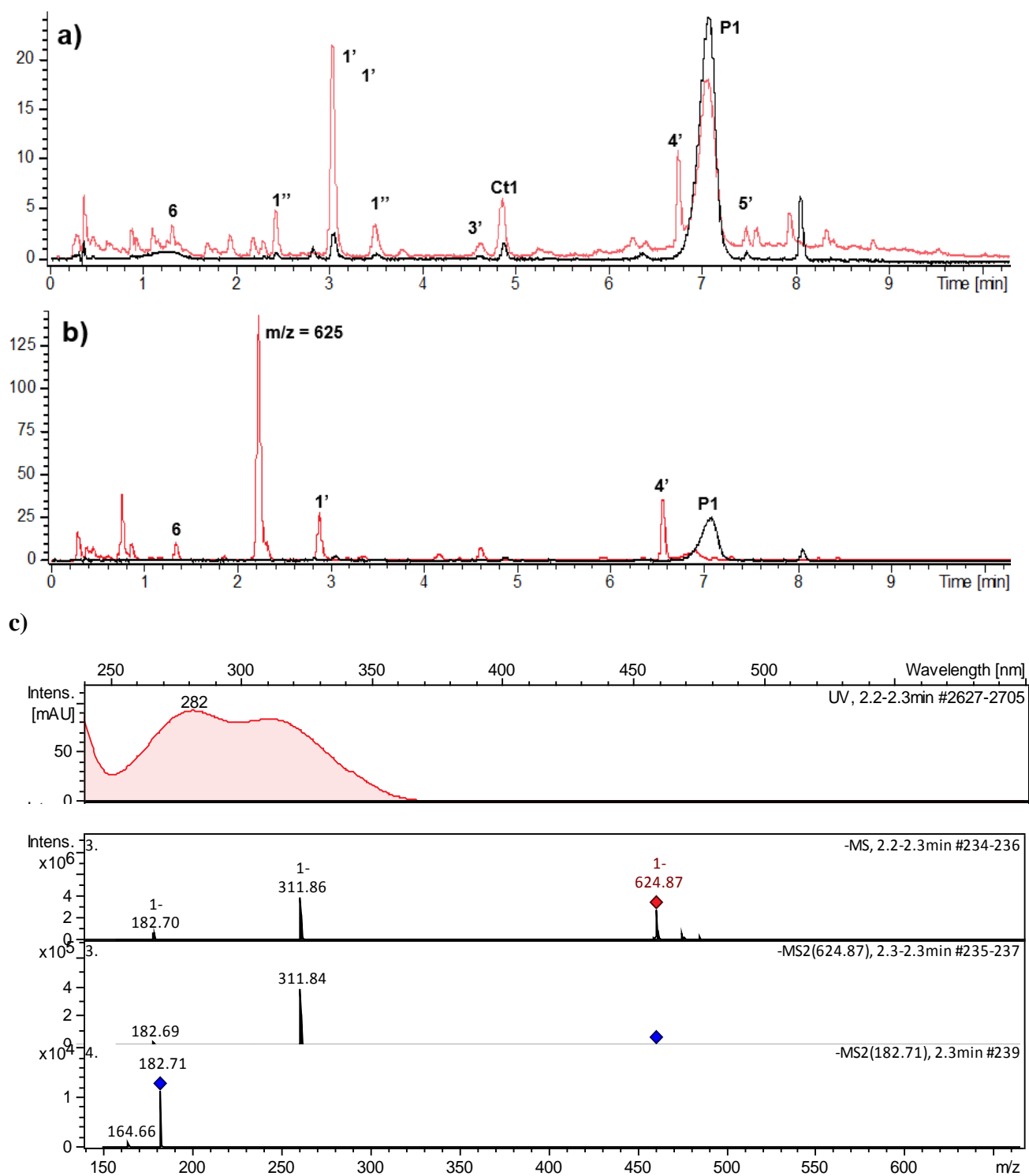


Fig. 11-SI. Chromatograms at 280 nm of P1 solution after 24h at pH 7, 50°C without and with added H₂O₂; a) 1 molar equiv.; b) 10³ molar equiv. c) DAD spectrum, MS and MS2 data of compound at m/z 625.

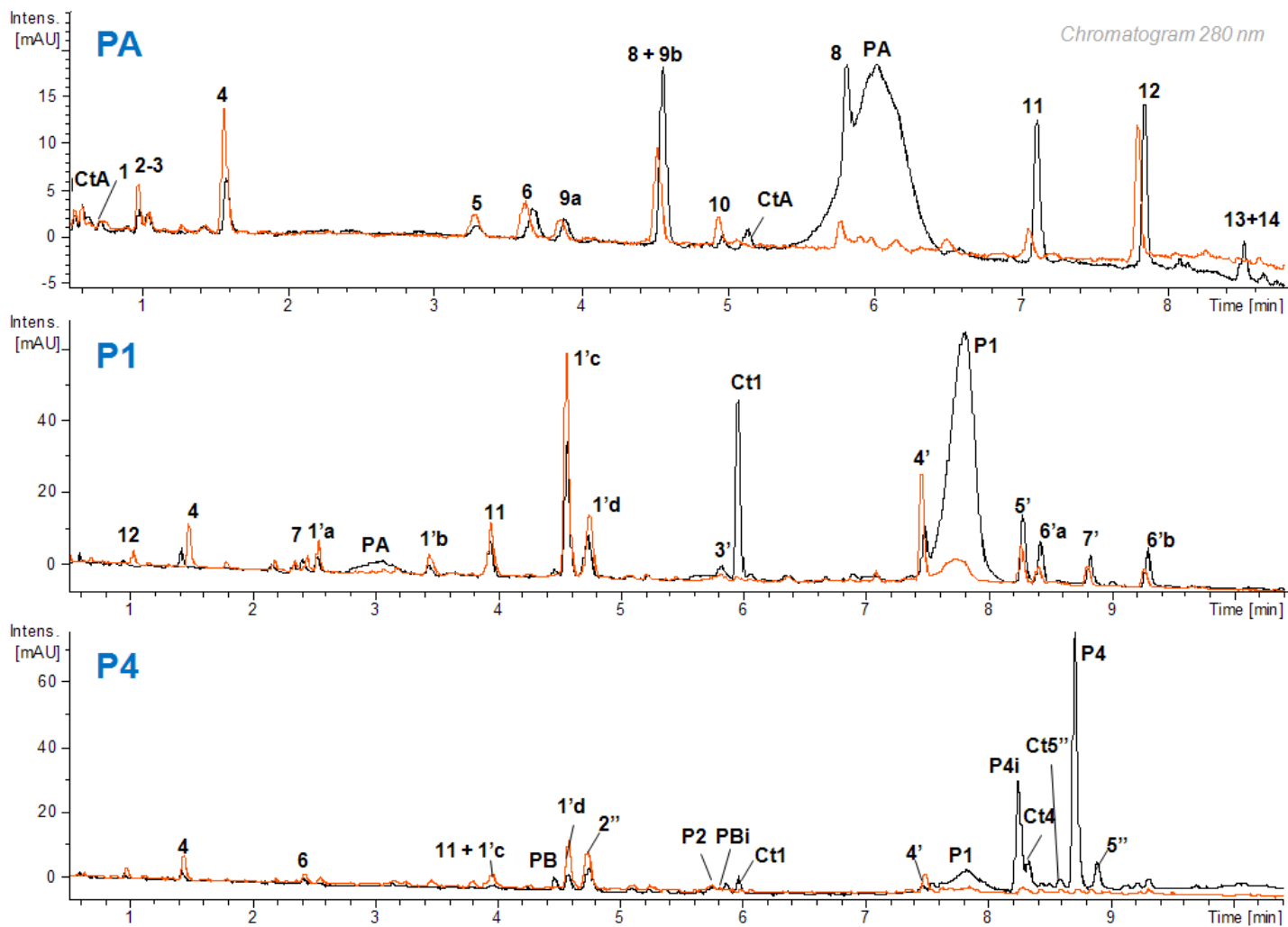


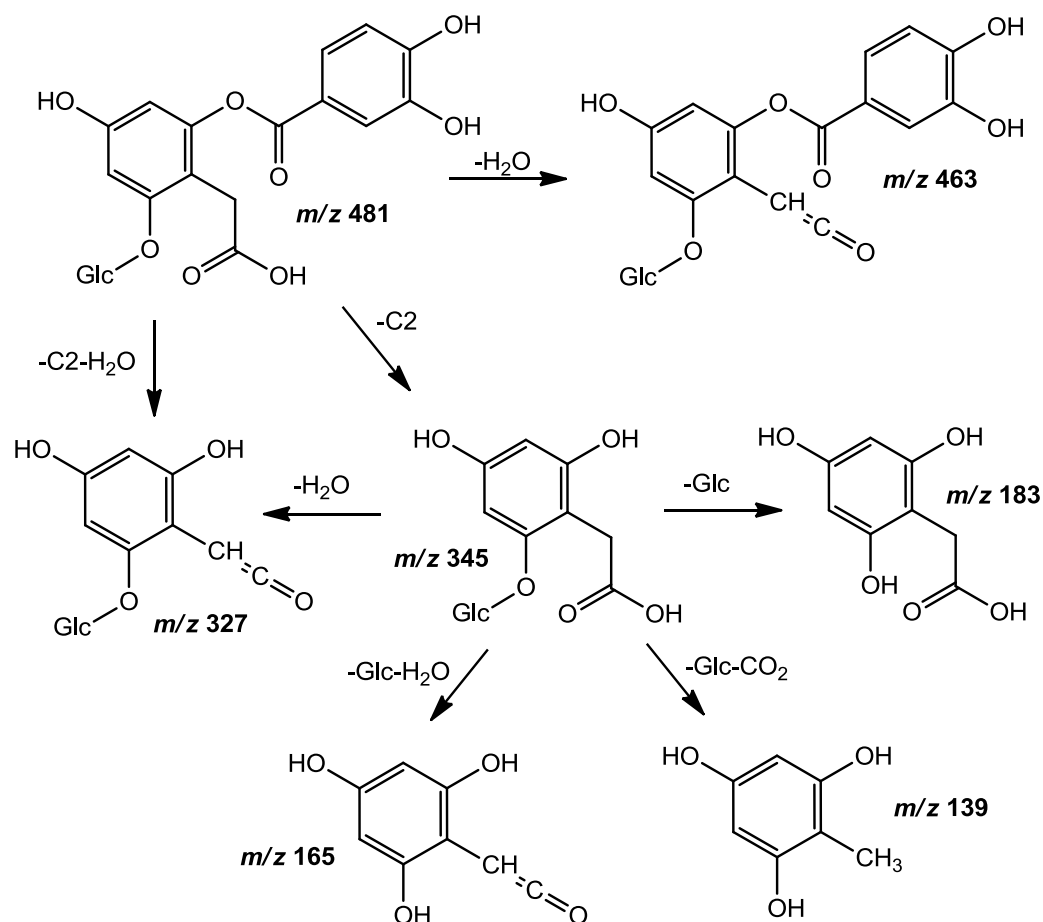
Fig. 12-SI. Chromatograms of the pigment solutions after prolonged thermal degradation: 24h (in black) vs. 72h (in red)

Table 1-SI. Product quantification in PA, P1 and P4 solutions after 24h at pH 7, 50°C

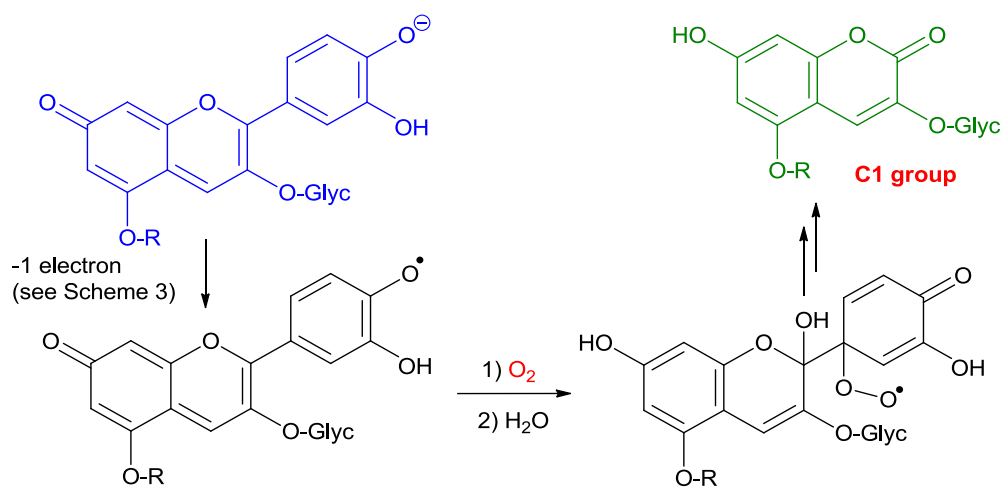
#	Compound	Reference	Concentration at 24h (% of initial pigment concentration)		
			PA	P1	P4
1'	pC-Soph	pC equiv.	NA	8.6	1.3
4	C2	C2 equiv.	2.1	1.3	0.7
6	C4-Glc	C4 equiv.	8.7	10.6	9.5
1''	<i>p</i> -Coumaric acid	pC equiv.	NA	3.8	0.4
5	C1-Soph,Glc derivatives	pC equiv.	0.8	0.7	0.8
5'	C3-C2-Soph derivatives	pC equiv.	6.6 ^a	0.4	ND ^b

^a As protocatechuic acid equivalent

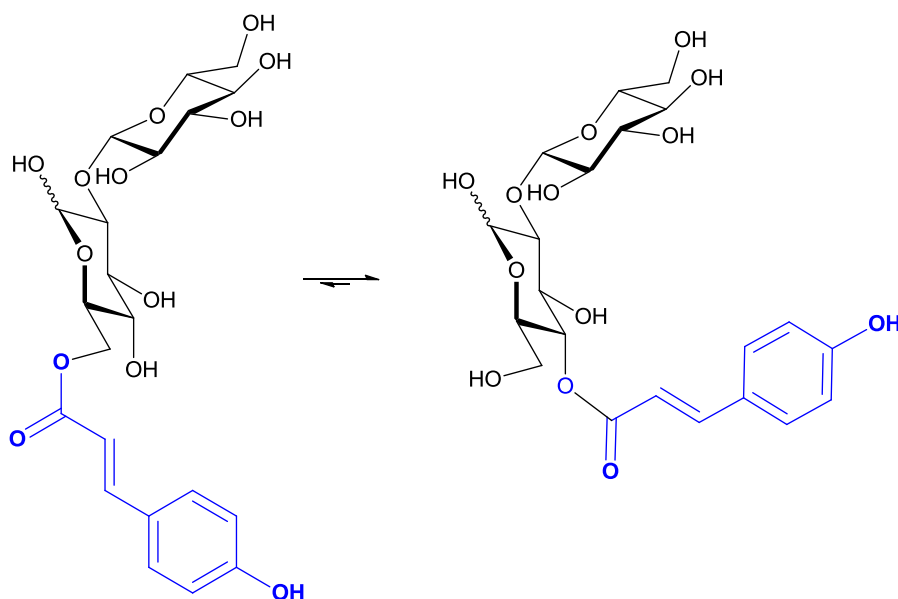
^b Coelution prevented quantification



Scheme 2-SI. Proposed fragmentation pattern for compound 12 (C3(Glc)-C2) from PA.



Scheme 3-SI. A possible mechanism for the formation of the coumarin derivatives



Scheme 4-SI. Possible intramolecular transesterification of the pC residue at C6-OH to the neighboring C5-OH position in the pC-sophorose. Both species are present as α and β anomers, and are in apparent equilibrium (in a stable ratio over time). When bound to the chromophore, the pC was not mobile.

Chapter 4. Acylated anthocyanins from Red Cabbage and Purple Sweet Potato can bind metal ions and produce stable blue colors



International Journal of
Molecular Sciences

Open Access Article

Acylated Anthocyanins from Red Cabbage and Purple Sweet Potato Can Bind Metal Ions and Produce Stable Blue Colors

by  Julie-Anne Fenger ^{1,*}  ,  Gregory T. Sigurdson ² ,  Rebecca J. Robbins ³ ,  Thomas M. Collins ³ ,
 M. Mónica Giusti ²   and  Olivier Dangles ^{1,*}  

¹ Avignon University, INRAE, UMR408, 84000 Avignon, France

² Department of Food Science and Technology, The Ohio State University, 2015 Fyffe Ct., Columbus, OH 43210, USA

³ Mars Wrigley, 1132 W Blackhawk Street, Chicago, IL 60642, USA

* Authors to whom correspondence should be addressed.

Academic Editor: Joana Oliveira

Int. J. Mol. Sci. **2021**, *22*(9), 4551; <https://doi.org/10.3390/ijms22094551>

Received: 13 March 2021 / Revised: 19 April 2021 / Accepted: 23 April 2021 / Published: 27 April 2021

(This article belongs to the Special Issue Anthocyanins: Chemistry and Bioactivity)

Abstract

Red cabbage (RC) and purple sweet potato (PSP) are naturally rich in acylated cyanidin glycosides that can bind metal ions and develop intramolecular π -stacking interactions between the cyanidin chromophore and the phenolic acyl residues. In this work, a large set of RC and PSP anthocyanins was investigated for its coloring properties in the presence of iron and aluminum ions. Although relatively modest, the structural differences between RC and PSP anthocyanins, i.e., the acylation site at the external glucose of the sophorosyl moiety (C2-OH for RC vs. C6-OH for PSP) and the presence of coordinating acyl groups (caffeoyl) in PSP anthocyanins only, made a large difference in the color expressed by their metal complexes. For instance, the Al^{3+} -induced bathochromic shifts for RC anthocyanins reached ca. 50 nm at pH 6 and pH 7, vs. at best ca. 20 nm for PSP anthocyanins. With Fe^{2+} (quickly oxidized to Fe^{3+} in the complexes), the bathochromic shifts for RC anthocyanins were higher, i.e., up to ca. 90 nm at pH 7 and 110 nm at pH 5.7. A kinetic analysis at different metal/ligand molar ratios combined with an investigation by high-resolution mass spectrometry suggested the formation of metal–anthocyanin complexes of 1:1, 1:2, and 1:3 stoichiometries. Contrary to predictions based on steric hindrance, acylation by noncoordinating acyl residues favored metal binding and resulted in complexes having much higher molar absorption coefficients. Moreover, the competition between metal binding and water addition to the free ligands (leading to colorless forms) was less severe, although very dependent on the acylation site(s). Overall, anthocyanins from purple sweet potato, and even more from red cabbage, have a strong potential for development as food colorants expressing red to blue hues depending on pH and metal ion.

1. Introduction

The color of red cabbage (RC) and purple sweet potato (PSP) is due to closely related anthocyanins displaying a cyanidin or peonidin (3'-O-methylcyanidin) 3-O-sophoroside-5-O-glucoside structure [1,2]. Cyanidin derivatives (the major RC pigments) are especially interesting colorants owing to their ability to bind metal ions (via their catechol B-ring) in neutral or mildly acidic solution. Indeed, metal-induced cyanidin deprotonation leads to a quinonoid chromophore that can express intense purple to blue colors [3,5]. Another

important consequence of metal–anthocyanin binding is increased color stability. Indeed, through the electrophilic flavylum ion (main colored form in acidic solution), anthocyanins, unlike their metal chelates, are vulnerable to water addition with the concomitant reversible formation of colorless forms (hemiketal and chalcones) [6]. A remarkable feature of RC anthocyanins is that the sophorosyl moiety is typically acylated by one or two residue(s) of *p*-hydroxycinnamic acid (HCA = *p*-coumaric, ferulic, caffeic, or sinapic acid). Phenolic acyl groups are known to favor folded conformations in which the anthocyanidin (chromophore) and the acyl residues develop π -stacking interactions. Like metal binding, this phenomenon, called intramolecular copigmentation, causes a bathochromic shift (BS) in the visible absorption band and protects the chromophore against water addition [1,7,8]. The combination of π -stacking interactions and metal binding is actually required to achieve maximal blue color stability with anthocyanins. Indeed, phenolic acyl groups stacked onto the cyanidin nucleus could either directly participate in metal binding (e.g., caffeic acid residues through their catechol ring) or at least strengthen metal binding by building a hydrophobic pocket around the metal–cyanidin complex. Recently, a remarkable RC anthocyanin (called pigment B or PB), displaying a single ideally located sinapoyl residue, was shown to form an aluminum(III) complex of 1:3 stoichiometry in which the three PB ligands in octahedral coordination to Al^{3+} adopt a chiral arrangement, causing an intense positive Cotton effect in the visible part of its circular dichroism spectrum [9]. The $Al(PB)_3$ complex is strongly stabilized by the π -stacking interactions taking place between each cyanidin chromophore and the sinapoyl residue of an adjacent ligand. Moreover, this original supramolecular structure imposes a large torsion angle around the bond connecting the B- and C-rings of the three cyanidin nuclei. This unique combination of structural characteristics results in an intense vibrant blue color of high stability, making PB and its metal complexes potential lead compounds for the replacement of artificial blue colorants by natural alternatives.

In this work, a selection of acylated cyanidin glycosides from red cabbage (including PB) and purple sweet potato is revisited for its affinity for aluminum and iron ions. In particular, the influence of the acyl groups on the binding kinetics, color stability, and rate of oxidative degradation of the complexes is systematically addressed. Indeed, the addition of iron ions was shown to accelerate the oxidative degradation of nonacylated cyanidin glycosides, while the presence of phenolic acyl groups tends to cancel this effect [10]. In this work, the conditions (pH, metal type, and concentration) permitting the optimal development of a blue color is also explored.

2. Results and Discussion

Metal–anthocyanin binding is of great importance for plants, not only because it is an efficient way to express blue colors to attract pollinating insects [8], but also as a detoxification mechanism against metal excess [11], which can operate with a variety of metal ions (e.g., Fe, Al, Pb, Cd, Mo, Mg, Ni, and V in corn roots). With Cu^{2+} , the binding is followed by Cu^{2+} reduction and anthocyanin oxidation [12]. However, quantitative physicochemical investigations of metal–anthocyanin binding are scarce. Such approaches have to address the structural transformations of anthocyanins in aqueous solution, the kinetics of metal binding and its stoichiometry, the critical influence of pH, and the possible influence of phenolic acyl groups and even of the selected buffer (depending on its own affinity for metal ions). This is the specific focus of this work, based on a large series of diversely acylated cyanidin glycosides and two of the most important metals (Al, Fe) in terms of blue color development [8].

2.1. The Color and Spectral Properties of the Metal Complexes

Anthocyanins under their flavylium form (AH^+) are typically diacids undergoing a first proton loss from C7-OH ($\text{p}K_{\text{a}1} \approx 4$), followed by a second one from C4'-OH around neutrality [13]. Thus, at pH 7, cyanidin glycosides from RC or PSP are a mixture of neutral (A_7) and anionic ($\text{A}_{4'7}$) bases ($\text{p}K_{\text{a}2} = 7.0\text{--}7.3$ [1,14]), in agreement with the broad absorption band observed (Figure 1). From the experimental spectra at pH 5–7, the $\text{p}K_{\text{a}}$ values, and the spectrum of the pure flavylium ion (pH 1), the spectra of the pure neutral and anionic bases can be calculated [14]. Compared to the neutral base, the anionic base not only has a much higher λ_{max} , but also a higher molar absorption coefficient at λ_{max} (Figure 1).

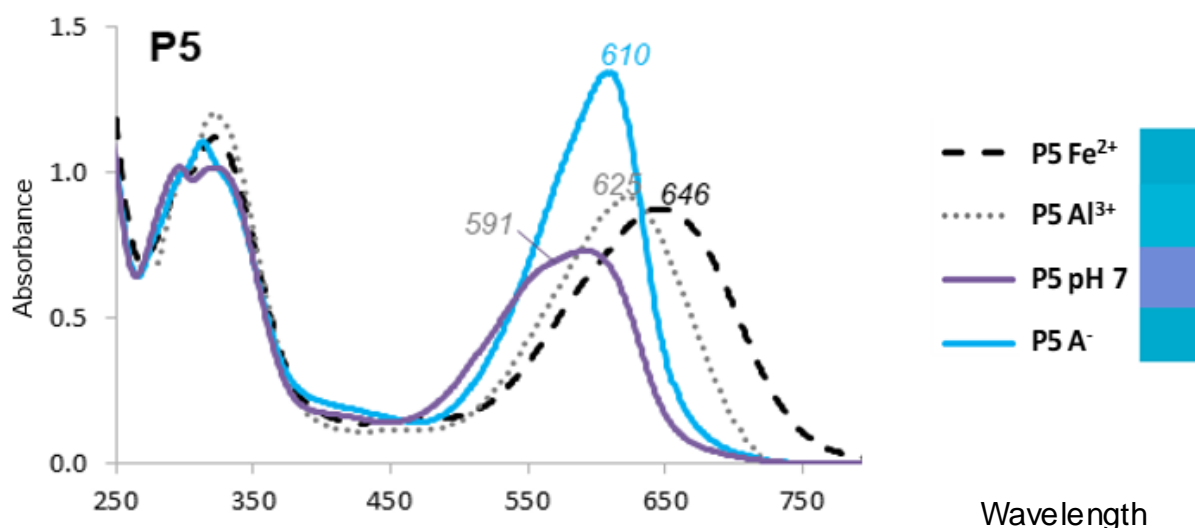


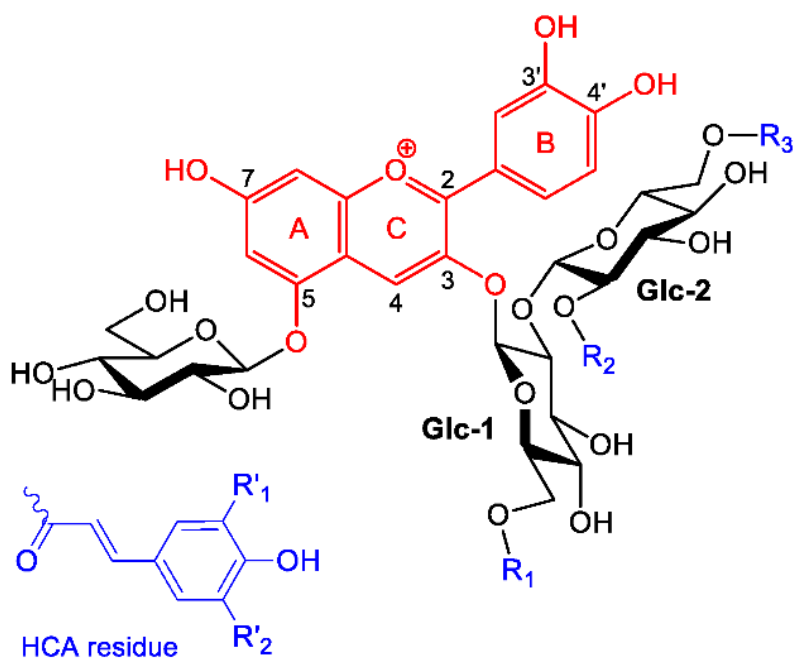
Figure 1. UV-VIS spectra of Pigment 5 (50 μM) at pH 7, its pure anionic base (A^- , calculated), and its Fe^{2+} and Al^{3+} complexes (1 equiv.). Right: color patches from the $L^*a^*b^*$ coordinates calculated from the visible spectra.

The major PSP anthocyanins are acylated peonidin glycosides, which do not bind metal ions through their chromophore. However, cyanidin glycosides are also present in PSP. Unlike the RC anthocyanins, the HCA residues of the PSP anthocyanins are only located at the primary C6-OH positions of the sophorosyl moiety (Scheme 1). In particular, the acyl residue borne by Glc-2 (R_3) is expected to be more mobile than its homolog in red cabbage ($\text{R}_2 = \text{sinapoyl}$). This happens to make a large difference in terms of color variation: the Al^{3+} -induced bathochromic shifts for PB (red cabbage) are ca. 50 nm at pH 6 and pH 7 vs. at best ca. 20 nm for P4' ($\text{R}_3 = \text{feruloyl}$, Table 1). The flexible acyl residue of P4' is probably much less apt to develop π -stacking interactions with the cyanidin nucleus than the more rigid sinapoyl residue of PB. Consistently, it has been demonstrated that RC anthocyanins having a single HCA residue at R_1 (P1–P3) are much more susceptible to water addition than PB [9] as a consequence of the latter adopting folded conformations in which the cyanidin and HCA moieties are in molecular contact. However, PSP pigments have a specific advantage over RC pigments: the presence of caffeoyl residues at Glc-1 and/or Glc-2, which themselves can bind metal ions.

Table 1. *Spectral* characteristics of the metal complexes of red cabbage and purple sweet potato anthocyanins (1 equiv. metal ion). $\Delta\lambda_{\text{max}} = \lambda_{\text{max}}(+\text{metal}) - \lambda_{\text{max}}(\text{no metal})$. $\Delta A = A(+\text{metal}) - A(\text{no metal})$.

		Fe^{2+}				Al^{3+}			
Red Cabbage Pigments		PA	P2	P5	PB	PA	P2	P5	PB
pH 6	$\lambda_{\text{max}}(+\text{metal})$ (nm)	559	569	640	656	no	571	587	629
	$\Delta\lambda_{\text{max}}$ (nm)	21	25	87	76	binding	27	34	49

	$\Delta A/A(\text{no metal})$ at λ_{max} (%)	-25	-15	3	65		-15	-9	16
	$\lambda_{\text{max}}(+\text{metal})$ (nm)	596	592	646	656	583	585	625	637
pH 7	$\Delta\lambda_{\text{max}}$ (nm)	14	-4	55	71	4	5	34	52
	$\Delta A/A(\text{no metal})$ at λ_{max} (%)	-7	-3	19	43	3	-1	17	25
Purple Sweet Potato Pigments						P4'	P6'	P7'	P9b'
	$\lambda_{\text{max}}(+\text{metal})$ (nm)	/	/	/	/	563	574	575	581
pH 6	$\Delta\lambda_{\text{max}}$ (nm)	/	/	/	/	16	26	23	29
	$\lambda_{\text{max}}(+\text{metal})$ (nm)	/	/	/	/	580	591	598	598
pH 7	$\Delta\lambda_{\text{max}}$ (nm)	/	/	/	/	8	21	22	16



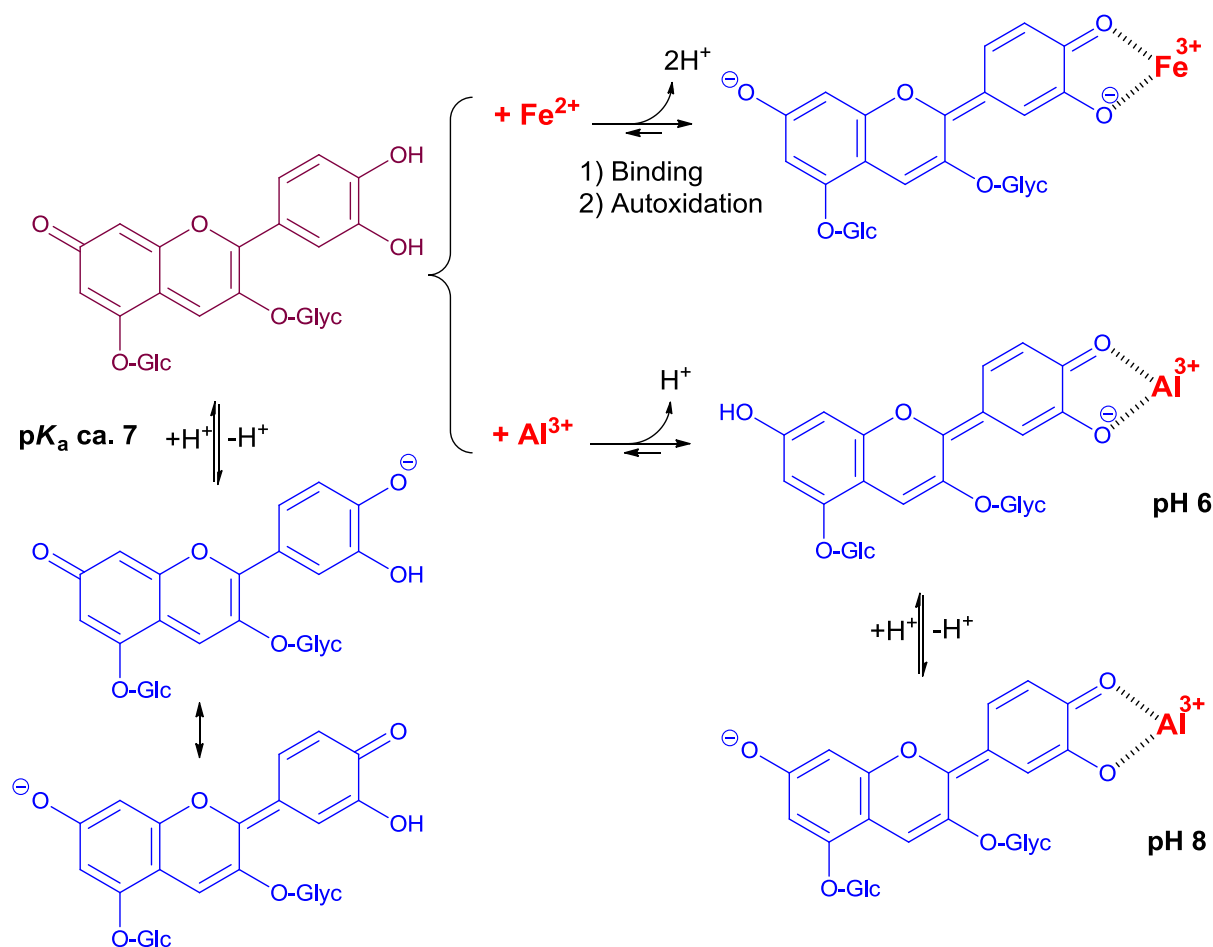
HCA Residue	R' ₁	R' ₂
pC	H	H
Cf	OH	H
Fl	OMe	H
Sp	OMe	OMe

Pigment	R ₁	R ₂	R ₃
PA a)	H	H	H
P1 a)	pC	H	H
P2 a)	Fl	H	H
P3 a)	Sp	H	H
PB a)	H	Sp	H
P4 a)	pC	Sp	H
P5 a)	Fl	Sp	H
P6 a)	Sp	Sp	H
P4' b)	H	H	Fl
P6' b)	Cf	H	H
P7' b)	Cf	H	Cf
P9b' b)	Cf	H	Fl

Scheme 1. Structure of the RC and PSP anthocyanins studied. When present, hydroxycinnamoyl residues R₁, R₂, and R₃ are *p*-coumaroyl (pC), feruloyl (Fl), caffeoyl (Cf), and/or sinapoyl (Sp). Note: a) from red cabbage; b) from purple sweet potato.

Our recent work [14] suggests that such pigments, in which the cyanidin and caffeoyl units tend to stack onto each other, can actually sequester Fe^{2+} and Al^{3+} by the simultaneous involvement of both catechol rings, thereby largely increasing the metal-induced bathochromic shift. This was confirmed in the current work: the bathochromic shifts induced by Al^{3+} (1 equiv.) at pH 7 were 8, 21, and 22 nm for P4' ($\text{R}_3 = \text{feruloyl}$), P6' ($\text{R}_1 = \text{caffeoyl}$), and P7 ($\text{R}_1 = \text{R}_3 = \text{caffeoyl}$), respectively (Figure S1A, Table 1). It was also clear that the caffeoyl residue at R_1 was critical to promote the bluing effect, while the other one at R_3 was not. By contrast, P9b ($\text{R}_1 = \text{caffeoyl}$, $\text{R}_3 = \text{feruloyl}$) was clearly less efficient (BS = 16 nm), possibly pointing to a less-favorable binding because of the relatively bulky feruloyl residue.

The pH dependence of the λ_{max} values in the pH range 6–8 for the free forms (Table S1) was consistent with the conversion of the neutral base (A_7) to the anionic base ($\text{A}_{4'7}$, proton loss from C4'-OH), in full agreement with the corresponding $\text{p}K_{\text{a}2}$ value of the RC and PSP anthocyanins [1,14]. As Al^{3+} also triggers proton loss from C4'-OH, the bathochromic shift (BS) induced in the free forms by increasing the pH from 6 to 8 should be close to the one accompanying Al^{3+} binding at pH 6. Additionally, only small BS were expected upon Al^{3+} binding at pH 8. While the latter prediction was well-verified experimentally for all PSP pigments (Al^{3+} -induced BS at pH 8 < 10 nm, Table S1), the former was not: indeed, the pH-induced BS (*ca.* 50 nm) were much larger than the Al^{3+} -induced BS at pH 6 (from 16 nm for P4' to 29 nm for P9b'). Moreover, bathochromism was clearly observed in the complexes' visible band when the pH was increased from 6 to 8 (BS = 25–33 nm, Table S1). Hence, it can be proposed that C7-OH in the complexes was not dissociated at pH 6, and lost its proton when the pH is raised to 8 (Scheme 2). This proposal is consistent with the theoretical visible spectrum calculated on the $\text{Al}(\text{PB})_3$ complex, which, while involving 3 ligands undissociated at C7-OH, were found fully consistent with the experimental spectrum [9]. Moreover, comparing the neutral base of the 7-O- β -D-glucosyloxy-4'-hydroxyflavylium ion (proton loss from C4'-OH) with that of its 4'-O- β -D-glucosyloxy-7-hydroxyflavylium regioisomer (proton loss from C7-OH) also showed that the former displayed a λ_{max} value that was 20 nm higher [15] and a molar absorption coefficient almost 3 times as large. Finally, DFT calculations on pyranoanthocyanins [16] confirmed that the neutral base formed by proton loss from C4'-OH ($\text{A}_{4'}$, a very minor species) displayed an intense absorption band at higher wavelengths than the major tautomer (proton loss from C7-OH). Overall, turning A_7 into $\text{A}_{4'}$ upon metal binding is actually expected to promote both bathochromism and hyperchromism.



Scheme 2. Metal–anthocyanin binding.

Red cabbage anthocyanins with $R_2 = \text{sinapoyl}$, whether mono- or diacylated, were distinct from the PSP anthocyanins and the other RC pigments in that the Al^{3+} -induced BSs were larger, especially at pH 7 (36 and 52 nm for P5 and PB, respectively, vs. barely 5 and 8 nm for P2 and P4', respectively) (Table 1, Figures 1 and S1B). The λ_{max} values of the complexes were even higher than that of the anionic base. Thus, even if proton loss from C7-OH was not complete at pH 7 for the Al^{3+} complexes, the strong π -stacking interactions occurring between the cyanidin nucleus and $R_2 = \text{sinapoyl}$ and the concomitant torsion imposed between the B- and C-rings [9] effectively turned the color to an intense cyan hue (Figure 1) close to the one expressed by the major synthetic blue food colorants Brilliant Blue (E133) and indigotine (E132), 630 nm and 608 nm respectively [9].

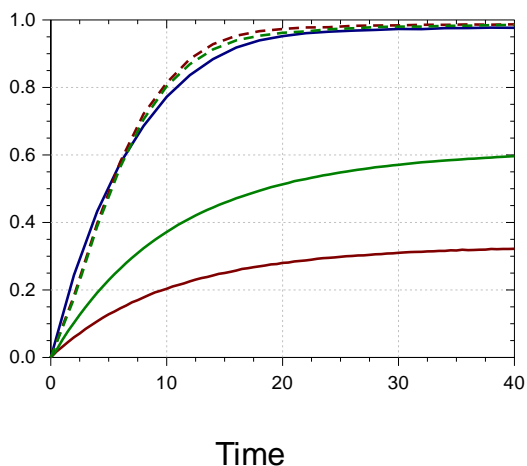
With Fe^{2+} , the BSs were even larger: at pH 7, 87 and 76 nm for P5 and PB, respectively, vs. 25 nm for P2 (Table 1, Figures 1 and S1B). As already reported for other Fe^{2+} -polyphenol complexes [17,18], bound Fe^{2+} was rapidly autoxidized to Fe^{3+} . This reaction was: (a) promoted by the higher affinity of catechols for Fe^{3+} (vs. Fe^{2+}); (b) confirmed by the

similarity of the final spectra, whether Fe^{2+} or Fe^{3+} was added [14]; and (c) consistent with the broad absorption band of the iron complexes and their high λ_{max} , which both suggest ligand-to- Fe^{3+} charge transfer. However, iron autoxidation clearly followed metal binding. Indeed, despite the higher intrinsic affinity of catechols for Fe^{3+} , anthocyanins bound Fe^{2+} much more rapidly in our model (Figures 2 and S2) [14], as competition between anthocyanins and the phosphate anions for the metal was much less severe with Fe^{2+} .

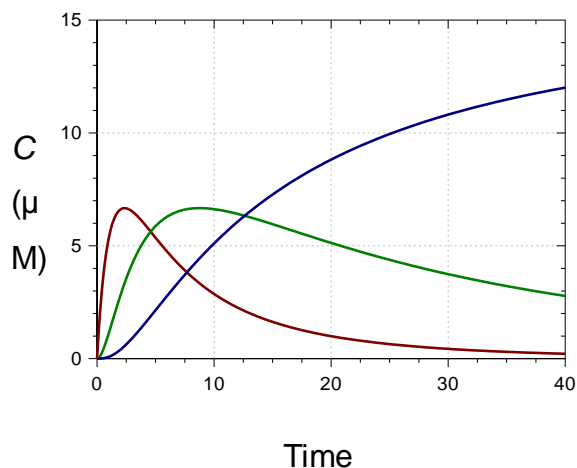
While the visible band of the Al^{3+} complexes of the RC anthocyanins showed the same pH dependence as for the PSP anthocyanins, the visible band of their Fe^{3+} complexes was remarkably insensitive to pH in the subgroup with $\text{R}_2 = \text{sinapoyl}$ (Figure S1B). In particular, the BS featuring iron–PB binding at pH 5.68 hit a record high of ca. 110 nm, i.e., twice as much as with Al^{3+} at the same pH. Hence, it can be proposed that C7-OH in the iron complexes is dissociated even at low pH (Scheme 2).

The colorimetric data of the PSP cyanidin glycosides and their Al^{3+} complexes (Table S2) provide additional evidence of the bluing effect induced by raising the pH from 6 to 8, or adding increasing Al^{3+} concentrations at a given pH. For comparison, a hue angle of 207.3 was recorded for the PB- Al^{3+} complex at pH 7, i.e., a close match for that of the synthetic triarylcation colorant Brilliant Blue ($h^0 = 209.4$), regarded as a reference for a vibrant cyan hue in the confectionary industry [9]. No such match was observed with the PSP anthocyanins and the best result recorded, i.e., the P6'- Al^{3+} complex at pH 8 ($h^0 = 221.7$) remained off target. However, it confirmed that a single caffeoyl residue at R_1 was sufficient to promote a strong bluing effect.

(A)



(B)



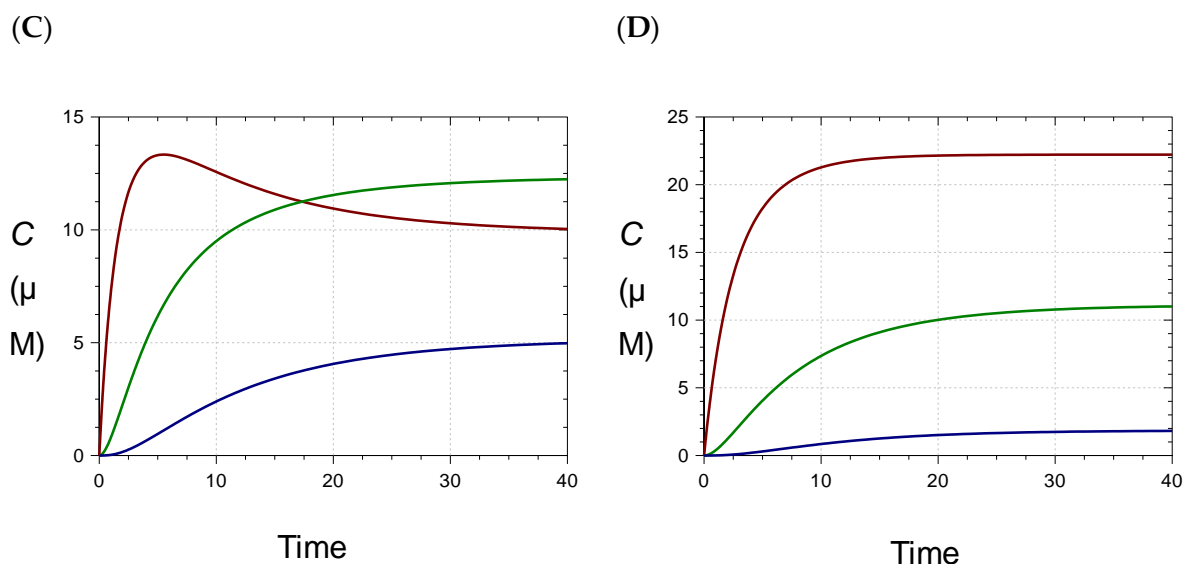


Figure 2. (A) Kinetics of Fe^{2+} -Pigment B binding (pH 7, 25 °C). Pigment concentration = 50 μM , metal/pigment molar ratio = 0.05 (—), 0.1 (—), 0.3 (—), 0.6 (—), 1 (—). (B–D) Speciation diagrams of Fe^{2+} -Pigment B complexes. (B) 0.3 equiv. Fe^{2+} . C) 0.6 equiv. Fe^{2+} . (D) 1 equiv. Fe^{2+} . ML (—), ML_2 (—), ML_3 (—). ML_n : metal–ligand complex having a 1:n metal/ligand stoichiometry.

2.2. Kinetic Analysis and Stoichiometry of Metal Binding

When small volumes of concentrated Fe^{2+} or Al^{3+} aqueous solutions were added immediately after diluting the RC pigments into pH 6–8 phosphate buffers, a relatively fast metal–anthocyanin binding occurred (Figures 2 and S2). Contrary to predictions based on steric hindrance, the observed trend was that acylation by noncoordinating HCA residues favored metal binding. For instance, nonacylated PA weakly bound Al^{3+} at pH 7 and 8 (weak spectral changes preventing the kinetic analysis), and strong Al^{3+} -P2 binding only occurred at pH 8. By contrast, P5 strongly bound Al^{3+} at both pHs.

The minimal metal/ligand molar ratio to reach full binding (saturation of the visible band of the complex) is an indicator of the complex's stoichiometry. This ratio lay between 1/3 and 2/3 for PA, PB, P2, and P5 (Figures 2 and S3), as already observed with iron [10]. Thus, mixtures of 1:1, 1:2, and 1:3 complexes were expected in variable proportions according to the metal/ligand molar ratio. Consistently, in our recent work, the $\text{Al}^{3+}(\text{PB})_3$ and $\text{Al}^{3+}(\text{P6})_3$ complexes were evidenced by high-resolution mass spectrometry in a dilute ammonium acetate buffer, but not the $\text{Al}^{3+}(\text{P3})_3$ homolog [9]. This was confirmed in the present work (Table S3). Under the same conditions, 1:1 and 1:2 iron–anthocyanin complexes were detected with P5 and PB (Table 2, Figure S4). With monoacylated P2, only the 1:1 complex was detected, whatever the M/L molar ratio between 1/6 and 1. The detection of 1:3

complexes is more challenging, as the corresponding ions must bear at least 3 charges for the m/z ratio to fall below 1500, the upper limit of detection. Satisfying agreements between experimental and theoretical m/z values were observed for the main ions and their major isotopes. Moreover, HRMS data were consistent with iron having a +3 oxidation degree in the complexes. For instance, the FeP5 monocation (exp. m/z 1208.2307, 1209.2352, 1210.2398) is proposed to be $[P5 - 3H^+ + Fe^{3+}]^+$ (P5 referring to the flavylum cation, theoretical m/z 1208.2302, 1209.2335, 1210.2362). The corresponding complex involving Fe^{2+} would be $[P5 - 2H^+ + Fe^{2+}]^+$ (m/z 1209.2381, 1210.2414, 1211.2440). Despite the possible match of the experimental spectrum with isotopes of the Fe^{2+} complex having one or two ^{13}C -atoms, the intense signal at m/z 1208.2307 (Figure S4) clearly required an Fe^{3+} ion. Unexpectedly, varying the M/L molar ratio between 1/6 and 1 did not strongly impact the signal intensity of the 1:1 complex relative to free ligand (Table S4). Moreover, the signal intensities of the 1:1; 1:2, and 1:3 complexes could not be compared due to the charge-specific ion sensitivity of the MS detector.

A simple model assuming stepwise 1:1, 1:2, and 1:3 binding was tested to account for the kinetics of metal binding as a function of the metal concentration. To keep the number of adjustable parameters to a minimum, the rate constants of the first, second, and third steps were assumed to be $3k$ (3 available binding sites), $2k$ (2 available binding sites) and k (1 available binding site), respectively. Moreover, the molar absorption coefficients of the ML, ML_2 , and ML_3 complexes (M = metal, L = ligand) were assumed to be ϵ , 2ϵ , and 3ϵ , respectively. Satisfactory curve-fittings of the $A(670\text{ nm})$ vs. time curves for different M/L molar ratios were thus obtained, leading to optimized values for parameters k and ϵ , and permitting the plotting of the time dependence of the concentrations of the 3 complexes (Table 3, Figure S5).

Table 2. Ions detected for the iron complexes of pigments P5 = Cya-3-(Fl)Glc-2-(Sp)Glc-3-Glc and PB = Cya-3-Glc-2-(Sp)Glc-3-Glc from red cabbage (metal/ligand molar ratio = 1).

Compound	Formula	Th. m/z (rel. abundance) (a)	Exp. m/z (rel. abundance) (b)	δ (ppm)
P5 ⁺	C ₅₄ H ₅₉ O ₂₈	1155.3187	1155.3198	1.0
		1208.2302 (100)	1208.2307 (100)	0.4
[P5 - 3H ⁺ + Fe ³⁺] ⁺	C ₅₄ H ₅₆ O ₂₈ Fe	1209.2335 (62.4)	1209.2352 (98)	1.4
		1210.2362 (25.2)	1210.2397 (46)	2.9
		604.6188 (100)	604.6189 (100)	0.2
[P5 - 2H ⁺ + Fe ³⁺] ²⁺	C ₅₄ H ₅₇ O ₂₈ Fe	605.1204 (62.0)	605.1211 (83)	1.2
		605.6217 (24.9)	605.6227 (32)	1.7
		788.1856 (84.1)	788.1836 (87)	2.5
[2P5 - 2H ⁺ + Fe ³⁺] ³⁺	C ₁₀₈ H ₁₁₆ O ₅₆ Fe	788.5199 (100)	788.5183 (100)	2.0
		788.8542 (69.8)	788.8537 (35)	0.6
PB ⁺	C ₄₄ H ₅₁ O ₂₅	979.2714	979.2722	0.8
		1032.1829 (100)	1032.1836 (100)	0.7
[PB - 3H ⁺ + Fe ³⁺] ⁺	C ₄₄ H ₄₈ O ₂₅ Fe	1033.1862 (51.4)	1033.1888 (71)	2.5
		1034.1887 (18.4)	1034.1921 (25)	3.3
		516.5951 (100)	516.5952 (100)	0.2
[PB - 2H ⁺ + Fe ³⁺] ²⁺	C ₄₄ H ₄₉ O ₂₅ Fe	517.0967 (51.1)	517.0969 (53)	0.4
		517.5980 (18.2)	517.5982 (16)	0.4
		1005.7273 (100)	1005.7277 (63)	0.4
[2PB - 3H ⁺ + Fe ³⁺] ²⁺	C ₈₈ H ₉₉ O ₅₀ Fe	1006.2289 (98.5)	1006.2304 (100)	1.5
		1006.7303 (59.0)	1006.7320 (80)	1.7
		1007.2317 (26.2)	1007.2343 (45)	2.6
[PB - 2H ⁺] ⁻	C ₄₄ H ₄₉ O ₂₅	977.2563	977.2570	0.7
		1030.1683 (100)	1030.1684 (100)	0.1
[PB - 5H ⁺ + Fe ³⁺] ⁻	C ₄₄ H ₄₆ O ₂₅ Fe	1031.1716 (51.4)	1031.1723 (53)	0.7
		1032.1741 (18.4)	1032.1752 (16)	1.1
		514.5806 (100)	514.5807 (100)	0.2
[PB - 6H ⁺ + Fe ³⁺] ²⁻	C ₄₄ H ₄₅ O ₂₅ Fe	515.0822 (51.1)	515.0822 (47)	0.0
		515.5834 (18.2)	515.5837 (12)	0.6
		1003.7128 (100)	1003.7124 (100)	0.4
[2PB - 7H ⁺ + Fe ³⁺] ²⁻	C ₈₈ H ₉₅ O ₅₀ Fe	1004.2143 (98.5)	1004.2153 (93)	1.0
		1004.7157 (58.9)	1004.7166 (65)	0.9
		1005.2171 (26.2)	1005.2180 (40)	0.9

(a) Relative abundances calculated on the website <https://www.chemcalc.org> (accessed on March 2, 2021). (b) Relative abundances estimated with the Freestyle software (Thermo Fisher Scientific, Waltham, MA, USA).

Table 3. Kinetic analyses of metal–anthocyanin binding according to the stepwise formation of ML, ML₂, and ML₃ complexes (25 °C, monitoring at 670 nm). ML_n: metal–ligand complex having a 1:n metal/ligand stoichiometry. For simplicity, the successive binding steps are described by rate constants 3*k*, 2*k*, and *k*, respectively, and each bound ligand by the same molar absorption coefficient ϵ . Some repetitions are shown. Values between brackets are standard deviations for the curve-fitting procedure.

M/Pigment	k ($\times 10^3$) ($M^{-1} s^{-1}$)	ϵ ($\times 10^3$) ($M^{-1} cm^{-1}$)
Pigment A + Fe ²⁺ , pH 7		
0.3	4.1 (0.1)	9.5 (0.1)
0.6	4.0 (0.3), 3.2 (0.2), 3.7 (0.2)	8.6 (0.2), 8.8 (0.2), 9.0 (0.1)
1.0	3.1 (0.3), 4.0 (0.4), 3.7 (0.3)	9.9 (0.4), 8.4 (0.2), 9.1 (0.2)
Pigment B + Fe ²⁺ , pH 7		
0.3	2.03 (0.15), 4.16 (0.36)	38.3 (1.4), 26.1 (0.4)
0.6	6.17 (0.15), 2.32 (0.13)	22.6 (0.1), 21.7 (0.2)
1.0	0.90 (0.02), 1.18 (0.04), 1.03 (0.04)	23.6 (0.1), 23.1 (0.1), 23.2 (0.1)
Pigment A + Al ³⁺ , pH 7 <i>Weak binding</i>		
Pigment B + Al ³⁺ , pH 7		
0.3	0.81 (0.01)	15.4 (0.1)
0.6	0.92 (0.01), 0.47 (0.01)	15.0 (0.1), 15.6 (0.1)
1	0.42 (0.01), 0.51 (0.01), 0.39 (0.01)	14.5 (0.1), 16.0 (0.1), 14.6 (0.1)
P5 + Fe ²⁺ , pH 7		
0.3	2.7 (0.1)	24.5 (0.1)
0.6	2.5 (0.1)	22.1 (0.1)
1	3.1 (0.1)	24.9 (0.1)
P5 + Fe ²⁺ , pH 8		
0.3	13.6 (0.3)	13.5 (0.1)
0.6	6.4 (0.1)	12.9 (0.1)
1	6.6 (0.3)	12.8 (0.1)
P2 + Fe ²⁺ , pH 7		
0.3	16.6 (0.8)	6.7 (0.1)
0.6	4.4 (0.1)	8.7 (0.1)
1	2.5 (0.1)	10.0 (0.1)
P2 + Fe ²⁺ , pH 8		
0.3	14.1 (1.5)	12.4 (0.4)
0.6	9.1 (0.7)	14.0 (0.3)
1	5.5 (0.4)	13.6 (0.2)
P5 + Al ³⁺ , pH 7 a)		
0.3	3.7 (0.1), 1.3 (0.1), 0.39 (0.05)	16.7 (0.2)
0.6	0.58 (0.03), 0.14 (0.06) b)	17.6 (1.1)
1	0.50 (0.01) c)	14.0 (0.1)
P5 + Al ³⁺ , pH 8		
0.3	5.5 (0.1)	10.3 (0.1)
0.5	6.1 (0.1)	8.9 (0.1)
1	1.7 (0.1)	7.4 (0.1)
P2 + Al ³⁺ , pH 7 <i>Weak binding</i>		

P2 + Al ³⁺ , pH 8		
0.3	4.1 (0.1)	3.4 (0.1)
0.6	3.1 (0.1)	3.7 (0.1)
1	1.2 (0.1)	3.8 (0.1)

Note: a) 3 optimizable rate constants; b) $k_3 = 0$; c) $k_2 = k_3 = 0$.

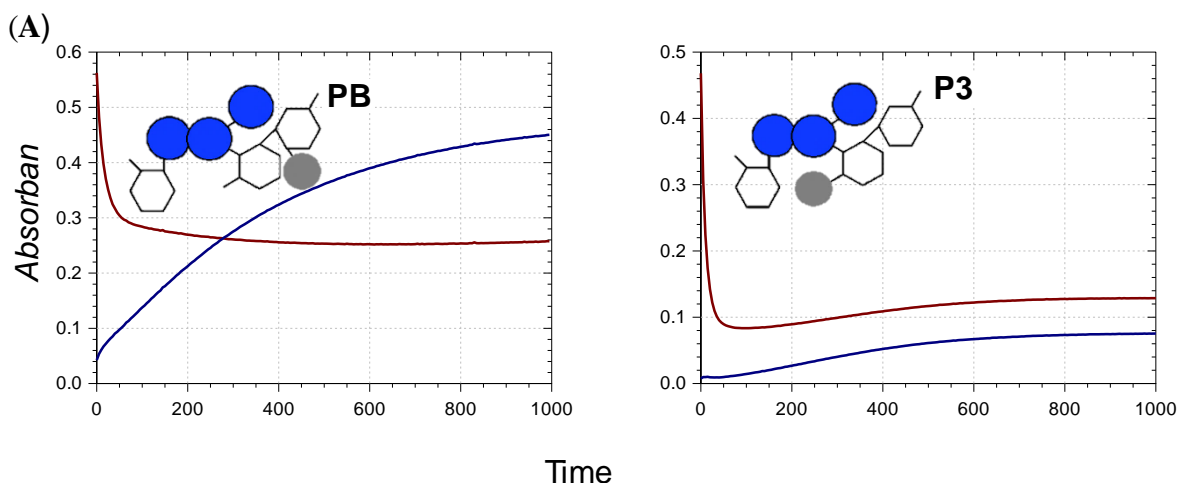
For given pigment and metal ion, the optimized ε values were fairly stable when the metal concentration was varied, which was satisfactory. This was less true for the optimized k values, which suggests that the model of independent binding steps was too simple. With the P5–Al³⁺ pair at pH 7, much better curve-fittings were actually obtained by implementing 3 optimizable rate constants in the model. Despite its crude approximations, the model offered a simple way to quantitatively assess the influence of pH, metal type, and acylation pattern on the rate of metal–anthocyanin binding. Overall, binding was faster at pH 8 than at pH 7, and faster with Fe²⁺ than with Al³⁺. Overall, under our conditions, acylation did not impede metal binding. Most importantly, pigments having R2 = sinapoyl (PB, P5) formed complexes with much higher molar absorption coefficients (typically, a factor 2–3), which was an obvious advantage for color development.

2.3. Competition between Metal Binding and Water Addition

Metal binding is accompanied by the removal of the B-ring's phenolic protons. In other words, protons and metal ions compete for the O-atoms of the B-ring. Hence, lowering the pH gradually destabilizes the complexes and a minimal pH for the onset of metal binding is expected. Also, a weaker stability for the complexes could mean reversibility in their formation and thus competition with water addition to the free form (flavylium ion), which leads to color loss.

The influence of pH on iron binding was investigated with the two isomers PB and P3. For a given pH, the UV-VIS spectra were recorded immediately after pigment addition to buffer in the absence of Fe²⁺ and after maximal binding in the presence of Fe²⁺. A rise in visible absorbance in the range 600–700 nm, which is typical of metal binding, could be perceived with both pigments at pH ≥ 3 (data not shown). Although P3 and PB could not be clearly distinguished by the pH for the onset of iron binding, it was obvious that the hyperchromic and bathochromic shifts in mildly acidic solution (pH 4.24) were much more spectacular with PB than with P3 (Figure 3A,C). Part of the interpretation is rooted in the higher susceptibility of P3 to color loss by reversible water addition, which was both faster and more complete

than for PB (Figure 3B). Indeed, when the pigment and Fe^{2+} (1 equiv.) were added to the acetate buffer, a sharp drop of visible absorbance at 530 nm (free pigment) was observed with P3 over the first minute, whereas the increase of visible absorbance at 670 nm (iron complex) was negligible (Figure 3A). In a second phase, the onset of iron binding occurred, and $A(670\text{ nm})$ slowly increased. In this case, the first step corresponding to the flavylum hydration (fast) was clearly decoupled from the second step (slow) of iron binding. By contrast, with PB, the drop of $A(530\text{ nm})$ over the first minute was limited and accompanied by a rise of $A(670\text{ nm})$, which was then amplified along the second phase. This is evidence that hydration and metal binding now compete from the beginning. It is interesting to note that if hydration was faster than metal binding in the case of P3, the higher affinity of the colored forms (vs. colorless forms) for the metal ion eventually permitted the reversal of the hydration equilibrium and the slow development of metal binding. However, even with PB, the intensity of the complex's band in the pH range 3–6 remained much lower than in neutral solution, where it reached saturation even in the presence of substoichiometric iron concentrations. As the λ_{max} of the iron–PB complex's visible band was pH-independent, the spectrum at pH 7 (Figure S1B) could be used to calculate the percentage of iron complex at equilibrium at pH 4.24: 47%. A similar calculation with P3 gave only 24%.



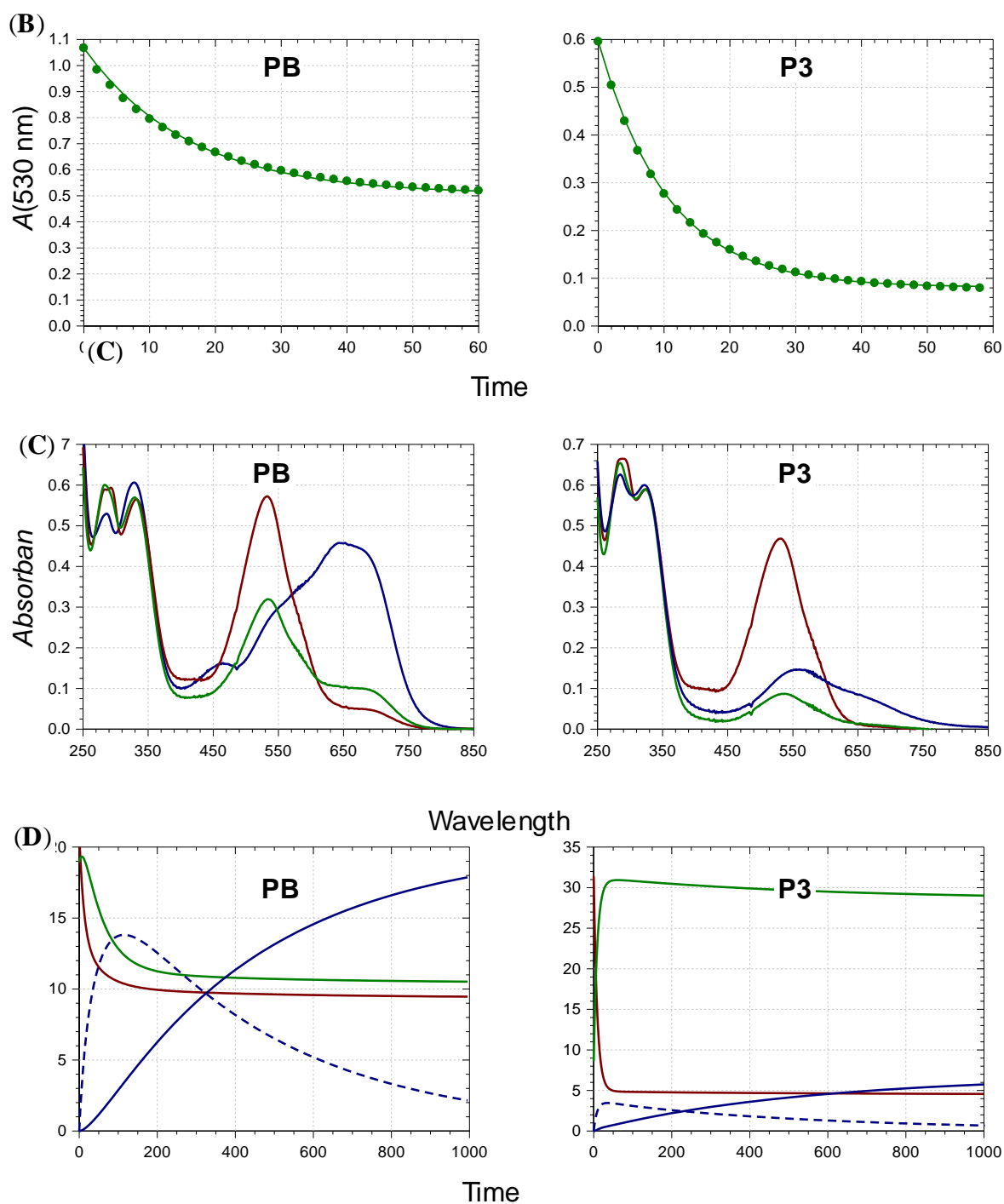


Figure 3. Iron–anthocyanin binding in a pH 4.24 acetate buffer (successive addition of pigment (40 μM) and Fe^{2+} (1 equiv.)), Left: Pigment B; right: Pigment 3. Simplified schemes are provided as a reminder of the key structural differences. (A) Spectral monitoring at 530 nm (free pigment, —) and at 670 nm (iron complex, —). (B) Control in the absence of iron (solid lines are the result of the curve-fitting procedure). (C) Spectra at time zero (—), after ca. 1 min (—) and at the end of the kinetic run (—). (D) Time dependence of the species distribution: free colored forms (—); free colorless forms (—); Fe^{2+} complex (—); Fe^{3+} complex (—).

Attempts to fit the spectral changes observed at 530 nm (free form) and 670 nm (iron complex) to a simple kinetic model, assuming competition with water addition and reversible iron binding, failed. However, a more sophisticated scheme assuming reversible Fe^{2+} binding by the colored forms, followed by irreversible autoxidation of bound Fe^{2+} with concomitant formation of a Fe^{3+} complex (in equilibrium with the free species), provided perfect curve-fittings and acceptable rate constants for the different steps (Table S5). Overall, PB bound Fe^{2+} twice as rapidly as P3 did, and the Fe^{2+} -PB complex seemed less susceptible to autoxidation than the Fe^{2+} -P3 complex. Finally, the blue color development was much more intense with PB, as the molar absorption coefficient of the PB- Fe^{3+} complex in the blue domain was ca. twice as large than that of the P3- Fe^{3+} complex. These remarkable improvements only reflected the shift of the single sinapoyl residue from the 6 position of Glc-1 to the 2 position of Glc-2. This is a spectacular example of the crucial importance of strong anthocyanidin-hydroxycinnamoyl π -stacking interactions in the development of vibrant blue colors.

2.4. Long-Term Stability of the Metal Complexes

Acylation promoted a moderate increase in color stability upon heating at 50 °C, again with an advantage conferred on pigments with R2 = sinapoyl (Table S6, Figure S6). This trend was hugely emphasized after Fe^{2+} addition (0.6 equiv.), a clear indication that the sinapoyl residue on Glc-2 was very efficient for the long-term stabilization of the metal complexes. Again, the comparison between the P3 and PB isomers was striking: a 25% color loss of the Fe^{2+} -P3 complex was reached in 15–20 min vs. 4.5 h for the Fe^{2+} -PB complex. As already observed [10], the spectroscopic titration of the residual pigment (after acidification to pH 1 for total dissociation of the iron complex and total conversion of the colorless forms into the flavylum ion) provided a more contrasted picture: in the absence of added iron, acylation offered to protect, and this so-called “acylation paradox” [10] could be interpreted by assuming that the colorless forms (hemiketal and chalcones) were much less susceptible to oxidative degradation than the electron-rich anionic base. In other words, being more vulnerable to reversible water addition, nonacylated PA and anthocyanins having a single HCA residue at R1 (P1, P3) were protected against autoxidation at the cost of losing their color. However, after Fe^{2+} addition, autoxidation was strongly accelerated for PA because the corresponding iron complex was not stable enough, and the protection offered by iron binding was significant for P4 and PB only. In our recent work, adding Fe^{2+} also was shown to increase the yield in some major degradation products of PA and P1 [19]. In summary, strong π -stacking

interactions within the complexes ensured an efficient iron sequestration, thus preventing the pro-oxidant activity of loosely bound iron ions [17]. The tight metal binding also explained the total inhibition of intramolecular acyl transfer, normally occurring when solutions of P4 or PB are heated [19].

3. Materials and Methods

Red cabbage (*Brassica oleracea* var. *capitata* f. *rubra* L.) and purple sweet potato (*Ipomoea batatas* L.) anthocyanin-rich extracts were provided by Mars Wrigley Confectionary (Hackettstown, NJ, USA). Anthocyanin individual pigments were isolated by preparatory LC according to already-published procedures [3,4]. Their structures are presented in Scheme 1.

3.1. Metal-Binding Experiments

3.1.1. Red Cabbage Anthocyanins

Metal–anthocyanin binding experiments were carried out according to previously reported procedures [14]. Fresh 5 mM solutions of Fe^{2+} and Al^{3+} were respectively prepared from $\text{FeSO}_4 \cdot 7\text{H}_2\text{O}$ and $\text{AlCl}_3 \cdot 6\text{H}_2\text{O}$ (Sigma-Aldrich, St-Quentin Fallavier, France) in 1 mM aqueous HCl. Concentrated stock solutions of pigment (5 mM) were prepared in 50 mM aqueous HCl. Absorption spectra were recorded on an Agilent 8453 diode-array spectrometer in thermostated and magnetically stirred quartz cuvettes (pathlength = 1 cm). The following solutions were directly added to the cuvette in this order: 2 mL of 10 mM phosphate buffer (pH 7 or 8), 20 μL of anthocyanin stock solution and, after a few seconds (negligible formation of colorless forms), a small volume of the 5 mM Fe^{2+} or Al^{3+} solution (final iron/anthocyanin molar ratio = 1 or 2). The full UV-VIS spectra were recorded in kinetic mode for 1 to 2 min. For an optimal sensitivity, the detection in the visible range was set at 550 or 610 nm for Al^{3+} (close to the complex's λ_{max}) and at 670 nm for Fe^{2+} (charge-transfer contribution of the Fe^{3+} complexes). The hyperchromic and bathochromic shifts were calculated from the initial (free ligand) and final (metal complex) spectra as $(A_{\text{max},f} - A_{\text{max},0})/A_{\text{max},0}$ and $\lambda_{\text{max},f} - \lambda_{\text{max},0}$, respectively.

Binding experiments were also carried out in the pH range 2–6 (50 mM acetate buffer) to determine the pH for the onset of metal binding and investigate the competition with water addition to the flavylum ion.

3.1.2. Purple Sweet Potato Anthocyanins

The anthocyanin isolates were diluted to a 50 μM concentration in buffers of pH 6 (0.1 M sodium acetate), 7, and 8 (0.25 M TRIS). Small volumes of concentrated $\text{Al}_2(\text{SO}_4)_3$ solutions were then added to reach metal/anthocyanin ratios of 0.5, 1, and 5. Samples were equilibrated for 30 min at room temperature in the dark prior to analysis (in triplicates). UV-VIS spectra were collected from 380 to 700 nm using 300 μL samples in poly-D-lysine-coated polystyrene 96-well plates with a SpectraMax 190 Microplate Reader (Molecular Devices, Sunnyvale, CA, USA).

3.2. Kinetic Analyses

The kinetic curves were analyzed with the Scientist software (Micromath, St. Louis, MO, USA). Sets of differential equations characteristic of the different kinetic processes (metal binding, water addition to the flavylum ion) were implemented in the models, as well as initial concentrations. Optimized values for the adjustable parameters (rate constants, molar absorption coefficients) and their standard deviations are reported.

3.3. Colorimetric Data

Color characteristics were expressed in the $L^*a^*b^*$ coordinates. L^* corresponds to the light intensity, varying from 0 (no light) to 100. Parameters a^* and b^* quantify the contribution of four colors: green ($-a^*$), red ($+a^*$), blue ($-b^*$) and yellow ($+b^*$). With RC anthocyanins, the method to generate the $L^*a^*b^*$ coordinates and the corresponding color patches was as described in our recent work [14]. With PSP anthocyanins, the colorimetric data were generated as previously reported [4].

3.4. High-Resolution Mass Spectrometry (HRMS)

Stock solutions of anthocyanins P2, PB, and P5 were diluted to 0.1 mM in a 50 mM ammonium acetate buffer at pH 7. A 0.5 μL volume was injected in the same solvent (flow injection analysis) over 1 min into an Orbitrap Exploris 480 mass spectrometer Exploris 480 (Thermo Fisher Scientific, Waltham, MA, USA) equipped with an H-ESI source. A static spray voltage of -3.5 kV in positive mode and of 2.5 kV in negative mode was applied with an ion-transfer tube temperature of 280 $^\circ\text{C}$, a vaporizer temperature of 300 $^\circ\text{C}$, and a N_2 sheath gas pressure of 40 psi. The full scan was recorded at a resolution of 24×10^4 and corrected with an internal mass calibrant. Ions were searched between m/z 400 and 1600. The elution lasted ca. 0.3 min and an average spectrum was determined with the Freestyle 1.6 software based on the 20–30 spectra of intensities higher than 10%. A targeted detection of

the Fe^{2+} , Fe^{3+} , and Al^{3+} complexes of stoichiometries 1:1, 1:2, and 1:3 and with charges ranging from -3 to $+4$ was carried out. Based on proposed raw formulae, the theoretical isotopic patterns were calculated with the <https://www.chemcalc.org/web> tool (accessed on March 2, 2021).

3.5. Thermal Degradation

Thermal degradation was performed at pH 7 and 50 °C in a thermostated water bath. The pigments were diluted to 50 μM in the phosphate buffer at 50 °C and UV-VIS spectra were recorded over 24 h. The residual fraction of color species at pH 7 (a mixture of neutral and anionic bases) was determined at λ_{max} as % Color = $100 \times A_{\lambda_{\text{max}}}(t)/A_{\lambda_{\text{max}}}(t = 0)$. Aliquots of 1.5 mL were taken up at time zero, at regular time intervals over 8 h, and finally at $t = 24$ h. They were cooled down, acidified to pH 1, and stabilized at room temperature for 15 h (nonacylated anthocyanins) to 48 h (diacylated anthocyanins) (to ensure complete regeneration of the flavylium ion from the colorless forms). The absorption spectra were then recorded and the residual fraction of flavylium ion was calculated as % $\text{AH}^+ = 100 \times A_{\lambda_{\text{max}}}(t)/A_{\lambda_{\text{max}}}(t = 0)$ and plotted as a function of time. The time periods for a 25% color loss, or a 25% pigment loss (noted t_{25}), were determined from the theoretical curves generated by exponential curve-fitting.

4. Conclusions

Anthocyanins acylated by hydroxycinnamic acid residues are prone to develop inter- and intramolecular π -stacking interactions that make the flavylium nucleus less vulnerable to water addition. However, the acylation site plays a critical role, and among the red cabbage anthocyanins, it is clear that the sinapoyl residue at C2-OH of Glc-2 is by itself sufficient to provide resistance to water addition. Enhanced π -stacking interactions result from the ideal positioning of the sinapoyl residue (external Glc + C2 position), which probably reaches an optimal compromise between rigidity and flexibility.

The present work shows that optimal cyanidin–hydroxycinnamoyl π -stacking interactions can also exert a critical and favorable influence on metal binding. Indeed, only the metal complexes having $\text{R}_2 = \text{sinapoyl}$ (pigments B, 4, 5, and 6) are deeply blue and thermally stable over long periods of time. Not only the sinapoyl residue (although noncoordinating by itself) does not compromise metal binding by steric hindrance, it also shifts the visible band to

the blue domain and increases its intensity, and stabilizes the metal complexes and prevents the release of free pro-oxidant iron in the medium.

Based on these results, the impact of metal – anthocyanin binding on the absorption and biological activity of acylated anthocyanins could be assessed. In summary, anthocyanins having a 3',4'-dihydroxy substitution (cyanidin, delphinidin and petunidin glycosides) with adequately located hydroxycinnamoyl residues offer bright prospects for further development as natural food colorants.

Supplementary Materials:

Author Contributions: Conceptualization, methodology, formal analysis, investigation, writing—original draft, visualization, J.A.F.; formal analysis, investigation (aluminum–PSP anthocyanin binding), G.T.S.; resources, funding acquisition, R.J.R.; resources, funding acquisition, T.M.C.; conceptualization, supervision (aluminum–PSP anthocyanin binding), M.M.G.; conceptualization, methodology, formal analysis, writing—review and editing, supervision, O.D. All authors have read and agreed to the published version of the manuscript.

Funding: This research received no external funding

Acknowledgments: The authors gratefully thank the Polyphenols analytical platform (UMR SPO, INRAE, Montpellier SupAgro, Montpellier University, France) for the HRMS analyses; Raphaël Plasson (UMR408, Avignon University) for developing the program converting UV-VIS spectra into L*a*b* coordinates; and Olivia Rossi (Avignon University) for her experimental assistance during her undergraduate internship.

Conflicts of Interest: The authors declare no conflict of interest.

References

1. Moloney, M.; Robbins, R.J.; Collins, T.M.; Kondo, T.; Yoshida, K.; Dangles, O. Red cabbage anthocyanins: The influence of D-glucose acylation by hydroxycinnamic acids on their structural transformations in acidic to mildly alkaline conditions and on the resulting color. *Dyes Pigm.* **2018**, *158*, 342–352. doi:10.1016/j.dyepig.2018.05.057
2. Terahara, N.; Shimizu, T.; Kato, Y.; Nakamura, M.; Maitani, T.; Yamaguchi, M.; Goda, Y. Six Diacylated Anthocyanins from the Storage Roots of Purple Sweet Potato, *Ipomoea Batatas*. *Bioscience, Biotechnology, and Biochemistry* **1999**, *63*, 1420–1424, doi:10.1271/bbb.63.1420.
3. Sigurdson, G.T.; Robbins, R.J.; Collins, T.M.; Giusti, M.M. Evaluating the role of metal ions in the bathochromic and hyperchromic responses of cyanidin derivatives in acidic and alkaline pH. *Food Chem.* **2016**, *208*, 26–34, doi:10.1016/j.foodchem.2016.03.109.

4. Sigurdson, G.T.; Robbins, R.J.; Collins, T.M.; Giusti, M.M. Molar absorptivities (ϵ) and spectral and colorimetric characteristics of purple sweet potato anthocyanins. *Food Chem.* **2019**, *271*, 497–504, doi:10.1016/j.foodchem.2018.07.096.
5. Sigurdson, G.T.; Robbins, R.J.; Collins, T.M.; Giusti, M.M. Effects of hydroxycinnamic acids on blue color expression of cyanidin derivatives and their metal chelates. *Food Chem.* **2017**, *234*, 131–138, doi:10.1016/j.foodchem.2017.04.127.
6. Pina, F. Chemical Applications of anthocyanins and related compounds. A source of bioinspiration. *J. Agric. Food Chem.* **2014**, *62*, 6885–6897, doi:10.1021/jf404869m.
7. Trouillas, P.; Sancho-García, J.C.; De Freitas, V.; Gierschner, J.; Otyepka, M.; Dangles, O. Stabilizing and modulating color by copigmentation: Insights from theory and experiment. *Chem. Rev.* **2016**, *116*, 4937–4982, doi:10.1021/acs.chemrev.5b00507.
8. Yoshida, K.; Mori, M.; Kondo, T. Blue flower color development by anthocyanins : From chemical structure to cell physiology. *Nat. Prod. Rep.* **2009**, *26*, 884–915, doi:10.1039/B800165K.
9. Denish, P.R.; Fenger, J.-A.; Powers, R.; Sigurdson, G.T.; Grisanti, L.; Guggenheim, K.G.; Laporte, S.; Li, J.; Kondo, T.; Magistrato, A.; et al. Discovery of a natural cyan blue: A unique food-sourced anthocyanin creates a replacement for brilliant blue. *Science Adv.* **2021**, *7*, eabe7871, doi:10.1126/sciadv.abe7871.
10. Fenger, J.-A.; Moloney, M.; Robbins, R.J.; Collins, T.M.; Dangles, O. The influence of acylation, metal binding and natural antioxidants on the thermal stability of red cabbage anthocyanins in neutral solution. *Food Funct.* **2019**, *10*, 6740–6751, doi:10.1039/C9FO01884K.
11. Fedenko, V.S.; Shemet, S.A.; Landi, M. UV–vis spectroscopy and colorimetric models for detecting anthocyanin-metal complexes in plants: An overview of in vitro and in vivo techniques. *J. Plant Physiol.* **2017**, *212*, 13–28, doi:10.1016/j.jplph.2017.02.001.
12. Smyk, B.; Pliszka, B.; Drabent, R. Interaction between cyanidin 3-glucoside and Cu(II) ions. *Food Chem.* **2008**, *107*, 1616–1622, doi:10.1016/j.foodchem.2007.10.037.
13. Dangles, O.; Fenger, J.-A. The chemical reactivity of anthocyanins and its consequences in food science and nutrition. *Molecules* **2018**, *23*, 1970, doi:10.3390/molecules23081970.
14. Fenger, J.-A.; Roux, H.; Robbins, R.J.; Collins, T.M.; Dangles, O. The influence of phenolic acyl groups on the color of purple sweet potato anthocyanins and their metal complexes. *Dyes Pigm.* **2021**, *185*, 108792, doi:10.1016/j.dyepig.2020.108792.
15. Al Bittar, S.; Mora, N.; Loonis, M.; Dangles, O. A simple synthesis of 3-deoxyanthocyanidins and their O-glucosides. *Tetrahedron* **2016**, *72*, 4294–4302, doi:10.1016/j.tet.2016.05.076.
16. Vallverdú-Queralt, A.; Biler, M.; Meudec, E.; Le Guernevé, C.; Vernhet, A.; Mazauric, J.-P.; Legras, J.-L.; Loonis, M.; Trouillas, P.; Cheynier, V.; et al. *p*-Hydroxyphenyl-pyranoanthocyanins: An experimental and theoretical investigation of their acid–Base properties and molecular interactions. *Int. J. Mol. Sci.* **2016**, *17*, 1842, doi:10.3390/ijms17111842.
17. Nkhili, E.; Loonis, M.; Mihai, S.; El Hajji, H.; Dangles, O. Reactivity of food phenols with iron and copper ions: Binding, dioxygen activation and oxidation mechanisms. *Food Funct.* **2014**, *5*, 1186–1202, doi:10.1039/C4FO00007B.
18. Perron, N.R.; Brumaghim, J.L. A Review of the antioxidant mechanisms of polyphenol compounds related to iron binding. *Cell Biochem. Biophys.* **2009**, *53*, 75–100, doi:10.1007/s12013-009-9043-x.
19. Fenger, J.-A.; Robbins, R.J.; Collins, T.M.; Dangles, O. The fate of acylated anthocyanins in mildly heated neutral solution. *Dyes Pigm.* **2020**, *178*, 108326, doi:10.1016/j.dyepig.2020.108326.

**Acylated anthocyanins from red cabbage and purple sweet potato
can bind metal ions and produce stable blue colors**

Julie-Anne Fenger,* Gregory T. Sigurdson, Rebecca J. Robbins, Thomas M.
Collins, M. Mónica Giusti, Olivier Dangles*

Supplementary Information

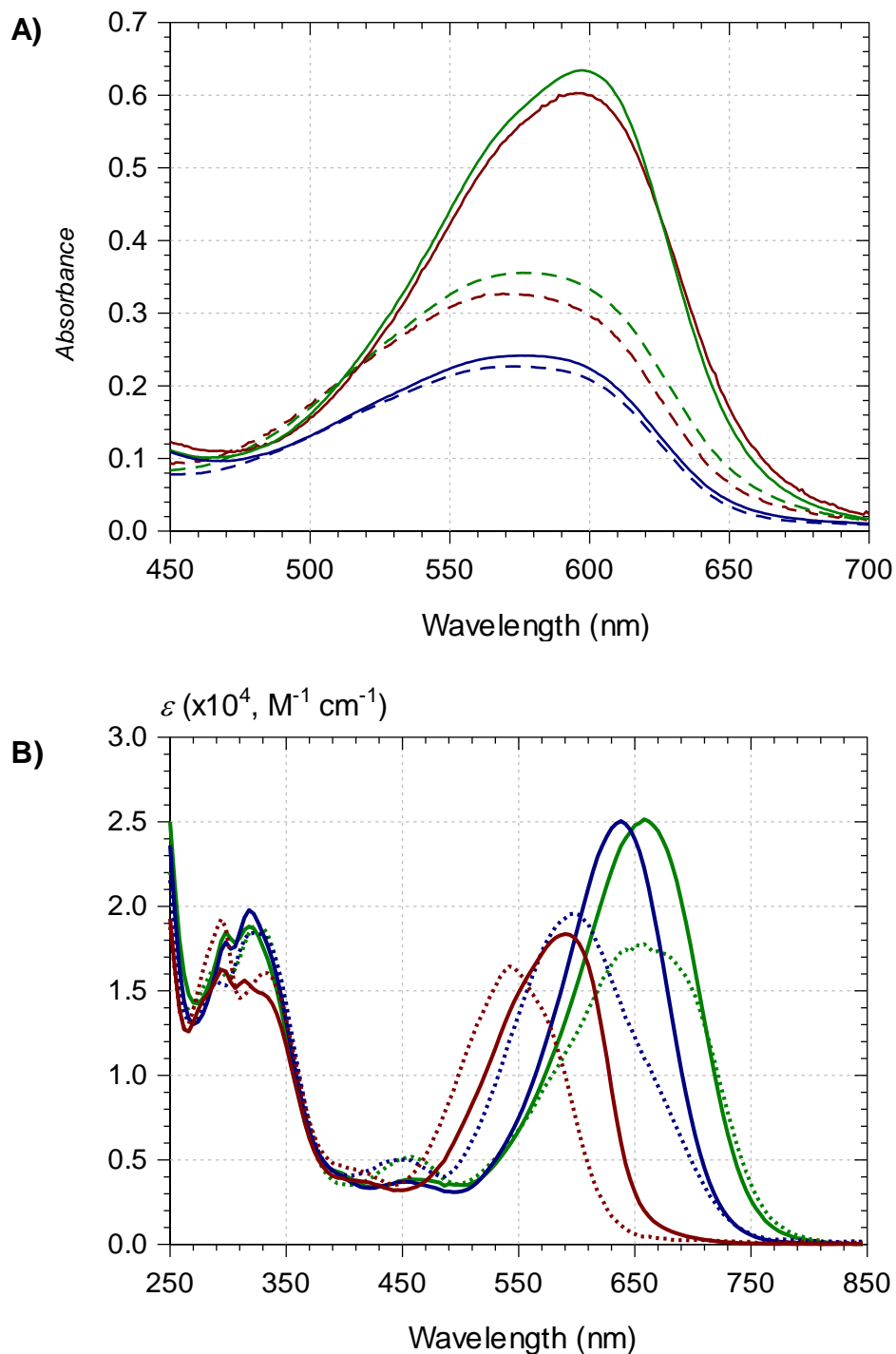


Figure S1. **A)** Visible spectra of Purple Sweet Potato (PSP) anthocyanins (solid curves) and their Al^{3+} complexes (dotted curves, 1 equiv. Al^{3+}) recorded at pH 7 30 min after sample preparation. Pigment 4' (—, acyl = Fl), Pigment 6' (—, acyl = Cf), Pigment 7 (—, acyl = Cf, Cf). **B)** UV-visible spectra of pigment B at pH 7.0 (solid curves) and at pH 5.68 (dotted curves). red: control, green: + Fe^{2+} (1 equiv.), blue: + Al^{3+} (1 equiv.).

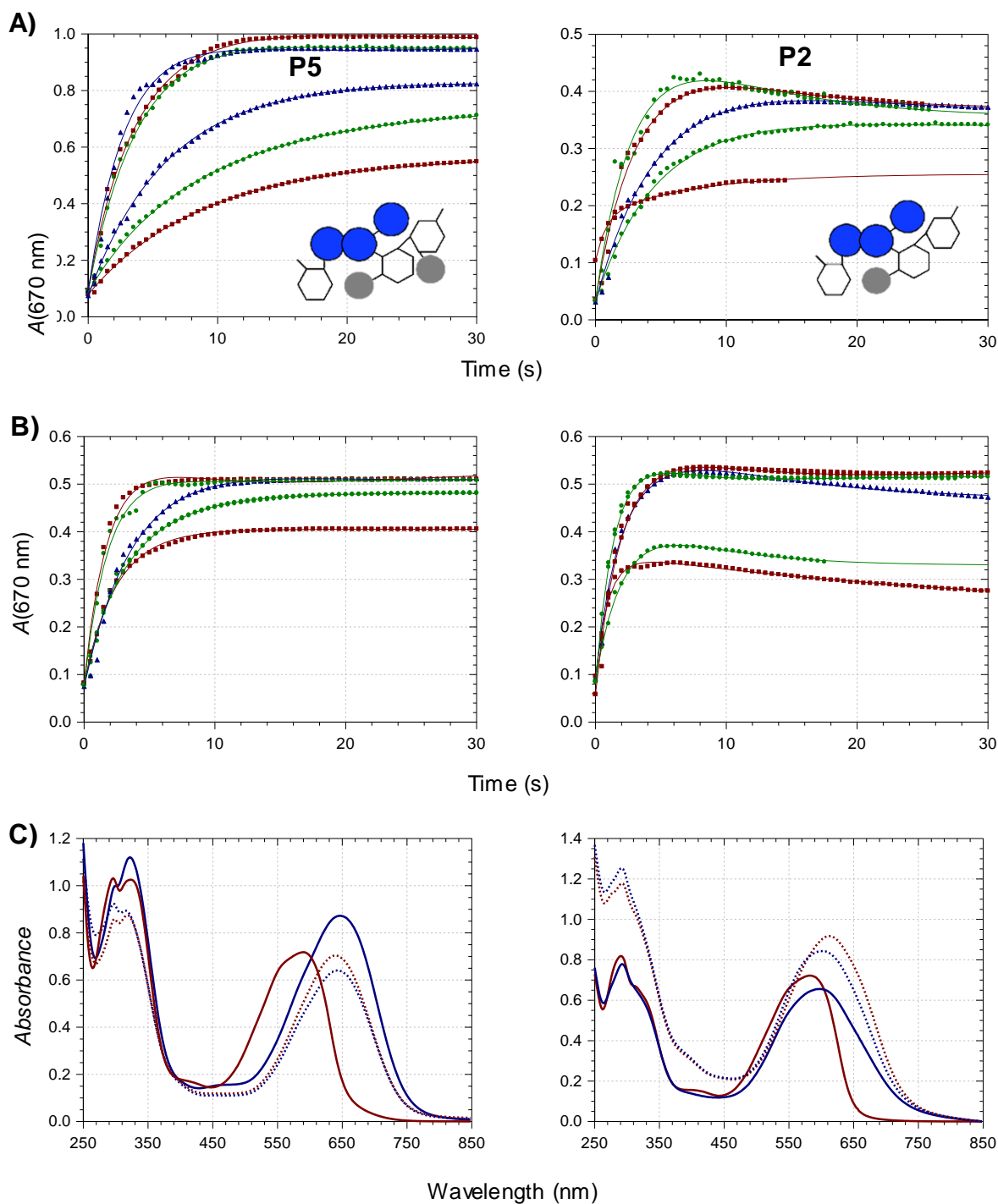


Figure S2. Iron - anthocyanin binding (successive addition of pigment (40 μM at pH 7, 20 μM at pH 8) and Fe^{2+}), inserts: schemes of the pigment structure are displayed. **A & B)** Kinetic monitoring at pH 7 (A) or pH 8 (B). Iron/pigment molar ratio (from bottom to top curves) = 0.1, 0.3, 0.6, 1, 1.5, 2 (Pigment 5, pH 7), 0.3, 0.6, 1, 2, 4 (Pigment 2, pH 7), 0.1, 0.3, 0.6, 1, 2 (Pigments 2 and 5, pH 8). **C)** Spectra at time zero (—) and at the end of the kinetic run (—). 1 equiv. Fe^{2+} . Solid curves: pH 7. Dashed curves: pH 8.

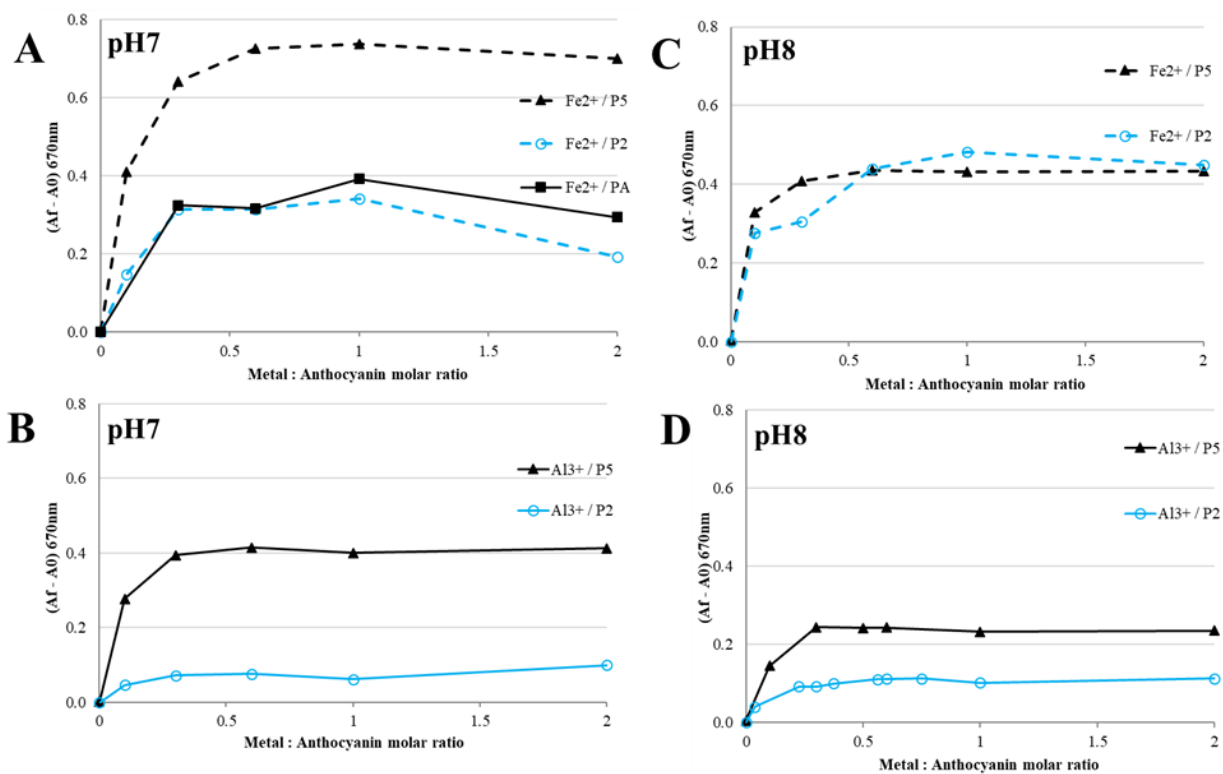
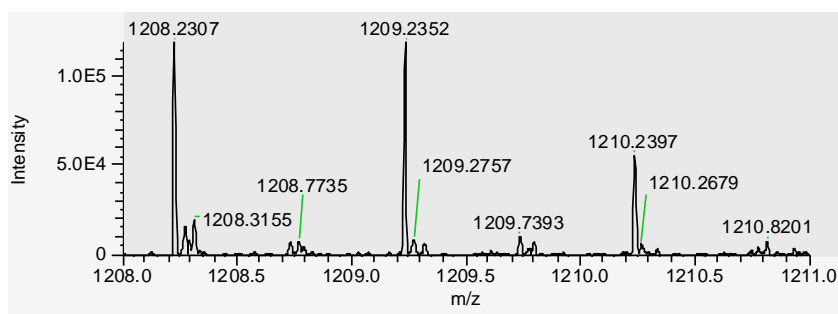
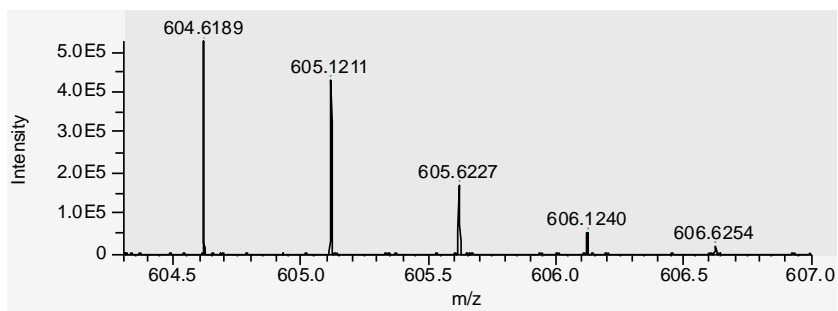


Figure S3. Amplitude of the complex's visible band as a function of the metal/ligand molar ratio. Pigment 2 (○), Pigment 5 (▲).

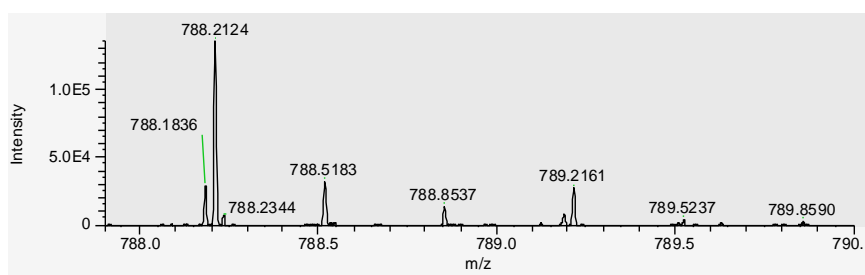
A)



[P5 - 3H⁺ + Fe³⁺]⁺



[P5 - 2H⁺ + Fe³⁺]²⁺



[2P5 - 2H⁺ + Fe³⁺]³⁺

(+ unidentified signals
at m/z 788.2124 and
789.2161)

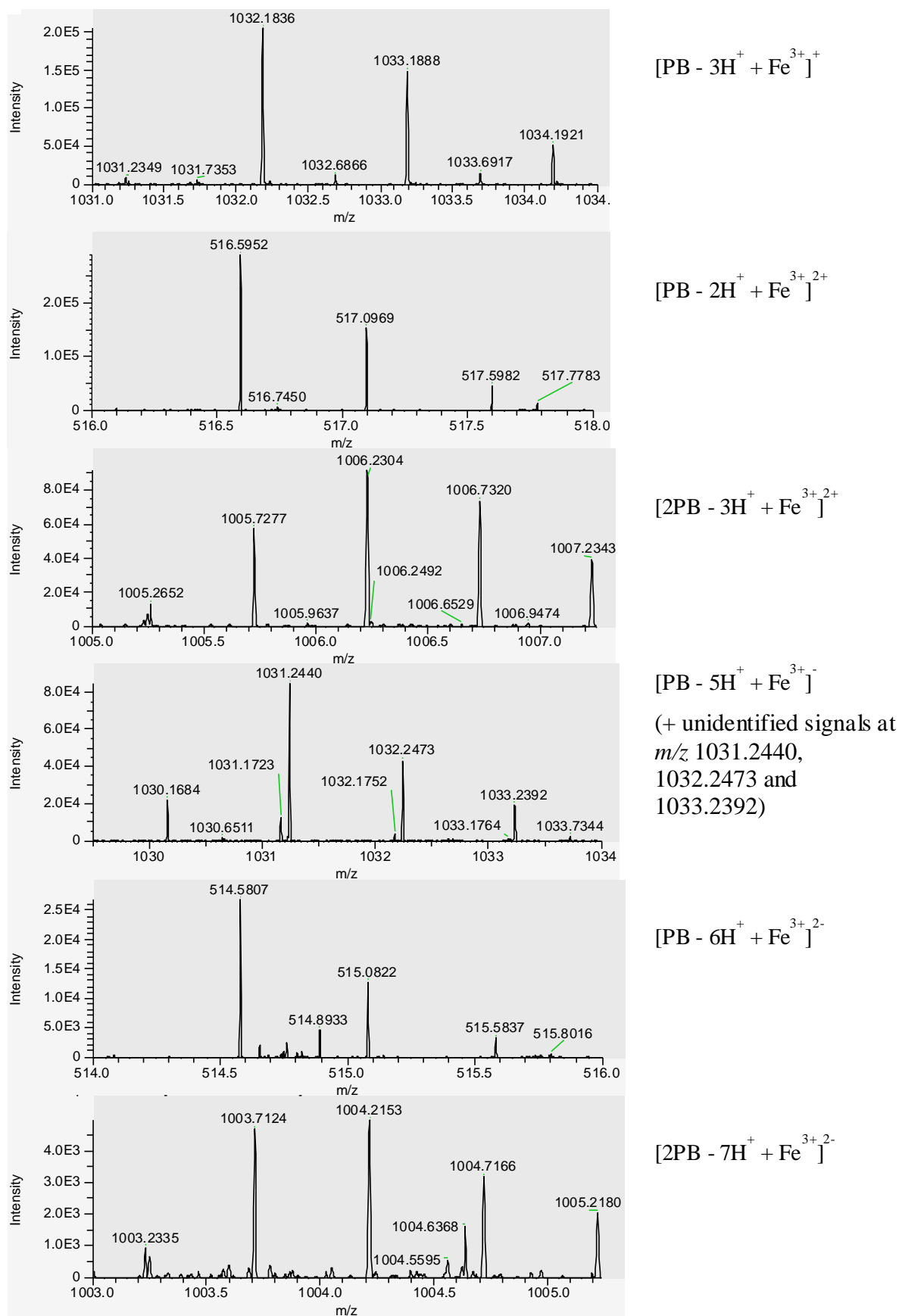
B)

Figure S4. HRMS analyses of iron – anthocyanin complexes (pH 7 ammonium acetate buffer, metal/ligand molar ratio = 1). **A)** Pigment 5, **B)** Pigment B.

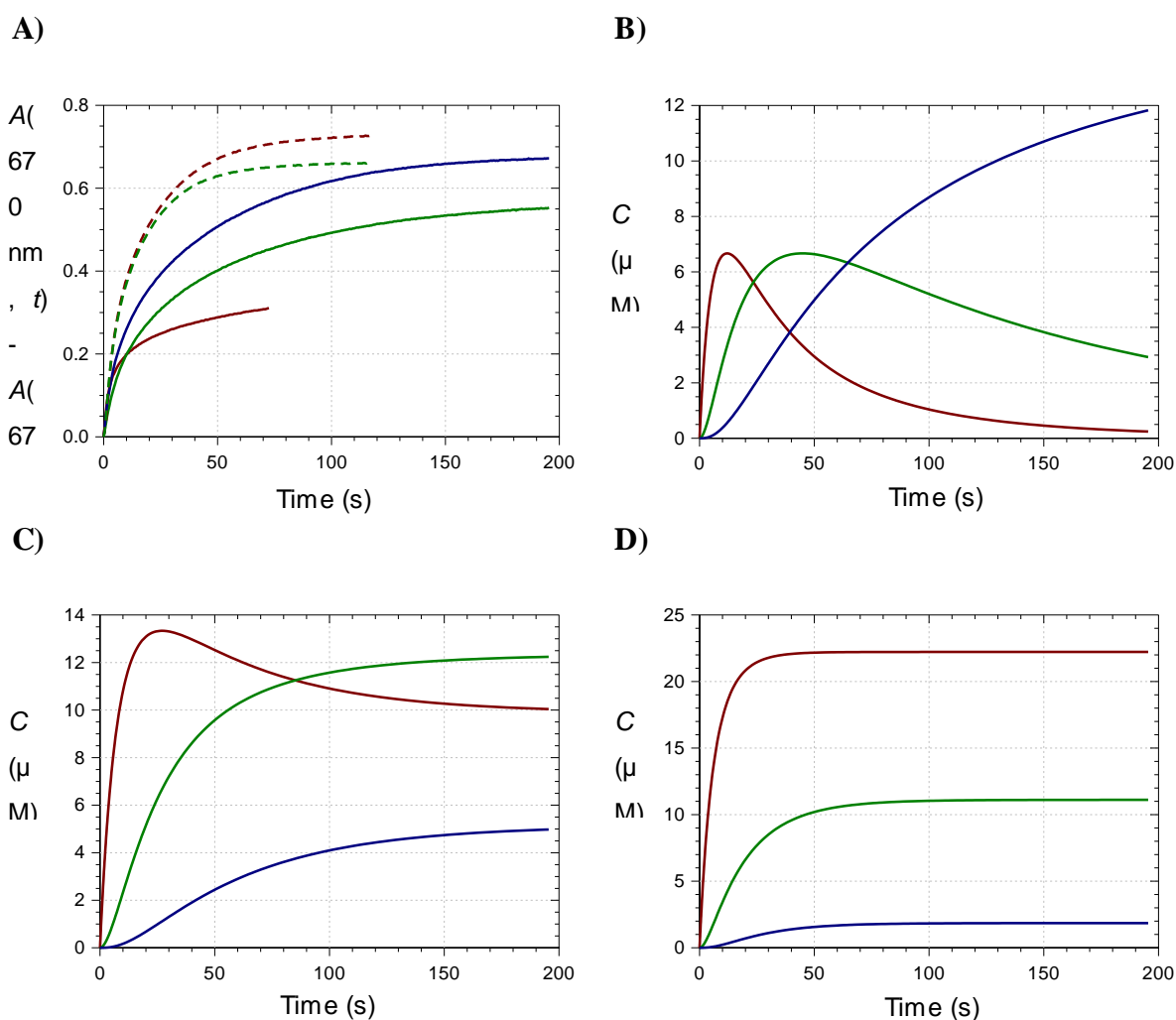


Figure S5. **A)** Kinetics of Al^{3+} – pigment B binding (pH 7, 25°C). Pigment concentration = 50 μM , metal / pigment molar ratio = 0.1 (—), 0.3 (—), 0.6 (—), 1 (---), 2 (---). **B-D)** Speciation diagrams of Al^{3+} - pigment B complexes. **B)** 0.3 equiv. Al^{3+} . **C)** 0.6 equiv. Al^{3+} . **D)** 1 equiv. Al^{3+} . ML (—), ML_2 (—), ML_3 (—). ML_n : metal-ligand complex having a 1:n metal/ligand stoichiometry.

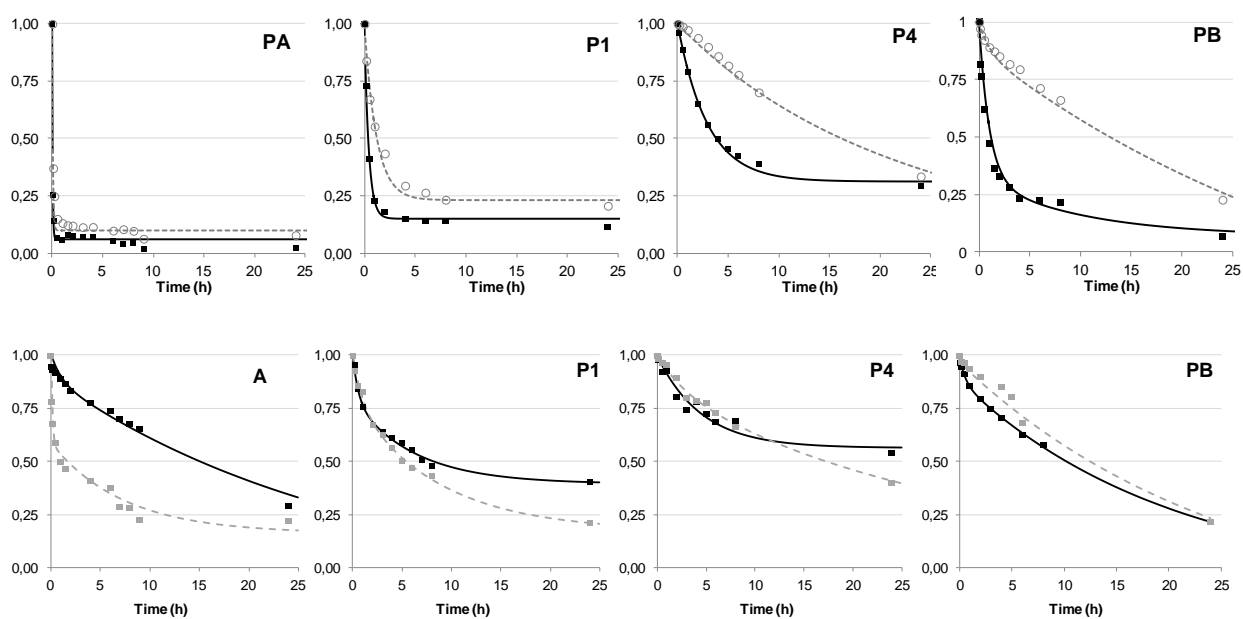


Figure S6. Rate of color loss (*top*) and pigment loss (*bottom*) in solutions of Pigments A, 1, 4 and B at pH 7, 50°C, in the absence (black plain line) or presence (grey dashed line) of 0.6 equiv. Fe^{2+} .

Table S1. Wavelengths of maximal visible absorption (λ_{\max} , in nm) of PSP anthocyanins (50 μM) in the absence or presence of Al^{3+} , 25°C, $n = 3$.

Pigment	No Al^{3+}	0.5 equiv. Al^{3+}	1 equiv. Al^{3+}	5 equiv. Al^{3+}
pH 6				
P4'	547 (2)	562 (1)	563 (1)	569 (1)
P6'	548 (3)	572 (2)	574 (1)	581 (1)
P7'	552 (1)	570 (0)	575 (3)	584 (1)
P9b'	552 (3)	584 (1)	581 (1)	589 (7)
pH 7				
P4'	572 (2)	583 (1)	580 (0)	576 (3)
P6'	570 (1)	591 (3)	591 (2)	590 (1)
P7'	576 (1)	594 (0)	598 (1)	595 (0)
P9b'	582 (3)	598 (2)	598 (1)	597 (5)
pH 8				
P4'	598 (0)	596 (1)	596 (1)	594 (4)
P6'	600 (1)	602 (2)	601 (1)	597 (3)
P7'	603 (0)	603 (0)	601 (0)	602 (1)
P9b'	604 (1)	607 (1)	606 (1)	606 (2)

Table S2. Hue angle (h^0) of PSP anthocyanins (50 μM) treated with Al^{3+} , 25°C, $n = 3$.

Pigment	No Al^{3+}	0.5 equiv. Al^{3+}	1 equiv. Al^{3+}	5 equiv. Al^{3+}
pH 6				
P4'	332.1 (1.1)	308.7 (1.2)	302.6 (0.9)	295.7 (0.9)
P6'	325.1 (0.6)	277.7 (1.5)	273.4 (0.4)	269.1 (0.2)
P7'	311.6 (0.2)	285.9 (0.2)	280.7 (2.2)	271.4 (0.0)
P9b'	308.1 (0.8)	265.3 (0.2)	265.1 (0.2)	263.3 (0.5)
pH 7				
P4'	291.6 (0.2)	271.6 (0.4)	272.3 (0.6)	269.4 (1.7)
P6'	293.0 (0.2)	253.8 (0.4)	247.8 (0.2)	249.9 (0.3)
P7'	285.9 (0.1)	261.2 (1.1)	254.6 (0.4)	249.6 (0.4)
P9b'	284.0 (0.3)	247.7 (1.2)	248.2 (0.9)	248.7 (1.2)
pH 8				
P4'	241.6 (0.2)	238.4 (0.3)	239.3 (0.2)	239.7 (0.6)
P6'	245.5 (0.2)	221.7 (0.1)	228.0 (0.7)	231.8 (0.3)
P7'	245.1 (0.1)	235.8 (0.3)	239.2 (1.2)	238.5 (0.5)
P9b'	243.4 (0.4)	232.9 (0.2)	234.0 (0.3)	235.4 (0.3)

a) h^0 (PB- Al^{3+} complex, pH 7) = 207.3 vs. 209.4 for Brilliant Blue [9]

Table S3. Ions detected for the aluminum complexes of Pigment B (metal/ligand molar ratio = 1).

Compound	Formula	Th. m/z ^{a)}	Exp. m/z	δ (ppm)
PB ⁺	C ₄₄ H ₅₁ O ₂₅	979.2714	979.2722	0.8
[PB + Al ³⁺ - 3H] ⁺	C ₄₄ H ₄₈ O ₂₅ Al	1003.2295	1003.2301	0.6
[PB + Al ³⁺ - 2H] ⁺²⁺	C ₄₄ H ₄₉ O ₂₅ Al	502.1184	502.1184	0.0
[2PB + Al ³⁺ - 3H] ⁺²⁺	C ₈₈ H ₉₉ O ₅₀ Al	991.2504	991.2510	0.6
[PB - 2H] ^{+,-}	C ₄₄ H ₄₉ O ₂₅	977.2563	977.2570	0.7
[PB + Al ³⁺ - 5H] ^{+,-}	C ₄₄ H ₄₆ O ₂₅ Al	1001.2149	1001.2151	0.2
[PB + Al ³⁺ - 6H] ^{+2,-}	C ₄₄ H ₄₅ O ₂₅ Al	500.1038	500.1016	4.4
[2PB + Al ³⁺ - 7H] ^{+2,-}	C ₈₈ H ₉₅ O ₅₀ Al	989.2359	989.2363	0.4
[3PB + Al ³⁺ - 8H] ^{+2,-}	C ₁₃₂ H ₁₄₅ O ₇₅ Al	1478.3679	1478.3765	5.8
[3PB + Al ³⁺ - 9H] ^{+3,-}	C ₁₃₂ H ₁₄₄ O ₇₅ Al	985.2429	985.2385	4.5
[3PB + Al ³⁺ - 10H] ^{+4,-}	C ₁₃₂ H ₁₄₃ O ₇₅ Al	738.6803	738.6790	1.8

^{a)} Calculations carried out on website <https://www.chemcalc.org/>

Table S4. Relative signal intensity (percentage of the free flavylum signal) with varying metal/pigment molar ratios.

Ion	Exp. m/z	Relative signal intensity			
		0	1/6	1/3	1
[P2 - 3H ⁺ + Fe ³⁺] ⁺	1002.1731	0.01%	0.80%	0.90%	0.90%
[P5 - 3H ⁺ + Fe ³⁺] ⁺	1208.2307	0.40%	1.1%	1.2%	4.1%
[PB - 3H ⁺ + Fe ³⁺] ⁺	1032.1836	0.03%	0.77%	0.90%	0.87%

Table S5. Competition between iron binding and water addition in a pH 4.24 acetate buffer
a). Simultaneous kinetic analysis of the spectral changes at 530 nm (free pigment) and 670 nm (iron complexes). k'_h and k'_{-h} : apparent rate constants for hydration and dehydration (determined from control experiments in the absence of iron). k_f and k_d : rate constants for the formation and dissociation of the complexes. k_{autox} : rate constant for the autoxidation of the Fe^{2+} complex.

Pigment	PB	P3
k'_h ($\times 10^{-3}$, s^{-1})	33.1 (\pm 0.1)	82.4 (\pm 0.2)
k'_{-h} ($\times 10^{-3}$, s^{-1})	29.8 (\pm 0.2)	13.0 (\pm 0.1)
$k_f(\text{Fe}^{2+})$ ($\text{M}^{-1} \text{s}^{-1}$)	680 (\pm 7)	346 (\pm 16)
$k_d(\text{Fe}^{2+})$ ($\times 10^{-4}$, s^{-1})	53 (\pm 1)	-
k_{autox} ($\times 10^{-4}$, s^{-1})	49.5 (\pm 0.3)	187 (\pm 9)
$k_f(\text{Fe}^{3+})$ ($\text{M}^{-1} \text{s}^{-1}$) b)	10^4	10^4
$k_d(\text{Fe}^{3+})$ ($\times 10^{-3}$, s^{-1})	91.9 (\pm 0.6)	211 (\pm 5)
ε ($\times 10^3$, $\text{M}^{-1} \text{cm}^{-1}$)	$\text{Fe}^{\text{II}}\text{-PB}$ (670 nm): 3.6 (\pm 0.1) $\text{Fe}^{\text{III}}\text{-PB}$ (670 nm): 24 c)	$\text{Fe}^{\text{III}}\text{-PB}$ (530 nm): 10.9 (\pm 0.1) $\text{Fe}^{\text{III}}\text{-PB}$ (670 nm): 13.5 d)

a) Successive addition of pigment (40 μM) and Fe^{2+} (1 equiv.). The concentrations of free colored and colorless forms at the time of iron addition were estimated from the molar absorption coefficient of the free colored forms at 530 nm: 26.7×10^3 (Pigment B) and 14.9×10^3 (Pigment 3) $\text{M}^{-1} \text{cm}^{-1}$. b) Set constant (values from previous work with synthetic flavylum ions [20]). c) Deduced from the spectrum at pH 7 assuming total binding. d) Deduced from the spectrum at pH 8 assuming total binding), 14900 (free pigment, 530 nm).

Table S6. Period of time for 25% loss in color or in total pigment (residual flavylum content assessed after acidification) at pH 7, 50°C.

	PA	P1	P3	P4	PB
t_{25} color (h), no metal added	0.02	0.15	0.18	1.4	0.29
t_{25} color (h), 0.6 equiv. Fe^{2+}	0.03	0.47	0.29	4.6	4.5
t_{25} pigment (h), no metal added	4.5	4.4	2.0	3.7	2.6
t_{25} pigment (h), 0.6 equiv. Fe^{2+}	0.12	1.4	1.9	5.2	5.5

t_{25} pigment (h), no metal added vs t_{25} pigment (h), 0.6 equiv. Fe^{2+}

Chapter 5. The influence of phenolic acyl groups on the color of purple sweet potato anthocyanins and their metal complexes

Julie-Anne Fenger,^a Hugo Roux,^a Rebecca J. Robbins,^b Thomas M. Collins,^c
Olivier Dangles^{a*}

^a Avignon University, INRAE, UMR408, 84000 Avignon, France

^b Mars Wrigley, 1132 W Blackhawk Street, Chicago, IL 60642, USA

^c Retired



Dyes and Pigments
Volume 185, Part A, February 2021, 108792



Highlights

- Diacylated anthocyanins from purple sweet potato are resistant to water addition.
- PSP anthocyanins bind metal ions through their cyanidin and/or caffeoyl moieties.
- Concomitant binding of cyanidin and caffeoyl to iron favors blue color expression.
- Autoxidation of caffeoyl residues at pH 7 accelerates anthocyanin degradation.
- Evidence for oxidative anthocyanidin - caffeoyl coupling.

*Corresponding author.

E-mail address: olivier.dangles@univ-avignon.fr

Abstract

Anthocyanins from purple sweet potatoes (PSP, *Ipomoea batatas* L.) are peonidin and cyanidin glycosides acylated by *p*-hydroxycinnamic and *p*-hydroxybenzoic acids.

For six individual PSP pigments, the thermodynamic constants of proton transfer and water addition were determined, from which the speciation diagrams for the colored and colorless forms (pH range 1 – 10) and the UV-visible spectra of individual colored forms could be constructed. The data confirm that acylation by phenolic acids protects the chromophore against water addition (a consequence of acyl – anthocyanidin π -stacking interactions) and that this protection depends on the type and number of acyl residues, diacylation being much more efficient than monoacylation, and *p*-hydroxycinnamoyl more efficient than *p*-hydroxybenzoyl.

Most PSP anthocyanins can bind metal ions (Fe^{2+} , Al^{3+}) through their cyanidin chromophore and/or their caffeoyl residue(s). At pH 7, cyanidin and caffeoylated derivatives bind metal ions, inducing respectively a bluing effect (bathochromic shift) or a pale yellow contribution to the color. The simultaneous binding of the same metal ion to both ligands was observed. The additional presence of a caffeoyl residue allows the simultaneous binding of the metal ion to both ligands.

Although the caffeoyl residues efficiently slow down color loss through their π -stacking interactions with the chromophore, their redox activity actually accelerates the thermal degradation of anthocyanins. Consistently, two-electron autoxidation of anthocyanins bearing caffeoyl residues could be evidenced by UPLC-MS/DAD analysis. These new pigments possibly stem from intramolecular coupling between the chromophore and *o*-quinones derived from the caffeoyl residues.

1. INTRODUCTION

Anthocyanins are plant pigments that typically exhibit bright red, purple and blue colors as the pH is changed from 1 to 9. This property makes them potential natural food colorants. However, color fading in the pH range 4 - 7 greatly limits the industrial applications of anthocyanins. Color loss results from a combination of reversible (water addition) and irreversible (autoxidation, hydrolysis) mechanisms [1]. Polyacylation by phenolic acids, *i.e.* hydroxycinnamic acids (HCAs) or hydroxybenzoic acids (HBAs), efficiently increases the color stability owing to π -stacking interactions between the anthocyanidin chromophore and the acyl residues. Within the compact conformations (intramolecular copigmentation) and/or aggregates (self-association) thus formed, the anthocyanidin is less available to attacks by bleaching agents, such as water, bisulfite and hydrogen peroxide [2]. Polyacylated anthocyanins, which are common in flower petals, can also be found in edible sources, especially in intensely colored vegetables, such as red cabbage (RC) and purple sweet potato (PSP), and the corresponding extracts bear great potential for application as food colorants.

RC and PSP anthocyanins are both 3-O-sophorosyl-5-O-glucosylcyanidin and peonidin derivatives bearing a variety of acyl groups on the sophorosyl moiety. In RC, acylation occurs at C6-OH of the first D-glucose unit (Glc-1) and/or at C2-OH of the second D-glucose unit (Glc-2). By contrast, acylation in PSP anthocyanins only occurs at the C6-OH positions of both Glc units (Scheme 1). Diacylation of RC and PSP anthocyanins provides a remarkable protection against water addition to the C2 position (C-ring) of the flavylum ion (AH^+), which leads to a colorless hemiketal (B) in equilibrium with minor concentrations of *cis*- and *trans*-chalcones (Cc and Ct) (Scheme 1-SI) [3,4]. Sandwich-type conformations with the chromophore intercalated between the two acyl residues are assumed to be involved in this gain in color stability [5].

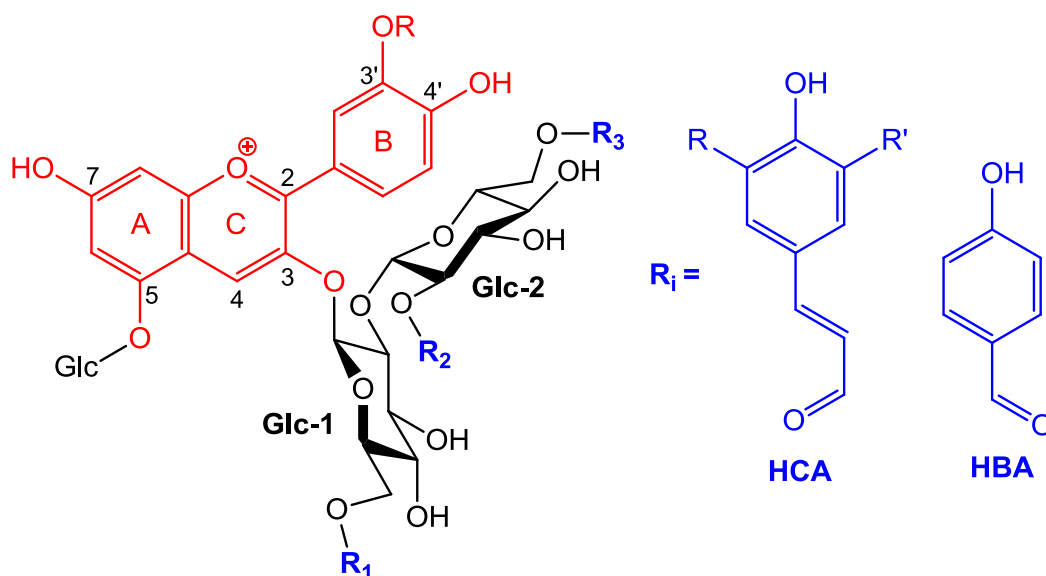
While PSP anthocyanins are peonidin (major) and cyanidin (minor) derivatives, RC are essentially cyanidin derivatives, which were shown to bind metal ions above pH 5 with concomitant intense bathochromic shifts in the visible band and color stabilization [6]. Unlike their RC cabbage homologs, some major PSP pigments have a caffeic acid residue, which itself can bind metal ions. Hence, depending on the PSP anthocyanin selected, metal binding can occur via the chromophore (RCE anthocyanins) or acyl group (P9a, P10, P11, P12) or both (P9b) (Scheme 1).

In this work, from a selection of individual PSP anthocyanins differing by the number and type (HCA *vs.* HBA) of acyl residues, the influence of acylation on the color loss by reversible water addition was quantitatively investigated. The superiority of anthocyanins bearing two HCA residues is clearly demonstrated. The relative affinity of the cyanidin and caffeoyl binding sites for metal ions and its consequences on the color expressed was investigated at pH 7 with Fe^{2+} and Al^{3+} . Finally, the impact of the caffeoyl residues, free or coordinated to Fe^{2+} , on the irreversible color loss (autoxidation) was also assessed. Evidence for the formation of new pigments derived from intramolecular caffeoyl – anthocyanidin oxidative coupling is provided.

2. MATERIALS AND METHODS

2.1. Chemicals

Anthocyanin extracts and isolated anthocyanins from purple sweet potato and red cabbage (Scheme 1) were provided by Mars Wrigley. They are acylated derivatives of cyanidin- or peonidin-3-O-sophorosyl-5-O-glucoside. HPLC-grade water was used for all aqueous solutions. Caffeic acid, $\text{FeSO}_4 \cdot 7\text{H}_2\text{O}$, $\text{AlCl}_3 \cdot 6\text{H}_2\text{O}$, KCl, $\text{NaH}_2\text{PO}_4 \cdot 2\text{H}_2\text{O}$ and $\text{Na}_2\text{HPO}_4 \cdot 7\text{H}_2\text{O}$ were all purchased from Sigma-Aldrich. Acetic acid (VWR), trace metal grade HCl (Fisher Scientific) and NaOH (Alpha Aesar) were also used. Concentrated stock solutions (5 mM) of pigment were prepared in 0.05 M HCl.



	R	R₁	R₂	R₃
PA'	Me	H	H	H
P9a ^a	Me	Caffeoyl	H	H
P9b ^b	H	Caffeoyl	H	Feruloyl
P10 ^b	Me	Caffeoyl	H	Caffeoyl
P11 ^b	Me	Caffeoyl	H	<i>p</i> -Hydroxybenzoyl
P12 ^b	Me	Caffeoyl	H	Feruloyl
PA ^c	H	H	H	H
P4 ^c	H	<i>p</i> -Coumaroyl	Sinapoyl	H

p-Coumaroyl (pC): R = R' = H

Caffeoyl (Cf): R = OH, R' = H

Feruloyl (Fl): R = OMe, R' = H

Sinapoyl (Sp): R = R' = OMe

^a Structure inferred from those of the PSP DAAs. ^b Structures from [7].

^c From red cabbage [3].

Scheme 1. Structure of the purple sweet potato anthocyanins studied

2.2. Structural transformations of anthocyanins

Nonacylated, monoacylated and diacylated anthocyanins (NAAs, MAAs, DAAs, resp.) were compared through the thermodynamic and kinetic parameters characteristic of their structural transformations in acidic to mildly alkaline solution (Scheme 1-SI). Whereas the first and second acidity constants are weakly impacted by the acylation with no clear trend emerging, the overall acidity constant, which includes the hydration component, is strongly affected: the pK'_a value increases from NAA to DAAs, with a gap more marked when a second acyl residue is introduced. As expected, this trend is translated in the pK'_h value, the global thermodynamic constant of water addition to the flavylium ion. The DAAs of purple

sweet potato appear much more resistant to water addition than the NAA and MAAs, meaning that the second acyl residue triggers a better protection of the flavylum ion against water addition than the first one, as observed with the red cabbage anthocyanins [3]. This is consistent with the hypothesis of DAAs adopting sandwich conformations with the anthocyanidin intercalated between the 2 acyl residues for optimal protection. The second acylation also occurs on the external sugar of the sophorose, and thus displays a higher flexibility. This may result in more efficient π -stacking interactions.

The speciation diagrams express the calculated fractions of flavylum, neutral base, anionic base and the mixture of colorless forms, plotted for each pigment over the pH range 1 – 10. They show that the fraction of colored forms in mildly acidic solution (pH 5 - 7) ranges from *ca.* 1% for PA' to *ca.* 60% for P9b. As for the red cabbage anthocyanins [3], the coloring potential of the diacylated anthocyanins far outreaches that of the non- and monoacylated homologs at all pHs. This protection against hydration is mostly rooted in smaller hydration rate constants (a factor *ca.* 30 between the k_h values of PA' and P12). As DAAs make a large contribution to PSP anthocyanin extracts, representing 48% to 75% or more according to the cultivar [10,11], these pigments are mostly responsible for the color of the extract at the typical food pHs.

$$x_{AH^+} = \frac{1}{1 + 10^{pH-pK'a} + 10^{2(pH-pKa1-pKa2)}}$$

$$x_A = \frac{10^{pH-pKa1}}{1 + 10^{pH-pK'a} + 10^{2(pH-pKa1-pKa2)}}$$

$$x_{A^-} = \frac{10^{2(pH-pKa1-pKa2)}}{1 + 10^{pH-pK'a} + 10^{2(pH-pKa1-pKa2)}}$$

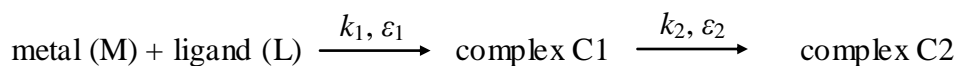
$$x_{B+Cc+Ct} = 1 - x_{AH^+} - x_A - x_{A^-}$$

2.3. Metal binding experiments

Fresh 5 mM solutions of Fe^{2+} and Al^{3+} were prepared from $\text{FeSO}_4 \cdot 7\text{H}_2\text{O}$ and $\text{AlCl}_3 \cdot 6\text{H}_2\text{O}$ in 1 mM HCl. In the quartz cuvette of the UV-visible spectrometer, the following solutions were added in this order: pH 7 phosphate buffer, 20 μL of anthocyanin stock solution and, after a few seconds, a small volume of the 5 mM Fe^{2+} solution (iron/anthocyanin molar ratio = 1 or 2). The full absorption spectra were recorded in kinetic mode. The duration of acquisition varied between 1 and 2 minutes. For an optimal sensitivity, the detection in the visible range was set at 550 or 610 nm with Al^{3+} (close to the complex's λ_{max}) and at 670 nm with Fe^{2+} (charge transfer contribution of the Fe^{3+} complexes). For free and bound caffeic acid, absorbance was recorded at 350 nm and 370 nm, respectively. When applicable, the hyperchromic and bathochromic shifts were calculated from the initial (free ligand) and final (metal complex) spectra as $(A_{\text{max},f} - A_{\text{max},0})/A_{\text{max},0}$ and $\lambda_{\text{max},f} - \lambda_{\text{max},0}$, respectively.

2.4. Kinetic modeling

The kinetic curves were analyzed with the Scientist[®] software (Micromath, St Louis, USA). A two-step process was usually observed which is interpreted as follows:



with k_1 a second-order rate constant, k_2 a first-order rate constant and ε the molar absorption coefficients. Optimized values for the rate constants and molar absorption coefficients are reported.

2.5. Thermal degradation

Thermal degradation was performed at pH 7 and 50°C in a thermostated water bath according to a method previously reported [2]. Briefly, the pigments were diluted to 50 μM in the phosphate buffer at 50°C and UV-vis spectra were recorded regularly over 8h. The residual fraction of color species at pH 7 (a mixture of neutral and anionic bases) was determined at λ_{max} as % Color = $A_{\lambda_{\text{max}}}(t) / A_{\lambda_{\text{max}}}(t = 0) \times 100$. Aliquots of 1.5 mL were taken up at time zero, at regular time intervals over 8h, and finally at $t = 24$ and 48h. They were cooled down, acidified to pH 1 and stabilized at room temperature for 15h (NAA) to 48h (DAA) (to ensure complete regeneration of the flavylium ion from the colorless forms). The absorption

spectra were then recorded and the residual fraction of flavylum ion was calculated as $\% \text{AH}^+ = A_{\lambda_{\text{max}}}(t) / A_{\lambda_{\text{max}}}(t = 0) \times 100$ and plotted as a function of time. Finally, the percentage of degradation products was simply deduced from $\% \text{D} = 100 - \% \text{AH}^+$.

2.6. Product identification and quantification

The acidified and stabilized samples were analyzed with an Acquity UPLC (Waters Corporation, Milford, USA) equipped with a diode array detector (DAD) and a ESI-Q-trap HCT Ultra mass spectrometer (Bruker Daltonics, Bremen, Germany) in ultrascan mode. Samples (5 μL) were injected onto an Acquity UPLC BEH C18 reversed phase column (50x2.1 mm, 1.7 μm) at 30°C. Phase A (1% HCO_2H in H_2O) and B (1% HCO_2H in MeCN) were used for elution at 0.4 mL/min. Gradient for P12 was %B: 0 min: 6%, 3 min: 12%, 9 min: 18%, 11 min: 24%, 14 min: 80%, 15-18 min: 6%. Gradient for P4 was %B: 0 min: 6%, 5 min: 12%, 10 min: 24%, 12-13 min: 80%, 15-18 min: 6%. The capillary voltage was -1.8 kV (positive mode) or 2.2 kV (negative mode) with a 120-2200 m/z scanning interval at a speed of $26 \times 10^3 m/z s^{-1}$. Desolvation was conducted with N_2 at 365°C, 40 psi, 540 L/h. The cone voltage was 40 V and the fragmentation amplitude was 1.2 V.

3. RESULTS AND DISCUSSION

3.1. Structural transformations of PSP anthocyanins

Nonacylated, monoacylated and diacylated anthocyanins (NAAs, MAAs, DAAs, resp.) were compared through the thermodynamic and kinetic parameters characteristic of their structural transformations in acidic to mildly alkaline solution (Scheme 1-SI). Whereas the first and second acidity constants are weakly impacted by the acylation with no clear trend emerging, the overall acidity constant, which includes the hydration component, is strongly affected: the pK'_a value increases from NAA to DAAs, with a gap more marked when a second acyl residue is introduced. As expected, this trend is translated in the pK'_h value, the global thermodynamic constant of water addition to the flavylium ion. The DAAs of purple sweet potato appear much more resistant to water addition than the NAA and MAAs, meaning that the second acyl residue triggers a better protection of the flavylium ion against water addition than the first one, as observed with the red cabbage anthocyanins [3]. This is consistent with the hypothesis of DAAs adopting sandwich conformations with the anthocyanidin intercalated between the 2 acyl residues for optimal protection. The second acylation also occurs on the external sugar of the sophorose, and thus displays a higher flexibility. This may result in more efficient π -stacking interactions.

The speciation diagrams express the calculated fractions of flavylium, neutral base, anionic base and the mixture of colorless forms, plotted for each pigment over the pH range 1 – 10. They show that the fraction of colored forms in mildly acidic solution (pH 5 - 7) ranges from *ca.* 1% for PA' to *ca.* 60% for P9b. As for the red cabbage anthocyanins [3], the coloring potential of the diacylated anthocyanins far outreaches that of the non- and monoacylated homologs at all pHs. This protection against hydration is mostly rooted in smaller hydration rate constants (a factor *ca.* 30 between the k_h values of PA' and P12). As DAAs make a large contribution to PSP anthocyanin extracts, representing 48% to 75% or more according to the cultivar [10,11], these pigments are mostly responsible for the color of the extract at the typical food pHs.

Table 1. Thermodynamic and rate constants for the structural transformations of the PSP anthocyanins (25°C).

	Pigment	pK'_a	pK_{a1}	pK_{a2}	pK'_h ^a	pK_h ^b	k_h (s ⁻¹)	k_{-h} (M ⁻¹ s ⁻¹)
PA'	Peo	2.04 (± 0.04)	4.21 (± 0.08)	7.08 (± 0.04)	2.04 (± 0.04)	2.55 (± 0.17)	0.33 (± 0.01)	116 (± 7)
P9a	Peo(Cf)	2.43 (± 0.02)	4.06 (± 0.12)	7.11 (± 0.02)	2.44 (± 0.02)	2.82 (± 0.32)	0.132 (± 0.011)	87.8 (± 6.6)
P9b	Cya(Cf,Fl)	3.71 (± 0.07)	3.93 (± 0.04)	7.15 (± 0.06)	4.11 (± 0.02)	3.91 (± 0.40)	0.049 (± 0.004)	394 (± 24)
P10	Peo(Cf,Cf)	3.53 (± 0.03)	4.11 (± 0.06)	7.16 (± 0.05)	3.66 (± 0.06)	3.95 (± 0.69)	0.028 (± 0.004)	251 (± 25)
P11	Peo(Cf,HB)	3.25 (± 0.03) ^c	3.99 (± 0.06) ^c	7.29 (± 0.02) ^c	3.34 (± 0.05)	3.74 (± 0.62)	0.030 (± 0.004)	162 (± 16)
P12	Peo(Cf,Fl)	3.85 (± 0.04)	4.34 (± 0.07)	7.49 (± 0.05)	4.02 (± 0.09)	4.25 (± 1.1)	0.010 (± 0.002)	176 (± 27)

^a $K'_h = K'_a - K_{a1}$ (Ct included), ^b $K'_h = k_h / k'_{-h}$ (Ct excluded). ^c From Oliveira et al., 2019 (phosphate / citrate / borate buffer): $pK'_a = 3.15$, $pK_{a1} = 4.2$, $pK_{a2} = 7.8$. Peo(HB): $pK'_a = 2.69$, $pK_{a1} = 4.1$, $pK_{a2} = 7.5$.

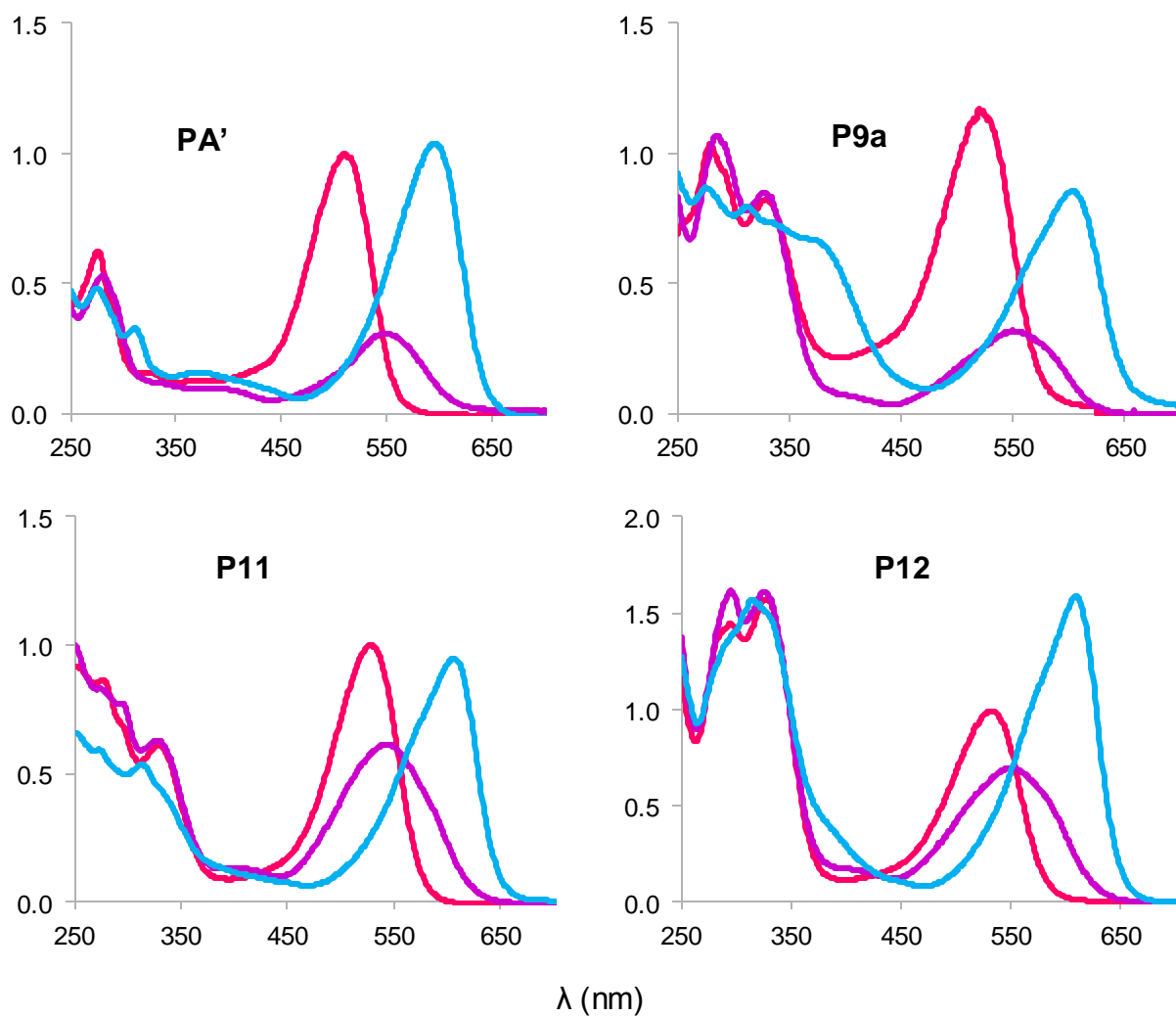
Among the diacylated anthocyanins of PSP, P11 bears a *p*-hydroxybenzoyl residue, which is much less common than the hydroxycinnamoyl residues. This peculiarity makes P11 more vulnerable to water addition than the other DAAs (P9b, P10 and P12), which display 2 HCA residues. For instance, the percentage of colored forms at equilibrium at pH 7 is *ca.* 40% for P12, *vs.* only 10% for P11. In addition, the formation of the colorless species (hydration) is 3 times as fast with P11 as for P12. This is consistent with HBAs being less potent copigments than HCAs [5] and suggests that the HBA residue of P11 develops weaker π -stacking interactions with the anthocyanidin than the wider more polarizable HCA residues.

The spectra of the pure neutral and anionic bases can be calculated from the experimental spectra at pH 1 (pure flavylum), 5.5 and 7.5 (recorded before significant hydration) and the pK_{a1} and pK_{a2} values. It permits to rigorously compare the coloring properties for a selection of peonidin derivatives from PSP as a function of their acylation pattern (Fig. 1). As usual, acylation results in a shifting of the visible band to higher wavelengths but this phenomenon, typically associated with acyl – anthocyanidin π -stacking interactions, is more significant with the flavylum ion and the anionic base. Acylation by a *p*-hydroxybenzoyl *vs.* *p*-hydroxycinnamoyl residue has no consequence on the flavylum

spectrum (same λ_{\max} for P11 and P12) but results in slightly lower λ_{\max} values for the neutral and anionic bases (Fig. 1).

The spectra of the anionic bases of P9a, P9b and P12 all show a narrow asymmetric absorption band, which is associated with a high chromaticity (Fig. 3-SI), which is an advantage in terms of color expression. Based on our previous work [3], purple sweet potato and red cabbage DAAs (except for P11) cannot be discriminated by their sensitivity to water addition. Thus, the position on Glc-2 of the second HCA residue (C6-OH in PSP *vs.* C2-OH in RC) has little influence on its capacity to hinder water addition to the flavylum ion.

From the spectral changes in the UV range at higher pH, the pK_a of the P9a's caffeoyl moiety was estimated at 8.27 ± 0.05 , *i.e.* a little more acidic than free caffeic acid ($pK_a = 8.48$, [12]) and chlorogenic acid (5-caffeoylquinic acid, $pK_{a2} = 8.42$ [13]). The dissociation of the HCA residues is thus largely negligible at food pHs.



max (nm)	Flavylium ion	Neutral base	Anionic base
PA' (no acyl)	511	548	597
P9a (acyl = Cf)	522	542	603
P11 (acyl = Cf, HB)	528	543	607
P12 (acyl = Cf, Fl)	528	553	610

Fig. 1. UV-visible spectra of pure colored forms for peonidin derivatives PA', P9a, P11 and P12. —: flavylium ion, —: neutral base, —: anionic base; color patches (L*a*b*coordinates).

3.2. Metal binding

In our study of metal – anthocyanin binding, a neutral moderately concentrated (10 mM) phosphate buffer was used to set the pH constant and also simply mimic the competition polyphenols may encounter in natural media with other common oxygenated ligands (organic acids, phosphate and phosphatidyl groups) for metal ions. Aluminum and iron binding is an important mechanism of color variation in plants, especially for the expression of blue colors in flowers [14]. In PSP anthocyanins, the cyanidin nucleus and/or the caffeoyl residues can bind metal ions owing to their catechol rings. For comparison, non acylated pigment PA and free caffeic acid were also studied. The spectral modifications of the PSP pigments (Fig. 2, Table 1-SI) are highly dependent on pH, the metal ion, and the presence, number and position of the acyl residues.

3.2.1. ALUMINUM BINDING

Caffeic acid does not bind to 1 molar equiv. of Al^{3+} at pH 7, whether free or as the single acyl group of peonidin derivative P9a (Glc-1). However, in P10, the presence of the second caffeoyl residue (Glc-2) allows Al^{3+} binding (Fig. 2, Table 1-SI). The binding of 1 or 2 equiv. Al^{3+} is primarily manifested by weak modifications in the UV band of the acyl residues (the appearance of a shoulder at *ca.* 400 nm), while the visible band remains mostly unaffected. Besides, reaching saturation in the spectral modifications requires an excess Al^{3+} , which suggests that Al^{3+} - P10 binding is reversible under our conditions.

P9b combines two potential binding units, the cyanidin nucleus and the caffeoyl residue on Glc-1 (inert to Al^{3+} as observed with P9a). Its binding to Al^{3+} is slightly slower than for P10 (Fig. 4), which suggests that both binding units participate. Indeed, the spectral changes in the UV range are the same as for P10, but the visible band is now shifted to higher wavelengths and broadened (Fig. 2). Moreover, the final spectra with 1 and 2 equiv. Al^{3+} are close. Overall, these observations suggest a simultaneous binding of 1 equiv. Al^{3+} for the cyanidin and caffeoyl moieties. The absorption spectrum of the P9B - Al^{3+} complex is actually close to the calculated spectrum of the pure anionic base (Fig 2). From the tautomers of A^- , deprotonated at C4' or C7-OH, the coordination of Al^{3+} induced an additional proton loss from C3'-OH, which has an overall weak hypsochromic impact, that may involve the caffeoyl moiety.

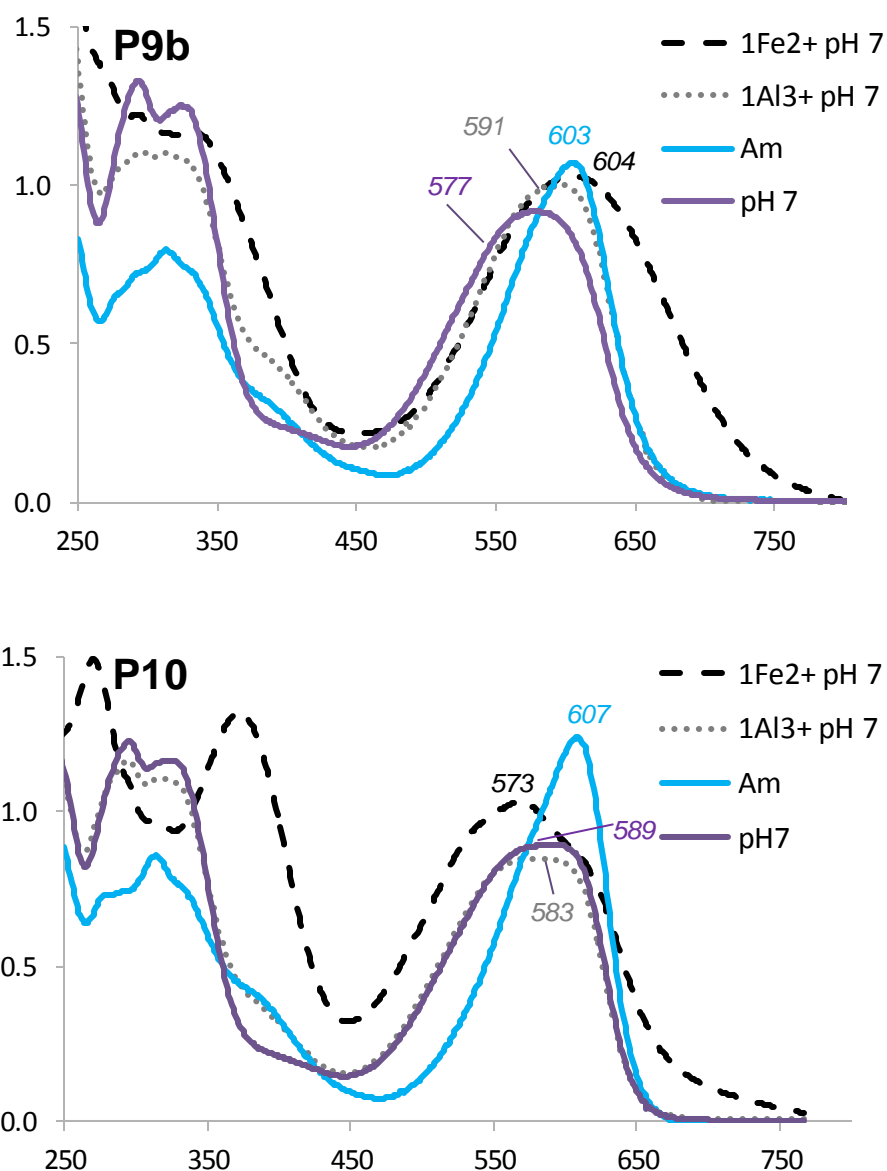


Fig 2. UV-visible spectra of pigment P9b (Cya, Acyl = Cf, HB) and P10 (Pn, Acyl = Cf, Cf), at pH 7, its pure anionic base (Am, calculated) and its Fe²⁺ and Al³⁺ complexes (1 equiv.).

3.2.2. IRON BINDING

In a neutral dilute phosphate buffer, natural catechols typically bind Fe³⁺ much more slowly than Fe²⁺ because of the strong competition between phosphate and phenol for Fe³⁺ [14]. However, fast Fe²⁺ binding is typically followed by fast autoxidation of Fe²⁺ within the complexes, which was confirmed by Fe²⁺ titration (ferrozine test). Independent experiments with RC anthocyanins (unpublished data) confirmed the much faster binding to Fe²⁺ in a 10⁻² M phosphate buffer. Moreover, the final spectra were actually the same, whether Fe²⁺ or Fe³⁺ was added, thus confirming iron autoxidation during binding (Fig. 4-SI). Although free Fe²⁺ is

already quite prone to autoxidation in neutral solution, its conversion to Fe^{3+} is expected to be accelerated by binding to catechols, given the much higher intrinsic affinity of these ligands for Fe^{3+} ($\log K_b = 20$ for Fe^{3+} , vs. 8 for Fe^{2+} , [16]).

Fe^{2+} binding to caffeic acid or P9a results in the formation of a characteristic shoulder (between 350 and 370 nm) from the UV band. By contrast, full deprotonation of caffeic acid (pH *ca.* 10) shifts the absorption band to 344 nm (Fig. 5-SI). With caffeic acid, a new absorption band typical of ligand-to-iron charge transfer is also observed at $\lambda_{\text{max}} \approx 610$ nm (Fig. 5-SI) with a weak molar absorption coefficient ($\epsilon \approx 900 \text{ M}^{-1} \text{ cm}^{-1}$). Fe^{3+} being a much stronger electron acceptor than Fe^{2+} , the development of the charge transfer band is another evidence of Fe^{2+} autoxidation within the complex [14,15]. With P10, the spectral changes in the UV range are much more intense and a true new absorption band at $\lambda_{\text{max}} = 374$ nm emerges (Fig. 2). Its extension into the visible range adds a yellow component to the P10's color. This new band points to cooperation between the two Cf residues in iron binding. Although the peonidin nucleus has no metal binding ability, iron shifts the visible band to shorter wavelengths (Fig. 2, Table 1-SI). This hypsochromic shift could reflect the perturbation of the peonidin – acyl π -stacking interactions (a consequence of the iron-induced perturbation of the electron density on the caffeoyl residues) and is also another evidence of the compact folded conformations adopted by diacylated anthocyanins.

Caffeic acid - Fe^{2+} binding results in a weak shoulder at 370 nm (Fig. 5-SI), which is not further increased by higher Fe^{2+} concentrations. In the presence of iron, the visible spectrum of PA exhibits a weak bathochromic shift of 9 nm (Fig. 5-SI). Both bindings occur with similar kinetics (Table 2). In comparison to PA and caffeic acid, the spectral modifications induced by Fe^{2+} - P9b binding are much more spectacular (a bathochromic shift of 27 nm and a more intense shoulder at 370 nm) and indicate that both binding sites participate (Fig. 2, Scheme 2).

3.2.3. BINDING STOICHIOMETRY

In the presence of increasing Fe^{2+} concentrations, the bathochromic shift of P9b's visible band reaches saturation at 1 equivalent (Fig. 6-SI). This is evidence of a dominant 1:1 binding, which is the stoichiometry typically evidenced with other iron – flavonoid complexes [15–17]. However, 1:2 binding was also reported with quercetin and kaempferol [18]. In agreement with a 1:1 iron – anthocyanin binding, the same final UV-visible spectra were recorded with P9b, whether 1 or 2 equiv. Fe^{2+} were added (data not shown). The same

observation holds for P10 and Fe^{2+} . By contrast, with caffeic acid, saturation was reached at lower iron concentrations, 1/3 to 2/3 equiv. (Fig. 6-SI), suggesting its possible involvement in 1:2 and 1:3 coordination complexes.

3.2.4. QUANTITATIVE KINETIC ANALYSIS

Simple binding models were used to simultaneously analyze the spectral changes in the visible (anthocyanidin) and UV (acyl) domains (Table 2, Fig. 3).

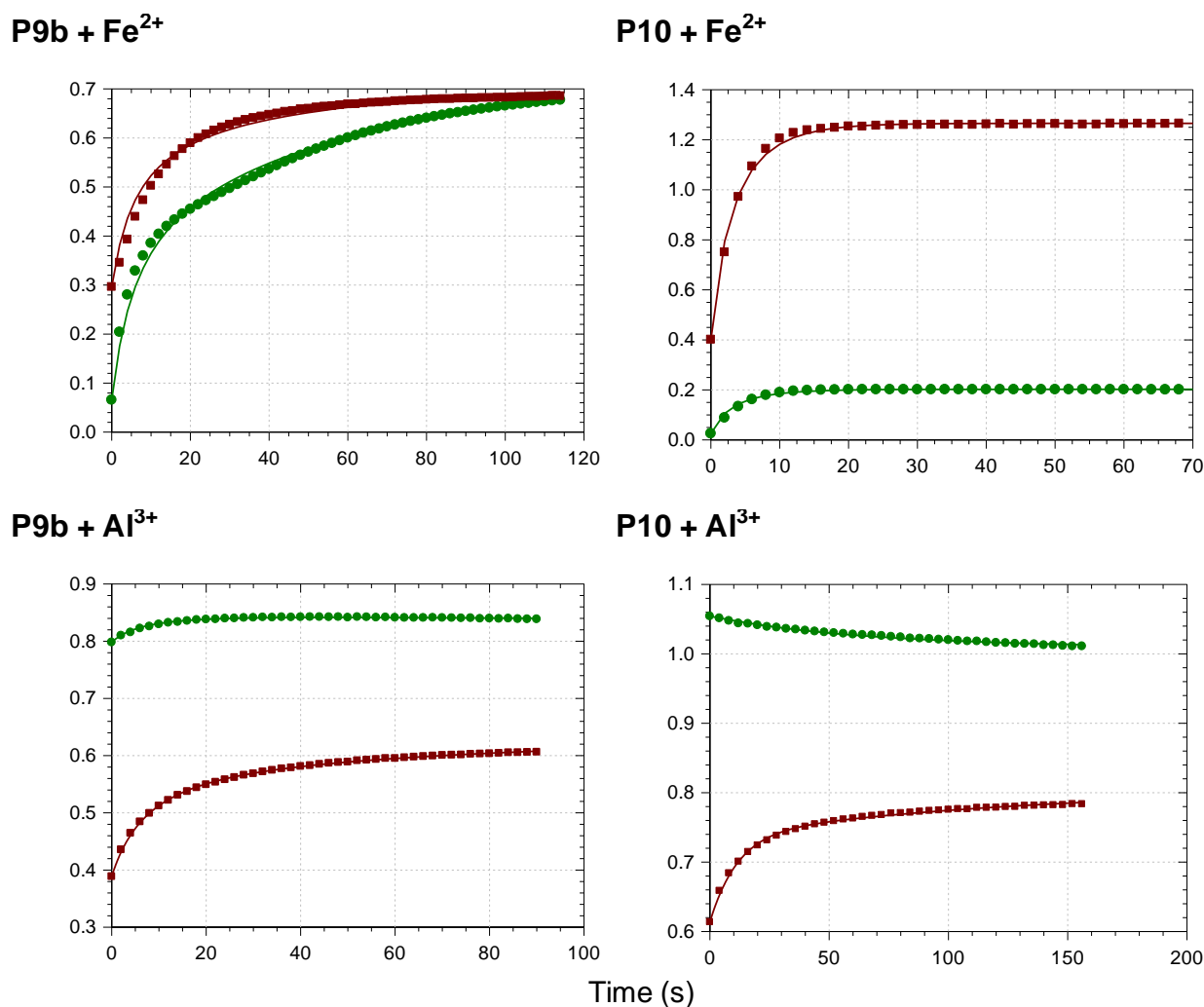


Fig. 4. The kinetics of metal binding to P9b and P10 (pH 7, 2 equiv. metal ion). ■: Monitoring in the UV range (370 nm), ●: Monitoring in the visible range (Fe^{2+} : 670 nm, Al^{3+} : 550 nm).

When metal binding is observed, this is often through a two-step kinetic process (Fig. 3). The 2 kinetic steps can be evidenced at the same monitoring wavelength, either by an increase in absorbance followed by a decay (*e.g.*, caffeic acid + Fe^{2+} , P9a + Fe^{2+} , P9b + Al^{3+}), or a clearly biphasic (fast, then slow) increase in absorbance (*e.g.*, P9b + Fe^{2+} , P10 + Al^{3+}). With ligands having a single binding site (caffeic acid, P9a), the second step (following a

second-order step of metal binding) is assumed to reflect a rearrangement in the coordination sphere (possibly involving the phosphate ions) to a more stable complex. With P9b, the two steps could in principle be ascribed to sequential metal binding to the two binding sites. However, as the UV band (Cf) and the visible bands (Cya) show a bathochromic shift at a similar rate (Fig.3), it is thus proposed that P9b binds a single Fe^{2+} equivalent simultaneously through its two binding units (cyanidin and Cf) and that the second (first-order) step most likely reflects a rearrangement in the coordination sphere. This double coordination should occur at a minimal reorganization cost as the two moieties are already in π -stacking interaction in the free pigment.

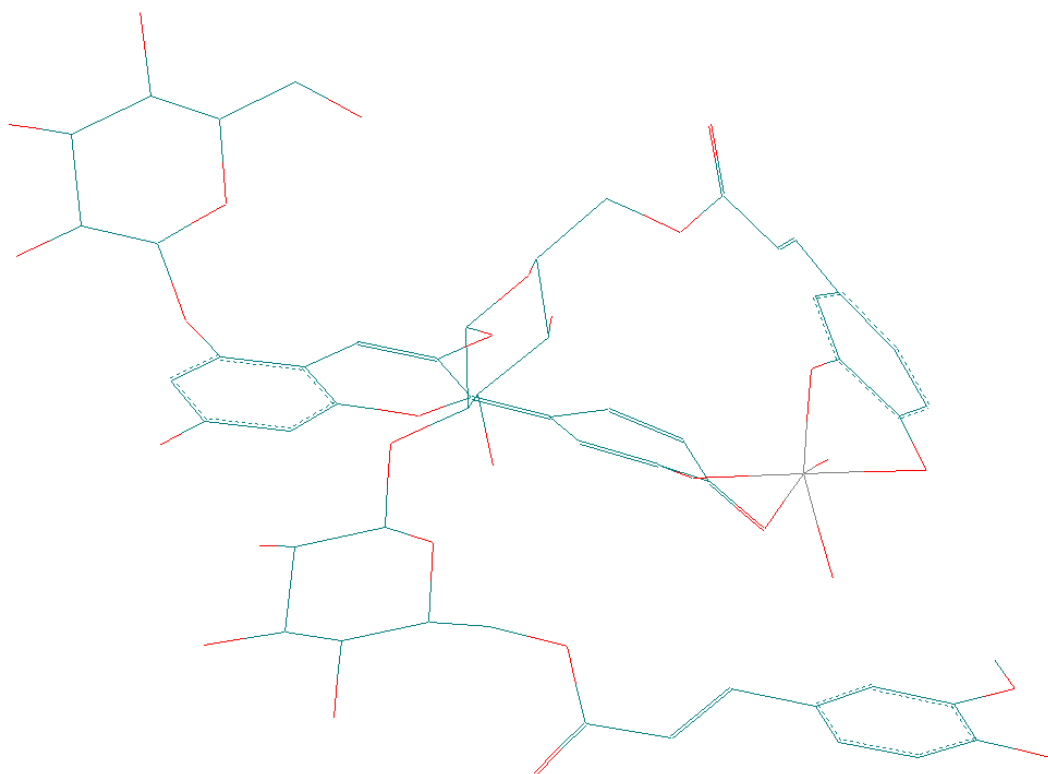
Similarly, as the free caffeic acid and pigments PA and P9a do not bind Al^{3+} under our conditions, Al^{3+} -P9b binding is probably driven by the joined coordination of Al^{3+} by the cyanidin and caffeoyl moieties stacked onto each other by intramolecular copigmentation. In the case of a double caffeoylation (P10), the fast coordination to Al^{3+} (at least as fast as with the cyanidin derivative P9b) emphasizes the specific affinity of the external caffeoyl residue for Al^{3+} . As the same residue is critical to providing protection against water addition to the peonidin nucleus (Table 1), it can be proposed that the strong π -stacking interactions developed by these two moieties are key to the affinity of P10 for Al^{3+} .

The spectral changes observed in iron - cyanidin binding combine the bathochromic shift featuring the complete conversion of the ligand to the anionic base and the underlying ligand-to-metal charge transfer. As the latter effect is absent with aluminum, the overall bathochromic shift is much weaker (for P9b, 8 nm, *vs.* 36 nm with iron) (Table 1-SI). With Al^{3+} , a small fraction of unbound pigment may also remain in solution (reversible binding). The influence of the acyl residues is critical and, for instance, the iron-induced bathochromic shift drops to 9 nm for nonacylated PA. It is thus proposed that the simultaneous binding of Fe^{2+} by cyanidin and the caffeoyl residue of P9b is the driving force in the intense bluing effect observed with this pigment. By comparison, the highest bathochromic shift achieved by adding Fe^{3+} (1 equiv.) to a neutral solution of red cabbage anthocyanins (non-coordinating HCA residues) is *ca.* 20 nm (8 nm with Al^{3+}) [6].

Table 2. Kinetic analysis of metal – ligand binding (pH 7, 0.01 M phosphate buffer, 25°C).

Metal, Pigment	M equiv.	$10^3 k_1$ ($M^{-1} s^{-1}$) ^a	k_2 (s^{-1}) ^a	λ (nm) ^a $10^3 \varepsilon_1$ ($M^{-1} cm^{-1}$)	λ (nm) ^a $10^3 \varepsilon_2$ ($M^{-1} cm^{-1}$)
Fe, P9a	1	10.6 (\pm 0.7)	0.17 (\pm 0.01)	370: 29.9 (\pm 0.7) 670: 5.9 (\pm 0.2)	370: 20.5 (\pm 0.1) 670: 3.7 (\pm 0.1)
Fe, P9b	1	2.4 (\pm 0.1)	-	370: 17.5 (\pm 0.1)	-
		7.2 (\pm 0.2)	16.9 (\pm 0.5) $\times 10^{-3}$	670: 10.8 (\pm 0.1)	670: 18.1 (\pm 0.1)
	^b	3.5 (\pm 0.1)	16.9 $\times 10^{-3}$	370: 16.2 (\pm 0.1) 670: 13.2 (\pm 0.2)	370: 17.5 (\pm 0.1) 670: 18.1 (\pm 0.1)
Fe, P9b	2	10.0 (\pm 0.2)	23.8 (\pm 0.4) $\times 10^{-3}$	370: 17.2 (\pm 0.1) 670: 12.3 (\pm 0.1)	370: 18.6 (\pm 0.1) 670: 17.7 (\pm 0.1)
Fe, P10	1	3.7 (\pm 0.1)	-	370: 29.6 (\pm 0.1) 670: 4.8 (\pm 0.1)	
Fe, P10	2	4.3 (\pm 0.1)	-	370: 31.6 (\pm 0.1) 670: 5.1 (\pm 0.1)	
Fe, Cf	1	13.0 (\pm 0.5)	39 (\pm 1) $\times 10^{-3}$	370: 4.7 (\pm 0.1) 670: 0.92 (\pm 0.01)	370: 1.9 (\pm 0.1) 670: 0.32 (\pm 0.01)
Fe, PA	1	5.10 (\pm 0.6)	199 (\pm 14) $\times 10^{-3}$	670: 26.3 (\pm 0.22)	670: 5.19 (\pm 0.05)
Al, P9a	1	No binding			
Al, P9b	1	1.3 (\pm 0.1)	-	370: 12.6 (\pm 0.1) 610: 21.4 (\pm 0.1)	-
Al, P9b	2	1.9 (\pm 0.1)	19 (\pm 1) $\times 10^{-3}$	370: 13.3 (\pm 0.1) 550: 20.3 (\pm 0.1)	370: 14.9 (\pm 0.1) 550: 20.2 (\pm 0.1)
Al, P10	1	2.2 (\pm 0.1)	-	370: 13.7 (\pm 0.1)	-
Al, Cf	1	No binding			
Al, PA'	1	No binding			

^a k_1 : bimolecular rate constant of metal binding leading to complex 1, k_2 : first-order rate constant for possible evolution of complex 1 to complex 2, ε_1 , ε_2 : molar absorption coefficients of complex 1 and complex 2. ^b Final (refined) curve-fitting at both wavelengths.



Scheme 2. Geometry optimization of the P9b-Al(OH)₂³⁻ complex in vacuum by molecular mechanics (MM+) followed by semi-empirical quantum mechanics calculations (PM3). HyperChem 5.1 software (Hypercube, Waterloo, Canada).

3.3. Thermal stability

3.3.1. RATE OF DEGRADATION

The stability of individual anthocyanins was investigated at pH 7, 50°C (Fig. 4). In the peonidin series, P10 (Peo-Cf,Cf) is more resistant to color loss than PA', a protection afforded by the acyl-peonidin π -stacking interactions (Fig. 4a). In the presence of caffeic acid (2 equiv.), the rate of color loss for PA' is unchanged, thus suggesting that intermolecular copigmentation is ineffective under such conditions. Unexpectedly, total pigment determination (after acidification) shows that P10 is much less resistant to true (irreversible) degradation than its non-acylated counterpart PA' (Fig. 4b). P11 and P12, which also display caffeoyl residues, have similar degradation rates as P10 (Fig. 7-SI). Moreover, the addition of caffeic acid (2 equiv.) also accelerates the degradation of PA' (Fig. 4b). By contrast, the irreversible degradation of the red cabbage anthocyanins (acyl = pC, Fl, Sp) is barely impacted by the acylation pattern [2]. Thus, it seems that the redox active caffeoyl residue [19] favors the oxidative degradation of PSP anthocyanins.

Iron – anthocyanin binding is major way of producing stable blue colors [6,20]. However, even moderate Fe^{2+} concentrations were shown to accelerate the degradation of red cabbage anthocyanins, specifically the non- and monoacylated ones [2]. Nonacylated PA' from PSP (Peo-3-O-Soph-5-O-Glc) and PA, its homolog from RC (Cya-3-O-Soph-5-O-Glc), undergo degradation at similar rates (Fig. 4b). However, PA is much more destabilized by Fe^{2+} addition than PA' ($t_{50} = 2\text{h}$ vs. 17h). This is consistent with a degradation initiated by iron binding followed by a two-electron transfer to O_2 . On the other hand, Fe^{2+} (1.5 equiv.) has no impact on the rate of P10 degradation (Fig. 7-SI). In this case, tight iron – caffeoyl binding cancels the pro-oxidant effect of Fe^{2+} , as observed with the diacylated anthocyanins of red cabbage [2].

In summary, caffeic acid, either free or bound to the glycosyl moieties, accelerates the degradation of PSP anthocyanins at pH 7 but this effect can be suppressed by iron - caffeoyl binding. More generally, the presence of redox-active catechols, such as catechins and caffeic acid esters, may contribute to the overall chemical instability of anthocyanin-rich extracts [21]. Indeed, in spite of its higher fraction in diacylated anthocyanins, the PSP extract is less stable than the RC extract at pH 7, 50°C (Fig. 8-SI).

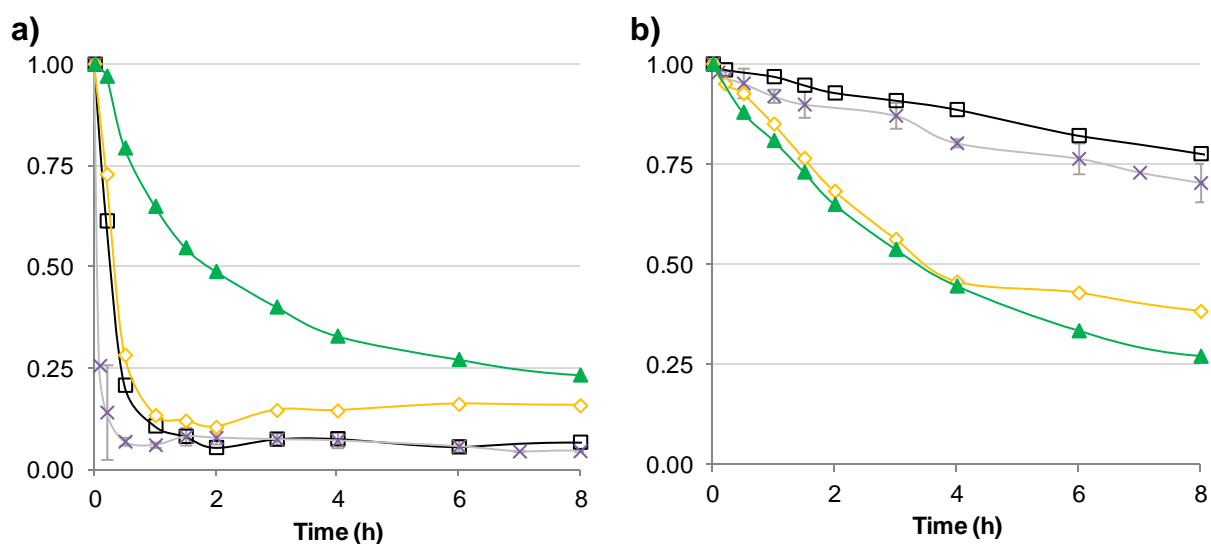


Fig 4. Kinetics of **a)** color loss and **b)** thermal degradation (pH 7, 50°C). PA (Cya, no acyl, grey), PA' (Peo, no acyl, black), P10 (Peo, Cf, Cf, green), PA' + equiv. 2 Cf (orange).

3.3.1. DEGRADATION PRODUCTS

The degradation products of P11 and P12 (diacylated peonidin derivatives having one caffeoyl residue) and of P4 (diacylated cyanidin derivative without caffeoyl residue) supplemented with caffeic acid (1 equiv.) were analyzed by UPLC-DAD-MS. The release of the diacylsophorose moieties was detected (m/z 623 from P11, m/z 679 from P12), as well as feruloylsophorose (2.8 μM in ferulic acid equiv. after 24h) and caffeoylsophorose (1.3 μM in caffeic acid equiv. after 24h) in low concentration. In similar degradation conditions, the *p*-coumaroylsophorose was detected as a major degradation product of red cabbage anthocyanins at pH 7 [1]. Pigments having lost the caffeoyl residue (m/z 905 from P11, m/z 961 from P12) were the sole hydrolysis products detected.

A group of new pigments was detected, corresponding to P11 – 2H and P12 – 2H. Similar two-electron oxidized products were not detected with red cabbage anthocyanins under the same conditions [1]. For instance, with P12, 2 isomers of **2** having a m/z of 1121 were observed at $R_t = 4.0$ and 5.2 min (Fig. 5a). Their λ_{max} of 536 nm corresponds to a shift of *ca.* +4 nm compared to P12 (Fig. 9-SI). Products **2** are probably formed by autoxidation of the caffeoyl residue (initiated by metal traces) with concomitant formation of a *o*-quinone and H_2O_2 [14]. The *o*-quinone could then evolve by intramolecular nucleophilic addition of the peonidin nucleus (under its nucleophilic anionic base or hemiketal form), as already observed in an intermolecular version [22,23]. As the *o*-quinone of a caffeoyl residue has several electrophilic centers and the peonidin nucleus (anionic base and/or hemiketal) has 2 nucleophilic centers (C6 and C8), the formation of several isomers is actually possible.

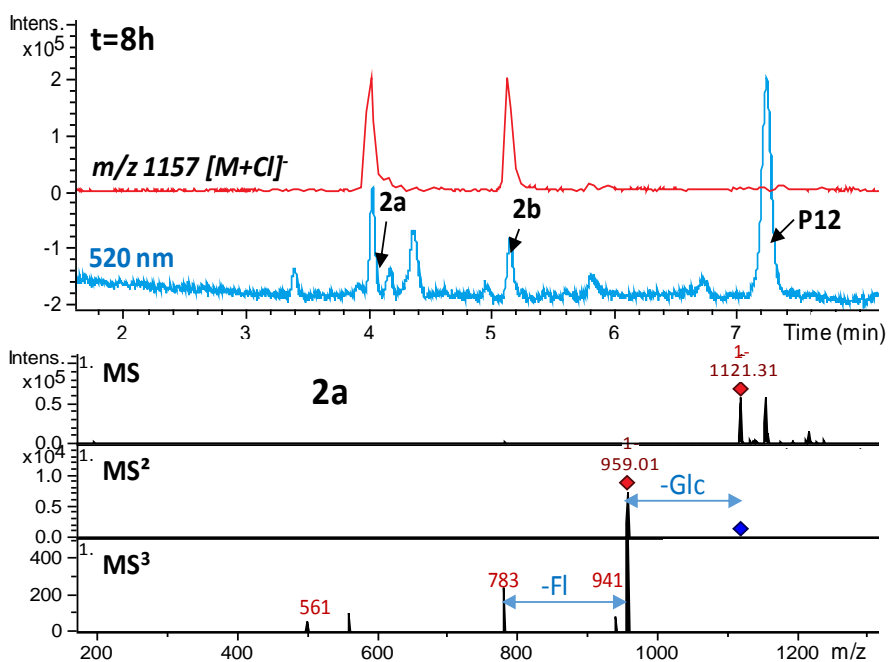
For comparison, a solution of red cabbage anthocyanin P4 (m/z 1123) supplemented with caffeic acid was heated under the same conditions. A new pigment noted **1** was detected with a λ_{max} of 525 nm (*vs.* 537 nm for P4) and a m/z of 1301 consistent with an oxidative coupling to caffeic acid (Figs 5b & 10-SI). This compound has 3 isomers ($R_t = 6.92$, 7.16 and 8.30 min) and yields an ion of m/z 1141, corresponding to the P4 hemiketal. Besides, **1** also losses CO_2 to yield ion m/z 1257. Product **1** is thus proposed to result from the nucleophilic addition of P4 to the caffeic acid *o*-quinone. Similar products have already been observed when nonacylated anthocyanins are treated by the *o*-quinone of caffeic or caffeoyltartric acid (generated by enzymatic oxidation).

Pigment **1** concentration after 24h at pH 7, 50°C was estimated at 5.2 μM (in cyanin equivalent), *i.e.* roughly equal to the residual P4 concentration (4.9 μM , *i.e.* *ca.* 10% of the

initial concentration). Interestingly, while P4 alone is very prone to isomerization (up to 53%) *via* intramolecular migration of its sinapoyl residue (at C2-OH of Glc-2) [1], addition of caffeic acid inhibits this phenomenon (only 19% under the same conditions).

In brief, acylation by caffeic acid or supplementation by free caffeic acid both concur to making anthocyanins more prone to autoxidation at neutral pH. The anthocyanin derivatives thus formed still absorb in the visible range (Figs 9-SI & 10-SI). Their contribution to the global color and its stability would deserve additional investigation.

a)



b)

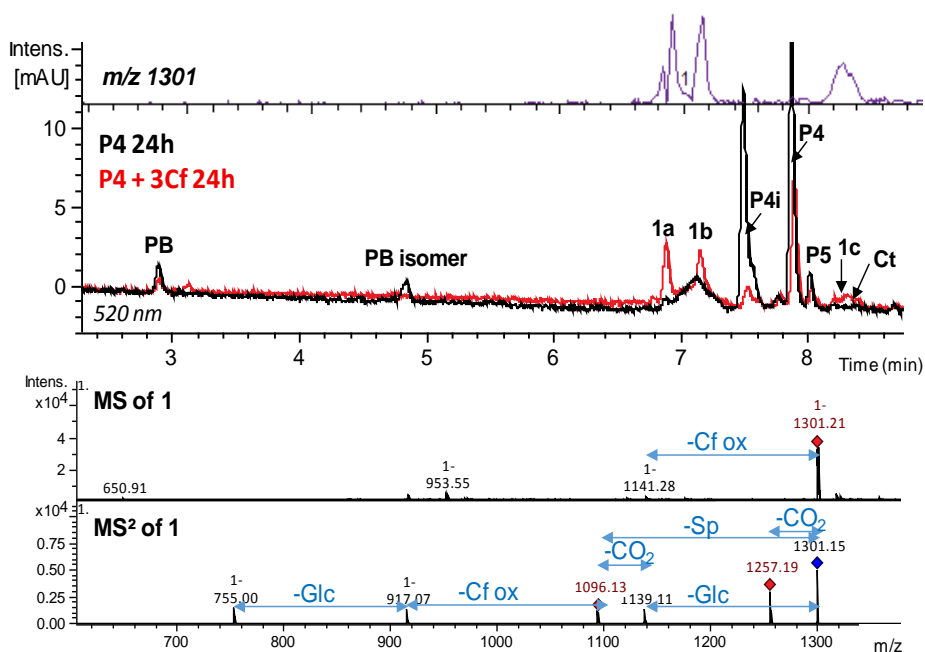


Fig. 5. UPLC-DAD-MS monitoring of thermal degradation at pH 7, 50°C (detection at 520 nm + ion current). **a)** P12 after 8h ($[M-2H]^-$ ion: m/z 1123). Detection of two-electron oxidized isomeric pigments 2a and 2b (m/z 1121). **b)** P4 after 24h ($[M-2H]^-$ ion: m/z 1123). Detection of pigments 1a and 1b (m/z 1301) resulting from oxidative coupling between P4 and caffeic acid (1 equiv.). P5: initial contamination. Ct: P4 trans-chalcone.

Conclusion

Diacylated PSP anthocyanins express more intense purple and blue colors in near neutral solution than non- and monoacylated ones. Their color is also more stable, thanks to efficient π -stacking interactions between the acyl residues and the anthocyanidin nucleus. However, a vulnerable point of the PSP anthocyanins evidenced in this work is the presence of redox-active caffeoyl residues that accelerate their oxidative degradation, thus making purple sweet potato extracts less stable than red cabbage extracts, despite the higher content in diacylated anthocyanins of the former. Thus, under moderate heating at pH 7, caffeoyl residues undergo autoxidation to electrophilic/oxidizing *o*-quinones produced by autoxidation of the caffeoyl residues, a reaction probably initiated by iron traces. Metal - caffeoyl binding only weakly modifies the color expressed through a modulation of the acyl - peonidin π -stacking interactions. Through a tight iron coordination, anthocyanins bearing two caffeoyl residues appear resistant to the pro-oxidant effect of moderate Fe^{2+} concentrations (10 to 100 times the trace concentrations in tap water). Al^{3+} binding could be an alternative to erase the redox activity of the caffeoyl residues. On the other hand, a minor PSP pigment combining a cyanidin nucleus and a caffeoyl residue can strongly bind iron through its two interacting catechol nuclei with concomitant strong bathochromism and blue color development.

In summary, diacylated PSP anthocyanins have a high potential for development as natural blue colors, provided that the reactivity of their caffeoyl residues be kept under control. To this purpose, food-grade nucleophiles and antioxidants (thiols, ascorbate) could be worth testing. In crude extracts, a purification step aimed at eliminating caffeoylquinic acids from the PSP extracts could help limit the oxidative degradation of anthocyanins.

REFERENCES

- [1] Fenger J-A, Robbins RJ, Collins TM, Dangles O. The fate of acylated anthocyanins in mildly heated neutral solution. *Dyes Pigments* 2020; 178:108326. <https://doi.org/10.1016/j.dyepig.2020.108326>.
- [2] Fenger J-A, Moloney M, Robbins RJ, Collins TM, Dangles O. The influence of acylation, metal binding and natural antioxidants on the thermal stability of red cabbage anthocyanins in neutral solution. *Food Funct* 2019; 10:6740–51. <https://doi.org/10.1039/C9FO01884K>.
- [3] Moloney M, Robbins RJ, Collins TM, Kondo T, Yoshida K, Dangles O. Red cabbage anthocyanins: The influence of d-glucose acylation by hydroxycinnamic acids on their structural transformations in acidic to mildly alkaline conditions and on the resulting color. *Dyes Pigments* 2018; 158:342–52. <https://doi.org/10.1016/j.dyepig.2018.05.057>.
- [4] Oliveira H, Basílio N, Pina F, Fernandes I, de Freitas V, Mateus N. Purple-fleshed sweet potato acylated anthocyanins: Equilibrium network and photophysical properties. *Food Chem* 2019; 288:386–94. <https://doi.org/10.1016/j.foodchem.2019.02.132>.
- [5] Trouillas P, Sancho-García JC, De Freitas V, Gierschner J, Otyepka M, Dangles O. Stabilizing and Modulating Color by Copigmentation: Insights from Theory and Experiment. *Chem Rev* 2016; 116:4937–82. <https://doi.org/10.1021/acs.chemrev.5b00507>.
- [6] Sigurdson GT, Robbins RJ, Collins TM, Giusti MM. Evaluating the role of metal ions in the bathochromic and hyperchromic responses of cyanidin derivatives in acidic and alkaline pH. *Food Chem* 2016; 208:26–34. <https://doi.org/10.1016/j.foodchem.2016.03.109>.
- [7] Terahara N, Shimizu T, Kato Y, Nakamura M, Maitani T, Yamaguchi M, et al. Six Diacylated Anthocyanins from the Storage Roots of Purple Sweet Potato, *Ipomoea batatas*. *Biosci Biotechnol Biochem* 1999; 63:1420–4. <https://doi.org/10.1271/bbb.63.1420>.
- [8] Torskangerpoll K, Andersen ØM. Colour stability of anthocyanins in aqueous solutions at various pH values. *Food Chem* 2005; 89:427–40. <https://doi.org/10.1016/j.foodchem.2004.03.002>.
- [9] CIE Standard. Colorimetry — Part 1: CIE standard colorimetric observers | CIE 2004. <http://www.cie.co.at/publications/colorimetry-part-1-cie-standard-colorimetric-observers-0> (accessed October 10, 2019).
- [10] Kim HW, Kim JB, Cho SM, Chung MN, Lee YM, Chu SM, et al. Anthocyanin changes in the Korean purple-fleshed sweet potato, Shinzami, as affected by steaming and baking. *Food Chem* 2012; 130:966–72. <https://doi.org/10.1016/j.foodchem.2011.08.031>.
- [11] Xu J, Su X, Lim S, Griffin J, Carey E, Katz B, et al. Characterisation and stability of anthocyanins in purple-fleshed sweet potato P40. *Food Chem* 2015; 186:90–6. <https://doi.org/10.1016/j.foodchem.2014.08.123>.
- [12] Silva FAM, Borges F, Guimarães C, Lima JLFC, Matos C, Reis S. Phenolic Acids and Derivatives: Studies on the Relationship among Structure, Radical Scavenging Activity, and Physicochemical Parameters. *J Agric Food Chem* 2000; 48:2122–6. <https://doi.org/10.1021/jf9913110>.
- [13] Tomac I, Seruga M. Electrochemical Properties of Chlorogenic Acids and Determination of Their Content in Coffee Using Differential Pulse Voltammetry. *Int J Electrochem Sci* 2016; 11:2854–76. <https://doi.org/10.20964/110402854>.

- [14] Yoshida K, Mori M, Kondo T. Blue flower color development by anthocyanins : from chemical structure to cell physiology. *Nat Prod Rep* 2009;26:884–915. <https://doi.org/10.1039/B800165K>.
- [15] Nkhili E, Loonis M, Mihai S, Hajji HE, Dangles O. Reactivity of food phenols with iron and copper ions: binding, dioxygen activation and oxidation mechanisms. *Food Funct* 2014;5:1186–202. <https://doi.org/10.1039/C4FO00007B>.
- [16] Perron NR, Brumaghim JL. A Review of the Antioxidant Mechanisms of Polyphenol Compounds Related to Iron Binding. *Cell Biochem Biophys* 2009;53:75–100. <https://doi.org/10.1007/s12013-009-9043-x>.
- [17] Moncada MC, Moura S, Melo MJ, Roque A, Lodeiro C, Pina F. Complexation of aluminum(III) by anthocyanins and synthetic flavylum salts: A source for blue and purple color. *Inorganica Chim Acta* 2003;356:51–61. [https://doi.org/10.1016/S0020-1693\(03\)00394-3](https://doi.org/10.1016/S0020-1693(03)00394-3).
- [18] Smyk B, Pliszka B, Drabent R. Interaction between Cyanidin 3-glucoside and Cu(II) ions. *Food Chem* 2008;107:1616–22. <https://doi.org/10.1016/j.foodchem.2007.10.037>.
- [19] Mira L, Fernandez MT, Santos M, Rocha R, Florêncio MH, Jennings KR. Interactions of Flavonoids with Iron and Copper Ions: A Mechanism for their Antioxidant Activity. *Free Radic Res* 2002;36:1199–208. <https://doi.org/10.1080/1071576021000016463>.
- [20] Hapiot P, Neudeck A, Pinson J, Fulcrand H, Neta P, Rolando C. Oxidation of caffeic acid and related hydroxycinnamic acids. *J Electroanal Chem* 1996;405:169–76. [https://doi.org/10.1016/0022-0728\(95\)04412-4](https://doi.org/10.1016/0022-0728(95)04412-4).
- [21] Malien-Aubert C, Dangles O, Amiot MJ. Color Stability of Commercial Anthocyanin-Based Extracts in Relation to the Phenolic Composition. Protective Effects by Intra- and Intermolecular Copigmentation. *J Agric Food Chem* 2001;49:170–6. <https://doi.org/10.1021/jf000791o>.
- [22] Kader F, Irmouli M, Nicolas JP, Metche M. Proposed mechanism for the degradation of pelargonidin 3-glucoside by caffeic acid o-quinone. *Food Chem* 2001;75:139–44. [https://doi.org/10.1016/S0308-8146\(00\)00301-0](https://doi.org/10.1016/S0308-8146(00)00301-0).
- [23] Sami-Manchado P, Cheynier V, Moutounet M. Reactions of polyphenoloxidase generated caftaric acid o-quinone with malvidin 3-O-glucoside. *Phytochemistry* 1997;45:1365–9. [https://doi.org/10.1016/S0031-9422\(97\)00190-8](https://doi.org/10.1016/S0031-9422(97)00190-8).

Chapter 5

The influence of phenolic acyl groups on the color of purple sweet potato anthocyanins and their metal complexes

SUPPLEMENTARY INFORMATION

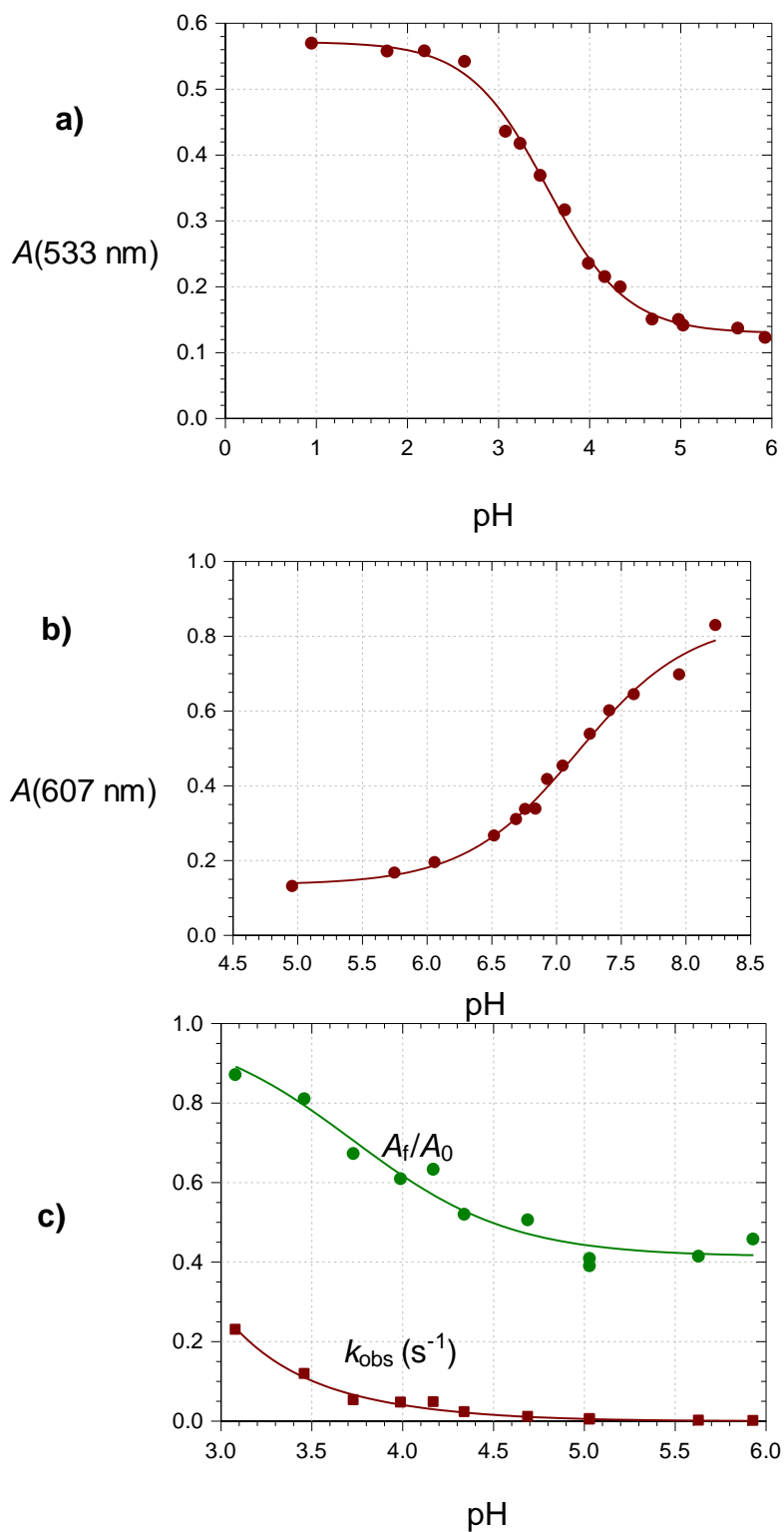


Fig. 1-SI. Spectroscopic titrations of P10 in the acidic pH range at equilibrium (a) and in near neutral solutions (b): $pK'_a = 3.53 (\pm 0.03)$, $pK_{a2} = 7.16 (\pm 0.05)$. pH dependence of the apparent rate constant of water addition and final-to-initial absorbance ratio (c): $pK_{a1} = 4.11 (\pm 0.06)$. The solid lines are the results of the curve-fitting procedures (Moloney et al., 2018).

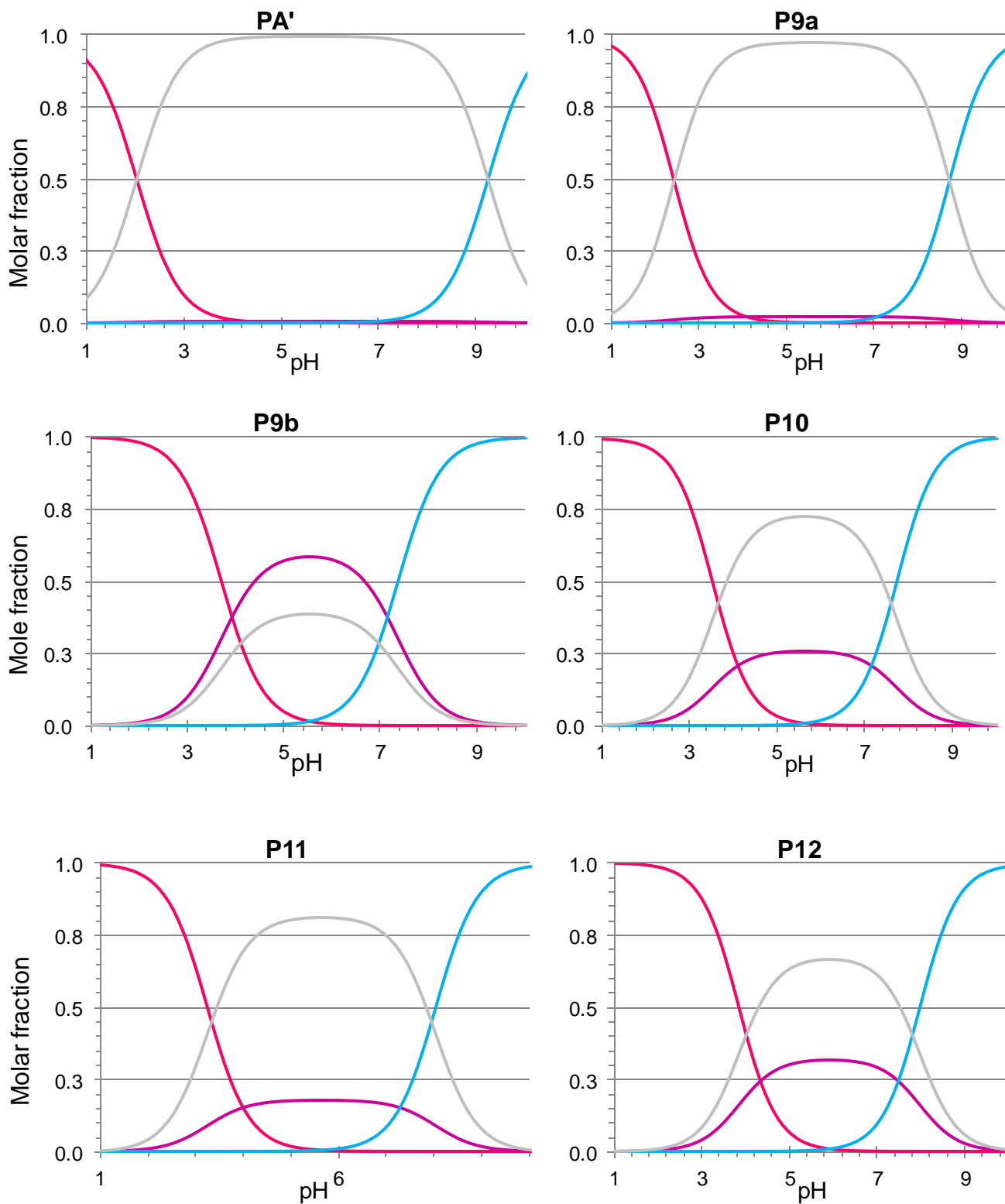
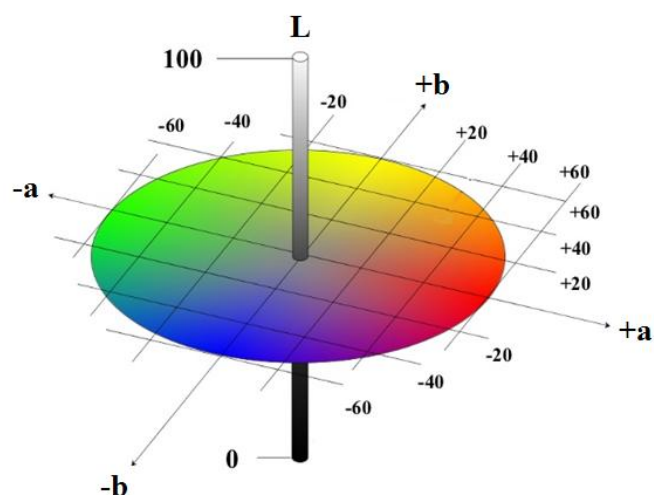


Fig. 2-SI. Speciation diagrams of PSP anthocyanins at equilibrium (calculated from the values of pK_{a1} , pK_{a2} and pK'_a). —: flavylium ion, —: neutral base, —: anionic base, —: total colorless forms.



Pigment	Species	L	a	b	Cab	Hab
PA'	Flavylium	81.52	47.81	10.33	48.9	12.2
	Neutral base	84.85	19.73	-15.76	25.3	321.4
	Anionic base	68.92	-8.23	-41.20	42.0	258.7
P9a	Flavylium	81.22	46.01	-4.11	46.2	354.9
	Neutral base	66.68	38.64	-29.50	48.6	322.6
	Anionic base	62.00	-18.43	-44.46	48.1	247.5
P9b	Flavylium	72.48	63.41	-13.31	64.8	348.1
	Neutral base	66.72	39.59	-29.23	49.2	323.6
	Anionic base	62.10	-19.15	-44.41	48.4	246.7
P10	Flavylium	73.09	62.28	-12.86	63.6	348.3
	Neutral base	65.85	41.66	-31.82	52.4	322.6
	Anionic base	66.17	-17.02	-41.62	45.0	247.8
P11	Flavylium	75.05	61.41	-12.94	62.8	348.1
	Neutral base	71.13	41.88	-28.59	50.7	325.7
	Anionic base	71.33	-13.84	-37.31	39.8	249.7
P12	Flavylium	75.59	60.23	-13.00	61.6	347.8
	Neutral base	66.25	38.91	-33.74	51.5	319.1
	Anionic base	62.93	-15.83	-47.08	49.7	251.4

Fig. 3-SI. L*a*b* coordinates for the pure colored forms of the 6 PSP anthocyanins used to elaborate the color patches in Fig. 1.

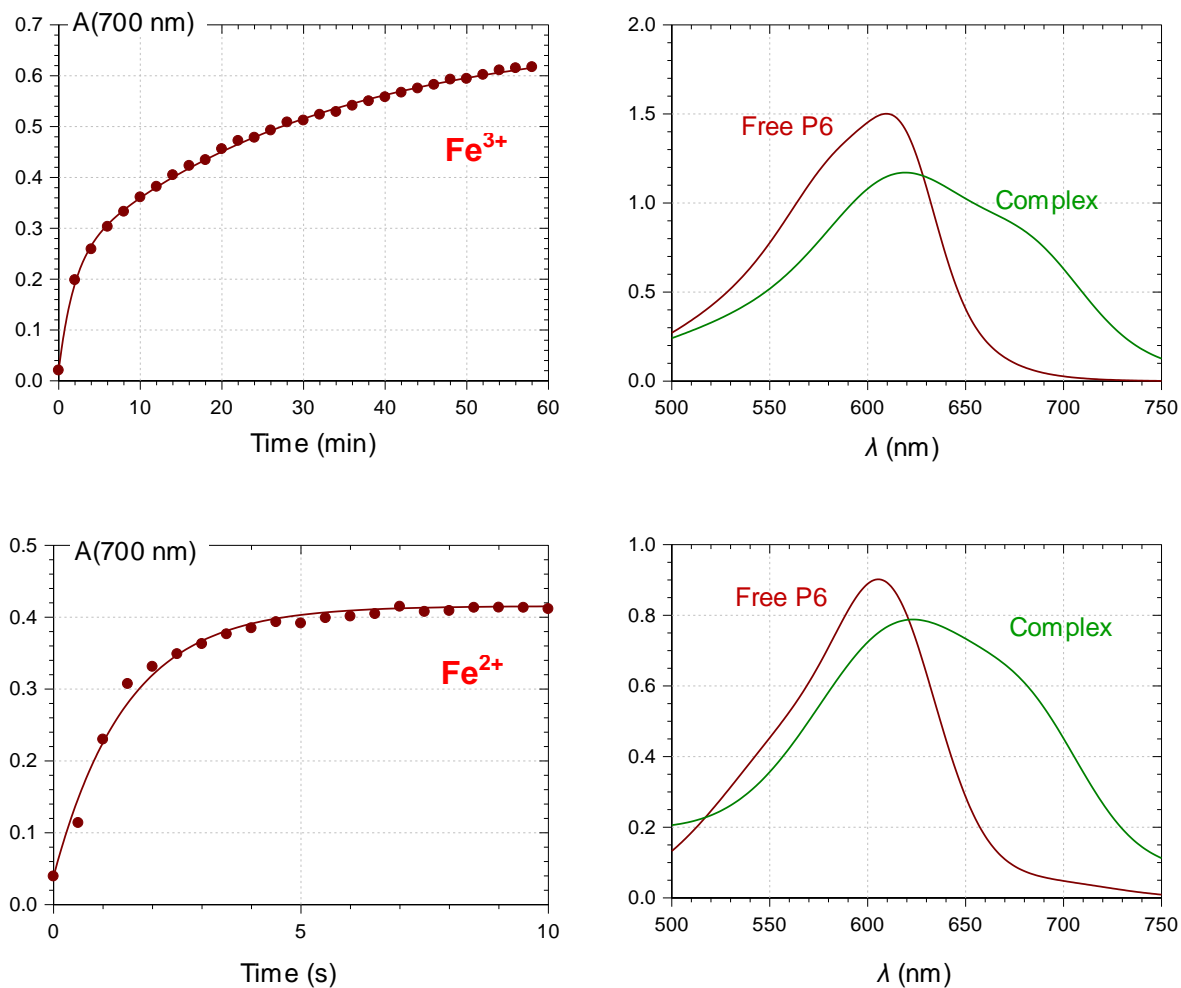


Fig. 4-SI. Iron - P6 binding at pH 8 (2 equiv. iron). *Top, left:* slow binding after addition of Fe³⁺. *Bottom, left:* fast binding after addition of Fe²⁺. *Right:* initial and final visible spectra (M. Moloney, Avignon University, unpublished results).

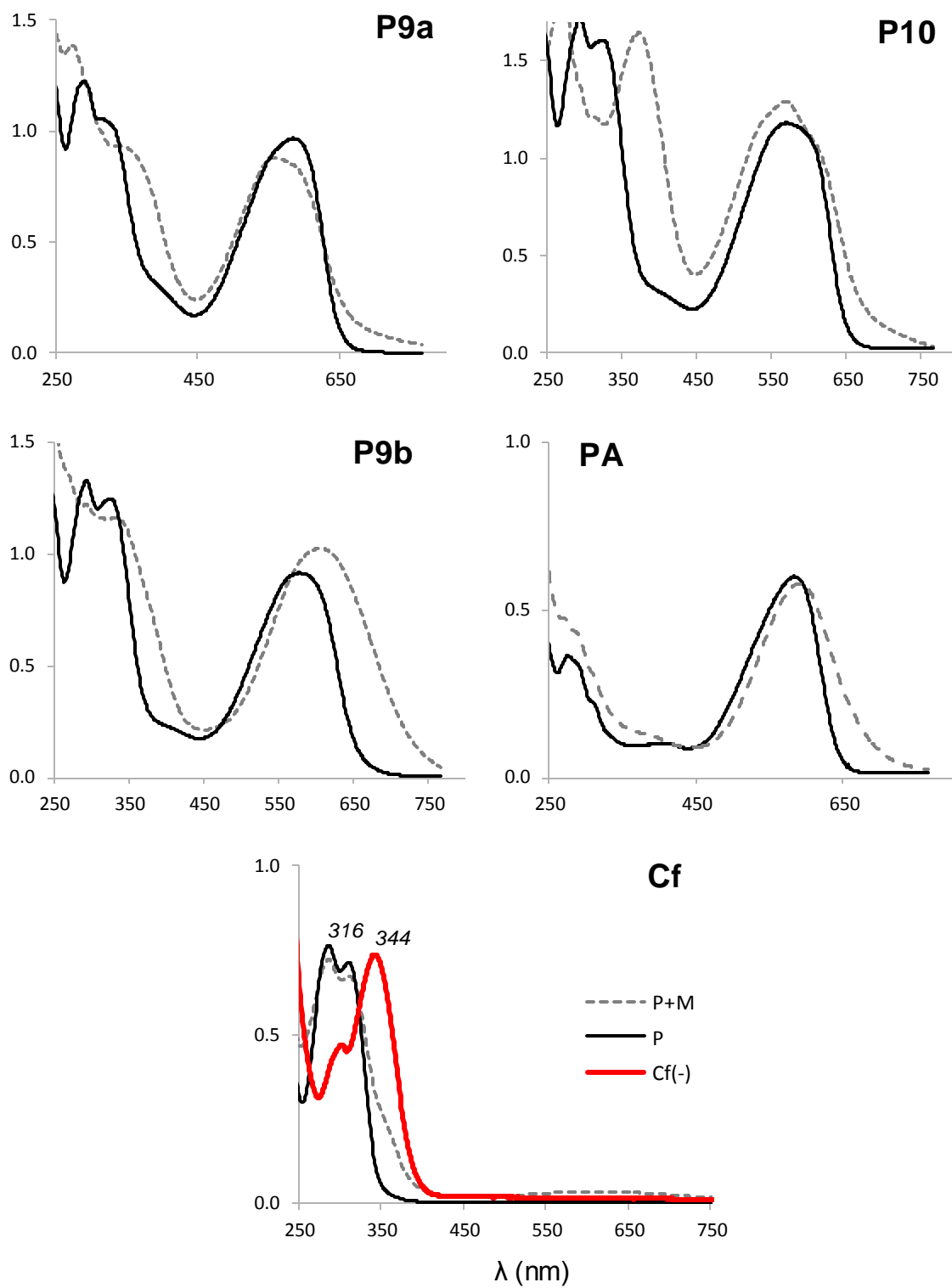


Fig. 5-SI. UV-visible spectra of caffeic acid, P9a, P9b, P10 (plain black lines) and their Fe^{2+} complexes (dashed gray lines) at pH 7. Red spectrum: caffeic acid trianion (pH ca. 10).

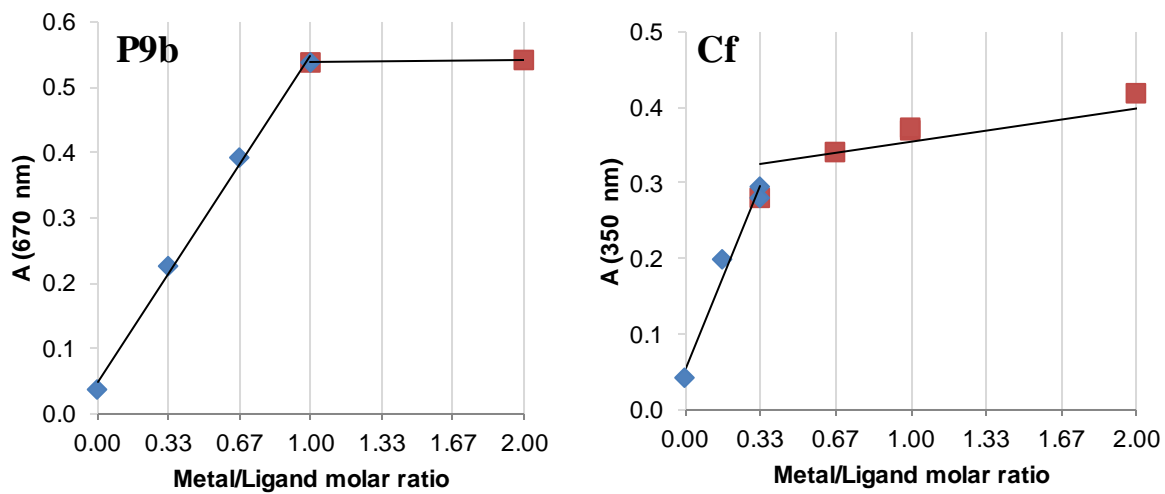


Fig. 6-SI. Plots of the final absorbance of iron complexes as a function of the iron/phenol molar ratio. *Left:* evidence for 1:1 binding with P9b. *Right:* evidence for 1:3 binding with caffeic acid.

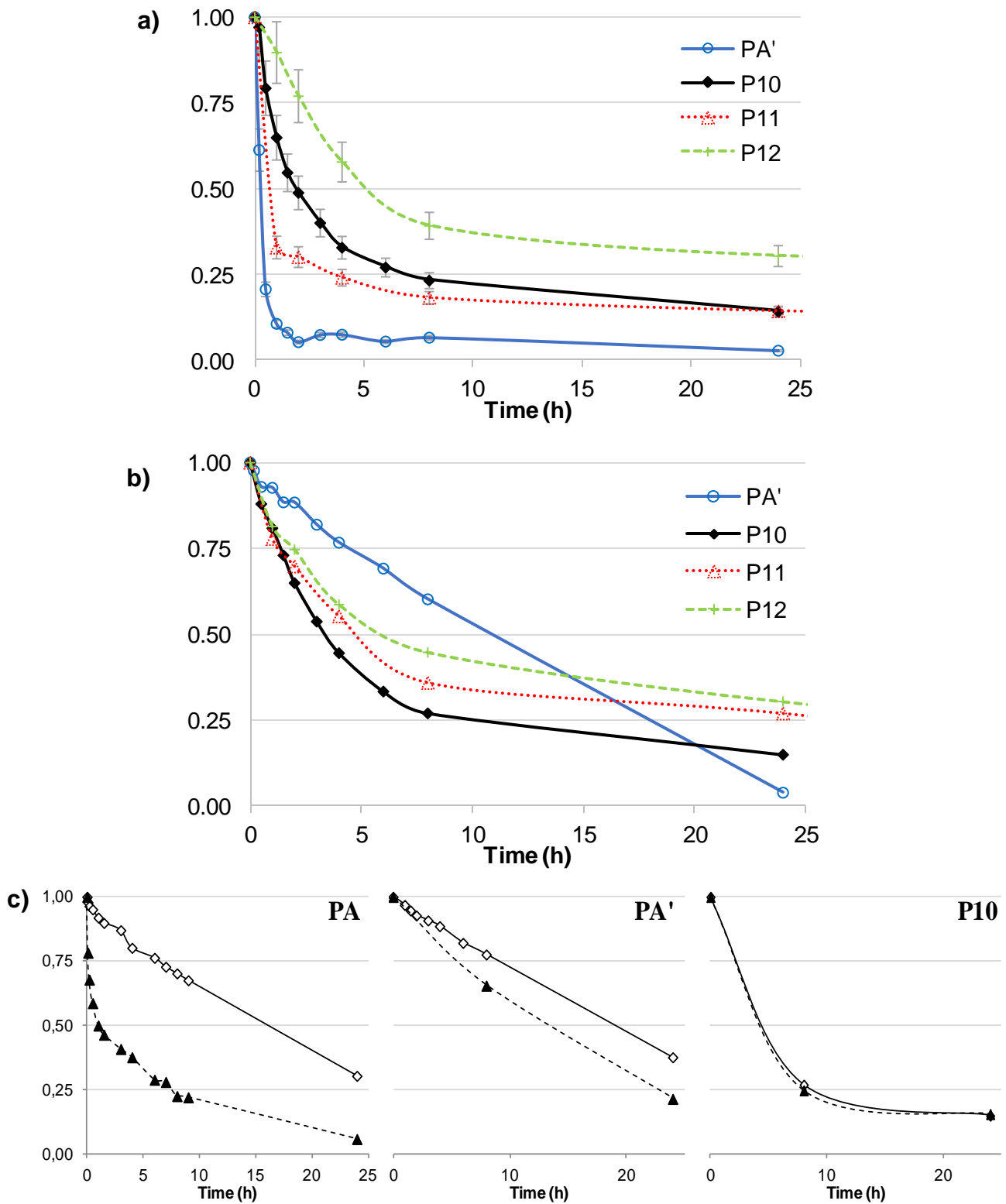


Fig. 7-SI. Thermal stability of four peonidin derivatives at pH 7, 50°C: PA' (no acyl), P10 (Cf, Cf), P11 (Cf, HB), P12 (Cf, Fl). **a)** Color loss. **b)** Pigment degradation. **c)** Pigment degradation of PA (Cya, no acyl), PA' and P10 in the presence (*dotted lines*) or absence (*solid lines*) of added Fe²⁺ (pH 7, 50°C). PA: 0.6 equiv. Fe²⁺; PA' and P10: 1.5 equiv. Fe²⁺.

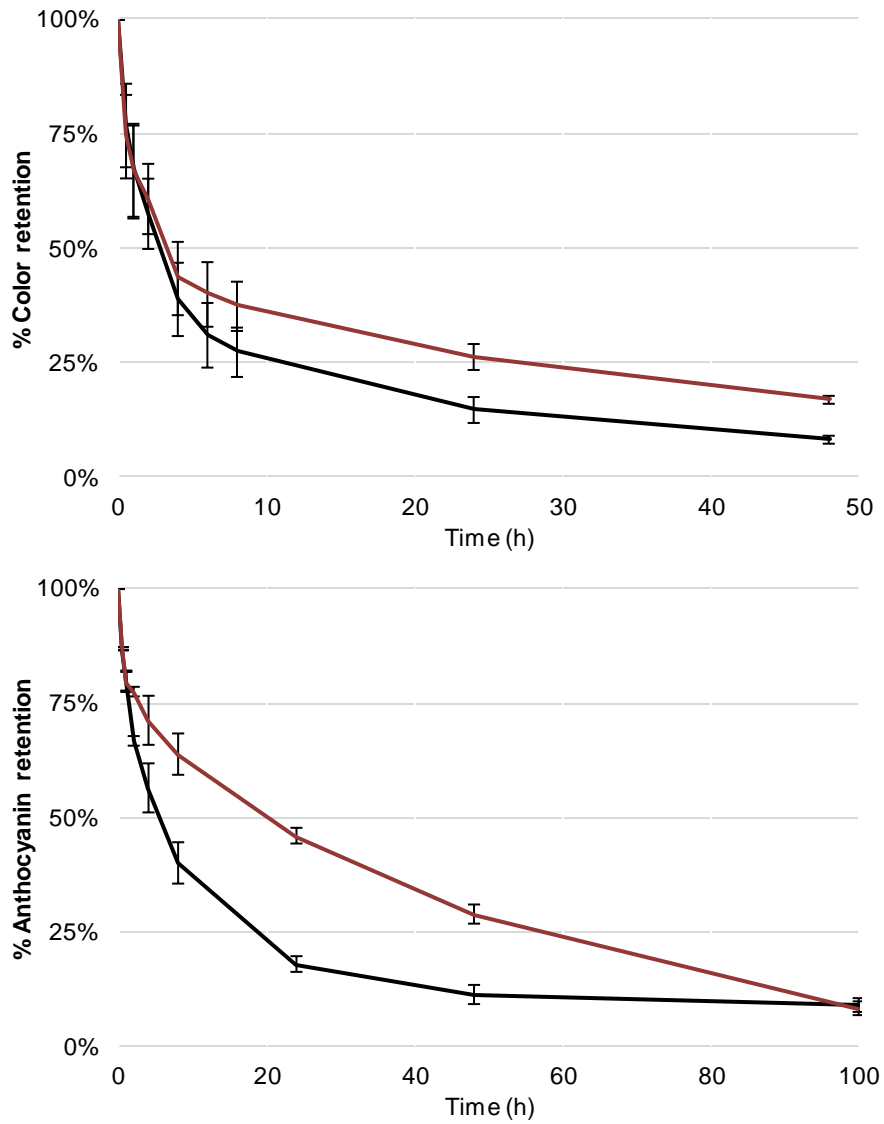


Fig. 8-SI. Color (top) and thermal (bottom) stability of red cabbage (red) and purple sweet potato (black) extracts (pH 7, 50°C).

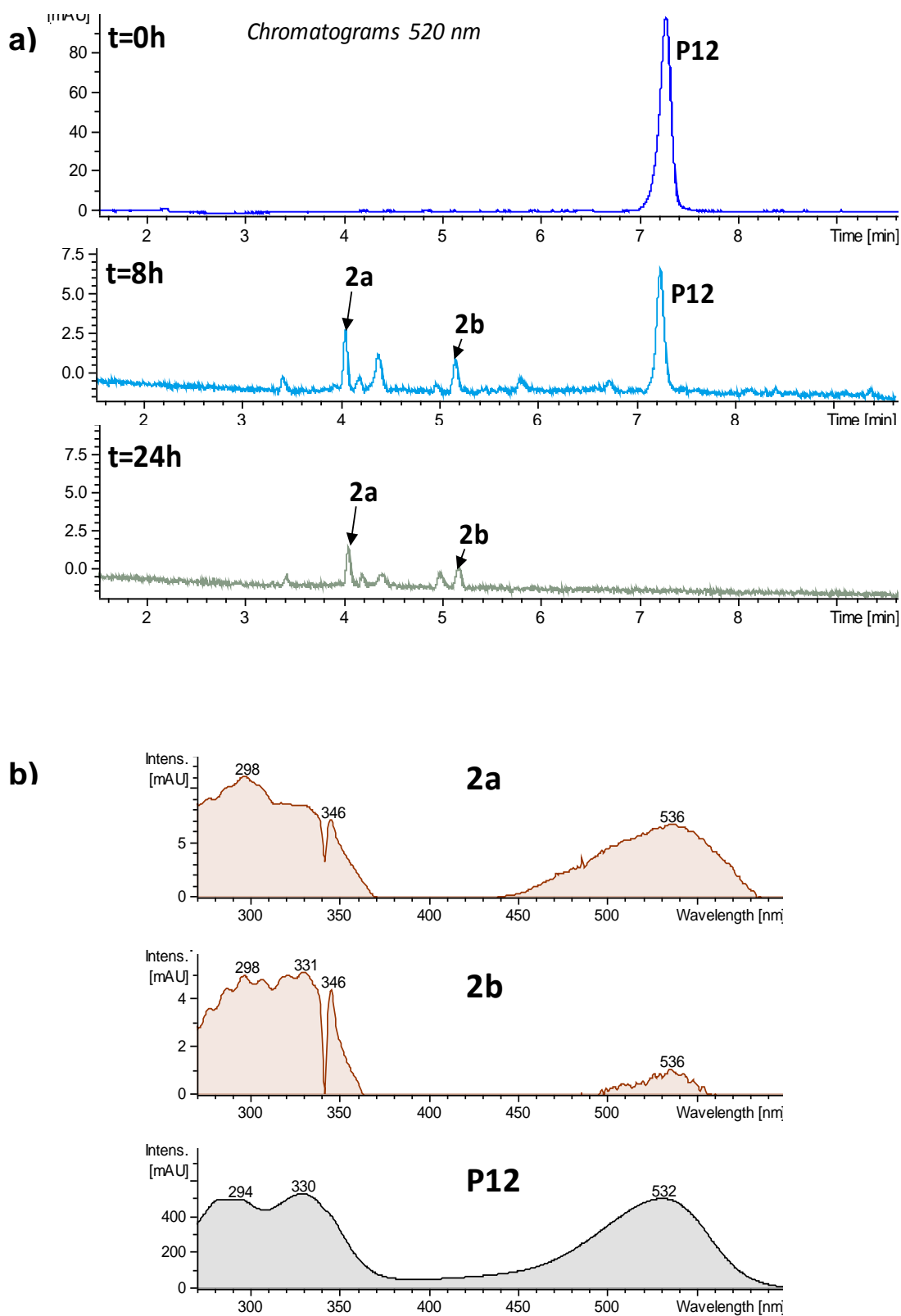


Fig. 9-SI. Thermal degradation of P12 (pH 7, 50°C). UPLC-DAD analysis showing the formation of new isomeric pigments (**2**) resulting from intramolecular P12 – caffeoyl oxidative coupling. **a)** Chromatograms with detection at 520 nm at $t = 0, 8$ and 24h. **b)** UV-visible spectra of P12 and pigments **2a** and **2b** (from DAD).

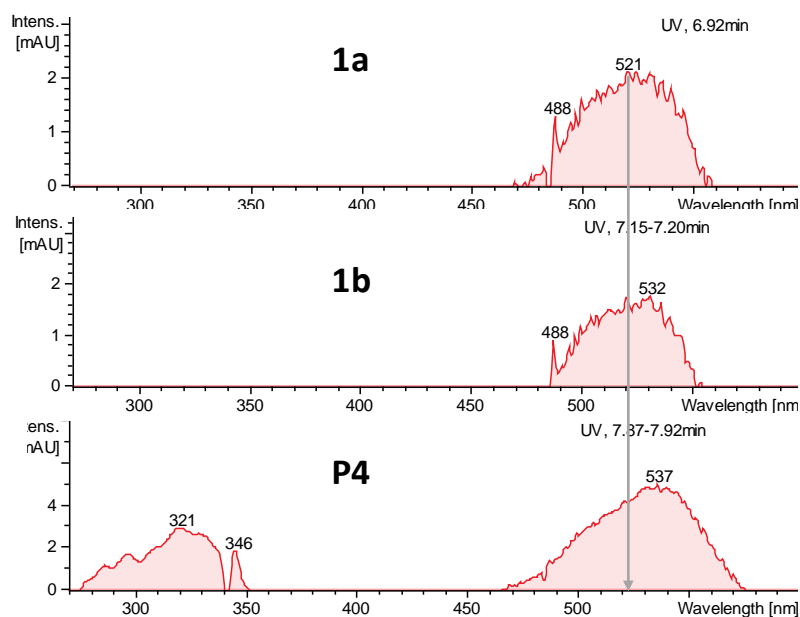
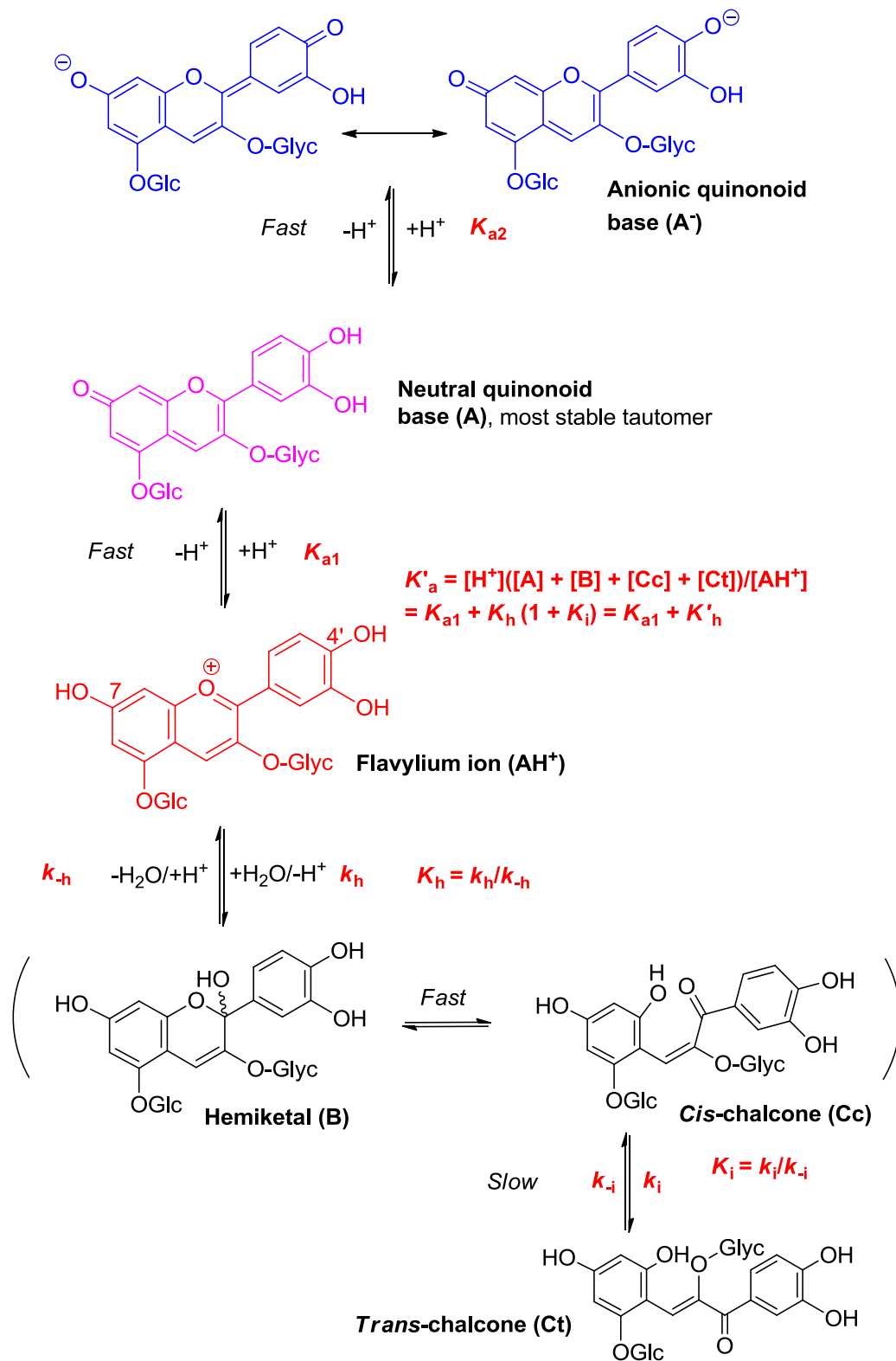


Fig. 10-SI. UV-visible spectra of P4 and its products of oxidative coupling with caffeic acid **1a** and **1b** (m/z 1301). From UPLC-DAD-MS analysis.

Table 1-SI. Spectroscopic data of selected ligands and their Fe^{2+} and Al^{3+} complexes deduced from the binding kinetics (initial vs. final spectra). Hyperchromic shift $\text{HS} = (A_{\text{max},f} - A_{\text{max},0})/A_{\text{max},0}$. Bathochromic shift $\text{BS} = \lambda_{\text{max},f} - \lambda_{\text{max},0}$. Metal/anthocyanin molar ratio = 1.

	Fe^{2+}				Al^{3+}			
	PA	P9a	P9b	P10	PA	P9a	P9b	P10
Aglycone	Cya	Peo	Cya	Peo	Cya	Peo	Cya	Peo
Acylation	-	Cf	Cf, Fl	Cf, Cf	-	Cf	Cf, Fl	Cf, Cf
$\lambda_{\text{max},0}$ (nm)	583	585	584	592	585		584	589
$\lambda_{\text{max},f}$ (nm)	592	558	620	571	596	No	592	573
HS (%)	-4	-9	17	13	-7	binding	10	-5
BS (nm)	9	-27	36	-21	11		8	-16



Scheme 1-SI. Structural transformations of anthocyanins in acidic to neutral aqueous solution.

Chapter 6. General discussion

The global research objective was to gain knowledge on the stability and reactivity of acylated anthocyanin in neutral aqueous solutions, in the absence and presence of metal ions. The material available, red cabbage anthocyanin extract (RCE) and purple sweet potato anthocyanin extract (PSPE), and 14 isolated compounds thereof, offered a broad range of acylated anthocyanins, including two aglycones (cyanidin and peonidin nuclei) and five types of acyl residues (pC, Fl, Sp, Cf, HB). The prior determination of the structures of each individual RCE pigment by NMR techniques (Moloney et al., 2018) and available literature data for PSPE (Terahara et al., 2009, Oliveira et al., 2019 and other unpublished data) enabled to investigate the link between structure and physico-chemical behavior.

The contribution of phenolic acyl groups to the pigment conformation and color stability through intramolecular copigmentation is well established (Moloney et al., 2018; Trouillas et al., 2016). The color expression of these pigments around neutral pH was also recently documented (Sigurdson et al., 2017; Sigurdson et al., 2019). In this context, the current work contributed to unveil the role of acyl residues in supramolecular associations, in particular within anthocyanin-metal complexes. Near-neutral pH is required to produce blue colors even in the presence of metal ions, but the phenols are particularly unstable in these conditions. The rich reactivity of these pigments at neutral pH was documented, as well as the impact of the acyl groups on the products distribution.

1. COLOR EXPRESSION

The target color for blue expression in this work was the synthetic pigment Brilliant Blue FCF, which exhibits a vibrant blue color ($\lambda_{\max} = 630 \text{ nm}$), with high a chromaticity. Based on spectral analysis, the UV-visible spectral features targeted were thus a narrow absorption band centered on 610 - 630 nm, with minimal absorption in the range 350 - 400 nm (yellow contribution, which could stem from metal-caffeic acid binding, contamination by flavones or flavonols, or the contribution of anionic chalcones or HCAs at pH 8). It resulted from screening various extracts and individual pigments that the best candidates for blue expression at pH 8 are the PSPE peonidins (e.g. P12), while the best candidates for blue

metal complexes at pH 7 are the anthocyanins bearing an acyl group on the external glucose of the sophorose (e.g. P4- Al^{3+}).

From the thermodynamic acidity and hydration constants, the speciation diagrams of each individual pigment were established (Fig. 9-A). In addition, based on the composition at each pH and spectra recorded at 3 different pH, the spectra for the 3 individual species were calculated (Method 2 in appendix, Fig. 8-A, 10-A). The full UV-visible spectra provide precious cues on the involvement of acyl moieties and the B-ring of the chromophore to the complex structure.

Based on these results and the literature, the best candidates for color expression among the known anthocyanins would be: i) those producing a blue anionic base: the 3-sophorosyl-5-glucosides (from RCE and PSPE); ii) those having a high fraction of colored species at equilibrium are the diacylated anthocyanins (DAAs) and PB (forming together “Group 2” or G2 anthocyanins); and iii) those exhibiting a high molar absorption coefficient (Moloney et al., 2018), i.e. the anionic bases of malvidin and peonidin (rather than cyanidin) (Cabrita et al., 2000). Including the criterion of color stability, a lower pH is preferred (Du et al., 2012), requiring metal binding to produce similar blue hues, therefore cyanidin would appear as the only candidates. In addition, the presence of caffeic acid residues are a source of instability through redox reactions, which is not the case of *p*-coumaric acid moieties. At pH 6, the affinity of cyanidin derivatives for Al^{3+} is insufficient to produce blue colors (Sigurdson et al., 2016; Chapter 5).

From the spectral data in the visible region, the chromatic coordinates $L^*a^*b^*$ and the corresponding digital color patches were calculated (Fig. 1). They reliably represent the color of anthocyanin solutions at 50 μM (Chapter 4, Fig 9-SI and 10-SI), with a higher reproducibility thanks to a standardized luminosity (that of the spectrophotometer vs. daylight). It results that the addition of 1 equiv. Fe^{2+} and Al^{3+} significantly closes the gap to the target Brilliant Blue at 50 ppm (calculated as ΔE).

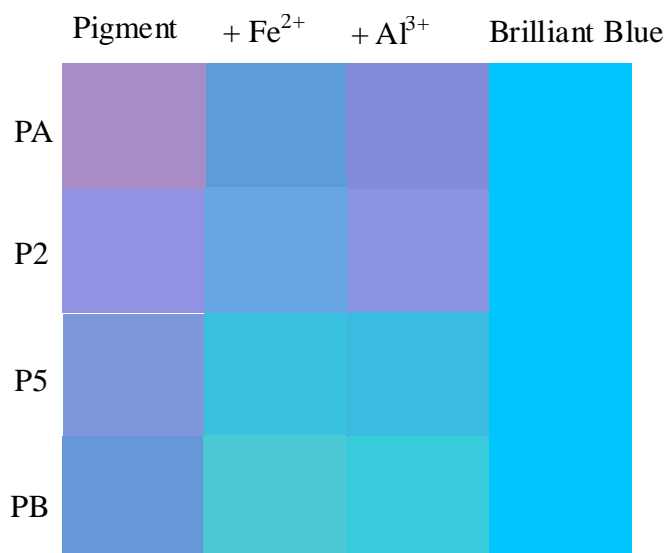
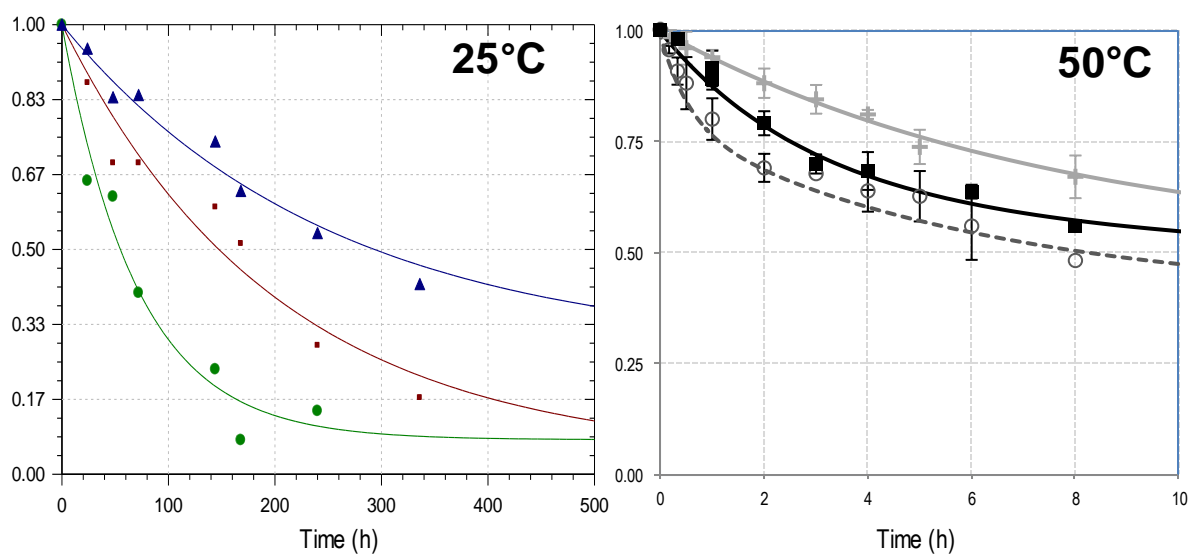


Fig 1. Color patches calculated from the L*a*b coordinates of 4 pigments and their metal complexes (1 molar equiv., 50 μ M).

2. COLOR STABILITY

For the study of anthocyanins degradation under realistic experimental conditions, their degradation was accelerated by increasing the temperature to 50°C. This accelerated the apparent rate of color loss (k_{obs}) by a factor *ca.* 10 (x7 for P1, x19 for P4). A higher temperature does not only increase the reaction rates but also weakens the copigmentation and self-association, which normally slow down the color loss. By contrast, the rate of pigment loss was accelerated by a factor 26 to 55 (Fig. 2), confirming that irreversible degradation is a significant contributor to the color loss.



k_{obs} (h^{-1})	PA	P1	P4
50°C	0.13	0.60	0.22
25°C	0.005	0.014	0.004
<i>Acceleration factor</i>	26	42	55

Fig. 2. a) Kinetics of residual color at 25°C and 50°C. b) Calculated apparent rates of pigment loss at 25°C and 50°C. NB: at 50°C, values are estimated for a first order kinetic model for the comparison of the order of magnitudes.

REVERSIBLE COMPONENT OF COLOR LOSS: HYDRATION

In mildly acidic solution, the rate of color loss at room temperature highly depends on the intensity of intra-/intermolecular copigmentation and self-association (Trouillas et al., 2016). In the pigments studied, the acylation pattern (type, number and position) strongly impacted the rate of hydration. With no surprise, the 4 hydroxycinnamic acids contributed similarly to the rate of hydration, except a lower contribution of *p*-hydroxybenzoic acid (Chapter 4), owing to its reduced electronic delocalization. However, the most impactful factor was the presence of an acyl moiety on the external glucose of the sophorose (G2 pigments). With DAAs, the hypothesis for strong color stabilization remains the sandwich-type conformation, with one acyl moiety on each side of the chromophore (Trouillas et al., 2016). However, this mechanism is not compatible with the presence of a single HCA. In the case of PB, its remarkable resistance to hydration in comparison to P3 and to the other DAAs must involve a combination of self-association and intramolecular copigmentation, even in the absence of metal ions. The rates of other nucleophilic additions, e.g. by bisulfite ions and hydrogen peroxide followed similar trends to the hydration rates (Chapter 2, Fig. 6).

The thermodynamic constants of acidity and hydration determined for 6 PSP anthocyanins (Chapter 5), the 8 major RC anthocyanins (Moloney et al., 2018), and the two extracts (Table 2-A in Appendix) were combined in a Table 2-A). In order to predict these constants (dependent variables) from the structures converted as quantitative variables (independent variables), a multiple linear regression was executed with the PSPP software (GNU project). The regression coefficients suggest a moderate impact of the acyl type on 3 color stability parameters tested ($\text{p}K'_a$, $\text{p}K'_h$, k_h , Table 1). More importantly, the 3 parameters appear better correlated to the position of the acylated sugar (Glc-1 or Glc-2) than to the acylation site (C2-OH or C6-OH) (Table 2). The difference is modest, but as compared to other structural parameters, it confirms the role of the sophorose as spacer in the

copigmentation process. And in particular, an acyl on Glc-2 contributes to the pK'_a with a coefficient of 1.16 vs. 0.28 (minor contribution) when the acyl is on the Glc-1.

Table 1. a) Coefficients of linear regressions correlating the physicochemical parameters of 16 anthocyanins with the type of phenolic acyl moieties. b) Coefficients of linear regressions correlating the pK'_a of 16 anthocyanins with the position of the phenolic acyl moieties.

	pK'_a	pK'_h	k_h
	Acyl type		
Cf	$0.79 \pm 0.16^{**}$	$0.86 \pm 0.23^*$	$-0.12 \pm 0.03^{**}$
pC	0.69 ± 0.26	0.66 ± 0.11 NS	$-0.15 \pm 0.04^{**}$
Fl	$0.84 \pm 0.20^{**}$	$1.0 \pm 0.28^{**}$	$-0.14 \pm 0.03^{**}$
Sp	$0.88 \pm 0.16^{**}$	$1.0 \pm 0.23^{**}$	$-0.16 \pm 0.03^{**}$

* p -value < 0.05; ** p -value < 0.01; NS = non-significant

pK'_a			Coeff.	SD	t	p -value
Acylation site		Primary	0.67	0.11	6.3	<0.001
	R^2	Secondary	1.11	0.18	6.3	<0.001
STD estimate	0.30	Constant	2.24	0.14	16.0	<0.001
Sugar position		Internal	0.35	0.14	2.6	0.022
	R^2	External	1.2	0.11	10.5	<0.001
STD estimate	0.20	Constant	2.2	0.12	17.8	<0.001

*STD = standard deviation, Estimate value: predicted pK'_a value by the model.

Besides, formation rate and degradation rate of the *trans*-chalcone of acylated anthocyanins is scarce in the literature (J. Mendoza et al., 2018). Actually, this information is required for the optimal recovery and quantification of the residual pigment (Chapter 2). The Ct → flavylum rate measured depends on the number of acyl residues. Together with previous data on the heavenly blue anthocyanin (Mendoza et al., 2018), we propose that the bulkiness of the glycoside at C3-OH determines the rate of the limiting step of E→Z isomerization of the chalcones. In addition, the kinetics of Ct accumulation at 50°C (which is simultaneous to its degradation) was measured for different anthocyanins (Fig. 5-A). The Ct accumulated much faster (and in higher proportion) in NAA vs. MAA vs. DAA, hence the criterion of C3-OH bulkiness must also impact the forward Z→E isomerization of the chalcones.

KINETIC ASPECTS

The experimental k_{obs} values of color loss at 25°C were confronted to the predictions based on k_{h} , $k_{\text{-h}}$, $\text{p}K_{\text{a1}}$ and $\text{p}K_{\text{a2}}$, assuming no degradation. The actual k_{obs} was 5-fold higher than the predicted value for P1, and 2.4-fold higher for P4. This difference was proposed to be the simultaneous irreversible degradation occurring over 24h, even at room temperature. In fact, other limits in the quantification of the constants could also explain this discrepancy. For example, the $\text{p}K_{\text{a1}}$ is determined with an uncertainty of *ca.* 0.2.

The kinetics of pure water addition to the flavylum ion follows a first-order kinetics. The first order is convenient to calculate half-life times with $t_{50} = \ln 2/k$. In the literature, the kinetics of anthocyanin degradation, often studied at acidic pH, is also generally reported to follow a first order (Dueñas et al., 2006; Dyrby et al., 2001; Kechinski et al., 2010; Kirca et al., 2006; Sinela et al., 2017; Torskangerpoll & Andersen, 2005), although the correlation factor may not always be satisfying (e.g. $R^2 = 0.972$ at 70°C in Kirca et al., 2006). These kinetics may actually hide more complex mechanisms of color loss. Unfortunately, the pigment quantification does not always refer to the total anthocyanin content, e.g. in “equivalent flavylum” but sometimes colorless species remain in the quantification system (e.g. at pH 3 to 4). Quantification in UPLC-DAD is a good tool for actual anthocyanin quantification, and more accessible than before. Alternatively, a UV-vis spectrum after acidification to pH 1 – 1.5 also quantifies the total flavylum content, and is simple and economical.

At pH 7, the rate of irreversible degradation is typically inferior to the rate of hydration. For example, t_{50} of color loss ranges between 0.2 - 3 h, and t_{50} of pigment consumption (irreversible component) ranges between 5 - 18 h. This combination of hydration and true degradation (autoxidation) explains why a clear first-order kinetics of color loss is not observed, and becomes more visible with the heating time. After 8h, the color loss becomes mainly driven by the irreversible degradation, until total discoloration (between 48h and 100h). Hence, a biexponential model was used to analyze the kinetics of color loss and pigment consumption (Fig 3). This type of curve fitting features two first-order processes, a fast one and a slow one. The fast one could correspond to the degradation of the colored species (with a contribution of hydration when color loss is monitored), and the slow one could involve the colorless species. The t_{50} was sometimes not reached, so an equivalent t_{75} (period of time required for a 25% decrease) was estimated (Table 2).

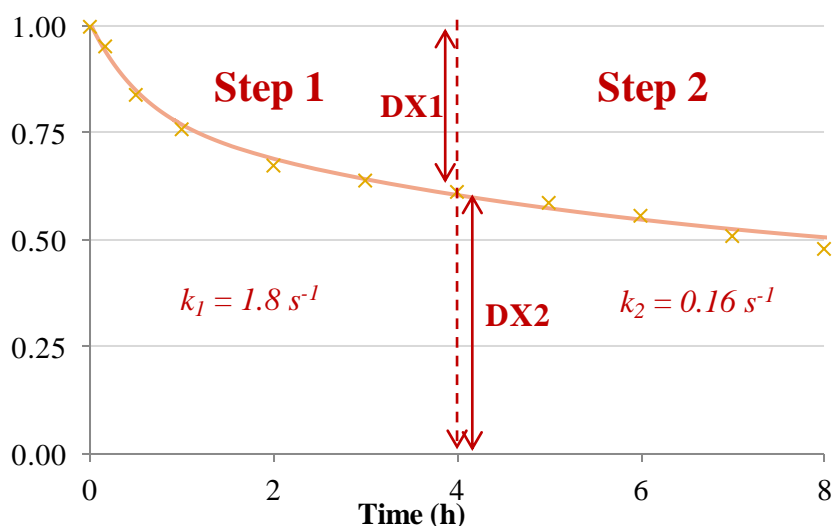


Fig 3. Example of biexponential fitting for the irreversible consumption of a monoacylated pigment, normalized absorbance at the flavylum λ_{\max} . Both step start at $t=0$, $DX = DX1 + DX2$. $X(t) = 1 - DX1(1 - e^{-k_1 t}) - DX2(1 - e^{-k_2 t})$.

Chemistry teaches that the most susceptible to oxidative degradation species among the flavylum ion, neutral base, anionic base, hemiketal, *cis*-chalcone, *trans*-chalcone is the anionic base. However, none of the methods used can quantify their relative contribution. It is difficult to determine experimentally, due to the existence of rapid equilibria, and due to the combined pH-dependence of the fraction of species, and the pH-dependence of their reactivity. In the literature, a correlation in the pH-dependence of hydration and degradation was observed: the rate of degradation increases between pH 2 and 6 (Dueñas et al., 2006), and the fraction of colorless species as well (speciation diagrams). This led many authors to propose the colorless species as intermediates in the degradation (Cabrita et al., 2014; Gradinaru et al., 2003).

In our work under neutral conditions, we confronted this hypothesis with a refined kinetic model (Chapter 2). The fractions of colored (neutral and anionic bases) and colorless forms (hemiketal and chalcones) and the fraction of degradation products were calculated from the differences between the curves of color loss and pigment degradation. Assuming a simultaneous degradation of the colored and the colorless species in the kinetic modeling, it was eventually shown that the time dependence of the different species' mole fractions could actually be correctly reproduced while neglecting the degradation of the colorless forms. The latter would thus not contribute to the irreversible degradation. This is chemically credible because the anionic base is probably a much better electron donor (more prone to

autoxidation) than any other (neutral) species present at pH 7 - 8. The mechanisms proposed based on the identification of major degradation products support this hypothesis: at pH 7 - 8, the anionic base is the major species undergoing degradation (Chapter 3).

Besides, the rates of color loss following H₂O₂ addition were compared between two solutions: a fresh solution pigment (before hydration, 100% colored forms), and a pre-hydrated solution containing 30% colorless forms (P5). The color loss induced by an excess of H₂O₂ at pH 7 was faster in the fresh pigment solution ($k_{\text{obs}} = 0.173 \pm 0.007 \text{ s}^{-1}$) than for the hydrated solution ($k_{\text{obs}} = 0.108 \pm 0.002 \text{ s}^{-1}$). Thus, the colored species appear more susceptible to degradation by H₂O₂. Other analyses could complete these observations, but all this data is in favor of the higher reactivity of the colored species and the higher stability of the colorless species at neutral pH.

The most interesting result may be the impact of the acylation pattern (mostly their position) on their sensitivity to Fe²⁺. Fe²⁺ ions have two major effects: i) anthocyanin binding, ii) the catalysis of the phenols oxidation (Perron & Brumaghim, 2009). However, the sinapoylation at C2s2 position (or G2 anthocyanins) actually protects the pigments from the irreversible degradation (decreased degradation rate *vs.* in absence of metal), and against the prooxidant effects of Fe²⁺ ions, observed with any other anthocyanin (Fig. 3. b).

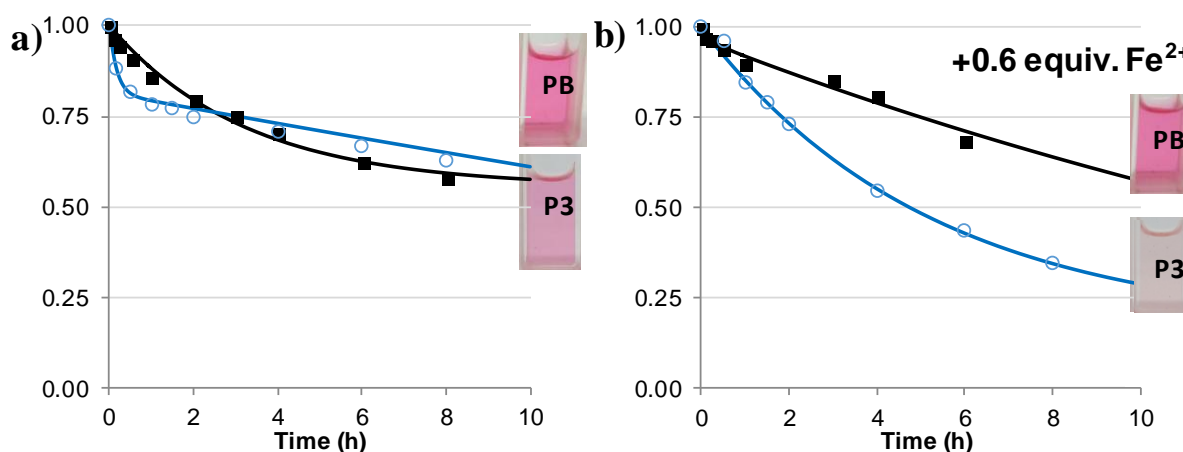


Fig. 3. Thermal degradation of pigments PB (■) and P3 (●) at 50°C, pH 7. Fraction of residual flavylum ion after acidification to pH 1. **a)** Pigment alone (50 μM pigment), **b)** Iron complex (0.6 equiv. Fe²⁺).

Table 2. t_{75} of pigment loss at pH 7 for various pigments. ^a Pigments alone, ^b in the presence of 0.6 or 1 equiv. Fe²⁺. *NB:* for several pigments, t_{50} was not reached over 24h.

	PA	P1	P3	P4	PB	PA'	P12	PB+Al ³⁺
t_{75} acid (h) ^a	4.0	2.0	2.0	2.5	2.6	11.0	2.1	-
+Fe ²⁺ ^b	0.1	1.1	1.9	7.5	5.2	-	-	5.0

3. COLOR STABILIZATION BY METAL BINDING

The combination of π -stacking interactions and metal binding is required to reach the highest level of blue color stability with anthocyanins (Trouillas et al., 2016a; Yoshida et al., 2009b). Metal binding induces the formation of the anionic base and stabilized it. This association likely lowers its electron-donating capacity.

The quantitative analysis shows that Fe²⁺ - anthocyanin binding generally occurs via a two-step mechanism. Following the fast bimolecular binding step (a few seconds), a slower first-order step can be evidenced, meaning the evolution of a first complex into a second one (Chapter 4 & 5). The two-step binding must reflect the combination of different phenomena: the autoxidation from Fe²⁺ to Fe³⁺ - polyphenol complexes [14], changes in the phosphate/water/pigment coordination around the metal, or the formation of quinones by two electron transfer (Perron & Brumaghim, 2009), or the hydration of an loosely bound fraction of pigment.

From the minimal M/L molar ratio for full binding (between 2/3 and 1 for PA, P2 and P5), we expect the presence of a mixture of 1:1 and 1:2 complexes. By contrast, this minimum ratio was lower for PB, *ca.* 1/3, suggesting tridentate complexes. The precision of this determination is modest, and a finer determination is feasible. The interpretation is consistent with the analysis of the metal complexes by high-resolution mass spectrometry (direct infusion). Indeed, a 1:3 Al³⁺-PB complex was detected, while the 1:1 and 1:2 complexes were not detected. With P5, 1:1 complexes with both metals were detected (Chapter 4).

Table 3. Spectroscopic features of the metal chelates formed from various cyanidin derivatives at pH 7 after addition of 1 equiv. Fe²⁺.

	PA	P2	P3	PB	P4	P5	P6	P9b
λ_{\max} final (nm)	596	592	607	639	627	622	619	620
$\Delta\lambda_{\max}$ (nm)	14	17	9	49	30	27	27	36
(A-A ₀)/A ₀ at λ_{\max} (%)	-7	-7	2	31	29	20	19	17

Several color stability parameters and the metal affinity revealed highly dependent on the position and number of the aromatic acyl residues (eg. Table 3 & 4). The 3 types of positions found in the RCE and PSPE anthocyanins are the C6s1-OH, C2s2-OH, C6s2-OH (Scheme 2). Besides, in the RCE, two major groups with similar behavior were distinguished, noted G1 (the unstable pigments, NAA and MAAs), and the G2 (stable pigments, including DAAs and the PB).

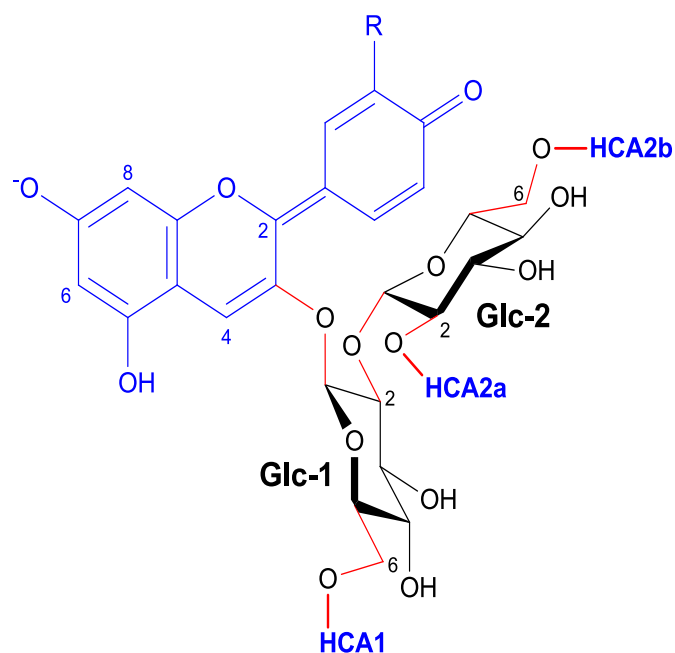
As the acylation at C2s2-OH is the common characteristic of the stable pigments, it was thus hypothesized that this feature (external Glc + C2 position) constitutes an ideal positioning for π -stacking interactions. It may be an optimal compromise between flexibility due to a relatively long spacer and sufficient number of freedom of rotation degrees; and rigidity due to acylation occurring at a C-atom of the pyrane ring, instead of the more flexible C5-C6 arm (Scheme 2).

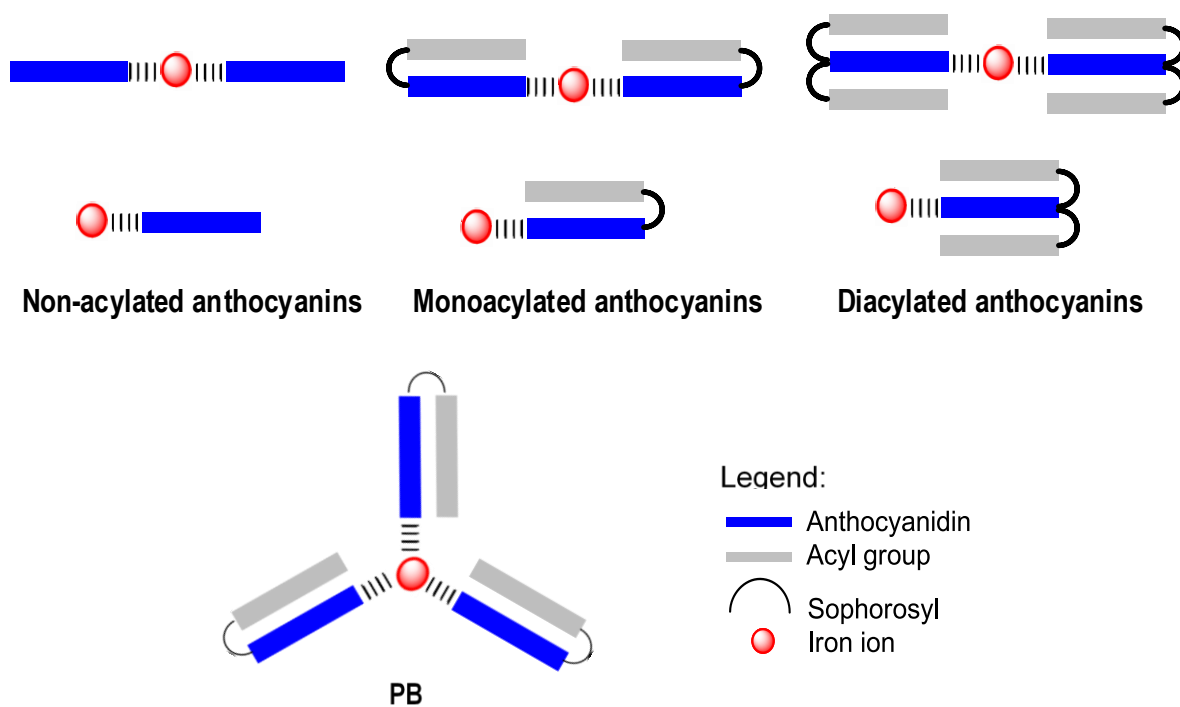
In addition, the bathochromic shift induced by PB Fe^{2+} - and Al^{3+} -binding (respectively +49 nm and +52 nm at pH 7) exceeds that of the other diacylated anthocyanins, denoting its peculiar behaviour with metal ions. Besides, unlike the DAAs, it cannot be stabilized in a “sandwich” conformation. There must thus exist other color stabilization mechanisms specific to PB. An interesting result was obtained in HRMS, a tridentate complex of Al^{3+} was detected, which is schematized in Scheme 3 (and modelled in Chapter 4, Scheme 2). Such propeller-like structure leaves a face of the chromophore free for self-association, e.g. with other complexes. This tendency of PB to form supramolecular metal assemblies is a credible hypothesis for its unique color expression and stability. The precise structural features that explain this behavior are investigated by a broader group of research teams, including in circular dichroism and using TD-DFT modelling.

Interestingly, P9b, which bears both acyl residues at C6-OH positions, also binds metal ions with high bathochromic shift (Table 3). Another peculiar stabilization mechanism is at work: the double complexation B-ring and caffeoyl residue stabilizes the complex. It is unsure if this results from an intra- or intermolecular stabilization mechanism.

Table 4. Compared behavior of 4 types of anthocyanins

	P1, P2, P3 (HCA1)	PB (HCA2a)	P4, P5, P6 (HCA1 + HCA2a)
Resistance to hydration	Weak	High	High
Metal-induced bathochromic shift	Low	High	Moderate
Acyl transfer at 50°C	None	Yes	Yes
Hydrolysis at 50°C	Yes	minor	Minor
Number of degrees of free rotation	5	6	5/6

**Scheme 2.** Hypothetical triacylated anthocyanin and the covalent bonds (in red) allowing free rotation for the development of π -stacking interactions between cyanidin and HCA moieties. The total number of degrees of free rotation is 5 (HCA1), 6 (HCA2a) and 7 (HCA2b).



Scheme 3. Probable organization of the metal complexes of NAA, MAA and DAA (mixtures of 1:1 and 1:2 complexes), and 1:3 complexes detected with PB.

4. BEHAVIOR OF TWO-GROUP EXTRACTS

OVERALL HYDRATION AND ACIDITY CONSTANT pK'_A

The pigments in RCE are prone to be classified into the group of unstable (G1: NAA + MAA) and stable (G2: DAA + PB) pigments (Table 5). The behavior of the entire extract can be studied as a sum of 2 groups (in the 60/40 ratio) and provide information on the kinetic and equilibrium position for each group. For example, the pK'_a of the two groups were determined for 4 different extracts characterized (Appendix 1), and are presented in Table 5. In RCE, the $pK'_{a1} = 2.39 (\pm 0.07)$ and $pK'_{a2} = 3.50 (\pm 0.10)$ were obtained with a satisfying fitting correlation ($R^2 = 0.994$), showing the presence of an important difference in the color stability between the 2 groups. For comparison, the mean pK'_a within each group is 2.54 for the G1 pigments (PA, P1, P2, P3) and 3.70 for the G2 (PB, P4, P5, P6). In the PSPE, the two groups also show a very distinct stability. In the partially purified extract, there was no non-acylated anthocyanins. The pK'_a of the diacylated group calculated from the model (3.55) is close to the average value for the DAAs from PSP (3.58). Overall, this simple method evidences subgroups with distinct pK'_a .

Table 5. Relative content in the RCE anthocyanins, and 2-groups classification by stability.

Pigment	(%)	By acylation (%)		By stability (%)	
PA	5	NAA	5	G1	61
P1+P2+P3	56	MAA	61		
PB	5	DAA	34	G2	39
P4+P5+P6	34				

Table 6. Fraction of anthocyanins based on their acylation number and calculated pK'_a values.

	pK'_a (NAA)	pK'_a (MAA)	pK'_a (DAA)	R^2
RCE*		2.39 (60%)	3.5 (40%)	0.998
PSPE**		2.04 (14%)	3.55 (86%)	0.999
Red radish		1.9 (12%)	3.41 (88%)	0.998
Black carrot	3.07 (35%)	4.05 (65%)		0.997

*Groups not directly determined on the acylation but on the particular pigment stability.

**Partially purified sample for contaminants elimination.

5. PERSPECTIVES

Anthocyanins are fascinating pigments, exhibiting a versatile reactivity and various applications. Plants are believed to produce anthocyanins - among other flavonoids - for defense purposes as well as for animal attraction or repulsion. Their richness in electron associated with their light absorption capacity (and the corresponding ecological interactions) is accompanied with a high electron-donating capacity, which is associated with their biological activity, both in plants and in the animals that ingest them (antiradical activity), in addition with other benefits : anti-inflammatory, antiseptic, antiviral activities, etc.

The different functions of anthocyanins in plants may well explain their diversity of structures. However, the extraction of anthocyanins from the plant cells has to destroy the natural stabilization systems : the vacuolar inclusions, where anthocyanins are protected from water, oxygen, light and other oxidants. In addition, the human society also desires ingredients with features beyond the natural possibilities, in particular a very long stability period, to make the products in which they are used compatible with economic and logistic constraints (long shelf-lives). As a consequence, the purpose of maintaining the pigment properties over months to a few years results challenging. However, our understanding of the chemical reactivity can help us devise fine-tuned stabilization techniques, within a frame of economical, regulatory and consumer acceptance criteria.

These perspectives aim at i) confirming the hypotheses proposed in this work, ii) assessing the potential of the two stabilization solutions proposed (addition of natural antioxidants and neutralization of the catechols with Al^{3+} ions) and iii) propose analytical methods for future research on the topic.

Without any constraints, the design of molecular cages with high affinity for anthocyanins (i.e. made of flat polarizable rings) of the size of acylated anthocyanins, e.g. dendromers, are a stabilization solution, but require chemical synthesis steps. Alternatively, among natural substances, clay offer layers where pigments can intercalate, in a low water-activity environment, and metal cations such as aluminum can contribute to the blue color expression and stability, however they are very opaque, and result only a light cyan color. Besides the use of mineral supports, the addition of pure aluminium salts in a buffered aqueous solution efficiently stabilizes the blue color, but require to work with slightly buffered deionized water, which is complex to manage industrially.

Among the solutions with good consumer acceptance, the micro-encapsulation in natural polymers or oils appears as a good option. Indeed, this range of techniques showed good results with both lipophilic and hydrophilic matrices, and it thus further detailed later.

In the current work, the possibility to work with individual pigments was exploited mainly to understand the relationship between their structure and their physico-chemical behavior, but it also enabled us to deepen the analysis of their reactivity and the structural characterization of the degradation compounds. However, all the perspective delivered here took into account the criterion of ingredients naturality: only biologically or physically-modified compounds were considered. Besides, the isolated pigments were in moderate quantity, for parsimony. Finally, each stabilization strategies was applied individually in order not to mix the effects, and to facilitate the interpretation. A few perspectives are suggested as a continuation of this research work.

PERSPECTIVES FOR FUNDAMENTAL RESEARCH

In the short term, the mechanisms a stake throughout the different phases following Fe^{2+} -complexation could be confirmed. In particular, the rate of Fe^{2+} autoxidation. Kinetic studies with Fe^{2+} and Fe^{3+} could be carried out with a G1 and a G2 pigments, but in the case of a very fast oxidation, a stopped-flow system may be necessary. The potential irreversible oxidation of the cyanidin B-ring may also have occurred. In this purpose, the pigment reacidification after a few minutes would dissolve the complex and enable to quantify the residual flavylum. The cyanidin *p*-quinones generated will not regenerate the flavylum ions.

A more systematic study of the metal complexes in HRMS could confirm the features enabling tridentate metal complexes (e.g. PB, P9b, optionally other catechols: chlorogenic acid, catechin...). An appropriate MS detector, targeting higher masses should be used. Besides, in the case of PB, the supposed intermolecular interactions between anthocyanin-metal complexes may contribute to decrease the complexes solubility. Therefore, to confirm this hypothesis, the limits of solubility could be investigated kinetically, and with increasing PB-metal ratios. Dynamic light scattering technique is unfortunately not accessible to blue complexes as it corresponds to the wavelength of the laser emission, and results in a very low sensitivity. A specific lamp should be purchased for this analysis.

Given the number of compounds that derive from each other (e.g. C1; C2-C3; C5; C6; C7 backbones), the MS data obtained for PA, P1 and P4 could be further analyzed with

molecular networks (Olivon et al., 2017). The online workflow Global Natural Products Social molecular networking (GNPS; <http://gnps.ucsd.edu>) represents ions in chemical maps related based on their fragmentation patterns (e.g. Scheme 1-A, 2 different datasets). The networks materialize non-obvious relationships, e.g. a link between ions 675 and 743 was not expected. The number of analyses (here resp. 29 and 25 spectra) should be higher for a good reliability.

Besides, higher anthocyanin-metal complexes in the presence of external copigments could be investigated, on the model of metallo-anthocyanins, as the copigments may increase the color stability (Kondo et al., 2005; Yoshida et al., 2009b). Preliminary results showed that Fe^{3+} decrease the pigment stability over long periods, but that an addition 10 equiv. NACys to this mixture compensates for this impact, and that an addition of 10 equiv. rutin provided an addition pigment stabilization that was maintained in the long term. However; in this case, the copigment used adds an undesirable yellow color, but other weaker copigments may provide a sufficient stabilization, e.g. the *p*-coumaric acid. This ternary system likely has a lower water-solubility than free acylated anthocyanins. In order to prevent color modifications due to self-association, a concentration of 20 - 50 μM was used throughout this work.

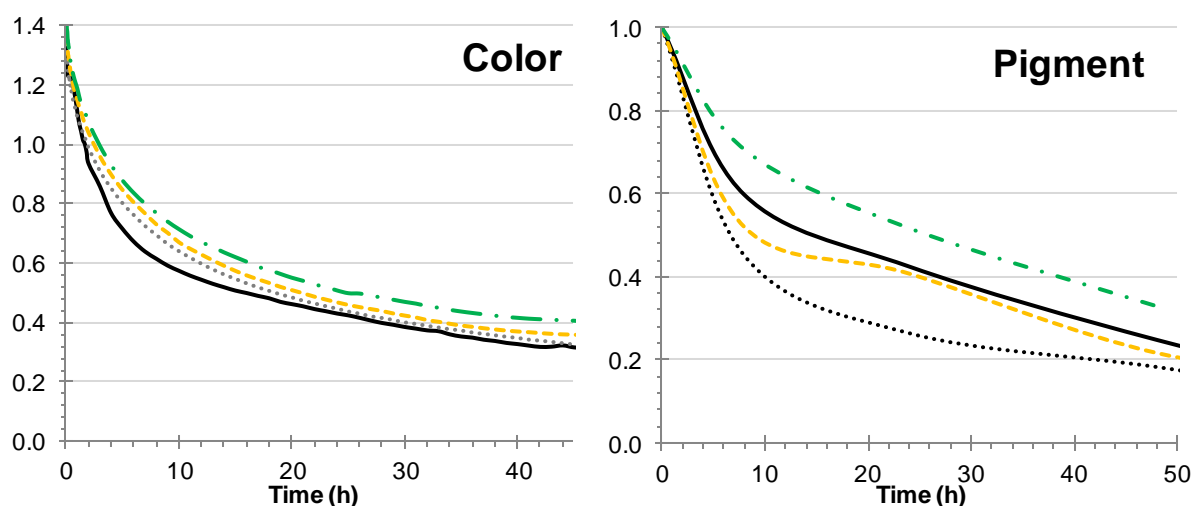


Fig 5. Rate of color loss (left) and pigment loss (right) of P6 at 50°C, in pH 7 phosphate buffer (black plain line), P6 with 1 equiv. Fe^{3+} (dotted line), P6 with 1 equiv. Fe^{3+} + 10 equiv. N-acetylcysteine (NAC, dashed yellow line), and P6 with 1 equiv. Fe^{3+} + 10 equiv. NAC + 10 equiv. rutin (dashed green line). The NAC compensates for the Fe^{3+} -induced degradation; and rutin further stabilizes the pigment and the color. initial absorbance with rutin = 1.42 vs. 1.32.

From the degraded samples, several known degradation products could be separated in UPLC: C3-C2 derivatives, C3-Glc, C2, acyl-sophorosides, and free acyl groups. For some of

them, the structure determination in nuclear magnetic resonance (NMR) was never carried out yet, namely the coumarins characterization of the C5 and C7 compounds for which a putative structure was proposed, may give access to a new group of degradation products from anthocyanins. In this purpose, higher amount of pigment should be degraded, to enable their isolation.

Large degradation products may as well be formed, especially once the 3-glycosyl moiety is released. Coupling mechanisms such as those in flavanol-anthocyanin and A-type anthocyanin-flavanol adducts detected in wine (Cheynier, 2005), However these compounds would not be detected with the current MS detectors due to their high mass ($> 2500 m/z$), but they could be relatively easily detected, in capillary zone electrophoresis coupled with DAD (CZE), confirming their family with their DAD spectrum. The preliminary analysis of the degraded pigment P6 in CZE revealed no dimers nor higher polymers. Its regioisomer and acyl-sophorose were detected. In the case of caffeoylated anthocyanins, the presence of cross-coupling compounds with the caffeoyl residue should be confirmed. A condensation product of Pg-3-Glc with the hydroxycaffeic acid *o*-quinone was reported previously (Kader et al., 2001). In this purpose, we could attempt their separation on different resins followed by NMR analysis.

Based on the degradation mechanisms, protection by other antioxidant could be further investigated. Preliminary results where several natural antioxidants and were added show the complexity of the redox properties of phenolic compounds. For instance, the phenolic acids gallic and caffeic acid increased the degradation rate, and induced a yellow color in the solution. In a recent copigmentation attempt in PSPE anthocyanins, the t_{50} of color and pigment degradation were actually significantly reduced in the presence of added F1 and Cf (Qian et al., 2017). Besides, the H_2O_2 released upon the autoxidation of gallols and catechols is highly deleterious for anthocyanins (hemiketal, anionic base and flavylium). Thiols such as N-acetylcysteine, DTT, GSH, cysteine, etc. are however promising, at least for *in vitro* applications. Besides, efficient metal chelatants were tested, so as to sequester the traces of pro-oxidant iron ions, and thus act as secondary antioxidants. Among the food-compatible ones, citric and oxalic acids are metal chelatants, and phosphates to a lesser extent.

OPPORTUNITIES FOR ANALYTICAL METHODS DEVELOPMENT

The screening of anthocyanin sources as potential colors is relevant for both fundamental and industrial applications. In this work, a rapid method of quantification of

anthocyanins' susceptibility to nucleophiles was used. It consists in the kinetic analysis of the bleaching rate of a pigment or extract, in presence of 5 eq. of bisulfite ion at room temperature. As the addition of sulfite or bisulfite onto the flavylum is reversible and fast, the rate bleaching rate should be correlated to the resistance to water addition. The ranking of the extracts should thus be the same as with a longer, more complex study of the hydration kinetics. The advantage of this test is its rapidity: the duration of the kinetic acquisition is 5 minutes, and requires a simple mono-exponential kinetic fitting. The first results showed that this method enables to discriminate the pigments (Chapter 2, Fig. 6. Indeed, the k_{obs} of bleaching is correlated to the pK'_{h} value (Moloney et al., 2018). With this method, new extracts could be screened for color stability, in a timely manner. It should first be validated that it accurately predicts the extracts color stability. Besides, another similar bleaching test was used, with an excess of H_2O_2 . It differs from the bisulfite test in that it combines the susceptibility of the flavylum to nucleophiles and to irreversible oxidation reactions. In this case, the duration in presence of 10^3 eq. of H_2O_2 is critical as it is relatively fast (ca. 1 h to reach 80% degradation at pH 7), and irreversible. Like the bisulfite test, this method could enable the screening of new extracts for both the color and pigment stability.

There are also opportunities for developing statistical data treatment. For example, an analysis would provide information on the relative degradation of each individual species. The initial composition of solutions over a pH range is calculated. From the constants of the individual pigments we get. The rate of irreversible degradation at this pH can be determined. The correlation between the two provides the dependence of the degradation rate on 1) the pH and 2) the species distribution, which cannot be distinguished. Now, using a combination of NAA, MAA, DAA provides very different species distribution at the same pH, which randomizes the pH/species fraction bias. From this dataset, a multilinear regression can be carried out, with as input, the fraction in each specie and the pH, and as output, the rate of irreversible degradation. The regression provides the relative contribution of each specie to the irreversible degradation. In order to warrant reliable results, the number of pigments analyzed should be sufficient, and balanced in their structural features, and the ionic strength and chelating capacity of the buffers should be homogenized.

Just as illustration and not for interpretation, a preview of this method was applied to degradation rates in presence of H_2O_2 at 3 different pH (Fig 6). The regression ($R^2 = 0.82$) concludes to a major contribution of A^- (coeff. = 0.78), of $[\text{B}+\text{C}]$ (0.47), then the flavylum (0.14), while the neutral base would not contribute to the degradation (0). This result does

obviously not provide the sufficient robustness for interpretation, but surprisingly makes sense from a chemical perspective, and given the pathways discussed previously.

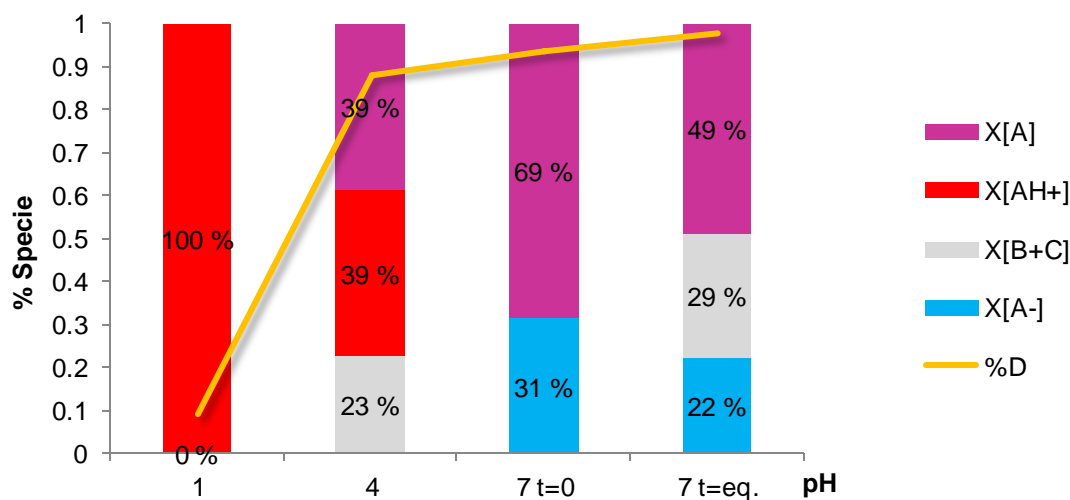


Fig 6. Fraction in each specie relatively to the flavylum, and k_{obs} of color loss in the presence of 10^3 equiv. H_2O_2 , at room temperature.

OPPORTUNITIES FOR APPLIED RESEARCH

The contribution of other components of the extracts in anthocyanins reactivity was not fully investigated. Acylated anthocyanins could be degraded in model solutions at pH 7 with e.g. 10 equivalents of flavanol-glycosides, esters of phenolic acids or catechins. These copigments are not expected to modulate the color of diacylated anthocyanins (at least in the absence of added metal ions), but similarly to the caffeic acid, they may contribute to the irreversible degradation of anthocyanins (Chapter 5). The comparison of their relative impact could orientate the partial purification of natural extracts towards specific gradients optimizing the chemical stability of the extracts.

Besides, reducing the pigment solubility by forming supramolecular complexes actually constitutes a stabilization strategy, like pigments aluminum lakes or anthocyanin vacuolar inclusions (Kallam et al., 2017). This is an option for dried applications (e.g. coatings, extruded and dried products), but causes processing challenges (homogeneity required for piping, nozzle clogging with large solid particles). For aqueous applications (most food and cosmetic products), pigment precipitation should be combined with the prevention of sedimentation, e.g. through the product gelation (feasible in soups, compotes, jams, yoghurts...).

The stability studies were executed in simple model systems, which modestly represent the actual matrices in which the pigments will eventually be used. In order to better

mimic the syrup application, similar stability studies could be extended to sugar syrups (50° or 60° brix, or sucrose content). Such solutions are transparent but viscous, enabling UV-vis spectroscopy analyses. It is difficult to predict the behavior of anthocyanins in high-sucrose syrups. Indeed, the impact of high levels of sucrose led to opposite conclusions (A. Patras, 2019). At 30 and 40°C, increasing the sucrose concentration between 20% ($a_w = 0.93$) and 60% ($a_w = 0.84$) at pH 3.2 significantly reduced the degradation index (A_{420}/A_{520}) of roselle anthocyanins, which was linked to the reduced water mobility (Tsai et al., 2004). In addition, preliminary results on RCE surprisingly indicated a faster hydration rate at room temperature, with $k_{obs\ 1} = 60 (\pm 5) 10^3\ s^{-1}$ in 60% sucrose syrup, vs. $20 (\pm 3) \times 10^3\ s^{-1}$ at pH 7 (Fig. 6-A). From the contribution of the water activity to the K_h , the fraction in colored species at the equilibrium is expected to decrease with a reduced a_w . In this preliminary experience, the position of the equilibrium was not significantly impacted by sucrose. Besides impact of water activity, the higher viscosity in high-brix solutions appears as a bias. Therefore, further studies should attempt to correlate the hydration rate with the kinematic viscosity.

Physico-chemical environments closer to the applications can be mimicked with semi-solid and mixed matrices (gels, dispersions, foams, emulsions). In particular, micro-encapsulation constitutes a promising stabilization strategy. Several recent reviews focus on the interaction of phenolic compounds with biomolecules: all phenols (Amoako & Awika, 2016; Munin & Edwards-Lévy, 2011; Ozdal et al., 2013; Papadopoulou & Frazier, 2004); flavonoids (Bordenave et al., 2014) and anthocyanins (Arroyo-Maya & McClements, 2015). The supramolecular interactions with the biomolecules include combinations of weak interactions: ion pairing, hydrogen bonding, electrostatic contributions, hydrogen bonding, π - π -stacking, dispersive forces and the hydrophobic effect (Biedermann & Schneider, 2016; X. Du et al., 2016). They can induce structural modifications in the macromolecule, in the phenol, or in both. For example, proteins interaction with flavonoids was shown to alter the protein charges, solubility and secondary structure. The technological functional properties may be affected as a result of the protein aggregation, namely their foaming, gelling and swelling capacities (Yan, Li, 2011). The quenching of fluorescence induced by protein-phenols interactions suggests the π -stacking interactions with amino-acids aromatic side chains (Tang et al., 2014).

For highly hydrophilic compounds, a lipidic membrane is an impermeable interface. Therefore, anthocyanins encapsulation in micelles of surfactants could provide a color stabilization, as well as a controlled kinetics of release. Several techniques have recently been explored. For example, anthocyanins co-micellization sodium dodecyl sulphate (SDS) micelles was investigated for purple sweet potato anthocyanins (Liu et al., 2014) as well as

lipophilized anthocyanins (Johan Mendoza et al., 2018). Anthocyanins incorporation in niosomal vesicles successfully enabled a controlled delivery, but used synthetic surfactants (Tween 20) (Fidan-Yardimci et al., 2019). Indeed, this area is poorly investigated for food applications. The challenge remains to identify natural, ideally cationic, available, surfactants.

Other analytical tools would be required to characterized the impact of anthocyanins-biopolymer interactions: light scattering, zeta-potential and electron microscopy to characterize the particle size, morphology and charge; differential scanning calorimetry, thermo-gravimetric analysis and infrared spectroscopy to characterize the molecular interactions; circular dichroism to provide insights on overall modifications of the protein structure; or X-ray diffraction to finely characterize the structure obtained.

Finally, anthocyanins are very easy to handle and innocuous. They are thus prone to experimenting with non-scientific persons, for example at a science fair. Simple experiments can show their potential (e.g. the typical “rainbow of colors” produced by a pH gradient). Combining this experimental ease with interview techniques to trigger people’s imagination may result in original ideas for future experimentation!

REFERENCES

- Arroyo-Maya, I. J., & McClements, D. J. (2015). Biopolymer nanoparticles as potential delivery systems for anthocyanins: Fabrication and properties. *Food Research International*, 69, 1–8. <https://doi.org/10.1016/j.foodres.2014.12.005>
- Biedermann, F., & Schneider, H.-J. (2016). Experimental Binding Energies in Supramolecular Complexes. *Chemical Reviews*, 116(9), 5216–5300. <https://doi.org/10.1021/acs.chemrev.5b00583>
- Bordenave, N., Hamaker, B. R., & Ferruzzi, M. G. (2014). Nature and consequences of non-covalent interactions between flavonoids and macronutrients in foods. *Food Funct.*, 5(1), 18–34. <https://doi.org/10.1039/C3FO60263J>
- Cabrita, L., Fossen, T., & Andersen, Ø. M. (2000). Colour and stability of the six common anthocyanidin 3-glucosides in aqueous solutions. *Food Chemistry*, 68(1), 101–107. [https://doi.org/10.1016/S0308-8146\(99\)00170-3](https://doi.org/10.1016/S0308-8146(99)00170-3)
- Cabrita, L., Petrov, V., & Pina, F. (2014). On the thermal degradation of anthocyanidins: cyanidin. *RSC Advances*, 4(36), 18939–18944. <https://doi.org/10.1039/C3RA47809B>
- Casanova, F., Chapeau, A.-L., Hamon, P., de Carvalho, A. F., Croguennec, T., & Bouhallab, S. (2017). pH- and ionic strength-dependent interaction between cyanidin-3-O-glucoside and sodium caseinate. *Food Chemistry*. <https://doi.org/10.1016/j.foodchem.2017.06.081>
- Cheyrier, V. (2005). Polyphenols in foods are more complex than often thought. *The American Journal of Clinical Nutrition*, 81(1), 223S–229S. <https://doi.org/10.1093/ajcn/81.1.223S>
- Chung, C., Rojanasathara, T., Mutilangi, W., & McClements, D. J. (2017). Stability improvement of natural food colors: Impact of amino acid and peptide addition on anthocyanin stability in model beverages. *Food Chemistry*, 218, 277–284. <https://doi.org/10.1016/j.foodchem.2016.09.087>
- Du, J., Sun, B., Zhang, J., & Guan, X. (2012). Parabola-Like Shaped pH-Rate Profile for Phenols Oxidation by Aqueous Permanganate. *Environmental Science & Technology*, 46(16), 8860–8867. <https://doi.org/10.1021/es302076s>
- Du, X., Li, Y., Xia, Y.-L., Ai, S.-M., Liang, J., Sang, P., Ji, X.-L., & Liu, S.-Q. (2016). Insights into Protein–Ligand Interactions: Mechanisms, Models, and Methods. *International Journal of Molecular Sciences*, 17(2), 144. <https://doi.org/10.3390/ijms17020144>
- Dueñas, M., Fulcrand, H., & Cheyrier, V. (2006). Formation of anthocyanin–flavanol adducts in model solutions. *Analytica Chimica Acta*, 563(1), 15–25. <https://doi.org/10.1016/j.aca.2005.10.062>
- Dyrby, M., Westergaard, N., & Stapelfeldt, H. (2001). Light and heat sensitivity of red cabbage extract in soft drink model systems. *Food Chemistry*, 72(4), 431–437. [https://doi.org/10.1016/S0308-8146\(00\)00251-X](https://doi.org/10.1016/S0308-8146(00)00251-X)
- Fenger, J.-A., Moloney, M., Robbins, R. J., Collins, T. M., & Dangles, O. (2019). The influence of acylation, metal binding and natural antioxidants on the thermal stability of red cabbage anthocyanins in neutral solution. *Food & Function*, 10(10), 6740–6751. <https://doi.org/10.1039/C9FO01884K>
- Fidan-Yardimci, M., Akay, S., Sharifi, F., Sevimli-Gur, C., Ongen, G., & Yesil-Celiktas, O. (2019). A novel niosome formulation for encapsulation of anthocyanins and modelling intestinal transport. *Food Chemistry*, 293, 57–65. <https://doi.org/10.1016/j.foodchem.2019.04.086>

- Gradinaru, G., Biliaderis, C. G., Kallithraka, S., Kefalas, P., & Garcia-Viguera, C. (2003). Thermal stability of *Hibiscus sabdariffa* L. anthocyanins in solution and in solid state: effects of copigmentation and glass transition. *Food Chemistry*, 83(3), 423–436. [https://doi.org/10.1016/S0308-8146\(03\)00125-0](https://doi.org/10.1016/S0308-8146(03)00125-0)
- Kader, F., Irmouli, M., Nicolas, J. P., & Metche, M. (2001). Proposed mechanism for the degradation of pelargonidin 3-glucoside by caffeic acid o-quinone. *Food Chemistry*, 75(2), 139–144. [https://doi.org/10.1016/S0308-8146\(00\)00301-0](https://doi.org/10.1016/S0308-8146(00)00301-0)
- Kallam, K., Appelhagen, I., Luo, J., Albert, N., Zhang, H., Deroles, S., Hill, L., Findlay, K., Andersen, Ø. M., Davies, K., & Martin, C. (2017). Aromatic Decoration Determines the Formation of Anthocyanic Vacuolar Inclusions. *Current Biology*, 27(7), 945–957. <https://doi.org/10.1016/j.cub.2017.02.027>
- Kechinski, C. P., Guimarães, P. V. R., Noreña, C. P. Z., Tessaro, I. C., & Marczak, L. D. F. (2010). Degradation Kinetics of Anthocyanin in Blueberry Juice during Thermal Treatment. *Journal of Food Science*, 75(2), C173–C176. <https://doi.org/10.1111/j.1750-3841.2009.01479.x>
- Kırca, A., Özkan, M., & Cemerog˘lu, B. (2006). Stability of black carrot anthocyanins in various fruit juices and nectars. *Food Chemistry*, 97(4), 598–605. <https://doi.org/10.1016/j.foodchem.2005.05.036>
- Kondo, T., Toyama-Kato, Y., & Yoshida, K. (2005). Essential structure of co-pigment for blue sepal-color development of hydrangea. *Tetrahedron Letters*, 46(39), 6645–6649. <https://doi.org/10.1016/j.tetlet.2005.07.146>
- Landi, M., Tattini, M., & Gould, K. S. (2015). Multiple functional roles of anthocyanins in plant-environment interactions. *Environmental and Experimental Botany*, 119, 4–17. <https://doi.org/10.1016/j.envexpbot.2015.05.012>
- Liu, S., Fu, Y., & Nian, S. (2014). Buffering colour fluctuation of purple sweet potato anthocyanins to acidity variation by surfactants. *Food Chemistry*, 162, 16–21. <https://doi.org/10.1016/j.foodchem.2014.04.029>
- Mendoza, J., Basílio, N., Pina, F., Kondo, T., & Yoshida, K. (2018). Rationalizing the Color in Heavenly Blue Anthocyanin. A Complete Kinetic and Thermodynamic Study. *The Journal of Physical Chemistry. B*, 122(19), 4982–4992. <https://doi.org/10.1021/acs.jpcc.8b01136>
- Mendoza, J., Pina, F., Basílio, N., Guimarães, M., de Freitas, V., & Cruz, L. (2018). Extending the stability of red and blue colors of malvidin-3-glucoside-lipophilic derivatives in the presence of SDS micelles. *Dyes and Pigments*, 151, 321–326. <https://doi.org/10.1016/j.dyepig.2018.01.007>
- Moloney, M., Robbins, R. J., Collins, T. M., Kondo, T., Yoshida, K., & Dangles, O. (2018). Red cabbage anthocyanins: The influence of d-glucose acylation by hydroxycinnamic acids on their structural transformations in acidic to mildly alkaline conditions and on the resulting color. *Dyes and Pigments*, 158, 342–352. <https://doi.org/10.1016/j.dyepig.2018.05.057>
- Nkhili, E., Loonis, M., Mihai, S., Hajji, H. E., & Dangles, O. (2014). Reactivity of food phenols with iron and copper ions: binding, dioxygen activation and oxidation mechanisms. *Food & Function*, 5(6), 1186–1202. <https://doi.org/10.1039/C4FO00007B>
- Olivon, F., Allard, P.-M., Koval, A., Righi, D., Genta-Jouve, G., Neyts, J., Apel, C., Pannecouque, C., Nothias, L.-F., Cachet, X., Marcourt, L., Roussi, F., Katanaev, V. L., Touboul, D., Wolfender, J.-L., & Litaudon, M. (2017). Bioactive Natural Products Prioritization Using Massive Multi-informational Molecular Networks. *ACS Chemical Biology*, 12(10), 2644–2651. <https://doi.org/10.1021/acschembio.7b00413>
- Patras, A. (2019). Stability and colour evaluation of red cabbage waste hydroethanolic extract in presence of different food additives or ingredients. *Food Chemistry*, 275, 539–548. <https://doi.org/10.1016/j.foodchem.2018.09.100>

- Perron, N. R., & Brumaghim, J. L. (2009). A Review of the Antioxidant Mechanisms of Polyphenol Compounds Related to Iron Binding. *Cell Biochemistry and Biophysics*, 53(2), 75–100. <https://doi.org/10.1007/s12013-009-9043-x>
- Qian, B.-J., Liu, J.-H., Zhao, S.-J., Cai, J.-X., & Jing, P. (2017). The effects of gallic/ferulic/caffeic acids on colour intensification and anthocyanin stability. *Food Chemistry*, 228, 526–532. <https://doi.org/10.1016/j.foodchem.2017.01.120>
- Sadilova, E., Stintzing, F. C., & Carle, R. (2006). Thermal Degradation of Acylated and Nonacylated Anthocyanins. *Journal of Food Science*, 71(8), C504–C512. <https://doi.org/10.1111/j.1750-3841.2006.00148.x>
- Satake, R., & Yanase, E. (2018). Mechanistic studies of hydrogen-peroxide-mediated anthocyanin oxidation. *Tetrahedron*, 74(42), 6187–6191. <https://doi.org/10.1016/j.tet.2018.09.012>
- Sheng, F., Wang, Y., Zhao, X., Tian, N., Hu, H., & Li, P. (2014). Separation and Identification of Anthocyanin Extracted from Mulberry Fruit and the Pigment Binding Properties toward Human Serum Albumin. *Journal of Agricultural and Food Chemistry*, 62(28), 6813–6819. <https://doi.org/10.1021/jf500705s>
- Sigurdson, G. T., Robbins, R. J., Collins, T. M., & Giusti, M. M. (2016). Evaluating the role of metal ions in the bathochromic and hyperchromic responses of cyanidin derivatives in acidic and alkaline pH. *Food Chemistry*, 208, 26–34. <https://doi.org/10.1016/j.foodchem.2016.03.109>
- Sinela, A., Rawat, N., Mertz, C., Achir, N., Fulcrand, H., & Domier, M. (2017). Anthocyanins degradation during storage of Hibiscus sabdariffa extract and evolution of its degradation products. *Food Chemistry*, 214, 234–241. <https://doi.org/10.1016/j.foodchem.2016.07.071>
- Tang, L., Zuo, H., & Shu, L. (2014). Comparison of the interaction between three anthocyanins and human serum albumins by spectroscopy. *Journal of Luminescence*, 153, 54–63. <https://doi.org/10.1016/j.jlumin.2014.03.004>
- Sadilova, E., Stintzing, F. C., & Carle, R. (2006). Thermal Degradation of Acylated and Nonacylated Anthocyanins. *Journal of Food Science*, 71(8), C504–C512. <https://doi.org/10.1111/j.1750-3841.2006.00148.x>
- Torskangerpoll, K., & Andersen, Ø. M. (2005). Colour stability of anthocyanins in aqueous solutions at various pH values. *Food Chemistry*, 89(3), 427–440. <https://doi.org/10.1016/j.foodchem.2004.03.002>
- Trouillas, P., Sancho-García, J. C., De Freitas, V., Gierschner, J., Otyepka, M., & Dangles, O. (2016). Stabilizing and Modulating Color by Copigmentation: Insights from Theory and Experiment. *Chemical Reviews*, 116(9), 4937–4982. <https://doi.org/10.1021/acs.chemrev.5b00507>
- Wang, S., Marcone, M. F., Barbut, S., & Lim, L.-T. (2013). Electrospun soy protein isolate-based fiber fortified with anthocyanin-rich red raspberry (*Rubus strigosus*) extracts. *Food Research International*, 52(2), 467–472. <https://doi.org/10.1016/j.foodres.2012.12.036>
- Wu, J., Guan, Y., & Zhong, Q. (2015). Yeast mannoproteins improve thermal stability of anthocyanins at pH 7.0. *Food Chemistry*, 172, 121–128. <https://doi.org/10.1016/j.foodchem.2014.09.059>
- Yoshida, K., Mori, M., & Kondo, T. (2009). Blue flower color development by anthocyanins : from chemical structure to cell physiology. *Natural Product Reports*, 26(7), 884–915. <https://doi.org/10.1039/B800165K>

APPENDICES

Table 1-A. Data for color repeatability and reproducibility of the absorbance in the visible region, for P5 at pH 7.

	Repeatability	Reproducibility
Number of repetitions (N)	6	7
Average	1,04	0,93
Standard deviation (SD)	0,037	0,094
% Variation	3,6%	10,1%
Absolute uncertainty U	3,0%	7,1%
Limit	0,074	0,19

Repeatability limit: $r = 2 * SD(\text{repeatability})$;

Absolute uncertainty U = Broadening value * N* $\sqrt{(SD)}$

Broadening value = 2 for a normal law distribution, at the risk $\alpha = 5\%$.

Table 2-A. Maximum wavelength (λ_{max}) and molar absorption coefficient (ϵ) of the pigments studied in pH 1 aqueous solutions.

	λ_{max} nm	ϵ L mol ⁻¹ cm ⁻¹
Cyanidin-3-Glc	510	26 900 ^a
Cyanin	510	30 175 ^a
PA	511	25 541 ^b
PB	528	13 714 ^b
P1	522	20 259 ^b
P2	521	18 203
P3	530	21 793 ^b
P4	517	16 870 ^b
P5	532	15 123 ^b
P6	533	12 730
PA'	510	21 918 ^c
P10	532	24 303 ^c
P9a	522	18 207 ^c
P9b	529	21 011 ^c
P11	527	21 968 ^c
P12	532	20 936 ^c

^a(Giusti et al., 1999), ^b(Ahmadiani et al., 2016), ^c(Sigurdson et al., 2019)

Table 3-A. Regulatory information of E 163 Anthocyanins ¹¹ as food color, (EU) No 231/2012.

Definition	Anthocyanins are obtained by maceration or extraction with sulfited water, acidified water, carbon dioxide, methanol or ethanol from the strains of vegetables and edible fruits, with subsequent concentration and/or purification if necessary. The resulting product can be transformed into powder by an industrial drying process. Anthocyanins contain common components of the source material, namely anthocyanin, organic acids, tannins, sugars, minerals etc., but not necessarily in the same proportions as found in the source material. Ethanol may naturally be present as a result of the maceration process. The coloring principle is anthocyanin. Products are marketed according to their color strength as determined by the assay. Color content is not expressed using quantitative units.		
Einecs	208-438-6 (cyanidin); 205-125-6 (peonidin); 208-437-0 (delphinidin); 211-403-8 (malvidin); 205-127-7 (pelargonidin); 215-849-4 (petunidin)		
Chemical name	3,3',4',5,7-Pentahydroxy-flavylium chloride (cyanidin) 3,4',5,7-Tetrahydroxy-3'-methoxyflavylium chloride (peonidin) 3,4',5,7-Tetrahydroxy-3',5'-dimethoxyflavylium chloride (malvidin) 3,5,7-Trihydroxy-2-(3,4,5-trihydroxyphenyl)-1-benzopyrylium chloride (delphinidin) 3,3',4',5,7-Pentahydroxy-5'-methoxyflavylium chloride (petunidin) 3,5,7-Trihydroxy-2-(4-hydroxyphenyl)-1-benzopyrylium chloride (pelargonidin)		
Chemical formula	Cyanidin: C ₁₅ H ₁₁ O ₆ Cl Peonidin: C ₁₆ H ₁₃ O ₆ Cl Malvidin: C ₁₇ H ₁₅ O ₇ Cl Delphinidin: C ₁₅ H ₁₁ O ₇ Cl Petunidin: C ₁₆ H ₁₃ O ₇ Cl Pelargonidin: C ₁₅ H ₁₁ O ₅ Cl	Molecular weight	Cyanidin: 322,6 Peonidin: 336,7 Malvidin: 366,7 Delphinidin: 340,6 Petunidin: 352,7 Pelargonidin: 306,7
Assay	E (1cm, 1%) = 300 for the pure pigment at 515-535 nm at pH 3,0		
Description	Purplish-red liquid, powder or paste, having a slight characteristic odour		
Identification			
Spectrometry	Cyanidin: 535 nm Peonidin: 532 nm Delphinidin: 546 nm Maximum in methanol with 0,01 % conc. HCl	Pelargonidin: 530 nm Malvidin: 542 nm Petunidin: 543 nm	
Purity			
Solvent residues	Methanol	Not more than 50 mg/kg	
	Ethanol	Not more than 200 mg/kg	
Sulfur dioxide	Not more than 1 000 mg/kg per percent pigment		
Arsenic	Not more than 3 mg/kg	Mercury	Not more than 1 mg/kg
Lead	Not more than 2 mg/kg	Cadmium	Not more than 1 mg/kg

¹¹ COMMISSION REGULATION (EU) No 231/2012 of 9 March 2012 laying down specifications for food additives listed in Annexes II and III to Regulation (EC) No 1333/2008 of the European Parliament and of the Council. *Aluminium lakes of this colour may be used.*

Table 4-A. List of the natural pigments authorized in foods in the European Union

COLOR	NAME	E-NUMBER	SOURCES
BROWN	Caramel	E150 a-d	Melanoidins from maillard reaction
BLACK	Carbon black	E153	carbonized vegetal organic matter
BLUE	Riboflavin (vitamin B2)	E101	vitamin B2
ORANGE/RED	Carotenoids: beta-carotene, lycopene	E160 a-g	Carotenoids (beta-carotene, lycopene) from apricots, carrots and tomatoes.
YELLOW	Curcumin	E100	Turmeric
INTENSE RED	Carminic acid	E120	Cochineal
GREEN	Chlorophyll, chlorophyllin, copper chlorophyll	E140-141	Plant leaves
BLUE/VIOLET/PINK	Anthocyanins	E163	Black Grapes, Blackcurrants, Cherries, Elderberries, Red Cabbage, Strawberries
RED/PINK	Betanin	E162	Beetroot
BLUE	Phycocyanin	E101	Spirulina microalgae

Table 5-A. Major patents on blue color made from anthocyanins

Applicant	Year	Patent n°	Name	Raw material
Chr. Hansen	2003	WO2003010240A1	Anthocyanin derivatives treated with an aluminum salt and used as food coloring substances	Red cabbage/purple carrot anthocyanin-aluminum sulfate lake, tasteless and/or odorless, at pH 6 - 8
Chr. Hansen	2005	US 6,881,430 B2	Food coloring substances and Method for their preparation	Red cabbage anthocyanin-aluminum sulfate lake, pH 7.9 with 5% ammonia, spray dried, 2 eq. Aluminium
Colormaker, Inc.	2006	US 2006/0003060 A1	Stabilized natural blue and green Colorants	Red cabbage, Aluminum sulfate:sodium bicarbonate 2:1. Blue and green applications in products of pH > 5
华东理工大学	2007	CN101104745B	Method for producing natural blue pigment	Genipin prepared by reaction of beta-glucosidase and natural gardenia blue pigment, an aminoacid and metal ions
Omnic GmbH	2009	WO2009031051A2	Stabilized anthocyanin compositions	Blackcurrant extract, aqueous solution stabilized by thiols (DHLA, glutathione, yeast extract, N-acetylcysteine, papain, bromelain, ficin, peptides containing cysteine, thiolated chitosans...)
Richard Rice	2010	WO2010115073A2	Natural blue flavorants and colorants	Viola extract and stannous chloride pH 3 - 7
Diana Naturals	2010	US20100121084A1	Modification of the color hue of anthocyanins for the obtention of color substances	red cabbage/purple carrot/elderberry + aldehyde (furaldehyde, glyoxylic acid) + polyphenol (chalcone, flavone, flavanol, flavanol, isoflavone)
Sensient	2011	US 2011/0129584A1	Natural, blue-shade colorants and methods of making and using same	Anthocyanin (RCE, PSP), divalent ion (Ca, Mg), TSPP, Na carbonate, bicarbonate.
NESTEC S.A.	2014	US 2014/0161938 A1	Food-grade blue encapsulate and process for the production thereof	globular proteins* + anthocyanin + metal ions (Fe/Cu/Al)
NESTEC S.A.	2014	WO2014023712A1	Anthocyanin colouring composition	Anthocyanins, metal ions (Al(III), Ca(II), Cu(II), Fe(II), Fe(III), Mg(II), Mn(II), Zn(II)), and at least one stabilizer (tannic acid/phospholipids), pH 3 - 10
Mars Inc.	2014	US9598581B2	Method of isolating blue anthocyanin fractions	Red cabbage (+PSPE, BCE, blue potato...) Ion exchange purification of anthocyanins fractions
Wild Flavors, Inc.	2017	WO2017062489A1	Natural colorants and processes of making the same	Genipin purified from Genipa americana, reacted with primary amines, Various colors expressed depending on the amino acid
Ohio State Innovation Foundation	2018	US 2018 / 0346731 A1	Formation of stable pyranoanthocyanins, and uses thereof as sources of natural color	Chromophore made from the reaction of an anthocyanin (chokeberries, blackberries...); with acetaldehyde, pyruvic acid or catechin into a pyranoanthocyanin, and the reaction with ascorbic acid.

Table 6-A. a) Structural features, b) Physico-chemical constants, of the 14 isolated anthocyanins studied. In PSPE and RCE: pondered constants based on the extract composition. Data used in the multiple linear regression.

Pigment	Cf	pC	Fl	Sp	I	II	Glc-1	Glc-2	Pn	Cy
PA'	0	0	0	0	0	0	0	0	1	0
P9a	1	0	0	0	1	0	1	0	1	0
P9b	1	0	1	0	2	0	1	1	0	1
P10	2	0	0	0	2	0	1	1	1	0
P11	1	0	0	0	1	0	1	1	1	0
P12	1	0	1	0	2	0	1	1	1	0
PSPE	1.1	0.0	0.6	0.0	1.7	0.0	0.99	0.99	0.8	0.2
PA	0	0	0	0	0	0	0	0	0	1
P1	0	1	0	0	1	0	1	0	0	1
P2	0	0	1	0	1	0	1	0	0	1
P3	0	0	0	1	0	0	1	0	0	1
PB	0	0	0	1	0	1	0	1	0	1
P4	0	1	0	1	1	1	1	1	0	1
P5	0	0	1	1	1	1	1	1	0	1
P6	0	0	0	2	0	1	1	1	0	1
RCE	0	0.06	0.06	0.59	0.1	0.4	0.9	0.4	0	1

Pigment	pK _a '	pK _{a1}	pK _{a2}	pK _h '	k _h (s ⁻¹)	k _h (M ⁻¹ s ⁻¹)
PA'	2.04	4.21	7.08	2.04	0.33	116
P9a	2.43	4.06	7.11	2.44	0.132	87.8
P9b	3.71	3.93	7.15	4.11	0.047	394
P10	3.53	4.11	7.16	3.66	0.028	251
P11	3.25	3.99	7.29	3.34	0.297	162
P12	3.85	4.34	7.49	4.02	0.0098	176
PSPE	3.6	4.1	7.3	3.8	0.1	234.1
PA	2.14	4.6	7.18	2.14	0.315	84
P1	2.65	4.2	6.95	2.66	0.132	149
P2	2.67	4.5	7.25	2.68	0.166	139
P3	2.69	4.2	7.09	2.7	0.143	154
PB	3.66	3.8	6.94	4.22	0.096	590
P4	3.77	4.6	7.34	3.84	0.01	124
P5	3.8	4	7.34	4.23	0.011	141
P6	3.57	4.3	7.2	3.66	0.006	149
RCE	2.59	4.29	7.15	2.6	0.106	163

Table 7-A. HR-MS data for the major identified compounds in PA, P1, P4, by identification level.

Peak	Compound detected	m/z (-)	λ_{\max}	Ion selected	Formula	Ion mass	Neutral mass	Detected mass	Error (ppm)	Ref.
1 5	Protocatechuic acid	109	258(293)	[M-CO ₂ H]-	C ₇ H ₆ O ₄	153.0186	154.0264	153.0203	11.1	Std
1"	p-coumaric acid	119	309	[M-CO ₂ H]-	C ₉ H ₈ O ₃	163.0393	164.0471	163.0401	4.9	Std
PA	PA	771	515	[M-2H]-	C ₃₃ H ₄₁ O ₂₁	771.1971	773.2127	771.1965	0.8	Std
P1	P1	917	524	[M-2H]-	C ₄₂ H ₄₇ O ₂₃	917.2337	919.2493	917.2331	0.7	Std
PB	PB	977	530	[M-2H]-	C ₄₄ H ₅₁ O ₂₅	977.2547	979.2703	ND		Std
2 2'	C1-3-Soph	517	330	[M-H]-	C ₂₁ H ₂₆ O ₁₅	517.1185	518.1263	517.1182	0.6	
6	C1-3-Soph-5-Glc	679	ND	[M-H]-	C ₂₇ H ₃₆ O ₂₀	679.1710	680.1788	679.1707	0.4	[1]
4'	C1-3-(pC)Soph-5-Glc	825	310	[M-H]-	C ₃₆ H ₄₂ O ₂₂	825.2076	826.2154	825.2071	0.6	[1]
2"	C1-3-(Sp,pC)Soph-5-Glc	1031	ND	[M-H]-	C ₄₇ H ₅₂ O ₂₆	1031.2652	1032.273	ND		
1'	pC-Soph	487	310	[M-H]-	C ₂₁ H ₂₈ O ₁₃	487.1443	488.1521	487.1454	2.3	[2]
CtA	PA trans-chalcone	789	328	[M-H]-	C ₃₃ H ₄₂ O ₂₂	789.2076	790.2154	789.2067	1.1	[3]
Ct1	P1 trans-chalcone	935	310	[M-H]-	C ₄₂ H ₄₈ O ₂₄	935.2442	936.252	935.2438	0.4	[3]
Ct4	P4 trans-chalcone	1141	320	[M-H]-	C ₄₂ H ₄₈ O ₂₄	1111.2913	1112.2991	ND		[3]
12	C3-Glc-C2	481	ND	[M-H]-	C ₂₁ H ₂₂ O ₁₃	481.0975	482.1053	481.0976	0.2	[4]
11	C3-Soph-Glc-C2	805	269(300)	[M-H]-	C ₃₃ H ₄₂ O ₂₃	805.2025	806.2103	ND		[4]
5'	C3-(pC-Soph)-Glc-C2	951	308	[M-H]-	C ₄₂ H ₄₈ O ₂₅	951.2391	952.2469	951.2438	4.9	[4]
7	C4-Glc	315	289	[M-H]-	C ₁₃ H ₁₆ O ₉	315.0711	316.0789	315.0714	1.0	[4]
3 13	Cy-5-Glc	447	330	[M-2H]-	C ₂₁ H ₂₁ O ₁₁	447.0921	449.1077	447.0927	1.3	-
1	C3-Glc	345	~275	[M-H]-	C ₁₄ H ₁₈ O ₁₀	345.0816	346.0894	345.0810	1.7	[4, 5]
4 8	C6-Soph	529	275	[M-H]-	C ₂₂ H ₂₆ O ₁₅	529.1185	530.1263	529.1190	0.9	-
7'	C6-(pC)Soph	675	278-285	[M-H]-	C ₃₂ H ₃₆ O ₁₆	675.1551	676.1629	675.1564	1.9	-
9	C7-Soph	597	278	[M-H]-	C ₂₆ H ₃₀ O ₁₆	597.1446	598.1524	597.1461	2.5	-
6'	C7-(pC)Soph	743	318	[M-H]-	C ₃₅ H ₃₆ O ₁₈	743.1812	744.189	743.1816	0.5	-
3"	C7-(Sp,pC)Soph	949	ND	[M-H]-	C ₄₆ H ₄₆ O ₂₂	949.2388	950.2466	ND		-
3'	Cy-5-Glc + H ₂ O ₂	498	ND	[M]-	C ₂₉ H ₂₃ O ₈	498.1002	498.1002	498.1323	64.4	[4]
14	C5-Glc	463	328	[M-H]-	C ₂₁ H ₂₀ O ₁₂	463.0870	464.0948	463.1051	39.1	[6]

Appendix 1. Composition of four anthocyanin extracts

1. Methods used

Table 1. LC-MS parameters used for the analysis of the four anthocyanin extracts.

LC system	Acquity UPLC System
Column	BEH Phenyl Acquity UPLC 100 x 2.1 mm, 1.7 μ m Spherical shape, 130Å pore size, 15% carbon load
Column temperature	30°C
Sample temperature	10°C
Flow rate	0.4 mL/min
Binary solvent system	
Mobile phase A	Water + 1% Formic acid
Mobile phase B	Acetonitrile + 1% Formic acid
Total run time	20 min
Injection volume	5 μ L, full loop
MS system	Bruker Daltonics HCT ultra
MS type	Ion trap
Ionization system	Electrospray ionization (ESI)
Collision gas	N ₂ (40 psi)
Capillary voltage	1800V (ESI+), 2000V (ESI-)
Desolvation temperature	365°C
Desolvation gas flow rate	9 L/min
Acquisition	Ultrascan mode
Precursor ion scans range	m/z 100-2000
Average target mass	m/z 500
Diode array detector :	
λ range	240-600 nm

Table 2. Gradient used in the binary system: %B = % Acetonitrile + 1% formic acid.

RCE		PSPE		BCE / EE	
Time (min)	%B	Time (min)	%B	Time (min)	%B
0	10	0	6	0	10
5	20	2	12	2	15
6	24	6	14	3	15
8	24	10	20	6	17
10	30	13	80	9	20
14	80	14	6	10	24
15	10	20	6	11	10
20	10			14	10

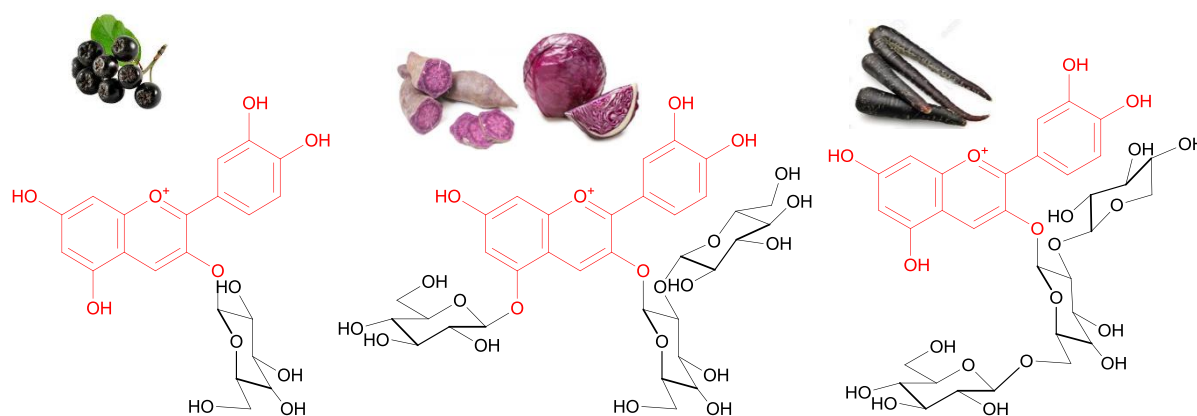
2. Results

Table 1. Composition of the four extracts studied: glycosylation pattern, acylation type.

Extract	Major aglycon	Glycosylation pattern	Acylation type	Average MW* (g/mol)
Red cabbage	Cyanidin	Glucose, Sophorose	pC, Fl, Sp	1060
Purple sweet potato	Cyanidin / Peonidin 48/52	Glucose, Sophorose	Cf, Fl, Sp, HBA	1079
Elderberry	Cyanidin	Glucose, galactose, Sambubiose	pC (50%), Ac (<1%), Ma (<1%)	660
Black carrot	Cyanidin	Xylose, Glucose, Galactose	pC, Fl (80%), Cf	874

*Calculated MW from the composition and mass of individual pigments (see tables 2,3,4,5).

Structures determined by RMN in the literature.



Scheme 1. Compared glycosylation patterns of the four extracts studied. a. Elderberry fruits, b. Red cabbage leaves and purple sweet potato roots, c. Black carrot roots.

Appendix 1.1. RED CABBAGE EXTRACT (*Brassica oleracea L., capitata rubra*)



Table 2. Anthocyanin composition of the crude red cabbage extract.

RT (min)	Compound	MW (g/mol)	λ_{\max} (nm)	Purity %*	% PA	% PB	Fraction %
1.1	PA	773	514	94%	-	-	5%
2.6	PB	979	531	98%	-	-	
6.5	P1	919	523	84%	4.5%	-	56%
7.0	P2	949	524	92%	5.3%	-	
7	P3	979	525	93%	3.3%	-	5%
7.55	P4	1125	536	75%	<	5.5%	6%
7.75	P5	1155	536	82%	<	5.0%	8%
7.8	P6	1185	538	90%	<	4.6%	20%

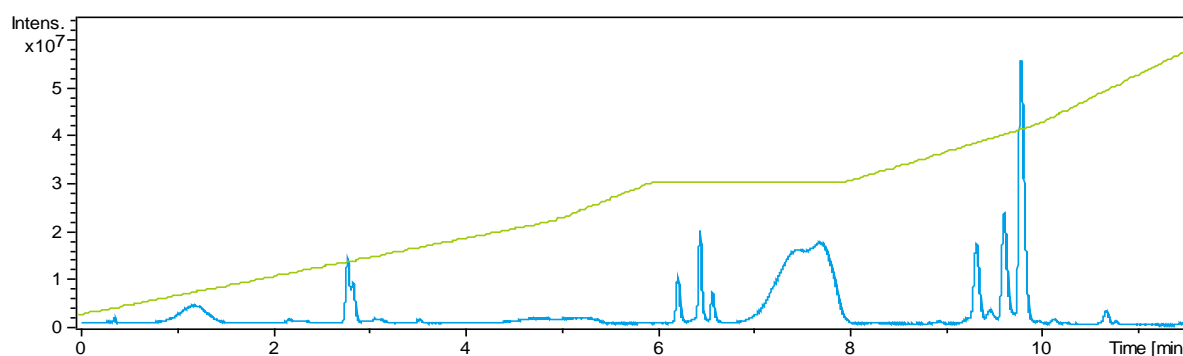


Fig 1. Chromatogram at 460-560 nm of the crude RCE with the phenyl column, and elution profile (% B, in green).

Appendix 1.2. PURPLE SWEET POTATO EXTRACT (*Ipomoea batatas* L.)



Table 3. Anthocyanin composition of the PSP extract.

#	RT (min)	Compound	MW (g/mol)	λ_{\max} (nm)	Area (%)
1	1	Pn-HB	907	524	1.10%
2	3.21	<i>Unidentified</i>	997	525	0.90%
3	3.96	Cya-Cf	935	525	3.70%
4	4.06	Cya-Cf ₂	1097	531	5.10%
5	4.20	Cya-Cf.HB	1055	525	4.80%
6	4.86	Pn-Cf (P9a)	949	525	6.40%
7	4.92	Pn-Cf ₂ (P10)	1111	531	10%
8	5.38	Cya-Cf.F1 (P9b)	1111	533	19%
9	5.59	Pn-Cf.HB (P11)	1069	528	22%
10	6.25	Pn-Cf.F1 (P12)	1125	533	25%
11	6.42	Pn-Cf	949	525	0.70%
12	7.39	Pn-F1	963	525	0.70%

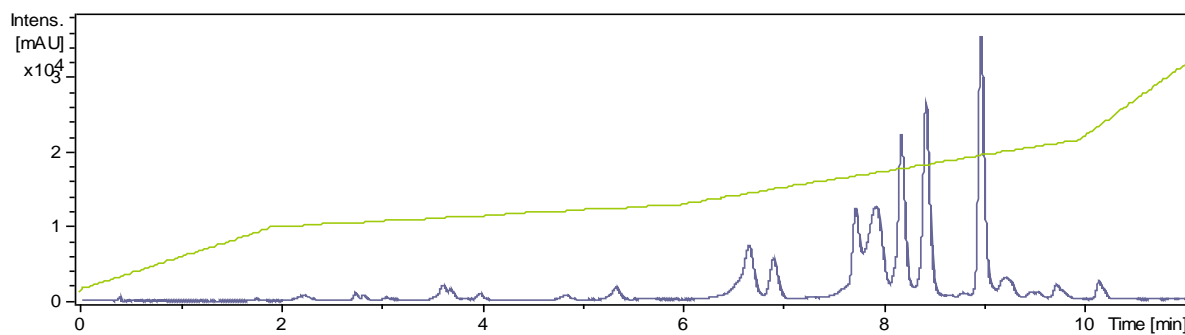


Fig 2. Chromatogram at 460-560 nm of the purified PSPE extract with the phenyl column, and elution profile (% B, in green).

Appendix 1.3. BLACK CARROT EXTRACT (*Daucus carota L.*)



Table 4. Anthocyanin and major phenols composition of the black carrot extract.

#	RT (min)	Compound	MW (g/mol)	λ_{\max} (nm)	Area (%)
1	1.6	Cy-3-Sb-5-Gal	743	521	7%
2	2.0	Cy-3-Xyl-Gal	581	521	36%
3	2.4	Cy-3-(Sp)Sb-5-Gal	949	534	15%
4	2.6	Cy-3-(Fl)Sb-5-Gal	919	530	35%
5	2.7	Cy-3-(pC)Sb-5-Gal	889	529	7%
6	2,2	Kaempferol 3-O-acetyl- glucoside	392	326	15%
7	4,8	Dihydrokaempferol-O-glucoside	452	328	1%

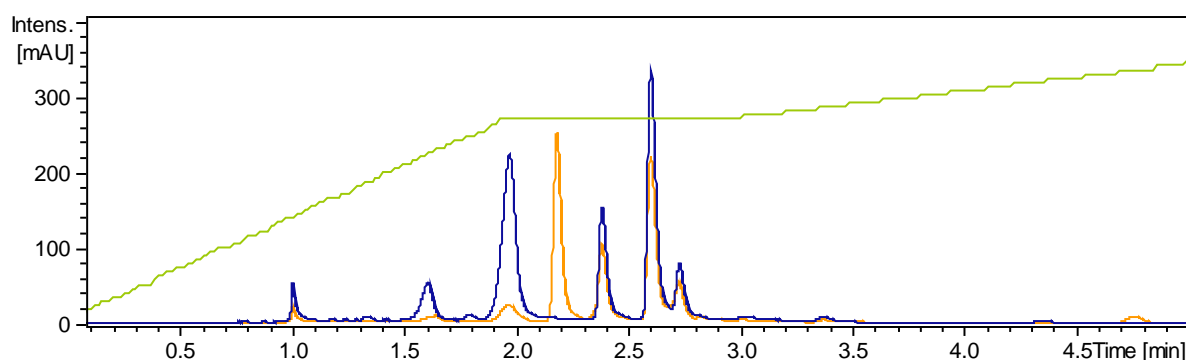


Fig 3. Chromatogram at 330 (orange) and 520 nm (purple) of the crude black carrot extract with the phenyl column, and elution profile (% B, in green).

Appendix 1.4. ELDERBERRY EXTRACT (*Sambucus nigra* L.)



Table 5. Anthocyanin composition of the elderberry extract.

#	RT (min)	Compound	MW (g/mol)	λ_{\max} (nm)	Area (%)	C (μM)
1	1.02	Unidentified	-	523	2%	6.7
2	1.49	Cyanidin 3-sambubioside-5-glucoside	743	514	8%	24.1
3	2.15	Cyanidin 3-sambubioside	581	519	49%	155
		Cyanidin 3-pC-sambubioside	717			
4	2.33	Cyanidin 3-glucoside	449	518	42%	134
5	4.73	Cyanidin 3, 5-diglucoside	611	356	0%	8.0
Total			266		100	328

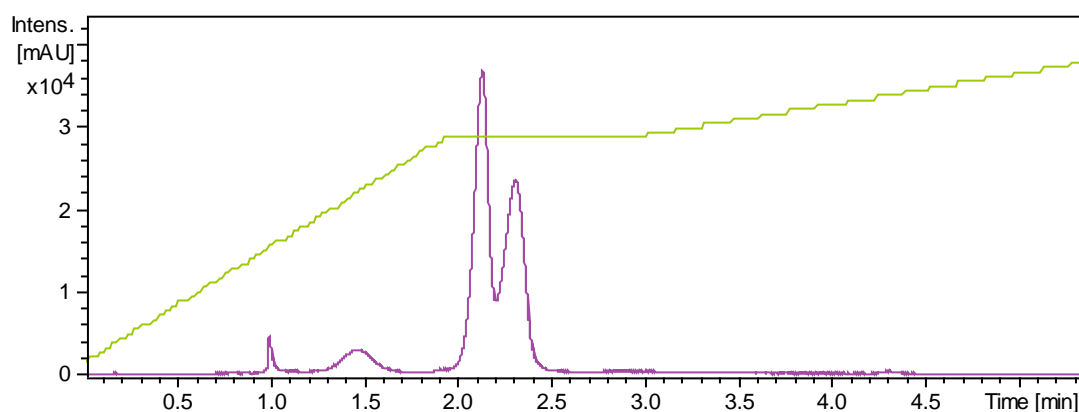
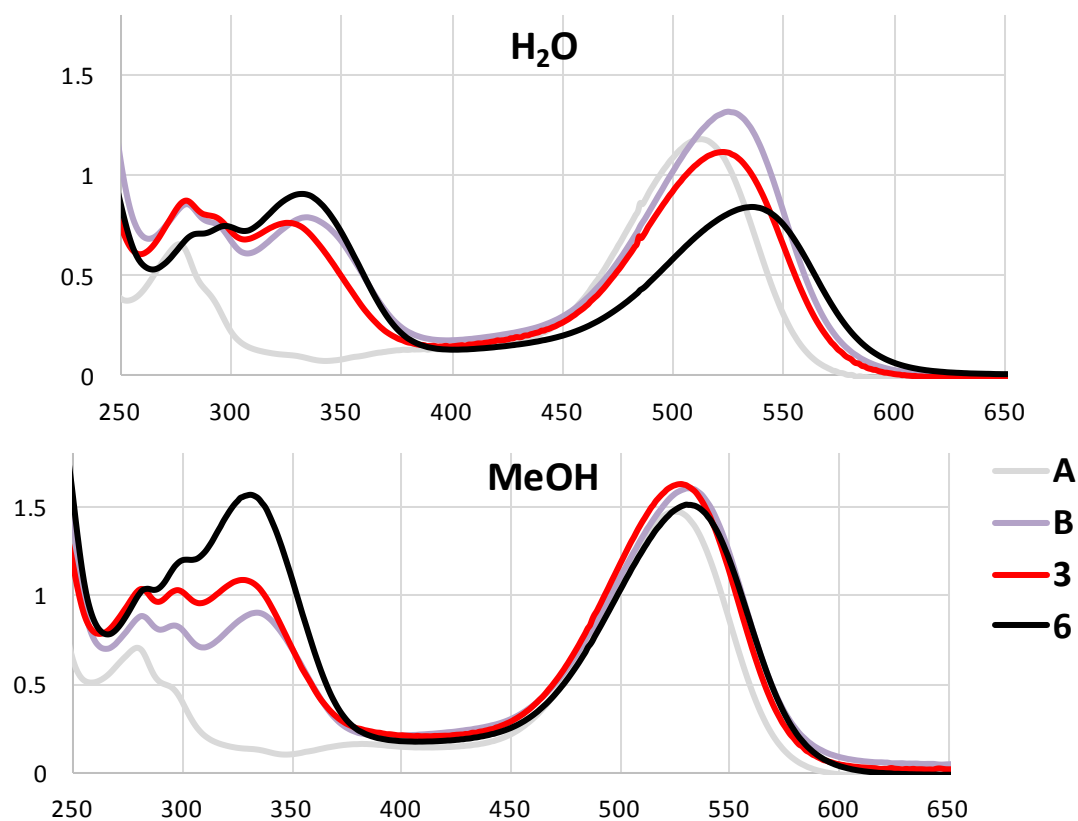


Fig 4. Chromatogram at 330 (orange) and 520 nm (purple) of the crude elderberry extract with the phenyl column, and elution profile (% B, in green).



Pigment	λ_{\max} (nm) H ₂ O	λ_{\max} (nm) MeOH	$\Delta\lambda_{\max}$ MeOH-H ₂ O
PA	512	525	13
PB	525	530	5
P3	522	525	3
P6	536	532	-4

Fig 5-A. Solvent effect on the UV-vis spectra of red cabbage anthocyanins acylated with sinapic acid: spectral features recorded at 0.1% aqueous HCl and 0.1% HCl methanol (MeOH), 50 μ M pigments. Anthocyanins show *negative solvatochromism*: as the excited state of the flavylum is less polar than ground state, in less polar solvents than H₂O (MeOH), the energetic gap between HOMO/LUMO is minimized, and the pigment λ_{\max} is superior (e.g. +13 nm for PA).

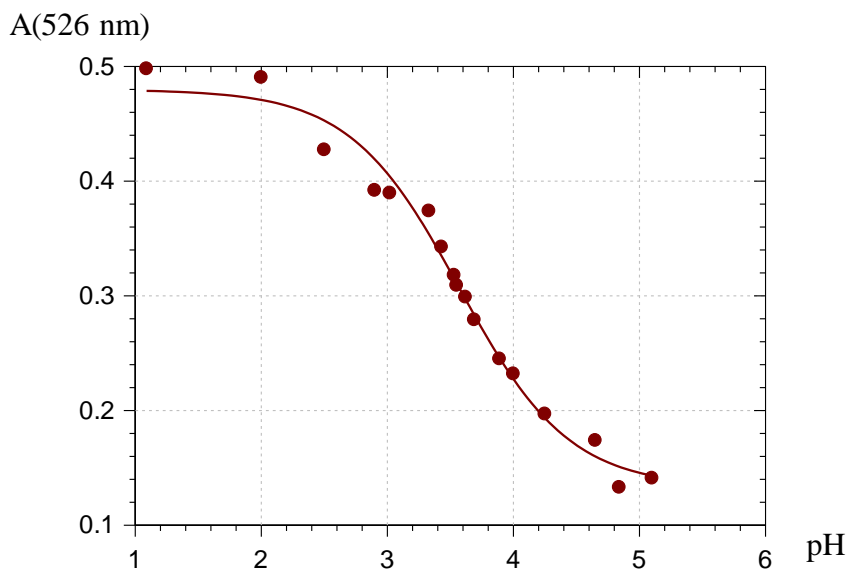
In water, acyl groups π -stacking dispersive interactions with the chromophore through a combination of solvation and hydrophobic effects induce a bathochromic shift (+11 and 13 nm in PB and P3, +24 nm in P6 vs. PA). In methanol, these π -stacking interactions are essentially dissociated, thus reducing the bathochromic effect due to acylation (+7 nm in P6 vs. PA).

Some interactions seem to remain in MeOH, for the pigments bearing an acyl at C2-OH of Glc-2 (+5 to +7 nm vs. PA), and long-range NOE (Nuclear Overhauser Effect) was detected for such pigments in MeOH (unpublished results).

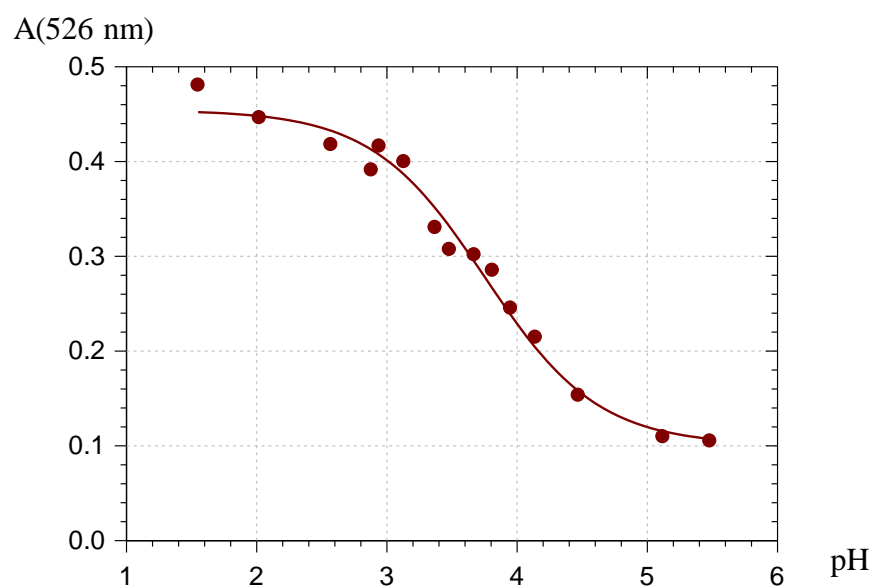
Table 7. pK'_a of pigment PB at 50 μM (in 10 mm quartz cuvette) and 500 μM (in 1 mm quartz cuvette), in 10 mM citrate buffer, with and without 0.1M KCl. The pK'_a values were slightly smaller at the 10-fold concentration (500 μM).

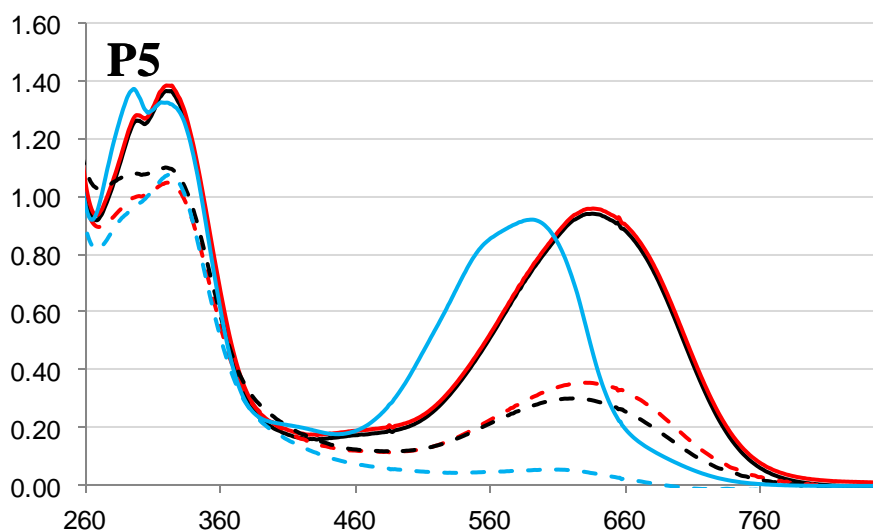
pK'_a		pK'_a difference
Diluted	Concentrated	
3.75 (± 0.06)	3.57 (± 0.05)	
3.68 (± 0.03)		
3.66 (± 0.06)		
3.70 (± 0.06)		0.13

- **C = 500 μM :** $r = 0.992$, $pK'_a = 3.57 (\pm 0.05)$, $A_0 = 0.48 (\pm 0.01)$, $r_A K_{a1} = 7.4 (\pm 1.3) \times 10^{-5}$



- **C = 50 μM :** $r = 0.992$, $pK'_a = 3.75 (\pm 0.06)$, $A_0 = 0.45 (\pm 0.01)$, $r_A K_{a1} = 3.9 (\pm 0.9) \times 10^{-5}$





Blue index	P5	Fe ²⁺	Fe ³⁺
t=0	60	113	116
t=20 days	4	35	42

Fig 6. Color stability of P5 at pH 7 in the absence or presence of Fe²⁺ or Fe³⁺ (1 equiv.). t=0 after complexation (plain lines), and after t=20 days at room temperature (dotted lines). P5 (blue), P5+Fe²⁺ (black), P5+Fe³⁺ (red). b) Blue index of the corresponding solutions: $\Sigma A(480 \text{ nm} - 750 \text{ nm})$. Similar spectra are interpreted as the fact that Fe²⁺ and Fe³⁺ lead to the same mixture of complexes, due to the fast autoxidation of Fe²⁺ into Fe³⁺ in the presence of anthocyanins. The color retention in aqueous solution is much better in the presence of iron ions.

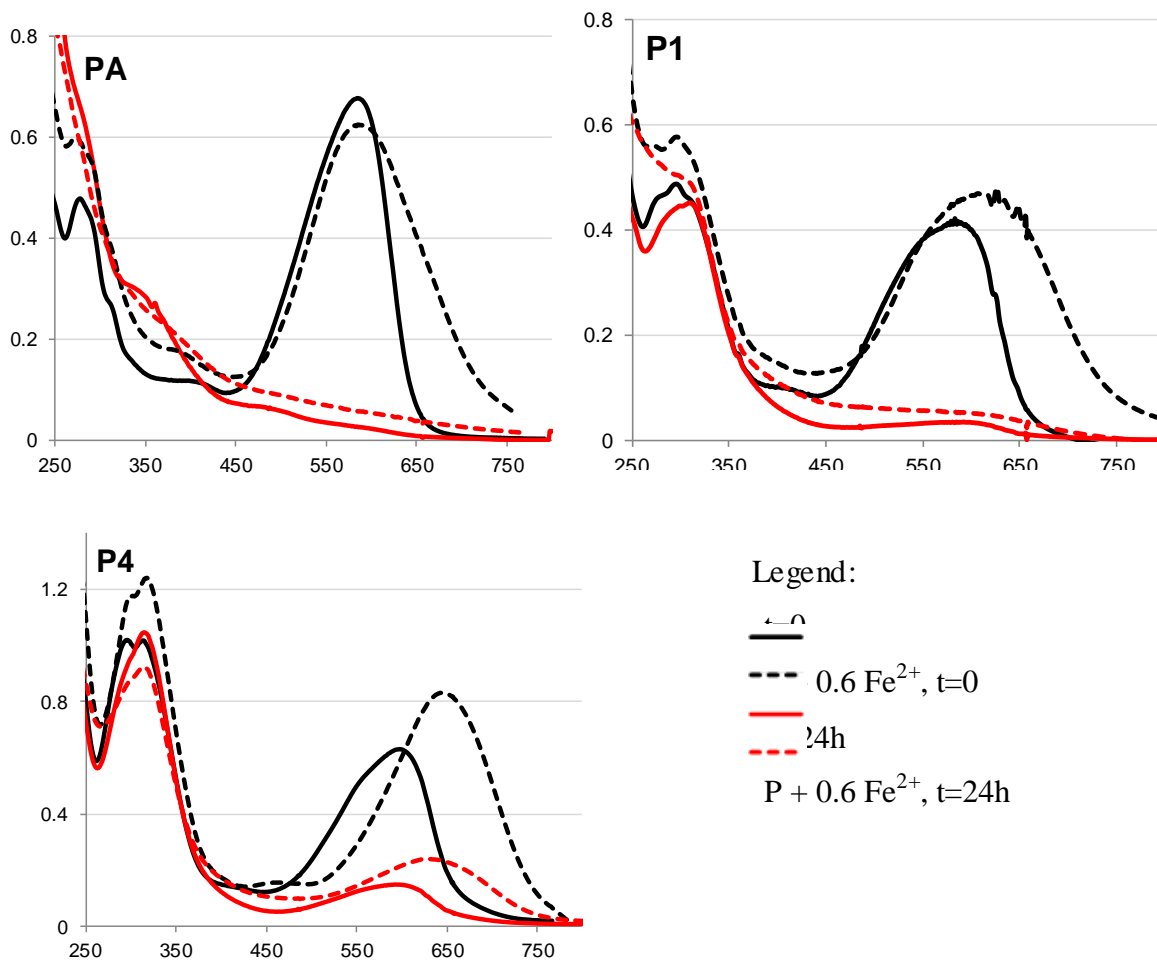


Fig 7-A. Spectra of the solutions at pH 7 of PA, P1 and P4 after 24h at pH7, 50°C, corresponding to the residual color in the absence and presence of 0.6 equiv. Fe^{2+} .

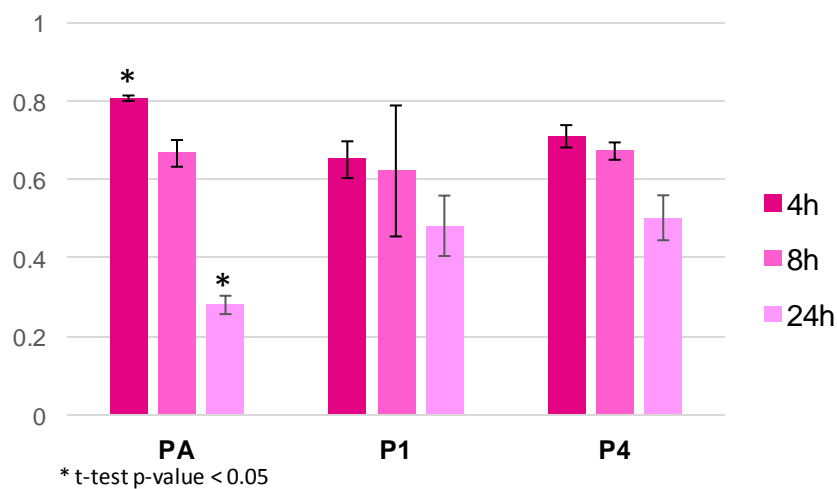


Fig. 8-A. ANOVA for the residual flavylum content after 4h, 8h and 24h at pH7, 50°C inter-pigment comparison: differences are significant at 4h and 24h.

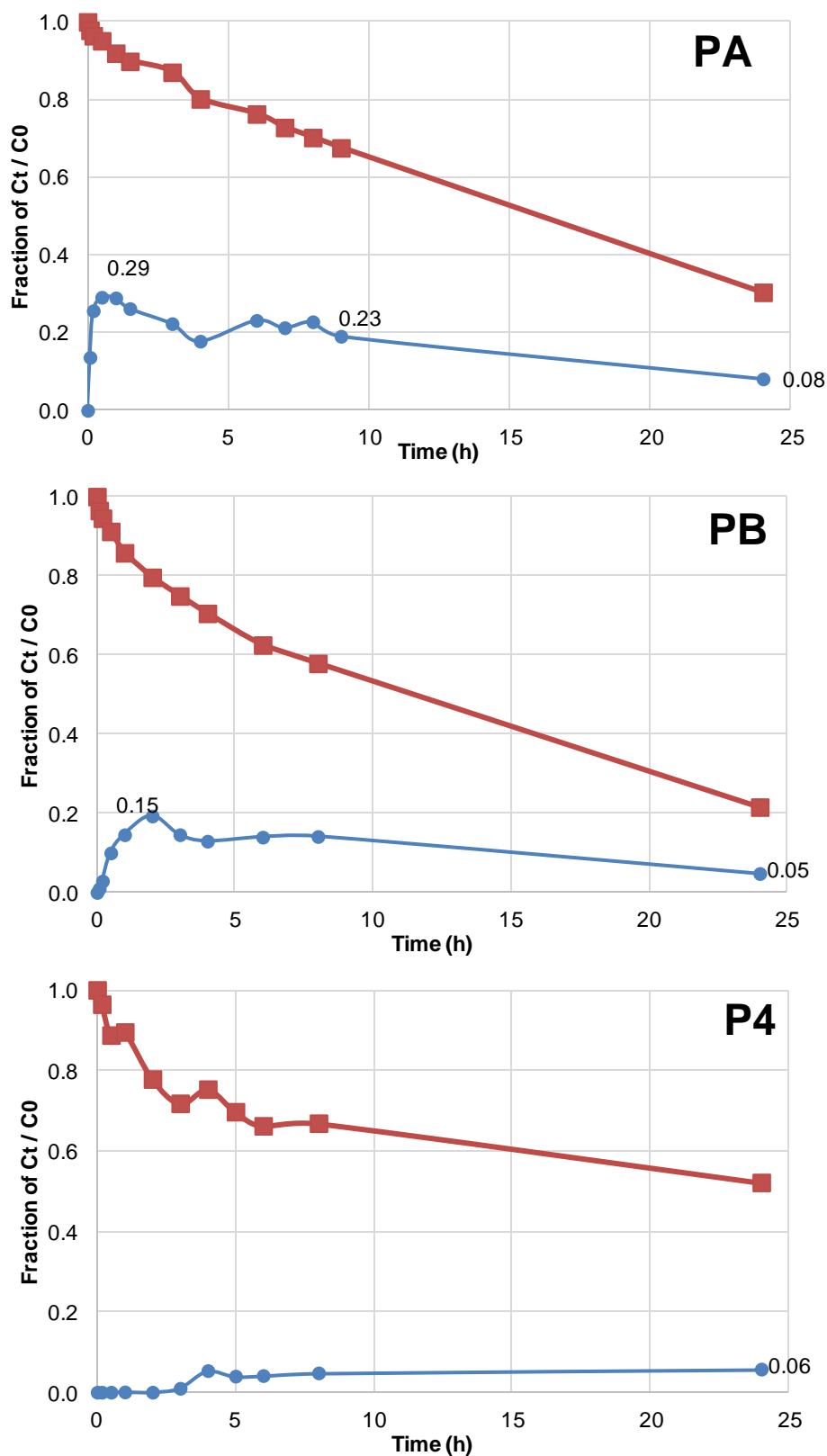


Fig 9-A. Kinetics of trans-chalcone accumulation at pH 7, 50°C for pigments PA, PB and P4, showing the very slow formation in the case of P4. Maximum Ct concentration is reached after 0.5-1 h for PA, 2h for PB and is not reached over 24h for P4 where the Ct formation is slower than its degradation.

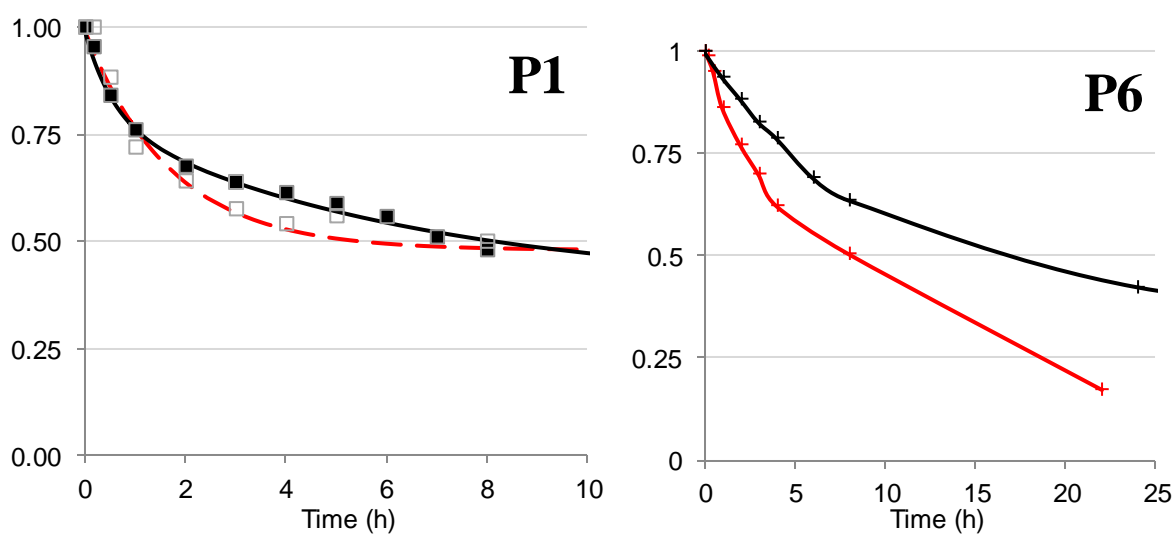


Fig 10-A. Kinetics of pigment loss of P1 and P6 at pH 7 (in black) and pH 8 (in red), at 50°C. The disinapoylated pigment P6 is more impacted by the pH variations than the p-coumaroylated pigment P1. P1 fraction in anionic base is 7.4% at pH 7 and 44% at pH 8 ($pK_{a2} = 7.2$). P6 fraction in anionic base is 13% at pH 7 and 60% at pH 8 ($pK_{a2} = 7.2$).

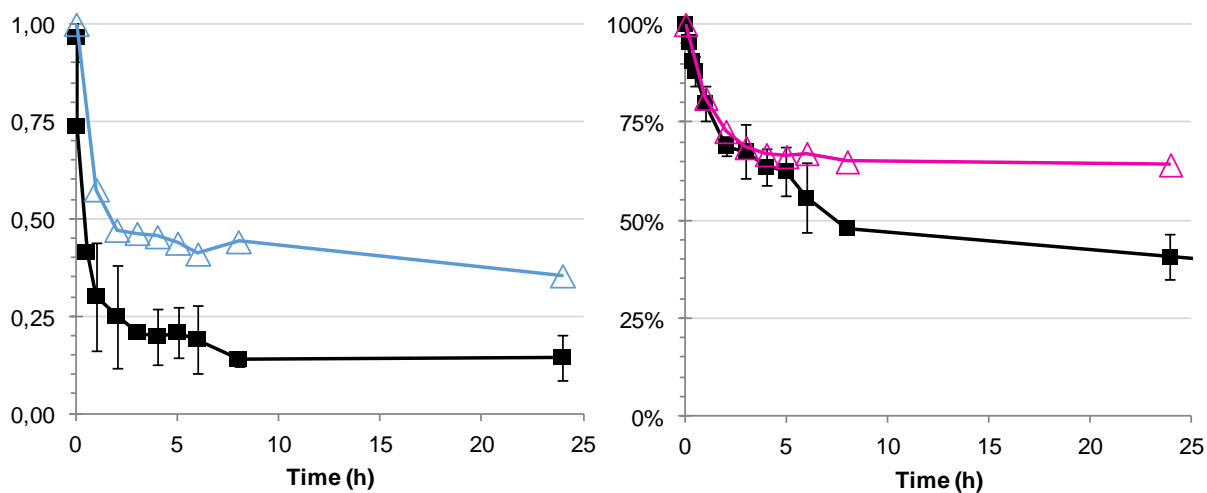


Fig 11-A. Rate of color loss (left) and pigment loss (right) of P1 under air (■) and under an inert atmosphere (△).

Pigment	λ_{\max} (nm)
Patented Blue	637
Brilliant Blue (FD&C 1)	629
Indigo carmine (FD&C 2)	647
Methylene Blue	662

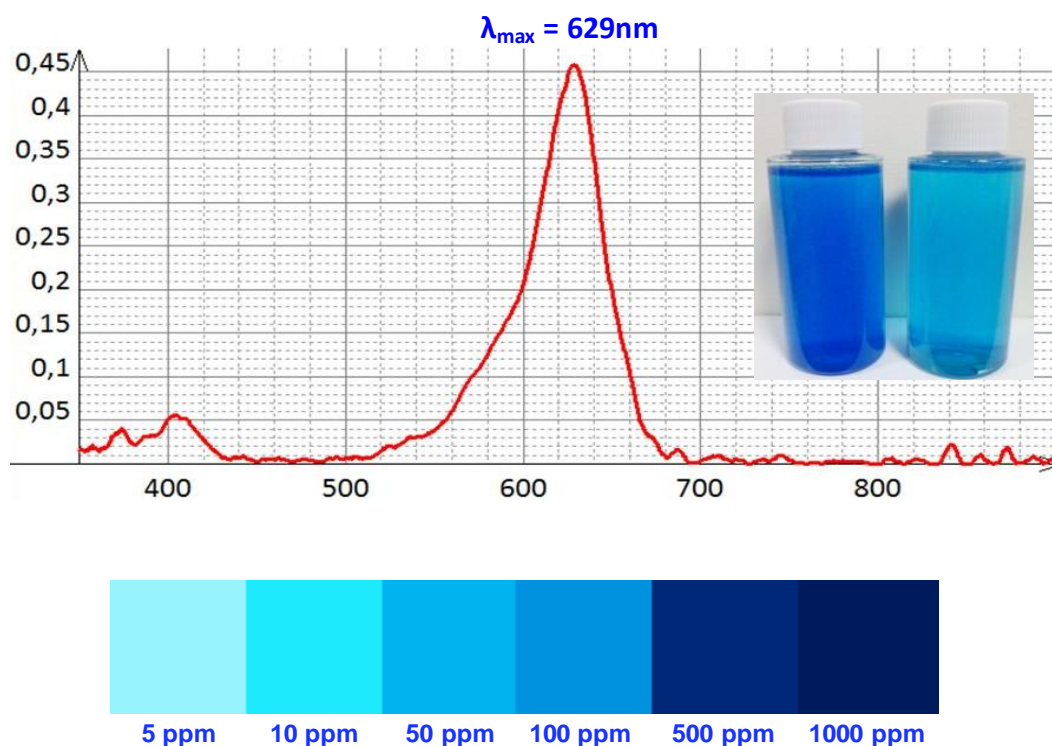
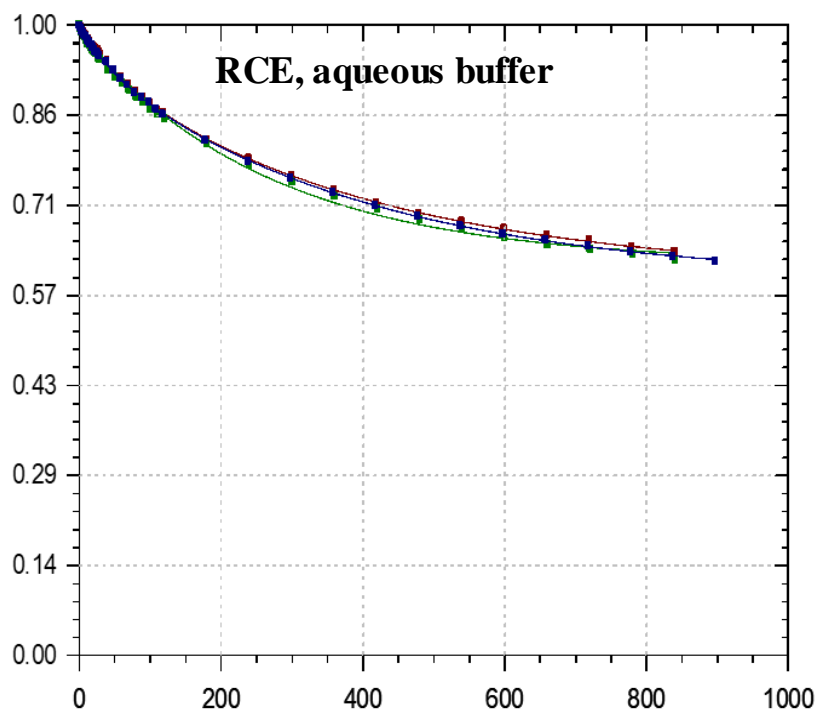
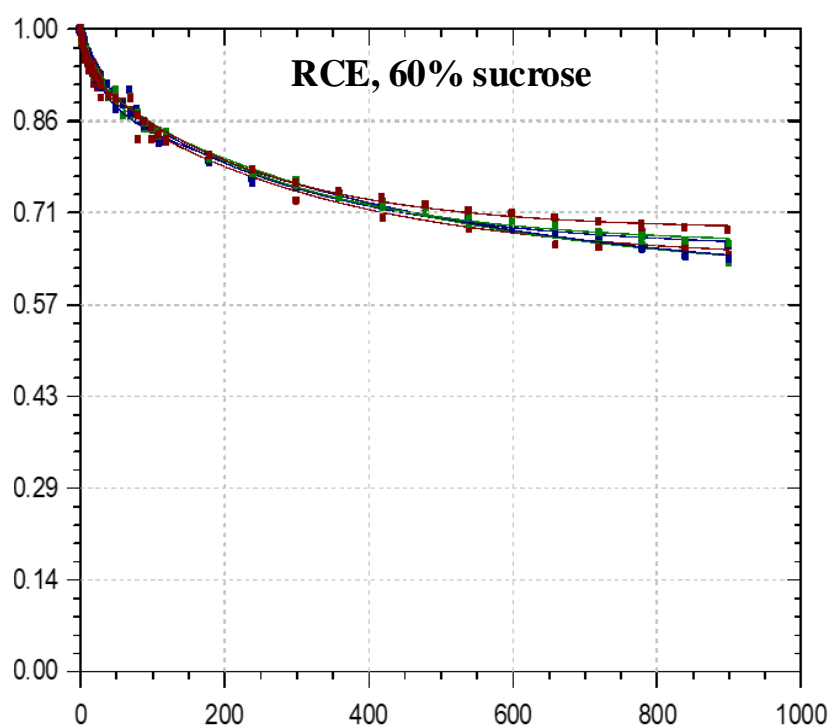


Fig 12-A. Spectral properties of common synthetic pigments and color patches calculated from the $L^*a^*b^*$ coordinates published in US 2016/0015067 A1.



$$k_{\text{obs } 1} = 20 \pm 3 \times 10^3 \text{ s}^{-1}, k_{\text{obs } 2} = 3.0 \pm 0.5 \times 10^3 \text{ s}^{-1}, A_f = 0.64 \pm 0.05 \text{ (N=3)}.$$



$$k_{\text{obs } 1} = 60 \pm 5 \times 10^3 \text{ s}^{-1}, k_{\text{obs } 2} = 3.1 \pm 0.4 \times 10^3 \text{ s}^{-1}, A_f = 0.70 \pm 0.1 \text{ (N=6)}.$$

Fig 13-A. Rate of color loss of RCE, in pH 7 phosphate buffer at room temperature. Top: aqueous buffer, bottom: 60% sucrose buffer. The apparent hydration rate was surprisingly 3-fold higher in sucrose syrup than in aqueous solution. The equilibrium is insignificantly shifted.

Script 1-A. Fitting model used to determine the k_h , k_{-h} and pK_{a1} , with the Scientist[®] software (Micromath, INC., Salt Lake City, USA).

Plot k_{obs} vs pH ($k_1 = k_h$, $k_2 = k_{-h}$)

1) Curve-fitting (pH 3 – 6)

// MicroMath Scientist Model File

IndVars: pH

DepVars: kobs

Params: pKa1,k1,k2

XAH=1/(1+10^{^(pH-pKa1)})

kobs=k1*XAH+k2*10^{^(-pH)}

pKa1=4

k1=0.2

k2=100

1bis) Double curve-fitting k_{obs} & $R = A_f/A_0$ vs pH (pH 3 – 6)

// MicroMath Scientist Model File

IndVars: pH

DepVars: kobs,R

Params: pKa1,k1,k2

XAH=1/(1+10^{^(pH-pKa1)})

kobs=k1*XAH+k2*10^{^(-pH)}

R=(10^{^(-pH)}+10^{^(-pKa1)})/(10^{^(-pH)}+10^{^(-pKa1)}+Kh)

Kh=k1/k2

pKa1=4

k1=0.2

k2=30

2) Simulation (pH 3 – 8)

// MicroMath Scientist Model File

IndVars: pH

DepVars: kobs

Params: k1

XAH=1/(1+10^{^(pH-pKa1)}+10^{^(2*pH-pKa1-pKa2)})

kobs=k1*XAH+k2*10^{^(-pH)}

pKa1=4

pKa2=7

pKh=2.5

k2=k1/10^{^(-pKh)}

k1=0.1

Script 2-A. Exponential models used with the Scientist[®] software.

$k = 1^{\text{st}}$ -order rate constant, $DA = \text{amplitude} = A_0 - A_f$

1) Biexponential decay (color loss, thermal degradation)

/ Modèle biexp1

Independent Variables: T

Dependent Variables: A

Parameters: k1,DA1,k2,DA2

$A = A_0 - DA_1 * (1 - \exp(-k_1 * T)) - DA_2 * (1 - \exp(-k_2 * T))$

$A_0 = 1$

$DA_1 > 0$

$k_1 > 0$

$DA_2 > 0$

$k_2 > 0$

// Parameter values:

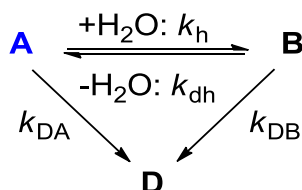
$DA_1 = 0.5$

$k_1 = 1$

$DA_2 = 0.2$

$k_2 = 0.1$

2) Exponential decay with 3 species



Scheme. A simplified model to analyze the color changes occurring in neutral solutions of acylated anthocyanins

A = mixture of colored forms (neutral & anionic bases in fast acid-base equilibrium)

B = mixture of colorless forms

NB: A and B may be (partially) isomerized (acyl transfer) or deacylated

D: mixture of degradation products

X_a : fraction of colored forms in *acidic* conditions (after reacidification), $X_a = A/A_0$ (typically plotted as a function of time on the pigment degradation graphs)

X_n : fraction of colored forms in *neutral* conditions (before reacidification), $X_n = A/A_0$ (typically plotted as a function of time on the color graphs)

X_h : fraction of colorless *hydrated* forms in neutral conditions (before reacidification)

X_d : fraction of colorless *degraded* forms in neutral conditions

$1 = X_a + X_d = X_n + X_h + X_d \Rightarrow X_a = X_n + X_h$

Independent Variables: T

Dependent Variables: X_n, X_h, X_d

Parameters: k_h, k_{dh}, k_{da}

$1 = X_a + X_d$

$1 = X_n + X_h + X_d$

$X_d = 1 - X_a$
 $X_h = 1 - X_n - X_d$
 $X_d' = k_{da} * X_n + k_{db} * X_h$
 $-X_n' = (k_{da} + k_h) * X_n - k_{dh} * X_h$
 $-X_h' = k_{db} * X_h - k_h * X_n - k_{db} * X_h - k_{dh} * X_h$
 $k_{da} > 0$
 $k_{db} = 0$
 $k_h > 0$
 $k_{dh} > 0$
// Parameter values:
 $k_{da} = 0.1$
 $k_h = 1$
 $k_{dh} = 1$
// Initial conditions:
 $T = 0$
 $X_h = 0$
 $X_d = 0$
 $X_n = 0$

Monoexponential growth (trans-chalcone back-isomerization; Job's method of determination of the metal-pigment binding stoichiometry)

Independent Variables: T
Dependent Variables: A
Parameters: k_1, DA_1, k_2, DA_2
 $A = A_0 + DA_1 * (1 - \exp(-k_1 * T)) + DA_2 * (1 - \exp(-k_2 * T))$
 $A_0 = 0.02$
 $DA_1 > 0$
 $k_1 > 0$
 $DA_2 > 0$
 $k_2 > 0$
// Parameter values:
 $DA_1 = 0.4$
 $k_1 = 0.2$
 $DA_2 = 0.3$
 $k_2 = 1E-2$

Script 3-A. Binding model followed by a first order decay

Independent Variables: T

Dependent Variables: A,M,Q,QM1,QM2

Parameters:k1,E1,k2,E2

$$A=A0*Q/5E-5+E1*QM1+E2*QM2$$

$$-Q'=k1*Q*M$$

$$-M'=k1*Q*M$$

$$QM1'=k1*Q*M-k2*QM1$$

$$QM2'=k2*QM1$$

$$k1>0$$

$$E1>0$$

$$k2>0$$

$$E2>0$$

$$A0=0.08$$

// Parameter values:

$$k1=3E3$$

$$E1=4E4$$

$$k2=0.1$$

$$E2=2E4$$

// Initial conditions:

$$T=0$$

$$M=5E-5*2$$

$$Q=5E-5$$

$$QM1=0$$

$$QM2=0$$

NB: The single step binding model is a particular case of this model, with a single QM complex.

Method 1. Determination of the overall hydration and acidity constant pK'_a of 2 groups within an extract

The pK'_a is determined from the pH-dependence of the absorbance of the flavylum ion at the pseudo-equilibrium, measured in UV-visible spectroscopy at room temperature. The presence of two populations with distinct pK'_a gives the following equation:

$$A = x \cdot A_1 \cdot (1 + r_1 \cdot 10^{pH}) / (1 + 10^{pH - pK'_{a1}}) + (1 - x) \cdot A_2 \cdot (1 + r_2 \cdot 10^{pH}) / (1 + 10^{pH - pK'_{a2}})$$

From a determined fraction x corresponding to group 1, the parameters are calculated :

$$\text{Group 1: } pK'_{a1}, A_1 = \varepsilon_1 C, r_1 = (r_A K_{a1})_1$$

$$\text{Group 2: } pK'_{a2}, A_2 = \varepsilon_2 C, r_2 = (r_A K_{a2})_2$$

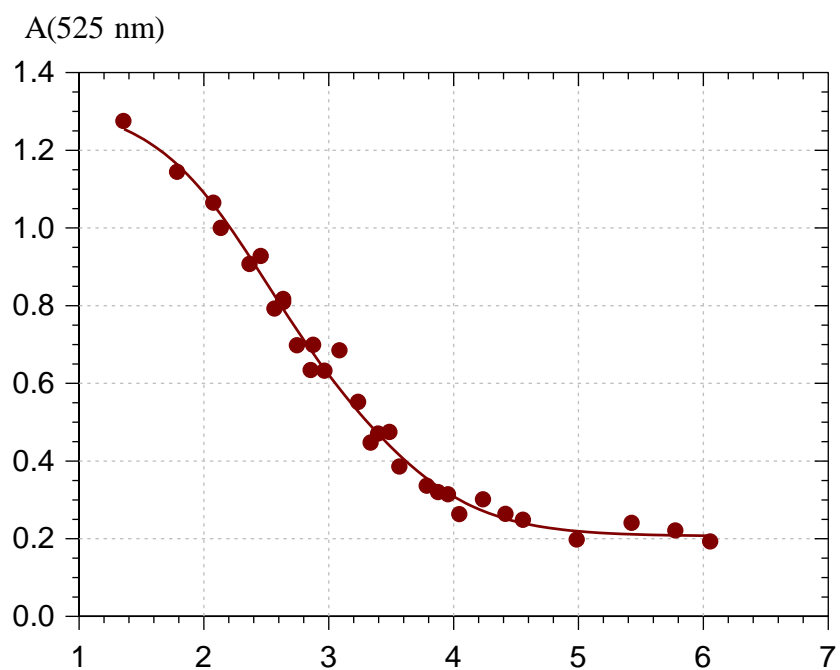
It was hypothesized that within a same group, all anthocyanins have the same K'_a value, and similar absorption coefficients: $A_1 = A_2$, $r_1 = r_2$. This method was used for 4 extracts. The composition of RCE and PSPE were determined in UPLC-DAD/MS (Appendix 3, p. 337), and the composition of the red radish and black carrot extracts were obtained from the literature respectively from (Pu Jing et al., 2012; Montilla et al., 2011) (references below). The results are presented in Table 6-A and Fig. 7-A.

Table. Calculated pK'_a values, fraction of acylated anthocyanins are in parenthesis.

	pK'_a (NAA)	pK'_a (MAA)	pK'_a (DAA)	R^2
RCE		2.39 (60%)	3.5 (40%)	0.998
PSPE**		2.04 (14%)	3.55 (86%)	0.999
Red radish		1.9 (12%)	3.41 (88%)	0.998
Black carrot	3.07 (35%)	4.05 (65%)		0.997

**Partially purified extract, for contaminants elimination.

Crude RCE



Purified PSPE

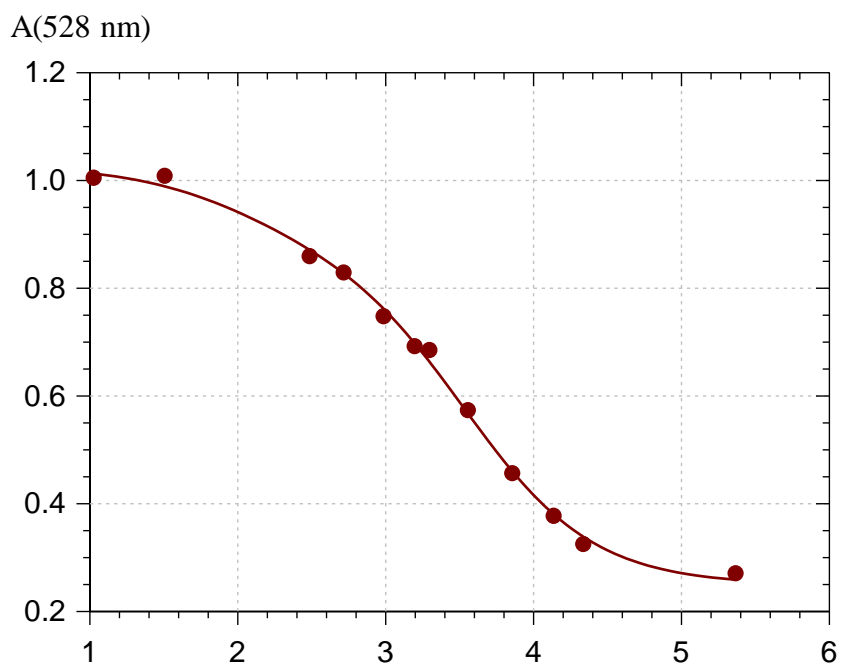
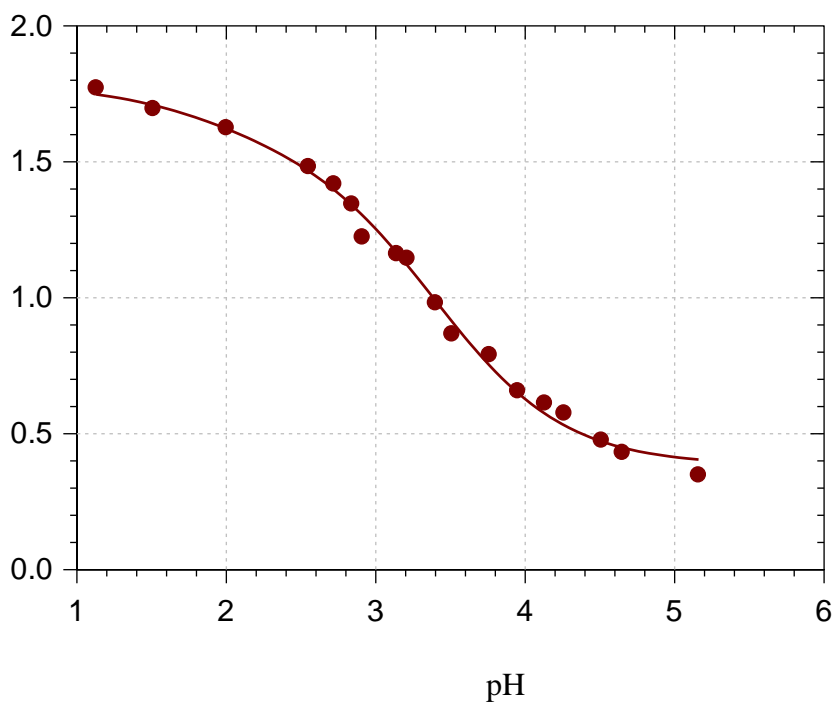


Fig 8-A. A(AH⁺) as a function of the pH used for the determination of pK'a of 2 groups within the extract. (continued next page)

Red Radish

A(512 nm)



Purple Carrot

A(521 nm)

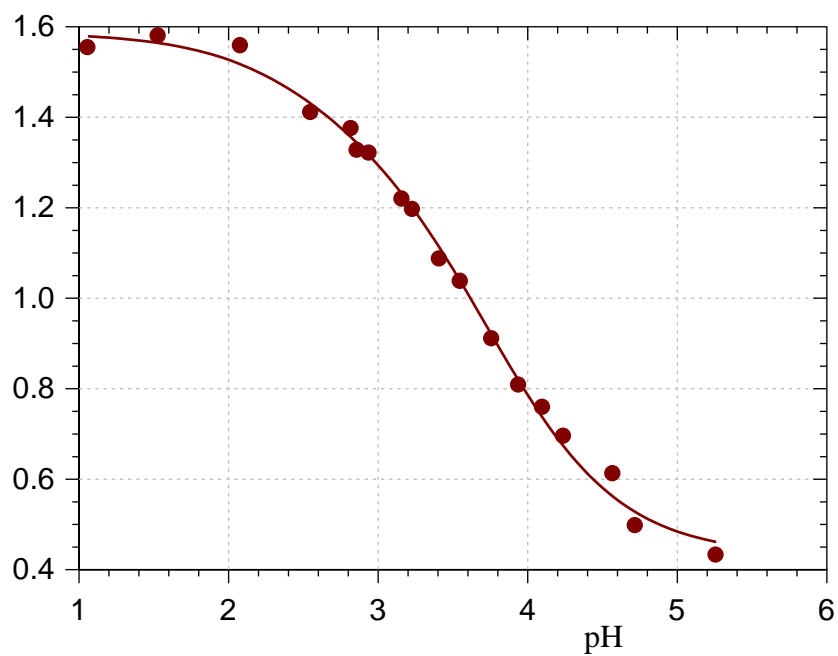


Fig 8-A. A(AH⁺) as a function of the pH used for the determination of pK'a of 2 groups within the extract.

Method 2. Calculation of the pure spectra of an individual anthocyanin.

For each individual pigment, spectra were measured at $\text{pH} \approx 1$; $\text{pH} \approx 5$ and $\text{pH} \approx 8$ at $t = 0$ (negligible hydration). The spectrum obtained at $\text{pH} 1$ corresponds to that of the pure flavylum ion: $A(\text{pH } 1) \approx A_{\text{AH}^+}$. The spectra of the pure neutral base and anionic base were determined from the fractions of colored species calculated from the two acidity constants.

At $\text{pH } 5$, because $\text{pH} \ll \text{p}K_{a2}$, the concentration in anionic base can be neglected:

$x_{\text{A}} = 1 - x_{\text{AH}^+}$. From the absorption spectrum measured at $\text{pH } 5$, thanks to the additive property of absorbance in the range studied, at each wavelength we can express the total absorbance as: $A(\text{pH } 5) = A_{\text{AH}^+} x_{\text{AH}^+} + A_{\text{A}} x_{\text{A}}$

Thus, we extract the spectrum of the pure neutral base: $A_{\text{A}} = \frac{A(\text{pH } 5) - A_{\text{AH}^+} x_{\text{AH}^+}}{1 - x_{\text{AH}^+}}$

with $x_{\text{AH}^+} = \frac{1}{1 + K_{a1}/[\text{H}^+]} = \frac{1}{1 + 10^{\text{pH} - \text{p}K_{a1}}}$.

Similarly, at $\text{pH } 8$ the concentration in flavylum can be neglected:

$A(\text{pH } 8) = A_{\text{A}} x_{\text{A}} + A_{\text{A}^-} x_{\text{A}^-}$

Thus, the spectrum of pure anionic base is deduced from: $A_{\text{A}^-} = \frac{A(\text{pH } 8) - A_{\text{A}} x_{\text{A}}}{1 - x_{\text{A}}}$

with $x_{\text{A}} = \frac{1}{1 + K_{a2}/[\text{H}^+]} = \frac{1}{1 + 10^{\text{pH} - \text{p}K_{a2}}}$

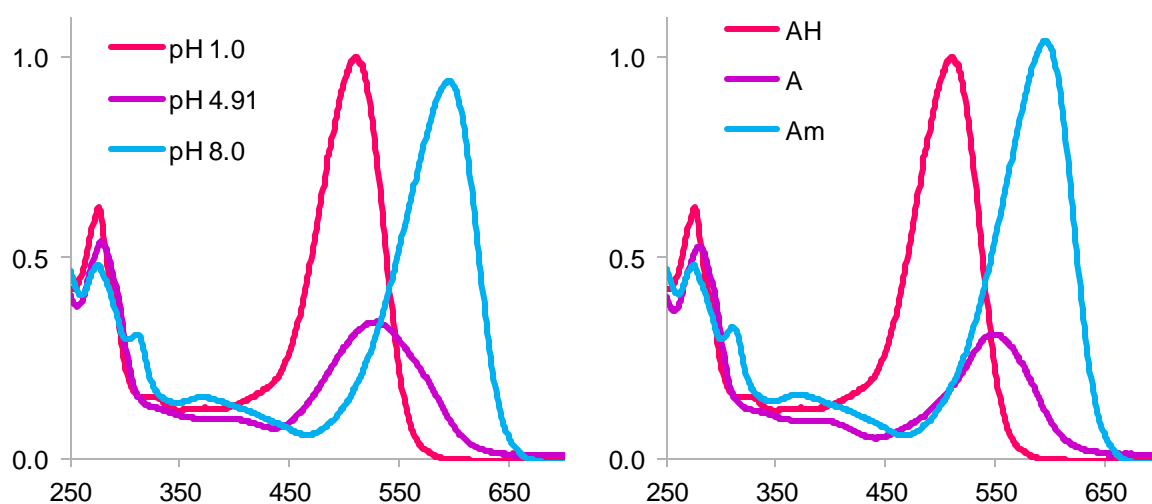


Figure. Comparison of the measured and calculated spectra of the individual species in PA'. AH = flavylum, A = neutral base, Am = anionic base. $\text{pH } 1 = \text{HCl } 0.1 \text{ M}$, $\text{pH } 4.91$ in acetate buffer, $\text{pH } 8.0$ in phosphate buffer. pH after pigment addition.

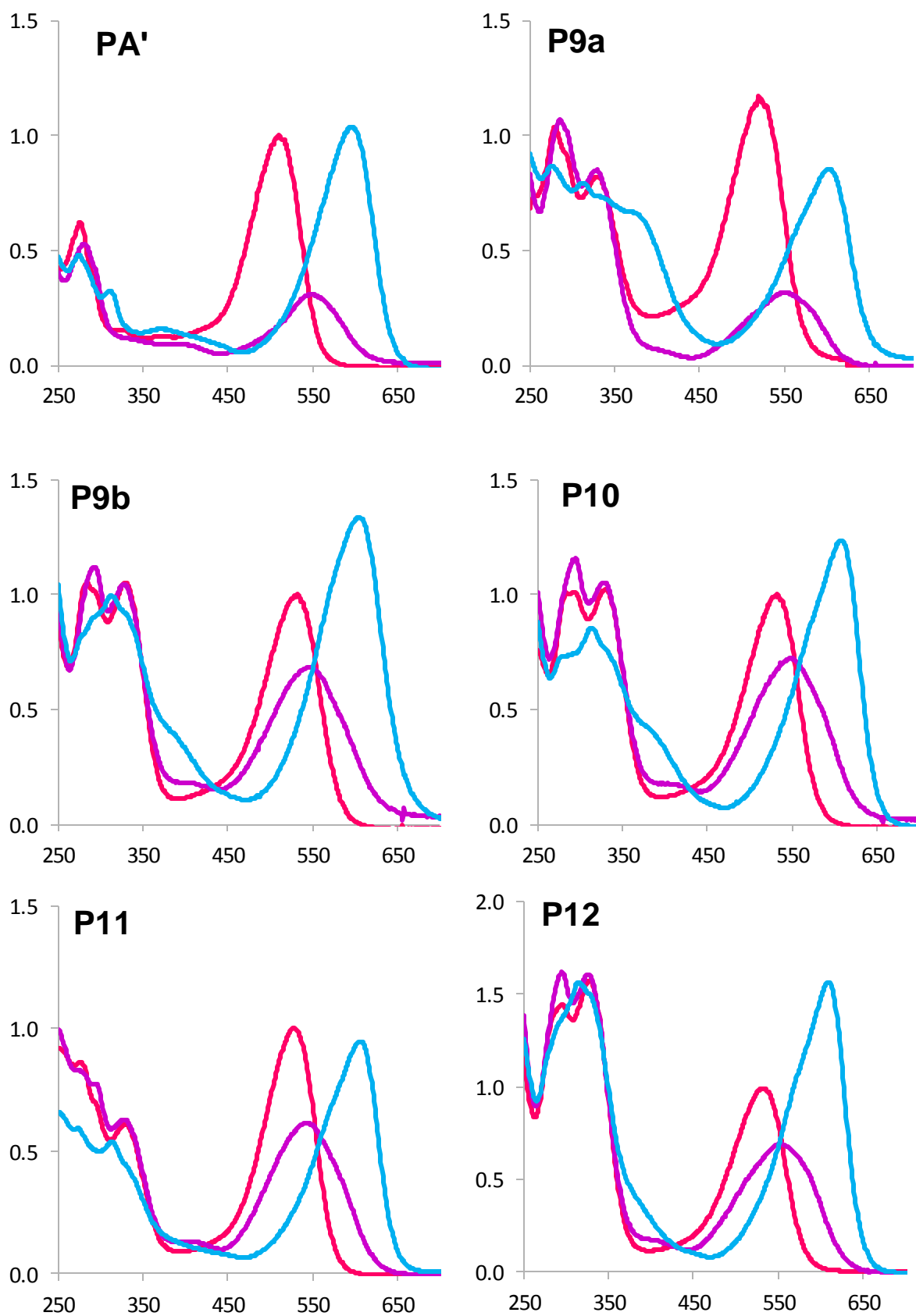
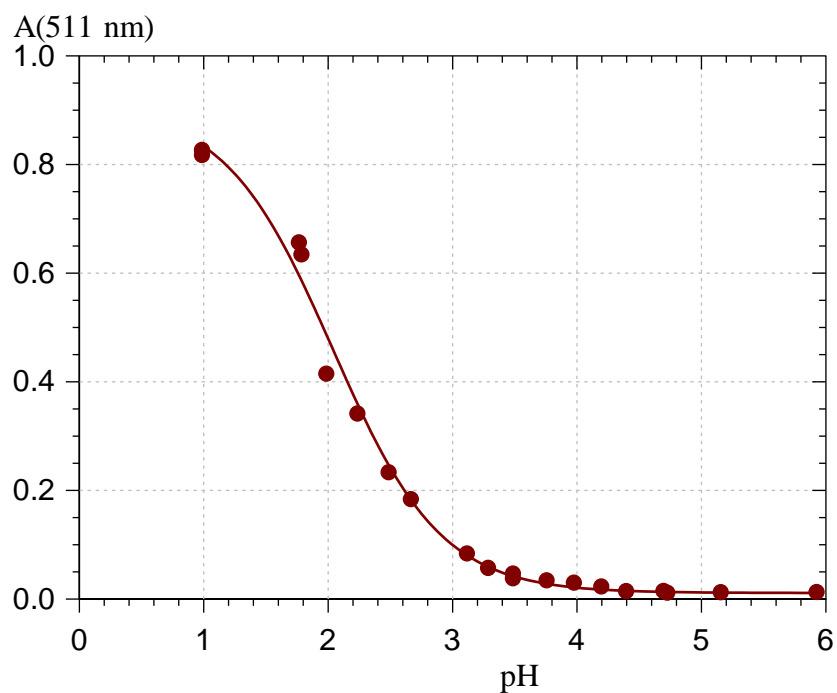
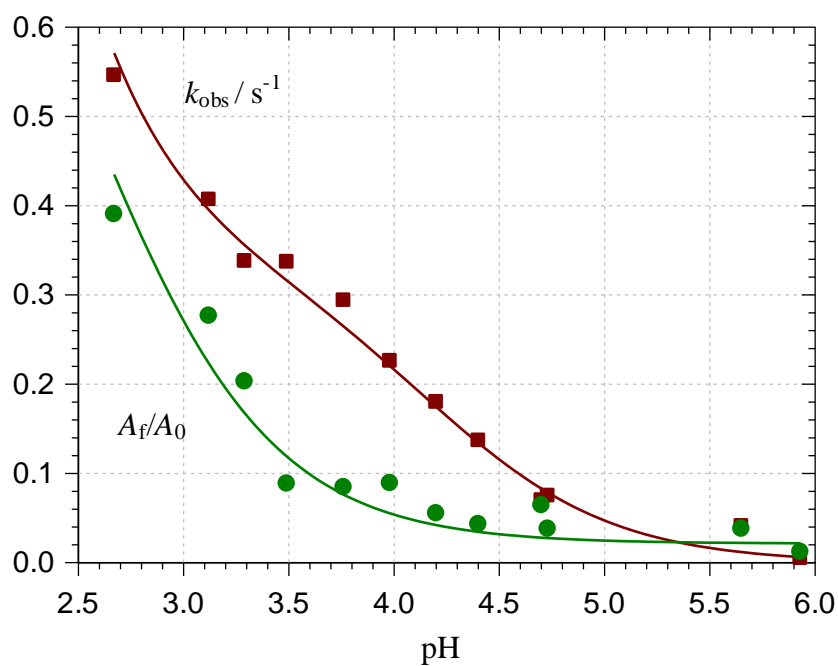


Fig 10-A. Calculated spectra the 3 forms: flavylum, neutral base and anionic base of 6 individual PSPE pigments, at $t=0$.

PA' = Peonidin-3-O-Soph-5Glc



$r = 0.996$, $\text{pK}'_a = 2.04 (\pm 0.04)$, $A_0 = 0.91 (\pm 0.02)$, $r_A K_{a1} = 11.3 (\pm 8.8) \times 10^{-5}$



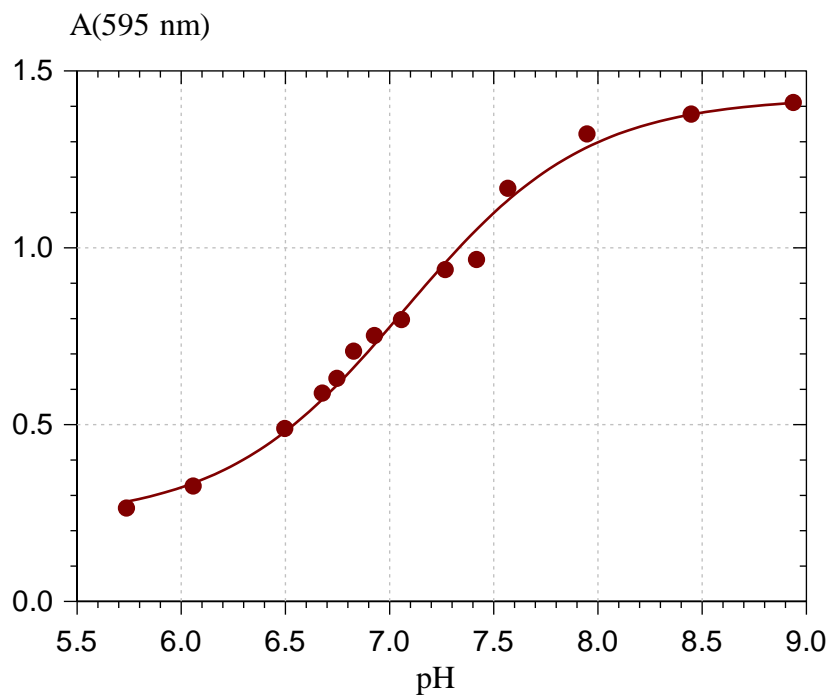
■: k_{obs} , $r = 0.995$. ●: A_f/A_0 , $r = 0.97$

$\text{pK}_{a1} = 4.21 (\pm 0.08)$, $k_h = 0.33 (\pm 0.01) \text{ s}^{-1}$, $k'_h = 116 (\pm 7) \text{ M}^{-1} \text{ s}^{-1}$

$\Rightarrow K_h = k_h/k'_h = 2.8 \times 10^{-3}$, $\text{pK}_h = 2.54$ (Ct excluded)

$K'_a = K'_h + K_{a1} \Rightarrow \text{pK}'_h \approx \text{pK}'_a = 2.04$ (Ct included)

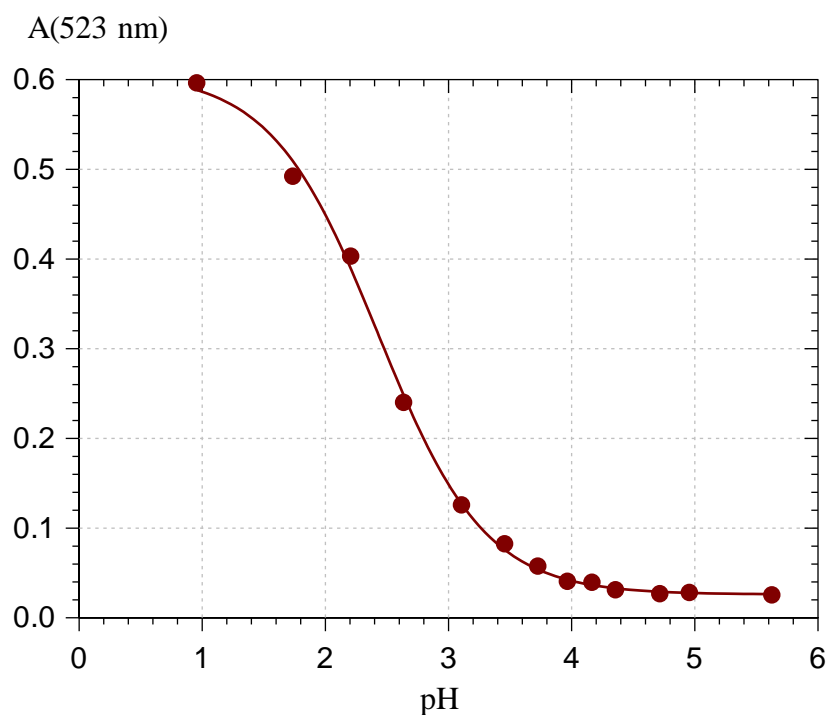
Fig 11-A. Data fitting for the determination of pK'_a , k_h , k'_h , pK'_h , pK_{a1} and pK_{a2} constants, for pigment PA' isolated from the purple sweet potato extract. (continued next page)



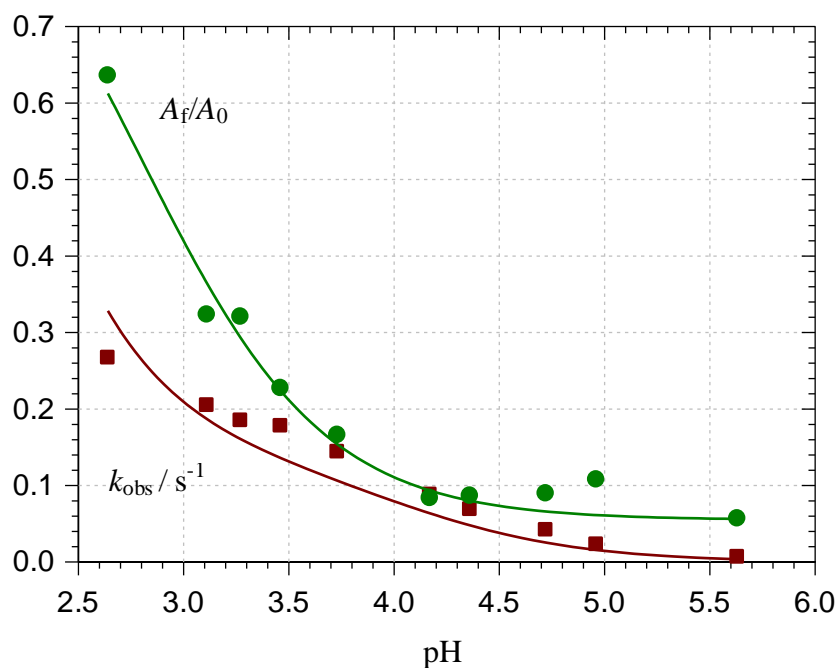
$r = 0.996$, $\text{p}K_{\text{a}2} = 7.08 (\pm 0.04)$, $A_0 = 0.23 (\pm 0.03)$, $r_A = 6.2 (\pm 0.8)$

Fig 11-A. Data fitting for the determination of $\text{p}K'_{\text{a}}$, k_{h} , $k_{\text{-h}}$, $\text{p}K'_{\text{h}}$, $\text{p}K_{\text{a}1}$ and $\text{p}K_{\text{a}2}$ constants, for pigment PA' isolated from the purple sweet potato extract.

P9a = Peonidin-3-O-Soph(Cf)-5Glc



$r = 0.999$, $\text{pK}'_a = 2.43 (\pm 0.02)$, $A_0 = 0.61 (\pm 0.01)$, $r_A K_{a1} = 16.0 (\pm 2.4) \times 10^{-5}$



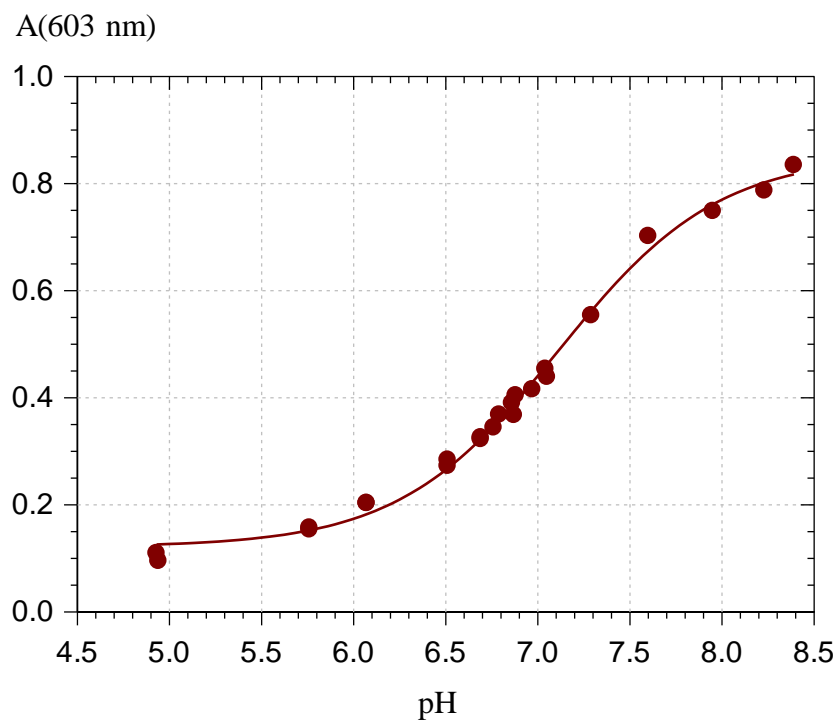
■: k_{obs} , $r = 0.96$. ●: A_f/A_0 , $r = 0.991$

$\text{pK}_{a1} = 4.06 (\pm 0.12)$, $k_h = 0.132 (\pm 0.011) \text{ s}^{-1}$, $k'_{-h} = 87.8 (\pm 6.6) \text{ M}^{-1} \text{ s}^{-1}$

$\Rightarrow K_h = k_h/k_{-h} = 1.5 \times 10^{-3}$, $\text{pK}_h \approx 2.82$ (Ct excluded)

$K'_a = K'_h + K_{a1} \Rightarrow \text{pK}'_h \approx \text{pK}'_a = 2.43$ (Ct included)

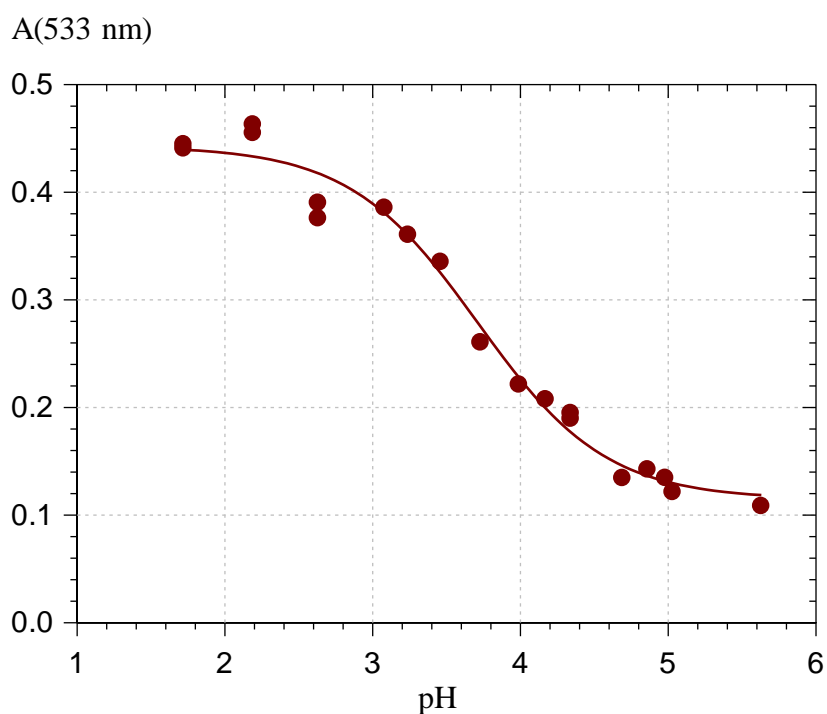
Fig 12-A. Data fitting for the determination of pK'_a , k_h , k_{-h} , pK'_h , pK_{a1} and pK_{a2} constants, for pigment P9A isolated from the purple sweet potato extract. (continued next page)



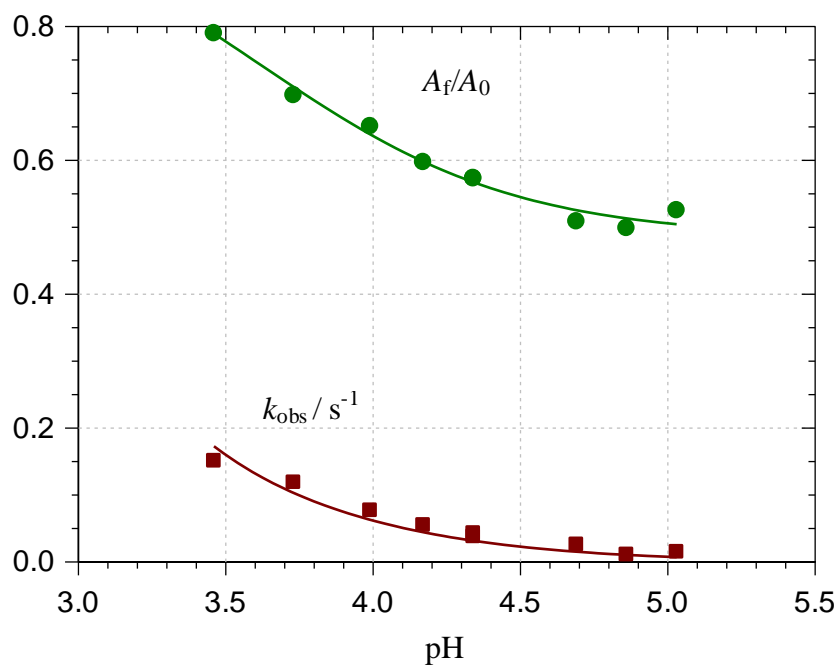
$r = 0.997$, $pK_{a2} = 7.11 (\pm 0.02)$, $A_0 = 0.12 (\pm 0.01)$, $r_A = 7.0 (\pm 0.4)$

Fig 12-A. Data fitting for the determination of pK'_a , k_h , k_{-h} , pK'_h , pK_{a1} and pK_{a2} constants, for pigment P9A isolated from the purple sweet potato extract.

P9b = Cyanidin-3-O-Soph(Cf,Fl)-5Glc



$r = 0.991$, $\text{pK}'_a = 3.71 (\pm 0.07)$, $A_0 = 0.44 (\pm 0.01)$, $r_A K_{a1} = 5.0 (\pm 1.1) \times 10^{-5}$



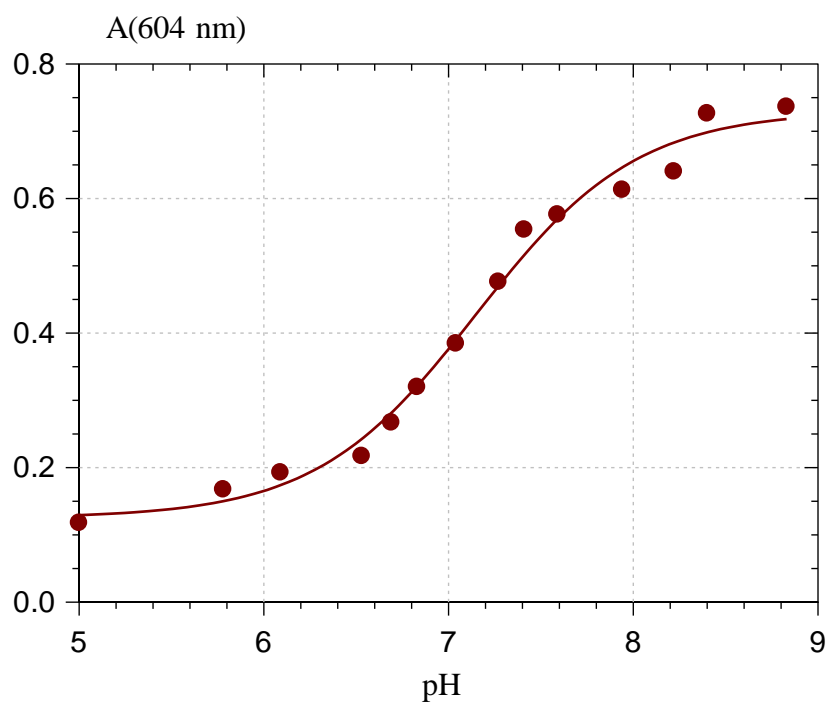
■: k_{obs} , $r = 0.98$. ●: A_t/A_0 , $r = 0.991$

$\text{pK}_{a1} = 3.93 (\pm 0.04)$, $k_h = 0.049 (\pm 0.004) \text{ s}^{-1}$, $k'_{-h} = 394 (\pm 24) \text{ M}^{-1} \text{ s}^{-1}$

$\Rightarrow K_h = k_h/k'_{-h} = 1.2 \times 10^{-4}$, $\text{pK}_h \approx 3.91$ (Ct excluded)

$K'_a = K'_h + K_{a1} \Rightarrow \text{pK}'_h \approx 4.11$ (Ct included, *should be lower than 3.9*)

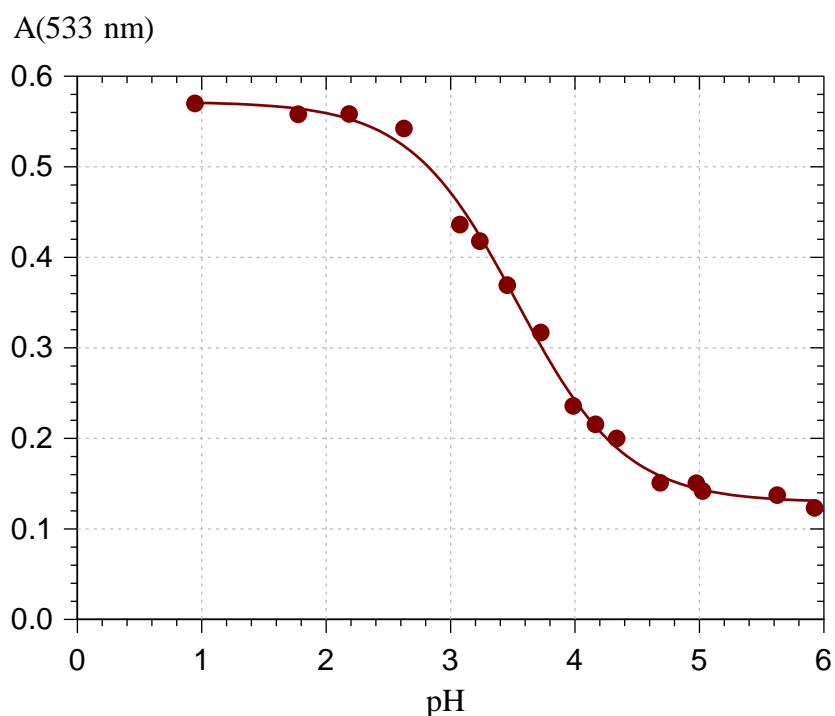
Fig 13-A. Data fitting for the determination of pK'_a , k_h , k_{-h} , pK'_h , pK_{a1} and pK_{a2} constants, for pigment P9b isolated from the purple sweet potato extract (*continued next page*)



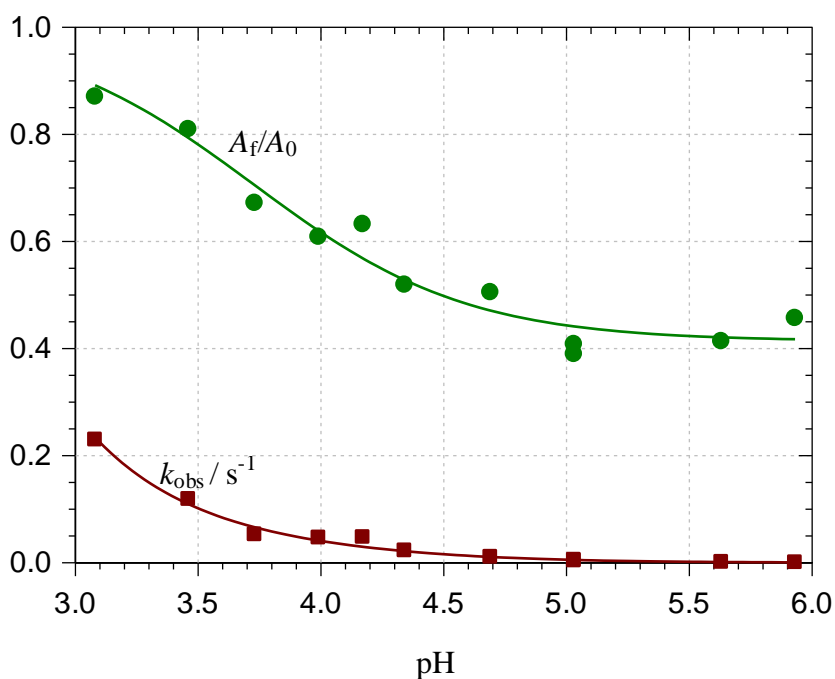
$r = 0.994$, $\mathbf{pK_{a2} = 7.15}$ (± 0.06), $A_0 = 0.13$ (± 0.02), $r_A = 5.8$ (± 0.7)

Fig 13-A. Data fitting for the determination of pK'_a , k_h , k_{-h} , pK'_h , pK_{a1} and pK_{a2} constants, for pigment P9b isolated from the purple sweet potato extract.

P10 = Peonidin-3-O-Soph(Cf,Cf)-5Glc



$r = 0.998$, $\text{pK}'_a = 3.53 (\pm 0.03)$, $A_0 = 0.57 (\pm 0.01)$, $r_A K_{a1} = 6.6 (\pm 0.6) \times 10^{-5}$



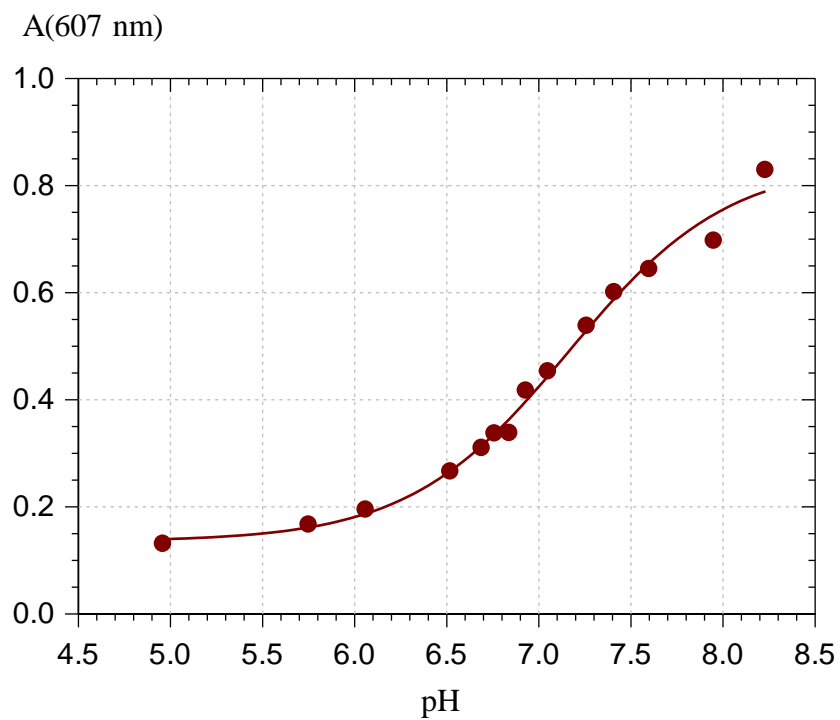
■: k_{obs} , $r = 0.994$. ●: A_i/A_0 , $r = 0.98$

$\text{pK}_{a1} = 4.11 (\pm 0.06)$, $k_h = 0.028 (\pm 0.004) \text{ s}^{-1}$, $k'_{-h} = 251 (\pm 25) \text{ M}^{-1} \text{ s}^{-1}$

$\Rightarrow K'_h = k_h/k_{-h} = 1.1 \times 10^{-4}$, $\text{pK}'_h \approx 3.95$ (Ct excluded)

$K'_a = K'_h + K_{a1} \Rightarrow \text{pK}'_h \approx 3.66$ (Ct included)

Fig 14-A. Data fitting for the determination of pK'_a , k_h , k_{-h} , pK'_h , pK_{a1} and pK_{a2} constants, for pigment P10 isolated from the purple sweet potato extract. (continued next page)

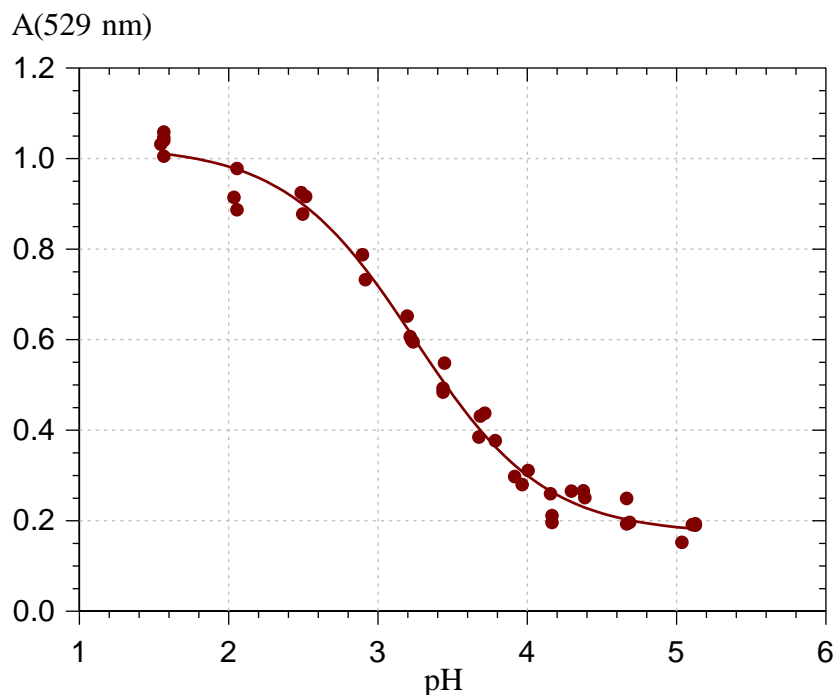


$r = 0.995$, $\text{p}K_{\text{a}2} = 7.16 (\pm 0.05)$, $A_0 = 0.14 (\pm 0.01)$, $r_A = 6.3 (\pm 0.6)$

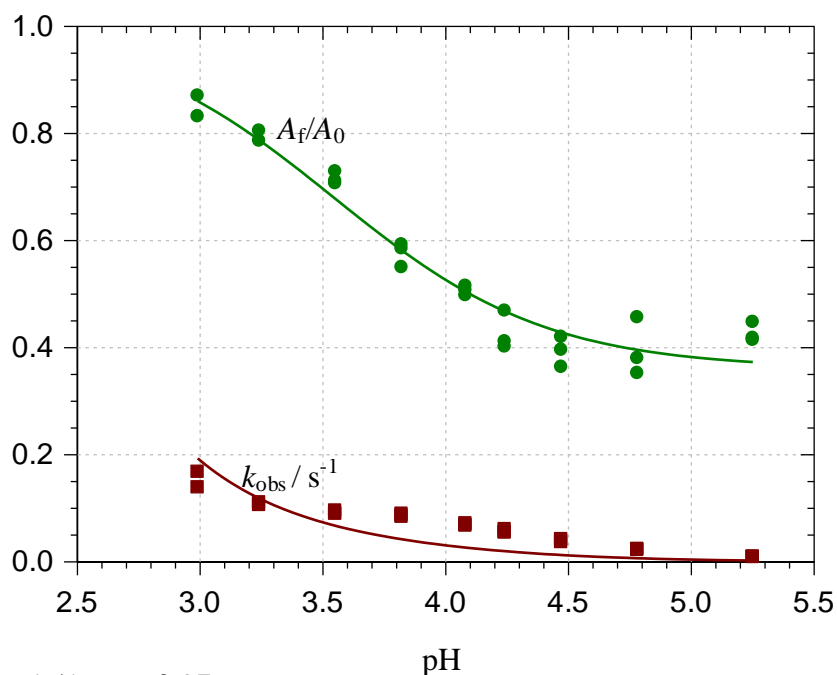
Fig 14-A. Data fitting for the determination of $\text{p}K'_{\text{a}}$, k_{h} , $k_{\text{-h}}$, $\text{p}K'_{\text{h}}$, $\text{p}K_{\text{a}1}$ and $\text{p}K_{\text{a}2}$ constants, for pigment P10 isolated from the purple sweet potato extract.

P11 = Peonidin-3-O-Soph(HB,Cf)-5Glc

3 repetitions



$r = 0.97$, $\text{pK}'_a = 3.25 (\pm 0.03)$, $A_0 = 1.03 (\pm 0.01)$, $r_A = 9.4 (\pm 1.1) \times 10^{-5}$



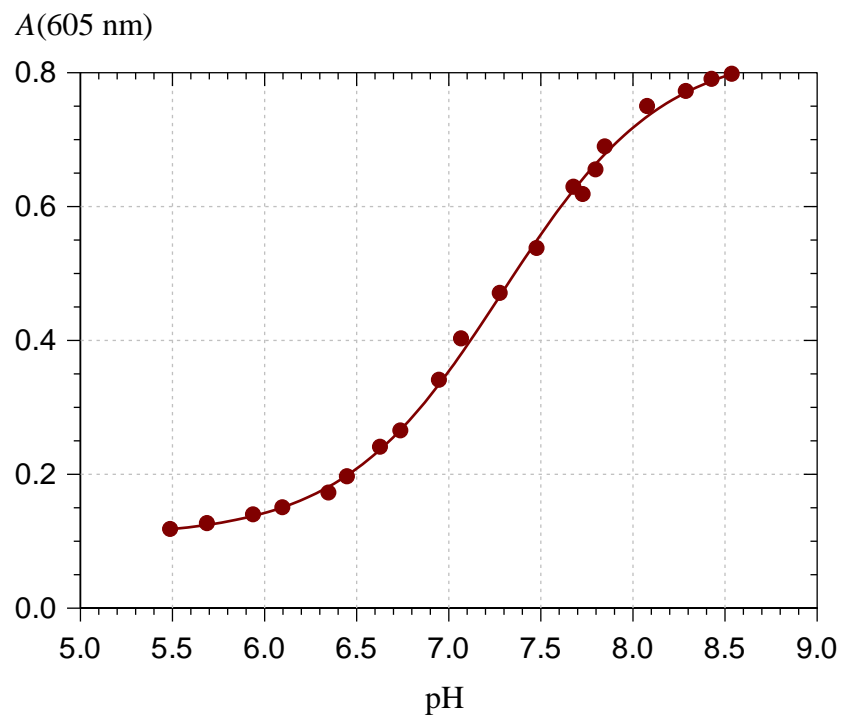
■: k_{obs} , $r = 0.91$. ●: A_f/A_0 , $r = 0.97$

$\text{pK}_{a1} = 3.99 (\pm 0.06)$, $k_h = 297 (\pm 37) \times 10^{-4} \text{ M}^{-1} \text{ s}^{-1}$, $k'_{-h} = 162 (\pm 16) \text{ s}^{-1}$

$\Rightarrow K_h = k_h/k'_{-h} = 1.8 \times 10^{-4}$, $\text{pK}_h = 3.74$ (Ct excluded)

$K'_a = K'_h + K_{a1} \Rightarrow K'_h = 4.6 \times 10^{-4}$, $\text{pK}'_h = 3.34$ (Ct included)

Fig 15-A. Data fitting for the determination of pK'_a , k_h , k_{-h} , pK'_h , pK_{a1} and pK_{a2} constants, for pigment P11 isolated from the purple sweet potato extract. (continued next page)

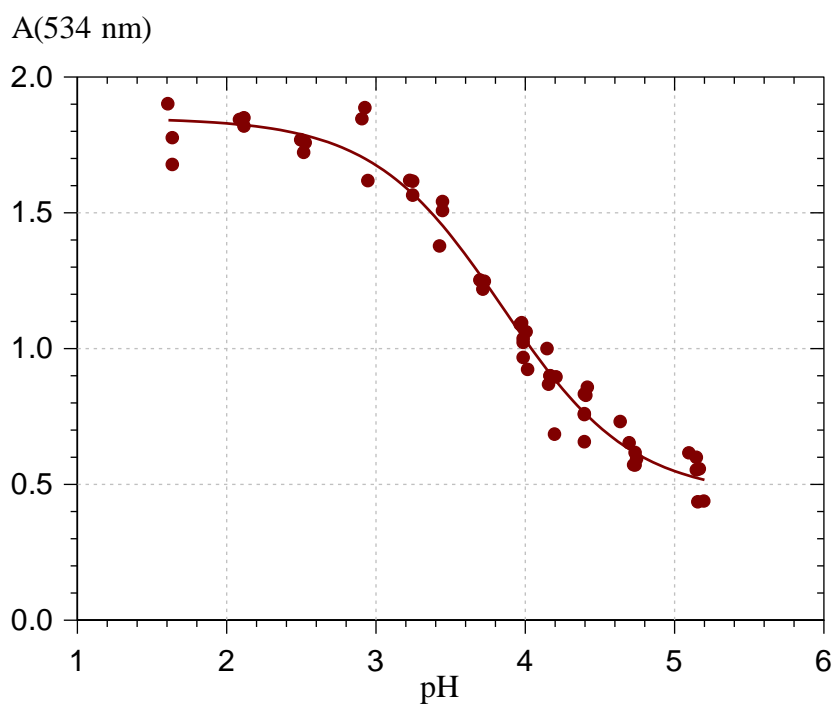


$\text{pK}_{a2} = 7.29 (\pm 0.02)$, $A_0 = 0.107 (\pm 0.05)$, $r_A = 7.85 (\pm 0.36)$, $r = 0.9993$

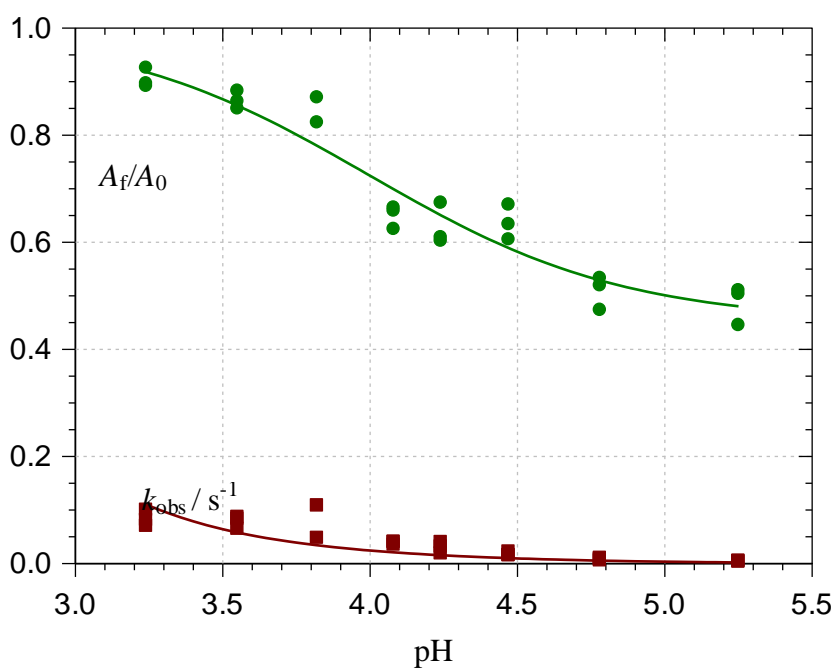
Fig 15-A. Data fitting for the determination of pK'_a , k_h , k_{-h} , pK'_h , pK_{a1} and pK_{a2} constants, for pigment P11 isolated from the purple sweet potato extract.

P12 = Peonidin-3-O-Soph(Fl,Cf)-5Glc

3 repetitions



$r = 0.988$, $\text{pK}'_a = 3.85 (\pm 0.04)$, $A_0 = 1.85 (\pm 0.02)$, $r_A = 3.5 (\pm 0.5) \times 10^{-5}$



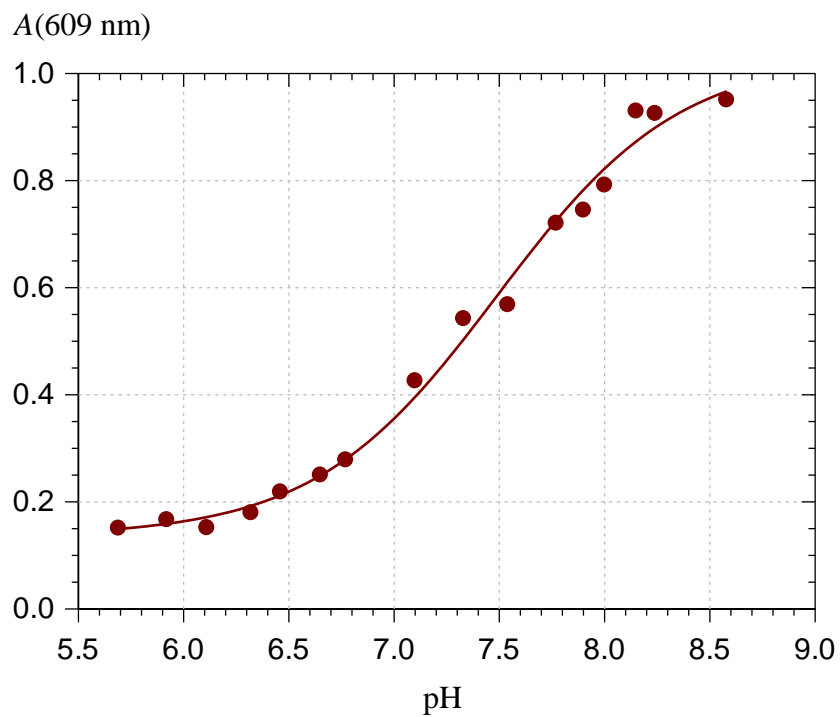
■: k_{obs} , $r = 0.81$. ●: A_f/A_0 , $r = 0.96$

$\text{pK}_{a1} = 4.34 (\pm 0.07)$, $k_h = 98 (\pm 17) \times 10^{-4} \text{ M}^{-1} \text{ s}^{-1}$, $k'_{-h} = 176 (\pm 27) \text{ s}^{-1}$

$\Rightarrow K_h = 5.6 \times 10^{-5}$, $\text{pK}_h = 4.25$ (Ct excluded)

$K'_a = K'_h + K_{a1} \Rightarrow K'_h = 9.6 \times 10^{-5}$, $\text{pK}'_h = 4.02$ (Ct included)

Fig 16-A. Data fitting for the determination of pK'_a , k_h , k_{-h} , pK'_h , pK_{a1} and pK_{a2} constants, for pigment P12 isolated from the purple sweet potato extract. (continued next page)



$\text{pK}_{a2} = 7.49 (\pm 0.05)$, $A_0 = 0.135 (\pm 0.015)$, $r_A = 7.64 (\pm 0.80)$, $r = 0.996$

Fig 16-A. Data fitting for the determination of pK'_a , k_h , k_{-h} , pK'_h , pK_{a1} and pK_{a2} constants, for pigment P12 isolated from the purple sweet potato extract.

Method 3. Prediction of acylated anthocyanin color in the pH range 1 - 8

Highlights

Based on the acidity and hydration kinetic and thermodynamic constants of isolated anthocyanins, their theoretical spectra at all pH in the range 1 to 8 could be generated, as well as the calculation of the L*a*b coordinated, and color patches.

The current method is able to predict the color at the equilibrium in aqueous applications, at pH between 1 and 8, for individual pigments from red cabbage and purple sweet potato, and any mixture thereof.

Method

- Determination of the pK'a acidity and hydration kinetic and thermodynamic constants of isolated anthocyanins (Table 2-A, under press (Moloney et al., 2018))
- Calculation of the spectra of the individual colored species (based on the spectra recorded at pH 1, 5, 8)
- Speciation at the target pH (Calculation of the fraction in flavylum ion; neutral base and anionic base)
- Spectral prediction at any pH (by combining the spectra of the pure species and their fraction at their hydration pseudo-equilibrium)
- Spectral conversion to L*a*b coordinates, and elaboration of a color patch

Domain of validity

- On any individual pigments among these tested from red cabbage or purple sweet potato, and extracts thereof.
- Within the pH range 1 - 8
- In aqueous solutions
- At room temperature

Examples of results: P2 and P5.

1. Calculation of the spectra

For the composition at $t=0$, from the pK_{a1} , pK_{a2} , the pH-dependence of the fraction in neutral base (x_A) and anionic base (x_{AM}) is determined with:

$$x_A(pH5) = \frac{1}{1 + 10^{pH - pKa1}} \quad \text{and} \quad x_{AM}(pH8) = \frac{1}{1 + 10^{pH - pKa1} + 10^{2(pH - pKa1 - pKa2)}}$$

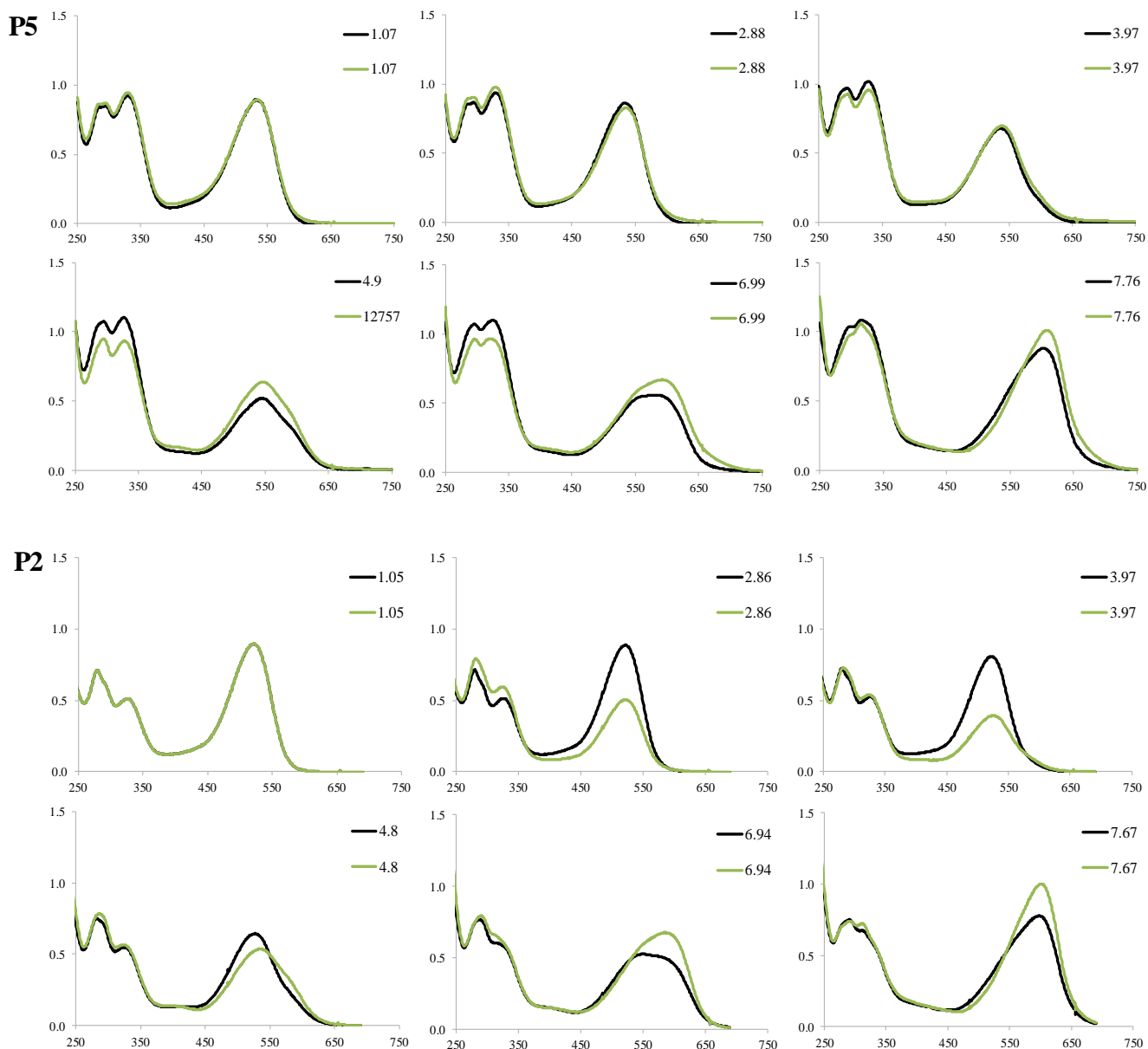


Fig 17-A. Predicted spectra vs. actual spectra for P5 (top) and P2 (bottom), at a theoretical $t=0$.

2) Spectral conversion to L^*a^*b coordinates, and elaboration of a color patch

Table. Predicted (top) vs. measured (bottom) L^*a^*b values for P5 at $t=0$.

pH	L^*	a^*	b^*	Cab^*	Hab^*
Prediction					
1.07	72.36	60.41	-15.31	62.32	345.8
2.88	72.21	58.64	-16.33	60.87	344.4
3.97	72.15	46.35	-21.15	50.95	335.5
4.9	73.59	30.80	-23.70	38.86	322.4
6.99	68.88	11.54	-32.40	34.39	289.6
7.76	64.09	-3.71	-39.54	39.71	264.6
Result					
1.07	65.84	67.06	-14.19	68.55	348.1
2.88	65.90	64.03	-17.91	66.48	344.4
3.97	63.37	53.45	-26.44	59.63	333.7
4.9	60.84	43.80	-33.95	55.41	322.2
6.99	57.23	8.98	-42.59	43.53	281.9
7.76	58.04	-15.95	-43.52	46.35	249.9

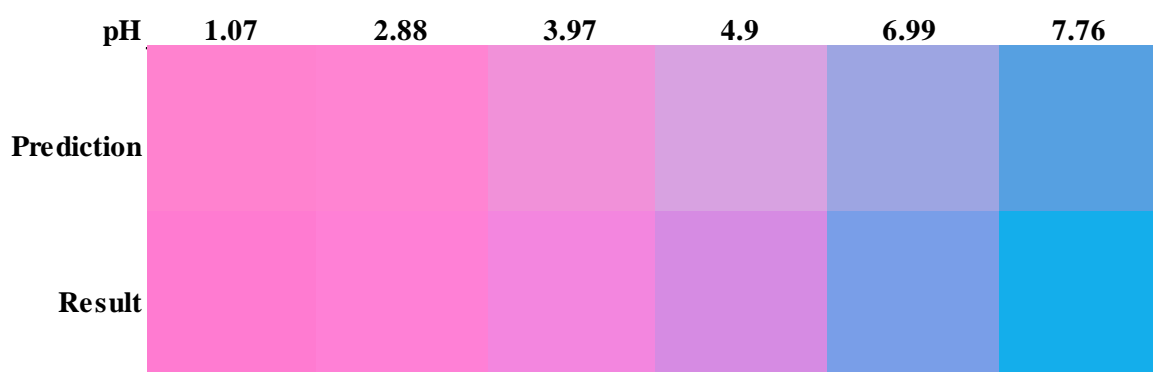


Fig 18-A. Color patches of pigment **P5** at $t=0$ (note: this pigments underwent metal complexation leading to a bathochromic shift (presence of trace metal in the water and buffers)).

Table. Predicted (top) vs. measured (bottom) L*a*b values for P5 at the pseudo-equilibrium.

pH	L	a	b	Cab	Hab
Prediction					
1,07	72,37	60,39	-15,31	62,30	345,8
2,88	72,91	57,29	-16,21	59,54	344,2
3,97	76,97	38,80	-18,26	42,88	334,8
4,9	81,43	21,70	-17,25	27,72	321,5
6,99	76,49	8,02	-25,10	26,35	287,7
7,76	67,82	-4,45	-36,03	36,30	263,0
Result					
1,07	72,37	60,39	-15,31	62,30	345,8
2,88	72,91	57,29	-16,21	59,54	344,2
3,97	76,97	38,80	-18,26	42,88	334,8
4,9	81,43	21,70	-17,25	27,72	321,5
6,99	76,49	8,02	-25,10	26,35	287,7
7,76	67,82	-4,45	-36,03	36,30	263,0

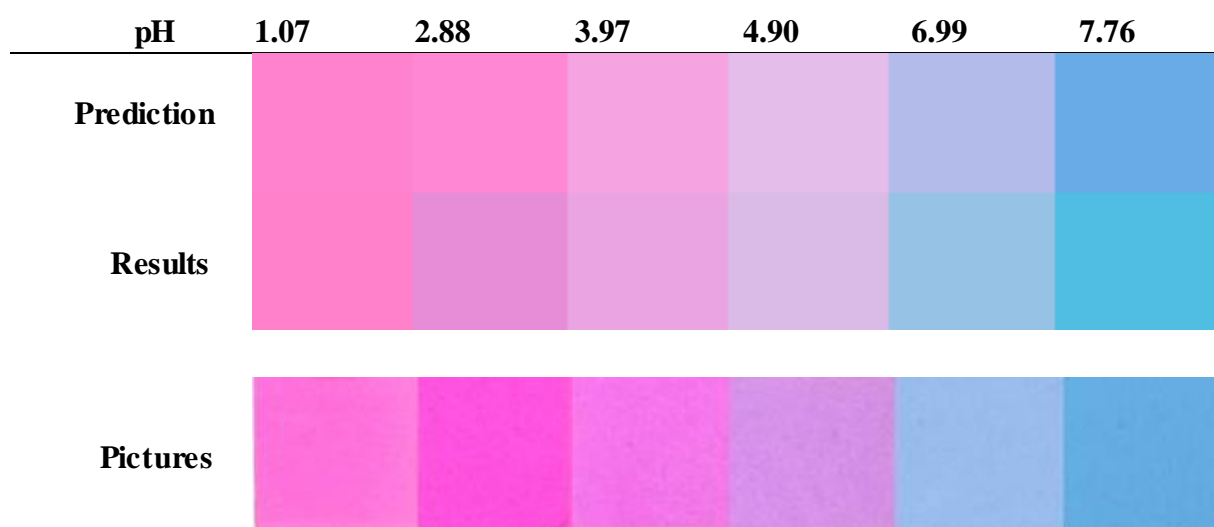


Fig 18-B. Color patches of **P5** at equilibrium (note: this pigments underwent slow metal complexation leading to a bathochromic shift (presence of trace metal in the water and buffers), c) Pictures of the cuvettes of P5, taken after 1 day, i.e. at the equilibrium

Table. Predicted (top) vs. measured (bottom) L*a*b values for P2 at t=0.

pH	L*	a*	b*	Cab*	Hab*
Prediction					
1.05p	77.25	54.81	-3.52	54.92	356.3
2.86p	77.11	54.58	-4.02	54.73	355.8
3.97p	75.95	52.21	-8.49	52.90	350.8
4.8p	74.34	45.32	-16.84	48.35	339.6
6.94p	69.12	21.70	-31.77	38.47	304.3
7.67p	66.05	3.30	-38.98	39.12	274.8
Result					
1.05	72.75	59.66	-15.28	61.58	345.6
2.86	85.80	31.38	-10.43	33.07	341.6
3.97	97.60	4.82	-2.04	5.23	337.0
4.8	99.24	1.13	-0.71	1.34	327.8
6.94	99.15	0.20	-0.96	0.98	281.7
7.67	97.53	-0.84	-3.04	3.15	254.6

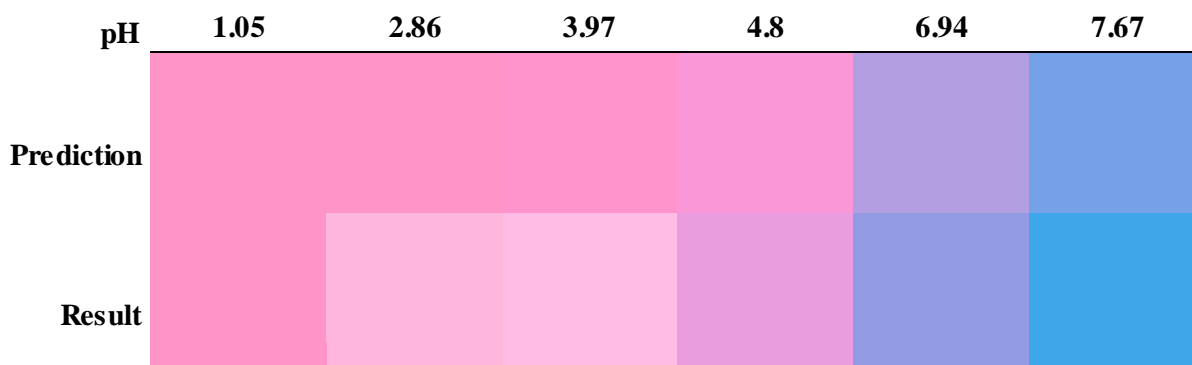


Fig 18-C. Color patches of **P2** at t=0, prediction and results. Note: the hydration was too fast for the picture, and even for spectrum record at low pH (2-5), so the pigment was partially hydrated in spite of the precautions.

Table. Predicted (top) vs. measured (bottom) L*a*b values for P2 at the pseudo-equilibrium.

pH	L*	a*	b*	Cab*	Hab*
Prediction					
1,05p	72.49	58.72	-15.73	60.79	345.0
2,86p	85.74	31.06	-10.54	32.80	341.3
3,97p	97.60	4.81	-2.05	5.23	337.0
4,8p	99.24	1.13	-0.71	1.34	327.8
6,94p	99.15	0.20	-0.96	0.98	281.7
7,67p	97.53	-0.84	-3.04	3.15	254.6
Result					
1,05	77.51	53.99	-3.75	54.12	356.0
2,86	88.14	28.45	-4.85	28.86	350.3
3,97	96.58	6.13	-2.18	6.51	340.4
4,8	97.06	2.69	-0.97	2.86	340.1
6,94	95.93	-0.53	-2.24	2.30	256.6
7,67	89.53	-6.66	-9.19	11.35	234.1

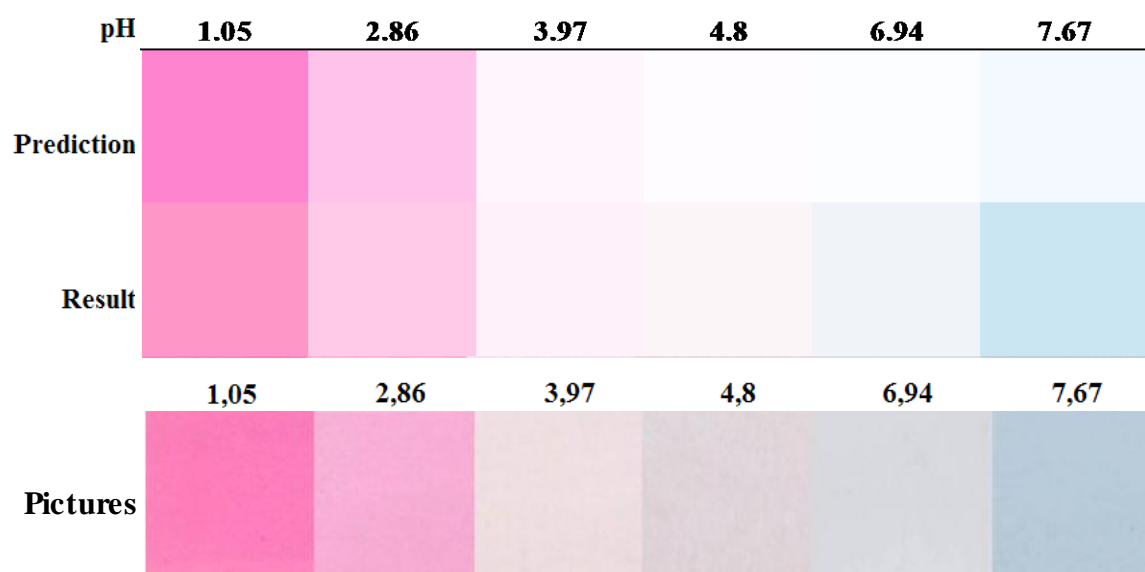


Fig 18.D. Color patches of pigment **P2** at the pseudo-equilibrium: prediction and obtained results (spectrum measurement and L*a*b* coordinates calculation (note: this pigments underwent slow metal complexation leading to a bathochromic shift (presence of trace metal in the water and buffers). Bottom: pictures of the cuvettes of P2 taken after 1 day.

Équipe d'encadrement

Pr. Olivier DANGLES, directeur de la thèse, Professeur, UMR 408 SQPOV (Sécurité et qualité des produits d'origine végétale), Equipe Micronutriments, Réactivité et digestion.

Abstract

Anthocyanins are ubiquitous plant pigments that exhibit bright colors from red to blue. Thus, they are good candidates to replace the synthetic food colors. However, the low stability of anthocyanin colors is a real hurdle to their industrial applications, especially under near neutral conditions required to express the blue color. A promising perspective is to resort to anthocyanins acylated by *p*-hydroxycinnamic acids, as these pigments develop color-stabilizing mechanisms (intramolecular copigmentation, self-association) based on strong π -stacking interactions between the anthocyanidin chromophore and the acyl residues. Therefore, this work investigates the structural transformations of acylated anthocyanins (proton transfer, water addition), their affinity to metal ions and their resistance to thermal degradation in the presence or absence of added metal ions. To that purpose, kinetic and thermodynamic studies by UV-visible spectroscopy are combined with the identification of degradation products by UPLC-DAD/MS.

The impact of the acyl residues (number, location, type) was deciphered from a series of isolated pigments from red cabbage and purple sweet potato. With the former, the acyl residue bound to the external glucose of the sophorose moiety provides a) optimal protection against attacks by H_2O , H_2O_2 and sulfite, b) improved affinity for metal ions, c) enhanced resistance against thermal degradation (for anthocyanins and their metal complexes). By contrast, caffeic acid, whether free or as an acyl residue (in purple sweet potato), accelerates the degradation of anthocyanins in spite of stabilizing the color.

Under moderate heating at pH 7, red cabbage anthocyanins were degraded into acylsophoroses, phloroglucinaldehyde-2-O-glucoside, protocatechuic acid, 3,5,7-trihydroxycoumarin derivatives, and 2,4,6-trihydroxyphenylacetic acid derivatives. Intramolecular acyl migration was also evidenced. The anionic base, a major colored form at pH 7, appears most vulnerable to autoxidation. The hydrogen peroxide thus produced is further involved in anthocyanin degradation. Overall, the tight binding of acylated anthocyanins to iron and aluminum ions and possibly the addition of natural antioxidants (e.g., N-acetylcysteine) are promising perspectives for the development of stable natural blue colors.

Résumé

Les anthocyanes sont des pigments d'origine végétale exprimant des couleurs vives allant du rouge au bleu. Ce sont donc de bons candidats pour remplacer les colorants alimentaires artificiels. Cependant, leur faible stabilité est un frein à ces applications, tout particulièrement en milieu neutre requis pour l'expression de la couleur bleue. Une perspective prometteuse est le recours aux anthocyanes acylées par les acides *p*-hydroxycinnamiques, car ces pigments développent des mécanismes protecteurs de la couleur (copigmentation intramoléculaire, auto-association) basés sur de fortes interactions d'empilement entre le chromophore et les résidus acyl. Ce travail étudie donc les transformations structurales d'anthocyanes acylées (transferts de proton, addition d'eau), leur affinité pour les ions métalliques et leur stabilité au cours d'un traitement thermique. Dans ce but, des études cinétiques et thermodynamiques par spectroscopie UV-visible sont combinées à l'identification de produits de dégradation par UPLC-DAD/MS.

L'impact des groupements acyl (nombre, position, type) a été étudié grâce à une gamme de pigments isolés du chou rouge et de la patate douce pourpre. Pour les premiers, les groupements acyl sur le sucre externe du groupement sophorose confèrent a) une protection optimale contre les attaques par H_2O , H_2O_2 and SO_3^{2-} , b) une plus grande affinité pour les ions métalliques, c) une plus grande stabilité thermique (pour les pigments et leurs complexes). En revanche, l'acide caféique, qu'il soit libre ou bien sous forme de résidu acyl (cas des anthocyanes de la patate douce violette), accélère la dégradation des anthocyanes, bien qu'il stabilise la couleur.

Un traitement thermique modéré à pH 7 a converti les anthocyanes du chou rouge en acylsophoroses, phloroglucinaldéhyde-2-O-glucoside, acide protocatéchique, dérivés de la 3,5,7-trihydroxycoumarine et de l'acide 2,4,6-trihydroxyphénylacétique. Un phénomène de migration intramoléculaire de résidus acyl a également été mis en évidence. La base anionique, une forme colorée majeure à pH 7, apparaît comme la plus vulnérable à l'autoxydation. Le peroxyde d'hydrogène ainsi formé est également impliqué dans la dégradation des anthocyanes.

Globalement, nos résultats montrent que la forte association des anthocyanes acylées avec les ions du fer et de l'aluminium, voire l'ajout d'antioxydants naturels (par ex., la N-acétylcystéine), constituent des voies d'avenir pour le développement de colorants bleus naturels stables.